

0061532



NASA CR-2629

F-8C DIGITAL CCV FLIGHT CONTROL LAWS


*Gary L. Hartmann, James A. Hauge,
and Russell C. Hendrick*

LOAN COPY: RETURN TO
AFWL TECHNICAL LIBRARY
KIRTLAND AFB, N. M.

Prepared by
HONEYWELL, INC.
Minneapolis, Minn. 55413
for Langley Research Center



NATIONAL AERONAUTICS AND SPACE ADMINISTRATION • WASHINGTON, D. C. • FEBRUARY 1976

1. Report No. NASA CR-2629		2. Government Accession No.		3. Report Number  0061532	
4. Title and Subtitle F-8C Digital CCV Flight Control Laws				5. Report Date February 1976	
				6. Performing Organization Code	
7. Author(s) Gary L. Hartmann James A. Hauge Russell C. Hendrick				8. Performing Organization Report No.	
				10. Work Unit No.	
9. Performing Organization Name and Address Honeywell, Inc. Systems and Research Center 2600 Ridgway Parkway Minneapolis, Minnesota 55413				11. Contract or Grant No. NAS1-12680	
				13. Type of Report and Period Covered Contractor Report October 1973 - Sept. 1974	
12. Sponsoring Agency Name and Address NASA Langley Research Center Hampton, Virginia 23665				14. Sponsoring Agency Code	
15. Supplementary Notes Contract Monitor: Mr. Joseph Gera Flight Dynamics and Control Division Final report.					
16. Abstract A set of digital flight control laws were designed for the NASA F-8C digital fly-by-wire aircraft. The control laws emphasize Control Configured Vehicle (CCV) benefits. Specific pitch axis objectives were improved handling qualities, angle-of-attack limiting, gust alleviation, drag reduction in steady and maneuvering flight, and a capability to fly with reduced static stability. The lateral-directional design objectives were improved Dutch roll damping and turn coordination over a wide range in angle-of-attack. An overall program objective was to explore the use of modern control design methodology to achieve these specific CCV benefits. Tests for verifying system integrity, an experimental design for handling qualities evaluation, and recommended flight test investigations have also been specified.					
17. Key Words (Suggested by Author(s)) F-8C Aircraft Digital Fly-by-Wire Optimal Control Flight Control Control Configured Vehicle			18. Distribution Statement Unclassified - unlimited Subject Category 08		
19. Security Classif. (of this report) Unclassified		20. Security Classif. (of this page) Unclassified		21. No. of Pages 457	22. Price* \$11.50

For sale by the National Technical Information Service, Springfield, Virginia 22161

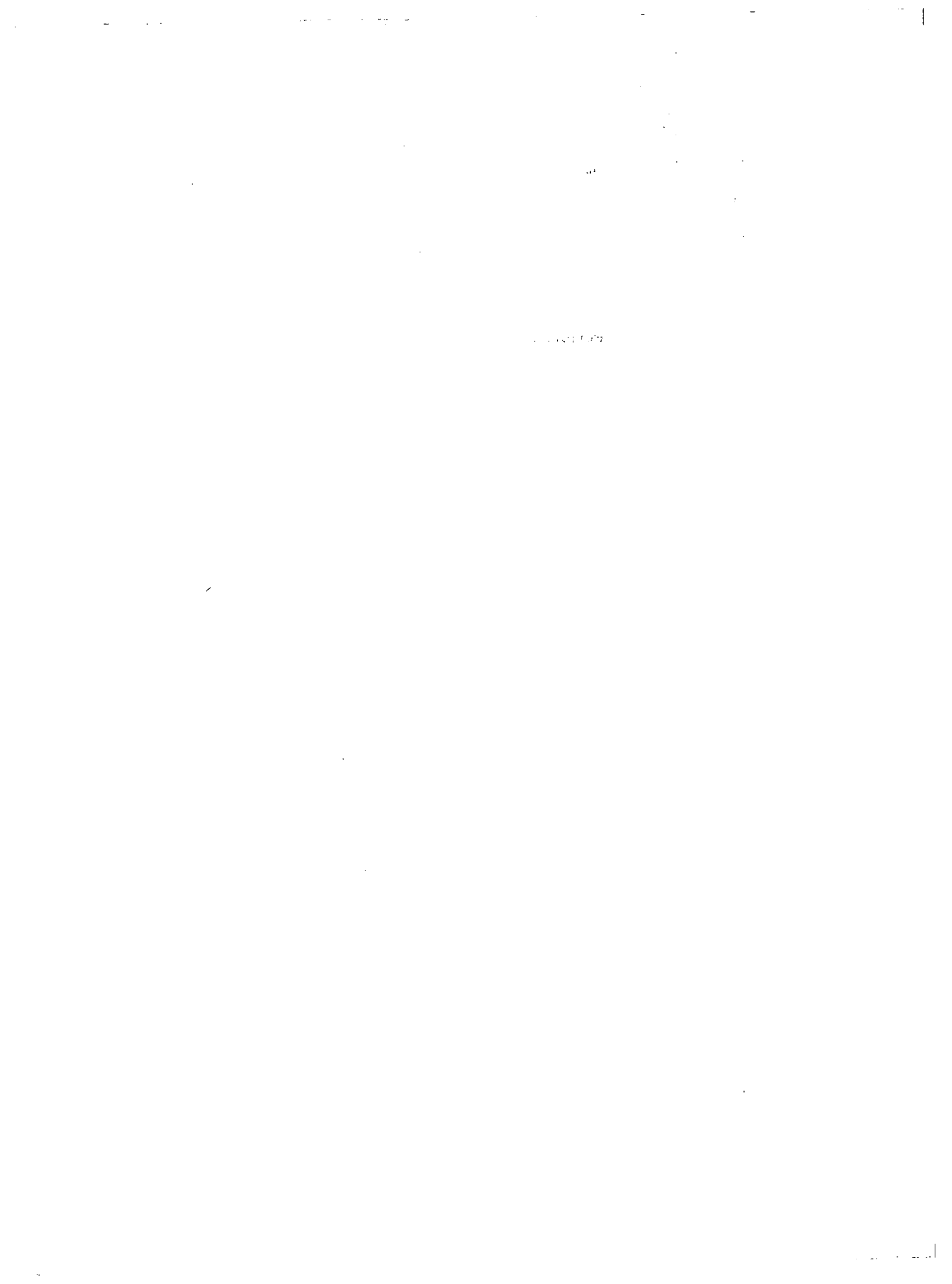


TABLE OF CONTENTS

Section		Page
1	PROGRAM OVERVIEW AND SUMMARY	1
	The Design Procedure	1
	Aircraft Modeling	1
	Quadratic Optimal Control Synthesis	2
	Digital Analysis	2
	Simulator Verification	2
	Control Law Functions	2
	Pitch CAS	2
	Lateral-Directional CAS	3
	Outer Loop Modes	3
	Performance Results	4
2	INTRODUCTION.	5
	Background	5
	Objectives	5
	Ground Rules	6
	Scope of Work	6
	Document Organization	6
3	SYMBOLS	7
4	CCV OBJECTIVES	12
	Longitudinal.	12
	Handling Qualities	12
	Angle-of-Attack Limiting.	13
	Good Control with Reduced Static Stability.	18
	Gust Effect Reduction.	19
	Maneuver Load Control (MLC)	19
	Transport-type MLC.	19
	Fighter-type MLC	21
	Lateral-Directional Objectives	22
	Handling Qualities.	22
	High Angle-of-Attack Performance.	23
5	DESIGN PROCEDURE.	26
	Overview	26
	Quadratic Design	28
	Continuous-Time Quadratic Formulation	28
	Discrete Quadratic Formulation	32
	Fixed Form Optimal Synthesis.	32
	Sampling Time Considerations	34
	Digital Analysis.	35
	Discrete Model for the Physical Plant	38
	Discrete Model for the Controller.	40
	General Frequency Response Software	42
	RMS Response of Plant to Continuous Stationary Inputs.	43

TABLE OF CONTENTS (Continued)

Section		Page
6	MODELING	45
	Linear Aircraft Model	45
	Actuator Dynamics.	50
	Gust (Turbulence) Model	51
	Augmented Model	53
	State Transformation	53
	Pitch Axis Model for Relaxed Static Stability.	54
7	SYNTHESIS OF PITCH AXIS CONTROL AUGMENTATION. . SYSTEM (CAS)	56
	Normal Elevator Controller	56
	Neutral Speed Stability Implementation	63
	Angle-of-Attack Boundary Controller Design.	63
	Mode Switching.	65
	Adaption over the Flight Envelope	68
	Mode I Results	68
	Reduced Static Stability Study	77
	Control Law Modifications	77
	Servo Actuator Requirements	78
	Symmetric Aileron Controller	98
	Minimum Drag Schedule	98
	Direct Lift Implementation	100
	Integration of Flap Schedule and Direct Lift	103
	Performance of Symmetric Aileron Controller.	105
	Pitch CAS Functional Block Diagram	110
	NASA/LRC Simulator Results	112
8	SYNTHESIS OF A LATERAL-DIRECTIONAL CAS WITH INERTIAL COORDINATION	125
	Linear Models for Lateral-Directional CAS Design	125
	Lateral-Directional Fixed Point Designs	128
	Gain Scheduling and Block Diagram Definition	131
	Roll Axis Gain Scheduling	132
	Yaw Axis Gain Scheduling	144
	Lateral-Directional Control Augmentation System	154
	Block Diagrams	
	Performance Summary	159
9	SYNTHESIS OF LATERAL-DIRECTIONAL CAS WITH REDUCED MEASUREMENT SET	170
	Fixed Point Designs	170
	Gain Scheduling and Block Diagram Definition	172
	Performance Summary	174

TABLE OF CONTENTS (Continued)

Section		Page
10	LATERAL-DIRECTIONAL SENSOR CONSIDERATIONS	196
	AND COMPARISON OF CAS DESIGNS	
	Sensor Considerations	196
	Application of Acceleration Plus Yaw Rate Control	197
	Benefits of Attitude-Referenced Yaw Control	199
	Performance Comparison	199
11	OUTER LOOP MODES	205
	Pitch Axis	205
	Lateral-Directional Outer Loops	210
12	SYSTEM INTEGRATION VERIFICATION	212
	Open-Loop Frequency Response Tests	212
	Gain Schedule Verification	212
	Closed Loop Ground Tests	273
	Surface Position Tests	273
	Structural Stability Tests	273
	Closed Loop Rigid Body Flight Function	274
13	SIMULATOR PROGRAM DEFINITION	278
	Overview	278
	Experimental Design	278
	Subjects	280
	Task	282
	Procedure	282
	Data Analysis	283
	Data Interpretation	284
14	FLIGHT TEST INVESTIGATION	286
	Digital Flight Control System (DFCS)	286
	Boundary Control	290
	Unaccelerated Limiting	290
	Accelerated Limiting	290
	Maneuver Load Control (Q-Flaps)	291
	MLC Plus Response Augmentation (Nz-Flaps)	291
	Autopilot Modes	292
	Pitch and Roll Attitude Hold	292
	Heading Hold	292
	Altitude Hold	292
	Mach Hold	293
15	CONCLUDING REMARKS	294

TABLE OF CONTENTS (Continued)

Appendix		Page
A	Definition of "A" Array Parameters Used in F8SIM . . .	295
B	Twenty Flight Conditions	303
C	F8SIM Program	405
D	F-8C Wing Root Loads	421
E	Experience Questionnaire and Global and Cooper- Harper Rating Scales	440
	REFERENCES	444

LIST OF ILLUSTRATIONS

Figure		Page
1.	C* Envelope	14
2.	Pitch Stick Gradient	15
3.	Angle-of-Attack Limiting	17
4.	Relaxed Static Stability Obtained by Shifting c.g. Aft	18
5.	Conventional Static Stability.	18
6.	Transport Aircraft Ideal Lift Distribution	20
7.	Fighter Aircraft Ideal Lift Distribution	21
8.	Sideslip Excursion Limitations	24
9.	Roll Rate Oscillation Limitations	24
10.	Design Process	27
11.	Quadratic Design Process	29
12.	Zero Order Hold with and without Phase Lead Compensation	36
13.	General Open Loop Frequency Response of Digital Controller	37
14.	State Diagram of the Digitized Controller	42
15.	The F-8C Aircraft	46
16.	Hysteresis Model	50
17.	Pitch CAS Structure	57
18.	States for Pitch CAS Design	58
19.	Block Diagram of Pitch CAS Optimal Design.	61
20.	NSS Implementation	64
21.	Boundary Controller Structure	65
22.	Block Diagram of Angle-of-Attack Limiting Controllers	67
23.	Mode Transition Logic	69
24.	K_C * Gain Schedule	70
25.	$K_{\alpha L}$ Gain Schedule	70
26.	Pitch CAS (Mode I)	71
27.	Pitch CAS and Boundary Control (Mach 0.67, 20,000 feet)	72
28.	Pitch CAS and Boundary Control (Mach 0.4, 20,000 feet)	73
29.	Pitch CAS and Boundary Control (Mach 0.8, 10,000 feet)	74
30.	Pitch CAS and Boundary Control (Mach 0.19, Sea Level)	75
31.	Pitch CAS RSS Controller	76
32.	RSS Response (FC 17; c.g. at 36%).	79
33.	RSS Response (FC 17; c.g. at 41%).	80

LIST OF ILLUSTRATIONS (Cont.)

Figure	Page
34. RSS Response (FC 17; c.g. at 48%)	81
35. RSS Response (FC 5; c.g. at 29%)	82
36. RSS Response (FC 5, c.g. at 40%)	83
37. RSS Response (FC 5, c.g. at 48%)	84
38. RSS Response (FC 1, c.g. at 29%)	85
39. RSS Response (FC 1, c.g. at 40%)	86
40. RSS Response (FC 1, c.g. at 48%)	87
41. RSS Response (FC 8; c.g. at 29%)	88
42. RSS Response (FC 8; c.g. at 48%)	89
43. RSS Response (FC 9, c.g. at 29%)	90
44. RSS Response (FC 9, c.g. at 40%)	91
45. RSS Response (FC 9; c.g. at 48%)	92
46. Analog Hysteresis Model.	94
47. Hysteresis Response (FC 5; c.g. at 48%)	95
48. Hysteresis Response (FC 9; c.g. at 48%)	96
49. Hysteresis Response (FC 1; c.g. at 48%)	97
50. Cruise Flap Schedule.	99
51. Accelerated Flight Condition.	99
52. Flap Schedule.	100
53. Gust Alleviation Controller Structure	102
54. N_Z Flap Compensation	103
55. Command and Gravity Compensation for N_Z Flap Mode.	104
56. Alternate N_Z Flap Compensation	105
57. Step Gust Response (FC 1)	106
58. Step Gust Response (FC 5)	107
59. Step Stick Response (FC 1)	108
60. Step Stick Response (FC 5)	109
61. Mode I Digital Controller.	111
62. Symmetric Aileron Digital Controller	113
63. FC 9 Open Loop Frequency Response 10 SPS	114
64. FC 9 Open Loop Frequency Response 20 SPS	115
65. FC 9 Open Loop Frequency Response 40 SPS	116
66. Transient Response (Mode I 20K; M = 0.67)	117

LIST OF ILLUSTRATIONS (Cont.)

Figure		Page
67.	Transient Response (N_Z , q Mode 20K; $M = 0.67$)	118
68.	Transient Response (Mode I 20K; $M = 0.4$).	119
69.	Transient Response (N_Z , q Mode 20K; $M = 0.4$).	120
70.	Transient Response (Mode I 10K; $M = 0.8$).	121
71.	Transient Response (N_Z , q Mode 10K; $M = 0.8$).	122
72.	Transient Response (Mode I, N_Z , q Mode 40K; $M = 1.1$)	123
73.	Transient Response (Mode I 3K; $M = 0.25$)	124
74.	Lateral CAS Structure	134
75.	Alternate Lateral CAS Structure	135
76.	Roll Rate Command	136
77.	Roll Rate Error Command	137
78.	Roll Axis Structure	139
79.	K_{Ar} Schedule	140
80.	$K_{A\dot{\beta}}$ Schedule	141
81.	K_{Ae} Schedule	142
82.	$K_{An_{syl}}$ Schedule	143
83.	$K_{R\varphi}$ vs. V	145
84.	K_{Rr} vs. α	146
85.	K_{21} vs. α	147
86.	$K_{Rn_{ysl}}$ Schedule	149
87.	$K_{Rn_{ysli}}$ Schedule	150
88.	$K_{R\delta_A}$ Schedule	151
89.	K_{Rp_m} Schedule	152
90.	K_{Ru_m} Schedule	153
91.	Roll Axis Lateral-Directional CAS with Inertial Coordination	155
92.	Yaw Axis Lateral-Directional CAS with Inertial Coordination	156
93.	Digitized Roll Axis Lateral-Directional CAS with Inertial Coordination	158
94.	Digitized Yaw Axis Lateral-Directional CAS with Inertial Coordination	159
95.	Stick and Gust Responses, Inertially Coordinated CAS, Mach .67, Altitude 20,000 ft.	162

LIST OF ILLUSTRATIONS (Cont.)

Figure	Page
96. Stick and Gust Responses, Inertially Coordinated CAS, Mach .4, Altitude 20,000 ft.	163
97. Stick and Gust Responses, Inertially Coordinated CAS, Mach .9, Altitude 20,000 ft.	164
98. Stick and Gust Responses, Inertially Coordinated CAS, Mach .7, Altitude 40,000 ft.	165
99. Stick and Gust Responses, Inertially Coordinated CAS, Mach 1.2, Altitude 40,000 ft.	166
100. Stick and Gust Responses, Inertially Coordinated CAS, Mach .7, Altitude 1,000 ft.	167
101. Stick and Gust Responses, Inertially Coordinated CAS, Mach .3, Altitude 1,000 ft.	168
102. Stick and Gust Responses, Inertially Coordinated CAS, Mach .189, Altitude 1,000 ft.	169
103. K'_{Au_m} Schedule	175
104. $-K'_{Ae}$ Schedule	176
105. K'_{Rr_w} Schedule	177
106. $K'_{Rn_{ysl}}$ Schedule	178
107. $K'_{Rn_{ysli}}$ Schedule	179
108. $K'_{R\delta_A}$ Schedule	180
109. K'_{Rp} Schedule	181
110. Roll Axis Lateral-Directional CAS with Reduced Measurements . . .	182
111. Yaw Axis Lateral Directional CAS with Reduced Measurements . . .	183
112. Digitized Roll Axis Lateral-Directional CAS with Reduced Measurements	184
113. Digitized Yaw Axis Lateral Directional CAS with Reduced Measurements	185
114. Stick and Gust Responses Reduced Measurement CAS (20,000 ft.; Mach .67)	188
115. Stick and Gust Responses Reduced Measurement CAS (20,000 ft.; Mach .4)	189
116. Stick and Gust Responses Reduced Measurement CAS (20,000 ft.; Mach .9)	190
117. Stick and Gust Responses Reduced Measurement CAS (40,000 ft.; Mach .7)	191

LIST OF ILLUSTRATIONS (Cont.)

Figure		Page
118.	Stick and Gust Responses Reduced Measurement CAS. (40,000 ft.; Mach 1.2)	192
119.	Stick and Gust Responses Reduced Measurement CAS. (1,000 ft.; Mach .7)	193
120.	Stick and Gust Responses Reduced Measurement CAS. (1,000 ft.; Mach .3)	194
121.	Stick and Gust Responses Reduced Measurement CAS. (1,000 ft.; Mach .189)	195
122.	3-g Pull-up with Inertial Lateral CAS h = 20,000 M = 0.6	201 - 202
123.	3-g Pull-up with Reduced Measurement Lateral CAS h = 20,000 M = 0.6	203 - 204
124.	Pitch Outer Loops	206
125.	Pitch Autopilot Gain Schedule	207
126.	Mach Hold Control	208
127.	Altitude Hold Dynamics	209
128.	Lateral Outer Loops	211
129.	Sensed Pitch Rate to Elevator	217
130.	Pitch Rate to Elevator Frequency Response (continuous)	218
131.	Pitch Rate to Elevator Frequency Response (32 sps)	219
132.	Sensed Normal Acceleration to Elevator	220
133.	Normal Acceleration to Elevator Frequency Response (continuous).	221
134.	Normal Acceleration to Elevator Frequency Response (32 sps)	222
135.	Pitch Stick to Elevator	223
136.	Pitch Stick to Elevator Frequency Response (continuous)	224
137.	Pitch Stick to Elevator Frequency Response (32 sps)	225
138.	Pitch Rate to Elevator and Flaps	226
139.	Pitch Rate to Elevator Frequency Response (continuous)	227
140.	Pitch Rate to Elevator Frequency Response (32 sps)	228
141.	Pitch Rate to Flaps Frequency Response (continuous)	229
142.	Pitch Rate to Flaps Frequency Response (32 sps)	230
143.	Pitch Stick to Flaps	231
144.	Pitch Stick to Flaps Frequency Response (continuous)	232
145.	Pitch Stick to Flaps Frequency Response (32 sps)	233
146.	Normal Acceleration to Flaps	234

LIST OF ILLUSTRATIONS (Cont.)

Figure		Page
147.	Normal Acceleration to Flaps Frequency Response (continuous)	235
148.	Normal Acceleration to Flaps Frequency Response (32 sps)	236
149.	Pitch Rate to Elevator	237
150.	Pitch Rate to Elevator Frequency Response (continuous)	238
151.	Pitch Rate to Elevator Frequency Response (32 sps)	239
152.	Angle-of-Attack to Elevator	240
153.	Angle-of-Attack to Elevator Frequency Response (32 sps)	241
154.	Angle-of-Attack to Elevator Frequency Response (continuous)	242
155.	Pitch Rate to Elevator (Boundary Function)	243
156.	Pitch Rate to Elevator Frequency Response (continuous)	244
157.	Pitch Rate to Elevator Frequency Response (32 sps)	245
158.	Roll Rate to Aileron and Rudder	246
159.	Roll Rate to Aileron Frequency Response (continuous)	247
160.	Roll Rate to Aileron Frequency Response (32 sps)	248
161.	Roll Rate to Rudder Frequency Response (continuous)	249
162.	Roll Rate to Rudder Frequency Response (32 sps)	250
163.	Roll Stick to Aileron	251
164.	Roll Stick to Aileron Frequency Response (continuous)	252
165.	Roll Stick to Aileron Frequency Response (32 sps)	253
166.	Yaw Rate to Rudder	254
167.	Yaw Rate to Rudder Frequency Response (continuous)	255
168.	Yaw Rate to Rudder Frequency Response (32 sps)	256
169.	Lateral Acceleration to Rudder	257
170.	Lateral Acceleration to Rudder Frequency Response (continuous) . . .	258
171.	Lateral Acceleration to Rudder Frequency Response (32 sps)	259
172.	Roll Rate to Rudder	260
173.	Roll Rate to Rudder Frequency Response (continuous)	261
174.	Roll Rate to Rudder Frequency Response (32 sps)	262
175.	Pitch Attitude to Elevator	263
176.	Pitch Attitude to Elevator Frequency Response (continuous)	264
177.	Pitch Attitude to Elevator Frequency Response (16 sps)	265
178.	Heading to Ailerons	266
179.	Heading to Aileron Frequency Response (continuous)	267

LIST OF ILLUSTRATIONS (Cont.)

Figure		Page
180.	Heading to Aileron Frequency Response (16 sps)	268
181.	Experimental Design	279
182.	Experimental Design for Comparison of Gust Effects on Pilot Performance	279
183.	Experimental Design for Comparison of Speed and Altitude Effects on Pilot Performance	281
184.	Typical Flight Profile	281
185.	Flight Control Test Conditions	287

LIST OF TABLES

Table	Page
1. C-5A Maneuver Load Control	20
2. DIGIKON-2 Subroutines	38
3. State Definition	47
4. Control Definition	47
5. Disturbance Vector	48
6. Output Vector , ,	48
7. Twenty Flight Conditions	49
8. Actuator Model Parameters	50
9. Augmented State Vector	53
10. RSS Modeling Summary	55
11. Pitch CAS Mode I Design Summary	60
12. Pitch CAS Parameters	62
13. Boundary Controller Design Summary	66
14. Boundary Controller Parameters	67
15. RSS Time Responses	78
16. Limit Cycle Characteristics with 0.01 Rad. Servo Hysteresis	93
17. RMS Gust Acceleration Response	110
18. Response Vector for Lateral CAS Design	127
19. Design Flight Conditions	128
20. Closed Loop Roots	160
21. Inertially Coordinated Lateral-Directional CAS Performance Summary	161
22. State Vector - Lateral - Directional	171
23. Measurement Vector	172
24. Closed Loop Roots, Reduced Measurements CAS	186
25. Lateral-Directional CAS with Reduced Measurements Performance Summary	187
26. Open-Loop Frequency Responses	213 - 216
27. Open-Loop Gain Schedule Tests	269 - 272
28. Closed-Loop Simulated Flight Functions	275 - 277
29. Analysis of Variance Output Format	285
30. Mode Test Sequence	286
31. DFCS Test Sequence	288

F-8C DIGITAL CCV FLIGHT CONTROL LAWS

Gary L. Hartmann, James A. Hauge, and Russell C. Hendrick

SECTION 1

PROGRAM OVERVIEW AND SUMMARY

NASA is conducting a flight control research program in digital fly-by-wire technology using a modified F-8C aircraft. The first phase of this program used Apollo hardware to demonstrate the practicality of digital fly-by-wire in an actual test vehicle. ^[1] For the second phase, conventional aircraft sensors and a large floating-point digital computer are being utilized to test advanced control laws and redundancy concepts.

As part of this research activity, Honeywell initiated work in 1973 under Contract NAS1-12680 to provide a system of digital flight control laws for flight test in Phase II. These control laws were to emphasize control configured vehicle (CCV) benefits. Specific pitch axis objectives were improved handling qualities, angle-of-attack limiting, gust alleviation, drag reduction in steady and maneuvering flight, and a capability to fly with reduced static stability. The lateral-directional design objectives were improved Dutch roll damping and turn coordination over a wide range in angle-of-attack. An overall program objective was to explore the use of modern control design methodology to achieve these specific CCV benefits.

The control laws were constrained to be compatible with the existing airframe without structural modification. Hence, the control laws use only existing elevator, rudder, and ailerons as control effectors, each powered by existing actuators. Altered control surfaces or new force producers were not considered. However, the ailerons are commanded symmetrically to provide an additional control input in the pitch axis. The control laws were also constrained to use available sensors. These were limited to pitch, roll, and yaw gyros and normal and lateral accelerometers. Air data measurements included angle-of-attack, Mach number, and pressure altitude.

The program successfully generated a package of CCV control laws that are ready for flight test. These control laws meet all handling quality requirements for the aircraft. They provide automatic boundary limiting, a 40 percent reduction in gust load accelerations, and a 15 percent maneuver load drag reduction. The capability for flying with reduced static stability have been provided. Tests for verifying systems integrity, an experimental design for handling qualities evaluation, and recommended flight test investigations have also been specified.

The remainder of this overview will summarize the design procedure, the control law functions, and performance results.

The Design Procedure

The major steps of the design process involved linear modeling, control law synthesis with optimal control theory, digital controller analysis, and design verification on a nonlinear six-degree-of-freedom simulation. The study utilized existing software design tools in the first three areas. The last task was conducted using the DFBW F-8C simulator at NASA/LRC. The major accomplishments of each task are summarized below.

Aircraft Modeling--NASA supplied nonlinear aerodynamic data for the F-8 as a function of Mach, altitude, angle-of-attack, and surface position. This data was used

directly in a generalized modeling program to quickly set up a nonlinear digital simulation. Linear models were obtained by numerically trimming the aircraft equations at selected conditions. Numerical differentiation, based on small perturbations in each of the states and controls, was used to compute the system matrices. The actuator models and gust filters were then appended to complete the modeling process. Use of this generalized modeling tool provides linear models about any flight condition including accelerated flight at very low cost. [2]

Quadratic Optimal Control Synthesis--Linear-quadratic optimal control methodology was extensively used in the design of the CCV control laws. A major portion of the CAS design was concerned with specifying performance within the framework of optimal control methodology. This involves the development of a problem structure and quadratic cost criteria such that the resulting feedback controller exhibits the desired performance. The criteria found most useful are in the form of response equations that include selected linear combinations of states and control inputs. [3]

Application of the quadratic procedure is an iterative process of choosing responses and weighting matrices. The choice of responses and weights is expedited by the designer's past experience and his understanding of the physics of the control problem. The procedure does not replace classical techniques but is a powerful design aid.

Digital Analysis--Major concerns in digital controllers are the effects of computational delays, sampling rates, and word lengths on performance. Since the Phase II computer has floating point arithmetic, word length is not a concern. Computational delays are minimized in the control software by proper sequencing of the computations. This leaves the sampling rate as the major digital control issue. Its effect on digital controller performance was evaluated with the aid of another software package (DIGIKON), which computes closed loop eigenvalues, transient responses to step commands, rms responses to random gusts, and open loop frequency responses of digital and hybrid systems. Frequency responses were used to check the controller bandwidth and to assess phase and gain margins. The sample rate was then selected on the basis of these margins. [4]

Simulator Verification--The CCV control laws were verified on NASA/LRC's F-8C simulator in four simulator sessions. The interface with LRC's real-time F-8C nonlinear simulation went smoothly. The package of CCV control laws was coded in FORTRAN as a separate subroutine, which resulted in rapid and easy procedures to check performance against predictions based on linear models.

Agreement between the complete nonlinear simulation results and linear model results has been good. This has instilled a high degree of confidence in the control laws and their design procedure.

Control Law Functions

The CCV control law package provides three control modes for the pitch axis, one basic mode for the lateral-directional axes, and several outer loops. These are described briefly below:

Pitch CAS--The pitch CAS consists of a basic elevator controller incorporating angle-of-attack limiting plus two additional modes that command symmetric aileron deflection in addition to the elevator.

- Basic Elevator Mode--The desired handling qualities were specified in the time domain in the form of a C* model response. The resulting controller is an explicit model-following design implemented with a second order C*

model. The C^* quantity is defined as a fixed ratio of normal acceleration and pitch rate. This criterion was chosen because it permits the designer to control one response with one forcing function (the elevator). At high dynamic pressures, the elevator produces primarily normal acceleration, and at low dynamic pressures, it produces primarily pitch rate; hence, the sum of these responses produces a composite variable that has significance at all flight conditions. [5, 6]

A separate elevator controller was designed to hold a reference angle-of-attack. This boundary controller, designed with quadratics, provides proportional plus integral action on the angle-of-attack error and uses pitch rate feedback for damping the short-period dynamics.

The two elevator controllers were integrated with a switching strategy which provides smooth transition from normal control to boundary control whenever the pilot commands an angle-of-attack higher than a preset reference limit. The mode transition also protects against unaccelerated stalls. The switching strategy is based on commanded elevator rates. This ensures smooth transitions and eliminates elevator trim problems.

- **Symmetric Aileron Modes**--Two modes for commanding symmetric ailerons are also provided. The first mode provides a minimum drag schedule. The second option combines elevator and symmetric ailerons dynamically to provide direct lift in addition to drag reduction. Direct lift provides a significant reduction in gust induced normal acceleration and achieves faster command responses.

Lateral-Directional CAS--The primary design objectives included good roll rate response, improved Dutch roll damping, and good turn coordination over a wide variation in angle-of-attack. Two lateral designs were produced with optimal control theory to meet these objectives. Both designs used explicit model-following to match a simple first order roll rate model. Additional response criteria were weighted to minimize sideslip and peak lateral acceleration for a roll stick command.

The first design used full-state feedback and achieved the best performance by commanding a theoretical yaw rate to perfectly coordinate a turn. Errors are used to damp the Dutch roll. The result is excellent coordination and good damping regardless of the angle-of-attack. Unfortunately these feedbacks require several difficult to measure signals. Angle-of-attack and true air speed are required in addition to rates and attitudes.

An alternate lateral-directional CAS was designed for applications not having an all-attitude platform or true airspeed available. This design was based on minimizing the same performance index as the full state design but with a reduced set of sensor feedbacks. The design resulted in gains scheduled with angle-of-attack. It exhibits similar performance with minimum degradation at high angles-of-attack when compared to the full state design. The practicalization quadratic software used to reduce the measurement set permitted the design to be completed in one week. This software demonstrates a convenient and sensible basis on which to conduct tradeoffs on type and number of sensors to be used in controller mechanizations.

Outer Loop Modes--Conventional outer loop modes including altitude hold, attitude hold, and Mach hold were added to the pitch CAS. The lateral axis includes a roll attitude hold mode and a heading hold mode. These loops demonstrate that conventional autopilot modes are completely compatible with inner loops designed with optimal control methods.

Performance Results

The basic elevator controller provides improved handling qualities and automatic angle-of-attack boundary limiting. Mode transitions to the boundary without overshooting the boundary have been demonstrated on the nonlinear simulation. The C* elevator controller provides Level I (MIL 8785A) fighter handling qualities as defined by short-period frequency and damping characteristics.[7] The pitch CAS can accommodate reduced static stability caused by shifting the center of gravity aft. Variations in the center of gravity from 29 percent mean-aerodynamic-chord (nominal static stability margin) to 48 percent (very unstable) were studied. Such dramatic variations in the center of gravity are not experienced under normal loading conditions. Instead, they are meant to represent different airframe designs. The pitch CAS demonstrates that conventional handling qualities can be achieved for airframes designed for efficiency rather than unaugmented handling qualities.

A minimum drag schedule is included in both symmetric aileron modes. This schedule was determined from an analysis of the F-8C aerodynamic data augmented by NASA flight test results.[8] The predicted drag reduction ranges from 10 to 30 percent at various flight conditions. This amount of drag reduction provides increased sustained turn capabilities on the order of one incremental "g".

The first symmetric aileron mode mechanizes the drag schedule as a function of low passed pitch rate. The second mode combines symmetric ailerons with elevator to dynamically provide direct lift in addition to drag reduction. Direct lift provides about 40 percent reduction in acceleration due to wind gusts when compared to the unaugmented aircraft. This is a significant improvement in ride qualities. Direct lift also provides faster acceleration response to stick commands (for the same amount of pitch rate overshoot) than is obtainable with only the elevator. At low dynamic pressure flight conditions (e.g., 110 psf) the normal acceleration response of the direct lift mode is twice as fast as the basic elevator mode. This capability enhances the pilot's ability to perform precision tracking tasks.

The lateral-directional CAS meets Level I fighter handling qualities. It also demonstrates improvements in Dutch roll damping and turn coordination at high angle-of-attack. For high angle-of-attack turns, the peak value of sideslip is reduced by an order of magnitude when compared to the unaugmented airframe. In addition the full state feedback CAS demonstrates a feedback structure that can accommodate a statically unstable yaw axis. This will be required in future CCV aircraft to reduce tail surface area and perform decoupled maneuvers.

SECTION 2

INTRODUCTION

Background

NASA is presently conducting a research program in digital fly-by-wire technology using a modified F-8C aircraft as the test vehicle. In 1972-73 during the first phase of this program the F-8C made a number of successful flights using an Apollo guidance computer, an inertial measurement unit, an analog (electrical) backup system, and an electrohydraulic actuation system. These flights have demonstrated the practicality of a digital fly-by-wire flight control system in an actual test vehicle. [1]

The F-8 Digital Fly-By-Wire program has now entered a second phase which is intended to support technology development of advanced, reliable control systems for future aircraft. Primary objectives are to demonstrate benefits of advanced control laws and to study redundant flight control. [9]

In Phase II, the test aircraft will use a triplex AP-101 digital computer and triplex redundant aircraft gyros and accelerometers. Dual air data measurements of angle-of-attack, Mach number, and pressure altitude, and a single sideslip sensor are also provided. Of special importance is the extensive computing power offered by the large, floating-point computer in the test aircraft. This capability makes it possible to flight test advanced control laws without the usual time and memory constraints imposed by less capable flight control computers.

One of the control law packages to be flight tested during Phase II is the so-called "CCV Package." This package consists of a collection of control modes designed to demonstrate potential control-configured-vehicle (CCV) benefits for current and future aircraft. The design process, tradeoffs, and performance results for these control laws are the subject of this report.

Objectives

The objective of the work reported here was to provide a digital flight control augmentation system, suitable for flight test, which demonstrates significant CCV benefits. Also of interest was the exploration of the use of modern control theory in achieving these benefits.

Candidate CCV concepts included the following areas. All have been studied analytically on various aircraft; some have been flight tested. [10]

- Improved handling qualities (numerous)
- Flight envelope limiting (F-101, F-103)
- Reduced static stability (C-5A, F-4, YF-16)
- Gust acceleration reduction (B52, XB-70, B-1, C-5A, YF-12)
- Maneuver load control (MLC)
 - Fighter type - minimum drag during maneuvers (F4, YF-16)
 - Transport type - minimum structural fatigue (B-52, C5-A)
- Active control of structural modes (B-52, YF-12)

The first five CCV concepts were studied and implemented in the CCV control laws for the F-8C. Transport-type MLC and active structural control were not included because these require more detailed knowledge of the effects of the structural modes than was available for the airframe. Pitch axis handling qualities were specified in the time domain as an envelope of desirable "C*" time histories. Specific lateral-directional handling quality objectives were improved Dutch roll damping and turn coordination over a wide range in angle-of-attack.

Ground Rules

While CCV designs are ideally conducted in parallel with the design of an airframe, the CCV laws for the F-8C were constrained to be compatible with the existing airframe and the existing sensor complement. Hence, the control laws were to emphasize the CCV concepts that could be accommodated by the flight control system of the experimental aircraft without structural modification. The existing actuators were used and no altered control surfaces or added force producers were considered. The control laws developed use the existing elevator, rudder, and ailerons as control effectors. The ailerons are also commanded symmetrically to provide an additional control input in the pitch axis. The available sensors were limited to pitch, roll, and yaw gyros, and lateral and normal accelerometers. Air data quantities available include angle-of-attack, Mach number, pressure altitude, and dynamic pressure.

Scope of Work

The scope of the design effort included development of a nonlinear model of the F-8C from NASA supplied data, generation of linear models, design of pitch and lateral control augmentation systems (CAS), and the inclusion of outer loop (autopilot) modes. Modern control theory tempered with classical analysis was used for the bulk of the linear design effort.

The NASA-Langley nonlinear simulation of the F-8C was used to verify the final design. Recommendations for flight system verification, simulator evaluation of handling qualities, and recommended flight test investigations were also defined.

Document Organization

Section 1 presents a Program Overview and Summary. Section 2 is the Introduction. Section 3 defines the symbols used. The main body of the report is contained in Sections 4 through 14. It consists of a discussion of the design objectives, control law synthesis, verification checks, a simulator experimental program, and recommended flight test investigations. Concluding remarks are presented in Section 15 and a list of references appear in Section 16.

Appendix A defines the variables used in the F8SIM computer program. Appendix B presents the linear equations for 20 flight conditions. Appendix C describes the F8SIM computer program. Appendix D presents a derivation of the wing root bending due to rigid body motion. Appendix E contains pilot rating forms for the simulation experiments.

SECTION 3

SYMBOLS

A	-	discrete system matrix
A	-	transition matrix e^{FT}
a	-	hysteresis parameter
a_y	-	lateral acceleration
a_z	-	normal acceleration
B	-	discrete input matrix
C^*	-	a fixed sum of normal acceleration and pitch rate
\bar{c}	-	chord
CAS	-	control augmentation system
C_N	-	normal force coefficient
CSS	-	control stick steering
D	-	control response matrix
$E(\cdot)$	-	expectation operator
e	-	elevator command
e_B	-	elevator command on α boundary
$e^{F(\cdot)}$	-	exponential operator
e_N	-	normal elevator command
F_L	-	lift force
F	-	system matrix
F_D	-	drag force
F_T	-	thrust
$G_1(s)$	-	transfer function
G_1	-	control input matrix
G_2	-	disturbance input matrix

g	-	acceleration due to gravity
H	-	state response matrix
H^*	-	Hamiltonian
h	-	vertical displacement or altitude
I	-	identity matrix
I_i	-	moment of inertia about i^{th} axis
J	-	quadratic cost
j	-	imaginary number ($\sqrt{-1}$)
K	-	optimal gains for full state feedback
K^*	-	optimal gain matrix on measurements
$K_{\alpha L}$	-	gain schedule in α limiter
$K_{A\dot{\beta}}$	-	gain on derived $\dot{\beta}$ to aileron
K_{Ae}	-	gain on roll rate error to aileron
K_{FS}	-	q gain for flap schedule
K_{F2}	-	gain schedule in flap controller
K_{F4}	-	gain schedule in flap controller
$K_{Rn_{ysl}}$	-	gain on lagged n_y to rudder
$K_{Rn_{sli}}$	-	gain on integral of lagged n_y to rudder
K_{RP}	-	gain on roll rate to rudder
K_{RP_m}	-	gain on roll rate error to rudder
K_{RUM}	-	gain on pilot command to rudder
K_c	-	corrected gain value
K_i	-	arbitrary gain
K_{jk}^i	-	gain to j^{th} input from K^{th} state at i^{th} flight condition
K_p	-	predicted gain value
K_{qL}	-	gain schedule in α limiter
K^1	-	gains on selected measurements
K^2	-	gains on unwanted measurements

M	-	mach number
M	-	measurement matrix
M_{α}	-	pitching moment due to α
$M_{\dot{\alpha}}$	-	pitching moment due to $\dot{\alpha}$
M_{δ_e}	-	pitching moment due to δ_e
M_q	-	pitching moment due to q
m	-	aircraft mass
N_{δ_r}	-	yawing moment due to δ_r
NSS	-	neutral speed stability characteristic
N_z	-	normal acceleration
P_i	-	roll rate peaks
P_s	-	specific excess power
p	-	roll rate
Q	-	quadratic weighting matrix
\bar{q}	-	dynamic pressure
R	-	response covariance matrix
r	-	response vector
r	-	yaw rate
r_n	-	discrete response vector
r_s	-	stability axis yaw rate
S	-	wing area
s	-	Laplace transform operator
T	-	sample time
T_i	-	time constant
U_A	-	aileron command
U_{E_1}	-	elevator command
U_R	-	rudder command
U_n	-	discrete input vector

U_0	-	nominal velocity along x axis
u	-	input vector
u	-	perturbation velocity along x axis
V_{T_0}	-	Total velocity or true air speed
V_{co}	-	cross over velocity in C* parameter
V_0	-	nominal velocity along y axis
v	-	perturbation velocity along y axis
W	-	aircraft weight
W_0	-	nominal velocity along z axis
w	-	perturbation velocity along z axis
w_i	-	wind gust state
X	-	state covariance matrix
x	-	forward displacement
x	-	state vector
x_n	-	discrete state vector
Y_β	-	side force due to β
y	-	lateral displacement
Z_α	-	normal force due to α
ZOH	-	zero order hold
z	-	discrete operator (z^{-1} = delay of one sample time)
α	-	angle of attack
$\dot{\alpha}$	-	time rate of change of α
α_L	-	limiting value of α in pitch CAS
β	-	side slip angle
$\dot{\beta}$	-	time rate of change of β
$\dot{\gamma}$	-	$q - \dot{\alpha}$
δ_a	-	aileron
δ_e	-	elevator

δ_i	-	surface deflection
δ_r	-	rudder
ϵ	-	error
η	-	white noise process
θ	-	pitch attitude
θ_E	-	pitch attitude error
$\dot{\theta}$	-	q = pitch rate
λ	-	scalar parameter in fixed form optimization
ξ	-	damping ratio
π	-	pi (3.141596)
ρ	-	roll rate parameter for handling qualities
σ	-	rms value
τ	-	arbitrary time constant in first order lag
Φ	-	power spectral density
ϕ	-	bank angle
ψ	-	yaw angle
Ω	-	spatial frequency
ω	-	undamped natural frequency

SECTION 4

CCV OBJECTIVES

The goal of a control configured vehicle (CCV) design is to improve the performance of an aircraft through the use of active control. The benefits of active control are improved mission performance and reduced cost of the vehicle.

CCV concepts include the following areas. All have been studied analytically on various aircraft; some have been flight tested.

- Improved handling qualities
- Flight envelope limiting
- Good control with reduced static stability
- Gust acceleration reduction
- Maneuver load control
 - Fighter type - minimum drag during maneuvers
 - Transport type - minimum structural fatigue
- Active control of structural modes

The first five of these concepts were studied and implemented in the F-8C CCV control laws. Consideration of transport-type MLC required a more detailed knowledge than was available of the effects of the structural modes on wing bending. Damping of the structural modes with active control was not considered on this program.

This section defines the various CCV objectives considered for the unmodified F-8C and indicates the goals of the control synthesis to be discussed in later sections.

Longitudinal

The objectives of the longitudinal CAS are to provide acceptable handling qualities, accommodate reduced static stability (by c. g. movement), provide angle-of-attack limiting, and provide for gust alleviation and maneuver load control.

Handling Qualities

There are many and diverse specifications on handling qualities. The problem of generating meaningful performance criteria is one of determining the levels and types of handling qualities required by pilots for various missions. The C* criterion is an example of specifying short period handling qualities in terms of aircraft parameters familiar to a pilot. The concept implicitly includes the traditional short period frequency and damping requirements but is more general in its application. The usual definition for C* is

$$C^* = K_a N_z + K_b \dot{\theta} + K_c \ddot{\theta}$$

where K_a , K_b , K_c are dimensional constants. The $\ddot{\theta}$ term represents the normal acceleration increment at the pilot's location caused by the moment arm from vehicle center-of-gravity. Therefore, the expression can be written as

$$C^* = N_{z_{\text{Pilot}}} + V_{co} q$$

where V_{co} = "crossover" velocity. The steady-state perturbation relation between q and N_z is

$$q_{ss} = \frac{N_z}{U_0} \quad U_0 = \text{forward velocity}$$

The velocity at which the contribution of pitch rate equals the contribution of N_z to the C^* response is the so-called crossover velocity.

The C^* criteria for flight control has evolved because it allows the designers to control one response with one forcing function (the elevator). At high dynamic pressures the elevator produces primarily normal acceleration, and at low dynamic pressures it produces a composite variable that is significant at all flight conditions. [5, 6]

The handling qualities can be summarized as:

- The dominant short-period frequency as excited by a sharp-edged gust shall have a minimum damping ratio of 0.3.
- For a step pilot input the time response shall meet the C^* envelope of Figure 1 where the categories are defined as:
 - I - Optimum response (aerial combat, etc.)
 - II - Not as critical (refueling, cruise, etc.)
 - III - Categories for conditions not covered by I, II, IV
 - IV - Power approach
- The pitch CAS will produce a steady-state short period control stick gradient consistent with MIL SPEC 8785A requirements. [7] A C^* feedback permits the stick gradient requirements to be met without scheduling the stick gain (K_f). This is illustrated in Figure 2 for several points representing extremes in the F-8C data (note $\frac{N_z}{\alpha} \approx -Z_{\dot{\alpha}}$).

Angle-of-Attack Limiting

Angle-of-attack limits are associated with stall, buffet, loss of lateral, directional and/or longitudinal control, and extreme drag increases. By limiting angle-of-attack, the maneuvering capabilities of the aircraft are enhanced since the pilot can demand the full maneuver capabilities of his aircraft without fear of penetrating the boundary which can lead to pitch up, directional instability, and spins.

Angle-of-attack limiting also represents one method to prevent exceeding available surface authority. Hitting surface limits on an aircraft with a statically unstable pitch axis will result in upset and subsequent loss of control.

Future CCV aircraft, with their greater reliance on augmented stability, will need flight boundary control as part of their control law repertoire.

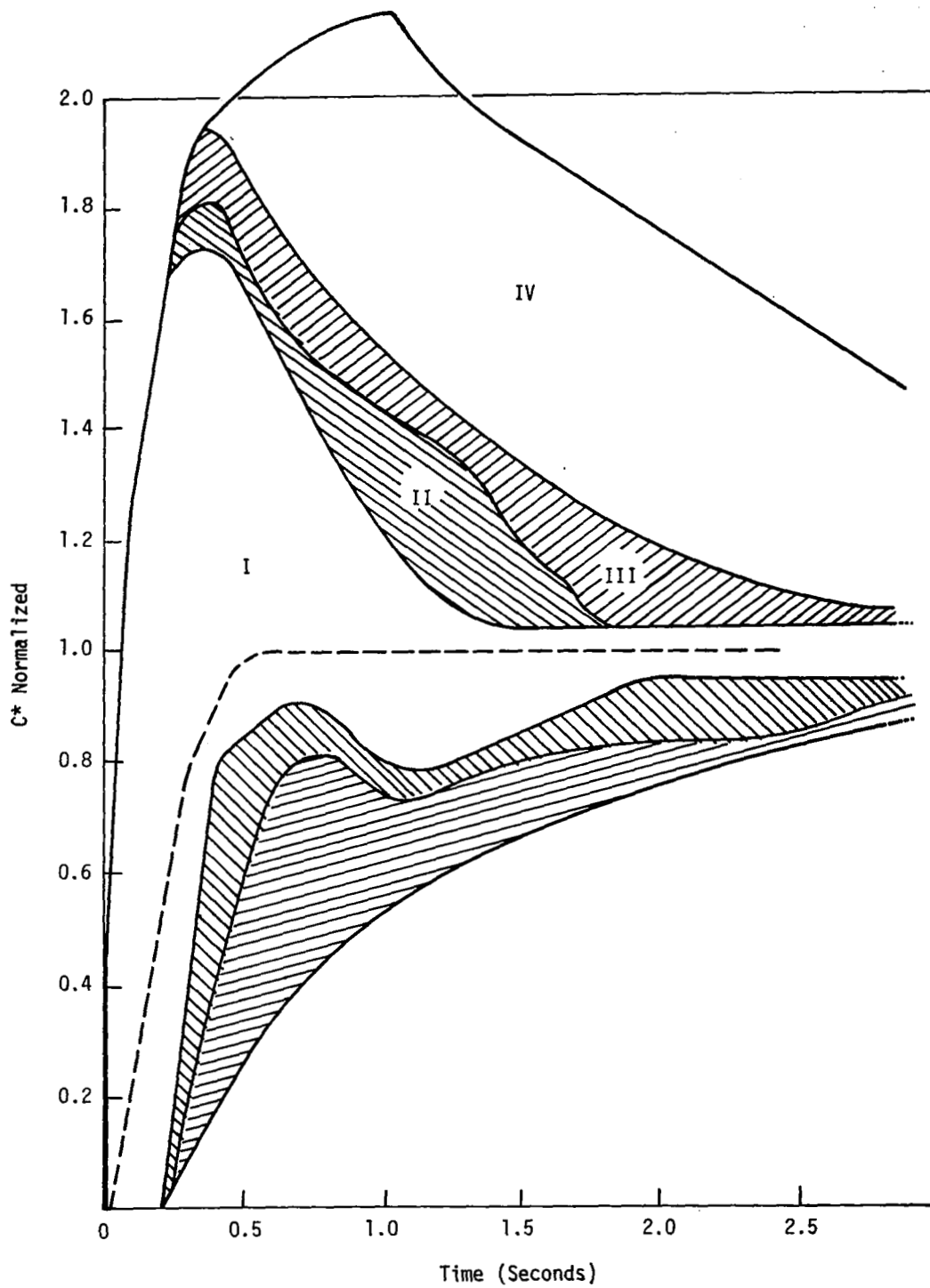
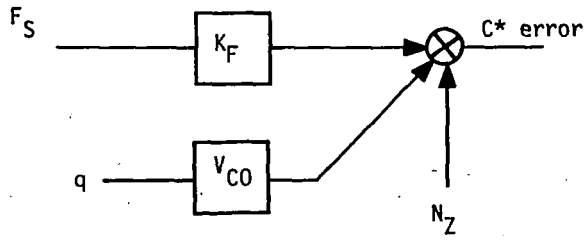


Figure 1. C* Envelope



$$\frac{F_S}{N_Z} = - \left(1 + \frac{V_{CO}}{V} \right) / K_F$$

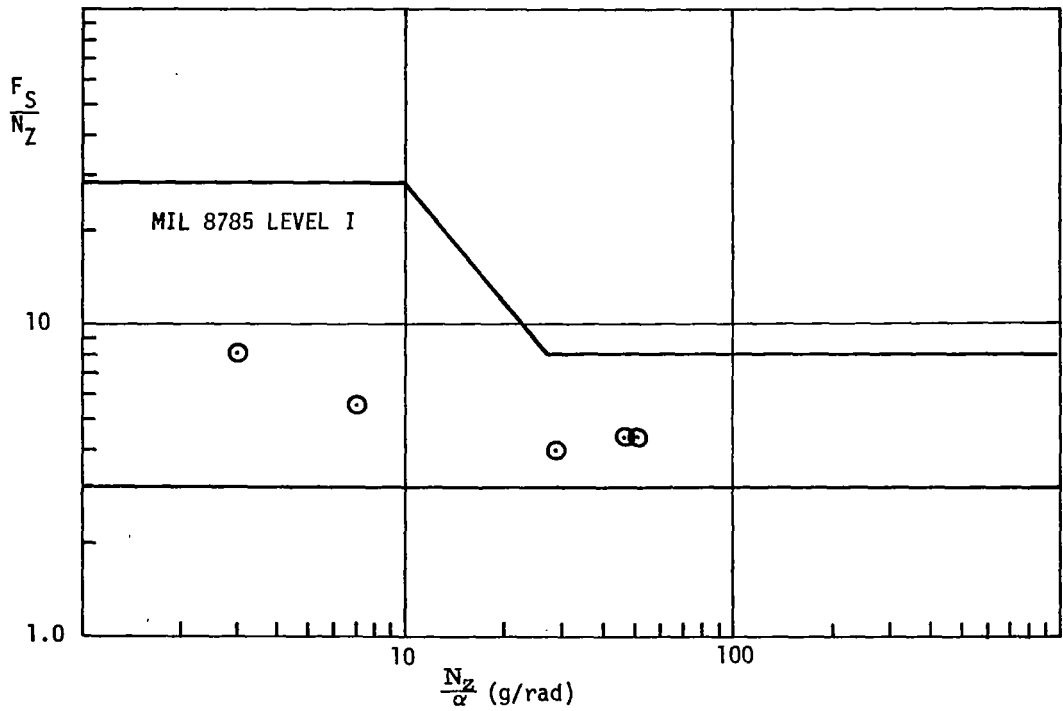


Figure 2. Pitch Stick Gradient

Implementing boundary control requires defining control laws suitable for boundary limiting and developing methods of transitioning between the boundary control laws and the normal control augmentation system. Boundary control will be implemented in the F-8C CCV control laws by mode switching linear controllers. A separate controller for the elevator is designed to hold the limit angle-of-attack. Mode switching is then used to effect transition smoothly from the normal elevator control to the angle-of-attack limiter. A mode transition occurs when α approaches α LIMIT. A "hard" limiting action will result in the boundary controller commanding the elevator to hold the limit angle-of-attack as long as the commanded angle-of-attack exceeds the limit.

By taking a linear combination of the limiter signal and the normal signal, a variety of "soft" limiting functions can be realized. The elevator command (U_E) can be a blended combination of the normal command (e_N) and the boundary command (e_B)

$$U_E = e_B + K_B(e_N - e_B).$$

Then

$$K_B = 1 = \text{No limiting}$$

$$= 0 = \text{Hard limit.}$$

A value of K_B in the range $0 < K_B < 1$ produces "soft" limits. Selection of a "hard" limit or a "soft" limit depends on one's motives for limiting α ; whether it is to prevent excessive drag or whether it is necessary to prevent entry into an undesirable stall region of the specific aircraft.

The effective "steady-state" limiting action of the boundary controller is determined by the parameter K_B as well as the feedback structure of the normal and boundary controller. For the structure shown in Figure 3 the parameter K_B produces an angle-of-attack relative to the set limit expressed as

$$\alpha = \frac{K_\alpha \alpha_L (1 - K_B) - \alpha_U K_B Z_\alpha (1 + \frac{V_{co}}{V_{T_o}})}{K_\alpha (1 - K_B) - K_B Z_\alpha (1 + \frac{V_{co}}{V_{T_o}})}$$

where α_L = set limit

α_U = unlimited α commanded by CAS

K_α = gain on α error

Then taking the derivative with respect to α_U results in the following expression for the stick gradient above the α limit.

$$\text{Gradient above } \alpha_L = \frac{-Z_\alpha (1 + \frac{V_{co}}{V_{T_o}})}{\frac{K_\alpha}{K_B} - K_\alpha - Z_\alpha (1 + \frac{V_{co}}{V_{T_o}})}$$

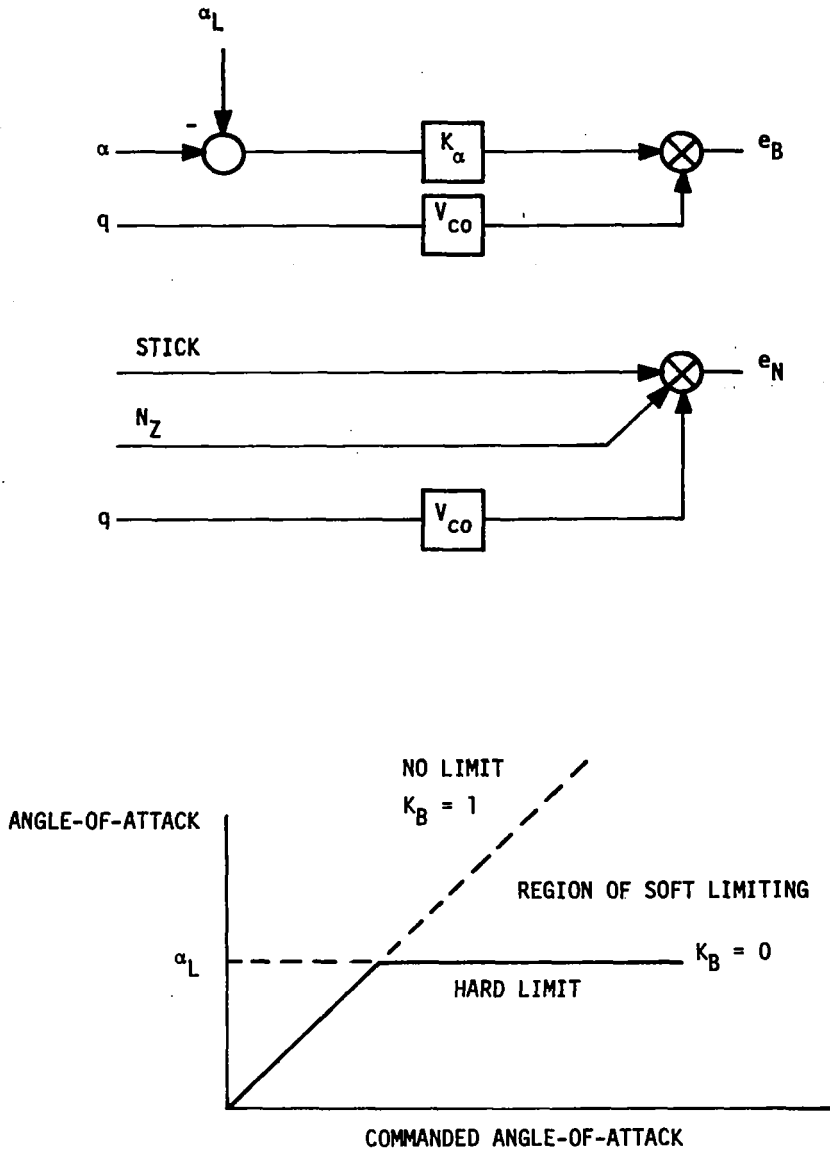


Figure 3. Angle-of-Attack Limiting

The above boundary limiting structure was selected because of its versatility in accommodating both "hard" and "soft" limits. Some candidate mechanizations for stall limiting attenuate the pilot's electrical command signal as the α boundary is approached. Unfortunately this strategy does not protect against an unaccelerated stall since for the latter condition the pilot's input is not significant. A further disadvantage is that this mechanization inherently produced a "soft" limiting function. Either limiting mechanization can be combined with cues to the pilot to inform him that limiting is taking place. The CCV control laws implemented only the "hard" limiting.

Good Control with Reduced Static Stability

One of the CCV objectives of this program is to examine reduced static stability (RSS) in the pitch axis by moving the c.g. aft. The RSS concept for a fighter aircraft is illustrated in Figure 4. For a conventionally designed aircraft, static stability and acceptable handling characteristics must be obtained through aerodynamic design which includes proper location of the c.g.. In maneuvering subsonic flight and in supersonic flight this usually results in significant tail down loads to provide the required moment balance for the aircraft, as shown in Figure 5. However, if a high authority feedback control system is used to provide artificial stability, then the unaugmented aircraft's longitudinal static stability can be relaxed. Relaxing the static stability by moving the c.g. aft results in a significant reduction in down tail loads (or possibly an uploaded tail). The wing loads are then reduced since the tail loads are not opposing the wing's lift. This enhances the maneuvering capability of the aircraft by reducing the drag.

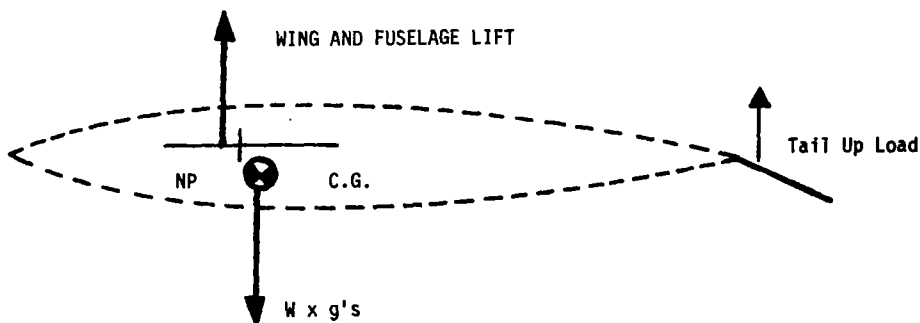


Figure 4. Relaxed Static Stability Obtained by Shifting c.g. Aft

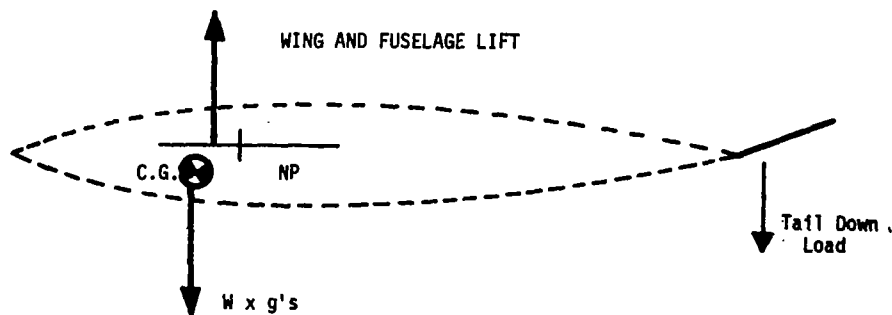


Figure 5. Conventional Static Stability

Gust Effect Reduction

Reduction of the aircraft accelerations due to wind gusts without deteriorating the response to pilot commands enhances the stability of the aircraft and results in improved mission performance. Such stability improves the ride qualities for the pilot as well as enhancing his ability to perform precision tracking tasks. It is well-known that the conventional elevator together with direct lift force producers (canards or flaps) can be effective in reducing gust induced accelerations. A mode combining the symmetric ailerons with the elevator controller to produce direct lift for gust alleviation is included in the F-8C CCV control laws. Only the rigid body response was considered. The flexible airplane was not modeled.

Maneuver Load Control (MLC)

One of the CCV objectives of the F-8C program was to study Maneuver Load Control (MLC). The basic performance improvement objectives to be achieved through the use of MLC are not the same for fighter aircraft as they are for bomber/transport aircraft and may not be compatible. A MLC system positions control surfaces with feedback to redistribute the loading on a wing in maneuvering flight. The objective for bomber/transport aircraft is to improve cruise efficiency (as measured by range and payload) and to reduce structural fatigue. For fighter aircraft, the design objective is to improve maneuvering performance as measured by such performance parameters as specific excess power (P_s) and maximum normal load factor ($n_{z_{max}}$). Whether or not a fighter-type MLC system also minimizes wing root bending depends on the location of the surfaces.

Transport-type MLC--For the large bomber or transport vehicle, the aircraft is designed so that at one g flight, the wing lift distribution associated with minimum drag is obtained. This type of aircraft is almost always at one g flight so there is no particular reason to minimize drag during maneuvering flight. Therefore, MLC for a bomber/transport is used to reduce the wing root bending moments during maneuvering flight to alleviate structural fatigue of the wing. This reduction in wing root bending is obtained by shifting the wing lift distribution inboard, as shown in Figure 6, through the proper deflection of inboard trailing edge flaps and possibly other wing control surfaces such as outboard spoilers. This type of control system can be illustrated by a recent study performed by Honeywell on the C-5A [11]. This system has been flight tested. The amount of MLC available can easily be computed using feedforward gains to the surfaces. Any feedback controller can do no better; however, a feedback mechanization is usually required to avoid the complexity of scheduling the feedforward gains with c. g. variation.

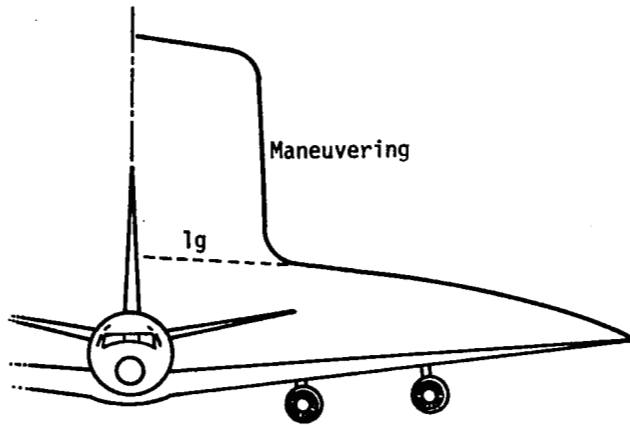


Figure 6. Transport Aircraft Ideal Lift Distribution

Table 1 illustrates transport-type MLC for the C-5A. Columns 1 and 2 show the peak and steady-state wing root stresses for a +1.5 incremental -g climb. Row 1 in Table 1 is for the free aircraft using only the elevator for maneuvering, Row 2 shows the reduction if the symmetric ailerons are deflected 25 degrees up; Row 3 shows that adding 10

Table 1. C-5A Maneuver Load Control

Peak Stress (10^3 psi)	Steady State Stress (10^3 psi)	δ_a Steady State (deg)	δ_{so} Steady State (deg)	Remarks	Stress Reduction (%)
-18.7	-17.4	0	0	Free aircraft	0
-12.1	- 9.81	-25	0		43.6
- 8.66	- 6.27	-25	-10		64.0

degrees of up spoiler provides further reductions. Stress relief is linear with surface deflection; hence results may be used to determine the MLC with different amounts of aileron and/or spoiler deflection. The amount of stress reduction can be illustrated for the case of elevator plus symmetric aileron (Table 1, Row 2). Steady state MLC relief is

$$1 - \frac{9810}{17,400} = 43.6\%.$$

Fighter-type MLC--In contrast, a fighter aircraft must maintain an efficient wing lift distribution in maneuvering flight as illustrated in Figure 7. Therefore, a fighter MLC system employs aerodynamic devices such as leading edges and maneuver flaps. The object is to redistribute the wing loading in maneuvers to improve performance through drag reduction and delayed buffet onset. The drag penalty at maneuvering flight conditions is of paramount importance for a fighter aircraft. Development of the fighter wind design is predicted on this fact, since the wing area is dictated by transonic or supersonic maneuverability and the wing is optimized for minimum attainable drag at high lift coefficients during high g maneuvers. The fighter aircraft's lifting capability at high maneuvering angles-of-attack is important since the more lift capability it has the more g's it can pull in maneuvers. Therefore, the primary aerodynamic parameters used to evaluate MLC are lift and drag at representative maneuvering flight conditions. [8, 11, 12]

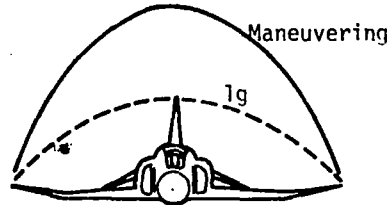


Figure 7. Fighter Aircraft Ideal Lift Distribution

The aerodynamic benefits can be expressed in terms of parameters that show the performance benefits of MLC at maneuvering flight conditions. The trim drag benefits can be shown in terms of specific excess power, P_s , where

$$P_s = \frac{T-D}{W} V$$

and

T = thrust (lb)

D = drag (lb)

W = aircraft weight (lb)

V_{T_0} = aircraft velocity (ft/sec)

The lift benefits of MLC can be shown in terms of maximum usable normal load factor, $n_{z_{max}}$, where

$$n_{z_{max}} = \frac{C_{N_{max}} \bar{q} S}{W}$$

with

- C_N = normal force coefficient
- \bar{q} = dynamic pressure (lb/ft²)
- S = wing area (ft²)
- W = aircraft weight (lb)

Normal load factor is a measure of the aircraft's apparent acceleration normal to its body axis. Specific excess power and normal load factor can be measured in flight test to determine the benefits of a flap schedule in reducing buffet onset, wing rock and in reducing drag. This is discussed in more detail in references 8 and 12.

For minimum drag the optimal position of the trailing edge devices were obtained by evaluating the performance of a systematically varied set of fixed flap deflections. This set point optimization problem can be solved using the nonlinear aerodynamics. Predictions can then be checked with flight test investigations. [8, 12, 13, 14] Movement of the leading edge flap was not considered in this investigation.

Lateral-Directional Objectives

Handling Qualities--The major performance specifications are concerned with:

- An acceptable roll-rate response
- Improved Dutch roll damping
- Reduced side-slip and peak lateral acceleration for good turn coordination in response to roll stick command

The performance specification for the lateral-directional axes control augmentation system is presented below. The specification is based on the handling qualities specification, MIL-F-8785B (ASG). [7] Additional criteria were added based on previous Honeywell experience in designing similar systems. [15] The specification meets or is better than those set in 8785B. In general, the specifications stated are those required for Class IV, Category A, Level I handling qualities.

Performance Specification:

1.0 The frequency and damping of the Dutch Roll mode shall satisfy:

$$\zeta_d > .19$$

$$\omega_{nd} > 1.0$$

$$\zeta_d \omega_{nd} > .35$$

2.0 If the spiral mode is unstable the time to double shall be greater than 20 sec.

3.0 The roll subsidence time constant τ_R shall be less than 1.0 sec.

4.0 Following a rudder pedals free step aileron command, the ratio of sideslip to the parameter k shall be less than specified below. The aileron command shall be held fixed until the bank angle has changed at least 90 degrees.

Category A $\beta/k < 6$ degrees for adverse sideslip
 $\beta/k < 2$ degrees for proverse sideslip

Category C $\beta/k < 10$ degrees for adverse sideslip
 $\beta/k < 3$ degrees for proverse sideslip

The parameter k is given by

$$k = \frac{\varphi_{1.3}}{90^{\circ}}$$

for category A and

$$k = \frac{\varphi_{1.0}}{30^{\circ}}$$

for category c, where φ_t is the bank angle achieved at t seconds after the step input.

For small inputs, aileron control commands which cause up to a 60 degree bank angle change within T_d (Dutch roll time constant) or 2 seconds, whichever is longer, the sideslip limitations are those given by Figure 8.

- 5.0 For a step aileron command, held until the bank angle has changed at least 90 degrees, the roll rate at the first minimum following the first peak shall be at least 60 percent of the peak value.

For step aileron commands up to the magnitude which causes a 60 degree bank in $1.7 T_d$ seconds, the parameter ρ_{osc}/ρ_{AV} shall be as specified in Figure 9, where the parameter is given by

$$\frac{\rho_{osc}}{\rho_{AV}} = \frac{P_1 + P_3 - 2P_2}{P_1 + P_3 + 2P_2}$$

where P_1 and P_3 are the first and second roll rate peaks, respectively, and P_2 is the first minimum.

- 6.0 For category A turn coordination, the lateral acceleration at the pilot shall be less than 0.15 g for a 60 deg/sec roll to a 60 degree bank.
- 7.0 Minimum stability margins for the complete control system, sensor dynamics, actuation dynamics, and rigid airplane of 6 dB gain margin and 35 degrees of phase margin for both the aileron command path (yaw at nominal) and the rudder command path (roll at nominal).

High Angle-of-Attack Performance

Poor lateral control at high angles-of-attack resulting from low directional stability is a problem for high-performance aircraft. Future aircraft, employing relaxed static stability in the yaw axis, will require significant directional stability augmentation to provide satisfactory high angle-of-attack turn coordination and to comply with pitch-roll-yaw coupling requirements.

The benefits of a statically unstable yaw axis in future aircraft are reduced tail sizes for less drag and improved decoupled maneuvering performance. These provide capabilities for:

- "Flat" turns - No side-slip or bank angle. A yaw rate is commanded proportional to lateral acceleration divided by airspeed.

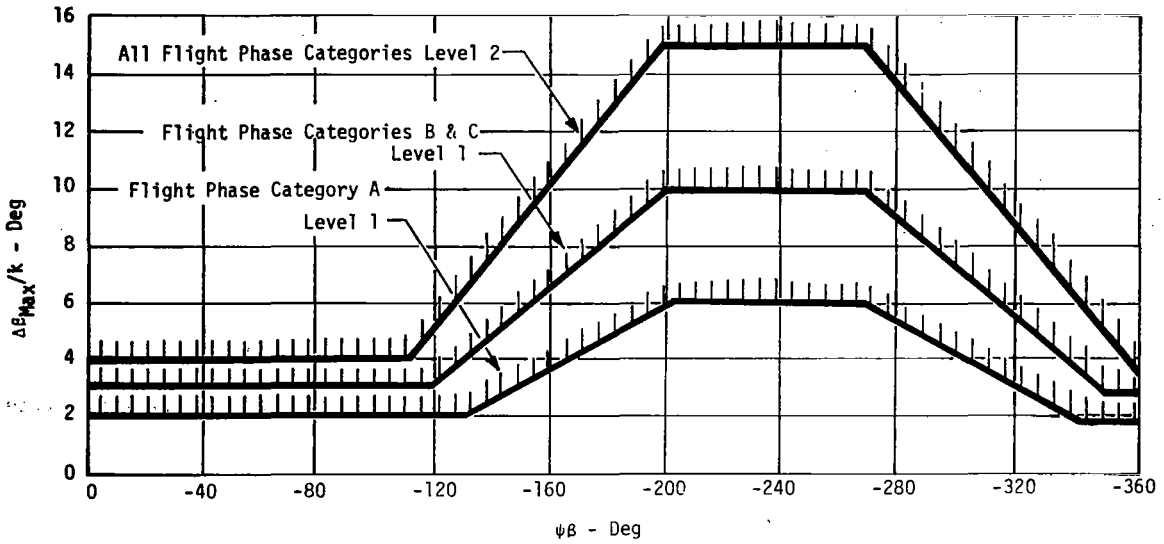


Figure 8. Sideslip Excursion Limitations

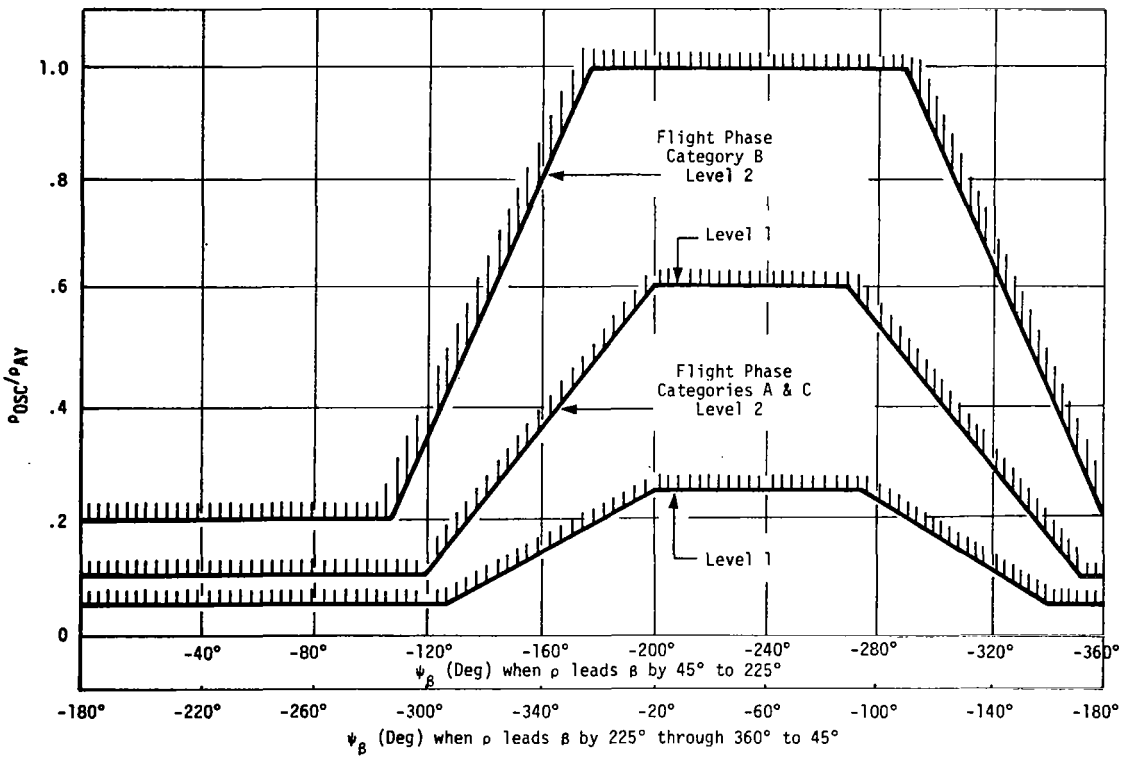


Figure 9. Roll Rate Oscillation Limitations

- "Lateral" translation - A sideslip is commanded without a bank angle or a heading change.
- Fuselage pointing - A yaw is commanded to obtain a heading change without changing the direction of the velocity vector. The aircraft is then at a constant side-slip.

These advanced lateral modes were not considered for implementation in the F-8C CCV control laws because they required the addition of a side force producer. However, the improvement of handling qualities over a wide variation in angle-of-attack was a major concern during the lateral-directional design.

Conventional turn coordination via lateral acceleration, high-passed yaw rate, and aileron-to-rudder crossfeeds cannot cope with the large inertial coupling moments and dramatic changes in aerodynamics associated with high angles-of-attack operation. This effect is present at both high angle-of-attack maneuvers and at low speed flight.

Use of derived side-slip feedbacks and gain schedules with angle-of-attack were areas investigated on this program. Use of a derived side-slip feedback (or "inertial" coordination) recognizes that implementation of these feedbacks requires all-attitude information and a good quality true airspeed signal. Ultimately two quadratic lateral-directional CAS designs were produced. They minimized the same quadratic performance index with different measurement complements. The first design required an all-attitude platform and true airspeed in addition to a lateral accelerometer and yaw rate gyro. The second design eliminated the platform and true airspeed requirement.

SECTION 5

DESIGN PROCEDURE

Overview

The synthesis of the CCV control laws used linear quadratic control theory (both continuous and sample data) to design the CAS and nonlinear simulation results to specify mode switching requirements.

Operation over the flight envelope was accomplished by gain scheduling the linear controllers obtained at specific flight conditions. The gain schedules were obtained by plotting the gains corresponding to individual flight conditions and fitting the curves for these values to appropriate air data measurements.

Insight into the gain scheduling problem was obtained by identifying the transfer functions for the various feedback and command feedforward signals.

All filters required for high frequency gain attenuation were included in the quadratic formulation. Both the longitudinal and lateral CAS designs use an "explicit" model to obtain desired transient responses to pilot command.

The use of optimal control theory is considered to be an aid to classical design techniques rather than a replacement. In the design procedure, optimal control theory was combined with classical evaluation techniques to produce the final design.

The CCV control laws must be in a form suitable for programming on a digital computer. There are basically two approaches to synthesizing a discrete control system: direct digital synthesis and conversion of a continuous design to a discrete format. [4]

An outline of the two synthesis methods is shown in Figure 10. For direct digital synthesis, the aircraft equations of motion are converted to a sampled data model for the chosen sample time. This model includes sample-and-hold devices. The design is then accomplished in the discrete time domain using Honeywell's discrete quadratic optimal design programs and z- and w-plane synthesis. The result of the discrete design is a controller which is optimal for the chosen sampling rate at the sampling times. Even though the design is accomplished in the digital domain, the controlled system is continuous and the performance for all time must be considered. If the sample rate is changed, the design has to be initiated at the beginning, since the z-plane root locations for the equations of motion change.

In the second approach, the major design task is accomplished in the continuous time domain and the resulting controller converted to a discrete form after design. The design is accomplished with Honeywell's optimal quadratic design programs and s-plane synthesis. The result is an optimal continuous design and is not directly affected by choice of sample time. The next step is to select a sampling rate and transform the control laws to discrete form. This is best accomplished using Tustin's method and includes the effects of the necessary sample-and-hold units. For low sampling rates, the controller performance will be degraded to a degree due to the discretization process and the sampling effects. This may necessitate some gain tuning at this stage. Altering sample times is easier than in direct digital design, which may affect some design time savings when sample rates are critical and are to be minimized. Again,

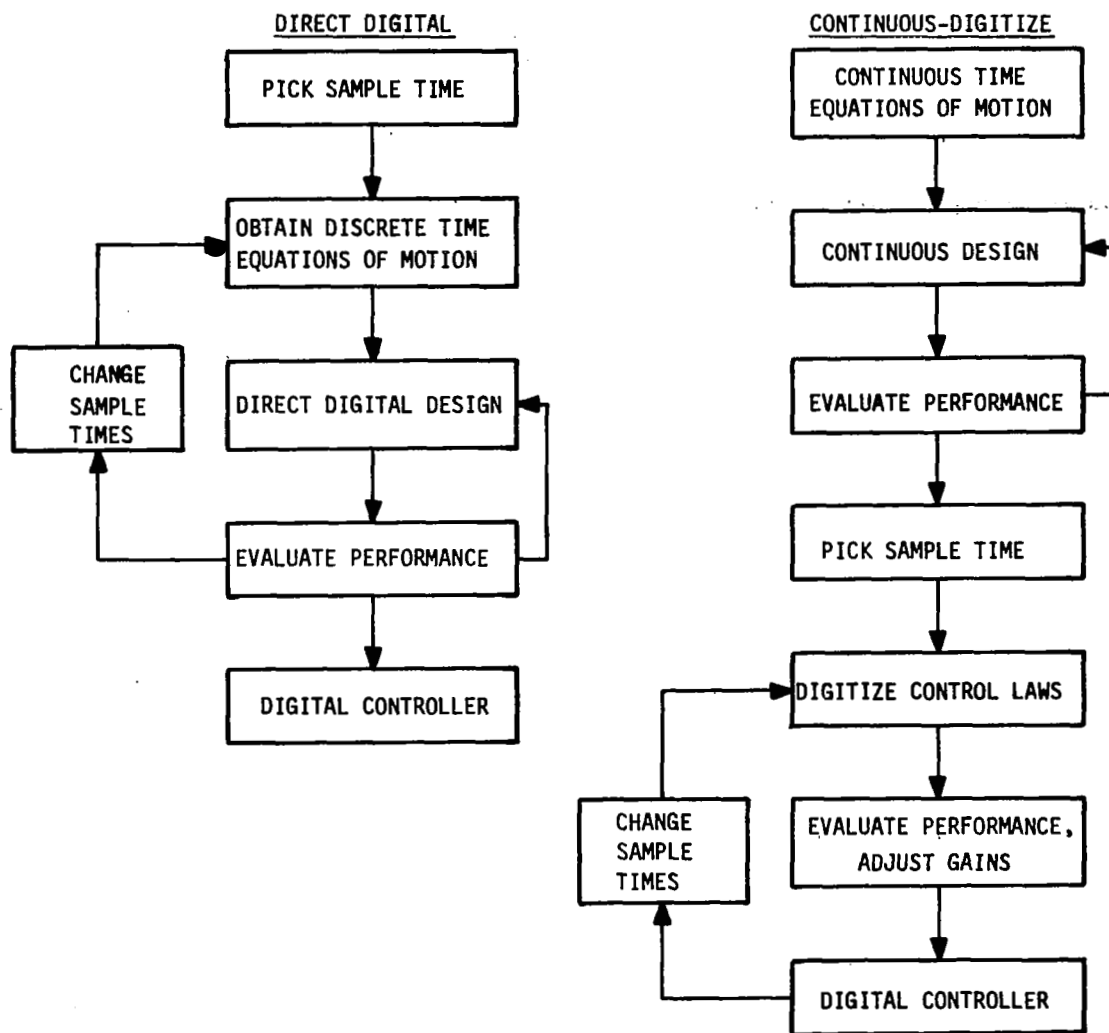


Figure 10. Design Process

the intersample response of the final system must be evaluated. This approach is more amenable to the design of systems where multiple sampling rates are required to conserve control computer requirements, e. g., outer loop sample rate need not be as high as the inner loop.

Both direct digital control laws and digitized control laws were designed. For these control laws and the range of sampling times, there is not a significant difference. The quadratic synthesis programs will now be discussed. Both the continuous time version and the sample data version are presented.

Quadratic Design

The application of quadratics is an iterative process of selecting responses and weighting matrices. The choice of responses and weights is expediated by the designer's past experience and his understanding of the physics of the control problem. The iterative nature of the procedure is illustrated in Figure 11.

The procedure can be summarized as:

- Step 1: Model the system as linear differential equations in state variable form $\dot{x} = Fx + G_1 u + G_2 \eta$
- Step 2: Define performance criteria and then define responses $r = Hx + Du$ to minimize that relate to performance goals.
- Step 3: Select initial weighting matrix Q and compute initial matrix of optimal gains.
- Step 4: Evaluate linear designs and adjust weighting matrix elements and/or responses until specifications are met.
- Step 5: Repeat steps 2, 3, and 4 for remaining flight conditions.
- Step 6: Schedule gains over flight envelope.
- Step 7: Evaluate the final design on a nonlinear simulation.

Continuous-Time Quadratic Formulation--The synthesis procedure for the unconstrained configurations is based on linear quadratic optimal control theory. [3, 16, 17] This approach results in an unconstrained or full-state feedback control law. The system is modeled by a set of first-order, linear, time-invariant differential equations

$$\dot{x} = Fx + G_1 u + G_2 \eta.$$

The vector x is the state vector of dimension n_x , u is the control input vector of dimension n_u , and η is a disturbance vector of dimension n_η . The disturbance input is assumed to be a zero mean white noise process where

$$E(\eta) = \bar{\eta} = 0$$

and

$$E\left([\eta(t) - \bar{\eta}] [\eta(\tau) - \bar{\eta}]'\right) = I\delta(t - \tau).$$

In these equations, E denotes the statistical expectation, x' is the transpose of the vector x , δ is the dirac delta function, and I the identity matrix. For this problem, η includes a random gust disturbance and a random command disturbance.

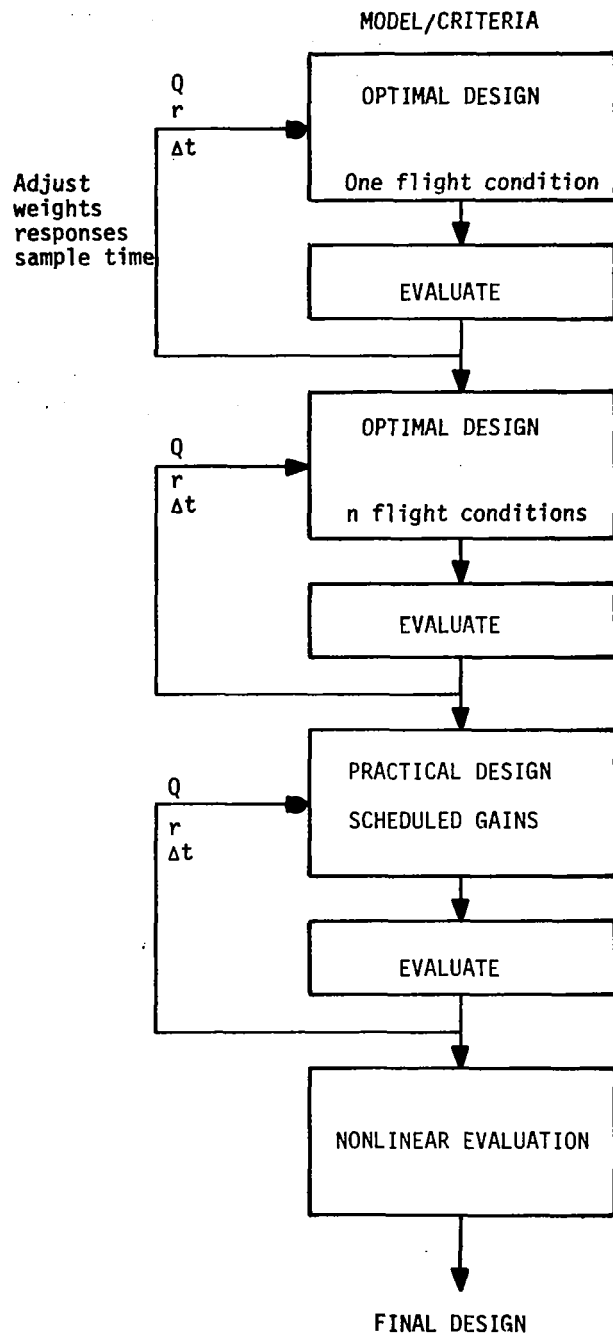


Figure 11. Quadratic Design Process

The model incorporates a low-pass filter operating on the process η , so the system is actually driven by a more realistic disturbance. The choice of the filter is discussed later in the text. The matrix F has dimensions $n_x \times n_x$, G_1 is $n_x \times n_u$, and G_2 is $n_x \times n_\eta$.

A set of n_r response equations is defined as

$$r = Hx + Du.$$

The derivation of the system models in this form is presented in Appendix B.

A quadratic cost function J is defined by

$$J = E(r' Q r)$$

where Q is a matrix of quadratic weights chosen during the design process. The cost function can be written

$$J = \text{tr } Q R$$

where tr is the trace operator and R the response covariance matrix

$$R = E [r(t) r'(t)].$$

Assume a feedback control law given by

$$u = Kx$$

Then,

$$r = (H + DK)x$$

and

$$R = E [(H + DK)x x'(H + DK)'] = (H + DK) X (H + DK)'$$

where

$$X = E [x(t) x(t)']$$

is the state covariance matrix.

The cost function is thus

$$J = \text{tr} [Q(H + DK) X (H + DK)'] = \text{tr} [(H + DK)' Q(H + DK)X]$$

For a white noise input, the closed-loop system must be stable if the steady-state variances of the states are to be finite. The system can be constrained to be stable by requiring that the steady-state covariances of the states have zero derivatives, implying the covariances are constant and finite.

The closed-loop state covariance equation is given by

$$\dot{X}(t) = \tilde{F} X(t) + X(t) \tilde{F}' + G_2 G_2'$$

where \tilde{F} is the closed-loop stability matrix

$$\tilde{F} = F + G_1 K$$

The optimal control problem formulation is to minimize the cost function J subject to the constraint

$$\dot{X} = \tilde{F} X + X \tilde{F}' + G_2 G_2' = 0$$

This constraint can be met by introducing a matrix of Lagrangian multipliers, P , such that

$$\text{tr } P \dot{X} = \sum_{i=1}^n \sum_{j=1}^n P_{ij} \dot{x}_{ij} = 0$$

if, and only if,

$$\dot{x}_{ij} = 0$$

Define the Hamiltonian by appending the multipliers to the cost functional; thus:

$$\begin{aligned} \bar{H} &= \text{tr}(H + DK)' Q(H + DK)X + \text{tr } P \dot{X} \\ &= \text{tr}(H + DK)' Q(H + DK)X \\ &\quad + \text{tr } P [(F + G_1 K)X + X(F + G_1 K)' + G_2 G_2'] \end{aligned}$$

Taking derivatives and setting equal to zero gives

$$\frac{\partial \bar{H}}{\partial P} = X(F + G_1 K)' + (F + G_1 K)X + G_2 G_2' = 0$$

$$\frac{\partial \bar{H}}{\partial X} = (H + DK)' Q(H + DK) + (F + G_1 K)' P + P(F + G_1 K) = 0$$

$$\frac{\partial \bar{H}}{\partial K} = 2D'Q(H + DK)X + 2G_1' P X = 0$$

If $D'QD$ and X are positive definite matrices, the last equation requires

$$2D'Q(H + DK) + 2G_1' P = 0$$

from which K is determined as

$$K = -(D'QD)^{-1} (D'QH + G_1' P)$$

Thus, only the matrix P must be determined to specify the gain matrix K . Substituting this equation into the equation for $\partial \bar{H} / \partial X$ yields, after algebraic manipulations,

$$\begin{aligned} 0 &= [F - G_1 (D'QD)^{-1} D'QH]' P + P [F - G_1 (D'QD)^{-1} D'QH] \\ &\quad + H'QH - H'QD(D'QD)^{-1} D'QH \\ &\quad - P G_1 (D'QD)^{-1} G_1' P \end{aligned}$$

This is an algebraic Riccati equation of the form

$$0 = \tilde{A}' P + P \tilde{A} + \tilde{Q} - P \tilde{E} P$$

This equation is solved for P, which thus determines the feedback gain matrix K by computer algorithms described in the sequel.

Discrete Quadratic Formulation--This section details the transformation process which takes place when the control function $u(t)$ in the linear continuous control system is required to be constant over intervals of length Δ ,

$$u(t) = u_n, \text{ for } t_n \leq t < t_{n+1}, n = 0, 1, 2, \dots, N-1$$

where $N = T/\Delta$ and $t_n = n\Delta$, $n = 0, 1, 2, \dots, N$.

A subsequent section will describe the use of DIGIKON to obtain the discrete quadruples

$$x_{n+1} = A x_n + B u_n + \xi$$

$$r_n = H x_n + D u_n$$

with

$$E(\xi) = 0 \quad E(\xi\xi') = V$$

Similar arguments as in the continuous case will show that

$$u_n = K x_n$$

minimizing $J = E(r'Qr)$ is obtained by computing K from

$$K = - [B'PB + D'QD]^{-1} [B'PA + D'QH]$$

where

$$P = [A + BK]' P [A + BK] + [H + DK]' Q [H + DK] \quad [18]$$

These equations are solved in DIAK-D.

Fixed Form Optimal Synthesis --For the lateral axis a quadratic design was produced using a constrained configuration of feedbacks to eliminate the requirement for all-attitude angular measurements. This design was produced using an algorithm that minimized a quadratic cost function subject to the preselected feedback structure. The optimum feedback gains are then determined with an incremental gradient algorithm. [19]

The starting point for the incremental gradient algorithm is the set of full-state feedback gains for the unconstrained controller. The algorithm then steps the gains not

allowed to zero, while correcting the remaining gains by a gradient optimization method to ensure that the constrained configuration controller satisfies necessary conditions for optimality with respect to the cost function and the specified configuration.

For the constrained control law, the control vector consists of feedback gains on a measurement vector, y , where

$$y = Mx$$

and thus

$$u = K*y = K*Mx$$

For the general problem, the equation

$$y = Mx$$

defines the sensor outputs. To include sensor dynamics, the original state vector may be augmented with states associated with sensor dynamics. If the measurement matrix M were invertible, the constrained gains matrix would easily be defined by $K^* = KM^{-1}$. This is not generally the case, however, and other means must be found to determine K^* .

The response covariance matrix is now

$$R = (H + DK^*M) X (H + DK^*M)'$$

and the performance index is

$$J = \text{tr}(H + DK^*M)' Q(H + DK^*M) X$$

Now, consider a gain matrix parameterized with a scalar, λ , in the form:

$$K(\lambda) = K^1(\lambda)M + \lambda K^2 \quad \text{and} \quad 0 \leq \lambda \leq 1$$

The matrix K^2 contains the gains that are to be forced to zero, and $K^1(\lambda)$ those gains to be retained and adjusted. The partial derivatives of the cost function with respect to the variable gains K^1 are set to zero as a necessary condition for optimality; that is,

$$\frac{\partial}{\partial K^1} J[K^1(\lambda)M + \lambda K^2]$$

or

$$\frac{\partial}{\partial K^1} J[K^1(\lambda), \lambda] = 0$$

The Implicit Function Theorem [19] states that the gains are defined by the differential equation in λ (assuming K^1 is represented as a vector):

$$\frac{d}{d\lambda} K^1(\lambda) = - \left[\frac{\partial^2 J(K^1, \lambda)}{\partial K^1 \partial K^{1T}} \right]^{-1} \left[\frac{\partial^2 J(K^1, \lambda)}{\partial \lambda \partial K^1} \right]$$

This equation can then be integrated from $\lambda = 1$ to zero and the gains at $\lambda = 0$ will be the desired ones. The starting gains or initial condition at $\lambda = 1$ can be defined by

$$K(1) = K \text{ (optimal full-state matrix)}$$

where

$$K^1(1) = KM' (MM')^{-1}$$

and

$$K^2 = K[I - M' (MM')^{-1} M]$$

If M is invertible, this reduces to

$$K^1(1) = KM^{-1}$$

as expected.

The integration process is a predictor-corrector scheme. In the algorithm used on this project, the gains are first predicted for a new (smaller) value of λ via the equation

$$K_p^1(\lambda_{j+1}) = K_c^1(\lambda_j) + [K_c^1(\lambda_j) - K_c^1(\lambda_{j-1})]$$

where the subscript "p" denotes predicted gains, and "c" the corrected gains. The predicted gains for λ_{j+1} are then corrected using a modified Newton-Raphson gradient search.

The gradient search corrects the gains to give the minimum cost for the present value of λ . The Newton-Raphson corrector would be

$$K_c^1 = K_p^1 - \left[\frac{\partial^2 J(K_p^1, \lambda_{j+1})}{\partial K^1 \partial K^{1T}} \right]^{-1} \left[\frac{\partial J(K_p^1, \lambda_{j+1})}{\partial K^1} \right]$$

Because the matrix of second partial derivatives is very costly to compute, it is approximated by dropping second-order terms. This requires more gradient steps, but, in practice, the additional steps are still less costly than the exact method. This corrector equation is cycled repeatedly until a convergence criterion of the form

$$|\partial J / \partial K^1| < \epsilon$$

is satisfied. At this point the gains are predicted for a new value of λ and the process repeated until $\lambda = 0$.

Sampling Time Considerations

In designing an aircraft digital control system, a major determinant of computer requirements is sample rate. Realization of adequate performance at minimum rate is the objective. When the control requirements are examined against this parameter, it is obvious that the high frequency properties are relevant. Both eigenvalues and frequency response specifications are candidates for sample rate selection. Statistical measures such as rms accelerations may be significant except that the dominant spectral content for typical random disturbances (i. e., gusts) is usually concentrated well below candidate sample rates.

A specification relative to describing the high frequency controller quality and consequently useful in selecting a sample rate is frequency response. There are three interrelated criteria of significance in the selection of a sampling rate:

- frequency aliasing (folding)
- phase lag over control frequencies
- output quantization effects (with time)

Each of the above effects is reduced by selecting higher sample rates.

To preclude excessive sample rates, some analog prefiltering is required to restrict the frequency content of the sensor signals. A conservative value for a first-order low pass prefilter is

$$\frac{1}{Ts + 1}$$

for a sample rate of T. The filter cutoff frequency is then a factor of π away from the half-sample frequency. This results in an attenuation of 10 db of the input signal at the half-sample frequency. If the phase lag presents a problem of the time constant can be reduced to a $\frac{T}{2}$ and/or phase compensation can be added in the computer.

The major difference between a continuous controller and its discrete counterpart is the gain and phase variation resulting from the hold circuit used for the D/A conversion at the servo interface. The frequency properties of a zero hold is shown in Figure 12. [20]

Adding a discrete function to provide phase correction over the control frequencies of interest is also illustrated in Figure 12.

Another constraining factor in practical digital system design is the effect of output quantization (i. e. , driving the servo actuator with a "staircase" function). The effect of excessive output quantization generally is manifested by a limit cycle during large transients. Although the practical impact of such operations is difficult to assess, it is an important subjective influence that has resulted in a variety of added functions to reduce the quantization amplitude. Most of these functions are analog post-filters or averagers operating with a zero-order hold.

For the CCV control laws a requirement for post-filtering is not necessary since the secondary servos are limited to a 10 Hertz bandwidth. This should provide adequate quantization correction. The CCV control laws were examined by breaking the loop (indicated in Figure 13) and computing the frequency response of the resulting discrete transfer function between 1 and 2 using the DIGIKON analysis software. This computation includes the phase lag of the zero-order hold. The resulting phase margin was checked using different sample rates. Examples are presented in Section 7.

Digital Analysis .

The analysis of the CCV Control Laws relied to a large degree on DIGIKON-2. [2] DIGIKON-2 is a software package, developed by Honeywell, for analyzing multi-loop, multi-input, multi-output systems. It provides frequency and time domain analysis tools for both continuous and sampled data systems. The subroutines used are listed in Table 2.

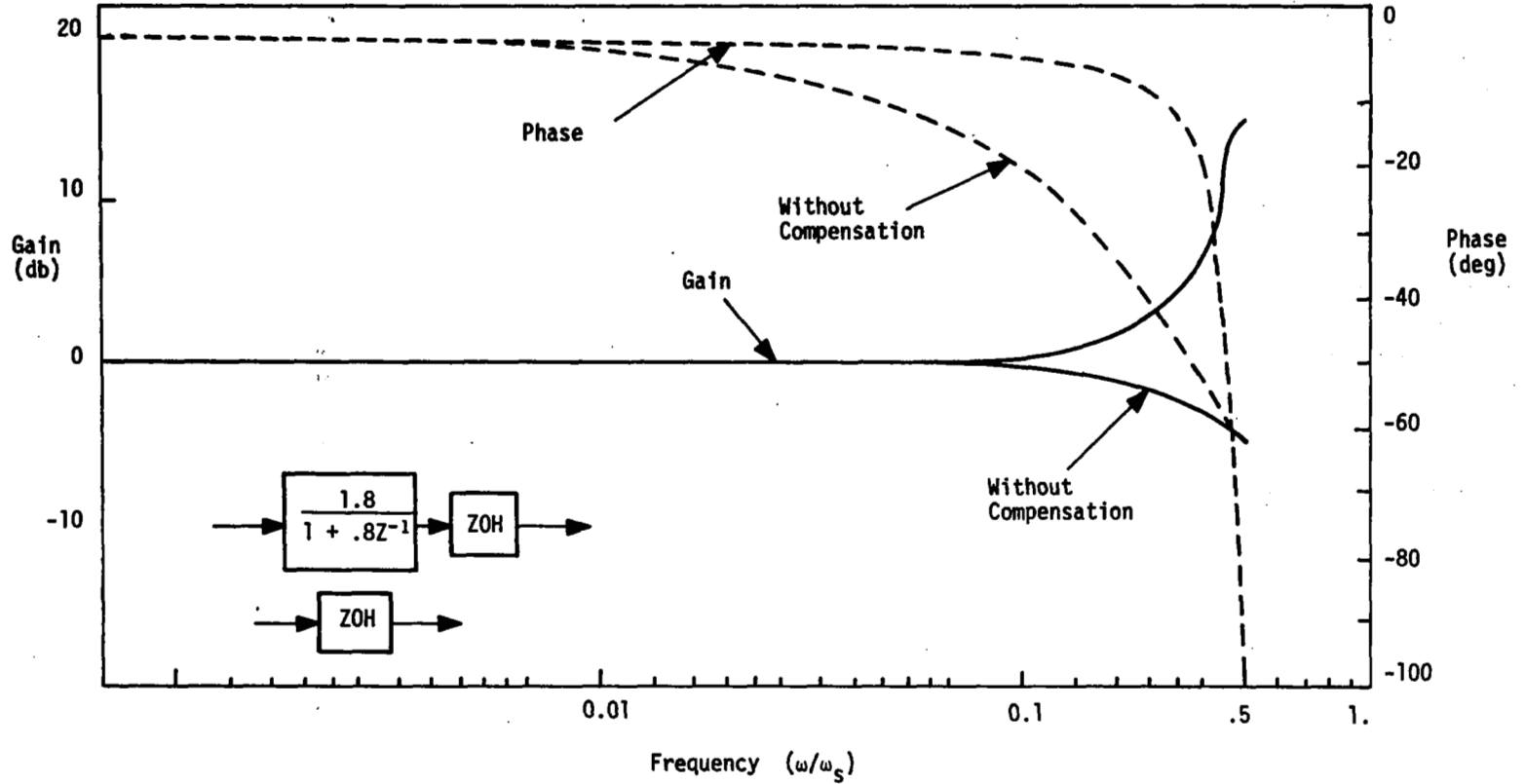
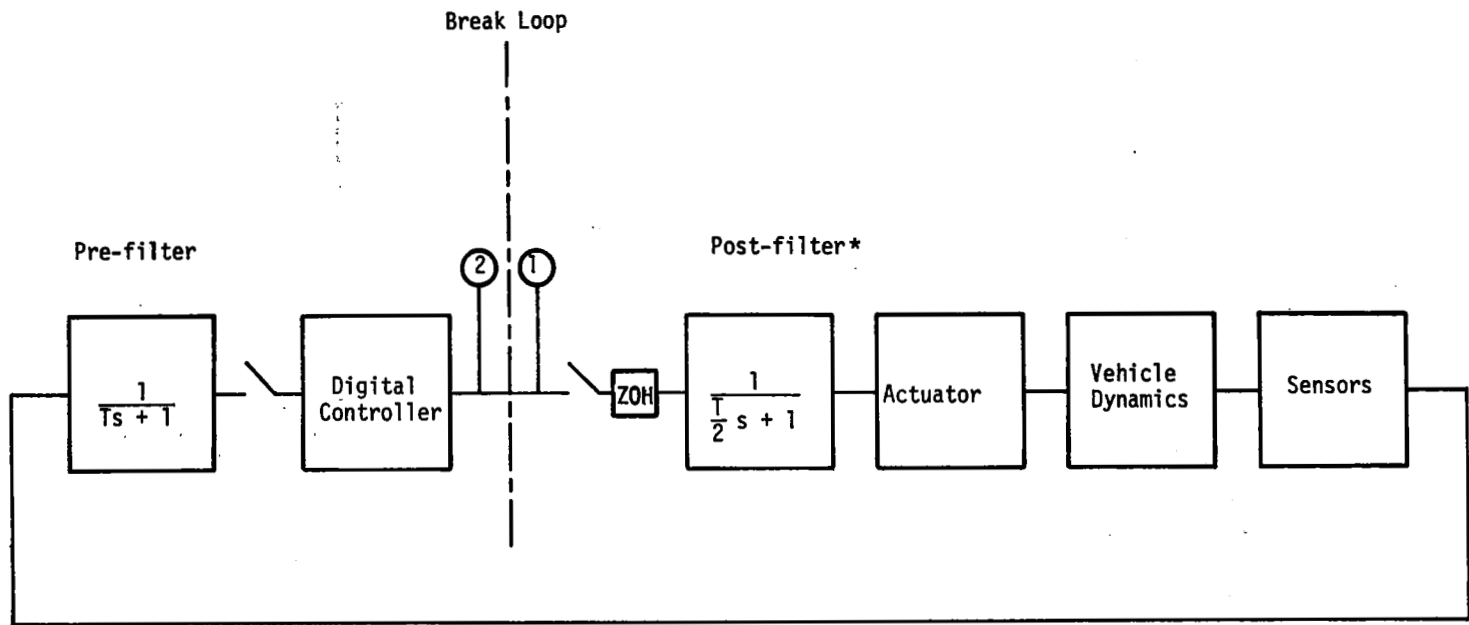


Figure 12. Zero Order Hold with and without Phase Lead Compensation



* Not required in F-8C application.

Figure 13. General Open Loop Frequency Response of Digital Controller

Table 2. DIGIKON-2 Subroutines

Subroutine	Description
EXPK	It computes discrete model of a continuous plant with digital inputs in the form of (F_p, G_p, H_p, E_p) for a given sample time.
WZK	It computes a discrete time model for the continuous controller dynamics using the Tustin algorithm.
POZK (Subprogram)	It computes poles and zeros of specified input-output pairs in the system using matrix quadruples input.
FREQK (Subprogram)	It computes frequency response of specified input-output points in the system. Analog as well as digital systems are handled. W-frequency response is also computed. Phase and Gain margins are computed.
TRESPK	It computes a transient response for a step input using the matrix quadruples.
PLOT	Using line printer it plots Bode diagrams.
POWK	It computes steady state RMS responses as well as power spectral density and its integral with respect to w . (Power contained in a given bandwidth.)

Discrete Model for the Physical Plant--The application here is to find the exact response of the plant states (aircraft plus actuators) at sample points as well as all other intersample time points with these inputs.

The analysis starts with the physical plant continuous matrix quadruples (A_p, B_p, C_p, D_p) . This quadruple is obtained from the simulation equations of the plant as discussed in Section 5. The physical plant equations are given by

$$\dot{x}_p = A_p x_p + B_p u_p$$

$$y_p = C_p x_p + D_p u_p$$

The state response is given by

$$x_p(t) = e^{A_p t} x_p(0) + \int_0^t e^{A_p(t-s)} B_p u_p(s) ds$$

The controller input from the hold unit to the plant remains constant between the sample intervals. For this case the state response of the plant is given by

$$\mathbf{x}_p(t) = e^{A_p t} \mathbf{x}_p(0) + \left(\int_0^t e^{A_p s} B_{pl} ds \right) u_p(0)$$

where $0 \leq t \leq T$.

At sample points we have

$$\mathbf{x}_p(K+1) = F_p \mathbf{x}_p(k) + G_{pl} u_{pl}(k)$$

where

$$F_p = e^{A_p T}$$

$$G_{pl} = \int_0^T e^{A_p s} B_{pl} ds$$

or

$$G_{pl} = \left(e^{A_p T} - 1 \right) A_p^{-1} B_{pl}$$

if the inverse exists.

If the inverse does not exist, the integrator states (x_h) are partitioned as

$$\begin{aligned} \dot{\mathbf{x}}_p &= A_p \mathbf{x}_p + B_p U_p, & \mathbf{x}_p(0) &= \mathbf{x}_{p0} \\ \dot{\mathbf{x}}_h &= 0 & \mathbf{x}_h(0) &= \mathbf{x}_{h0} \end{aligned}$$

This is equivalent to the homogeneous system

$$\dot{\mathbf{x}} = A_h \mathbf{x}$$

where

$$A_h = \begin{bmatrix} A_p & B_p \\ 0 & 0 \end{bmatrix}$$

The transition matrix for this system is given by

$$F_h = e^{A_h T}$$

where by definition

$$F_h = \begin{bmatrix} F_p & G_p \\ 0 & 1 \end{bmatrix}$$

To compute $F = e^{AT}$, subroutine EXPK uses the following algorithm:

$$e^{AT} \equiv \left(I + e^{-AT} \right)^{-1} \left(I + e^{AT} \right)$$

$$= \left[I + I - AT + \frac{(AT)^2}{2!} + \dots + (-1)^m \frac{(AT)^m}{m!} + E_0 \right]^{-1} \left[I + I - AT + \frac{(AT)^2}{2!} + \dots + (-1)^m \frac{(AT)^m}{m!} + E_0 \right]$$

where m is the maximum power used in the rational approximation.

The terms appearing in the above series are recursively computed.

The transition time T used in EXPK3 is computed from

$$T_k = 2^{-k} T_s$$

where

T_s = Sample interval over which matrix exponential is computed

k = integer ≥ 1

The subinterval index k is predicted using the maximum eigenvalue of the continuous system matrix A . The actual value of the parameter k and the intersample time interval are subsequently obtained using a relative error criteria.

Discrete Model for the Controller--To develop a discrete time model for the continuous controller dynamics, sub-routine WZK uses the matrix version of the Tustin algorithm. The z -transform could also be used (as above the the physical plant) to obtain somewhat different results. The analysis starts with the continuous controller

$$\dot{x}_c = A_c x_c + B_c u_c$$

$$y_c = C_c x_c + D_c u_c$$

Transforming the state equation

$$X_c(s) = (sI - A_c)^{-1} B_c U_c(s)$$

This can be written as

$$X_c(s) = \left(\frac{sT}{2} I - \frac{A_c T}{2} \right)^{-1} \left(\frac{B_c T}{2} \right) U_c(s)$$

Now replacing $\frac{sT}{2}$ by $\frac{z-1}{z+1}$ (Tustin's Rule),

$$X_c(z) = \left(\frac{z-1}{z+1} I - \frac{A_c T}{2} \right)^{-1} \frac{B_c T}{2} U_c(z)$$

Clearing the fractions and rearranging.

$$X_c(z) = (zI - F_1^{-1} F_2)^{-1} (zI+I) F_1^{-1} G_1 U_c(z)$$

where

$$F_1 = \left(I - \frac{A_c T}{2} \right)$$

$$F_2 = \left(I + \frac{A_c T}{2} \right)$$

$$G_1 = \frac{B_c T}{2}$$

Note here that F_1 and F_2 are analytic functions of A . Therefore, they commute with A .

$$Y_c(z) = \left[C(zI - F_1^{-1} F_2)^{-1} (F_1^{-2} G_1) + (C F_1^{-1} G_1 + D) \right] U_c(z)$$

The transformed system has a new set of states which we shall identify with the subscript d .

Letting

$$F_c = F_1^{-1} F_2$$

$$G_c = F_1^{-2} G_1$$

$$H_c = C_c$$

$$E_c = D_c + C_c F_1^{-1} G_1$$

one can write the state equations of the digital controller as follows:

$$x_d(k+1) = F_c x_d(k) + G_c u_c(k)$$

$$y_c(k) = H_c x_d(k) + E_c u_c(k)$$

The state diagram of the digitized controller is shown in Figure 14.

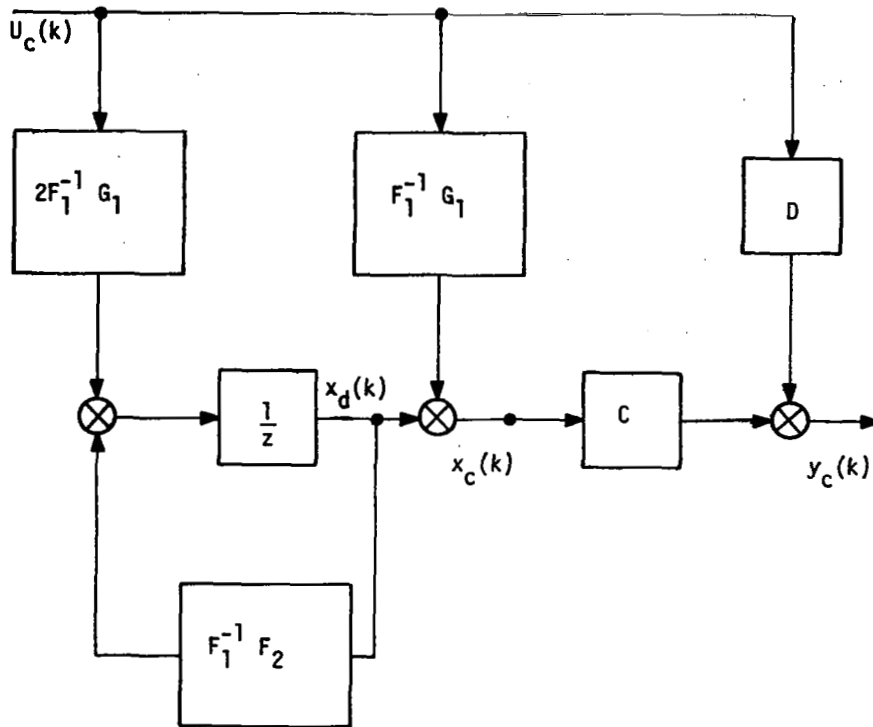


Figure 14. State Diagram of the Digitized Controller

$x_d(k)$ = State of the digitized controller

$x_c(k)$ = "Digitized state" of the continuous controller

$y_c(k)$ = "Digitized output" of the continuous controller

It can be shown that the steady state gain under the Tustin transformation is invariant. If the continuous system is prewarped for locating the critical frequencies, correction to gain term is made to maintain the steady-state gain invariance.

General Frequency Response Software--To determine the effects of sampling time on system frequency response (phase margin, gain margin), the complex system functions discussed below are implemented in program FREQK.

Two types of data inputs are considered: 1) continuous quadruple (F, G, H, D), and 2) discrete quadruple (A, B, H, D). For all types of frequency responses the transfer function is in the following generic form:

$$H(j\omega) = C[(\xi I - A) + i\eta I]^{-1} B + D$$

Where the (A, B, C, D) matrices correspond to continuous or discrete system matrix quadruples. The variables ξ and η depend upon the type of frequency response evaluation. The complex matrix is evaluated by using the complex matrix inversion subroutine.

For a given range of frequency (number of decades), the magnitude of the elements of $H(j\omega)$ are computed in units of db and phase angles in units of degree. These values are stored on tape for subsequent plotting. A simple plotting routine is used to see the trends in the response. Accurate plottings can be made on the "calcomp" plotter.

RMS Response of Plant to Continuous Stationary Inputs--Consider a plant characterized by the quadruple (F_p, G_p, H_p, E_p) . Input to plant consists of two parts:

$$u_p = \text{col}(u_{p1} \ u_{p2})$$

where

$$u_{p1} = \text{control input to plant}$$

$$u_{p2} = \text{disturbance input to plant}$$

The state of plant evolved as follows

$$\dot{x}_p = A_p x_p + B_{p1} u_{p1} + B_{p2} u_{p2}$$

Assuming a piecewise constant control input and a stochastic disturbance input,

$$u_{p1}(t) = u_{p1}(kT) \quad kT < t \leq (k+1)T$$

$$u_{p2}(t) = \eta_p(t) \quad \text{for all } t$$

the response is given by:

$$x(t) = F_p(t-kT)x_k + G_{p1}(t-kT)u_{p1}(kT) + \int_{kT}^t e^{(t-s)A_p} B_{p2} \eta_p(s) ds$$

When η_p is a white noise, the covariance response due to this input alone is given by

$$X(t) = F_p(t-kT)X_k F_p'(t-kT) + X_p(t)$$

where

$$X_p(t) = \int_{kT}^t e^{(t-s)A_p} B_p W_p B_p' e^{(t-s)A_p'} ds$$

with

$$kT < t \leq (k+1)T$$

and

$$W_p = \begin{bmatrix} 0 & | & \\ \hline & & \sigma_g^2 \end{bmatrix}$$

For the stationary inputs W_p is a constant matrix.

A change of independent variable simplifies the integral and yields

$$X_p(t) = \int_0^{(t-kT)} e^{\xi A} B_p W_p B_p' e^{\xi A'} d\xi$$

At sample points we obtain

$$X_{k+1} = F(T)X_k F'(T) + X_p(T)$$

where

$$X_p(T) = \int_0^T e^{\xi A} B_p W_p B_p' e^{\xi A'} d\xi$$

and T = output sample time.

The above set of equations define the discrete RMS response model corresponding to continuous stochastic inputs.

SECTION 6

MODELING

The LTV F-8C which is the test vehicle was designed as a supersonic shipboard day fighter which resulted in several special features: two position wing incidence, a speed break and a leading-edge cruise droop. The test aircraft has been modified for digital fly-by-wire and carries a triplex AP-101 computer, and triply redundant aircraft gyros and accelerometers. Dual air data measurements of Mach, pressure altitude and angle-of-attack are made. A single sideslip sensor is provided. Dynamic pressure and true air speed are derived from Mach assuming a standard atmosphere. The existing elevator, rudder, and ailerons are used as control effectors. The ailerons were also commanded symmetrically for an additional control surface in the pitch axis.

The DFBW F-8C is shown in Figure 15. [21] The aero data and the force and moment equations describing the DFBW F-8C were incorporated in a nonlinear simulation program in use at Honeywell. [2] The resulting software (F8SIM) is a six degree-of-freedom simulation and linearization program. It was used to:

- Generate linear models for controller synthesis.
- Assist in set point optimization (determination of steady state surface positions for minimum drag).

F8SIM is discussed in Appendix C.

Linear Aircraft Model

The output of F8SIM is a set of linear equations

$$\dot{\mathbf{x}} = \mathbf{F}\mathbf{x} + \mathbf{G}_1 \mathbf{u} + \mathbf{G}_2 \mathbf{w}$$

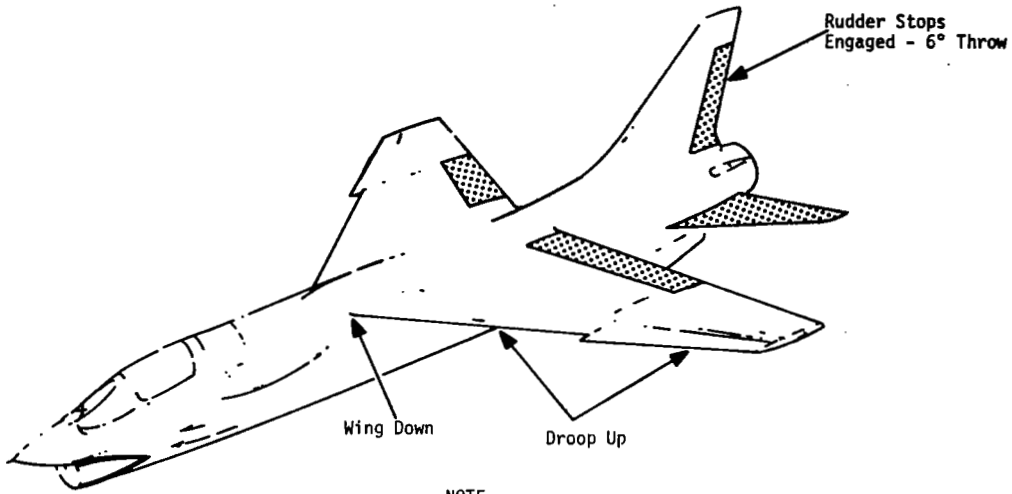
with output equations

$$\mathbf{y} = \mathbf{H}_x \mathbf{x} + \mathbf{H}_u \mathbf{u} + \mathbf{H}_w \mathbf{w}$$

The state (\mathbf{x}) is defined in Table 3, the control vector (\mathbf{u}) in Table 4, the disturbance vector (\mathbf{w}) in Table 5, and the output vector (\mathbf{y}) in Table 6. After the modeling is complete the gust vector and control vector will become elements of the state vector.

Using F8SIM linear models for the twenty flight conditions shown in Table 7 were obtained. The matrices corresponding to these flight conditions are contained in Appendix B.

CLEAN CONDITION



NOTE

When cruise droop selected - center section leading edge drooped 6.8° and outer panel leading edge drooped 7°.

LANDING CONDITION

Clean Condition Stops Disengaged
Aileron Throw Changed to 15° Up and
45° Down
Ailerons Drooped 20°

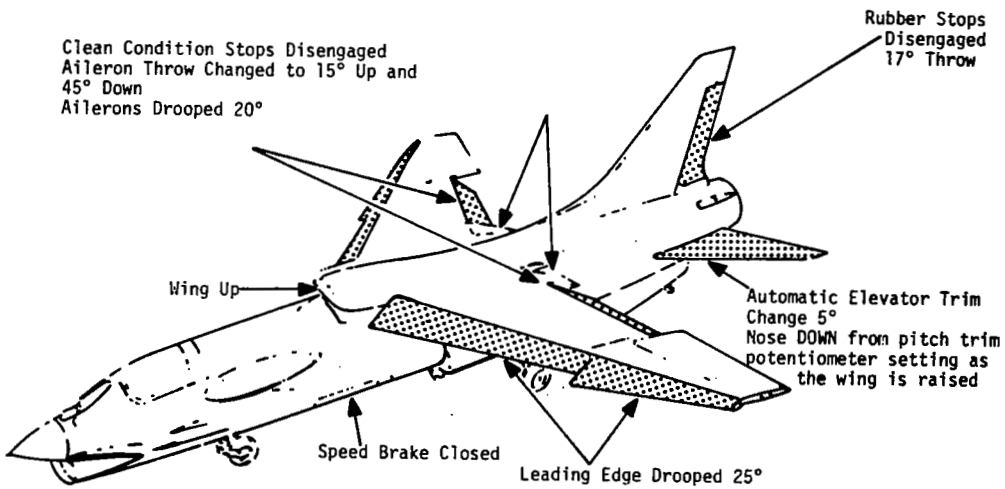


Figure 15 . The F-8C Aircraft

Table 3. State Definition

Symbol	Definition	
p	Roll rate (rad/sec)	Lateral Axis
r	Yaw rate (rad/sec)	
v	Lateral velocity (ft/sec)	
ϕ	Bank angle (rad)	
ψ	Yaw angle (rad)	
y	Lateral displacement (ft)	
q	Pitch rate (rad/sec)	Longitudinal Axis
w	Vertical velocity (ft/sec)	
u	Forward velocity (ft/sec)	
θ	Pitch angle (rad)	
h	Vertical displacement (ft)	
x	Forward displacement (ft)	

Table 4. Control Definition

Symbol	Definition	
δ_a	Differential aileron deflection (rad)	Lateral Axis
δ_r	Rudder deflection (rad)	
δ_{rt}	Differential elevator deflection (rad)	
δ_e	Symmetric elevator deflection (rad)	Longitudinal Axis
δ_f	Symmetric aileron deflection (rad)	
δ_{le}	Leading edge deflection (rad)	
δ_{sb}	Speed brake (rad)	
δ_g	Gear (%)	
δ_t	Throttle (%)	

Table 5. Disturbance Vector

Symbol	Definition
u	Forward gust (ft/sec)
v	Side gust (ft/sec)
w	Vertical gust (ft/sec)

Table 6. Output Vector

Symbol	Definition
β	Sideslip angle (rad)
a_y	Lateral acceleration (ft/sec ²)
α	Angle-of-attack (rad)
a_z	Normal acceleration (ft/sec ²)
V	Total velocity (ft/sec)
F_D	Total drag force (lbs)
F_L	Total lift force (lbs)
$C_{y\delta r}$	ΔC_y /rudder deflection
$C_{y\beta}$	ΔC_y /sideslip

Table 7. Twenty Flight Conditions

No.	h(ft.)	Mach	\bar{q} (psf)	V (ft/sec)	α_{TRIM} (deg)	CONDITION
1	20,000	.67	305	695	3.45	Cruise
2	20,000	.67	305	695	6.10	$\Delta N_z = 1g$ (Climb)
3	20,000	.67	305	695	12.12	$\Delta N_z = 3g$ (Climb)
4	20,000	.67	305	695	4.32	Cruise
5	20,000	.4	109	415	8.86	Cruise
6	20,000	.9	551	934	2.18	Cruise
7	40,000	.7	134	678	6.73	Cruise
8	40,000	1.2	395	1163	2.72	Cruise
9	10,000	.8	652	863	1.96	Cruise
10	0	.7	725	782	1.86	Cruise
11	0	.3	133	335	7.64	Cruise
12	0	.53	416	592	2.88	Cruise
13	20,000	.6	245	623	4.25	Cruise
14	20,000	.8	435	830	2.54	Cruise
15	40,000	.8	175	775	5.15	Cruise
16	40,000	.9	222	872	4.08	Cruise
17	0	.189	53	211	7.48	Power Approach Wing Up, $\delta_{Flap} = 20^\circ$ $\delta_{LE} = 25^\circ$ Gear down
18	0	.219	71	245	2.76	
19	20,000	.67	305	695	2.12	$\Delta N_z = 0.5g$ (Dive)
20	20,000	.6	245	623	15.45	$\Delta N_z = 3g$ (Climb)

Actuator Dynamics

The primary and secondary actuator dynamics were taken from unpublished NASA data and are presented in Table 8. The hysteresis model is defined in Figure 16.

Table 8. Actuator Model Parameters

Actuator	Primary (First Order)	Secondary (Second Order)
Pitch	$\tau_1 = 0.0800$ $2a = 0.25^\circ$ Rate limit = $25^\circ/\text{sec}$	$\omega = 62.8 \text{ rad/sec}$ $\zeta = 0.7$ $2a = 0.82^\circ$
Roll	$\tau_2 = 0.0333$ $2a = 0.35^\circ$ Rate limit = 140°	Same as above
Yaw	$\tau_3 = 0.0400$ $2a = 0.49^\circ$ Rate limit = $70^\circ/\text{sec}$	Same as above

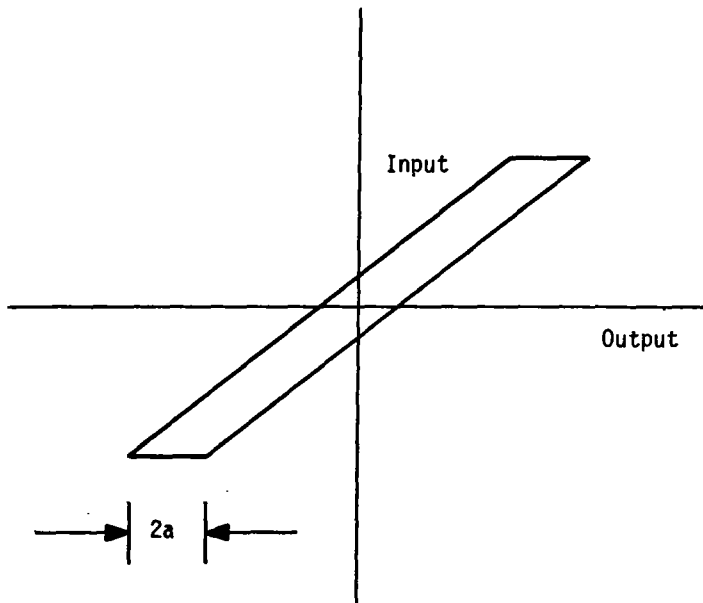


Figure 16. Hysteresis Model

Gust (Turbulence) Model

The gust model used in F8SIM is the form attributed to Dryden. In this form, it is assumed that gust velocities are locally isotropic (i. e., locally invariant with respect to position and orientation) and that time variations are statistically equivalent to distance variations in traversing the gust field. [2]

The translational gust velocity vector is defined as

$$\tilde{w} = \begin{pmatrix} u_g \\ v_g \\ w_g \end{pmatrix}$$

The power spectral densities for the translational gust velocity components are given by

$$\Phi_w(\Omega) = \begin{pmatrix} \phi_{ug}(\Omega) \\ \phi_{vg}(\Omega) \\ \phi_{wg}(\Omega) \end{pmatrix} \begin{bmatrix} \sigma_u^2 \left(\frac{2L_u}{\Omega} \right) \frac{1}{[1+(L_u\Omega)^2]} \\ \sigma_v^2 \left(\frac{L_v}{\Omega} \right) \frac{[1+3(L_v\Omega)^2]}{[1+(L_v\Omega)^2]^2} \\ \sigma_w^2 \left(\frac{L_w}{\Omega} \right) \frac{[1+3(L_w\Omega)^2]}{[1+(L_w\Omega)^2]^2} \end{bmatrix}$$

where

$$\Omega = \frac{2\pi}{\lambda} = \text{spatial frequency, (rad/ft)}$$

$$\lambda = \text{wavelength, (ft)}$$

$$L_i = \text{scales (ft)}$$

$$\sigma_i = \text{the root mean-square gust velocities (ft/sec)}$$

$$i = u, v, w$$

The mean-square gust velocities and the scales are related to each other through the following set of equations:

$$\frac{\sigma_u^2}{L_u} = \frac{\sigma_v^2}{L_v} = \frac{\sigma_w^2}{L_w}$$

The quantities appearing above have the following altitude dependence:

$$100 < h < 1750 \text{ ft}$$

$$L_w = h$$

$$L_u = L_v = 145.0 h^{1/3}$$

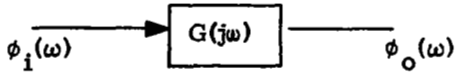
$$h > 1750 \text{ ft}$$

$$L_w = L_u = L_v = 1750 \text{ ft}$$

$$\sigma_w = 5.25 - \log_{10} \left(\frac{h}{10,000} \right)^{1.25}$$

This expression approximates the Mil 8785A values from 100 to 60,000 feet. For $0 < h < 100$, the value of $h = 100$ is used in the above equations.

Random velocities with above spectra are obtained by passing a gaussian random "white" noise through a linear system with a proper transfer function $G(s)$



It is known that

$$\phi_o(\omega) = |G(j\omega)|^2 \phi_i(\omega)$$

where the bars denote the magnitude of the complex variable. The power spectral densities given above are ratios of polynomials in ω^2 where ω is the temporal frequency given by

$$\omega = V_a \Omega \text{ rad/sec}$$

can be spectrally factored out. This process yields the proper transfer functions as follows: [2]

$$\begin{bmatrix} G_{ug}(s) \\ G_{vg}(s) \\ G_{wg}(s) \end{bmatrix} = \begin{bmatrix} \sigma_u \sqrt{\frac{2L_u}{V_a}} \frac{1}{[1 + \frac{L_u}{V_a} s]} \\ \sigma_v \sqrt{\frac{L_v}{V_a}} \frac{[1 + \frac{\sqrt{3}L_v}{V_a} s]}{[1 + \frac{L_v}{V_a} s]^2} \\ \sigma_w \sqrt{\frac{L_w}{V_a}} \frac{[1 + \frac{\sqrt{3}L_w}{V_a} s]}{[1 + \frac{L_w}{V_a} s]^2} \end{bmatrix}$$

Augmented Model

A separate program was written to decouple the lateral and longitudinal axes and append the actuator dynamics and wind gust models. This program also re-ordered the states and implemented the coordinate transformation discussed in the next section. The lateral and longitudinal states are tabulated in Table 9. W_1 , W_2 refer to the states associated with the second order gust model.

Table 9. Augmented State Vector

Lateral	Longitudinal
p	q
r	w
v	u
φ	θ
ψ	h
y	x
δ_a	δ_f
δ_r	δ_e
δ_{rt}	δ_{te}
W_1	W_1
W_2	W_2
	δ_t

State Transformation

The augmentation program also provided for a change of coordinates for the longitudinal and lateral models. This was accomplished as

$$\dot{\mathbf{x}} = \mathbf{F}\mathbf{x} + \mathbf{G}_1\mathbf{u} + \mathbf{G}_2\boldsymbol{\eta}$$

$$\mathbf{y} = \mathbf{H}\mathbf{x}$$

$$\mathbf{z} = \mathbf{T}\mathbf{x}$$

then

$$\dot{\mathbf{z}} = [\mathbf{T}\mathbf{F}\mathbf{T}^{-1}]\mathbf{z} + [\mathbf{T}\mathbf{G}_1]\mathbf{u} + [\mathbf{T}\mathbf{G}_2]\boldsymbol{\eta}$$

and

$$\mathbf{y} = [\mathbf{H}\mathbf{T}^{-1}]\mathbf{z}$$

where the products in brackets define a new set of quadruples at each flight condition.

States were selected for use with particular designs based on the sensor complement and the control objectives. To illustrate, consider the pitch CAS. Since the primary sensors are normal acceleration and pitch rate, the short period states were changed from w and q to N_z and q . Therefore, considering only the short period and actuator dynamics

$$\begin{bmatrix} \dot{q} \\ \dot{w} \\ \dot{\delta}_e \end{bmatrix} = \begin{bmatrix} F \end{bmatrix} \begin{bmatrix} q \\ w \\ \delta_e \end{bmatrix} + \begin{bmatrix} 0 \\ 0 \\ 12.5 \end{bmatrix} \begin{bmatrix} \delta_e \end{bmatrix}$$

Since N_z is one of the output quantities of F8SIM, an equation for N_z in terms of the original states and controls can be used to determine the transformation for

$$N_z = [K_1 \quad K_2 \quad K_3] \begin{bmatrix} q \\ w \\ \delta_e \end{bmatrix}$$

The transformation matrix T becomes

$$T = \begin{bmatrix} 1 & 0 & 0 \\ K_1 & K_2 & K_3 \\ 0 & 0 & 1 \end{bmatrix}$$

Pitch Axis Model for Relaxed Static Stability

Thirteen of the twenty flight conditions were studied with relaxed static stability in the pitch axis. Two conditions were considered: a shift to neutral stability and a further shift of the c.g. to 48 percent \bar{c} . The 48 percent \bar{c} location represents a 19 percent c.g. shift from the nominal 29 percent or a shift of 2.23 feet aft.

The pitching moment equation was modified to approximate the effect of a c.g. movement. Shifting the c.g. a distance $X_{c.g.}$ from the nominal modifies the pitching moment equation through Z_α and Z_{δ_e} :

$$\dot{q} = M_\alpha \dot{\alpha} + M_q q + M_{\delta_e} \delta_e + M_\alpha \alpha - \frac{X_{cg} m}{I_y} Z_\alpha \alpha - \frac{X_{cg} m}{I_y} Z_{\delta_e} \delta_e$$

where m is the airplane mass.

The same form of the equation can be kept by defining a new M_α (\bar{M}_α) and a new M_{δ_e} (\bar{M}_{δ_e}) that include the c.g. effect.

$$\bar{M}_\alpha = [M_\alpha - \frac{X_{cg} m Z_\alpha}{I_y}]$$

$$\bar{M}_{\delta_e} = [M_{\delta_e} - \frac{X_{cg} m Z_{\delta_e}}{I_y}] \text{ (this does not change much)}$$

Table 10 presents \bar{M}_α and \bar{M}_{δ_e} for the 48 percent \bar{c} condition.

Table 10. RSS Modeling Summary

F. C. No.	h(ft.)	Mach	\bar{q} (psf)	V_o (ft/sec)	NOMINAL c. g. (28.7% \bar{C})				CORRECTION		48% \bar{C}		Parameters	
					M_α	$M_{\delta e}$	Z_α	$Z_{\delta e}$	$\frac{X_{CG} m Z_\alpha}{I_y}$	$\frac{X_{CG} m Z_\delta}{I_y}$	\bar{M}_α	$\bar{M}_{\delta e}$	$\frac{\Delta M_\alpha}{M_{\delta e}}$	T_a
1	20,000	.67	305	695	- 6.8	-12.3	- 698.	- 89.1	-11.5	-1.47	4.7	-10.8	1.1	1.07
4	20,000	.67	305	695	- 6.38	-11.5	- 535.	- 68.3	-10.8	-1.38	4.4	-10.1	1.07	1.39
5	20,000	.4	109	415	- 2.12	- 4.54	- 233.	- 33.2	- 3.84	- .547	1.72	- 3.99	0.96	1.91
6	20,000	.9	551	934	-14.4	-21.6	-1422.	-158.	-23.5	-2.61	9.1	-19.0	1.2	0.71
7	40,000	.7	134	678	- 3.71	- 6.0	- 313.	- 39.3	- 5.15	- .648	1.44	- 5.4	0.96	2.35
8	40,000	1.2	395	1163	-24.1	-15.0	- 941.	-105.	-15.5	-1.73	- 8.6	-13.3	1.17	1.50
9	10,000	.8	652	863	-14.3	-22.9	-1577.	-190.	-26.0	-3.13	11.7	-19.8	1.3	0.59
10	0	.7	725	782	-14.4	-26.2	-1638.	-212.	-27.0	-3.5	12.6	-22.7	1.19	0.51
11	0	.3	133	335	- 2.32	- 5.65	- 281.	- 41.5	- 4.64	- .69	2.32	- 4.96	0.94	1.27
12	0	.53	416	592	- 8.03	-14.7	- 896.	-123.	-14.8	-2.03	6.8	-12.7	1.17	0.71
13	20,000	.6	245	623	- 5.40	- 9.79	- 544.	- 71.6	- 8.97	-1.18	3.57	- 8.61	1.04	1.23
16	40,000	.9	222	872	- 6.57	-10.4	- 592.	- 63.5	- 9.76	-1.05	3.19	- 9.3	1.05	1.58
17	0	.189	53	211	- .491	- 2.08	- 100.	- 18.3	- 1.13	- .207	.64	- 1.87	.60	2.2

SECTION 7

SYNTHESIS OF PITCH AXIS CONTROL AUGMENTATION SYSTEM (CAS)

The functional form of the pitch CAS is illustrated in Figure 17. The feedback sensors include a normal accelerometer, a pitch rate gyro, and an angle-of-attack sensor. This section will discuss the procedure and the rationale used to design the pitch CAS.

The design of the normal elevator controller will be discussed next followed by a discussion of the angle-of-attack limiting controller.

Normal Elevator Controller

The pitch CAS mode using only the elevator is referred to as Mode I. This controller provides improved handling qualities by model-following an explicit second order C* model. The feedback consists of normal acceleration and pitch rate with a low pass filter included in the accelerometer feedback for high frequency gain attenuation. Apparent neutral speed stability (no trim change with speed) is provided (except at power approach) by effectively including an integration in the forward loop. The integration is mechanized by a positive feedback of lagged elevator position. The advantages of this mechanization will be discussed in more detail later.

With only one forcing function (the elevator), the reduction of gust acceleration is limited to that resulting from the improved short period damping. After obtaining gain-scheduled controllers over the flight envelope, the changes necessary to accommodate reduced static stability were studied.

The problem is formulated as presented in Section 5. That is:

$$\dot{x} = Fx + G_1 u + G_2 \eta$$

$$r = Hx + Du$$

Five flight conditions (1, 5, 8, 9, and 17), spanning the variations across the envelope, were selected for preliminary design. The structure used for the quadratic design at each flight condition is shown in Figure 18.

The states were as follows:

$$x_1 = q, \text{ pitch rate (rad/sec)}$$

$$x_2 = N_z, \text{ sensed normal acceleration (ft/sec}^2\text{)}$$

$$x_3 = \text{integral of C* error}$$

$$x_4 = \text{gust state}$$

$$x_5 = \text{gust state}$$

$$x_6 = \delta_f, \text{ symmetric aileron position (rad, + trailing edge down)}$$

$$x_7 = \delta_e, \text{ elevator position (rad, + trailing edge down)}$$

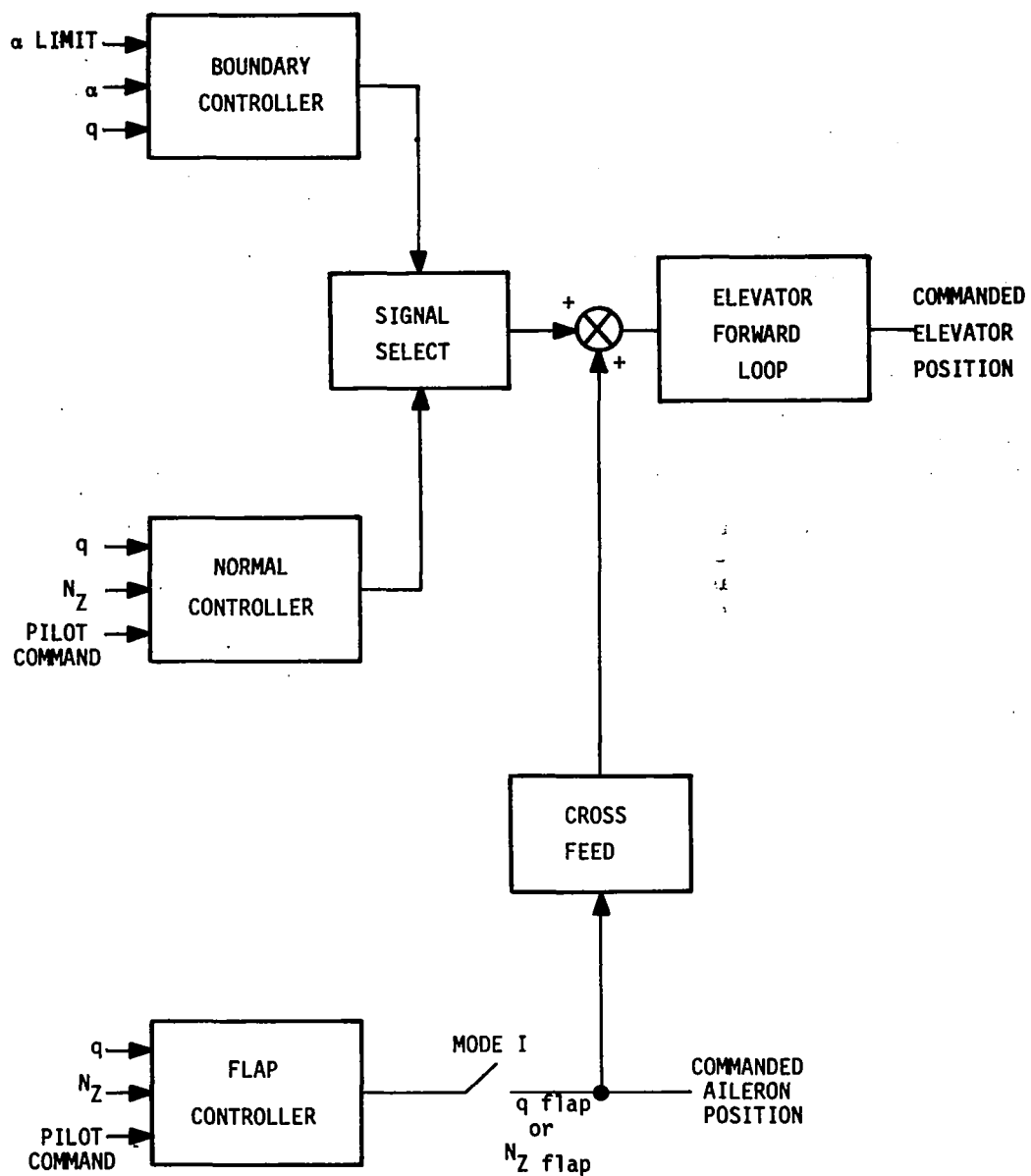


Figure 17. Pitch CAS Structure

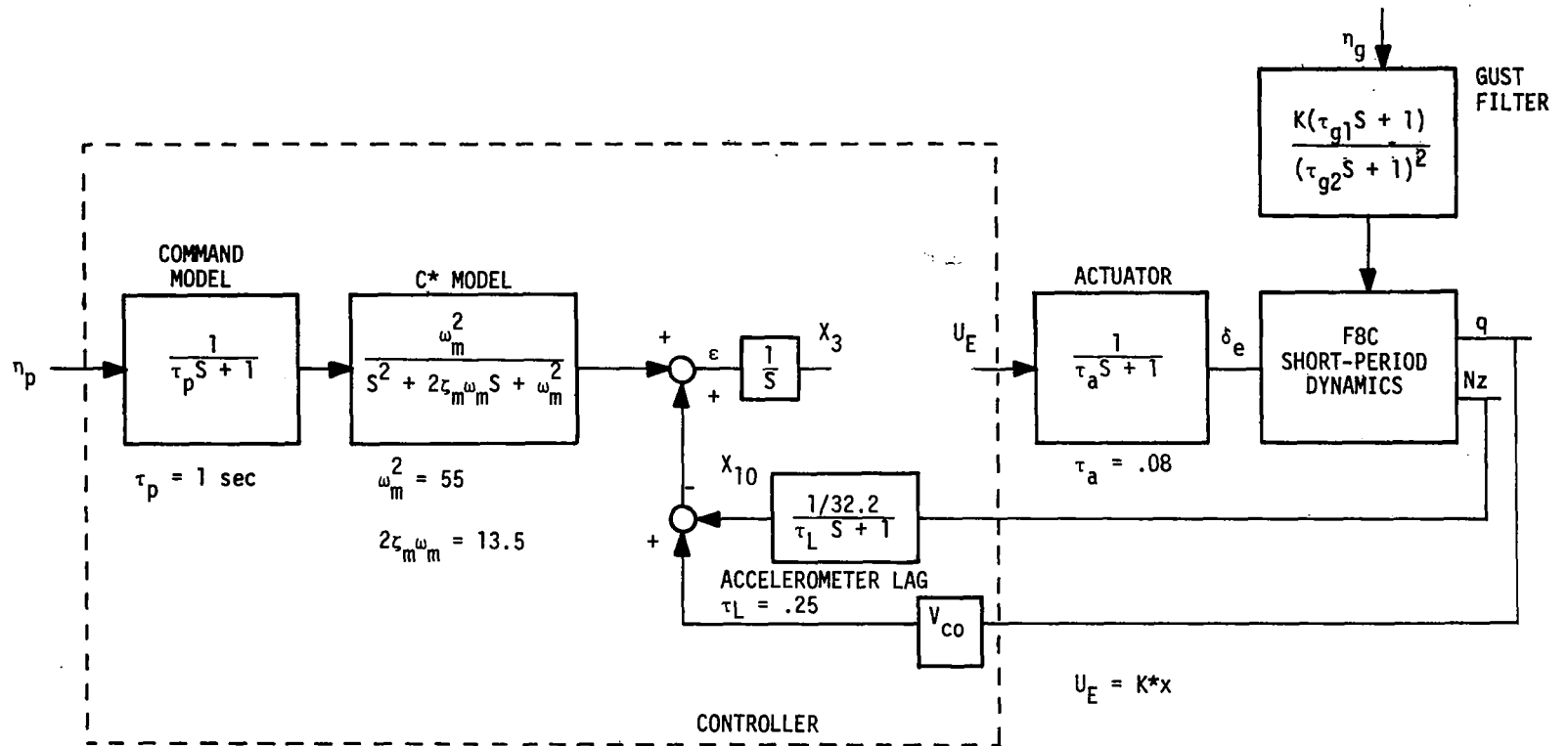


Figure 18. States for Pitch CAS Design

- x_8 = command model
- x_9 = lagged N_z (g's)
- x_{10} = C* model
- x_{11} = C* model rate

The gust model and the command model are driven by independent white noise processes. The gust filter was developed in Section 6. The command model was selected as a first order lag with a time constant of one second. Selection of the time constant is not critical as it does not affect the feedback gains.

After a number of trial and error iterations, four responses were found to be significant for the Mode I design. These responses together with the final weights are tabulated in Table 11. Also shown is the gain variation and the closed loop eigenvalues. Both DIAK (continuous) and DIAK-D (discrete) designs were checked at various flight conditions. No significant differences in performance were noted for a 32 sample/second rate.

The first response is the difference between the explicit C* model ($\omega = 7$ rad/sec $\xi = 0.9$) and the C* quantity formed by the sum of lagged normal acceleration and pitch rate. The second response is the integral of this C* error function. Weighting these two responses causes the C* response of the F-8C to match the C* response of the model. This provides a desirable stick response and suitable short period damping. The third response used is the elevator rate $\dot{\delta}$ obtained from the first order representation used for the power actuator. Weighting this response reduces the actuator state feedback to itself and helps to constrain the bandwidth of the controller. The final response ($u_{\bar{D}}$) is required for a solution to the optimal control problem to exist, and it also influences the system bandwidth.

Next, the controllers were put into a transfer function format where the inputs to the transfer functions are pitch rate, normal acceleration, and pilot command. The reasons for converting to a more "classical" or conventional structure are

- The normal/boundary limiting mode transition strategy requires isolation of a common proportional plus integral function. This is covered in greater detail in the discussion on mode transition.
- Insight to the gain scheduling requirements is obtained.

Therefore, the designs from Table 11 are redrawn in block diagram structure of Figure 19. In deriving this structure the gains on states 4, 5, 6 and 7 were set to zero. This did not change performance. The proportional plus integral function on the accelerometer was isolated. Since pitch rate and stick input had different proportional plus integral functions this resulted in adding lead-lag dynamics to these signals to maintain equivalent feedback.

The specific parameters for the flight conditions are listed in Table 12. Compromises in the gain as a result of gain scheduling are discussed in a later subsection.

Table 11. Pitch CAS Mode I Design Summary

Responses	Quadratic Weights				
	FC 1	FC 5	FC 8	FC 9	FC 17
$r_1 = C_A^* - C_M^*$.1E+3	.1E+4	.1E+4	.1E+3	.1E+5
$r_2 = \int (C_A^* - C_M^*)$.1E+2	.1E+3	.1E+3	.1E+1	.1E+4
$r_3 = \delta_e$.1E+4	.1E+4	.1E+5	.1E+4	.1E+4
$r_4 = u_E$.1E+4	.1E+4	.1E+4	.1E+4	.1E+4
Closed Loop	-1.59	-1.62	-1.67	-0.50	-0.76
Eigenvalues	-2.46+j2.52	-2.15+j2.257	-2.56+j2.18	-2.76+j4.26	-1.85
	-4.32+j4.09	-4.89+j4.92	-3.43+j6.02	-6.38+j5.72	-3.39
	-6.75+j3.11	-6.75+j3.11	-6.75+j3.11	-6.75+j3.11	-3.83+j3.70
					-6.75+j3.11
Gains					
k_1	.2974E00	.9552E00	.1920E00	.2361E00	.2793E+01
k_2	.8612E-02	.1050E-02	.1656E-02	.1172E-04	-.1680E-02
k_3	.3988E-01	.1261E00	.3998E-01	.1261E-01	.1694E00
k_4	.8781E-08	-.3792E-04	-.8762E-04	.8570E-05	.1908E-03
k_5	-.2055E-06	.1805E-04	.1212E-03	.8695E-05	-.4703E-04
k_6	-.1477E-01	-.6215E-02	.7655E-01	.03183E-01	-.4497E-01
k_7	.2331E00	.1079E00	.1342E00	.5640E-01	.3796E00
k_8	.1372E-01	.3883E-01	.1191E-01	.8977-02	.1421E00
k_9	.1660E-01	.5424E-01	.1735E-01	.1502E-01	.1253E00
k_{10}	.1885E-01	.6234E-01	.2013E-01	.1759E-01	.1384E00
k_{11}	.1336E-02	.4301E-02	.1384E-02	.1198E-02	.1063E-01

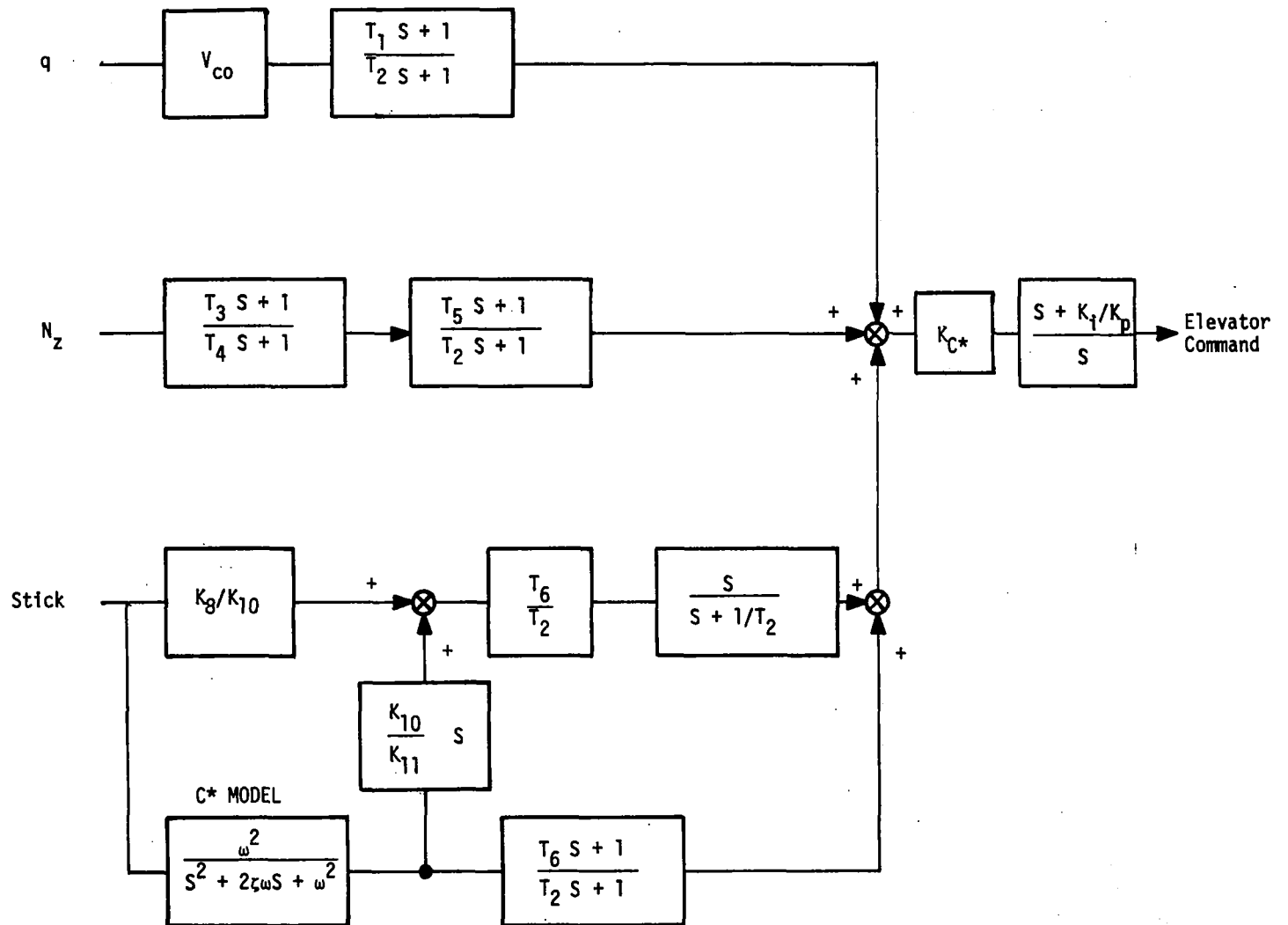


Figure 19. Block Diagram of Pitch CAS Optimal Design

Table 12. Pitch CAS Parameters

Parameter	Flight Condition				
	1	5	8	9	17
K_i/K_p	2.3	2.3	2.3	2.3	2.3
V_{co}	324	324	324	324	324
$1/T_2$	2.4	2.3	2.31	2.3	1.0
T_1/T_2	1.8	1.76	1.11	4.37	.380
$1/T_4$	4.	4.	4.	4.	4.
T_3/T_4	0	1.424	.563	0	1.62
T_5/T_2	0	-.43	-1.36	2.76	.055
K_c^* - elevator loop gain	.000515	.0017	.000538	.000167	.019
ω^2 C* Model	55	55	55	55	55
ζ	0.9	0.9	0.9	0.9	0.9
k_8/k_{10}	.729	.623	.511	.51	1.31
k_{11}/k_{10}	.0712	.069	.068	.068	.096
T_6/T_2	1.15	1.2	1.16	3.3	.414

Neutral Speed Stability Implementation

The neutral speed stability (NSS) characteristic is obtained by generating an integration in the forward path of the elevator control system. The integration maintains zero steady-state error between force command and the blended pitch rate and normal acceleration feedback. Neutral speed stability keeps the airplane in trim since any uncommanded pitch rate and acceleration are automatically reduced to zero by the action of the integral. For non-terminal flight conditions, only occasional trim inputs initiated by the pilot are required to offset electrical biases or to trim at other load factor levels. During terminal phases the integration function is removed when the wing is up or the landing gear is down. These flight phases will require conventional trimming action by the pilot.

The two secondary actuators are used to provide the integration function. This is accomplished by a positive feedback of the average of the two elevator positions. (Refer to Figure 20). Differential elevator position will cancel and hence will not be fed back. The secondary actuators still contain their internal feedback of ram position. The lag feedback is an additional feedback that will be mechanized in the computer.

For NSS the switch is open as shown in Figure 20 and the closed loop transfer function to the power actuator is

$$\frac{\tau S + 1}{\tau S}$$

if the secondary servo has a unity transfer function. τ is the time constant of the lag.

This mechanization was selected since it eliminates the need for synchronizing integrators in redundant computers and because it is less sensitive to secondary servo nonlinearities.

Angle-of-Attack Boundary Controller Design

As discussed in Section 4 under angle-of-attack limiting, a separate controller was designed using the elevator to hold angle-of-attack. The quadratic formulation of the design problem is presented followed by a discussion of the mode switching implementation.

The controller structure used for designing the angle-of-attack controllers is shown in Figure 21. For these designs the short period aircraft dynamics were modeled with w and q as the variables. The disturbance was modeled as filtered white noise to represent the control action of the normal controller. The filter was a 1 second lag.

The states were as follows:

- $x_1 = q$, pitch rate (rad/sec)
- $x_2 = w$, vertical velocity (ft/sec)
- $x_3 = \delta_e$, elevator surface position (rad, + trailing edge down)
- $x_4 =$ disturbance
- $x_5 =$ integral of α error (rad)

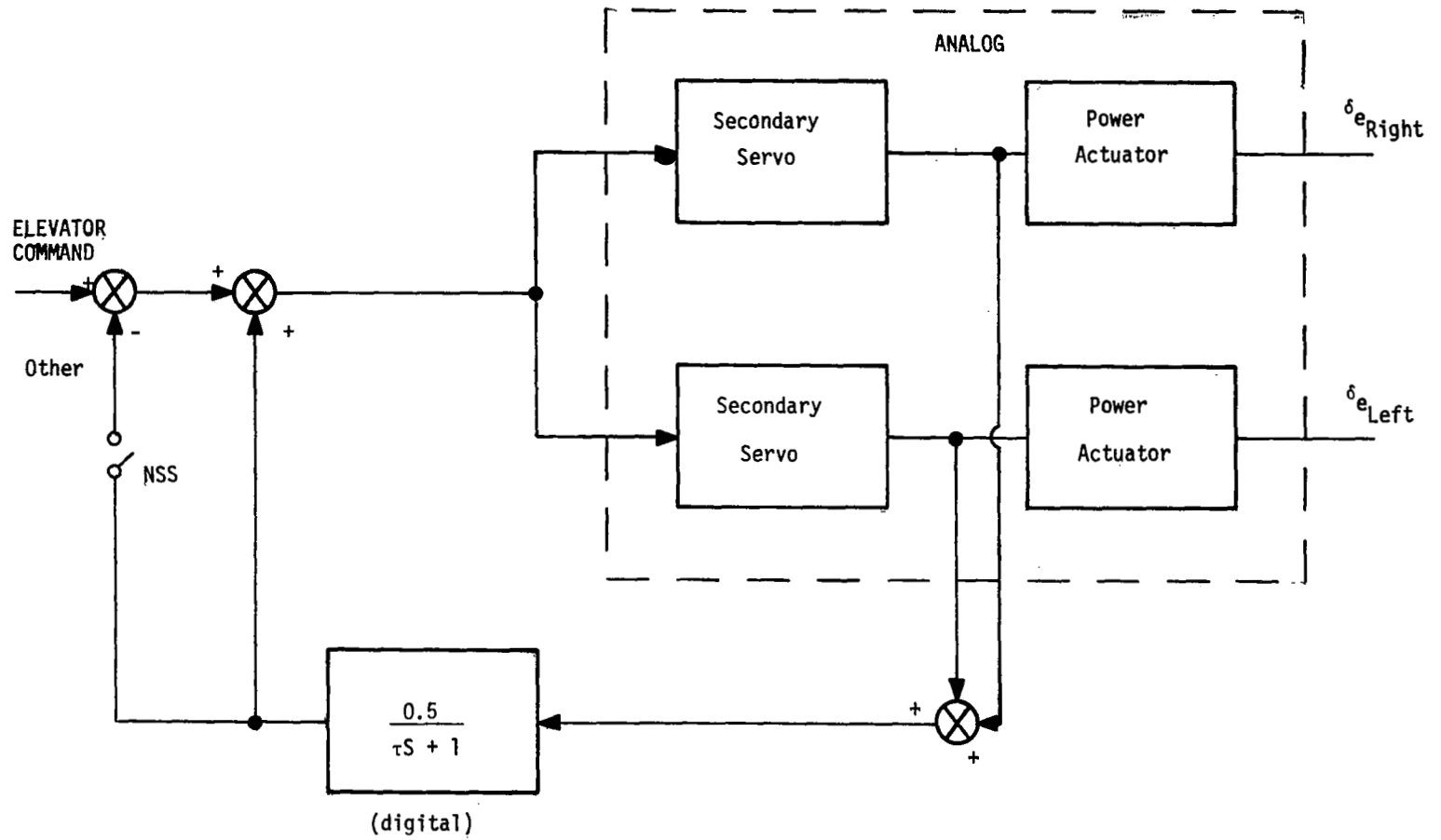


Figure 20. NSS Implementation

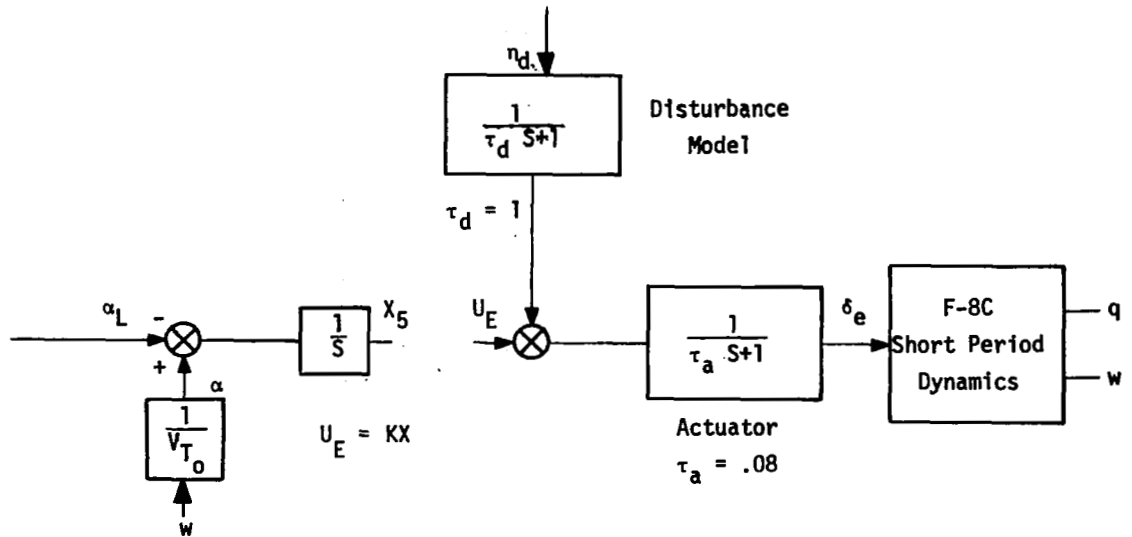


Figure 21. Boundary Controller Structure

The quadratic weights are selected to minimize the angle of attack error without extending the bandwidth of the actuator by actuator state feedback. In addition the maximum short-period damping is desirable to prevent boundary overshoot. The responses, weights and gains are tabulated in Table 13 for selected flight conditions. The angle of attack error and the integral of this error (responses 1 and 2) define a proportional plus integral function on the angle of attack error. Response 3, the elevator rate, is weighted to reduce the feedback around the elevator. Pitch rate (response 4) is weighted to provide maximum short period damping.

The block diagram form of the boundary controllers are shown in Figure 22. The parameters for the transfer functions are given in Table 14.

Mode Switching

The boundary controller is built around the normal elevator controller in such a manner as to effect a smooth transition from normal control to the boundary and vice versa. The transition is via a signal selector that alters the command applied to the actuator as the two functions become equal (cross each other). This prevents signal level discontinuities and their resulting transients.

Table 13. Boundary Controller Design Summary

Responses	Quadratic Weights			
	FC 1	FC 5	FC 9	FC 17
$r_1 = \alpha \text{ ref} - \alpha$.1E+1	--	.1E+10	--
$r_2 = \int (\alpha \text{ ref} - \alpha)$.1E+6	.1E+6	.1E+6	.1E+6
$r_3 = \dot{\delta}_e$.5E+8	.1E+9	.1E+9	.1E+9
$r_4 = q$.1E+10	.1E+11	.1E+10	.1E+13
$r_5 = u_E$.1E+8	.1E+7	.1E+7	.1E+7
Closed Loop	-1.94+j1.79	-.857+j0.753	-2.27+j1.83	-0.146
Roots	-5.26+j5.80	-4.60+j4.93	-5.45+j6.51	-0.459 -6.48+j6.51
Gains				
k_1	.4633E00	.8594E00	.2774E00	.7644E+01
k_2	.1171E-02	.1147E-02	.3345E-03	.1915E-02
k_3	-.1842E-01	.2064E00	.1973E-02	-.1645E-01
k_4	-.7909E-01	-.7806E-01	-.7869E-01	-.7877E-01
k_5	.3575E-02	.253E-2	.2530E-02	.2530E-02

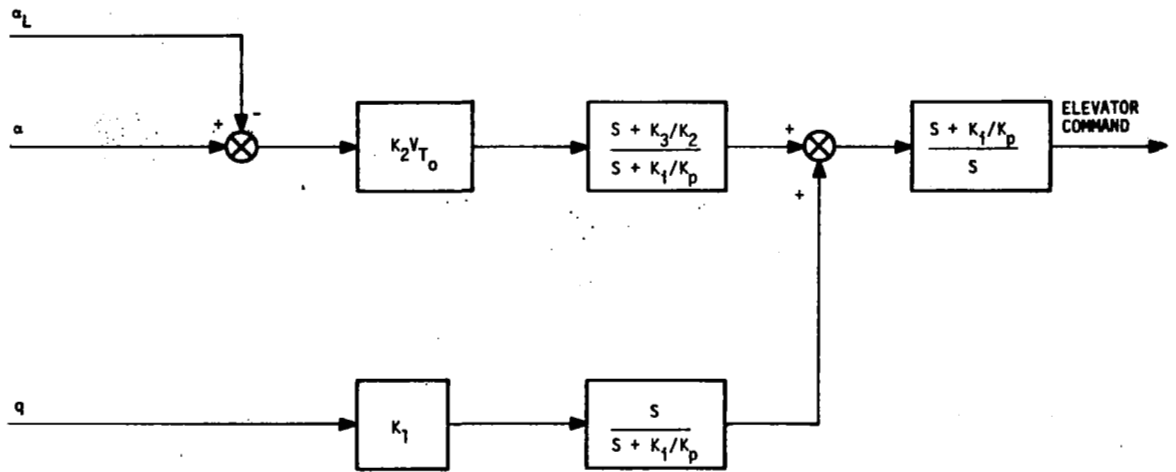


Figure 22. Block Diagram of Angle-of-Attack Limiting Controllers

Table 14. Boundary Controller Parameters

Parameter	Flight Condition			
	1	5	9	17
$K_2 V_{T_0}$.8115	.4703	.2883	.4673
K_3/K_2	3.053	2.206	7.563	1.32
K_1	.4633	.8594	.2774	7.64
K_1/K_p	2.4	2.4	2.4	2.4

The transition between the normal and the boundary elevator controller was implemented using a comparison of commanded elevator rate. A comparison of commanded elevator position is not practical because of the problem of accounting for the trim elevator position. Switching on elevator rate has been found to be a simple and effective transition means and it eliminates the trim question.

The mode switching is illustrated in Figure 23 where each intersection of the normal and boundary control represents a transition. The logic selects the "most nose down" signal so the resultant elevator rate command is shown as the dotted line. The input signal to the common proportional plus integral function can be considered a pseudo elevator rate. For low frequencies (less than K_I/K_P rad/sec) the signal actually is the elevator rate. For this reason the ratio of K_I/K_P is usually around 3 so that the input to the common block approximates the elevator rate satisfactorily over the frequencies of interest. The actual implementation used for mode switching permits switching on elevator rate even in power approach when the neutral speed stability characteristic is not used in the normal pitch CAS. This is mechanized by first subtracting and then adding the lagged feedback of the secondary servo.

Adaptation Over the Flight Envelope

With the structures given in Figure 19 and 22 for the normal and boundary controllers a number of compromises were assessed using a linear simulation to check their influence on transient response performance.

First a schedule for K_{C^*} was postulated using the dynamic pressure as the schedule variable (refer to Figure 24). Next the various filter time constants were modified to obtain fixed values over the flight envelope.

The boundary controller was compromised in a similar fashion. Gain schedules for K_{qL} and $K_{\alpha L}$ were obtained in the following manner. $K_{\alpha L}$ has been explicitly obtained as a function of true air speed (as a result of using q and w in the quadratic designs). $K_{\alpha L}$ was postulated as a scheduled gain by plotting gain values against dynamic pressure (refer to Figure 25).

After several iterations with fixed filter time constants the compromised system shown in Figure 26 was obtained. Figure 26 shows the analog representation of the controller with the gain schedules on the normal and boundary controller and with the signal select means included.

Mode I Results

Using the pitch CAS and angle of attack limiter (Figure 31) sample responses to pilot commands and step α gusts are shown for selected flight conditions. Transitions to the α boundary are also shown.

<u>Figure</u>	<u>Flight Condition</u>
27	1 (20,000, 0.67)
28	5 (20,000, 0.4)
29	9 (10,000, 0.8)
30	17 (0, 0.19 power approach)

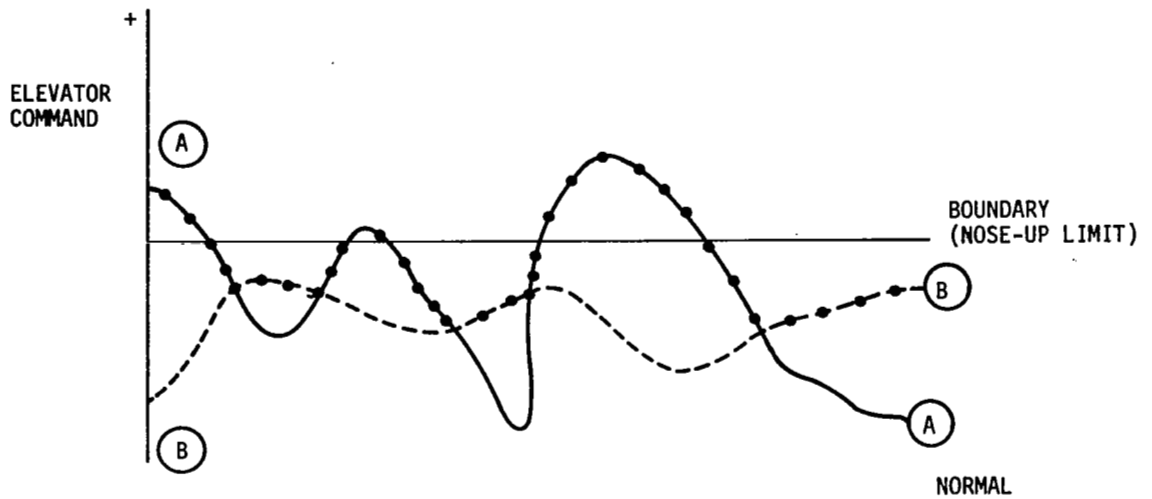
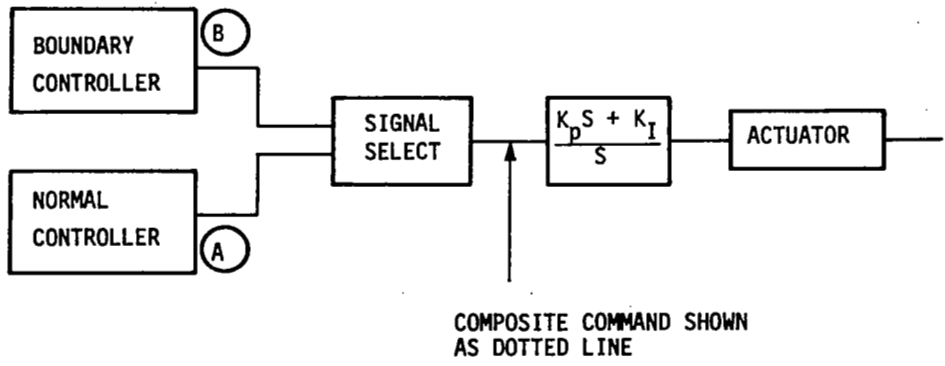


Figure 23. Mode Transition Logic

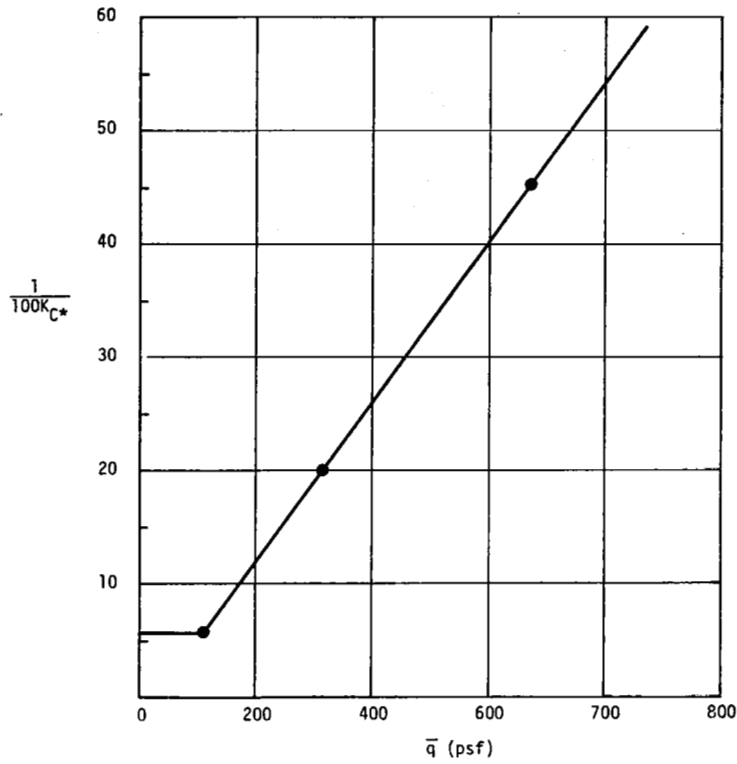


Figure 24. K_C * Gain Schedule

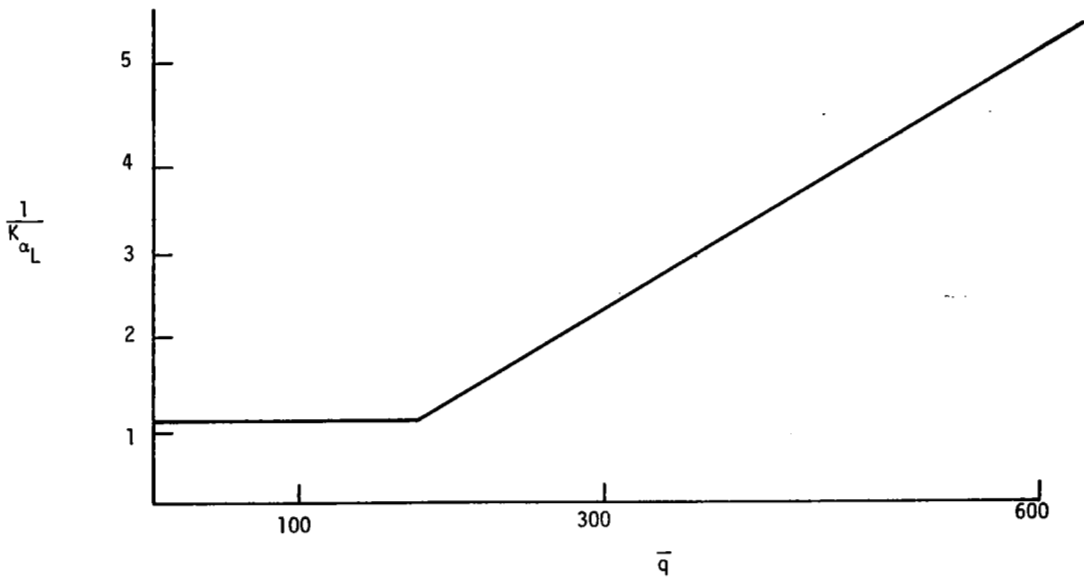


Figure 25. K_{α_L} Gain Schedule

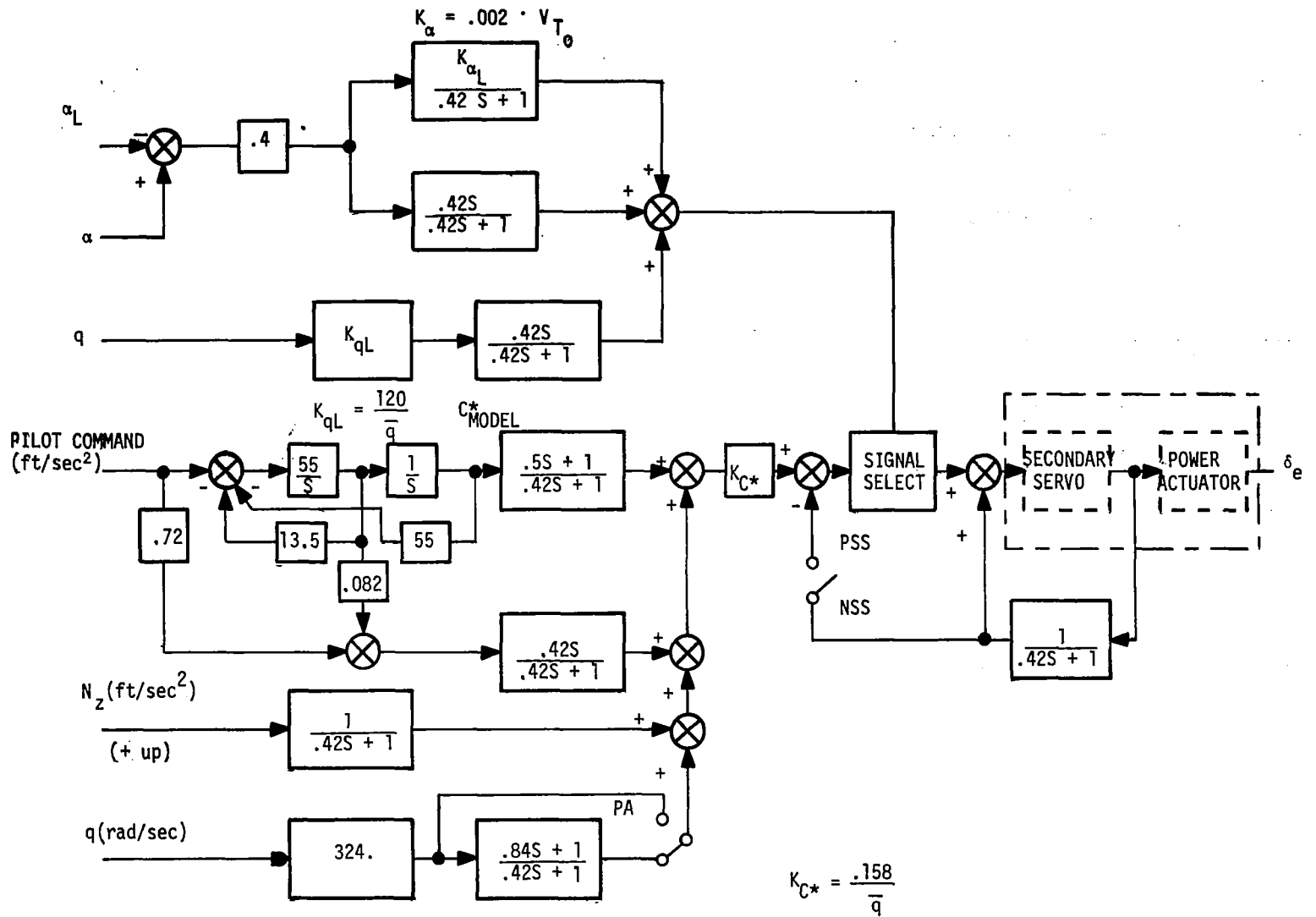


Figure 26. Pitch CAS (Mode I)

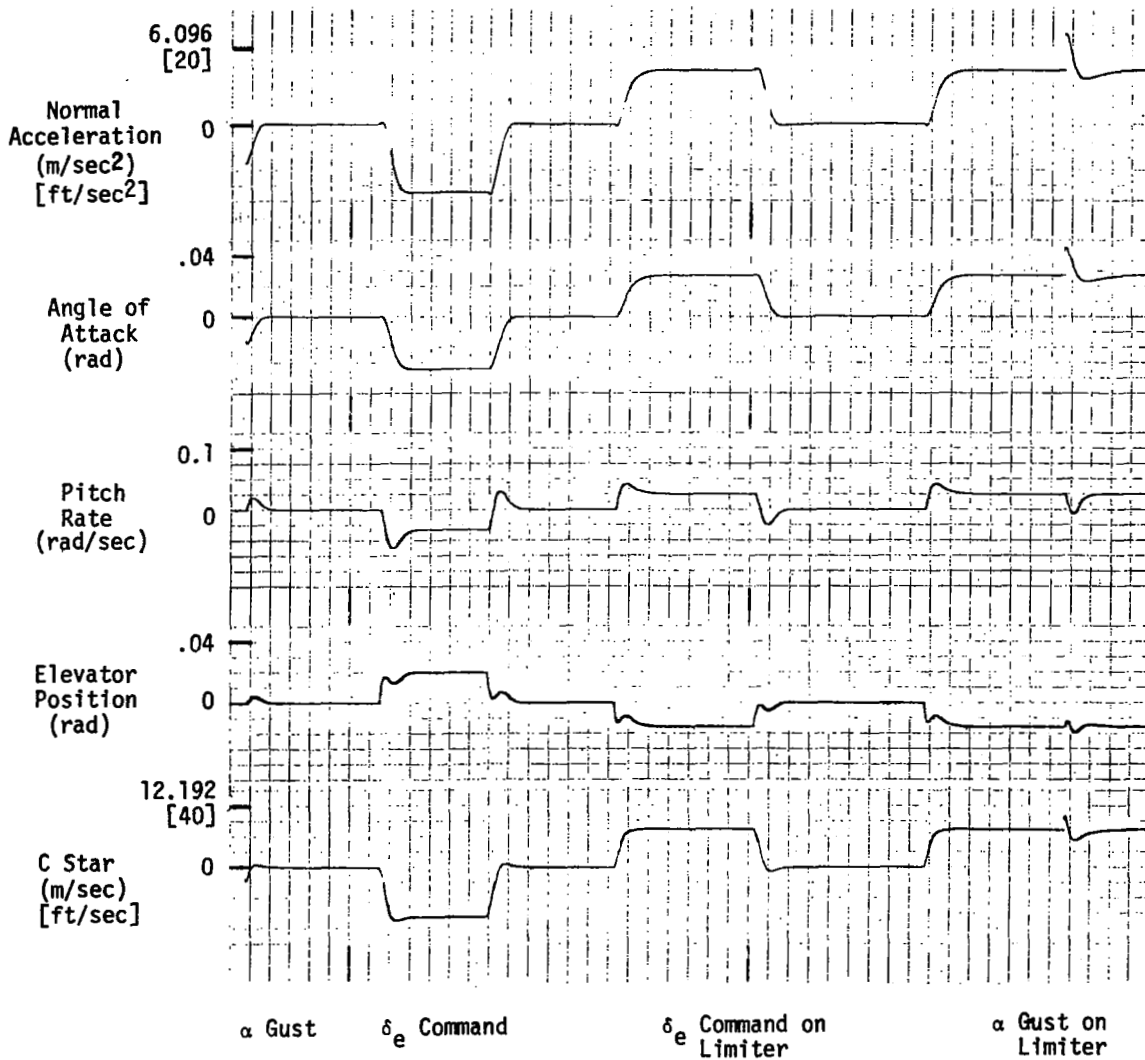


Figure 27. Pitch CAS and Boundary Control
(Mach 0.67, 20,000 feet)

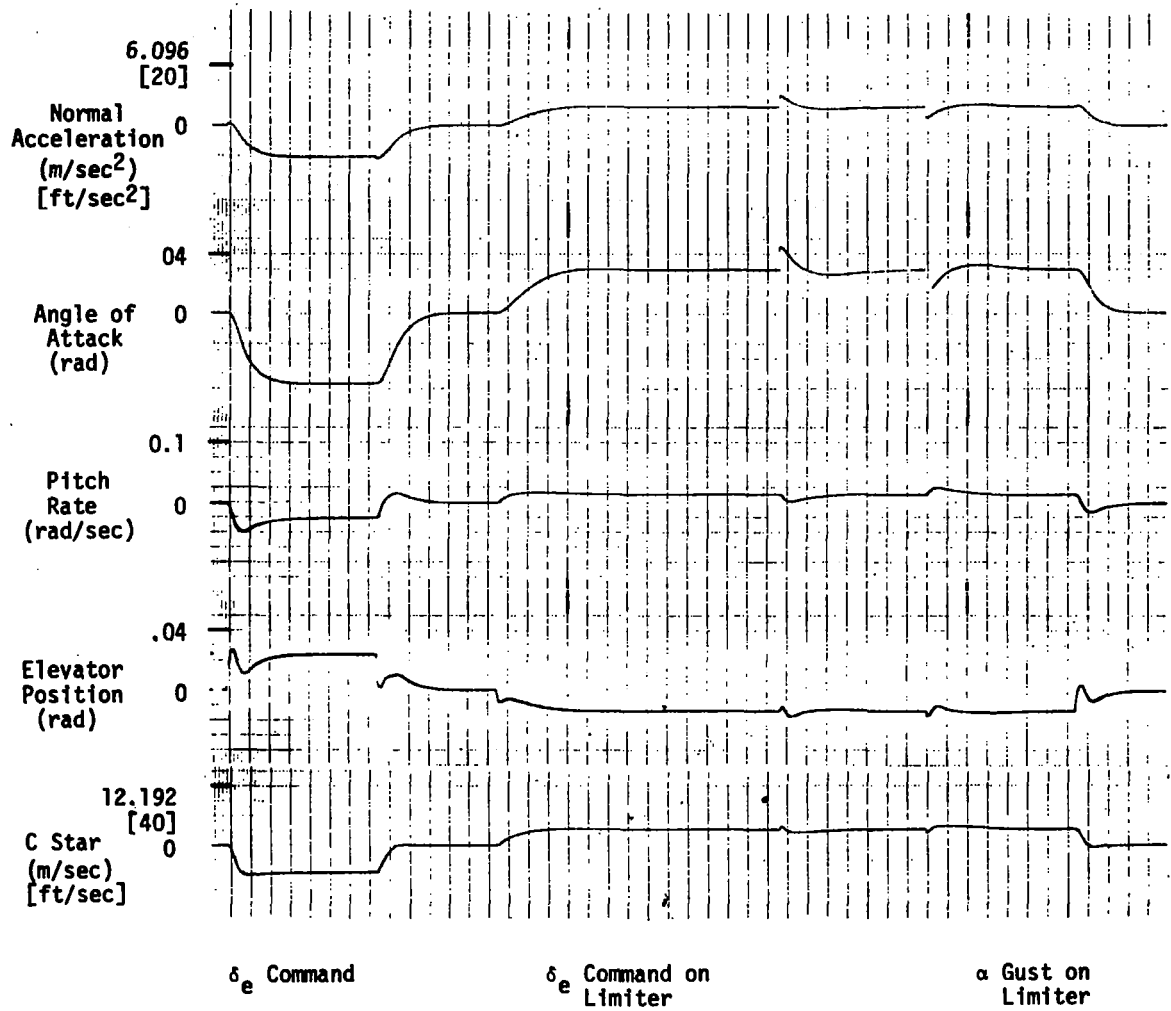


Figure 28. Pitch CAS and Boundary Control
(Mach 0.4, 20,000 feet)

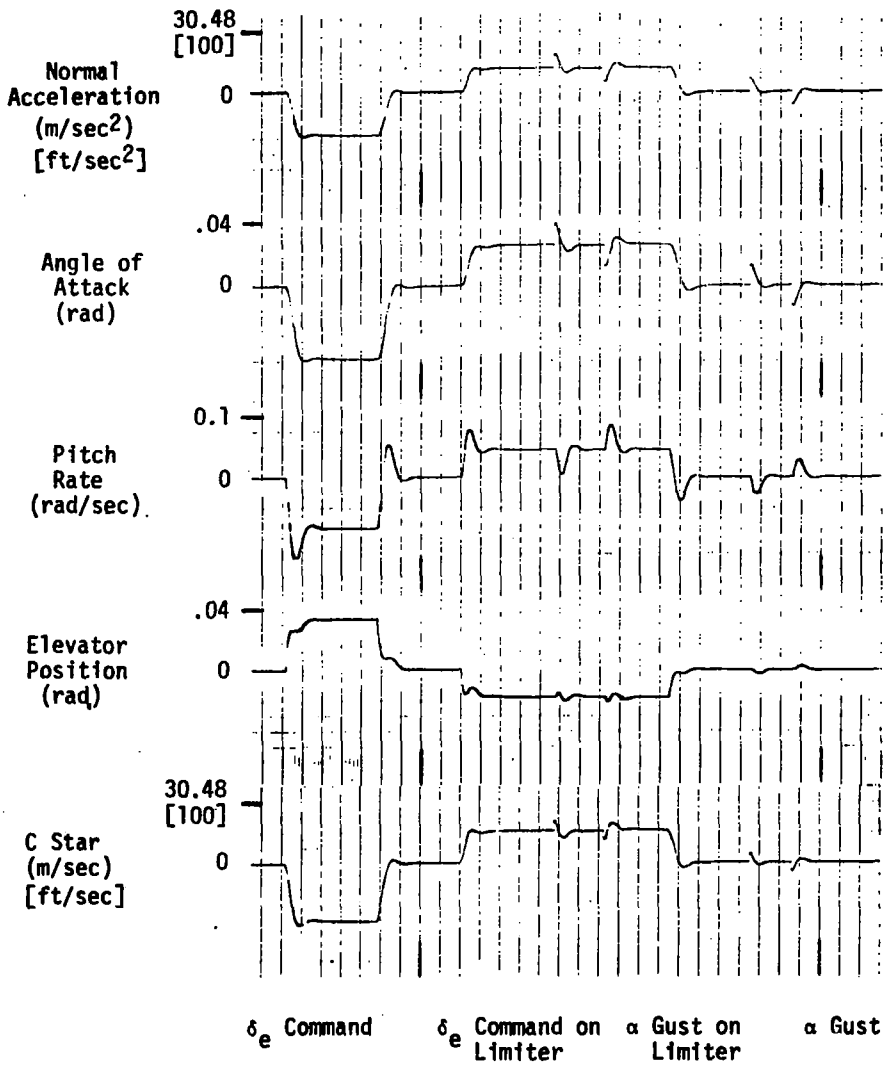


Figure 29. Pitch CAS and Boundary Control
(Mach 0.8, 10,000 feet)

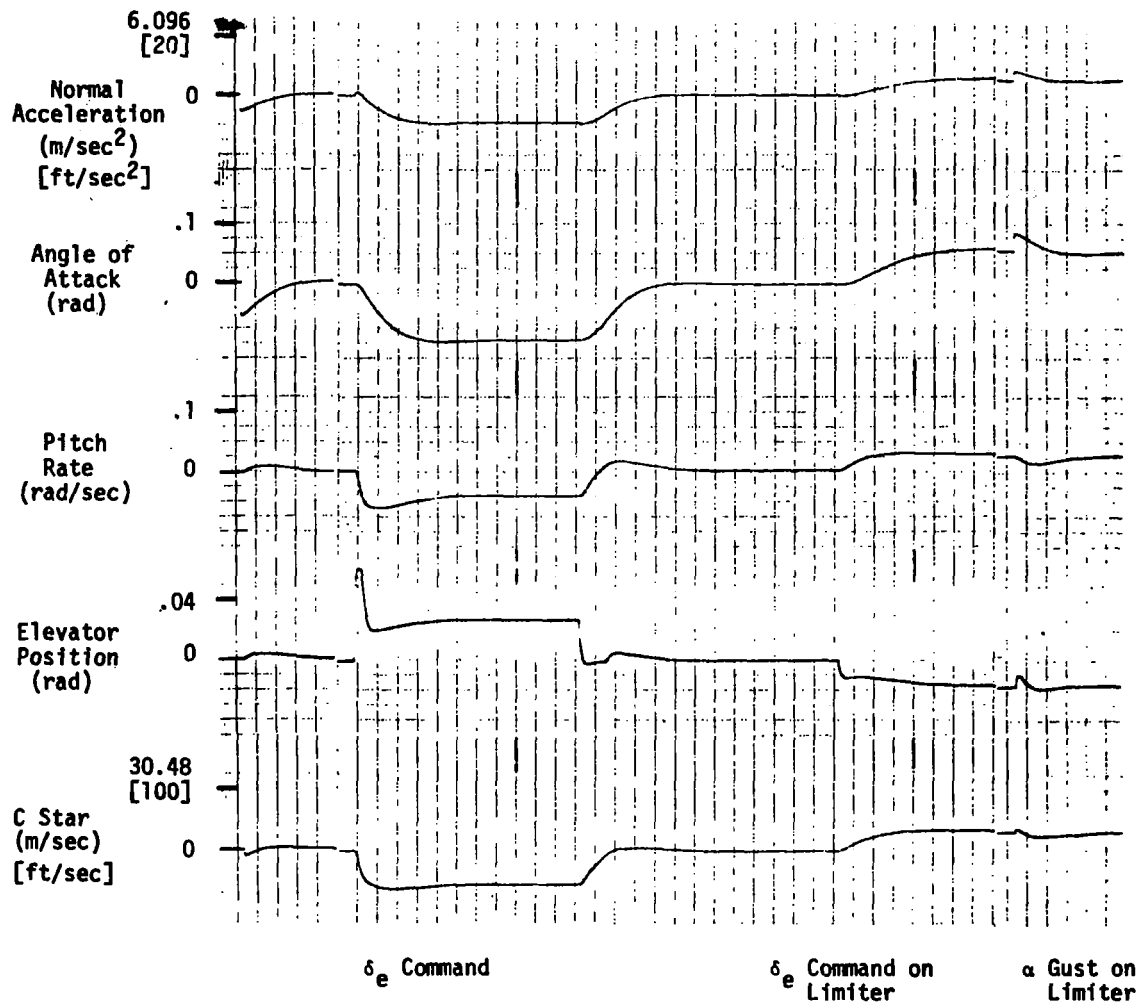


Figure 30. Pitch CAS and Boundary Control
(Mach 0.19, Sea Level)

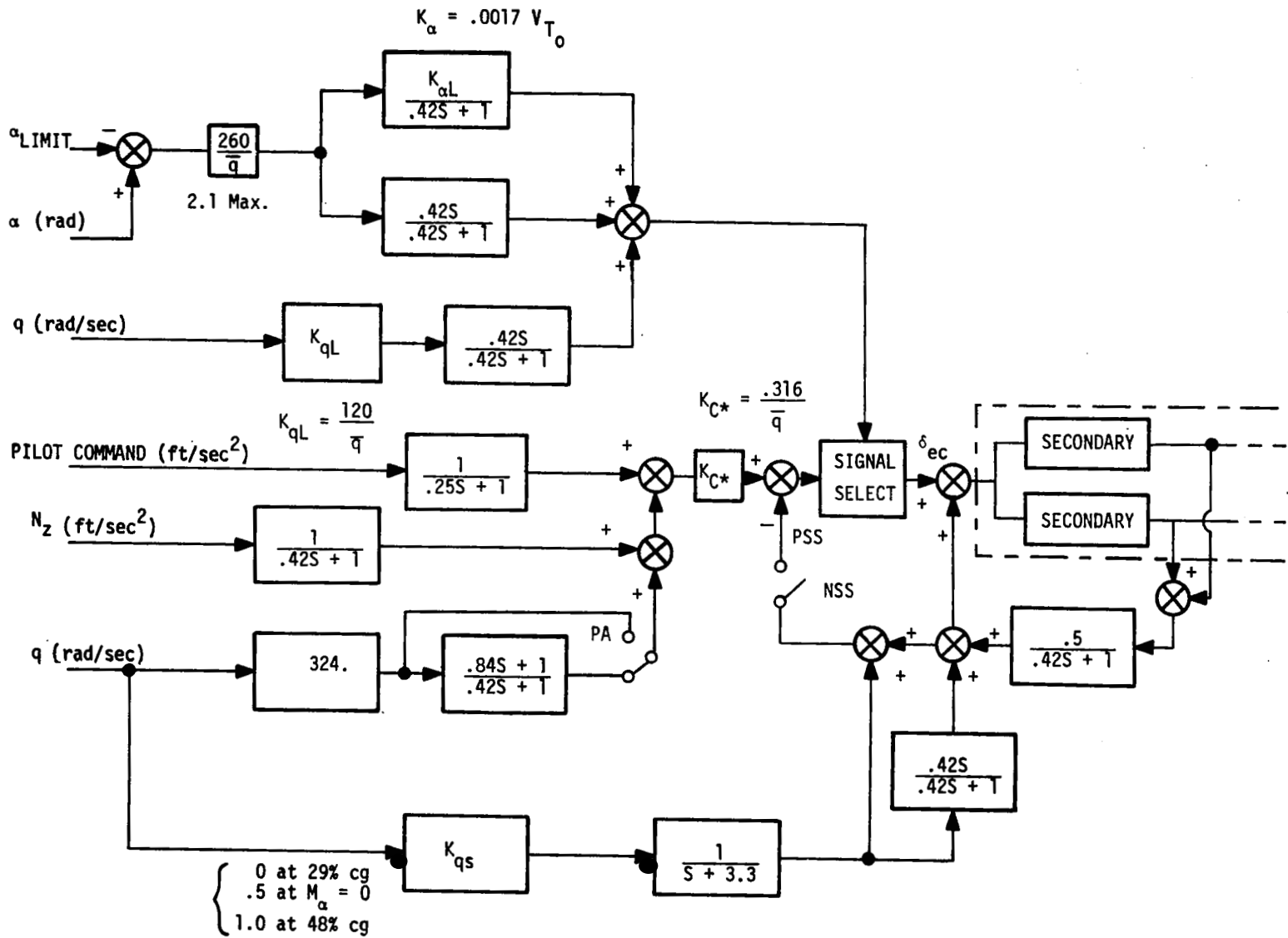


Figure 31. Pitch CAS RSS Controller

Reduced Static Stability Study

The short-period dynamics of the pitch axis were modified as explained in Section 5 to account for the effect of moving the center of gravity aft to reduce the static stability. The implication of reduced static stability on both the control laws and on the actuator requirements were determined.

Control Law Modifications--The primary modification to the nominal control laws to accommodate reduced static stability was the addition of another pitch rate feedback term to the elevator. This term is lagged pitch rate with a transfer function defined as

$$\frac{K_c/T_a}{S + 1/T_a}$$

where

$$K_c = \frac{\Delta M}{M_{\delta e}} \alpha$$

ΔM is the change in M associated with the c. g. shift and T_a is the flight path time constant. These values are listed in Table 10. This feedback in essence restores the stability lost by shifting the center of gravity. The gain, K_c , can be approximated by unity. The time constant, T_a , should be picked to give the best match at the highest short-period frequency. At this condition the short period starts to approach the bandwidth of the controller.

The RSS pitch CAS shown in Figure 31 appears to have a gain (K_q s) scheduled with "center-of-gravity" position. The range in center-of-gravity that was considered varied by about 20 percent of the mean aerodynamic chord. This dramatic a change in c. g. is not experienced under normal loading conditions (fuel, external stores, etc.) but represents different airframe designs. In actual practice the value of this gain would be fixed for a specific airframe configuration, and it could then accommodate the usual c. g. variations about nominal resulting from changes in loading.

Because of the importance of α limiting in a statically unstable airplane, the boundary controller was studied in detail. Proper mode transition required adding a scheduled gain on the ($\alpha - \alpha_{LIMIT}$) error.

The modifications to the nominal pitch CAS for RSS are shown in Figure 31. For convenience an analog representation is used. The changes are summarized below:

- Lagged pitch rate at aft c. g. added
- Stick shaping changed to 0.25 sec. lag (to reduce overshoot at FC9, 48 percent c. g. condition)
- K_c gain doubled at all conditions to attain better aft c. g. stability
- α gain \bar{q} schedule added and related airspeed gain schedule revised in the boundary controller for better aft c. g. control

These differences in the pitch controller will not affect the selection of a sample rate.

Time responses for flight conditions 17, 5, 1, 8 and 9 are shown in Figures 32 through 45. These responses show: (refer to Table 15)

- Step α gust response on CAS
- Step stick response
- Step stick response encountering α boundary limit
- Step α gust while on α boundary limit

These responses are given for stable (c.g. = 29 percent MAC) approximately neutrally stable ($M_{\alpha} = 0$) and unstable (c.g. = 48 percent MAC).

Table 15. RSS Time Responses

Figure	F. C.	c.g. (MAC)
32	17	36%
33	17	41%
34	17	48%
35	5	29%
36	5	40%
37	5	48%
38	1	29%
39	1	40%
40	1	48%
41	8	29%
42	8	48%
43	9	29%
44	9	40%
45	9	48%

Servo Actuator Requirements--An analog computer study was performed using the short-period F-8C dynamics to assess the impact of reduced static stability on the actuator performance requirements.

From the analysis on the servo/actuator nonlinearities such as hysteresis, it is evident that state-of-the-art actuator performance is necessary to achieve satisfactory performance levels. State-of-the-art is considered to correspond to magnitudes of nonlinearities below 0.05 degree of equivalent elevator deflection. With elevator effectiveness in excess of 1 g per degree at the higher dynamic pressures, control resolution is a concern for normal c.g. location; and with an unstable airframe, limit cycle amplitudes less than the 0.05 g. level are required.

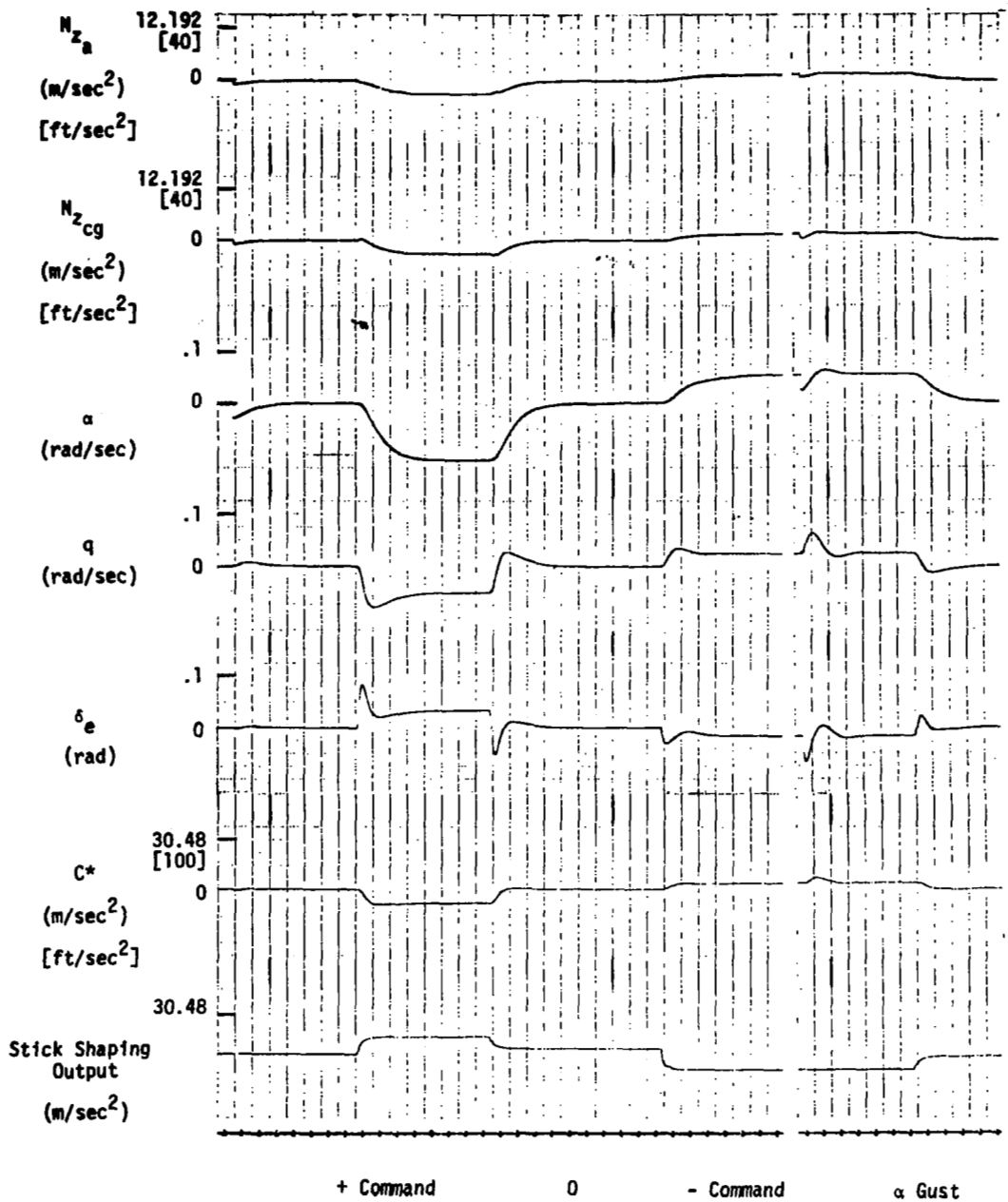


Figure 32. RSS Response (FC 17; c.g. at 36%)

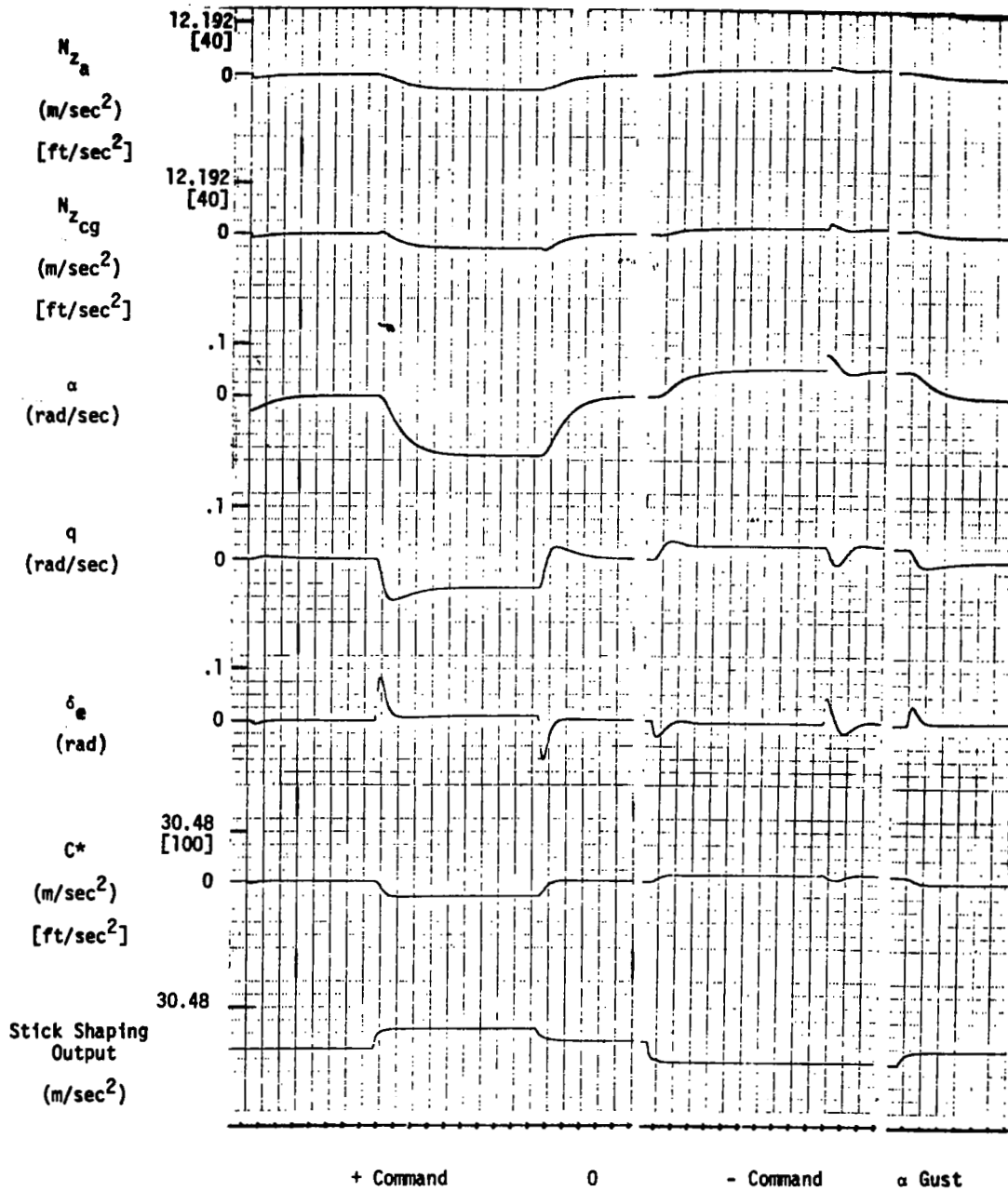


Figure 33. RSS Response (FC 17; c. g. at 41%)

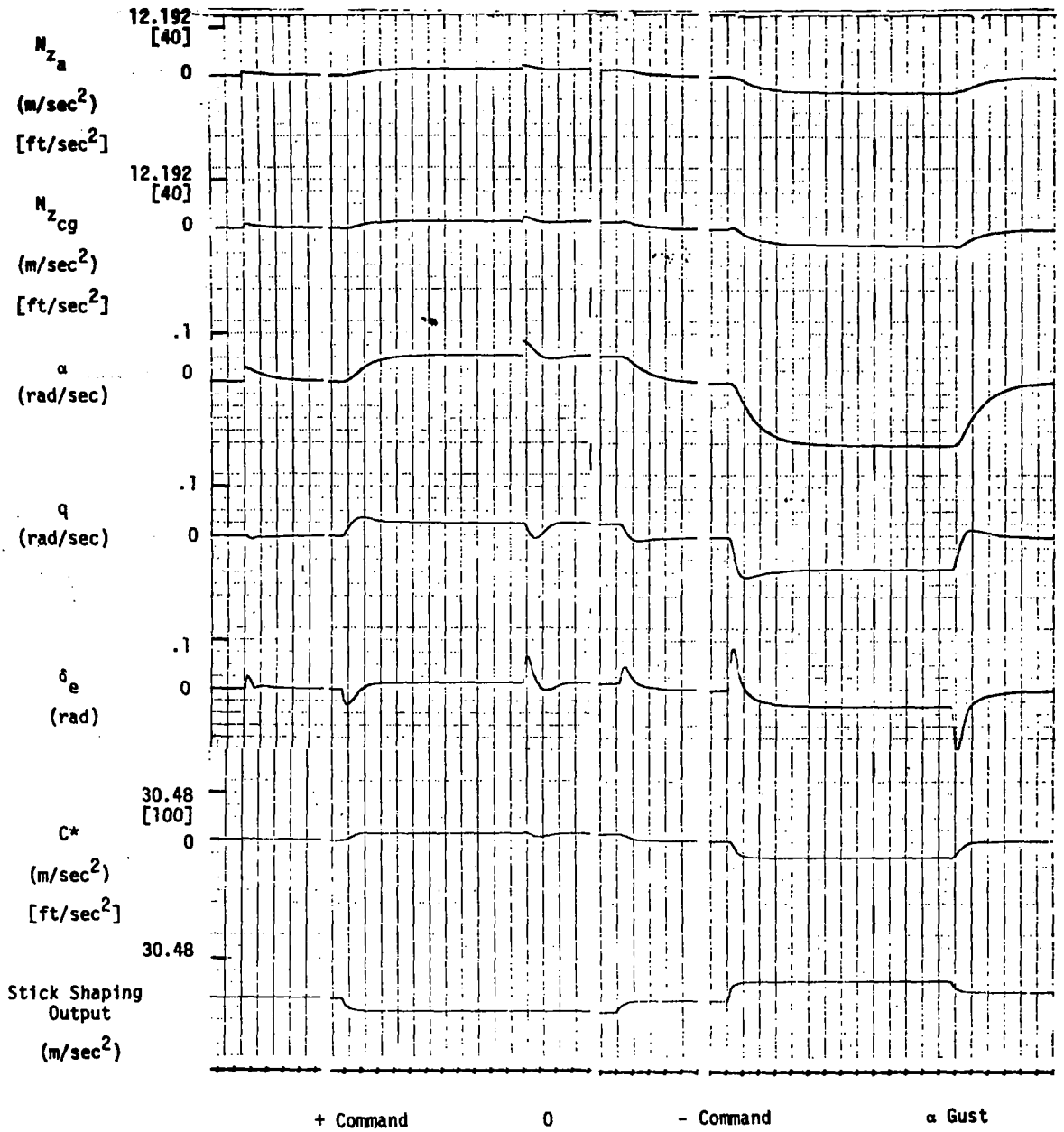


Figure 34. RSS Response (FC 17; c. g. at 48%)

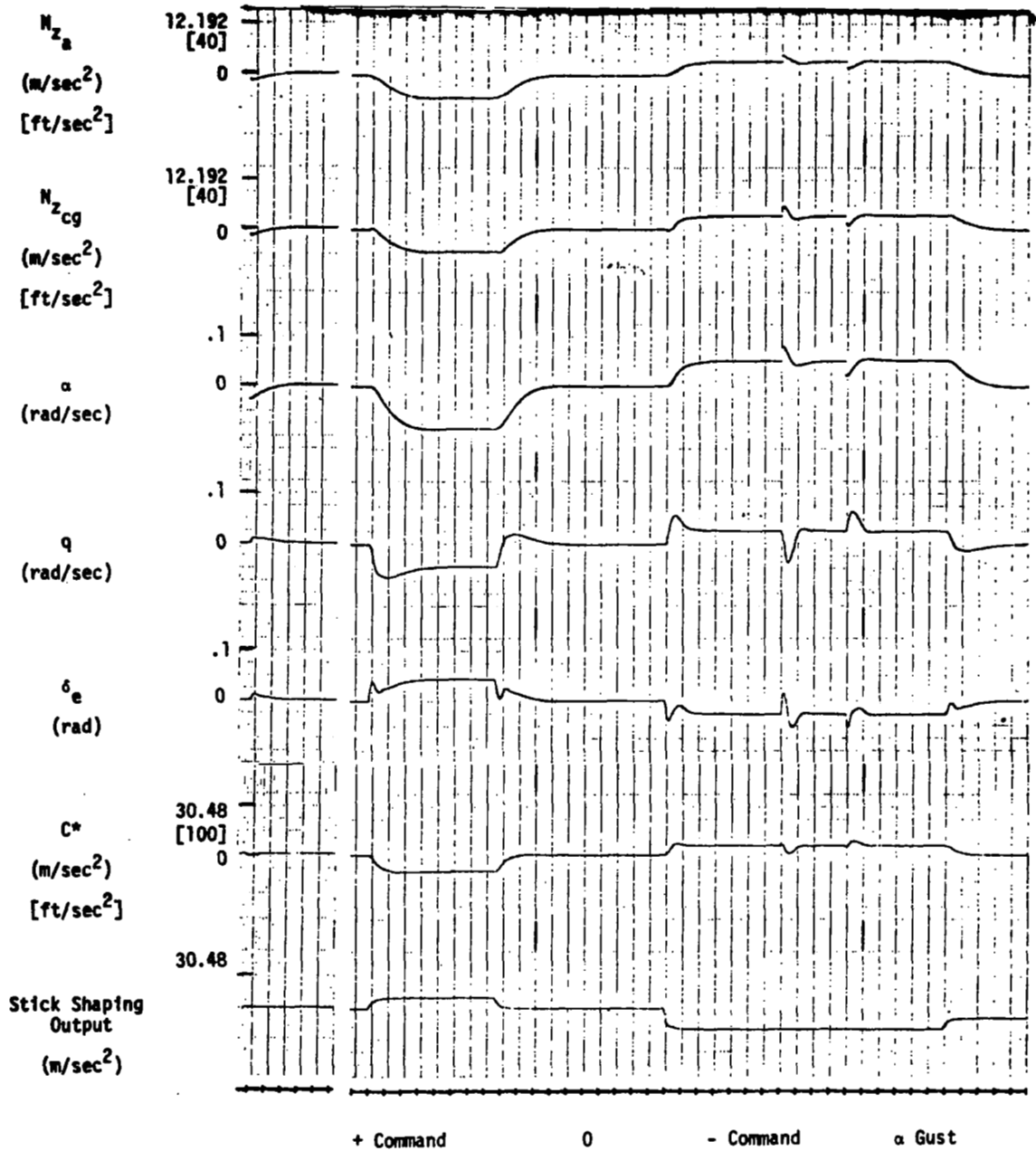


Figure 35. RSS Response (FC 5; c.g. at 29%)

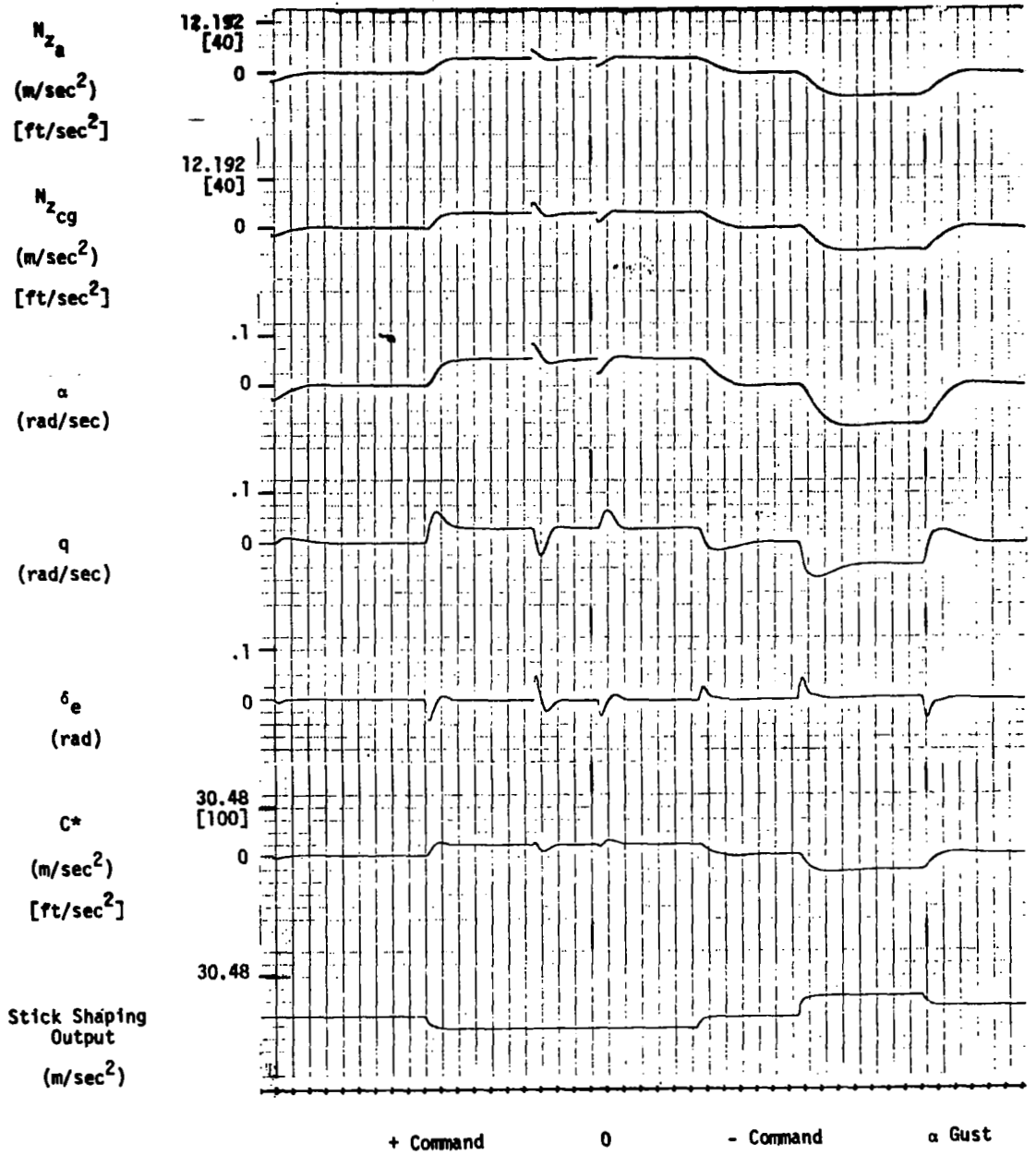


Figure 36. RSS Response (FC 5, c.g. at 40%)

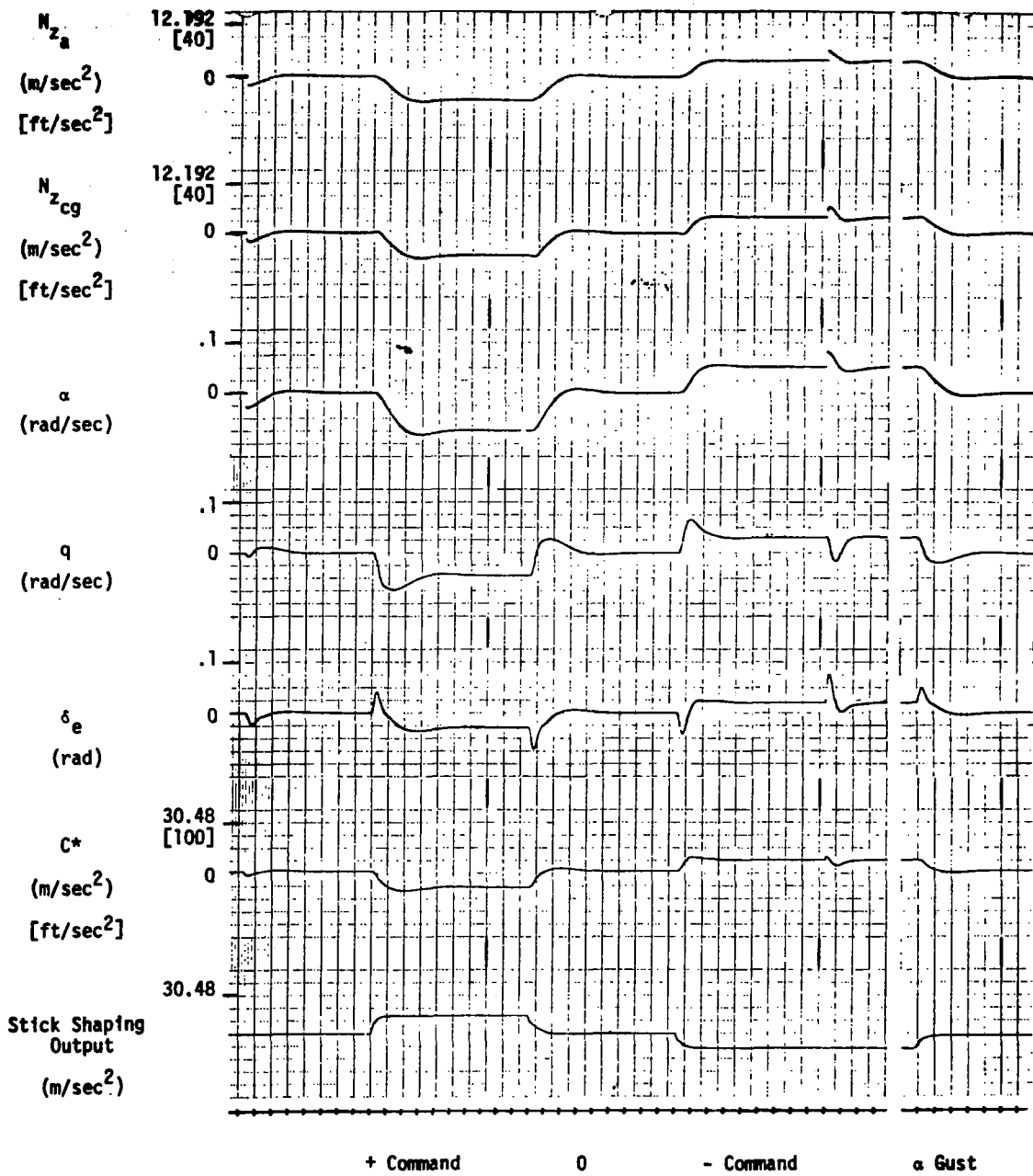


Figure 37. RSS Response (FC 5, c.g. at 48%)

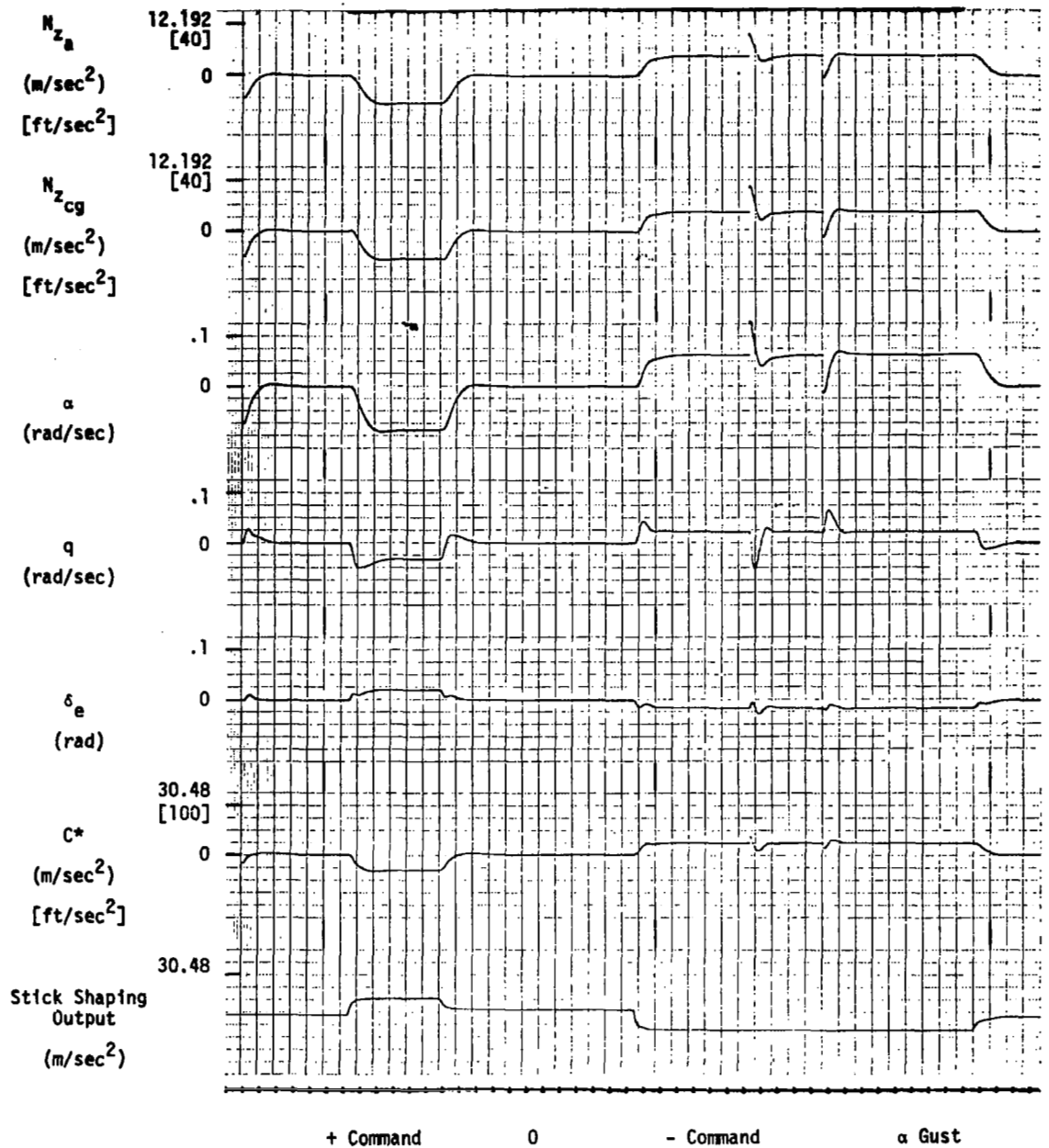


Figure 38. RSS Response (FC 1, c. g. at 29%)

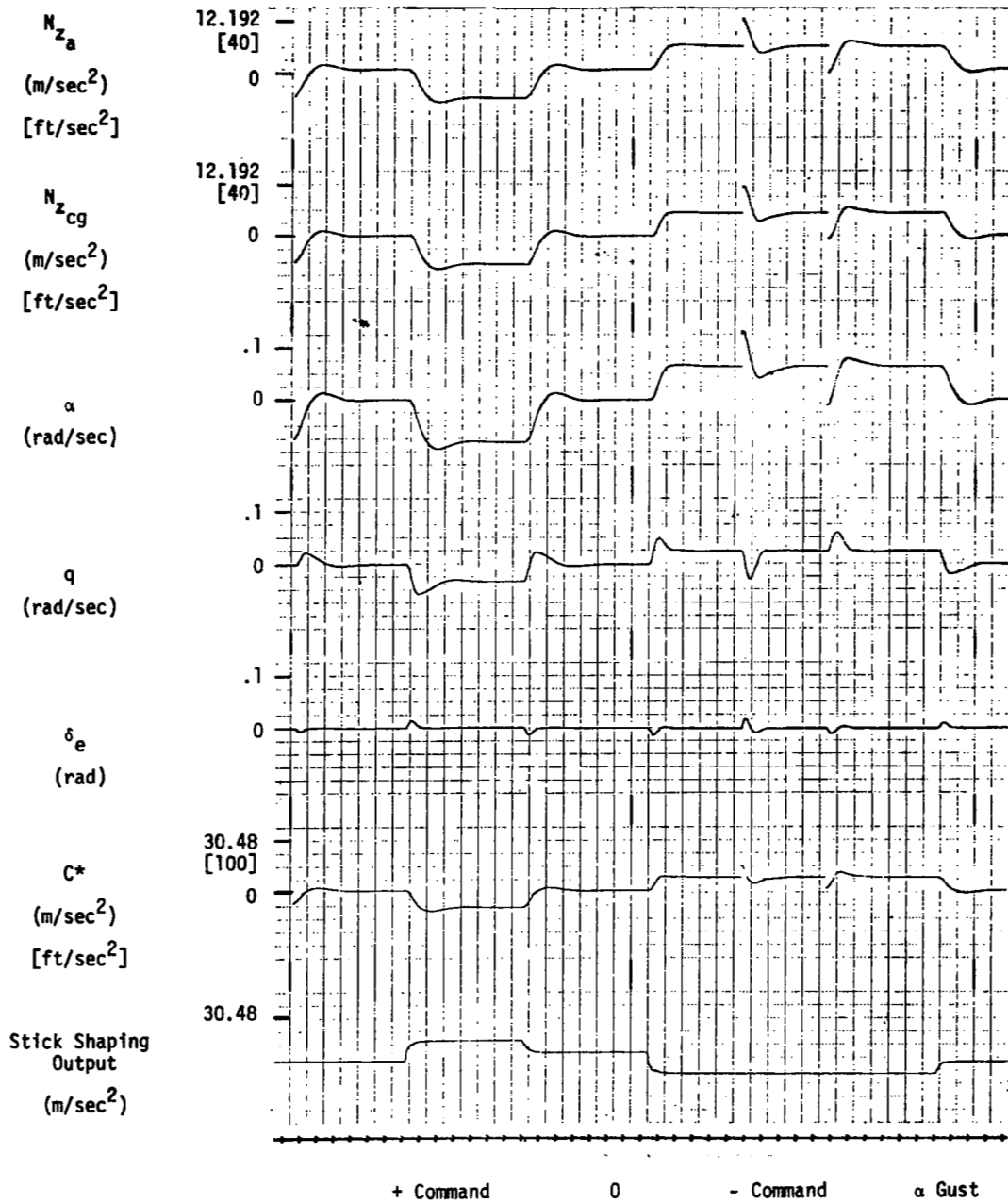


Figure 39. RSS Response (FC 1, c.g. at 40%)

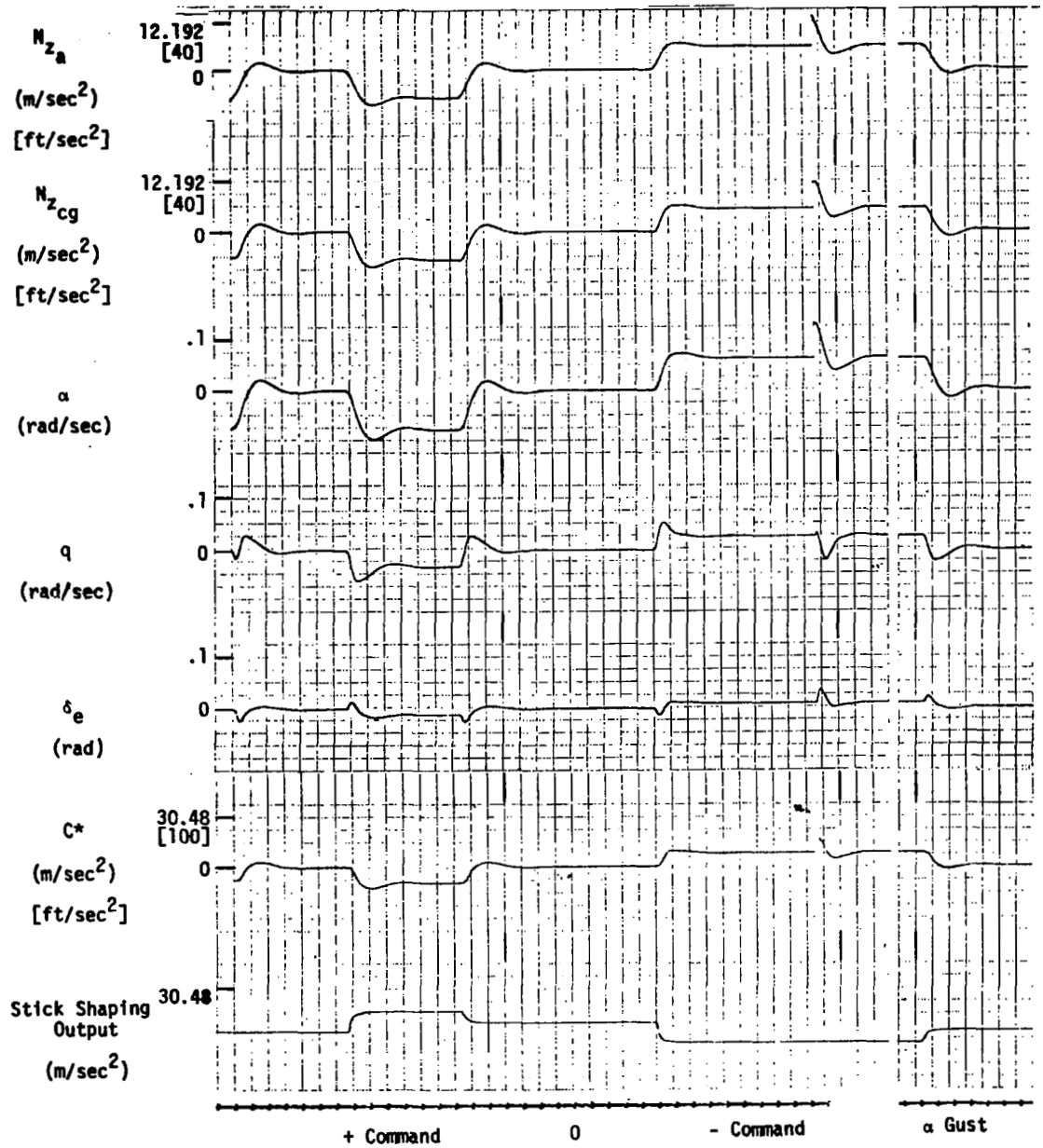


Figure 40. RSS Response (FC 1, c.g. at 48%)

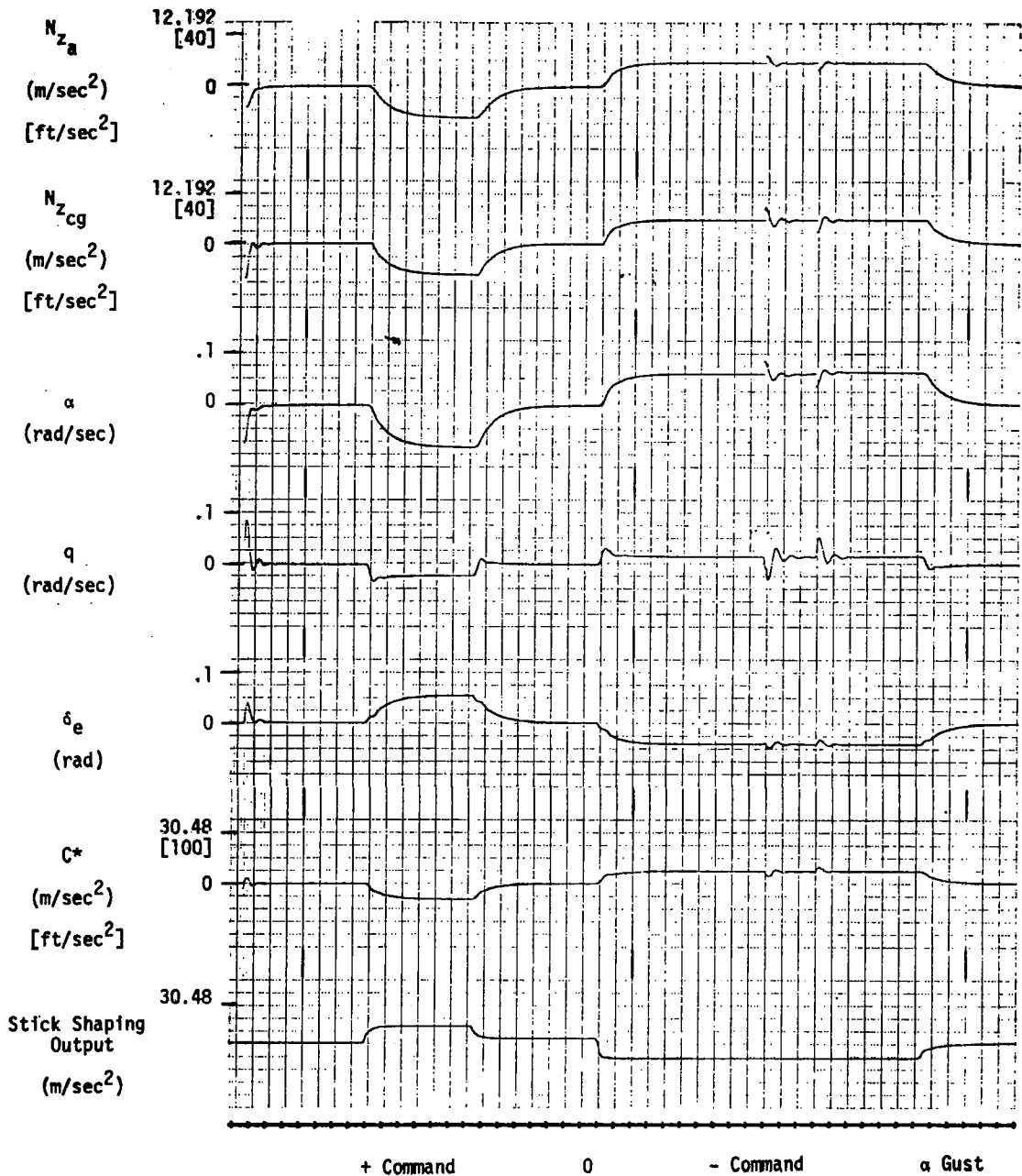


Figure 41. RSS Response (FC 8; c.g. at 29%)

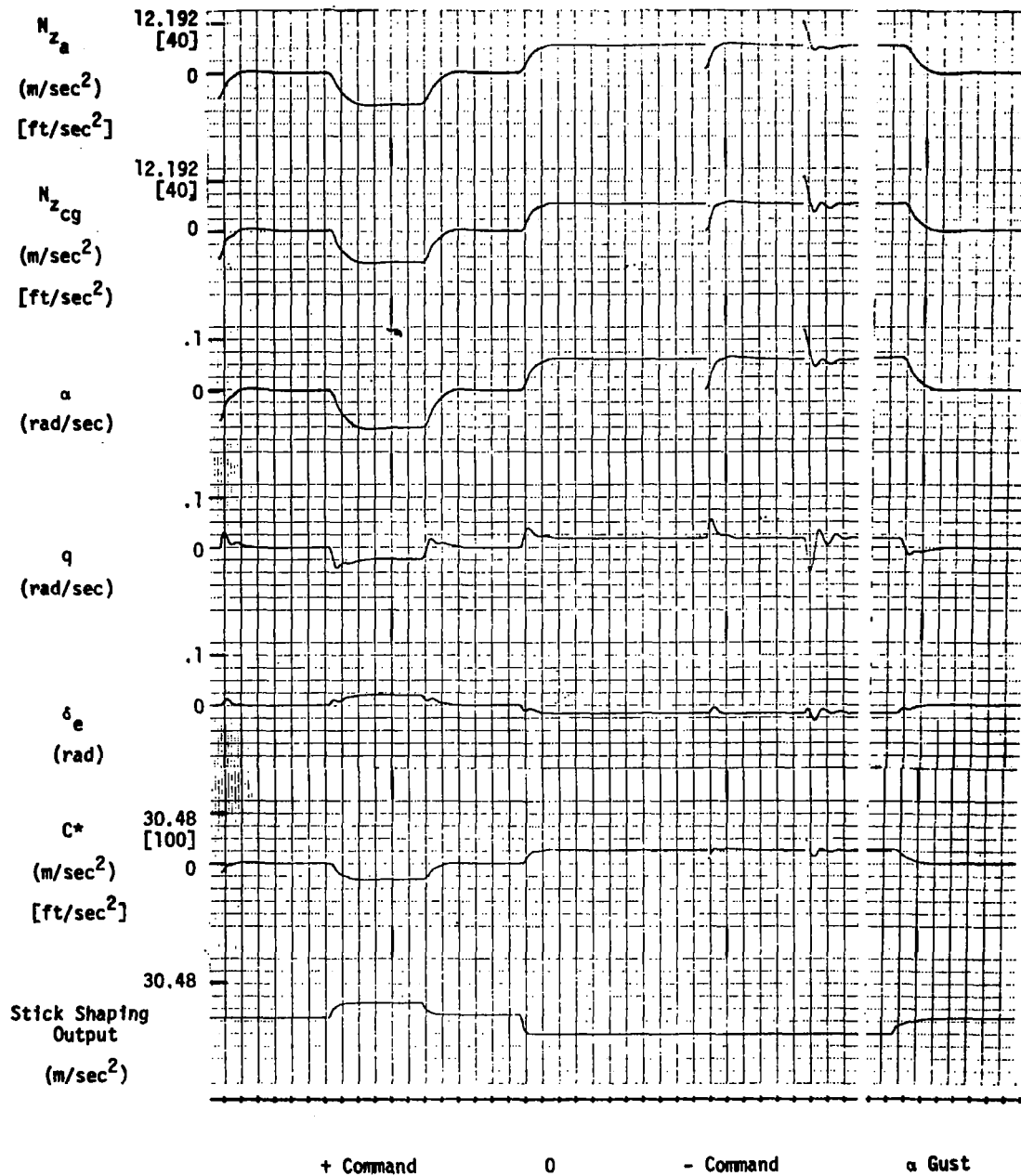


Figure 42. RSS Response (FC 8; c.g. at 48%)

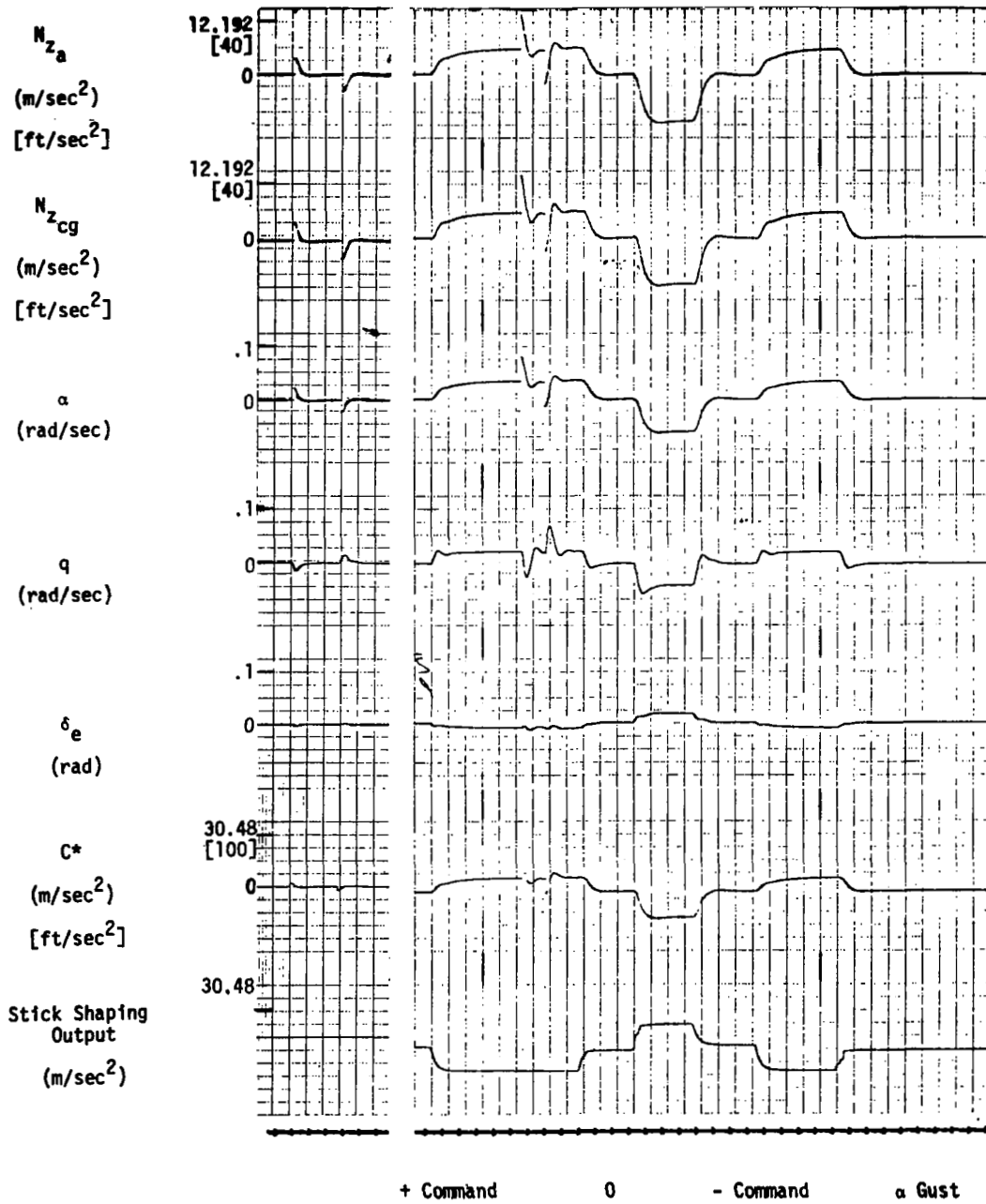


Figure 43. RSS Response (FC 9, c.g. at 29%)

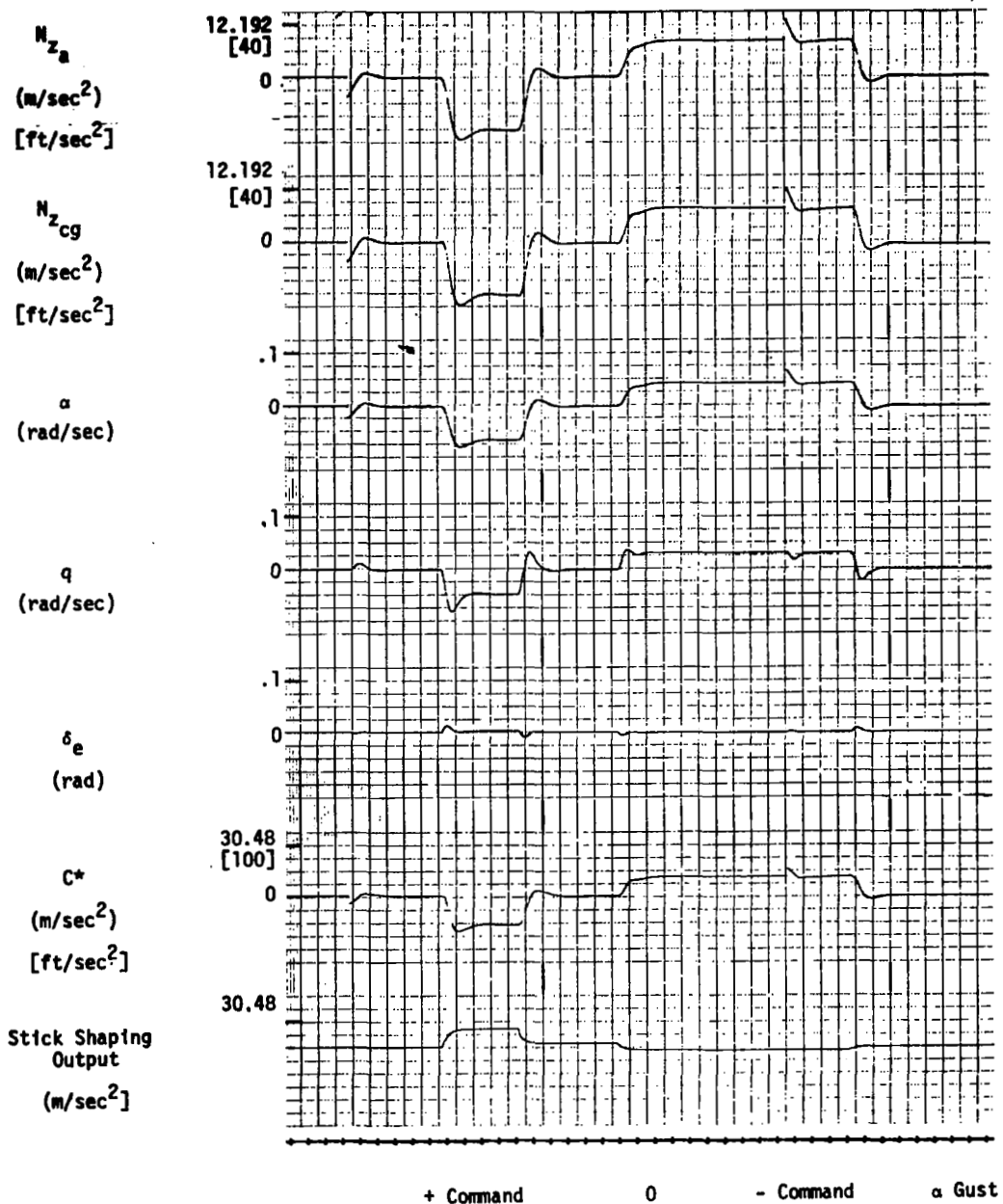


Figure 44. RSS Response (FC 9, c.g. at 40%)

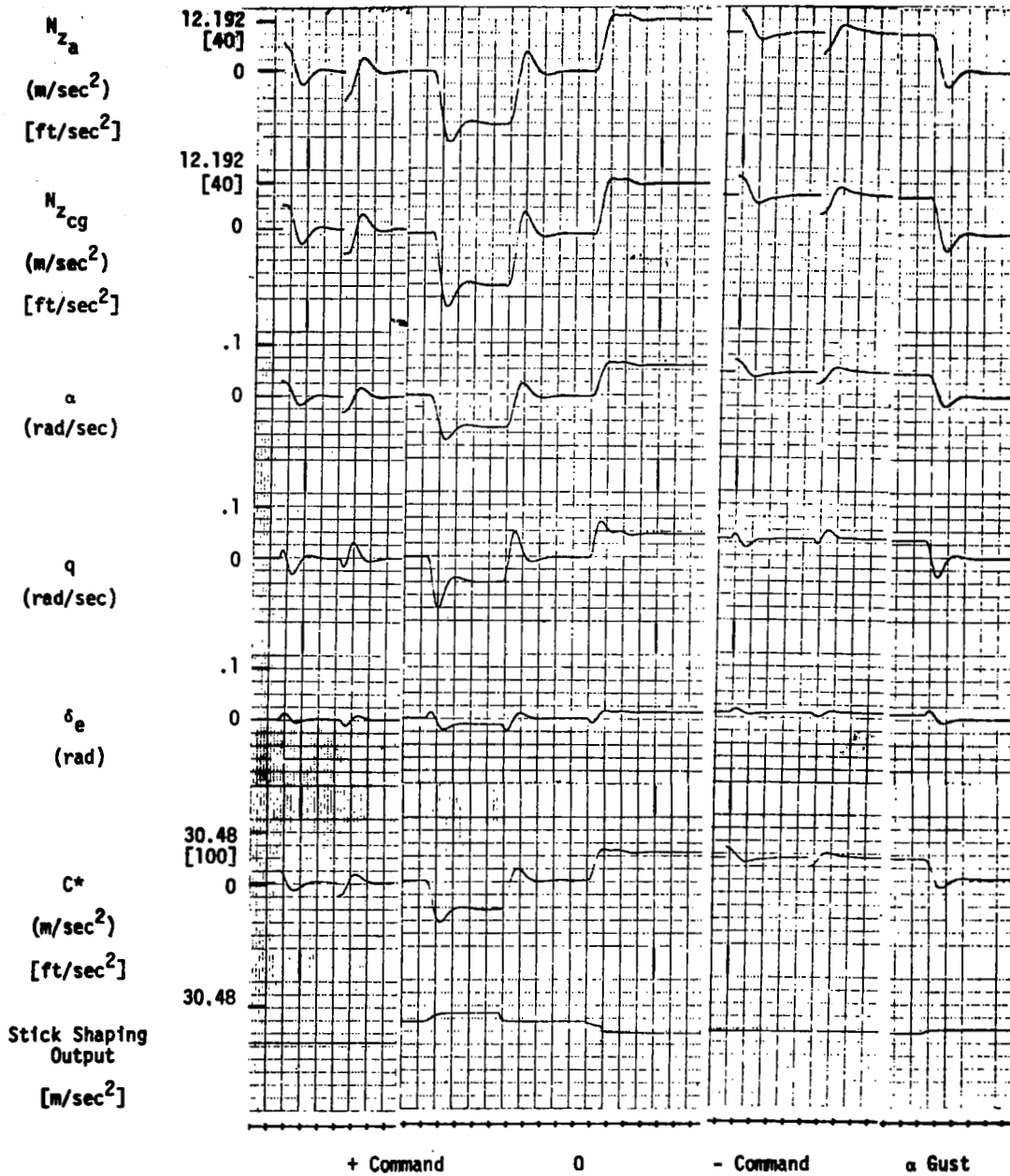


Figure 45. RSS Response (FC 9; c.g. at 48%)

Reports on the current F-8C servos suggest hysteresis levels considerably greater than the above requirement. [21] The inverse proportionality of hysteresis with servo loop gain indicates that the majority of the hysteresis is due to servo breakout forces. An increase in servo force gain is therefore apparently necessary. It is recognized that high force gains aggravate the force-fight problem in redundant servos of the subject type.

The elevator servo was modeled with an equivalent linear natural frequency of 10 Hz and a damping ratio of 0.7 with hysteresis of 0.01 rad. The analog hysteresis model is shown in Figure 46.

Results on the performance with this level of hysteresis is summarized in Table 16. As expected, 0.01 rad of hysteresis results in rather unacceptable limit cycles for the statically unstable configuration. Time responses are presented in Figure 47 through 49 for three selected flight conditions at the 48 percent c.g. condition.

Table 16. Limit Cycle Characteristics with
0.01 Rad. Servo Hysteresis

Flight Condition	C.G. Location	f_{LC} Hz	δe Amplitude (rad) Peak-to-peak	Nz_{cg} Amplitude m/sec ² Peak-to-peak	q (rad/sec) Peak-to-peak
1	29%	(1)	--	--	--
1	0 M_{α}	(1)	--	--	--
1	48%	0.208	0.0225	3.96	0.098
5	29%	(1)	--	--	--
5	0 M_{α}	(1)	--	--	--
5	48%	0.114	0.0125	2.14	0.032
9	29%	(1)	--	--	--
9	0 M_{α}	(1)	--	--	--
9	48%	0.444 (2)	0.0548	35.00	0.240

(1) No Limit Cycle

(2) Limit Cycle exceeds α_{Limit} boundary

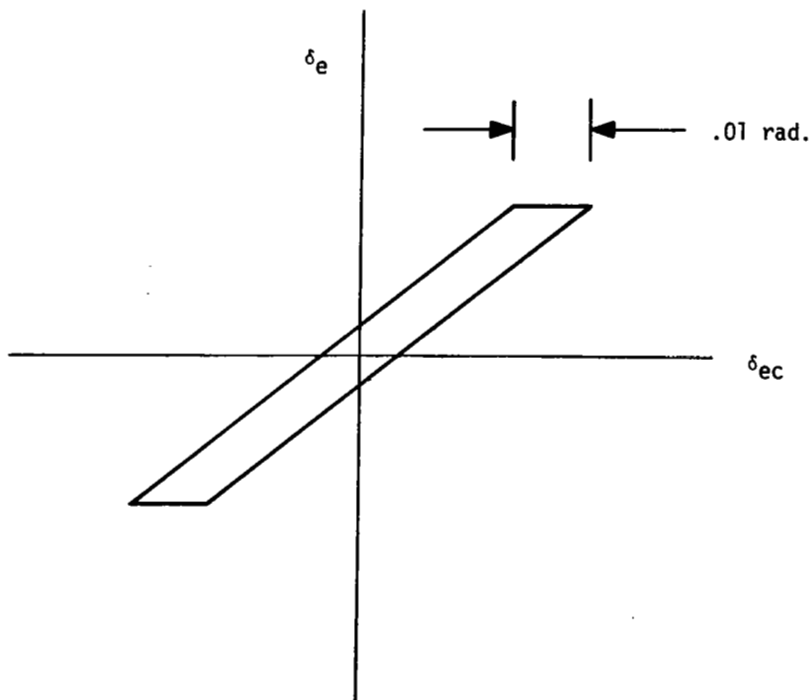
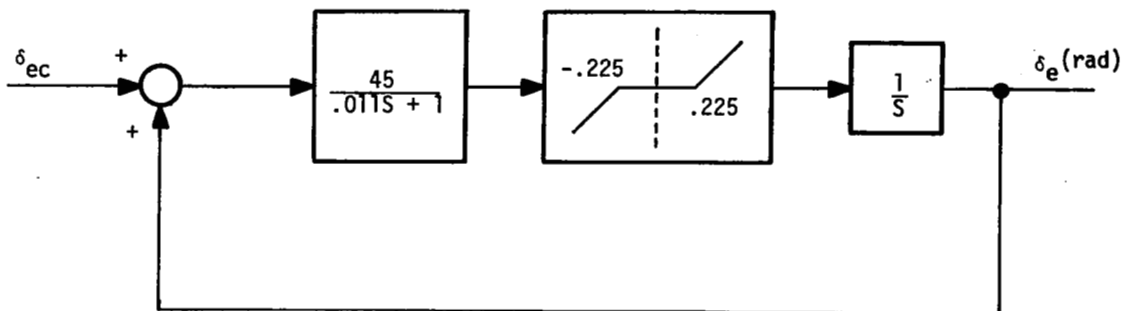


Figure 46. Analog Hysteresis Model

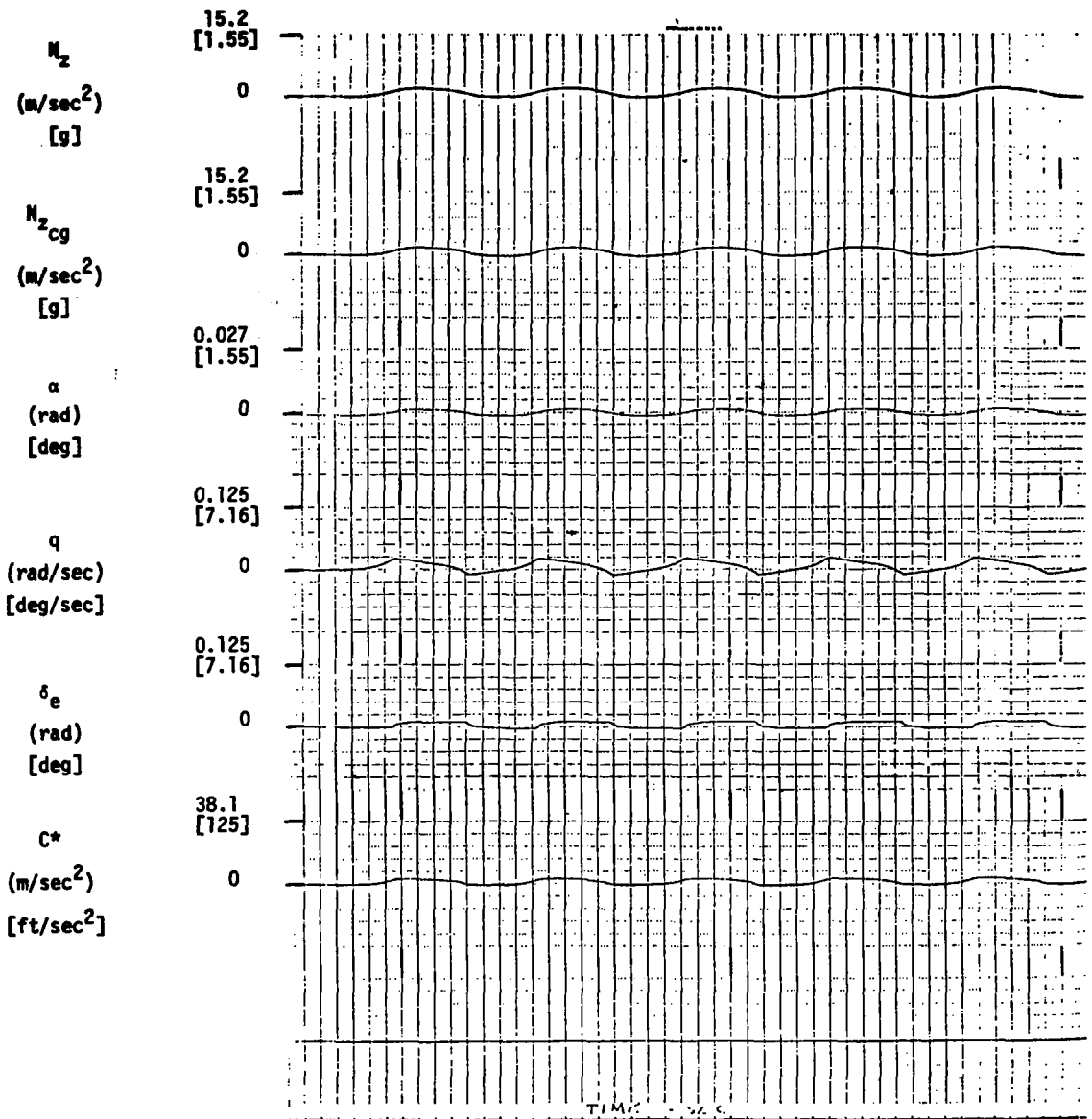


Figure 47. Hysteresis Response (FC 5; c.g. at 48%)

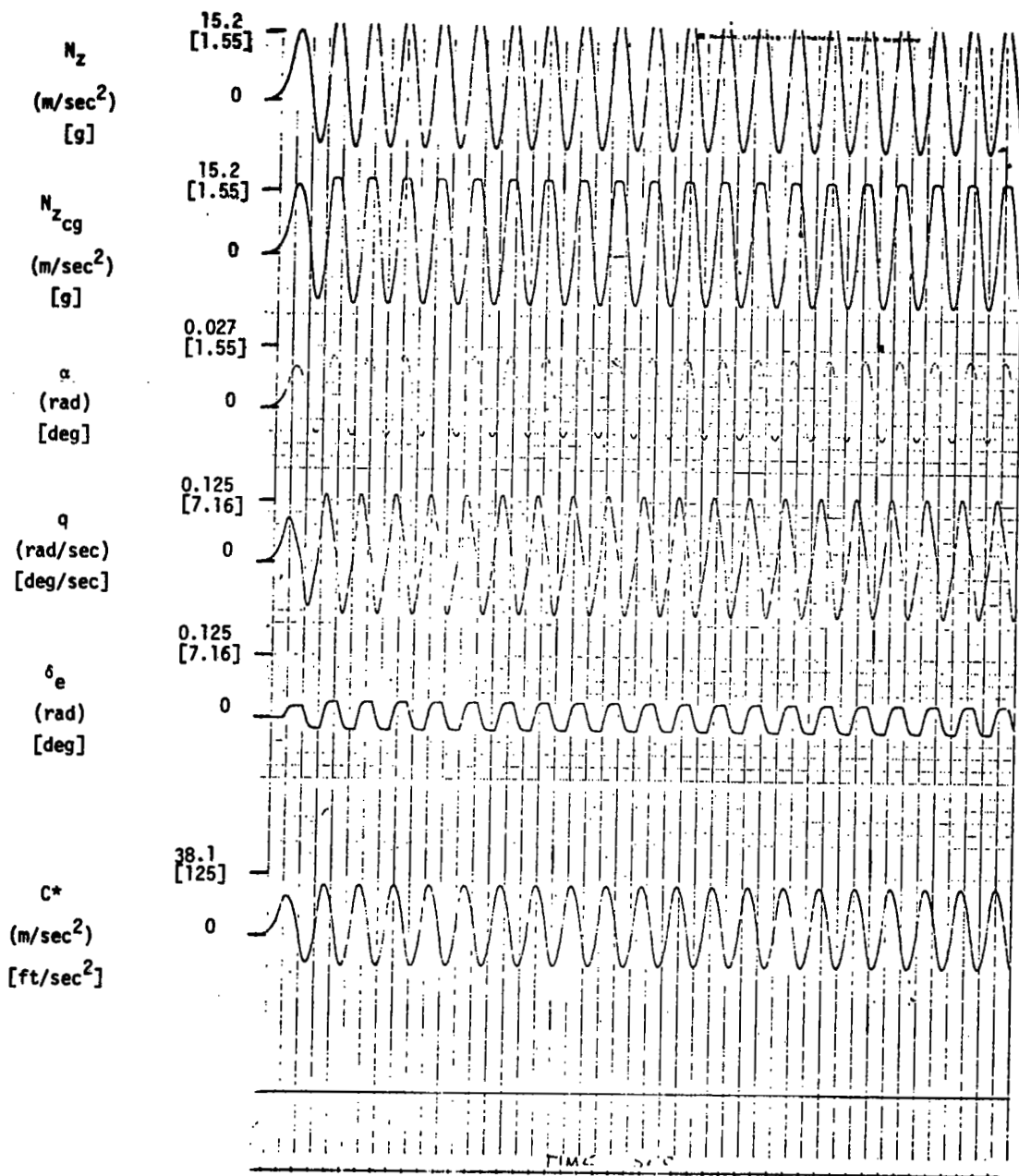


Figure 48. Hysteresis Response (FC 9; c.g. at 48%)

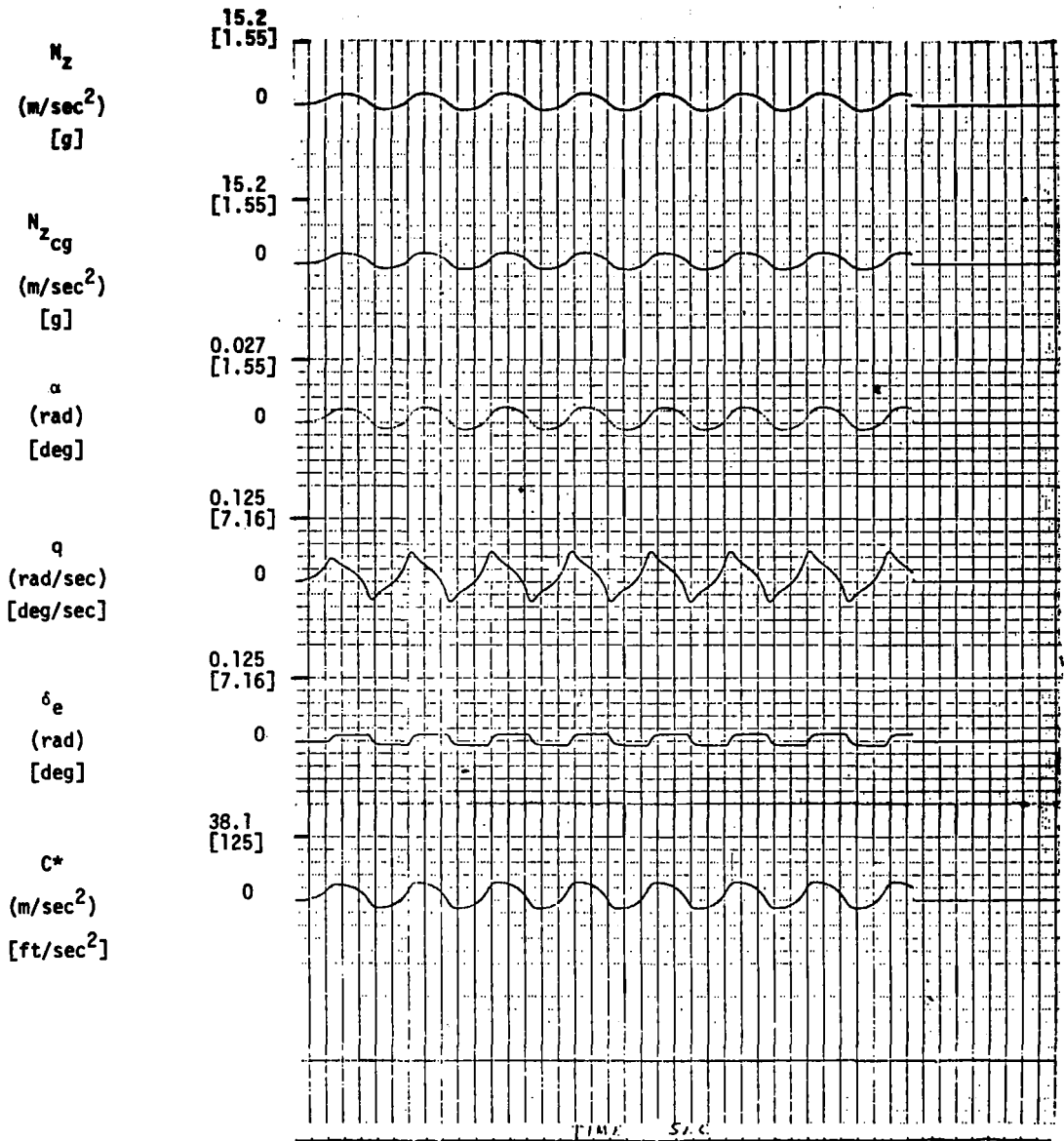


Figure 49. Hysteresis Response (FC 1; c. g. at 48%)

Symmetric Aileron Controller

Two controller modes have been provided in the CCV Control Laws for commanding symmetric aileron deflection. The two modes are referred to as a "q" mode and an "N_z" mode. The "q" mode implements a minimum drag schedule with pitch rate. The N_z mode combines direct lift with the same minimum drag schedule. The direct lift provides gust alleviation and improved command responses. The direct lift function is integrated with the elevator control such that the pitch stick automatically provides direct lift in the N_z mode.

The minimum drag schedule is discussed next, followed by a discussion of the direct lift controller for gust alleviation and command enhancement. Finally, the implementation details and predicted performance of the q and N_z modes are presented.

Minimum Drag Schedule--Predictions of aircraft drag can be obtained by analyzing a nonlinear model of the aerodynamics. Minimum drag configurations using symmetric aileron and leading edge deflections were determined for both 1-g flight (cruise) and maneuvering flight conditions. The schedules were determined from an analysis of the nonlinear aerodynamic functions using the F8SIM program. Those results were compared to NASA/FRC flight test results that considered the effects of the leading edge and flaps on drag reduction, buffet, and wing rock onset. [8, 11, 12, 13]

The drag reduction aspect was studied using the nonlinear (digital-non-real-time) simulation program. The leading and trailing edge surface positions were varied in a systematic manner. For each setting the simulation trimmed the airplane equations. The reduction of thrust required to trim was a convenient measure of the amount of drag reduction obtained for various surface positions. This approach is not restricted to trimming only in cruise; F8SIM can also trim the aircraft with commanded accelerations (i. e., 8-g pull-ups, etc.). This is quite useful in defining the flap schedule since many points can be inexpensively obtained.

In the transonic mach number range, zero flap deflection combined with some leading edge deflection defines a minimum drag configuration. This agrees with flight test data.

The schedule was obtained by systematically varying the leading-edge and flap positions in the nonlinear relations:

$$\text{Drag} = f_1 (\delta e, \delta l_e, \delta f, \alpha, M)$$

$$\text{Drag} = f_2 (\delta e, \delta l_e, \delta f, \alpha, M)$$

and then trimming the aircraft at the prevailing condition. At $\gamma = 0$ and $\dot{\gamma} = 0$ (cruise), the optimum flap position is zero except at low dynamic pressures requiring a high trim angle of attack. This is depicted below in Figure 50.

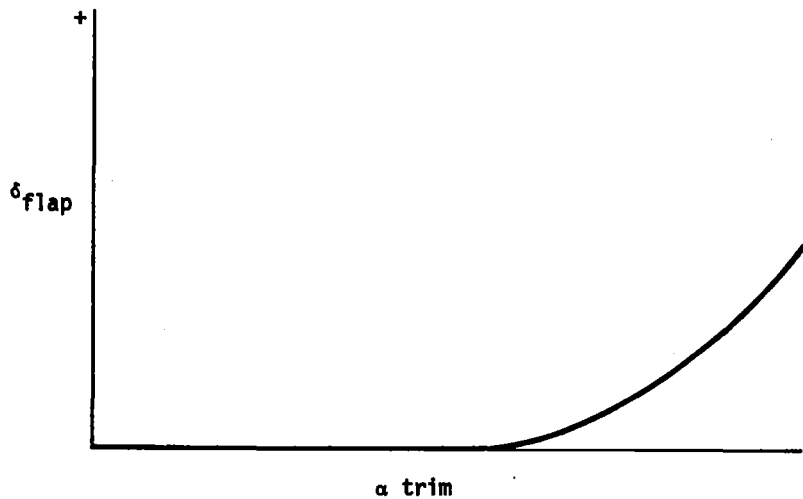


Figure 50. Cruise Flap Schedule

Since the flaps are already deflected in the wing-up conditions, the flap position recommended for cruise will be no deflection.

The flap position for minimum drag was studied for accelerated flight conditions ($\gamma = 0$, $\dot{\gamma} \neq 0$) as illustrated in Figure 51.

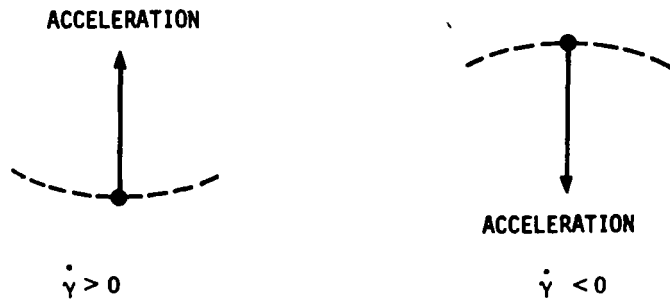


Figure 51. Accelerated Flight Condition

F8SIM predicts that the schedule for minimum drag for $\gamma = 0$ is

$\dot{\gamma} > 0$ down flaps

$\dot{\gamma} < 0$ up flaps

Next, the problem was considered at non-zero flight path angles. For $\dot{\gamma} = 0$ and a non-zero flight path angle, the gravity vector rotates appropriately and the trim angle-of-attack changes as required. When $\dot{\gamma} = 0$, zero flap deflection is shown to be desirable for minimum drag. For $\dot{\gamma}$ positive or negative, the same strategy as for $\gamma = 0$ applies.

The leading edge schedule (with mach number) used for cruise also applies to maneuvers. The optimal flap deflection determined by the nonlinear simulation is shown in Figure 52. The flap schedule is one that produces "direct lift" in a maneuver. As the altitude increases, additional flap deflection is required and the gains at low maneuver levels increase as shown. The maximum flap deflection considered was limited to 12 degrees due to limitations of the F-8C aero data. The fact that the schedule quickly saturates to the 12 degree maximum deflection correlates with other results. [8, 11]

The flap schedule was defined as a function of steady-state pitch rate, since at zero pitch rate no flap deflection is desired. A further advantage in defining a flap schedule based on pitch rate is that this provides minor gust alleviation as well as drag reduction. Therefore, a pitch rate schedule will be compatible with the gust alleviation provided by the N_z mode using normal acceleration feedback.

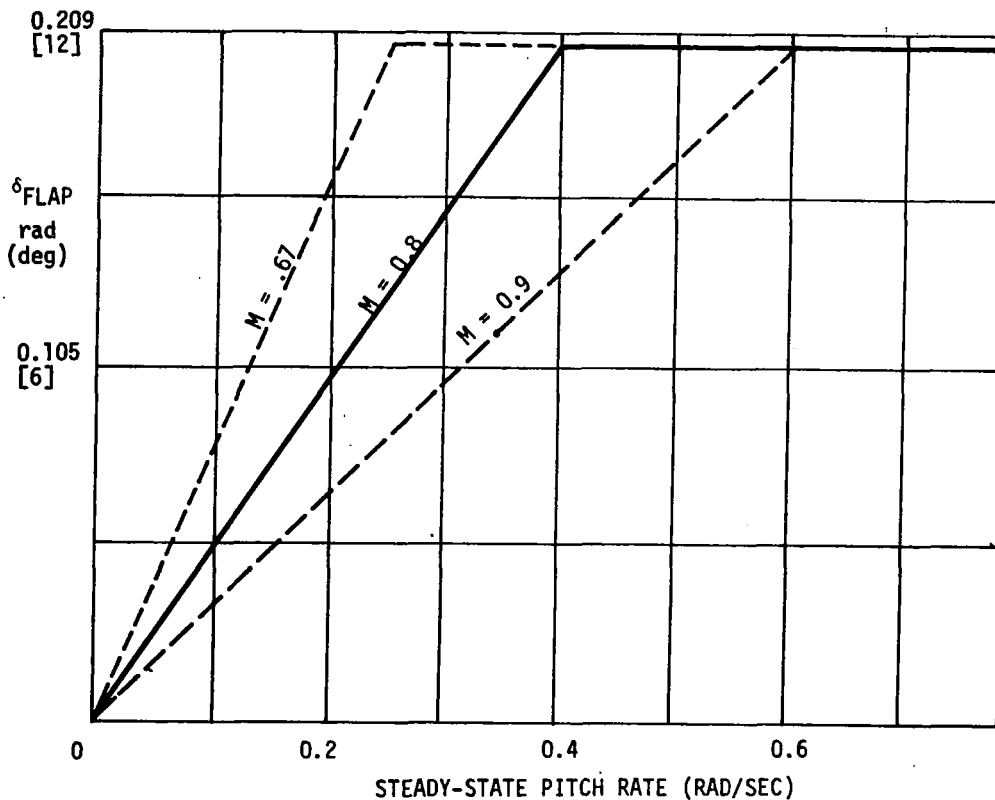


Figure 52. Flap Schedule

Direct Lift Implementation--The N_z flap mode was designed to provide direct lift through a combination of symmetric flap deflection and elevator deflection. The benefits of direct lift are gust alleviation and command augmentation. A significant reduction in rms acceleration due to gusts can be realized if lift can be produced "directly" rather than by changing the angle-of-attack with the elevator. Utilization of direct lift also provides "command augmentation" whereby the amount of pitch rate overshoot required to obtain a fast N_z response is reduced.

The formulation of the gust alleviation problem for quadratics used a "rate-model" following error quantity in pitch rate and normal acceleration. These two responses were defined as

$$\begin{aligned}\tilde{\dot{q}} &= \dot{q} - \dot{q}_m \\ \tilde{\dot{N}}_z &= \dot{N}_z - \dot{N}_{z_m}\end{aligned}$$

the \dot{q}_1, \dot{N}_z equations represent the short period dynamics of the F-8C driven by a command model and a wind gust model.

$$\begin{bmatrix} \dot{q} \\ \dot{N}_z \end{bmatrix} = [F] \begin{bmatrix} q \\ N_z \end{bmatrix} + [G1] \begin{bmatrix} \delta_f \\ \delta_e \end{bmatrix} + [G2] \begin{bmatrix} w_{gust} \\ w_{pilot} \end{bmatrix}$$

The \dot{q}_m and \dot{N}_{z_m} equations represent the same dynamics as the \dot{q}, N_z equations, except the vector corresponding to the wind gust input is set to zero. Weighting the rate model following errors ($\tilde{\dot{q}}$ and $\tilde{\dot{N}}_z$) forces the response of the aircraft driven by both commands and gusts to follow a similar dynamic model driven by commands but not by gusts.

The result of such a quadratic formulation results in gains from the gust state to the flap and elevator. This is easily explained if one considers the response of the short-period dynamics to gusts.

If the actuator dynamics are neglected

$$\begin{bmatrix} \dot{q} \\ \dot{N}_z \end{bmatrix} = [F] \begin{bmatrix} q \\ N_z \end{bmatrix} + [G1] \begin{bmatrix} \delta_e \\ \delta_f \end{bmatrix} + [g] w_{gust}$$

then for q and n_z and their derivatives to be zero yields

$$\begin{bmatrix} \delta_e \\ \delta_f \end{bmatrix} = -[G1]^{-1} [g] w_{gust}$$

The above feedforward gains from the gust state to the elevator and flap will minimize gust response. These gains depend on the inverse of the G1 matrix which describes the amount of normal force and pitching moment each surface produces. The disadvantage of the above formulation is that it requires measuring or estimating the w_{gust} state (or equivalently α gust).

To avoid feedback gains from the gust state, the direct lift controller structure was selected early in the design process by noting that the w_{gust} input excites only the N_z equation. Thus N_z feedback to the direct lift will provide significant gust reduction.

Furthermore the gain limits on this feedback can be computed from loop gain considerations. Implementation of direct lift requires a flap-to-elevator crossfeed to compensate for the pitching moment of the symmetric ailerons. This crossfeed is easily computed from the properties of the G1 matrix by comparing the relative magnitudes of the pitching moment and normal force of the elevator and flaps.

The direct lift mode for gust alleviation has the structure of Figure 53. The crossfeed (K_{XF}) is the ratio of pitching moments $-M_{\delta f}/M_{\delta e}$ which, fortunately, is nearly constant for all flight conditions. Its value is set at -0.16 . The gain K_{F2} was determined from the following loop gain considerations.

Consider

$$N_z = Z_\alpha \alpha + Z_{\delta f} (K_{F2} N_z) + \text{other terms}$$

$$N_z = \frac{Z_\alpha}{1 - Z_{\delta f} K_{F2}} \alpha$$

If the loop gain is set at unity (i. e. $-Z_{\delta f} K_{F2} = 1$) the effects of the gusts will be reduced 50 percent, and a loop gain of unity will not present any stability problem.

Approximating K_{F2} by $1/-Z_{\delta f}$ results in a gain scheduled with dynamic pressure over the flight envelope.

The gain schedule that results is

$$K_{F2} = 4.3/\bar{q}$$

The next section discusses the integration of the gust alleviation with the minimum drag schedule to produce a composite direct lift controller.

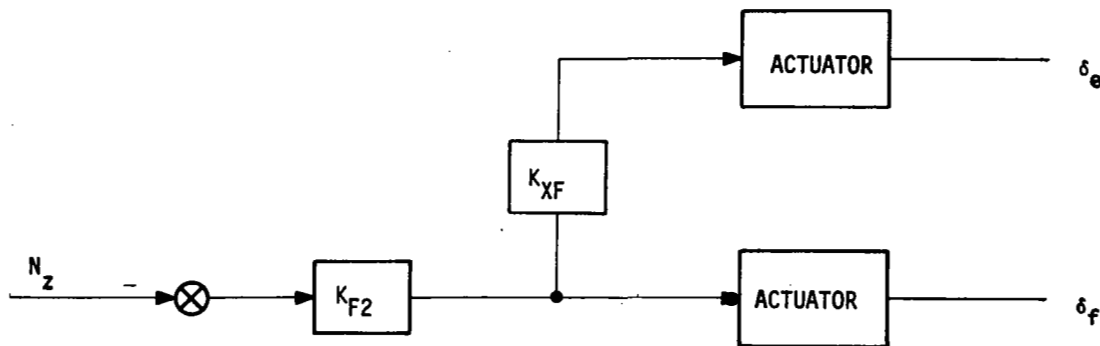


Figure 53. Gust Alleviation Controller Structure

Integration of Flap Schedule and Direct Lift--The fighter-type MLC has been implemented in two separate modes of the CCV Control Laws. The modes are referred to as "q flap" and " N_z flap". The implementation of both modes will be discussed. These modes are inhibited in the power approach condition.

The optimal schedule has the form of Figure 52 based on pitch rate. The schedule could also be based on angle-of-attack or normal acceleration. However, use of either of these variables would result in alpha gust aggravation. This means that a vertical gust would move the flaps to aid rather than oppose the gust. This would result in degraded ride qualities. The q flap schedule has been implemented with a two second lag on pitch rate to effectively decouple the schedule from the dynamics of the direct lift.

The schedule implemented uses a fixed ratio of flap deflection to pitch rate. This is a compromise but in view of the saturation of the flaps at 12 degrees and the approximate nature of the aerodynamic data, it is felt that this schedule is sufficient. There may be some effects that are not predicted by the F-8C aero data so that the above schedules may need to be modified as a result of wind tunnel data or additional flight test results.

For identical maneuvers both the q flap and the N_z flap modes produce the same steady-state flap deflection. This requires adding a stick input in the N_z mode. The q flap mode is scheduled with pitch rate. The N_z flap mode uses a combination of normal acceleration and stick input to be compatible with N_z gust alleviation feedbacks and still provide minimum drag in a maneuver.

The previous section discussed the implementation of the gust alleviation with normal acceleration feedback to the symmetric ailerons and an aileron-to-elevator crossfeed. The feedback is illustrated in Figure 54 where K_2 is the accelerometer gain scheduled with dynamic pressure. The following discussion will determine an input command signal (I) to be combined with the N_z feedback as shown. The object of this feedback is to obtain a steady state position of the flaps equal to the minimum drag schedule

$$\delta f = K_{FS}q$$

Then in the presence of no command the normal acceleration feedback remains for gust alleviation.

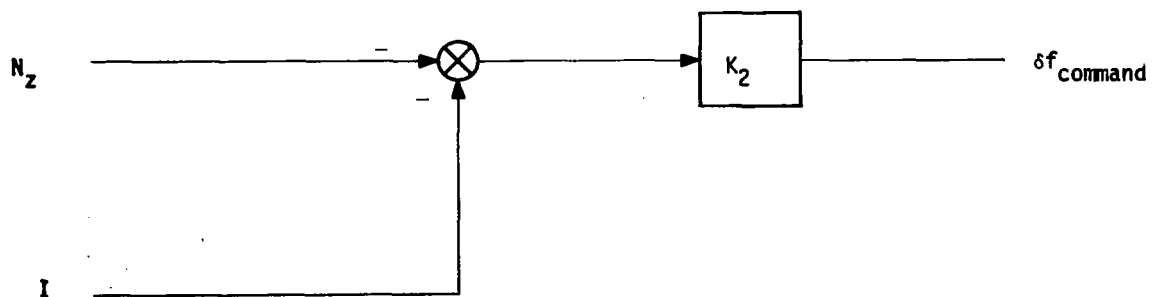


Figure 54. N_z Flap Compensation

Consider $\delta f = -K_2(N_z + I)$. The quantity N_z is accelerometer output biased by gravity ($N_z = 0$ in cruise), and I is an input command signal to be determined. The flap schedule desired for minimum drag is

$$\delta f = K_{FS} q$$

therefore

$$I = -\frac{K_{FS}}{K_2} q - N_z$$

The pitch CAS in NSS enforces

$$F + N_z + V_{CO} q = 0$$

and at steady state

$$N_z = V_{T_0} q + g(\cos \theta \cos \phi - 1)$$

Therefore, the elevator control maintains the following relation between F and N_z :

$$N_z = \frac{1}{\left(1 + \frac{V_{CO}}{V_{T_0}}\right)} \left[\frac{g V_{CO}}{V_{T_0}} (\cos \theta \cos \phi - 1) - F \right]$$

Combining the above relations and writing I in terms of F and g yields the structure of Figure 55.

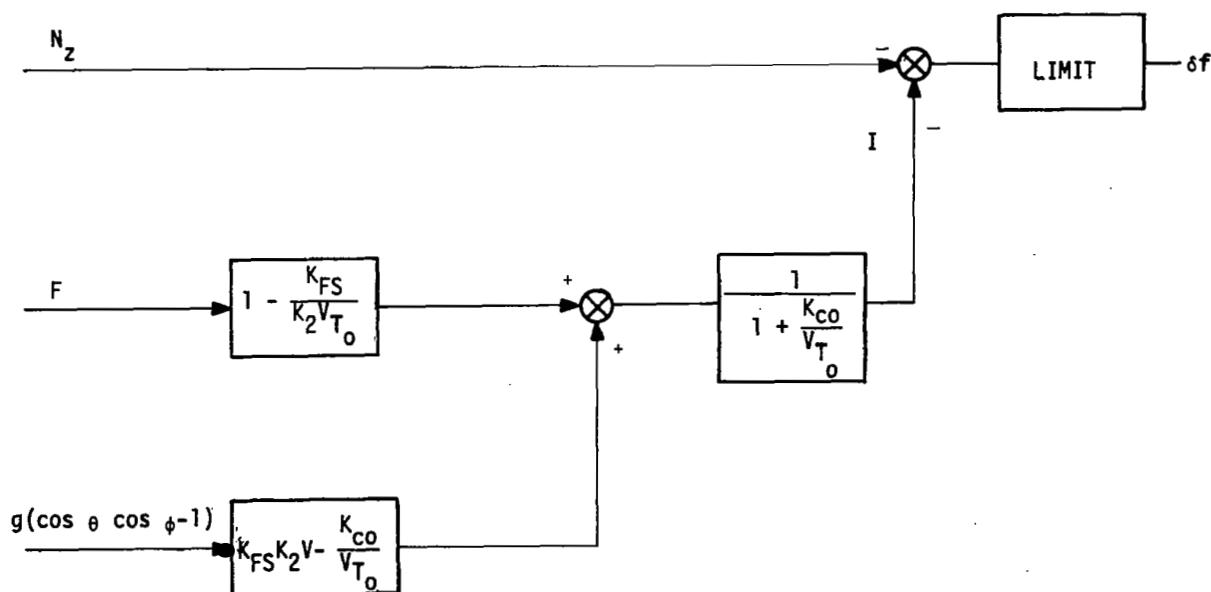


Figure 55. Command and Gravity Compensation for N_z Flap Mode

The computation of $g (\cos \theta \cos \varphi - 1)$ requires all-attitude θ and φ . This requirement can be circumvented by using a high-pass on N_z to remove the gravity effect. The command term I is then simplified to K_{F4} as shown in Figure 56. The N_z flap mode then has a complementary structure with the steady state flap deflection δ_f determined by pitch rate.

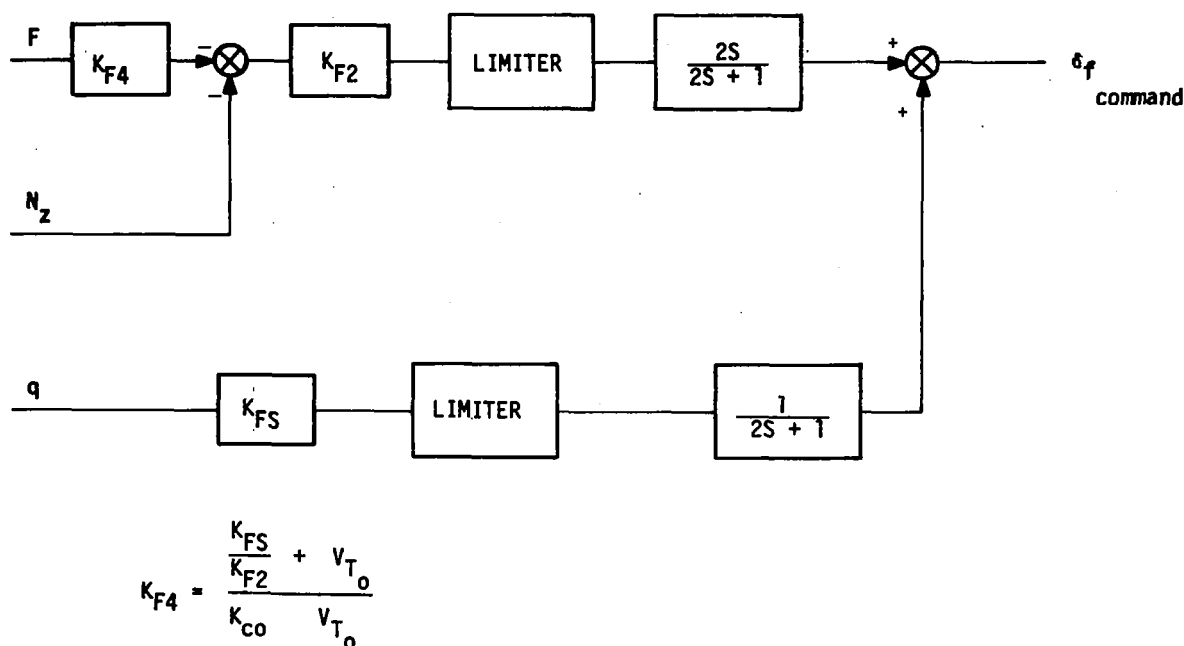


Figure 56. Alternate N_z Flap Compensation

Performance of Symmetric Aileron Controller

The performance of the N_z flap controller in reducing gust effects is summarized in Table 17. Three flight conditions covering low, medium, and high dynamic pressures are presented. The results have been normalized to the free aircraft response and are for a digital controller operating at 32 sps.

The transient response of the F-8C to a step alpha gust is shown in Figures 57 and 58 for a low and medium dynamic pressure flight condition. The time histories illustrate the response using only the elevator, then with the q flap mode engaged and finally with the N_z mode engaged.

The command augmentation provided by the direct lift is illustrated in Figure 59 and 60 for a step stick command. The enhancement of the stick response is apparent at the lower dynamic pressure flight condition. At the 20,000 feet Mach 0.4 condition the normal acceleration transient response is nearly twice as fast with slightly less pitch rate overshoot. The q -flap response is also shown for comparison. It verifies that the minimum drag schedule has been decoupled from the dynamic response by the inclusion of the two-second lag. Therefore, the transient responses to stick commands are

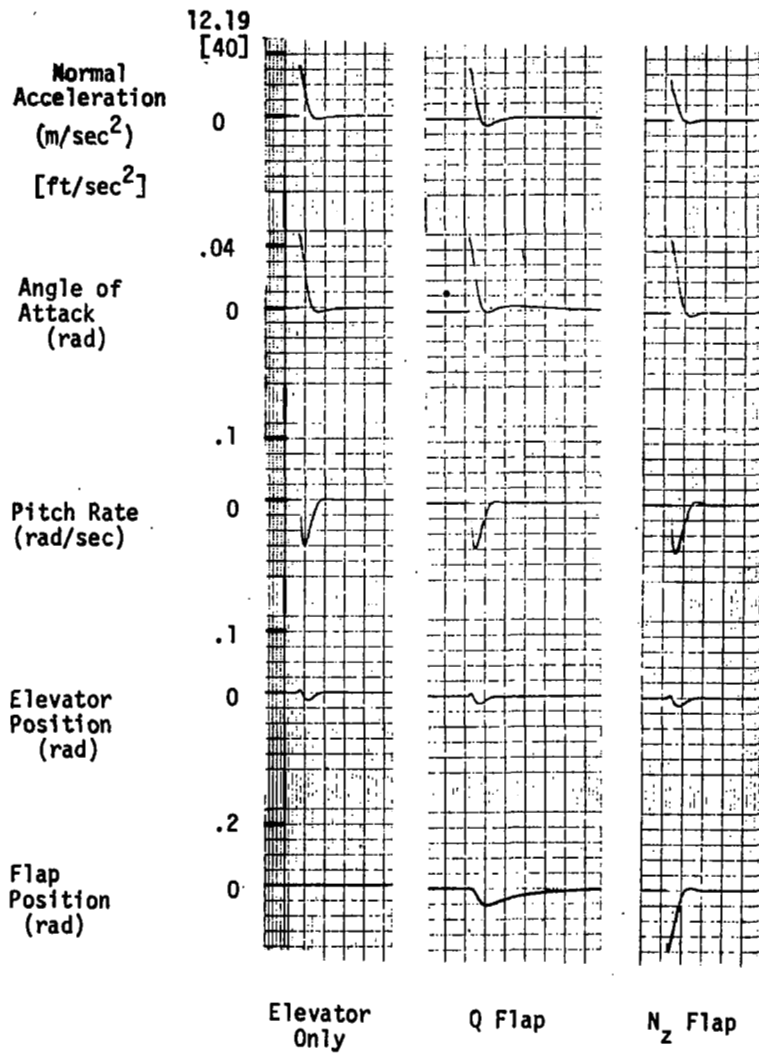


Figure 57. Step Gust Response (FC 1)

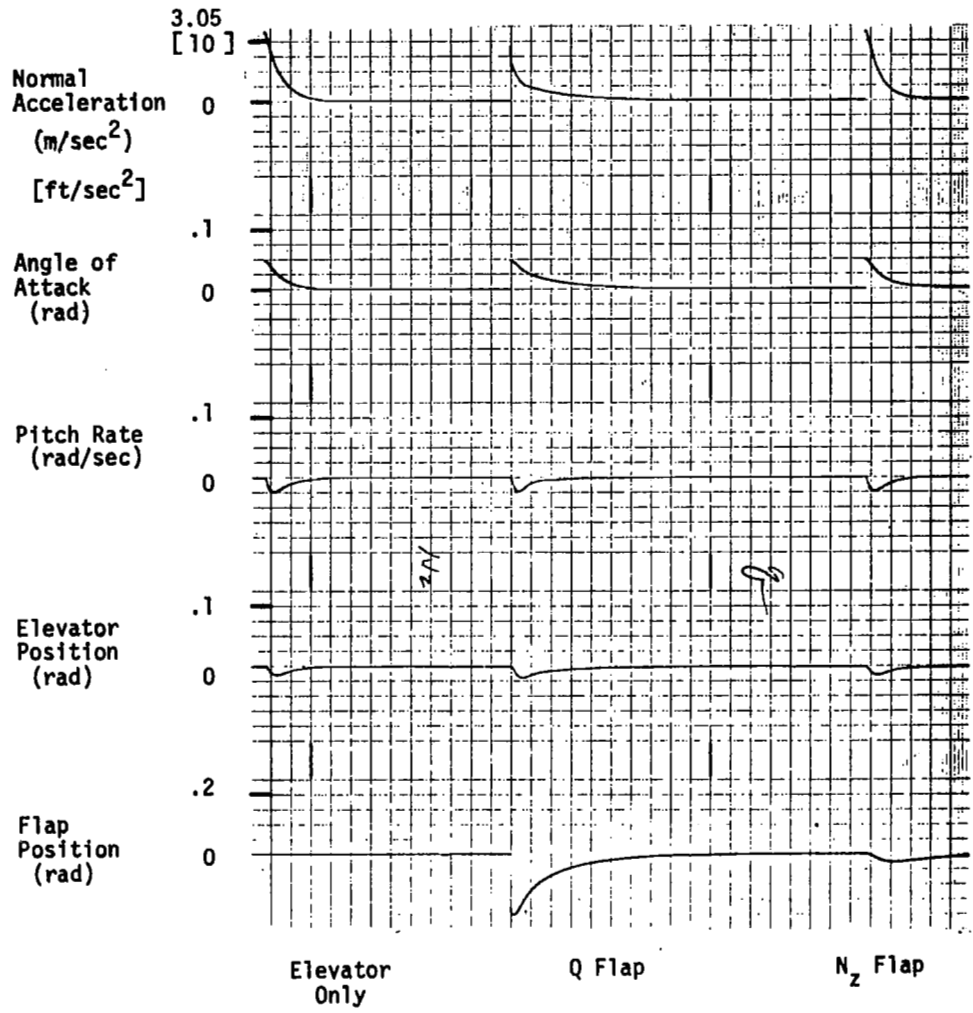


Figure 58. Step Gust Response (FC 5)

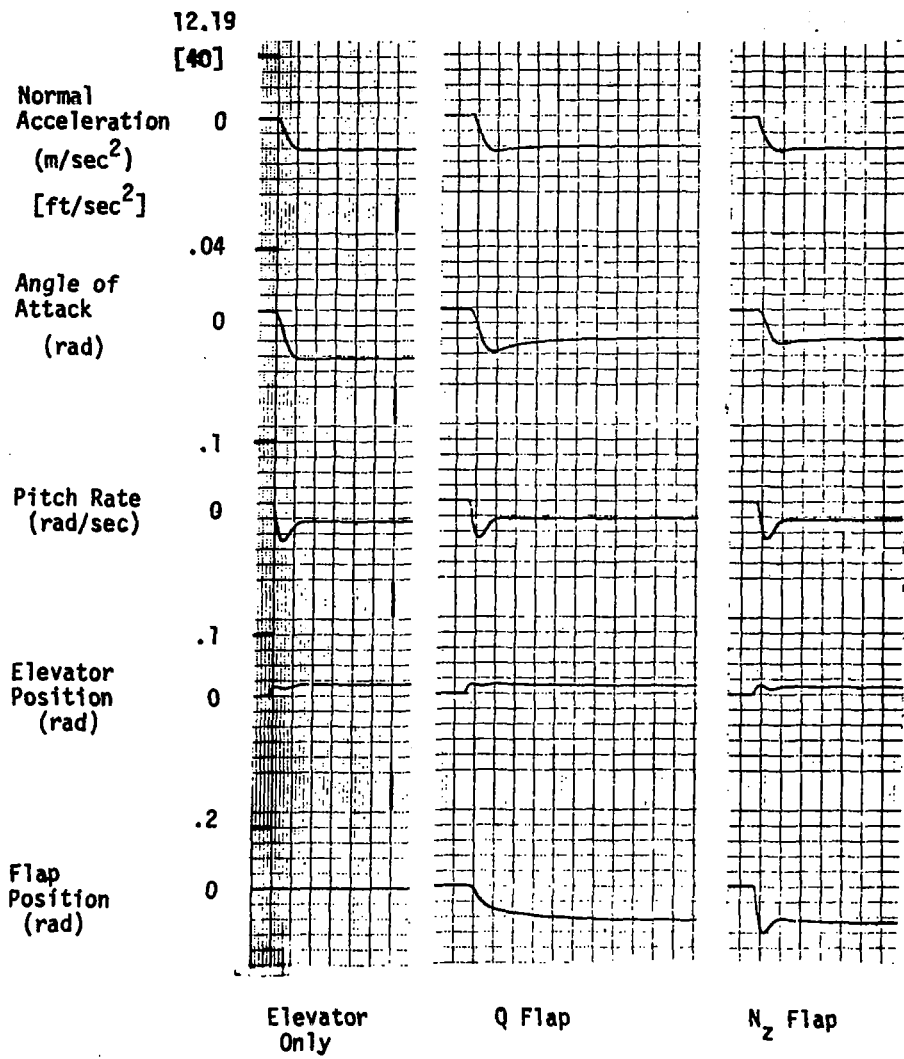


Figure 59. Step Stick Response (FC 1)

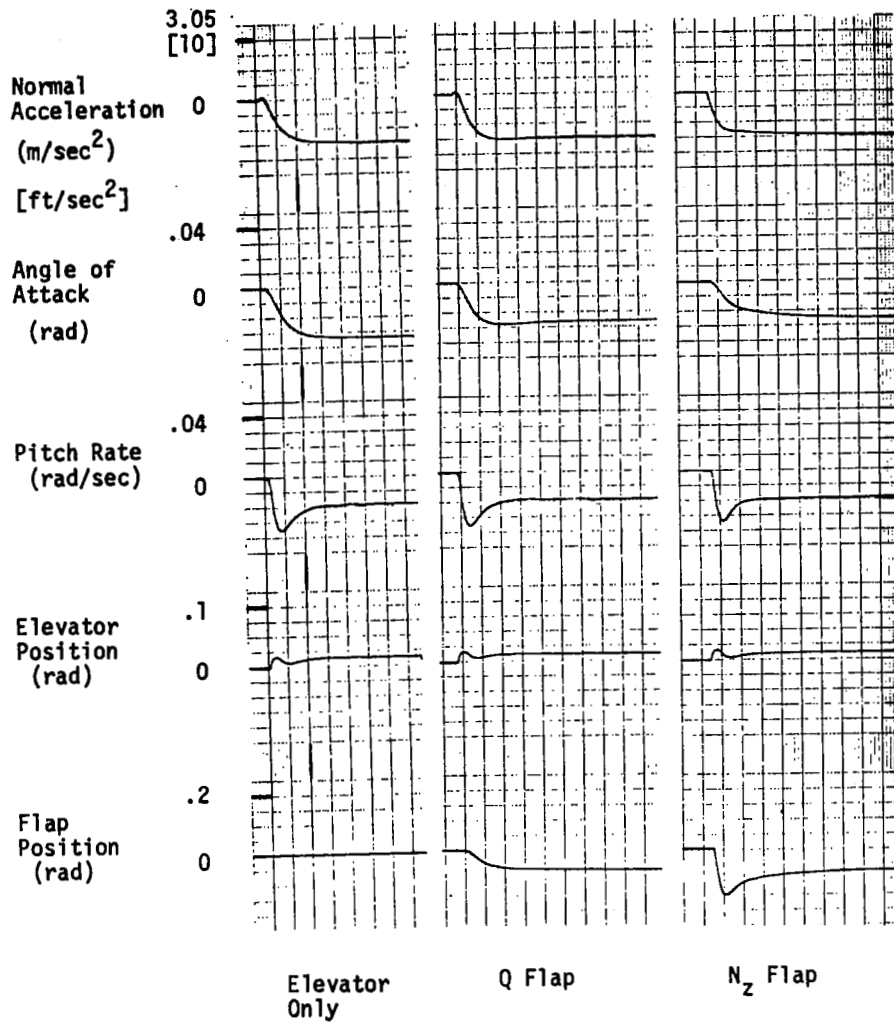


Figure 60. Step Stick Response (FC 5)

identical for the elevator only mode and the q flap mode. Note that the flap position is identical for either the q flap or the N_Z flap mode.

Table 17. RMS Gust Acceleration Response

Flight Condition	Free Aircraft	Elevator Only	Elevator plus Symmetric Aileron
5 ($\bar{q} = 109$)	1.0	0.89	0.59
1 ($\bar{q} = 305$)	1.0	0.85	0.61
9 ($\bar{q} = 654$)	1.0	0.87	0.70

Pitch CAS Functional Block Diagram

The results of the design process are summarized in Figure 61 which shows the digital controllers for the elevator and boundary controllers for a 32 sps rate. (The analog equivalent of this was illustrated previously in Figure 26). Also indicated are the summing points for the crossfeed from the direct lift controller and outer loop modes.

The angle-of-attack boundary controller uses true air speed (ft/sec) and dynamic pressure (psf) as scheduling quantities

$$K_{\alpha L} = 0.002 * V_{T_0}$$

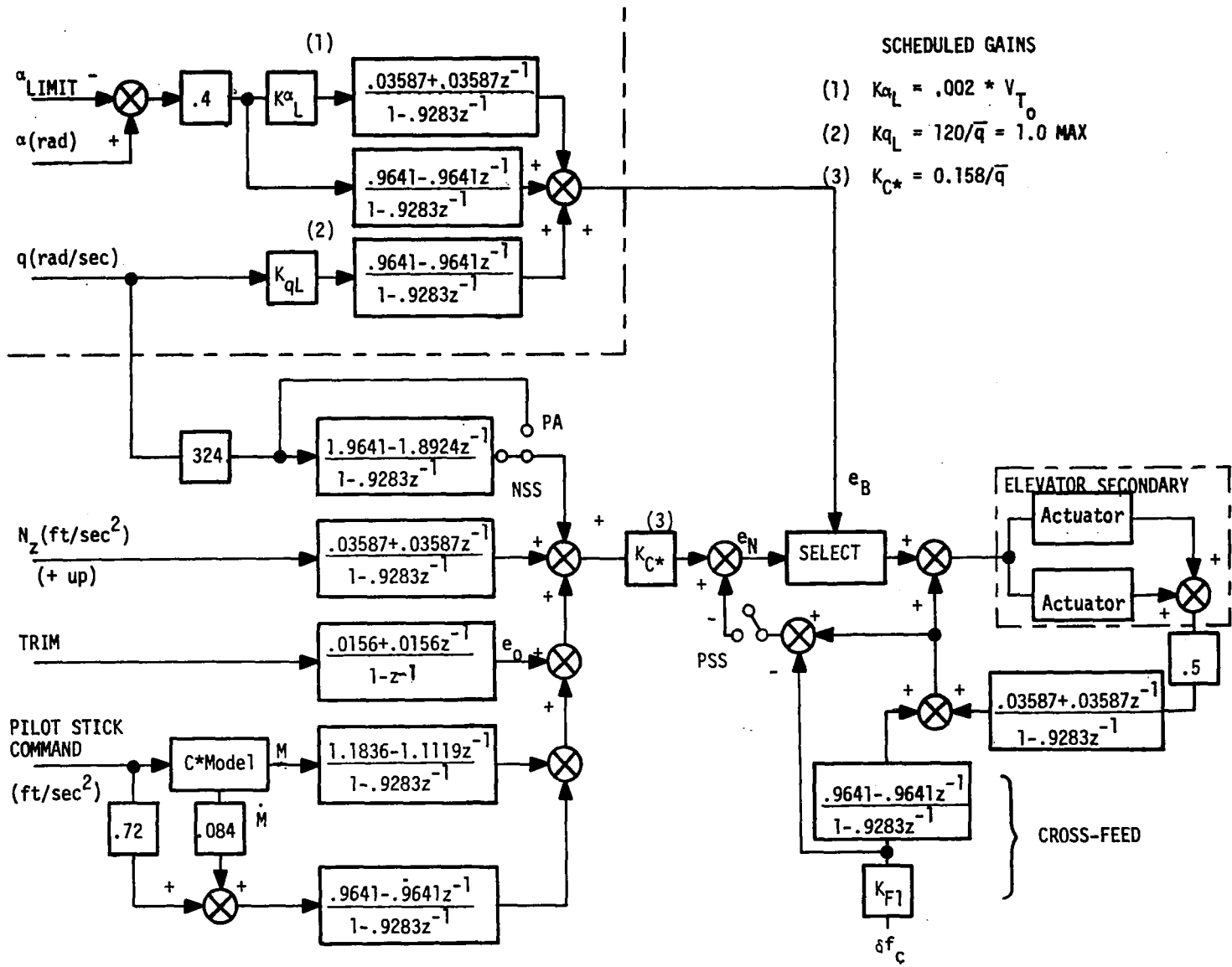
$$K_{qL} = 120/\bar{q}$$

The elevator controller schedules loop gain with dynamic pressure

$$K_C^* = \frac{0.158}{\bar{q}}$$

The minimum values of \bar{q} and V_{T_0} used for gain scheduling purposes are 100 psf and 100 ft/sec, respectively.

The explicit C^* model is a second order model with a frequency of 7 rad/sec and 0.9 damping ratio. The function of the signal select was previously explained; it selects the more positive (most nose down) of the two command signals e_B or e_N (refer to Figure 23).



- SCHEDULED GAINS
- (1) $K_{\alpha L} = .002 * V_{T_0}$
 - (2) $K_{qL} = 120/\bar{q} = 1.0 \text{ MAX}$
 - (3) $K_{C*} = 0.158/\bar{q}$

Figure 61. Mode I Digital Controller

The digital controller for the q flap and N_z flap modes is shown in Figure 62. Gains are scheduled with dynamic pressure and true air speed.

$$K_{F2} = \frac{4.3}{\bar{q}}$$

$$K_{F4} = \frac{\frac{K_{FS}}{K_{F2}} + V_{T_o}}{324 + V_{T_o}}$$

Fixed values of K_{FS} and K_{XF} are used.

Frequency responses of the elevator controller with the loop broken at the input to the elevator actuator were computed to check phase and gain margins as a function of sample rate. Results for flight condition 9 for sample rates of 10, 20, and 40 samples per second are shown as Figures 63, 64, and 65.

The complete pitch axis equations including four symmetric structural modes was used. The structural mode data and their influence on sensed pitch rate and normal acceleration were taken from reference 21. The prefilter was not included in these frequency responses. The gain crossover occurs between 3 and 4 rad/sec and shows a phase margin of about 70 degrees. The phase crossover occurs between 45 and 50 rad/sec and shows a gain margin of about 21 db.

From a consideration of phase and gain margins a sampling rate of 40 sps appears to provide sufficient phase margin such that an analog prefilter can be accommodated without adding additional compensation.

NASA/LRC Simulator Results

The digital control system presented in Figures 61 and 62 were programmed in FORTRAN and run as a control subroutine in the CDC 6600 simulation of the F-8C. The control system was checked out and "flown" throughout the flight envelope. Traces are presented below for eight selected flight conditions. The results from the LRC Simulator compared well with the linear simulation results. Time histories for the elevator mode and the "q" flap and N_z flap modes are presented for the following conditions.

Altitude	Mach	Condition
20,000	0.67	clean, medium \bar{q}
20,000	0.4	clean, low \bar{q}
10,000	0.8	clean, high \bar{q}
40,000	1.1	clean
3,000	0.25	Power Approach

For the N_z flap mode responses shown, the $2S/2S+1$ high pass was not included in the N_z feedback.

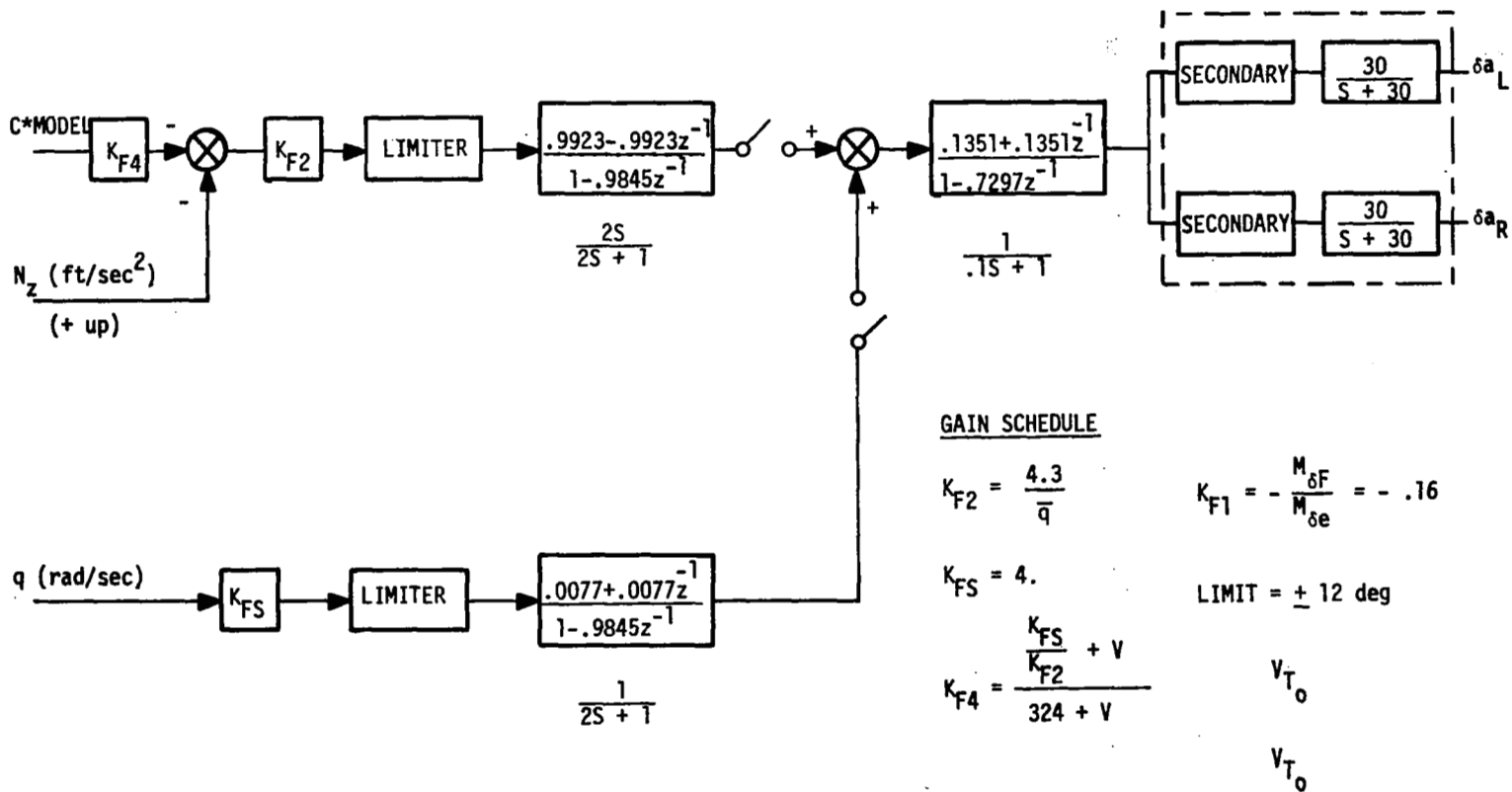


Figure 62. Symmetric Aileron Digital Controller

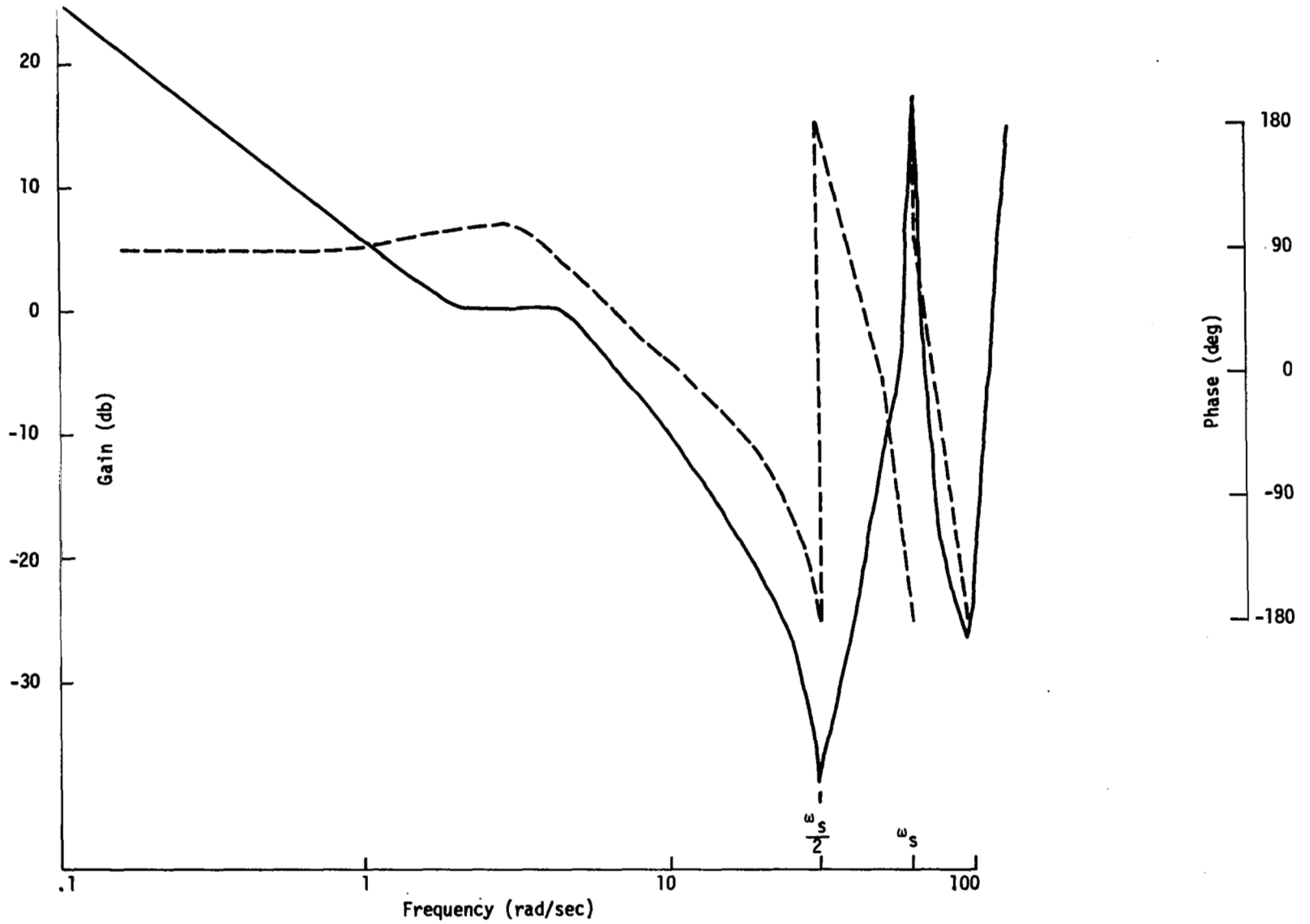


Figure 63. FC 9 Open Loop Frequency Response
10 SPS

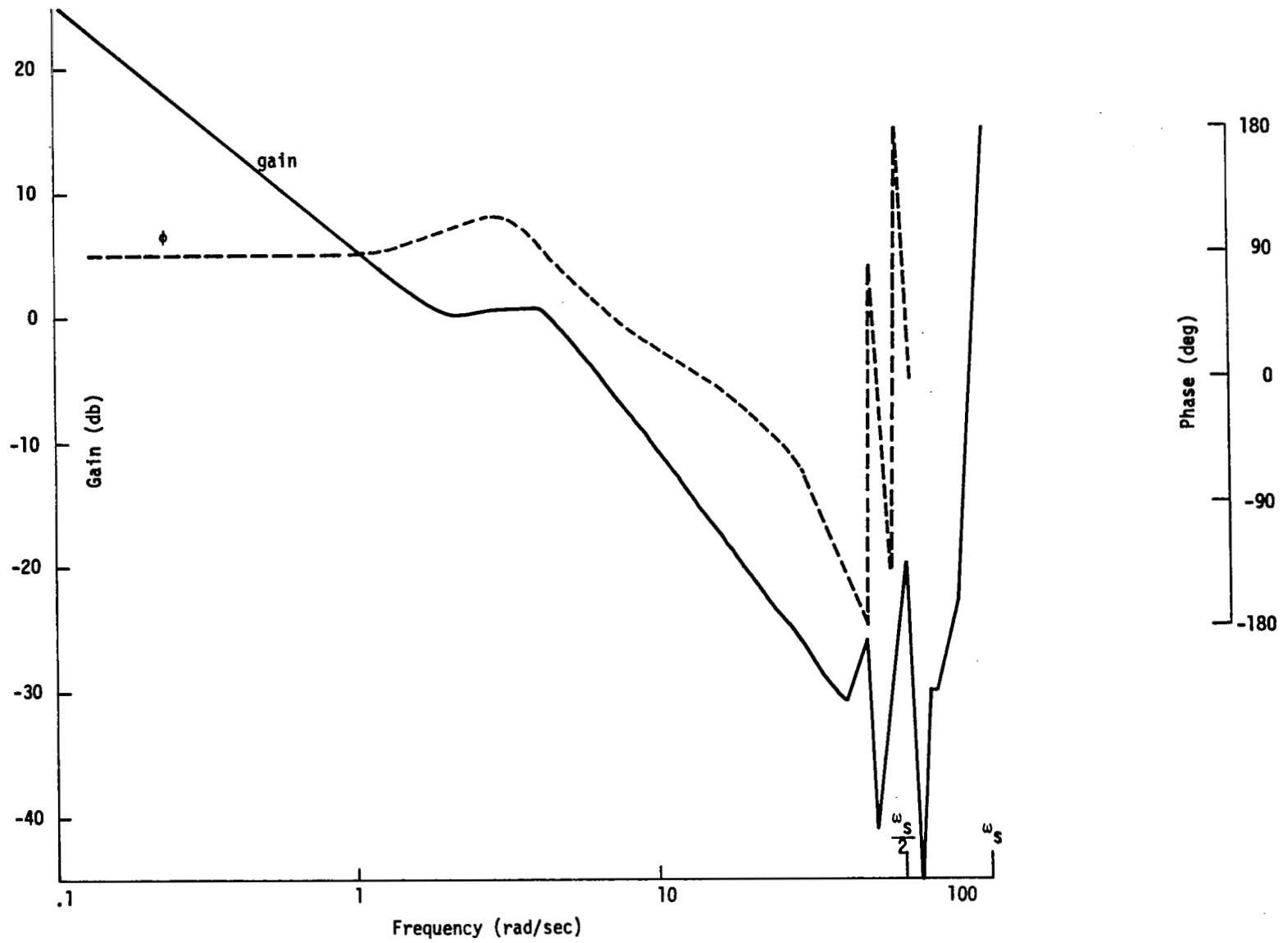


Figure 64. FC 9 Open Loop Frequency Response
20 SPS

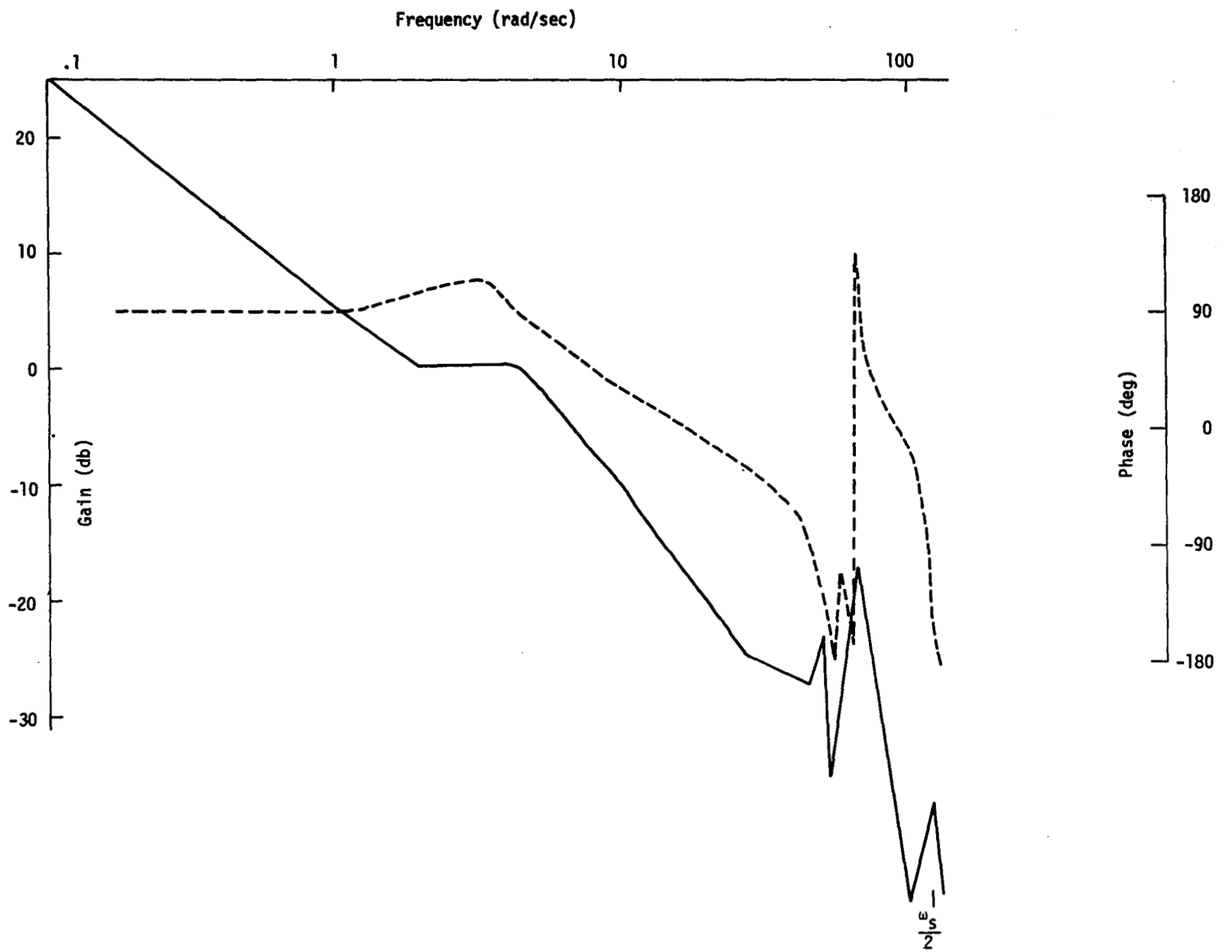


Figure 65. FC 9 Open Loop Frequency Response
40 SPS

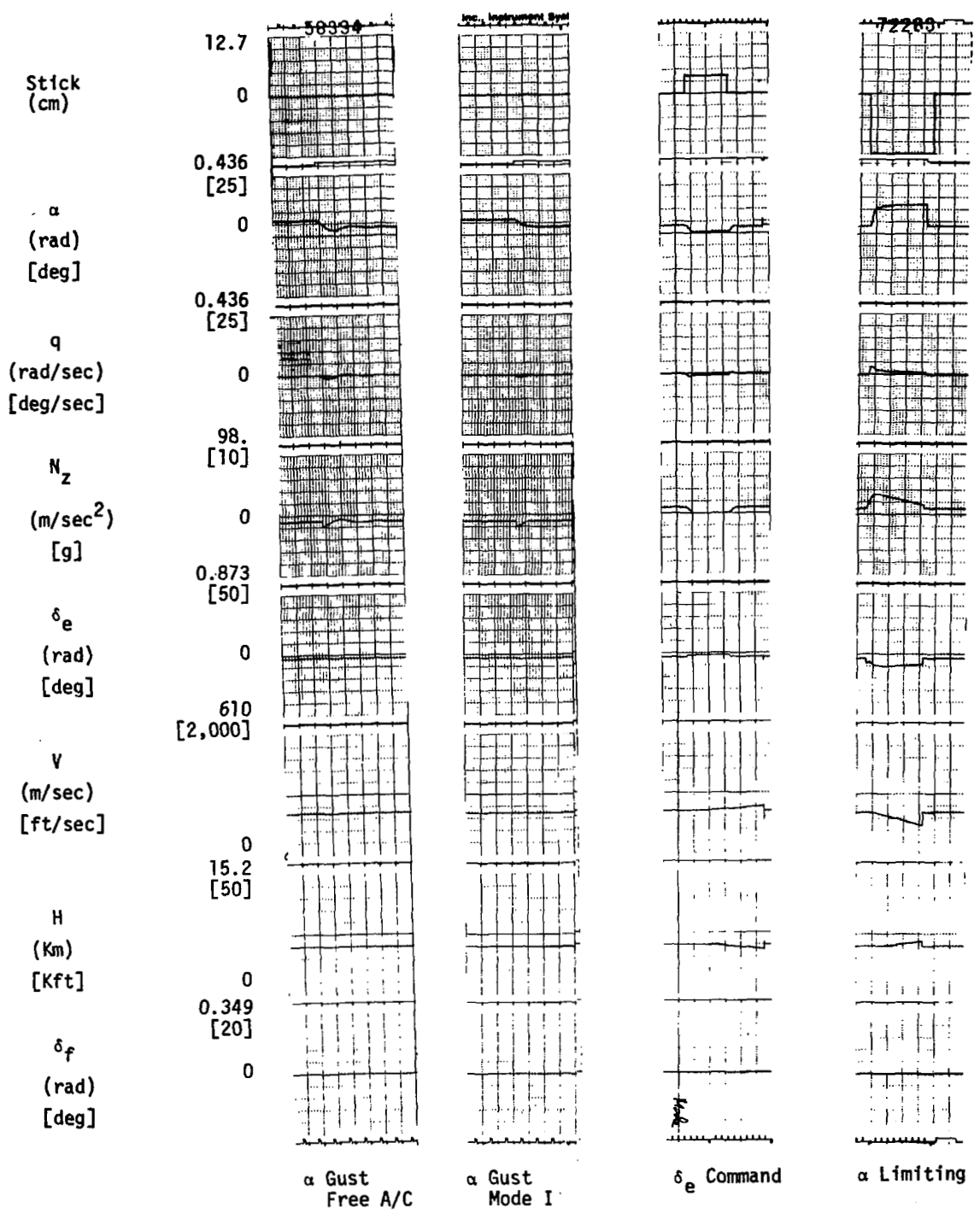


Figure 66. Transient Response (Mode I 20K; M = 0.67)

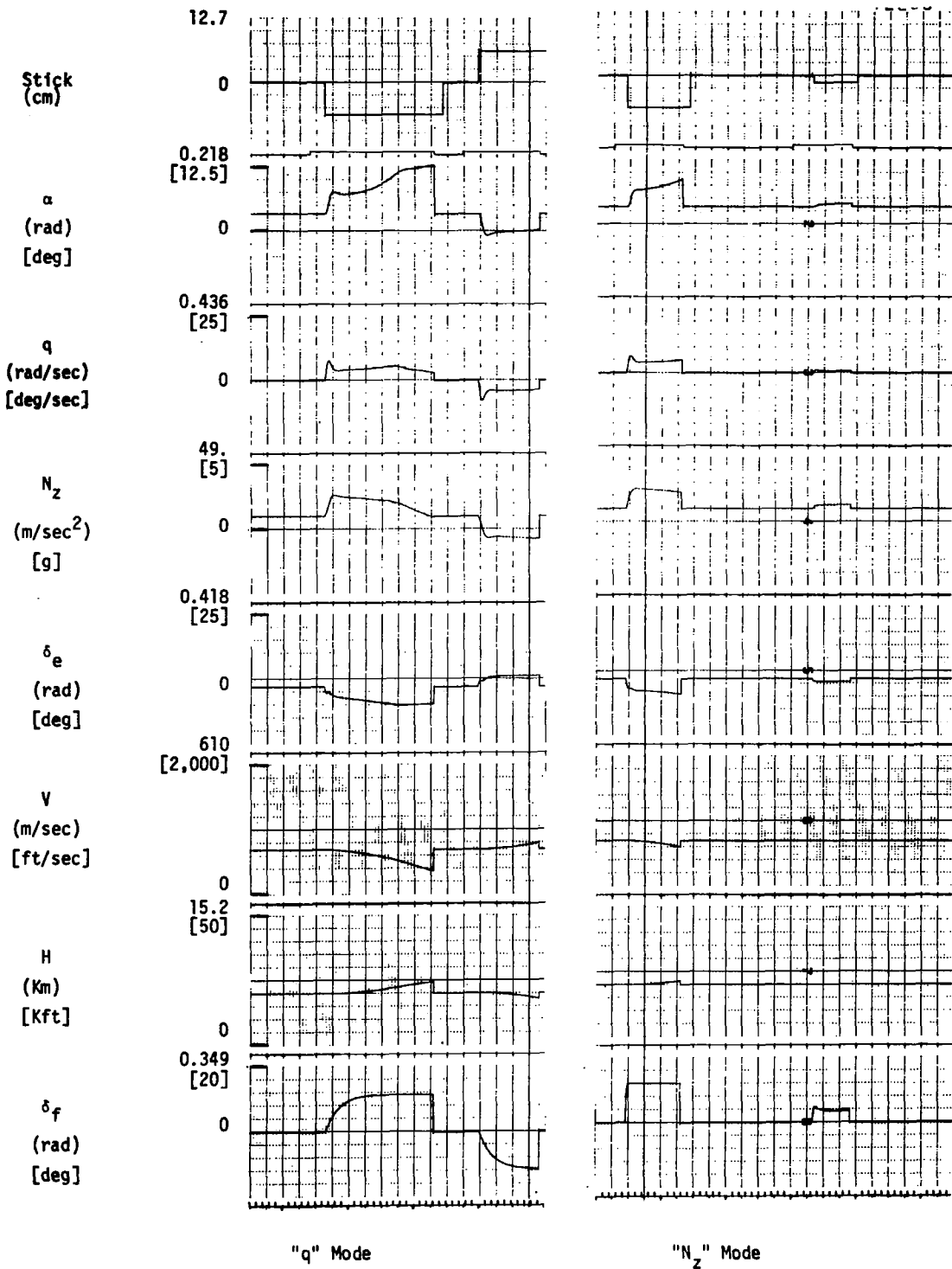


Figure 67. Transient Response (N_z , q Mode 20K; M = 0.67)

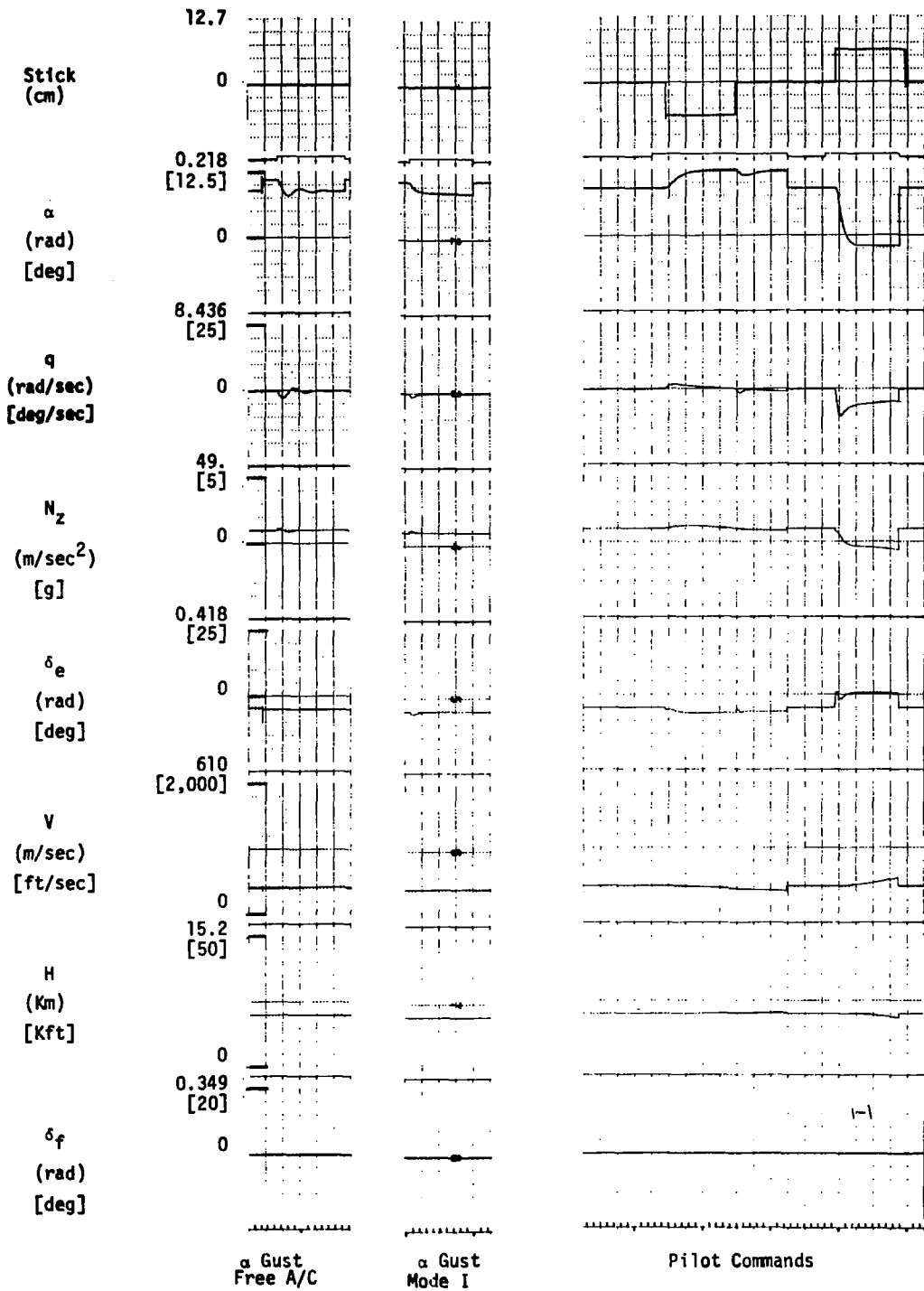


Figure 68. Transient Response (Mode I 20K; M - 0.4)

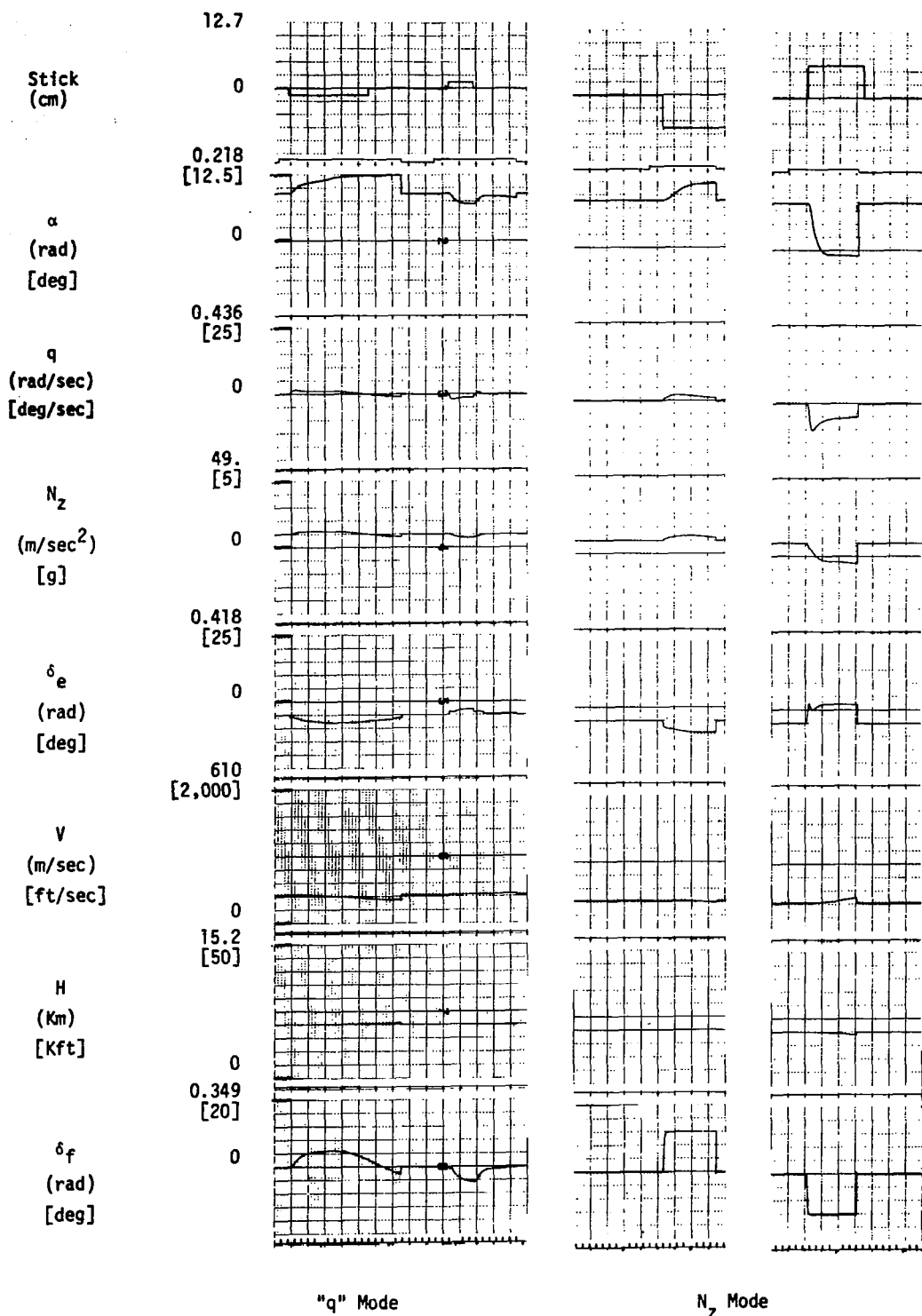


Figure 69. Transient Response (N_z , q Mode 20K; $M = 0.4$)

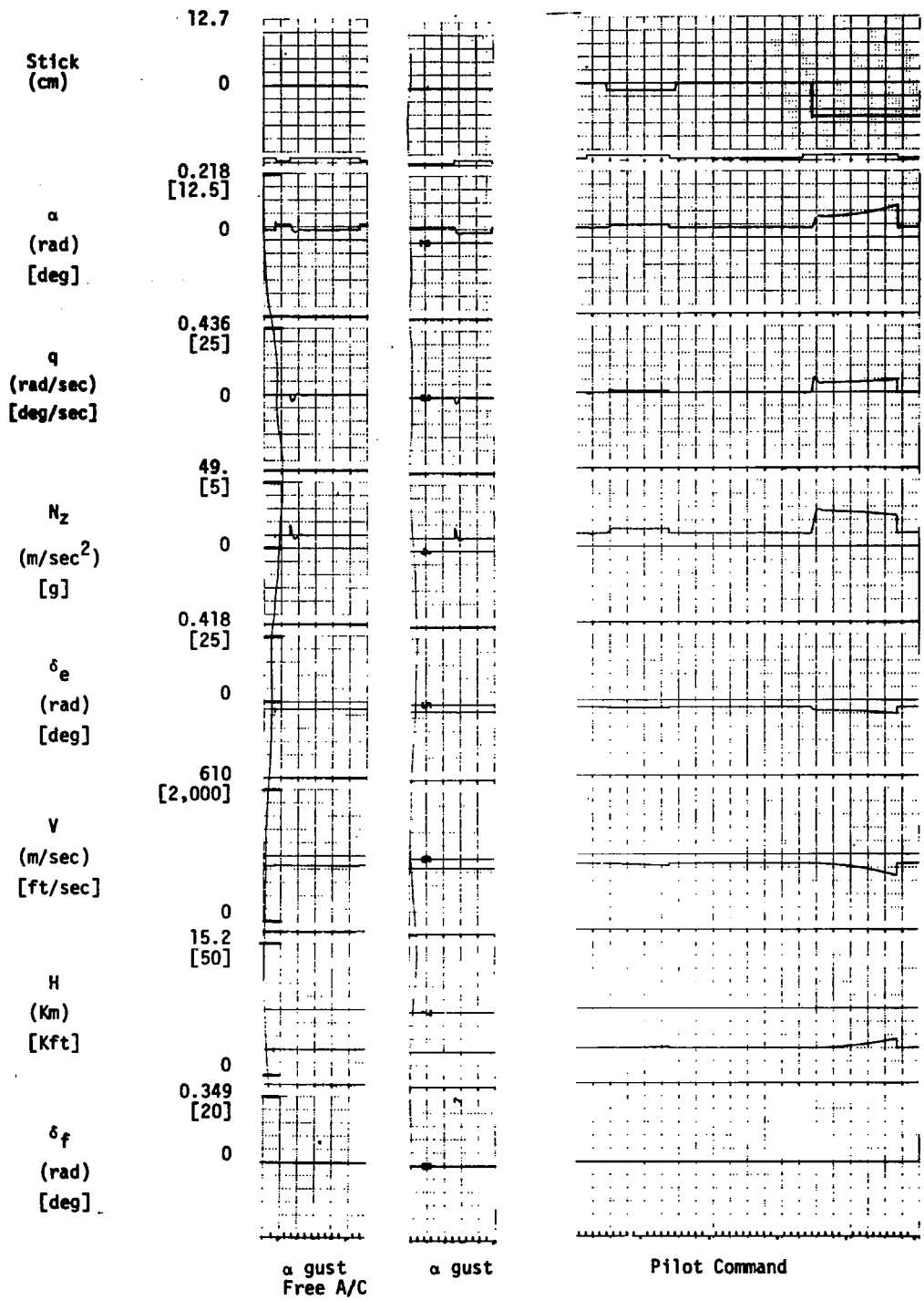


Figure 70. Transient Response (Mode I 10K; M = 0.8)

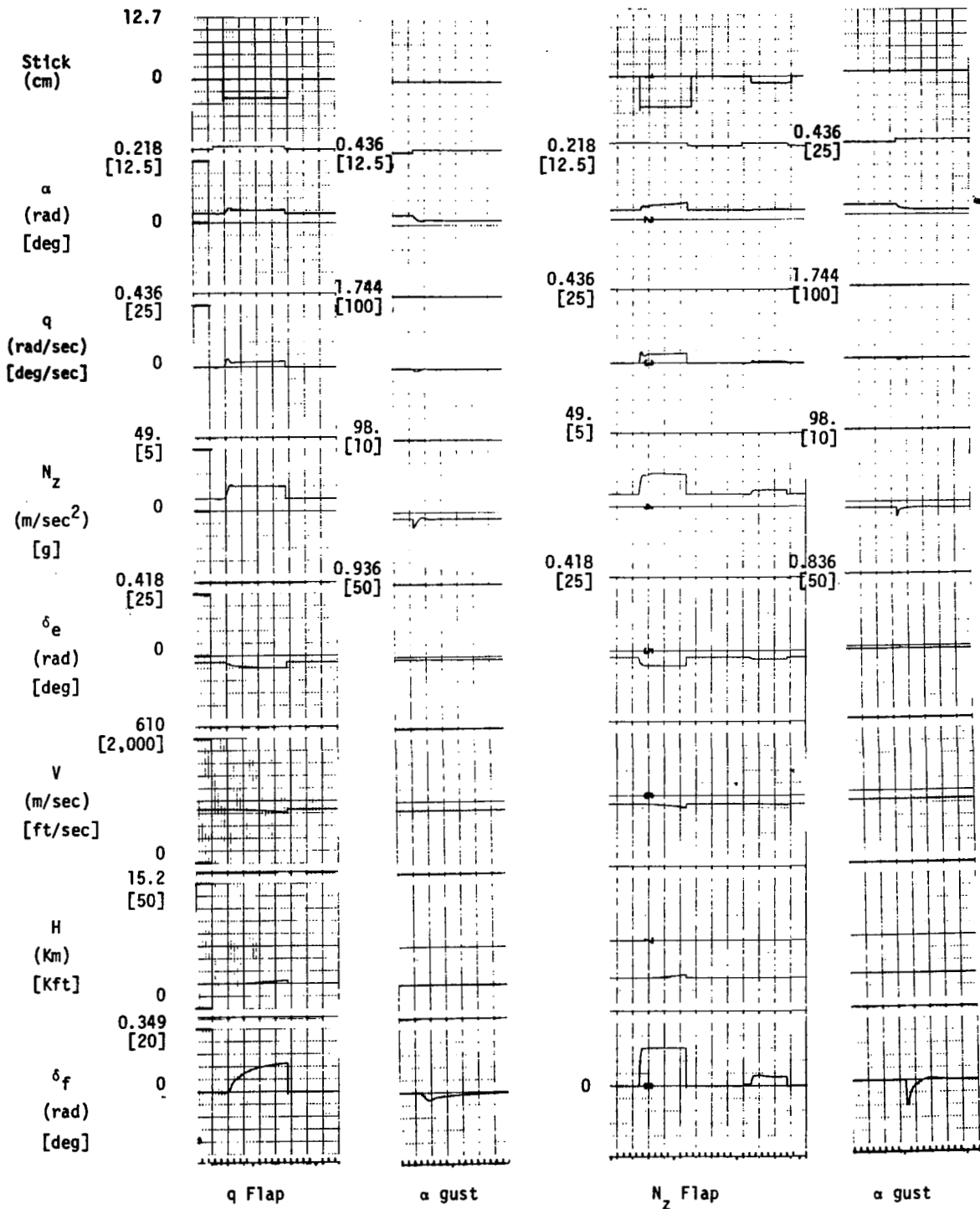


Figure 71. Transient Response (N_z , q Mode 10K; M = 0.8)

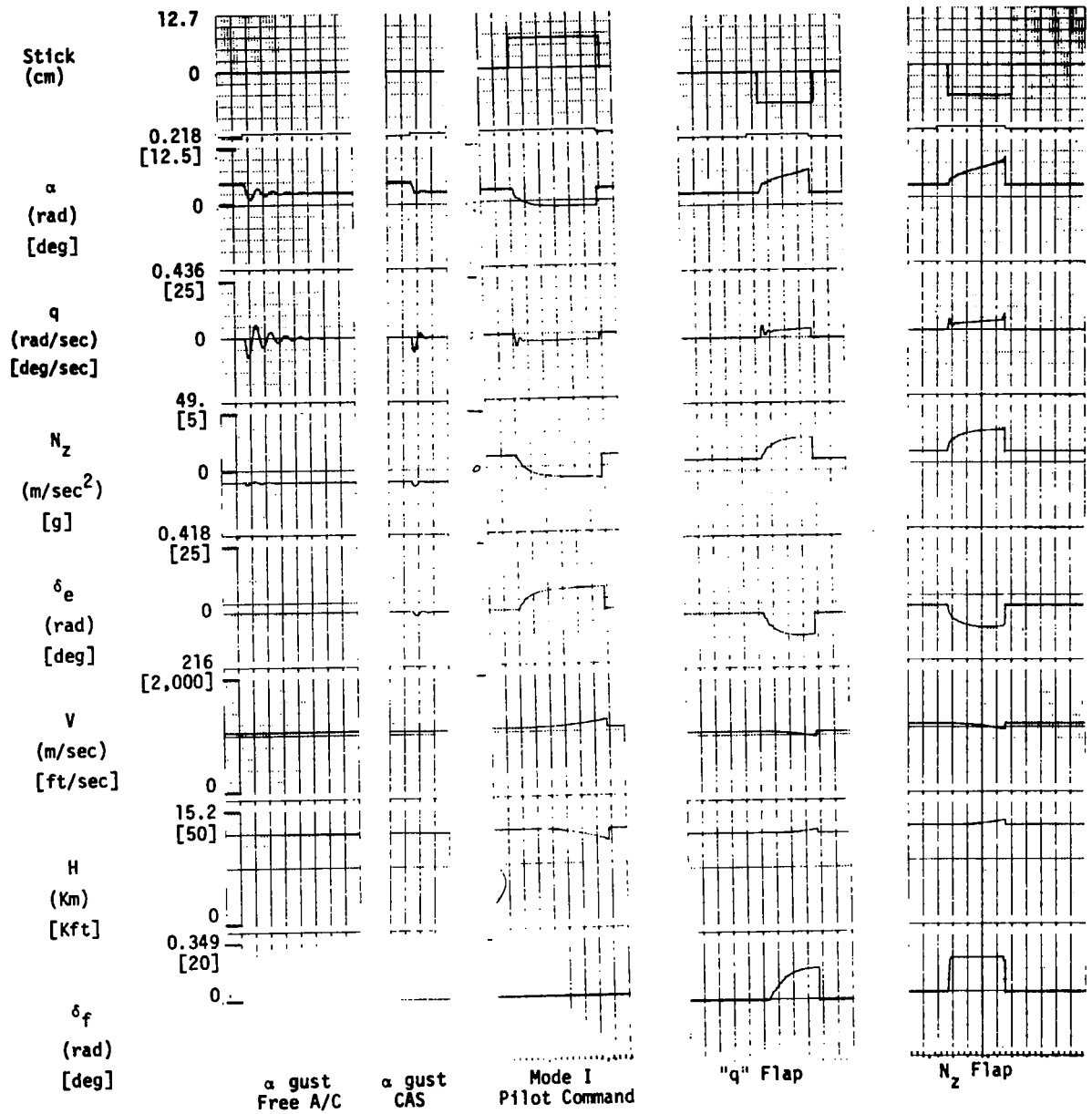


Figure 72. Transient Response (Mode I, N_z , q Mode 40K; M = 1.1)

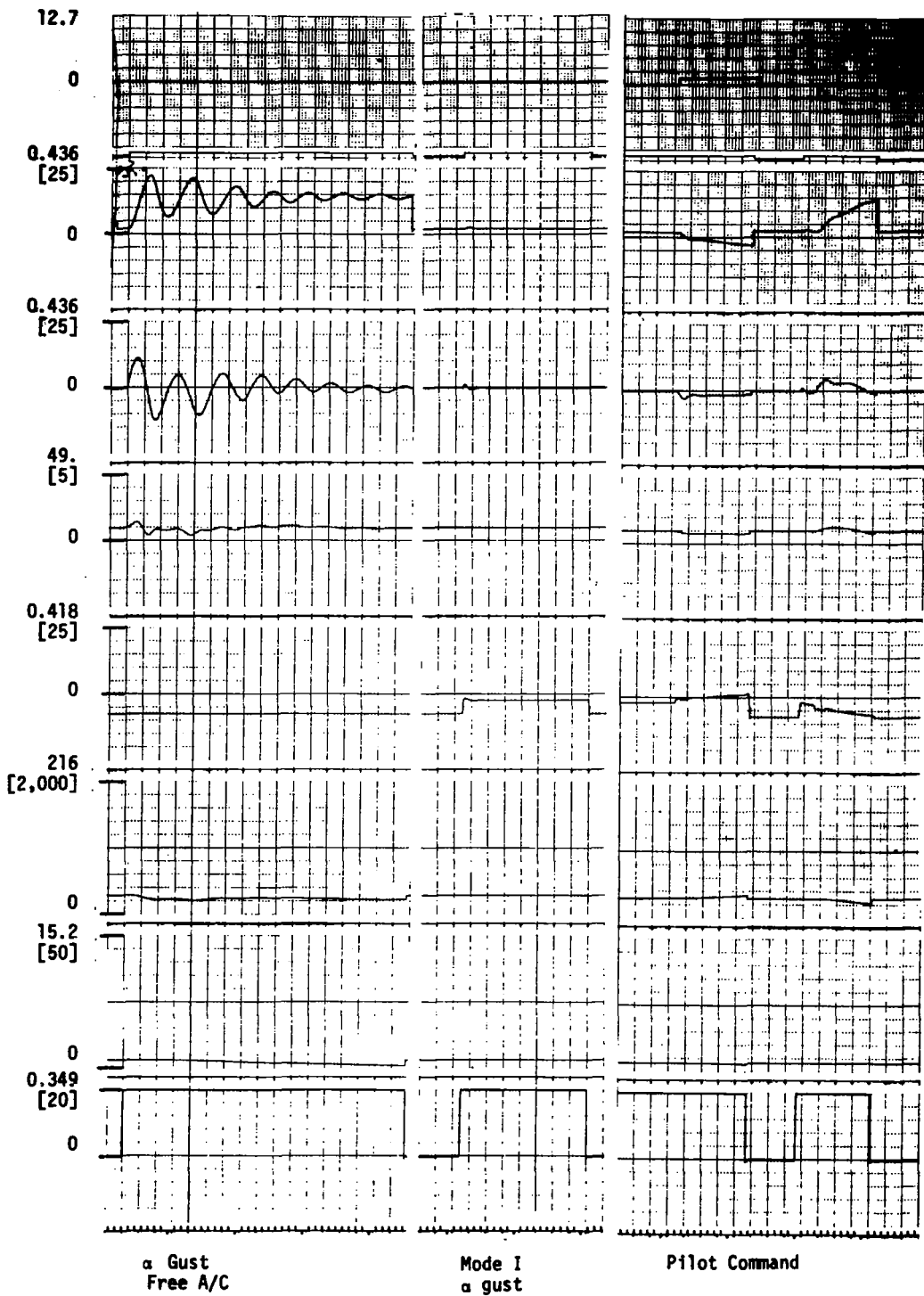


Figure 73. Transient Response (Mode I 3K; M = 0.25)

SYNTHESIS OF A LATERAL-DIRECTIONAL CAS WITH
INERTIAL COORDINATION

The linear quadratic optimal design methodology discussed in Section 5 was used to design a control augmentation system for the lateral-directional axes for the F-8C aircraft. Details of the designs which uses full state feedback are presented below. This design is denoted as "inertial coordination" since the full state vector is combined with a true air speed measurement to command a yaw rate that provides turn coordination (i. e., minimum sideslip). The design specification summary was presented in Section 4. The linear mathematical models are first described, followed by the fixed point design procedure and results. Gain scheduling of the fixed point designs over the flight envelope and the resulting control system structure are discussed next, followed by a summary of the system performance and sensor requirements.

Linear Models for Lateral-Directional CAS Designs

The quadratic design methodology requires linear state equations for synthesis. These linear models were obtained with the computer programs F8SIM and F8AUG. The lateral-directional rigid body states of the F8SIM output are p , r , v , ϕ , ψ , and y . The F8AUG program was used to add actuator dynamics and to transform the state. The lateral velocity state v was replaced by the lateral acceleration at the sensor station, n_{y_S} . By making this transformation all of the rigid body states are sensed quantities, and the full state design can be used directly for the inertial coordination CAS without the added design step of using the practicalization algorithm. For the design presented in Section 8 where inertial coordination was not used, the practicalization algorithm was employed to eliminate feedback gains from the nonmeasurable signals.

For the actual design the first four rigid body state equations were used (states p , r , n_{y_S} , ϕ). These state equations were augmented with the aileron and rudder actuator dynamics, states δ_A and δ_R , respectively. First order lags with time constants of 1/30 and 1/25 seconds, respectively, were used.

In addition to the aircraft dynamics, control system dynamics were added. A first order roll rate model was used for explicit model following, and a lag and integrator were added on the n_{y_S} signal. The lag is used for noise filtering and the integrator for rudder trim. The pilot command was modeled as filtered white noise. The filter is first order. The two control inputs are the aileron and rudder commands.

The states were as follows:

$$x_1 = p, \text{ roll rate, rad/sec}$$

$$x_2 = r, \text{ yaw rate, rad/sec}$$

$$x_3 = n_{y_S}, \text{ sensed lateral acceleration, ft/sec}^2$$

$x_4 = \phi$, bank angle, rad

$x_5 = \delta_A$, aileron position, deg, (left down, right up positive), $\delta_A = \frac{\delta_{A_L} - \delta_{A_R}}{2}$

$x_6 = \delta_R$, rudder position, deg (trailing edge left positive)

$x_7 = n_{y_{sl}}$, lagged sensed lateral acceleration, ft/sec²

$x_8 = \int n_{y_{sl}} = n_{y_{sli}}$ integral of lagged sensed acceleration, ft/sec

$x_9 = p_m$, roll rate model state (rad/sec)

$x_{10} = u_m$, noisy pilot input filter state (in)

The state equations are of the form

$$\dot{\mathbf{x}} = \mathbf{F}\mathbf{x} + \mathbf{G}_1\mathbf{u} + \mathbf{G}_2\boldsymbol{\eta}$$

where $\mathbf{u} = (u_A, u_R)^T$ is the control input vector of aileron and rudder commands to the servos (or actuators of this model). The noise input $\boldsymbol{\eta}$ is a white noise source representing the pilot's roll commands.

The state equations are thus

$\begin{bmatrix} \dot{p} \\ \dot{r} \\ \dot{n}_{y_s} \\ \dot{\phi} \\ \dot{\delta}_A \\ \dot{\delta}_R \\ \dot{n}_{y_{sl}} \\ \dot{n}_{y_{sli}} \\ \dot{p}_m \\ \dot{u}_m \end{bmatrix}$	=	Rigid body equations of motion		Surface effectiveness		0	0	0	0	$\begin{bmatrix} P \\ r \\ n_{y_s} \\ \phi \\ \delta_A \\ \delta_R \\ n_{y_{sl}} \\ n_{y_{sli}} \\ p_m \\ u_m \end{bmatrix}$	+	$\begin{bmatrix} 0 & 0 \\ 0 & 0 \\ x & x \\ 0 & 0 \\ 30 & 0 \\ 0 & 25 \\ 0 & 0 \\ 0 & 0 \\ 0 & 0 \\ 0 & 0 \end{bmatrix}$		$\begin{bmatrix} u_A \\ u_R \end{bmatrix}$	+	$\boldsymbol{\eta}$	$\begin{bmatrix} 0 \\ 0 \\ 0 \\ 0 \\ 0 \\ 0 \\ 0 \\ 0 \\ 0 \\ 30.4 \end{bmatrix}$							
		0	0	0	0	-30	0	0	0			0	0					0	0	0	0	0	0	
		0	0	0	0	0	-25	0	0			0	0					0	0	0	0	0	0	0
		0	0	4.0	0	0	0	-4.0	0			0	0					0	0	0	0	0	0	0
		0	0	0	0	0	0	1.0	0			0	0					0	0	0	0	0	0	0
		0	0	0	0	0	0	0	0			-5.0	5.0					0	0	0	0	0	0	0
		0	0	0	0	0	0	0	0			0	0					-1.0	0	0	0	0	0	30.4

The rigid body elements of the untransformed F and G₁ matrices are listed in Appendix B for the various flight conditions. The two nonzero elements in the third row of the G₁ matrix occur because of the transformation of the velocity state v to the acceleration state n_{ys}. The noise pilot filter of 30.4/(s + 1) was chosen to have a cut-off such that the free aircraft was reasonably excited. The d. c. gain of 30.4 was selected during the design process to give convenient rms response magnitudes. These parameters affect only the feedforward gains and are thus not important. The accelerometer lag and the roll rate model time constant were determined during the design process.

The final response vectors used for design and evaluation are shown in Table 18. Responses such as β, n_{yp}, p, r, etc., were used for evaluating the system performance with transient responses and rms responses. Other responses were used primarily for design via weighting in the quadratic cost function. The final designs were obtained with quadratic weights on p - p_m, n_{ysli}, r - pα - $\frac{g}{V_{T_0}} \varphi$, u_A and u_R. Several other combinations were investigated during the design process as will be discussed in the next section.

Table 18. Response Vector for Lateral CAS Design

Component	Definition
r ₁	β = sideslip, rad
r ₂	n _{yp} = lateral acceleration at pilot station, g's
r ₃	e = p - p _m = roll rate error, rad/sec
r ₄	p = roll rate, rad/sec
r ₅	r = yaw rate, rad/sec
r ₆	n _{ys} = sensed lateral acceleration, ft/sec ²
r ₇	φ = bank angle, rad
r ₈	δ _A = aileron surface position, deg
r ₉	δ _R = rudder surface position, deg
r ₁₀	n _{usl} = lagged sensed lateral acceleration, ft/sec ²
r ₁₁	n _{ysli} = integral of n _{ysl} , ft/sec
r ₁₂	$\dot{\delta}_A$ = aileron surface rate, deg/sec
r ₁₃	$\dot{\delta}_R$ = rudder surface rate, deg/sec
r ₁₄	u _A = aileron command input, deg
r ₁₅	u _R = rudder command input, deg
r ₁₆	r - pα - $\frac{g}{V_{T_0}} \varphi$ = coordination response, rad/sec

The lateral-directional control augmentation system was designed by first synthesizing systems at fixed points throughout the flight envelope, using quadratic methodology software and linear time-invariant models. Gain schedules were then defined based on the fixed point designs. There were linear models available at twenty flight conditions, obtained with the F8SIM and F8AUG programs. Five distinct flight conditions were chosen for iterative application of the quadratic methodology. After obtaining satisfactory designs at these five flight conditions, the selected quadratic weights were applied to all twenty flight conditions and this set of twenty gain matrices was used for determining the gain schedules, after checking to insure satisfactory performance was obtained at all twenty flight conditions.

As mentioned previously, the F8SIM program has the capability to linearize the equations of motion about nonequilibrium flight conditions. This feature was used to linearize about various pull-up maneuvers, resulting in linear models at high angle-of-attack conditions, with the associated decrease in directional stability. Even though the longitudinal and lateral-directional axes equations were decoupled after linearization, the dynamic characteristics of the linear equations reflect the decreased stability. The five flight conditions were chosen so that high and low dynamic pressure conditions and a high angle-of-attack at medium dynamic pressure were included, as well as a nominal medium dynamic pressure level flight situation. Since the aircraft configuration is unique in power approach, a power approach flight condition was chosen as the fifth. The five flight conditions chosen for design iteration were as listed in Table 19.

Table 19. Design Flight Conditions

Flight Condition No.	h(ft)	Mach	\bar{q} (psf)	V (ft/sec)	α_{TRM} (deg)	Condition
1	20,000	.67	305	695	3.45	Cruise
5	20,000	.4	109	415	8.86	Cruise
10	0	.7	725	782	1.86	Cruise
17	0	.189	53	211	7.48	PA, wing up, gear down
20	20,000	.6	245	623	15.45	$\Delta n_z = 3g$ (climb)

Flight Condition 1 is a nominal cruise, medium dynamic pressure condition. Flight Condition 5 was chosen because of the low dynamic pressure, and Flight Condition 10 because of the high value of dynamic pressure. Flight Condition 20 represents a high angle-of-attack, and Flight Condition 17 is a power approach flight condition. The high angle-of-attack flight conditions (20 and 5) also were chosen to insure that the augmentation system design met the goal of good handling qualities at those conditions.

The design objectives are stated in Section 4 on performance criteria. The method of meeting these handling quality objectives with the quadratic methodology is to select appropriate responses and associated quadratic weights which reflect and achieve the objectives. This is an iterative process just as any other design procedure. The steps that lead to the final set of responses and weights are summarized briefly.

To achieve a good roll rate response, a roll rate error consisting of the difference between the aircraft roll rate and the roll rate model response was defined. The roll rate model was a first order lag and is driven by the pilot stick input. In the design models this is set up by forcing the model state equation (state 9, p_m) with the output of the noisy pilot filter (state 10, u_m). Weighting this error response serves to establish the basic control objective, pilot stick input commands roll rate, and also introduces some Dutch roll damping in the resultant controller. This response was always weighted during the iterative design process. Two other responses that always had quadratic weights were the aileron and rudder servo command inputs u_A and u_R . These control inputs must have weights for a solution to the Ricatti equation to exist (it is a necessary condition for $[D'QD]^{-1}$ to exist), and these weights have a major effect on the system bandwidth and stability margins.

The initial responses selected to specify turn coordination and Dutch roll damping were the lateral acceleration at the pilot station, n_{y_p} , and sideslip, β . These two responses, weighted either individually or at the same time, tended to define controllers with good coordination and damping but with objectionable properties of the gains. The two major problems were the magnitudes of the gain on the sensed lateral acceleration (and the lagged signal) and the crossfeed gain from aileron to rudder. The gain on lateral acceleration must not be excessive because of the noise content of the accelerometer output. A general guideline, based on past experience with similar flight control systems that have been tested, was to keep this gain below .01 rad/(ft/sec²). The crossfeed gain should be avoided as much as possible, because achieving turn coordination primarily by crossfeeding aileron to rudder results in a system that is highly dependent on the aircraft model parameters. The performance of such a system will deteriorate under parameter variations which can be expected. It was felt that, with an inertial coordination system, the design should not have to depend on crossfeed for coordination. It was found that one or both of these problems occurred with any combination of quadratic weights on n_{y_p} and/or β , and that some other response should be used to enforce the coordination property.

A turn coordination measure was determined based on the force equation in the y-axis. The force equation is, in body axes,

$$\frac{\dot{v}}{V_{T_0}} + r - p \frac{w}{V_{T_0}} - \frac{g}{V_{T_0}} \cos \theta \sin \varphi = \frac{n_y}{V_{T_0}}$$

which is approximately

$$\dot{\beta} + r - p\alpha - \frac{g}{V_{T_0}} \cos \theta \sin \varphi = \frac{n_y}{V_{T_0}}$$

The objective of turn coordination is to have lateral acceleration, a_y , and sideslip β zero during a maneuver. Assuming a_y and $\dot{\beta}$ are zero results in

$$r - p\alpha - \frac{g}{V_{T_0}} \cos \theta \sin \varphi = 0.$$

Turn coordination will be achieved if this expression is held at, or near zero. Linearizing the expression, a response was defined as

$$r_{16} = r - p\alpha_o - \frac{g}{V_{T_o}} \phi$$

where α_o is the trim angle-of-attack. Weighting this response will result in control system designs which tend to regulate the response to zero as desired.

In terms of applying quadratics, this is a good coordination response because the lateral acceleration n_{y_s} does not appear explicitly in the equation, which appeared to be the cause of the two problems mentioned above. Weighting this response worked well. Good controllers resulted without the undesirable gains experienced with the weights on n_{y_p} and β .

In addition to these responses one additional quadratic weight was used on the integral of lateral acceleration. This insures that the rudder trim function will be implemented. The final set of responses and weights were thus:

<u>Response</u>	<u>Quadratic Weight</u>
$p - p_m$	50
$\int n_{y_{Bl}}$	0.01
$r - p\alpha_o - \frac{g}{V_{T_o}} \phi$	2.5×10^3
u_A	1×10^3
u_R	3×10^3

Initially, independent designs were obtained for each of the five flight conditions studied. The quadratic weights turned out to be very close to the above values for all five flight conditions. Thus, these weights were used on all twenty flight conditions for the final designs. It might be conjectured that this set of responses and quadratic weights would be applicable to all similar aircraft. Experience has shown that the responses chosen for weighting are the correct responses for other aircraft, but the quadratic weights must be determined for each aircraft and, in general, are markedly different from application to application.

The primary responses used for evaluation during the design process were, p , r , n_{y_p} , ϕ , β , δ_A and δ_R . Generally, transient and frequency responses were obtained for each weight variation, and these responses along with the eigenvalues were used to evaluate the design with respect to the performance criteria.

During the course of the design, parametric variations were made in the roll rate model time constant and the sensed acceleration signal lag time constant to determine the best values. As presented in the discussion of the linear models, the model was chosen to have a time constant of 1/5 second and the lag a time constant of 1/4 second. Faster responding models tended to result in higher peak lateral accelerations at the pilot station because of the z-axis moment arm associated with roll rate, and slower models produced sluggish roll rate responses. The lag on the accelerometer was chosen to give the best turn coordination.

The effects of variations in each of the quadratic response weights can be summarized. Increasing the weight on roll rate error results in a sharper roll rate response with attendant increases in gain magnitudes and a deterioration in turn coordination. Increasing the weight on the coordination response ($r - p\alpha - g\phi/V$) improves coordination at the expense of higher gain magnitudes and, in the extreme, a deterioration in roll rate response. The weights on the controls u_A and u_R directly affect the gains to each control input and the stability margins of the system. Decreasing these weights results in high gains and good performance if stability considerations are ignored.

Gain Scheduling and Block Diagram Definition

The selected control dynamics, responses, and quadratic weights were used to obtain feedback gain matrices at all twenty of the flight conditions at which linear models had been derived. The result was thus a set of twenty fixed point controllers of the form

$$u = K^i x, \quad i = 1, 2, \dots, 20$$

$$u_A = K_{11}^i p + K_{12}^i r + K_{13}^i n_{y_s} + K_{14}^i \phi + K_{15}^i \delta_A + K_{16}^i \delta_R + K_{17}^i n_{y_{s1}} \\ + K_{18}^i n_{y_{sli}} + K_{19}^i p_m + K_{110}^i u_m$$

$$u_R = K_{21}^i p + K_{22}^i r + K_{23}^i n_{y_s} + K_{24}^i \phi + K_{25}^i \delta_A + K_{26}^i \delta_R + K_{27}^i n_{y_{s1}} \\ + K_{28}^i n_{y_{sli}} + K_{29}^i p_m + K_{210}^i u_m$$

$$i = 1, 2, 3, \dots, 20,$$

where the superscript i on the gains indicates the flight condition. The task at this point is to define a control system which operates throughout the flight envelope based on these gain matrices at specific flight conditions. The problem is basically one of determining gain schedules, where the gains are scheduled on acceptable (for mechanization) quantities which identify the flight condition for each gain. This could be done with the controller in the structure given above--that is, determine a schedule for each gain and implement the system as $u = K^i x$ where the elements of K^i are each a function of a flight condition parameter. Because of uncertainties in the models always associated with control designs and for mechanization reasons, a better approach is to consider the system structure prior to gain scheduling. A general rule of thumb is that it is better to specify gain schedules on error feedbacks rather than separate schedules on the component signals that are used to derive the error. In this way, the system will be less sensitive to compromises introduced when deriving the gain schedules and to uncertainties in the models used for design. Thus it is preferable to schedule a gain on $p - p_m$ rather than to define individual gain schedules on the p and p_m gains. As will be seen below, by considering the physics of the situation, the gains on r , p and ϕ constitute a synthesis of a $\dot{\beta}$ signal which is an error in turn coordination. Thus a structure which first synthesizes an estimate for $\dot{\beta}$ with a schedule on this quantity is better than implementing the system in the form $u = Kx$ with separate schedules on each component of the $\dot{\beta}$ signal.

The result of the application of the linear quadratic optimal control algorithms is a feedback gain matrix with a nonzero gain on every state to every control input. Several

of these gains are generally insignificant and can be set to zero without affecting performance. This also simplifies the controller structure. For the inertial coordination designs this was accomplished by arbitrarily zeroing gains and evaluating the performance. The practicalization algorithm, discussed in Section 5 and used on the second lateral-directional CAS design presented in the following section, could be used for this process, but this algorithm is really required only when modifying the basic structure or character of the system which is not being done here. In addition to arbitrarily zeroing insignificant gains, the gain on the accelerometer output n_{y_s} was transferred to the lagged accelerometer signal $n_{y_{sl}}$. The lag was included basically for noise filtering and phase compensation. Because of the structural noise content of the accelerometer output, this signal should not be fed directly to a surface actuator without prior filtering. Because this modification could affect system performance a careful check was made to determine any resulting performance differences. If there had been a significant change, the solution would have been to use the practicalization algorithm to effect the transfer. This was not required.

The gains which were arbitrarily set to zero for the reasons discussed above were:

- K_{15} - feedback around aileron actuator
- K_{16} - crossfeed from rudder surface position to aileron
- K_{18} - gain on $n_{y_{sli}}$ to aileron
- K_{26} - feedback around rudder actuator

A negative feedback around the actuator will effectively place a lead ahead of the actuator when implemented. This would cause mechanization problems and is to be avoided. During the design, this was not a problem as the gains were always very small. In a case where significant feedbacks do occur, weighting the actuator rate will eliminate them. Since the actuator feedbacks were negligibly small, they were eliminated.

The general procedure for obtaining gain schedules was to plot each gain value over the twenty flight conditions against candidate scheduling quantities. Any plot of a gain versus a parameter which is well behaved (not scattered), or in particular, monotonic identifies a potential for scheduling the gain on that parameter. There were five candidate parameters considered for scheduling. These were dynamic pressure (q), Mach number, true air speed, altitude (h) and angle-of-attach (α). In the quadratic optimal control formulation of the problem, the pilot stick input was modeled as a filtered white noise process. In defining the controller structure, the output of the filter becomes the pilot input, and the filter dynamics are dropped. Thus the gains on state 10, u_m , are the feedforward gains from the pilot stick input.

Roll Axis Gain Scheduling

Prior to determining schedules for the gains from the states to the aileron, the potential structure of the roll axis CAS was investigated. As mentioned above, three of the gains in this axis were initially set to zero with no performance difference ($K_{15} = K_{AA}$, $K_{16} = K_{A\delta_R}$, $K_{18} = K_{An_{y_{sli}}}$, where $K_{A\delta_R}$ is the gain from the rudder position, δ_R , to the aileron input u_A). This leaves six gains

$$K_{11} = K_{Ap} = \text{roll rate to aileron}$$

$$K_{12} = K_{Ar} = \text{yaw rate to aileron}$$

$K_{13} = K_{A_{n_{ys}}}$, transferred to $K_{17} = K_{A_{n_{ysi}}}$

$K_{14} = K_{A_{\phi}}$ = bank angle to aileron

$K_{17} = K_{13}$ = lateral acceleration to aileron

$K_{19} = K_{A_{p_m}}$ = roll rate model to aileron

$K_{110} = K_{A_{u_m}}$ = pilot stick input to aileron

Because of the significant gains on r and ϕ to the aileron, it is possible that the gains on r , ϕ , and part of the p gain constitute a synthesis of a β signal. If lateral acceleration is assumed to be negligibly small, the y -force equation becomes

$$-\dot{\beta} = r - p\alpha - \frac{g}{V_{T_0}} \cos \theta \sin \phi.$$

The linearized equation is

$$-\dot{\beta} = r - p\alpha_0 - \frac{g}{V_{T_0}} \phi.$$

The feedback structure as defined by the gains matrix is shown in Figure 74. If the gains do constitute a synthesis of β , then the gain on ϕ for the linear case should have a factor of g/V_{T_0} , and a component of the roll rate feedback should appear as $p\alpha$. Rearranging the block diagram, without changing any of the loop gains, results in the structure shown in Figure 75 where

$$K'_{14} = \frac{K_{14}}{g/V_{T_0}}$$

$$K'_{11} = K_{11} - \alpha \left(\frac{K_{14}}{g/V_{T_0}} \right)$$

$$K'_{12} = \frac{K_{12}}{-K'_{14}}$$

If a β feedback is being synthesized, then the yaw rate gain K'_{12} should be approximately constant and equal to one. This indeed is the case as will be seen from the schedules presented below. Note that the roll rate feedback has been split into two components, the first a $p\alpha$ term with a scheduled gain K'_{14} and the second the remainder of the original K_{11} gain specified. Figure 76 is a rearrangement of the stick input and the remaining roll rate feedback paths. The block diagram of Figure 76 is equivalent to the diagram shown in Figure 77, where

$$K_a = \frac{K_{110} + K_{19}}{-K'_{11}}$$

and

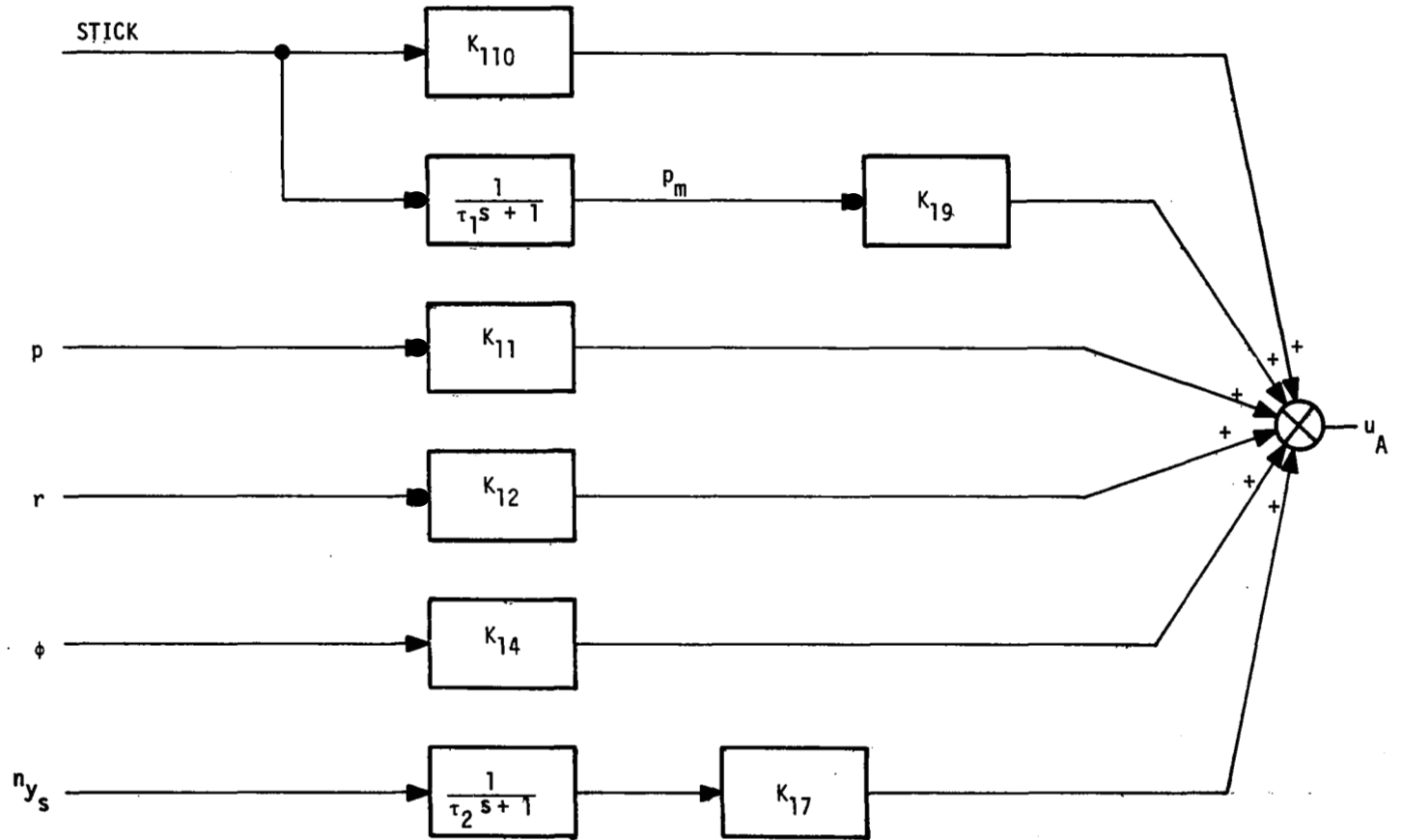


Figure 74. Lateral CAS Structure

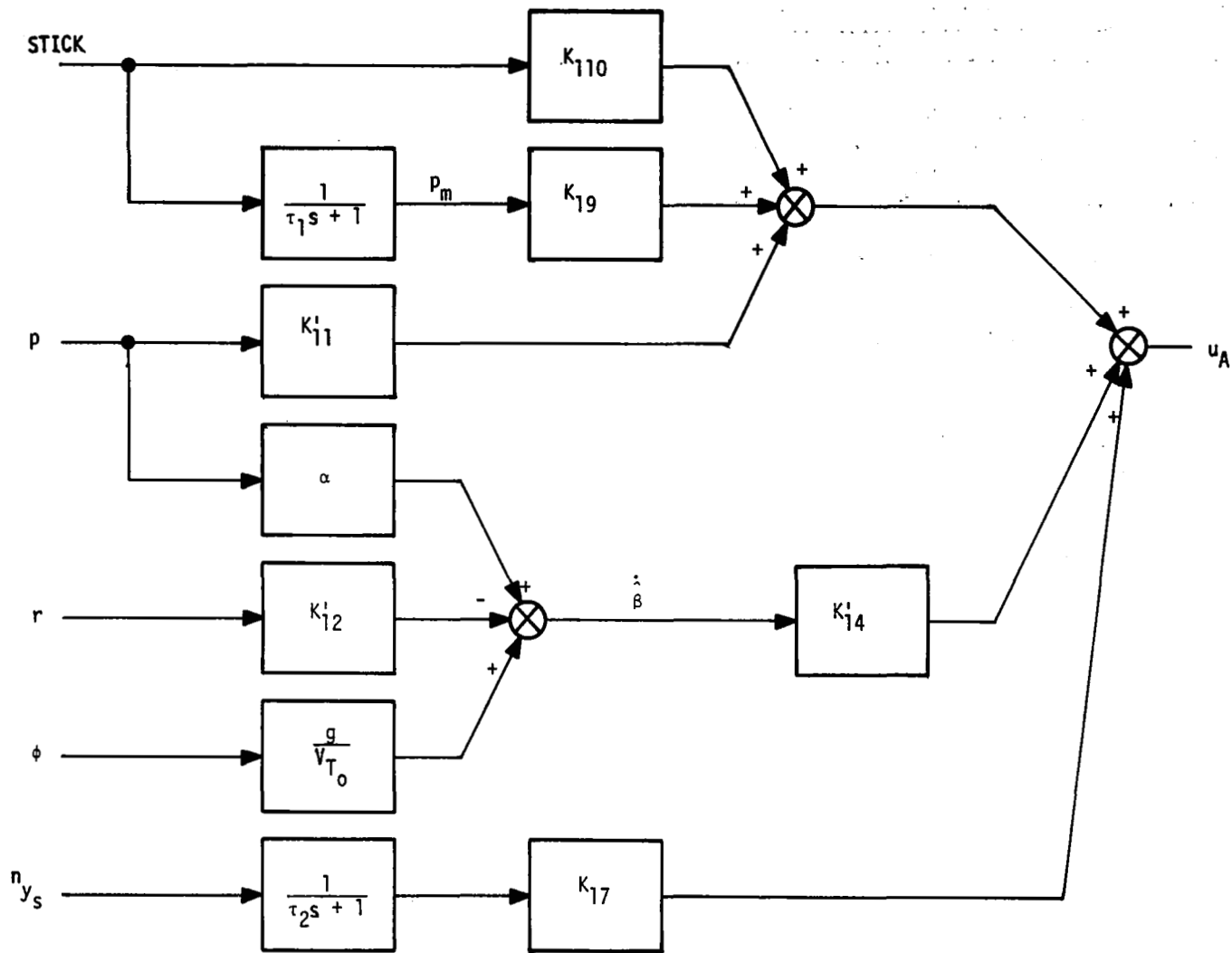


Figure 75. Alternate Lateral CAS Structure

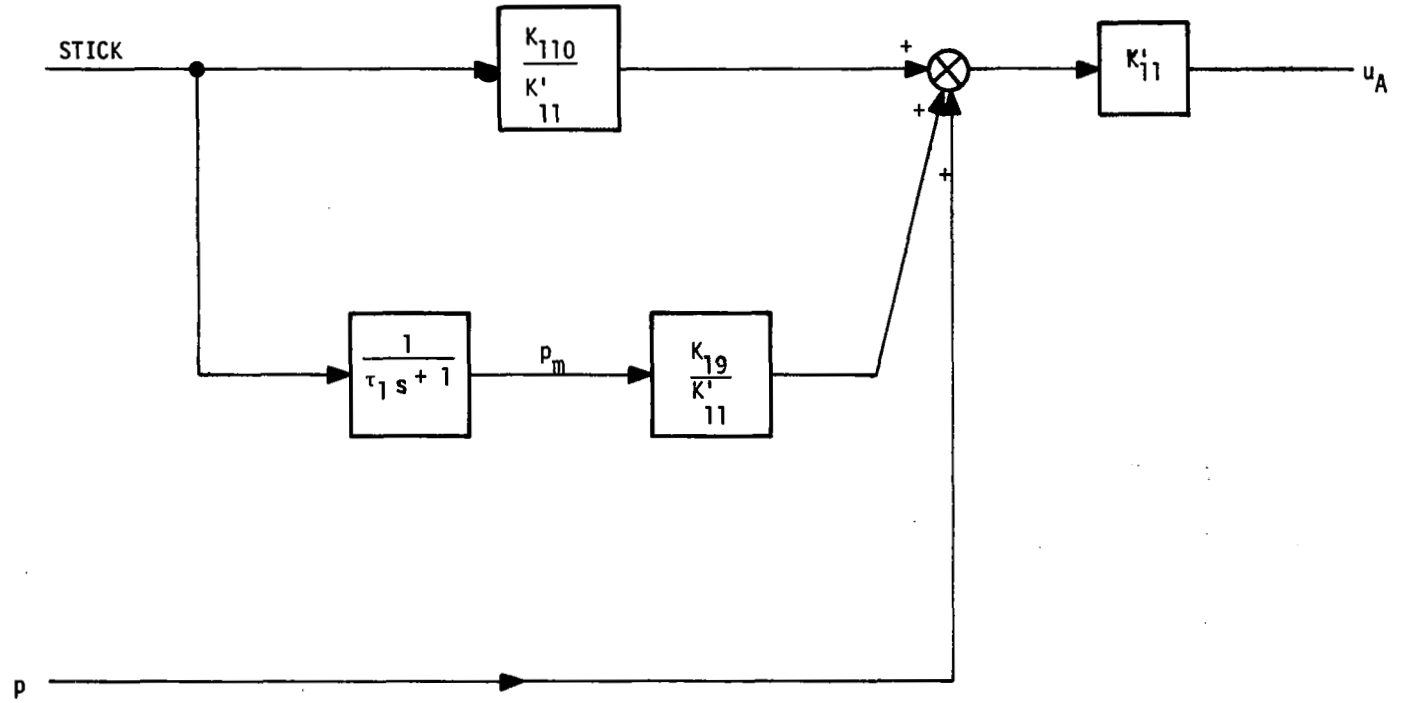


Figure 76. Roll Rate Command

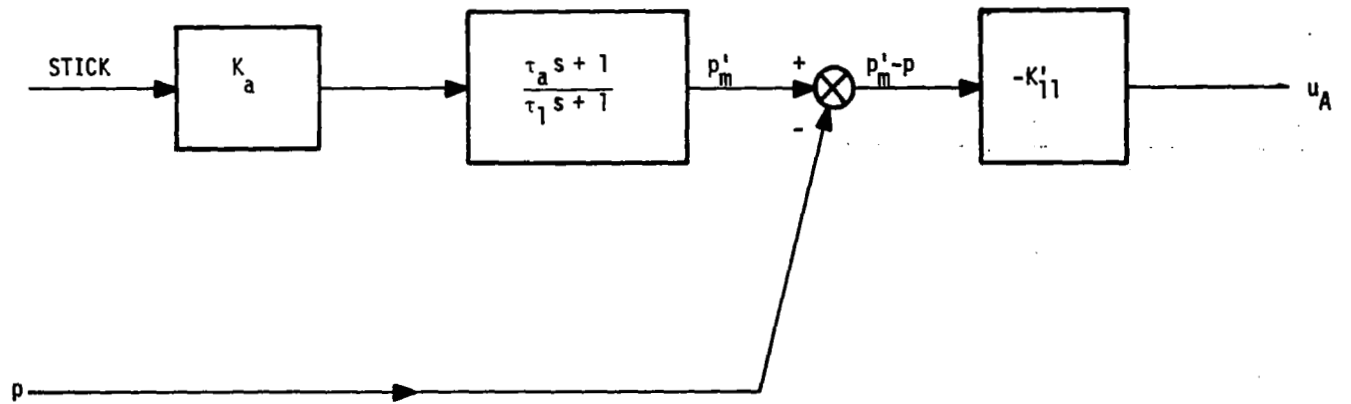


Figure 77. Roll Rate Error Command

$$\tau_a = \frac{K_{110}}{K_{110} + K_{19}} \tau_1$$

Up to this point no actual modifications to the original gains have been made. Two modifications are now made. With the present structure of driving the aileron with a roll rate error signal, stick shaping is implicitly provided. Thus the gain K_a , which can be identified as a stick shaping gain, was set to one. Because of the new structure imposed, this does not affect the dynamic performance of the system.

The second modification was to eliminate the zero in the equivalent roll rate model. The time constant τ_a was approximately constant and equal to $\tau_1/2$. The effect of the zero is thus to quicken the model response. Because initial lateral acceleration peaks at the pilot station for step stick inputs were relatively high (but still acceptable), this zero was eliminated. A check of transient responses without the zero showed no significant change in the roll rate response, and the initial lateral acceleration peak was reduced somewhat.

With these modifications the controller structure is now as shown in Figure 78. This is the final roll axis system structure used for scheduling the gains.

The five remaining gains were plotted against each of the potential scheduling parameters (\bar{q} , Mach, V_{T0} , h , α) to determine the best choice for scheduling. The gains are relabeled for clarity as follows:

$$K_{Ae} = -K'_{11}$$

$$K_{A\dot{\beta}} = K'_{14}$$

$$K_{Ar} = K'_{12}$$

$$K_{An_{y_{sl}}} = K'_{17}$$

A plot of each gain K_{Ar} versus angle-of-attack is shown in Figure 79. If the gains on r , ϕ and α are, in effect, synthesizing a $\dot{\beta}$ signal, the yaw rate gain should have a constant value of one. As can be seen from the figure, this is a fair approximation (except for two spurious points), and thus K_{Ar} was set to unity.

The gain $K_{A\dot{\beta}}$ was plotted against all the potential scheduling parameters. Most plots were quite random except for the plot against angle-of-attack which is shown in Figure 80. For this gain angle-of-attack was chosen as the scheduling parameter, and the schedule is shown in the figure.

The roll rate error gain was most uniform when plotted against angle-of-attack which is shown in Figure 81. A simple constant value was chosen for this gain. Finally the gain $K_{An_{y_{sl}}}$ is shown in Figure 82 plotted versus angle-of-attack. The gain variation was not well behaved for any of the candidate parameters. Because the gain was very small and not amenable to scheduling, it was dropped (set to zero). Little performance difference was noted. The resulting schedules are shown on the system block diagram, Figure 91.

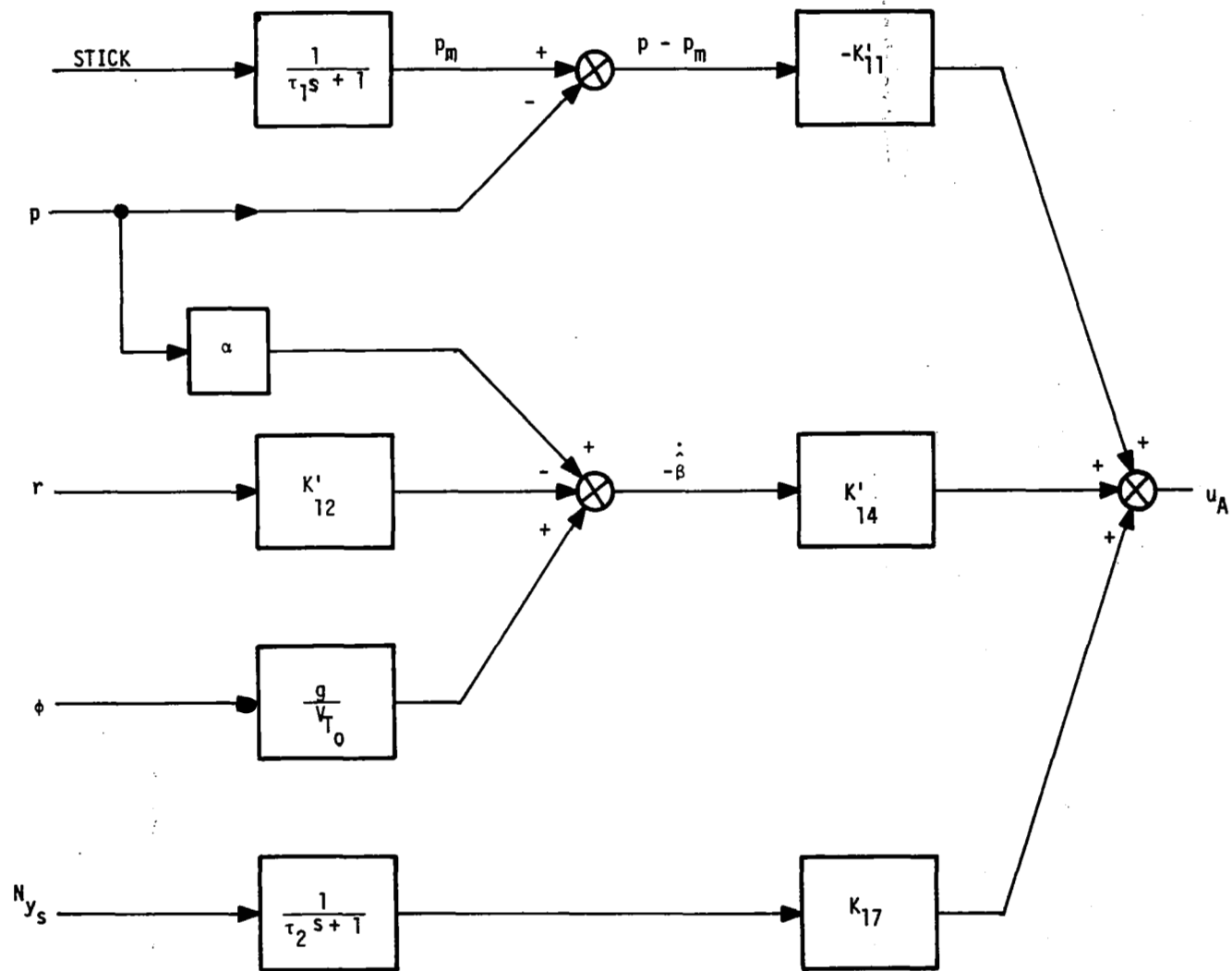
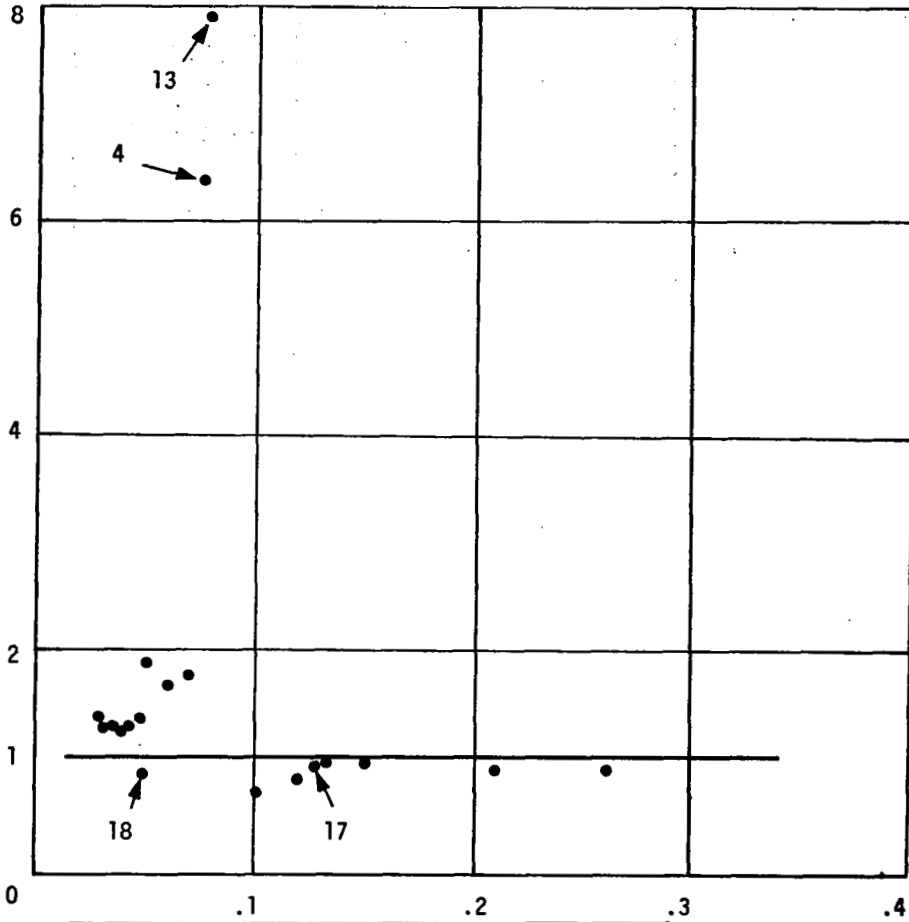


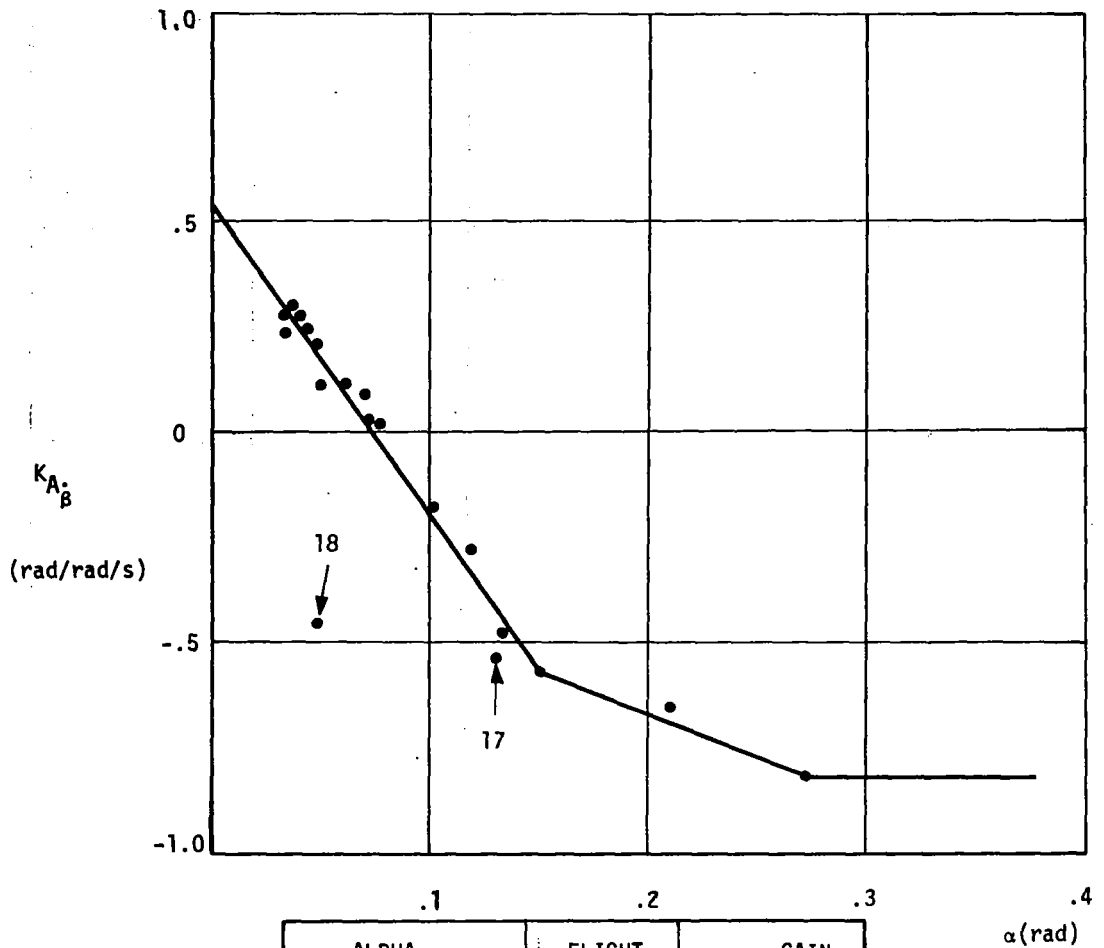
Figure 78. Roll Axis Structure

K_{Ar}
(rad/rad/s)



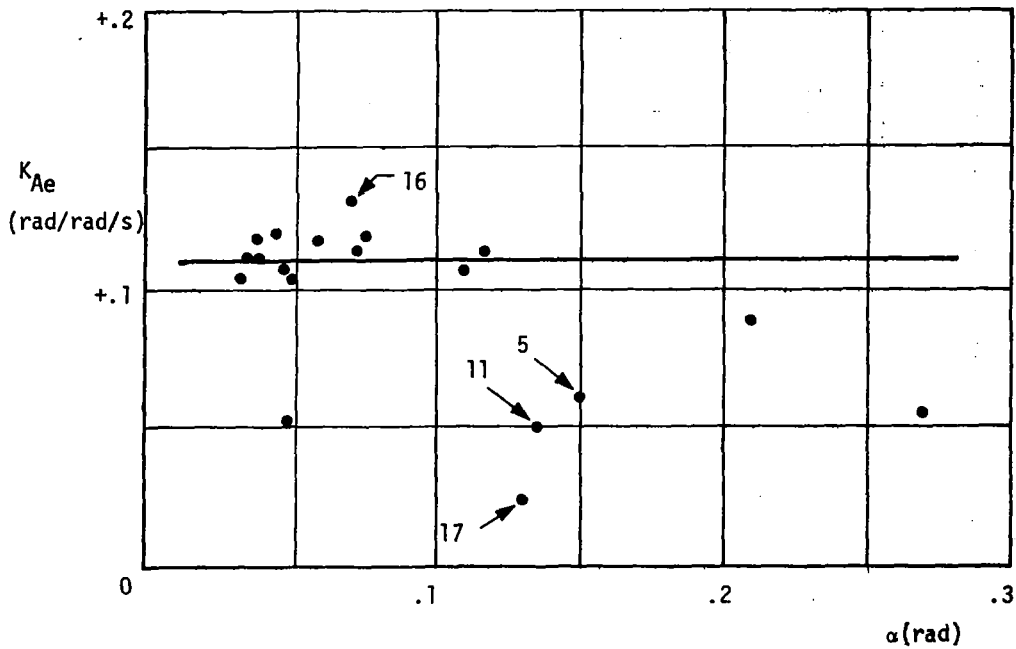
ALPHA	FLIGHT CONDITION	GAIN
.32463E-01	10	1.97
.34208E-01	9	1.30
.37001E-01	19	1.29
.38048E-01	6	1.28
.43310E-01	14	1.33
.47470E-01	8	1.39
.48171E-01	18	.837
.50265E-01	12	1.89
.60213E-01	1	1.66
.71209E-01	16	1.77
.74176E-01	13	7.93
.75398E-01	4	6.35
.10646E+00	2	.64
.11746E+00	7	.80
.13055E+00	17	.919
.13334E+00	11	.90
.15464E+00	5	.92
.21153E+00	3	.88
.26965E+00	20	.871

Figure 79. K_{Ar} Schedule



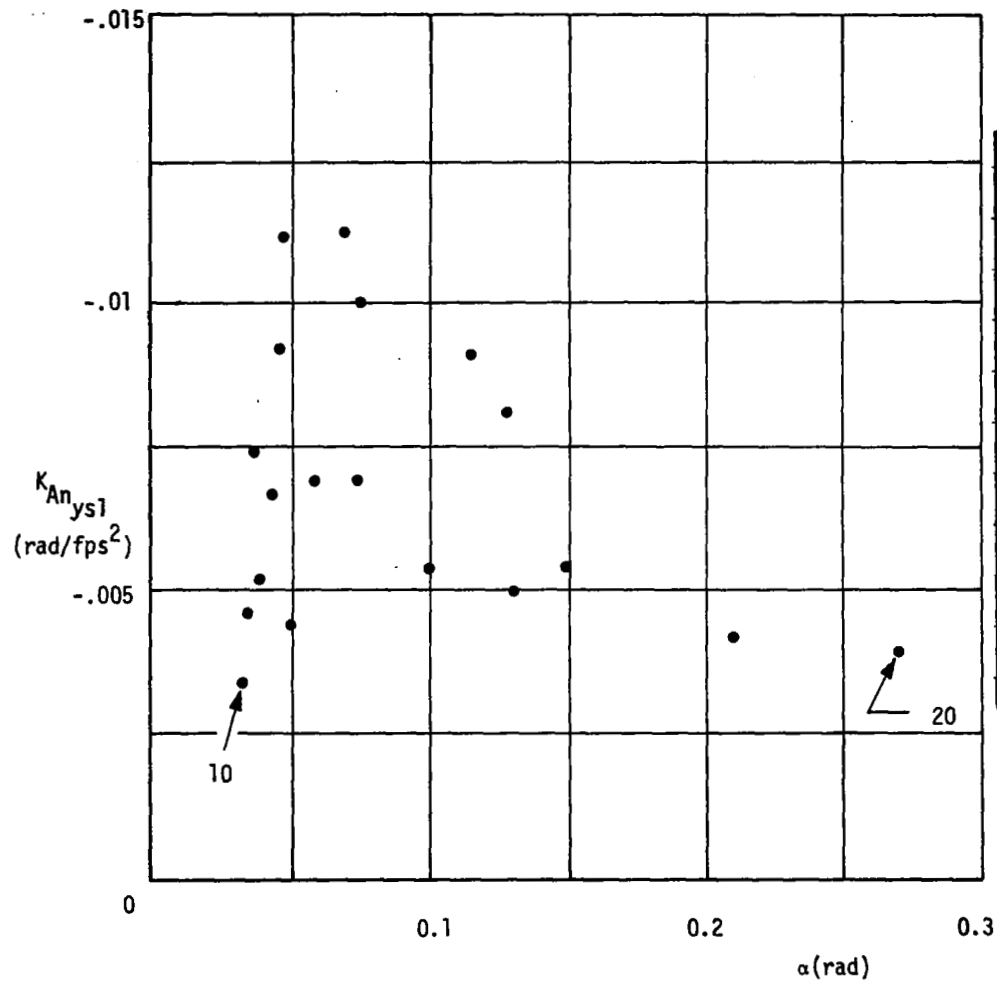
ALPHA	FLIGHT CONDITION	GAIN
.32463E-01	10	.243
.34208E-01	9	.276
.37001E-01	19	.281
.38048E-01	6	.285
.43310E-01	14	.241
.47470E-01	8	.218
.48171E-01	18	-.464
.50265E-01	12	.103
.60213E-01	1	.122
.71209E-01	16	.087
.74176E-01	13	.012
.75398E-01	4	.016
.10646E+00	2	-.200
.11746E+00	7	-.283
.13055E+00	17	-.588
.13334E+00	11	-.487
.15464E+00	5	-.571
.21153E+00	3	-.666
.26965E+00	20	-.829

Figure 80. $K_{A\beta}$ Schedule



ALPHA	FLIGHT CONDITION	GAIN
.32463E-01	10	.105
.34208E-01	9	.111
.37001E-01	19	.119
.38048E-01	6	.112
.43310E-01	14	.121
.47470E-01	8	.106
.48171E-01	18	.054
.50265E-01	12	.103
.60213E-01	1	.118
.71209E-01	16	.131
.74176E-01	13	.113
.75398E-01	4	.117
.10646E+00	2	.109
.11746E+00	7	.114
.13055E+00	17	.024
.13334E+00	11	.054
.15464E+00	5	.060
.21153E+00	3	.088
.26965E+00	20	.056

Figure 81. K_{Ae} Schedule



ALPHA	FLIGHT CONDITION	GAIN
.32463E-01	10	-.34871E-02
.34208E-01	9	-.46169E-02
.37001E-01	19	-.73665E-02
.38048E-01	6	-.51854E-02
.43310E-01	14	-.66217E-02
.47470E-01	8	-.92779E-02
.48171E-01	18	-.12313E-01
.50265E-01	12	-.44030E-02
.60213E-01	1	-.68930E-02
.71209E-01	16	-.11891E-01
.74176E-01	13	-.69875E-02
.75398E-01	4	-.10810E-01
.10646E+00	2	-.53894E-02
.11746E+00	7	-.90918E-02
.13055E+00	17	-.82444E-02
.13334E+00	11	-.49428E-02
.15464E+00	5	-.52729E-02
.21153E+00	3	-.41537E-02
.26965E+00	20	-.37656E-02

Figure 82. $K_{An_{syl}}$ Schedule

Yaw Axis Gain Scheduling

The procedure for scheduling the yaw axis gains was similar to the roll axis. The gains to be scheduled were

$$K_{21} = K_{Rp} = \text{roll rate to rudder}$$

$$K_{22} = K_{Rr} = \text{yaw rate to rudder}$$

$$K_{24} = K_{R\phi} = \text{roll angle to rudder}$$

$$K_{25} = K_{R\delta A} = \text{aileron to rudder crossfeed}$$

$$K_{27} = K_{Rn_{ysl}} = \text{lagged accelerometer output to rudder}$$

$$K_{28} = K_{Rn_{ysli}} = \text{integral of lagged accelerometer to rudder}$$

$$K_{29} = K_{Rp.m} = \text{roll rate model output to rudder}$$

$$K_{210} = K_{Ru.m} = \text{pilot stick input to rudder}$$

As with the roll axis, it was suspected that the feedback gains on roll rate, yaw rate, and bank angle determined by the quadratic design process constitutes a synthesis of an estimate for sideslip rate β . The roll angle gain was considered first. Figure 83 is a plot of $K_{R\phi}$ against true airspeed. The locus of points is seen to approximate an inverse dependency on V_{T_o} . Fitting a curve to these points results in

$$K_{24} = \frac{22}{V_{T_o}} + .003$$

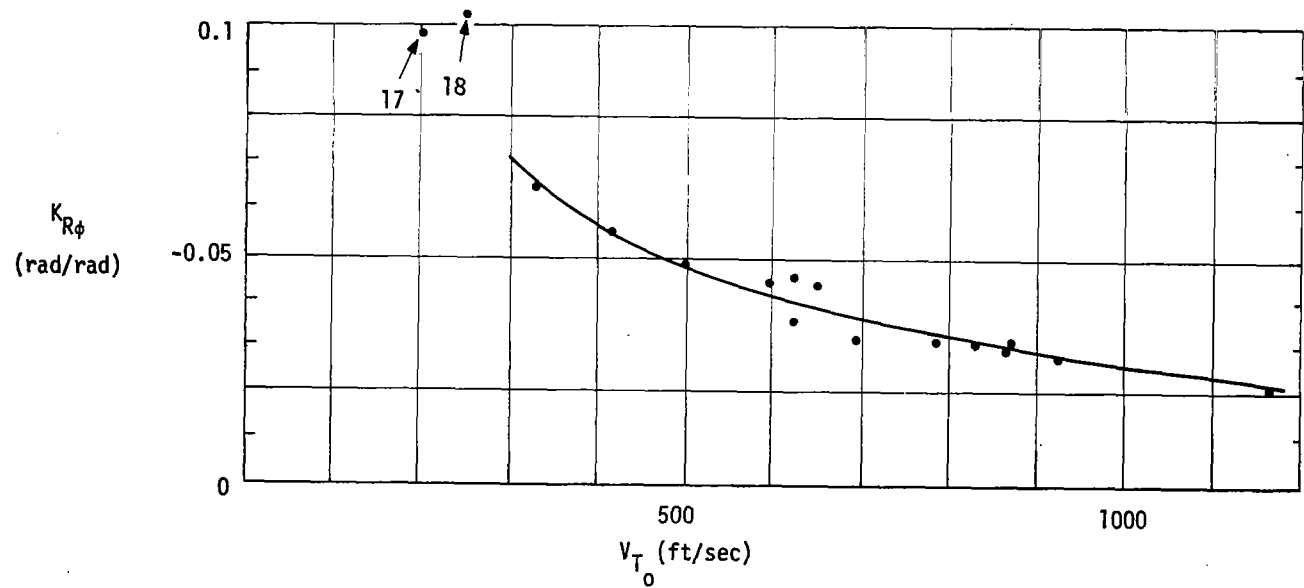
The ratio

$$\frac{g/V_{T_o}}{\frac{22}{V_{T_o}} + .003}$$

is approximately 1.4. Thus the $K_{R\phi}$ schedule was defined to be g/V_{T_o} which must then be followed by a gain of $1/1.4$ ($K'_{R\phi}$) to preserve the magnitude of the original roll angle gain. The structure is now specified if the yaw rate and roll rate gains have the expected variation, in which a β signal is synthesized followed by a constant gain of $K'_{R\phi}$.

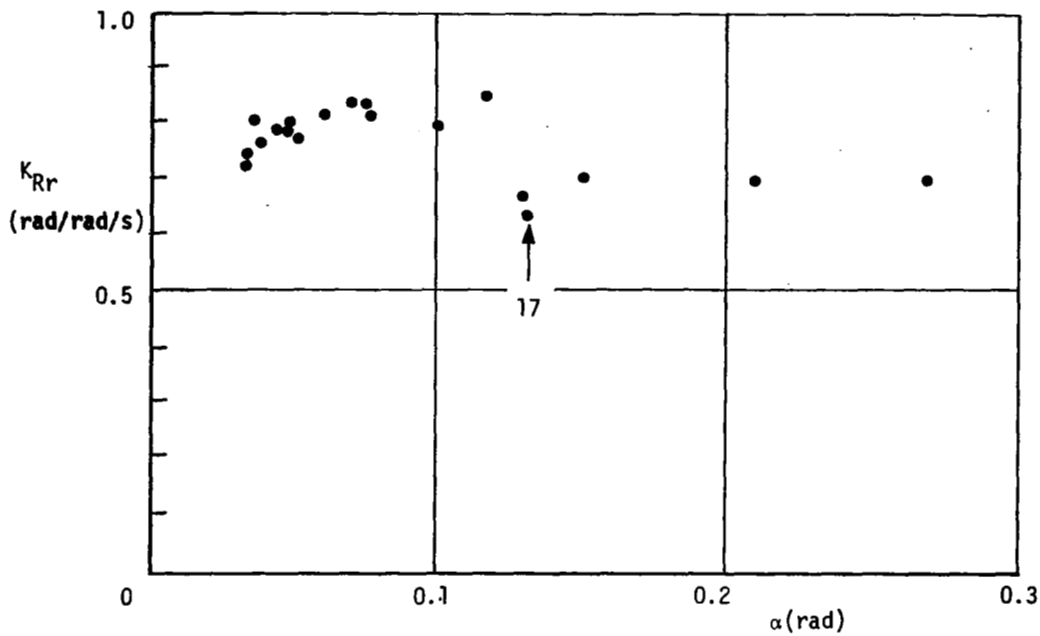
Consider the yaw rate gain first. Figure 84 is a plot of K_{22} versus α . The gain is approximately constant and equal to 0.77. Assuming that r is to be used to synthesize the β signal which is to have a gain on it of $K'_{R\beta}$ (determined by the K_{24} manipulation), K_{22} must be multiplied by 1.4.

This gives a constant value of 1.07 which was approximated by a unity gain. The roll rate gain to the rudder K_{21} plotted against α is shown in Figure 85. The gain is definitely linear with angle-of-attack, with a slope of 0.38 instead of 1.0 as expected. Rather than force the gain to be equivalent to angle-of-attack, the schedule shown was used which results in a feedback of the form $p(m\alpha + b)$ rather than $p\alpha$. After scaling by 1.4, as with yaw rate, the slope becomes 0.54 and the intercept 0.042. The final scheduled gain K_{Rp} is shown on the block diagram of Figure 92.



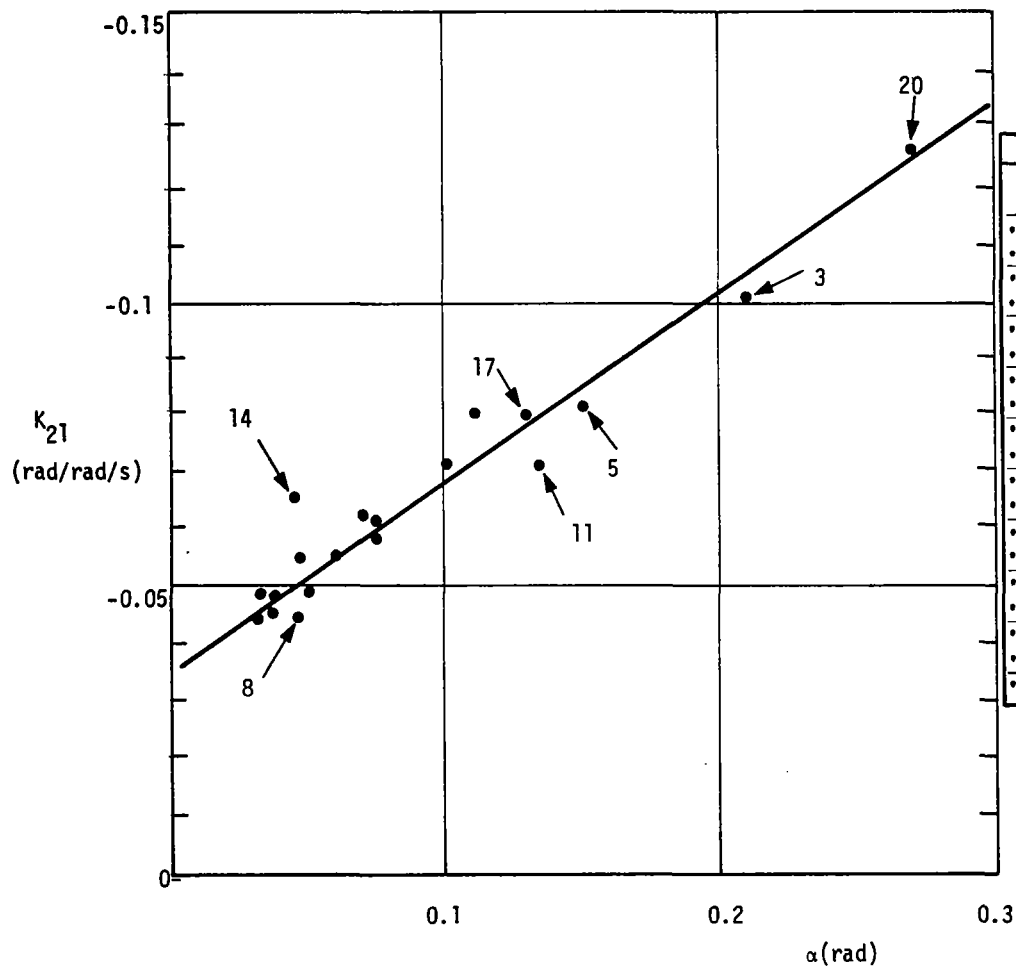
V (FT/SEC)	FLIGHT CONDITION	GAIN
.21100E+03	17	-.98160E-01
.24500E+03	18	-.10487E+00
.33500E+03	11	-.65870E-01
.41500E+03	5	-.54804E-01
.59200E+03	12	-.43964E-01
.62300E+03	13	-.44754E-01
.62300E+03	20	-.35807E-01
.67800E+03	7	-.40938E-01
.69500E+03	1	-.39292E-01
.69500E+03	2	-.38273E-01
.69500E+03	3	-.32742E-01
.69500E+03	19	-.38601E-01
.69500E+03	4	-.39590E-01
.78200E+03	10	-.32820E-01
.83000E+03	14	-.31809E-01
.86300E+03	9	-.29469E-01
.87200E+03	16	-.31957E-01
.93400E+03	6	-.27978E-01
.11630E+04	8	-.22858E-01

Figure 83. $K_{R\phi}$ vs. V_{T_0}



ALPHA	FLIGHT CONDITION	GAIN
.32463E-01	10	.73166E+00
.34208E-01	9	.73627E+00
.37001E-01	19	.80372E+00
.38048E-01	6	.76857E+00
.43310E-01	14	.78172E+00
.47470E-01	8	.79516E+00
.48171E-01	18	.80271E+00
.50265E-01	12	.77245E+00
.60213E-01	1	.82248E+00
.71209E-01	16	.84635E+00
.74176E-01	13	.84537E+00
.75398E-01	4	.82988E+00
.10646E+00	2	.80677E+00
.11746E+00	7	.85579E+00
.13055E+00	17	.64847E+00
.13334E+00	11	.66948E+00
.15464E+00	5	.70197E+00
.21153E+00	3	.69804E+00
.26965E+00	20	.69434E+00

Figure 84. K_{Rr} vs. α



ALPHA	FLIGHT CONDITION	GAIN
.32463E-01	10	-.43012E-01
.34208E-01	9	-.48447E-01
.37001E-01	19	-.45709E-01
.38048E-01	6	-.47066E-01
.43310E-01	14	-.51545E-01
.47470E-01	8	-.43030E-01
.48171E-01	18	-.54039E-01
.50265E-01	12	-.48013E-01
.60213E-01	1	-.55018E-01
.71209E-01	16	-.62236E-01
.74176E-01	13	-.60192E-01
.75398E-01	4	-.58804E-01
.10646E+00	2	-.70777E-01
.11746E+00	7	-.80196E-01
.13055E+00	17	-.80123E-01
.13334E+00	11	-.70723E-01
.15464E+00	5	-.81055E-01
.21153E+00	3	-.10262E+00
.26965E+00	20	-.12632E+00

Figure 85. K_{21} vs. α

The gain $K_{Rn_{ys1}}$ is plotted versus dynamic pressure in Figure 86. Recall that this gain is actually $K_{Rn_{ys1}} \bar{K}_{23}$ which was transferred to the lagged accelerometer signal. The gain magnitude on the lagged accelerometer signal specified by the quadratic design was very small. In transferring the feedback from the accelerometer to the lagged signal, the sign was reversed. The gain K_{27} was positive (but small) while K_{23} was negative. In previous designs with the same structure, this gain was positive. Test runs were made with both signs for $K_{Rn_{ys1}}$, and although little difference was noted, coordination was improved somewhat for the positive feedback. It is felt that the phase shift introduced by the lag accounts for this. As will be seen in the next section where the practicalization algorithm was used, the algorithm effectively reversed the sign. Because the gain is small and quite scattered for all candidate scheduling parameters, a constant value of 0.002 was chosen.

The integral gain $K_{Rn_{ysli}}$ plot versus dynamic pressure is shown in Figure 87. Because the gain is small a constant value of 0.0085 was chosen. The principle reason for the integral feedback was to permit automatic rudder trim. This criteria was not really reflected in the quadratic cost function. The gain shown is actually making a small contribution to turn coordination. From past experience the trim function is adequately provided by a gain of the magnitude selected.

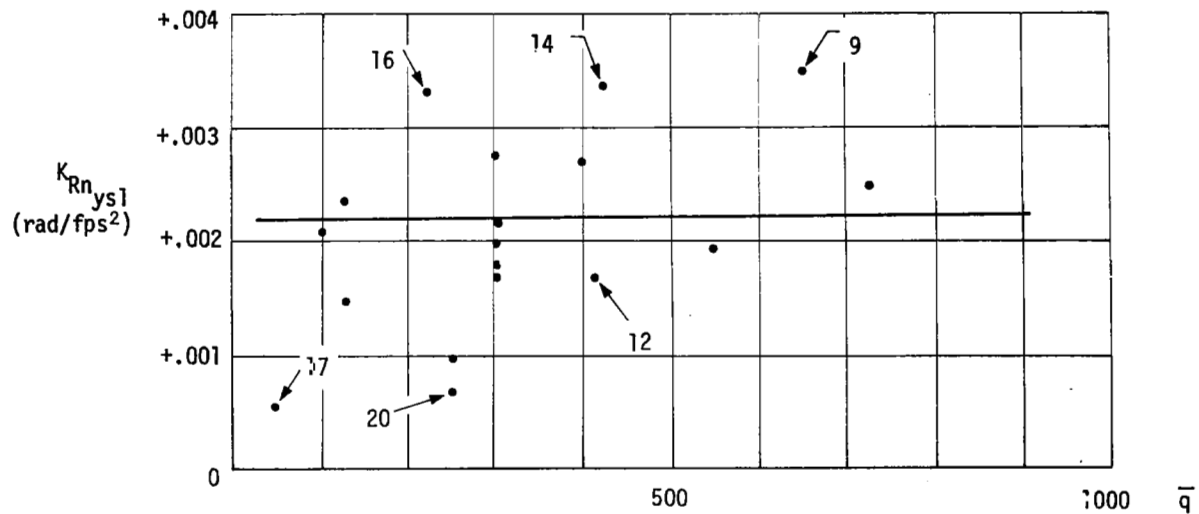
The fact that both the proportional and integral accelerometer gains decrease with increasing dynamic pressure or angle of attack is interesting. One would expect that as angle-of-attack increases and coordination becomes more difficult (or directional stability is lost) the gain would increase. This does not occur because for low dynamic pressures and thus high angles of attack mis-coordination is reflected predominately in sideslip rather than lateral acceleration. Thus the quadratic algorithms place a small gain on the signal since it is ineffective for coordination.

A constant value of 0.13 was chosen for the aileron to rudder crossfeed gain $K_{R\delta_A}$ shown in Figure 88. At high \bar{q} and low angles of attack this crossfeed had a small effect on turn coordination. For lower dynamic pressures it had essentially no effect, and no change was noted in setting it constant. The variation of the crossfeed with \bar{q} and α will be seen to be markedly different in the next section for the system without inertial coordination. There, the gain increases significantly with α or \bar{q} where it is required for coordination. For this design it is really not required and has small effect.

Two other crossfeeds from the roll axis are shown in Figures 89 and 90. The crossfeeds are from the roll rate model to rudder and from the pilot stick input to rudder. The gains are small and the main effects are to improve the roll rate response.

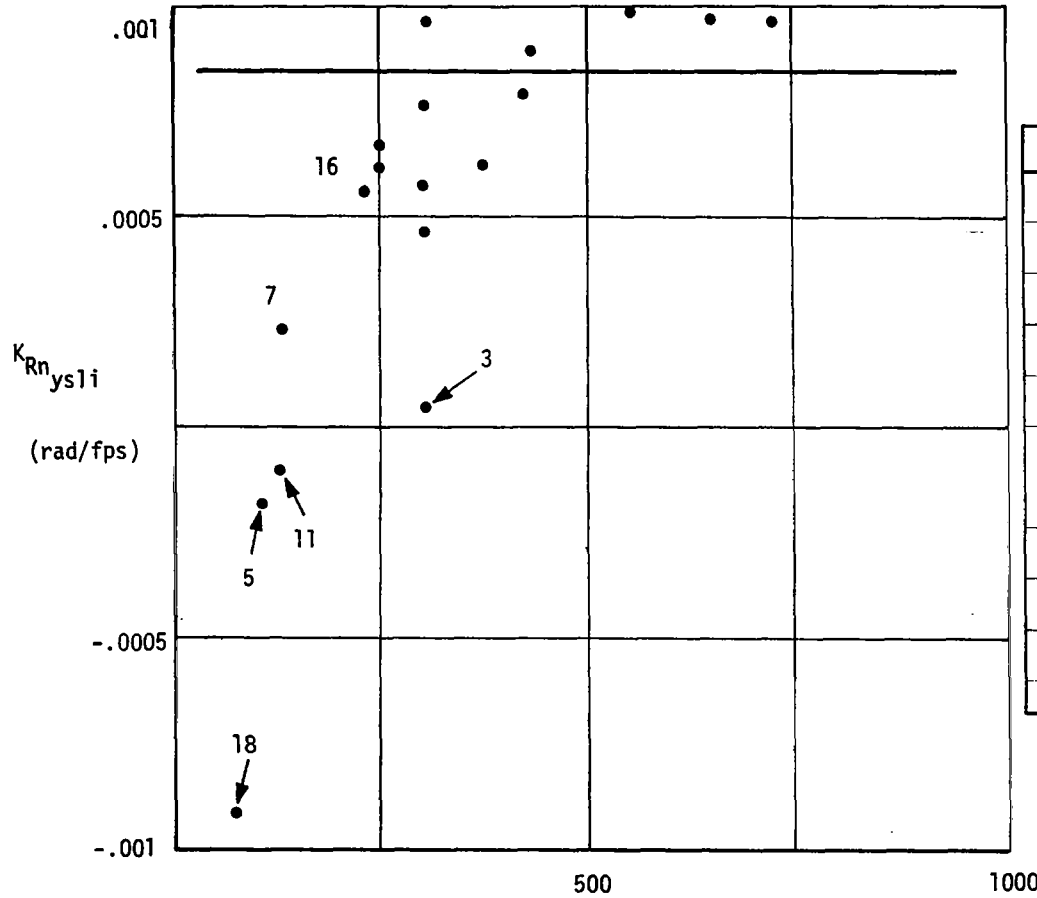
The formulation of the problem did not include the capability for a pilot rudder input since the control augmentation system's normal operation does not require any direct rudder control by the pilot. In order to provide for rudder control, primarily during landing, a direct path from rudder pedals to the rudder servos was added. The gain in this path initially was arbitrarily chosen as unity (rad/in). During the hardware simulator checkout this gain was found to be appropriate. Note that with the $\hat{\beta}$ feedback in the yaw axis, a rudder pedal input with no stick input is effectively a sideslip command.

The linear models and feedback gains determined via quadratics indicate a feedback of roll angle φ . By inspection of the $\hat{\delta}$ equation presented above it can be seen that this signal should be $\sin \varphi$, and an additional factor of $\cos \theta$ should be incorporated in the $g/\sqrt{V_T} \sin \varphi$ feedback term for completeness.



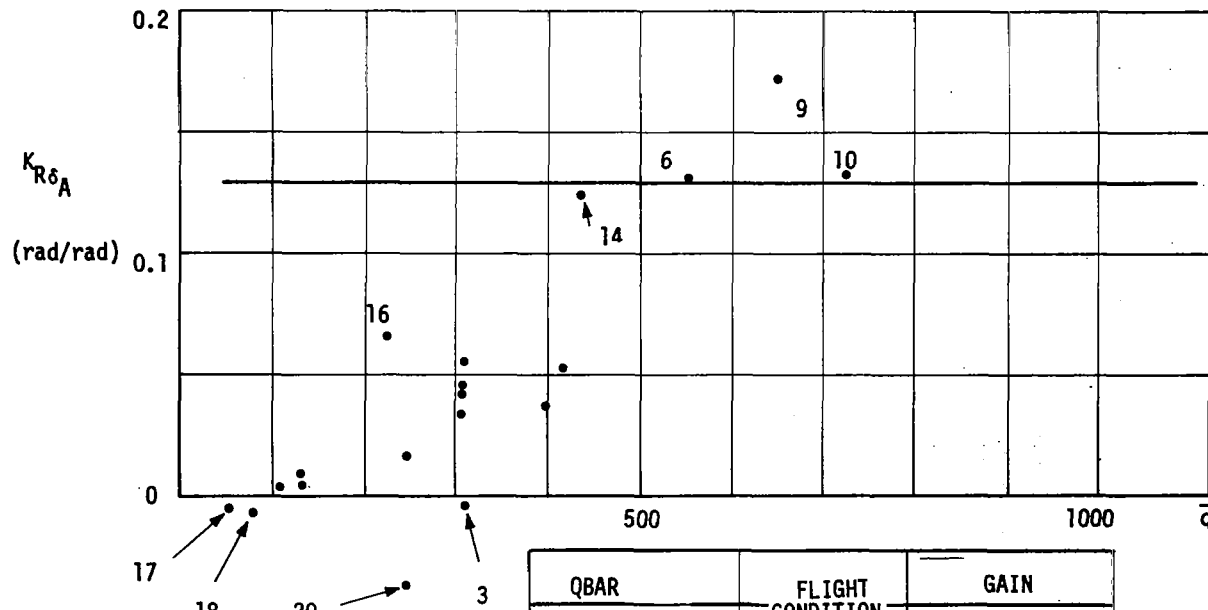
QBAR	FLIGHT CONDITION	GAIN
.53000E+02	17	+.54405E-03
.71000E+02	18	.93628E-03
.10900E+03	5	+.20907E-02
.13300E+03	11	+.23659E-02
.13400E+03	7	+.14596E-02
.22200E+03	16	+.33129E-02
.24500E+03	13	+.99048E-03
.24500E+03	20	+.62065E-03
.30500E+03	1	+.17521E-02
.30500E+03	2	+.19978E-02
.30500E+03	3	+.21569E-02
.30500E+03	19	+.18805E-02
.30500E+03	4	+.27475E-02
.39500E+03	8	+.26663E-02
.41600E+03	12	+.16407E-02
.43500E+03	14	+.33201E-02
.55100E+03	6	+.29228E-02
.65200E+03	9	+.34810E-02
.72500E+03	10	+.24167E-02

Figure 86. $K_{Rn_{ys1}}$ Schedule



QBAR	FLIGHT CONDITION	GAIN
.53000E+02	17	-.12234E-02
.71000E+02	18	-.82016E-03
.10900E+03	5	-.18021E-03
.13300E+03	11	-.11159E-03
.13400E+03	7	.23035E-03
.22200E+03	16	.57471E-03
.24500E+03	13	.66899E-03
.24500E+03	20	.62847E-04
.30500E+03	1	.76287E-03
.30500E+03	2	.45616E-03
.30500E+03	3	.37411E-04
.30500E+03	19	.92448E-03
.30500E+03	4	.57452E-03
.39500E+03	8	.62855E-03
.41600E+03	12	.79405E-03
.43500E+03	14	.88348E-03
.55100E+03	6	.98442E-03
.65200E+03	9	.97876E-03
.72500E+03	10	.97804E-03

Figure 87. $K_{Rn_{ysli}}$ Schedule



QBAR	FLIGHT CONDITION	GAIN
.53000E+02	17	-.64459E-02
.71000E+02	18	-.82206E-02
.10900E+03	5	.14823E-02
.13300E+03	11	.82865E-02
.13400E+03	7	.50270E-02
.22200E+03	16	.66829E-01
.24500E+03	13	.19112E-01
.24500E+03	20	-.38609E-01
.30500E+03	1	.44165E-01
.30500E+03	2	.32325E-01
.30500E+03	3	-.62145E-02
.30500E+03	19	.54720E-01
.30500E+03	4	.43335E-01
.39500E+03	8	.37720E-01
.41600E+03	12	.51696E-01
.43500E+03	14	.12443E+00
.55100E+03	6	.13142E+00
.65200E+03	9	.17382E+00
.72500E+03	10	.13167E+00

Figure 88. $K_{R\delta_A}$ Schedule

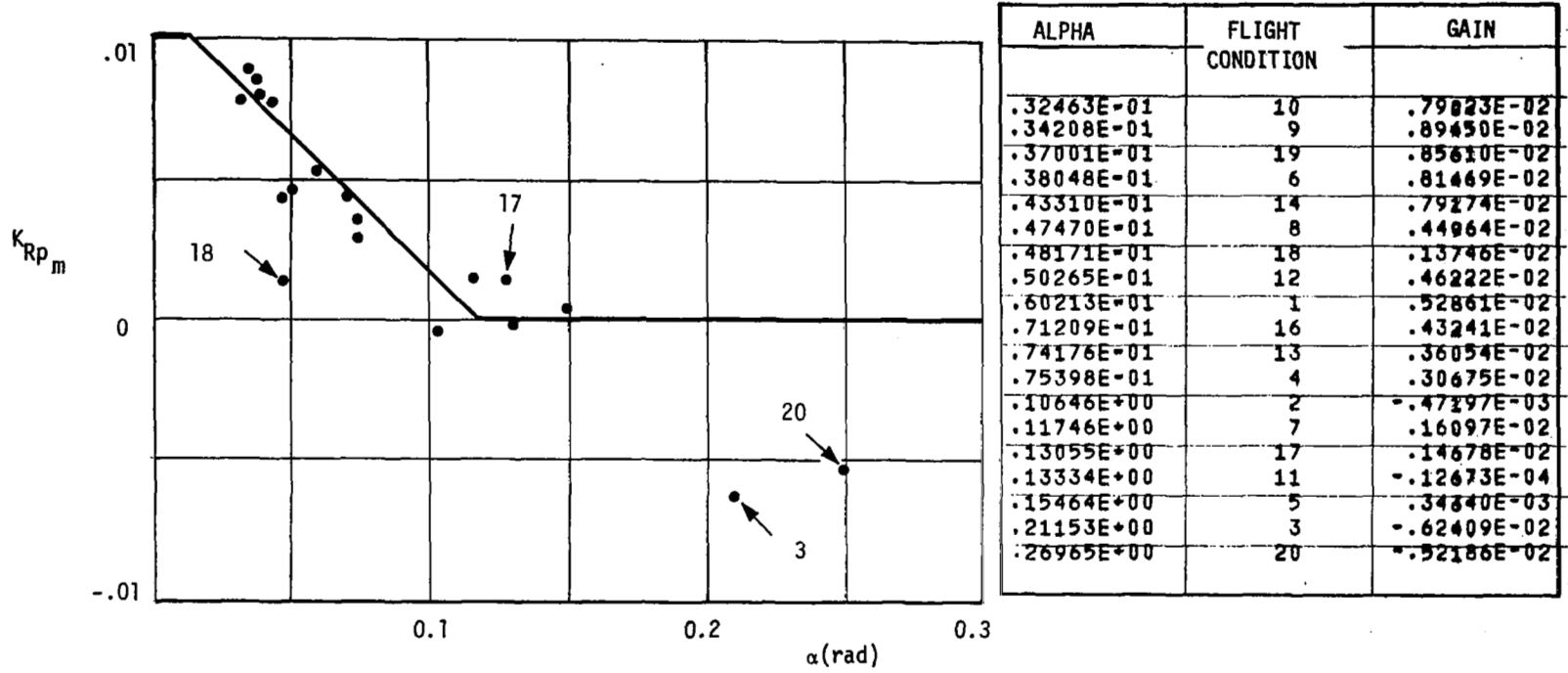
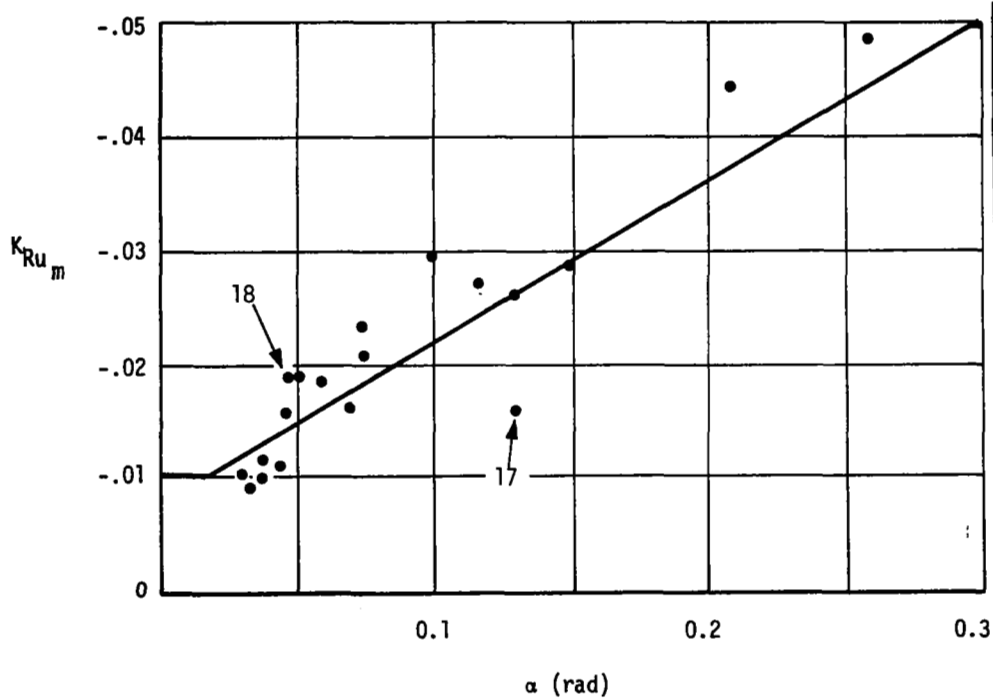


Figure 89. K_{Rp_m} Schedule



ALPHA	FLIGHT CONDITION	GAIN
.32463E-01	10	-.11074E-01
.34208E-01	9	-.95415E-02
.37001E-01	19	-.10241E-01
.38048E-01	6	-.12085E-01
.43310E-01	14	-.11198E-01
.47470E-01	8	-.16011E-01
.48171E-01	18	-.18971E-01
.50265E-01	12	-.18305E-01
.60213E-01	1	-.18992E-01
.71209E-01	16	-.16051E-01
.74176E-01	13	-.23401E-01
.75398E-01	4	-.21612E-01
.10646E+00	2	-.29944E-01
.11746E+00	7	-.27247E-01
.13055E+00	17	-.16644E-01
.13334E+00	11	-.26381E-01
.15464E+00	5	-.28586E-01
.21153E+00	3	-.42057E-01
.26965E+00	20	-.48022E-01

Figure 90. K_{Ru_m} Schedule

The reader will note that most of the scheduled gains are scheduled on angle-of-attack whereas conventionally the predominant scheduling parameter is dynamic pressure. The reason for this is straight-forward. Angle-of-attack is a prime lateral-directional axes rigid body dynamics variable. Variations with angle-of-attack were taken into account by designing at both cruise and maneuver conditions.

Lateral-Directional Control Augmentation System Block Diagrams

The block diagrams for the roll and yaw axis control augmentation systems are shown in Figures 91 and 92 for the roll and yaw axes, respectively. The system is shown in the continuous form. Digitized versions are presented below. Now that the system is in a conventional format the operation can be conveniently summarized. For the roll axis the pilot lateral stick command is shaped by a first order roll rate model and combined with roll rate for roll control. This roll rate error is fed to the aileron servos with a gain scheduled on angle-of-attack. In addition, a kinematic beta dot term is crossfed to the aileron. This crossfeed, in effect, partially counteracts the dihedral resistance to roll commands. This crossfeed is also scheduled on angle-of-attack.

The yaw axis augmentation system achieves turn coordination and Dutch roll damping with the beta dot feedback. In addition, a lagged lateral acceleration aids in turn coordination, and the integral provides automatic rudder trim. Small feedforwards of the roll rate model and pilot stick input are scheduled on angle-of-attack. A small rudder-to-aileron crossfeed is included. Because of the beta dot feedback, this crossfeed is not critical to turn coordination.

The complete beta dot signal would include a lateral acceleration term at the center of gravity. When incorporating sensed lateral acceleration, additional factors of \dot{p} and \dot{r} , due to the moment arms associated with the sensor location, must also be included. This acceleration factor is generally omitted from the beta dot signal for implementation reasons. The accelerometer output should be filtered--in this case a first order lag was used--to reduce the noise content of the signal, and hence the acceleration is not appropriate for inclusion as a contribution to beta dot.

Two switches have been incorporated in the block diagram. The first switches out the lateral acceleration feedback when the rudder pedals are deflected so that the acceleration feedback does not resist the desired sideslip maneuver. The second switch closes a feedback loop around the integrator when the aircraft is on the ground (weight on wheels) which slowly resets the integrator.

The sensor requirements will be discussed in detail following the presentation of the CAS without inertial coordination. In summary, the following signals are required for the inertially coordinated lateral-directional CAS.

p = roll rate

r = yaw rate

n_{y_s} = lateral acceleration

ϕ = roll angle

θ = pitch attitude

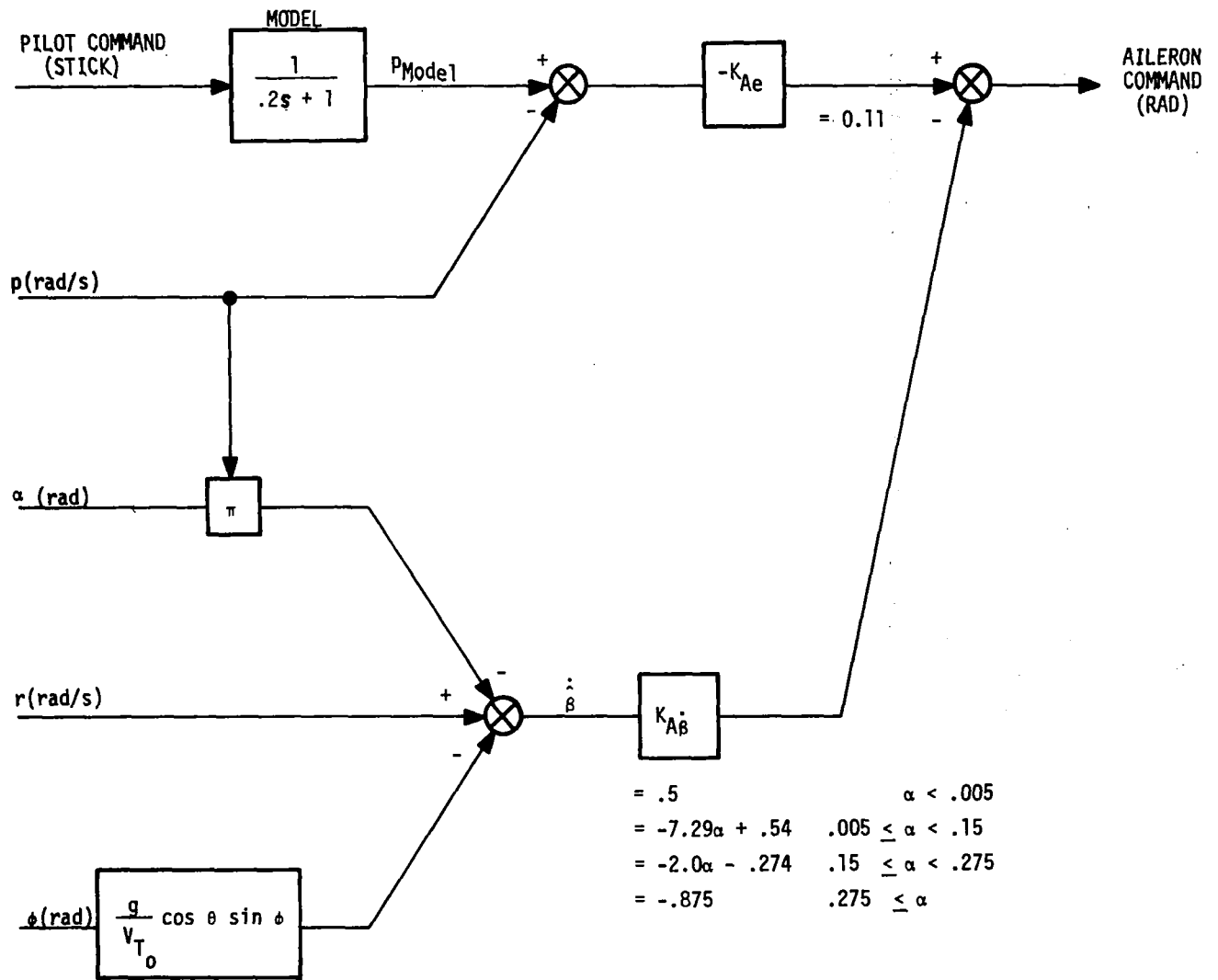


Figure 91. Roll Axis Lateral-Directional CAS with Inertial Coordination

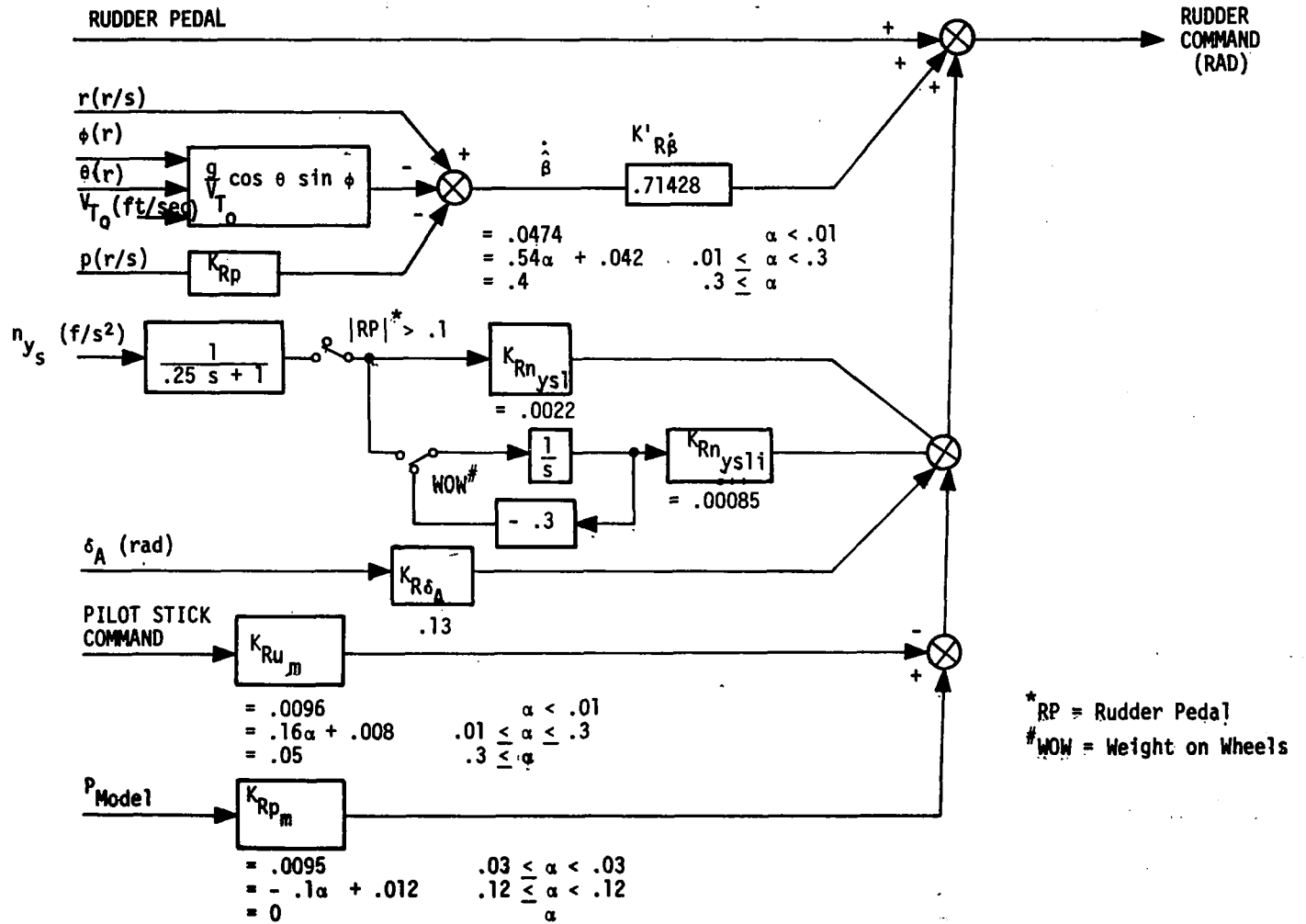


Figure 92. Yaw Axis Lateral-Directional CAS with Inertial Coordination

V_{T_0} = TAS = true airspeed

α = angle of attack

δ_A = aileron surface position

The last signals φ and θ imply that an all-attitude reference is included on the aircraft. The implications of using these additional signals over the conventional yaw damper plus accelerometer system will be discussed in Section 10.

Digitized versions of the augmentation system block diagrams are shown in Figure 93 for the roll axis and Figure 94 for the yaw axis. The Tustin transformation was used to digitize the continuous control laws at a sample rate of 32 samples per second. This is the sample rate used in the NASA-Langley Research Center Hardware Simulator for checkout.

Performance Summary

The digital control system presented in Figures 93 and 94 were programmed to run on the NASA-Langley Research Center F-8C hardware simulator. The system was programmed in FORTRAN and run as a control subroutine in the CDC 6600 simulation of the F-8C. For the responses presented below the simulated actuators were used.

The closed loop roots at flight conditions 1, 5, 10 and 20 are shown in Table 20. The eigenvalues are identified with the aircraft modes in the table. The identifications are estimated.

The control system was checked out and "flown" throughout the flight envelope. Traces are presented below for eight selected flight conditions. The flight conditions were numbers 1, 5, 6, 7, 8, 10, 11 and 17. Table 21 is a summary of the system performance at these flight conditions. The parameters describing the flight conditions are also included in the table. At each flight condition three responses were run, a step stick input, a closed loop β gust (v gust) response and the response of the free airplane to the same gust. The responses are presented in Figures 95 through 102. As evidenced by the responses and the summary table the control system performs well throughout the flight envelope, including high angle-of-attack flight conditions.

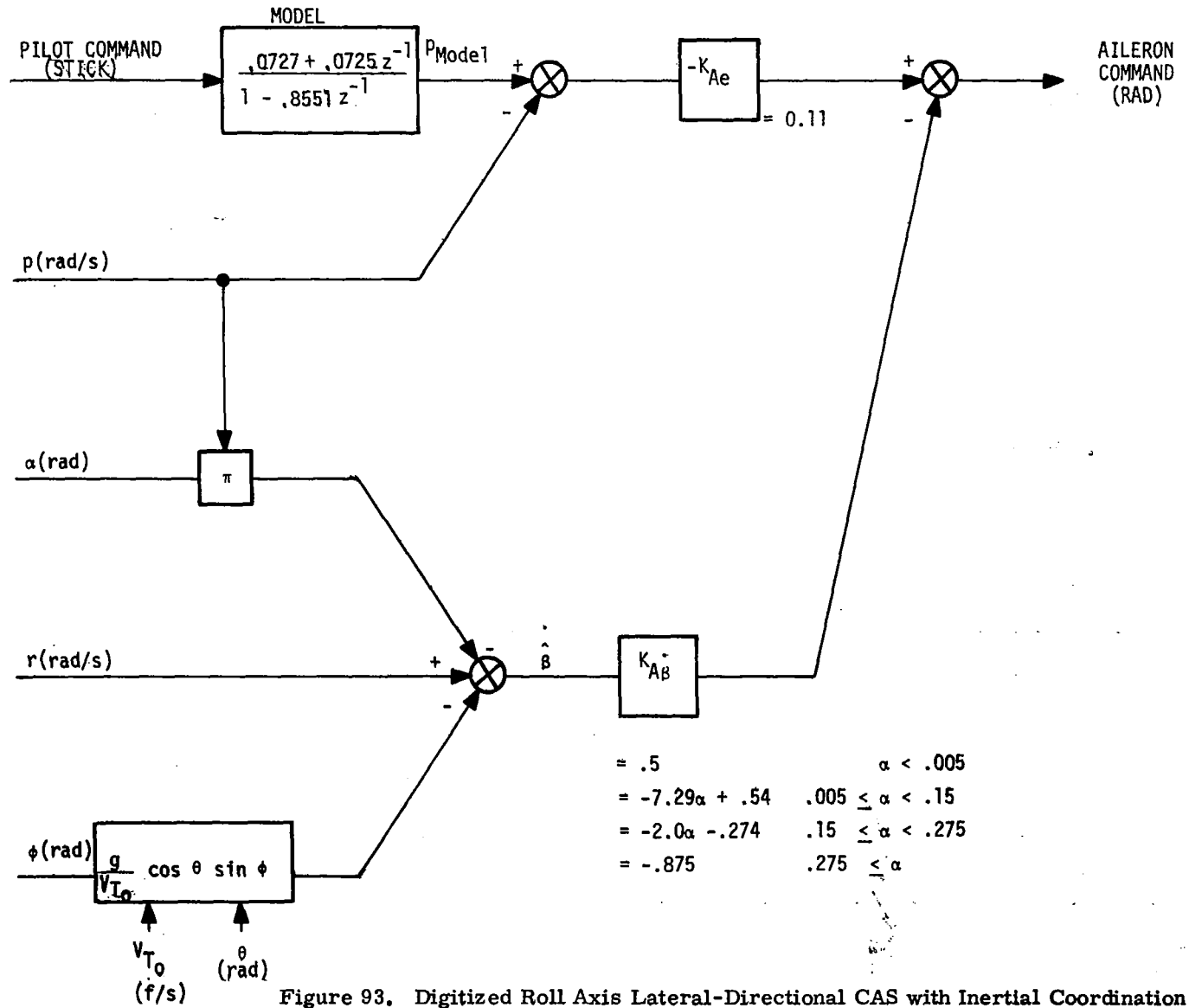


Figure 93. Digitized Roll Axis Lateral-Directional CAS with Inertial Coordination

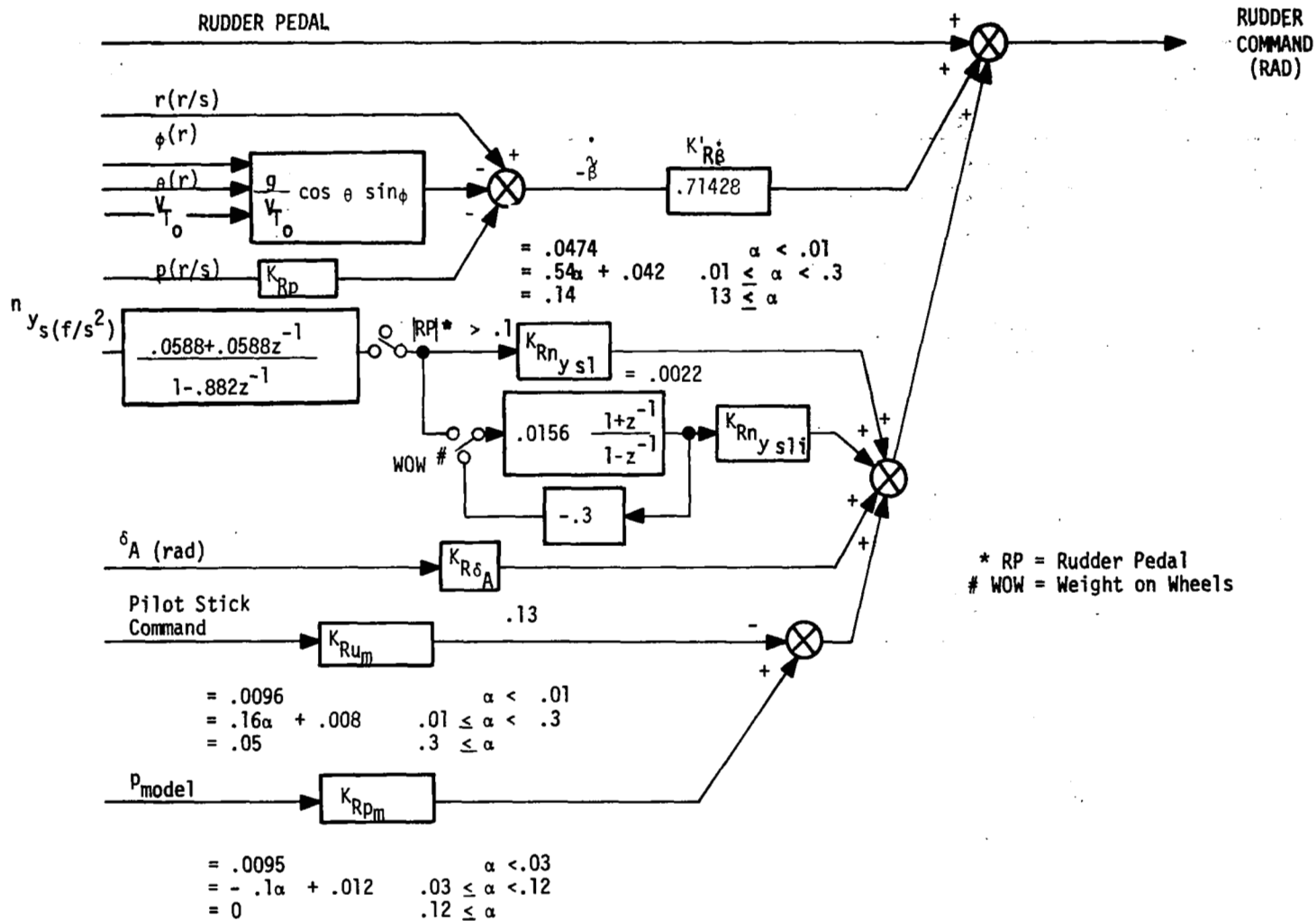


Figure 94. Digitized Yaw Axis Lateral-Directional CAS with Inertial Coordination

Table 20. Closed Loop Roots

Flight Condition	Eigenvalues				Mode Identification
	REAL	IMAG	FREQ	DAMP	
1	-5.00000000 -.00002912 -.02564684 -1.47230910 -3.49243913 -8.45422045 -19.05383277 -27.42263472	0.00000000 0.00000000 0.00000000 0.00000000 2.23132486 0.00000000 0.00000000 0.00000000	5.00000000 .00002912 .02564684 1.47130910 4.14438677 8.45422045 19.05383277 27.42263472	-1.00000000 -1.00000000 -1.00000000 -1.00000000 -.84269141 -1.00000000 -1.00000000 -1.00000000	Roll Rate Model Spiral ny Integrator Dutch Roll ny Lag Roll Subsidence Actuator Actuator
5	-5.00000000 .00033090 -.03381781 -1.36645315 -3.78048876 -21.81508930 -29.59745066	0.00000000 0.00000000 0.00000000 .82222308 .13846434 0.00000000 0.00000000	5.00000000 .00033090 .03381781 1.59475547 3.78302361 21.81508930 29.59745066	-1.00000000 1.00000000 -1.00000000 -.85684180 -.99932994 -1.00000000 -1.00000000	Spiral ny Integrator Roll Rate Model Dutch Roll, ny Lag Roll Subsidence Actuator Actuator
10	-5.00000000 -.00024189 -.02238666 -1.25322803 -5.84992873 -15.44849905 -24.01411432	0.00000000 0.00000000 0.00000000 0.00000000 3.97180977 6.44808031 0.00000000	5.00000000 .00024189 .02238666 1.25322803 7.07085136 16.74018705 24.01411432	-1.00000000 -1.00000000 -1.00000000 -1.00000000 -.82733018 -.92283909 -1.00000000	Roll Rate Model Spiral ny Integrator ny Lag, Roll Subsidence Dutch Roll Actuator Actuator
20	-5.00000000 -.00049404 -.05104369 -.88312817 -2.45504280 -4.30527431 -12.60850229 -29.01322890	0.00000000 0.00000000 0.00000000 0.00000000 0.00000000 0.00000000 5.58725596 0.00000000	5.00000000 .00049404 .05104369 .88312817 2.45504280 4.30527431 13.79100283 29.01322890	-1.00000000 -1.00000000 -1.00000000 -1.00000000 -1.00000000 -1.00000000 -.91425565 -1.00000000	Roll Rate Model Spiral ny Integrator Dutch Roll ny Lag Actuator, Roll Subsidence Actuator

Table 21. Inertially Coordinated Lateral-Directional CAS Performance Summary

FLIGHT CONDITION							PERFORMANCE							
No.	h ft	Mach	\bar{q} psf	V ft/s	α_{trim} deg.	Condition	p_{max} deg/sec	$n_{y_{max}}$ g's	$n_{y_{allowed}}^6$ g's	β_{max}^7 deg.	ϕ_t deg.	k	β/k deg.	β/k allowed (deg.)
1	20K	.67	305	695	3.45	Cruise	20	.025	<u>+0.05</u>	+ .25 - .1	21.6 ²	.24 ⁴	+1.04 - .42	+6 -2
5	20K	.4	109	415	8.86	Cruise	12	-	<u>+0.03</u>	+ .5 -	14.4 ²	.16 ⁴	3.12 -	+6 -2
6	20K	.9	551	934	2.18	Cruise	20	+ .05	<u>+0.05</u>	- - .07	20 ²	.22 ⁴	- - .33	+6 -2
7	40K	.7	134	678	6.73	Cruise	20	-	<u>+0.05</u>	+ .1 -	18 ²	.2 ⁴	+ .5	+6 -2
8	40K	1.2	395	1163	2.72	Cruise	20	+ .03	<u>+0.05</u>	- - .05	18 ²	.2 ⁴	- - .25	+6 -2
10	S.L.	.7	725	782	1.86	Cruise	20	+ .05	<u>+0.05</u>	- - .1	23 ²	.26 ⁴	- - .38	+6 -2
11	S.L.	.3	133	335	7.65	Cruise	12	-	<u>+0.02</u>	+ .5 -	14.4 ²	.16 ⁴	+3.12 -	+6 -2
17	S.L.	.189	53	211	7.48	PA ¹	6	-	<u>+0.01</u>	+ .5 -	4.0 ³	.13 ⁵	+3.85 -	+10 -3

¹ Power approach wing up, gear down

² $\phi_t = \phi_{1.3 \text{ sec.}}$

³ $\phi_t = \phi_{1.0 \text{ sec.}}$

⁴ $k = \phi_t/90$

⁵ $k = \phi_t/30$

⁶ $n_{y_{allowed}} = \frac{p_{max}}{60} (- .15)$

⁷ up to ϕ of 90°

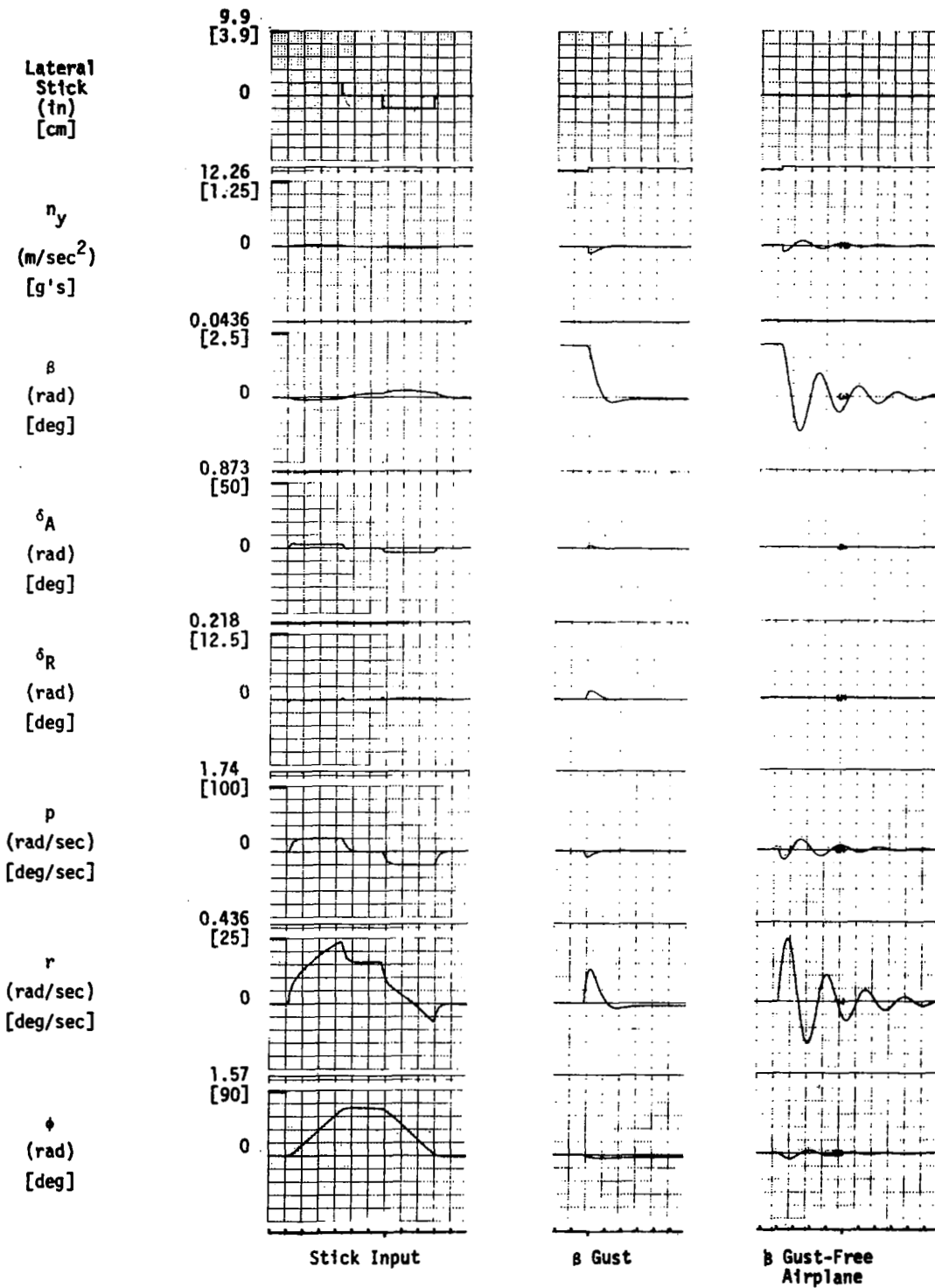


Figure 95. Stick and Gust Responses, Inertially Coordinated CAS, Mach .67, Altitude 20,000 ft.

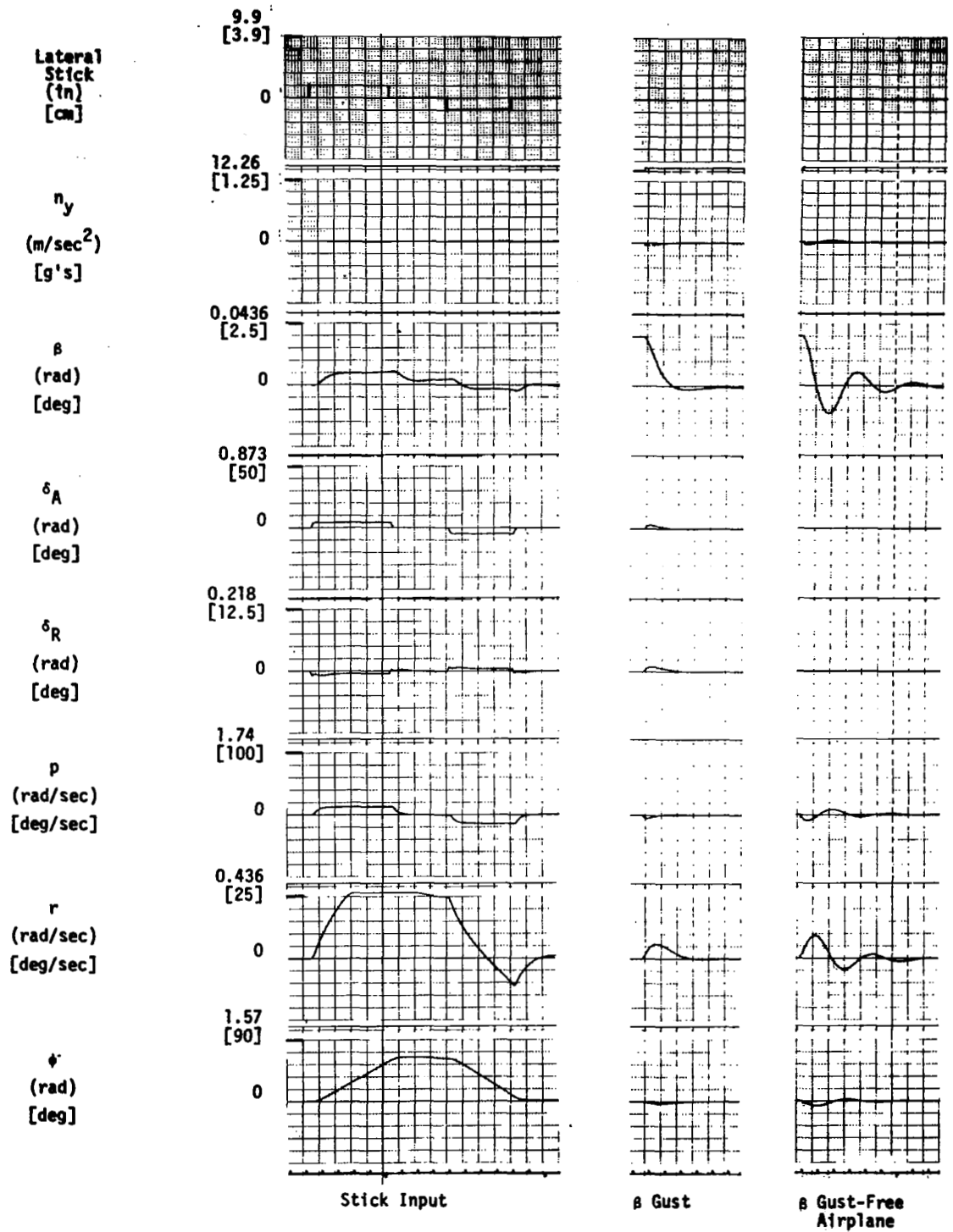


Figure 96. Stick and Gust Responses, Inertially Coordinated CAS, Mach .4, Altitude 20,000 ft.

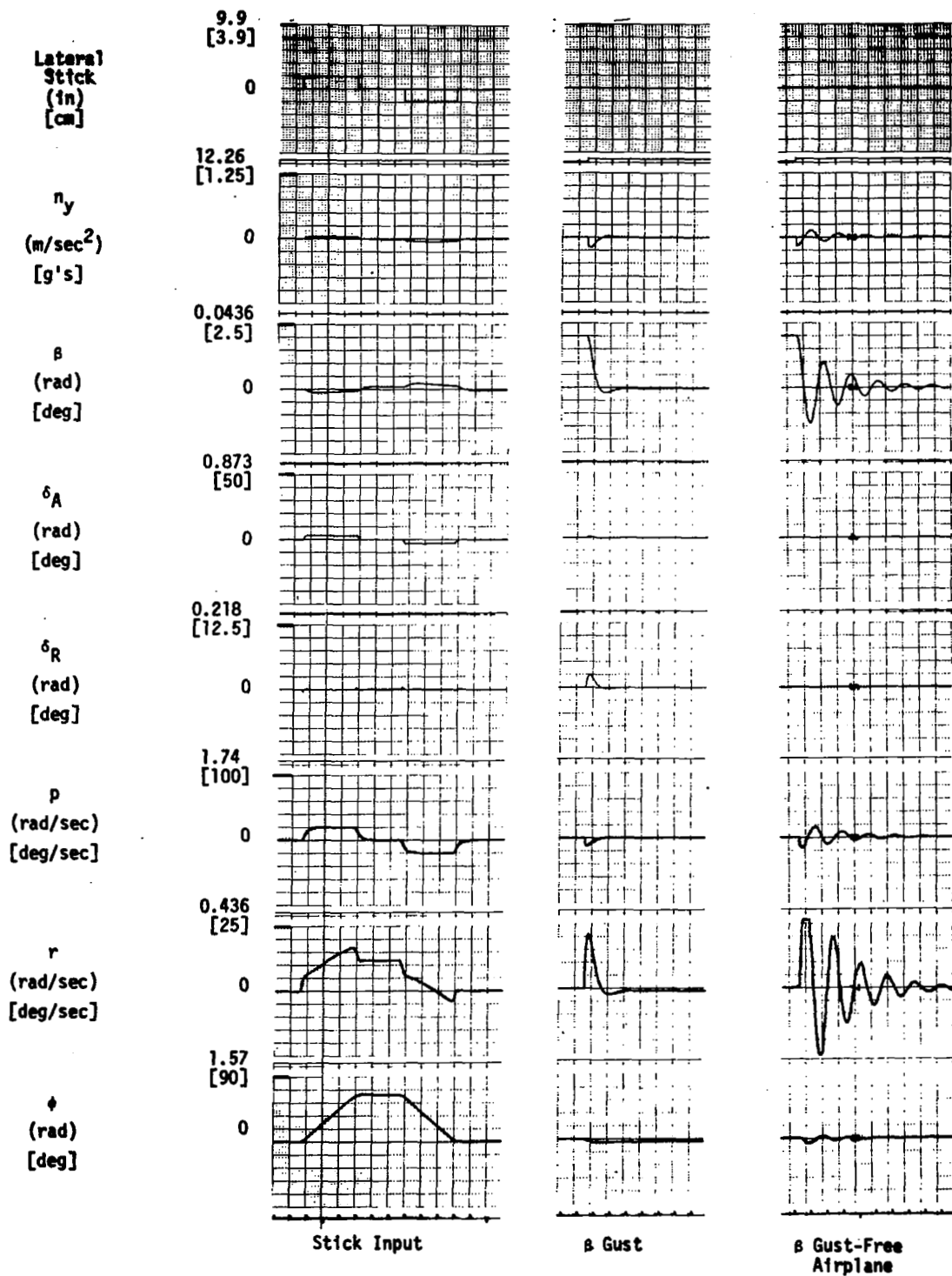


Figure 97. Stick and Gust Responses, Inertially Coordinated CAS, Mach .9, Altitude 20,000 ft.

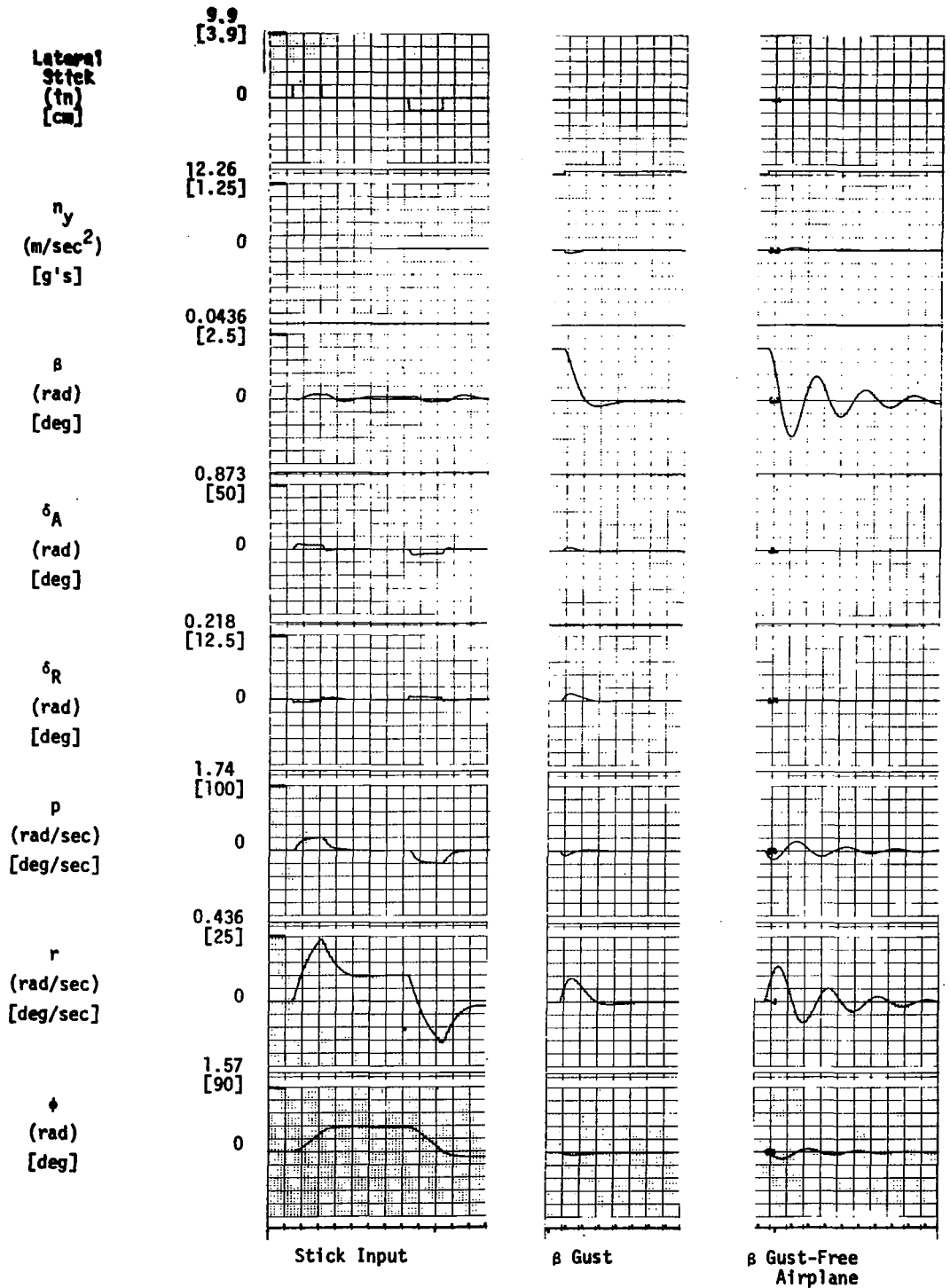


Figure 98. Stick and Gust Responses, Inertially Coordinated CAS, Mach .7, Altitude 40,000 ft.

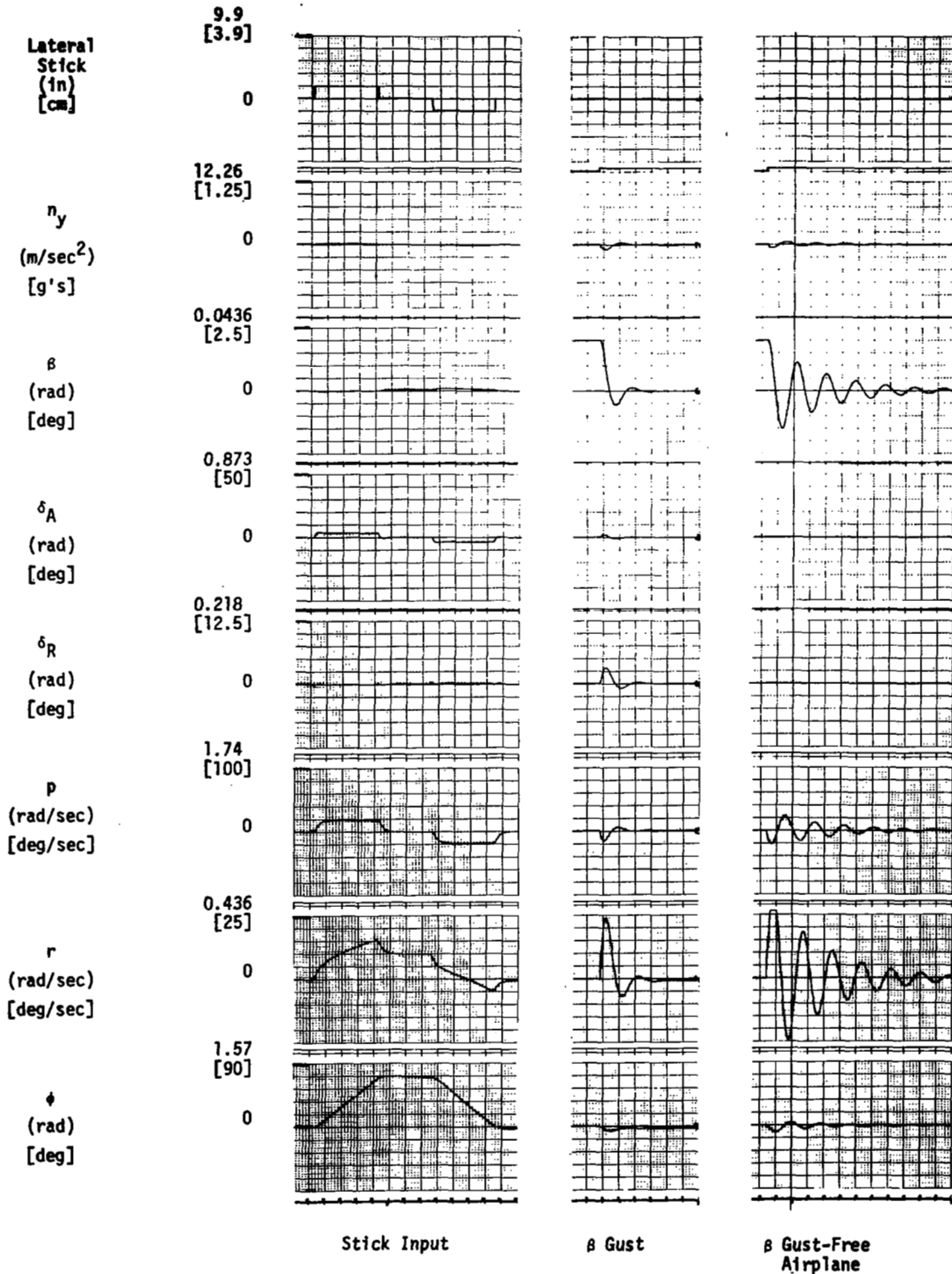


Figure 99. Stick and Gust Responses, Inertially Coordinated CAS, Mach 1.2, Altitude 40,000 ft.

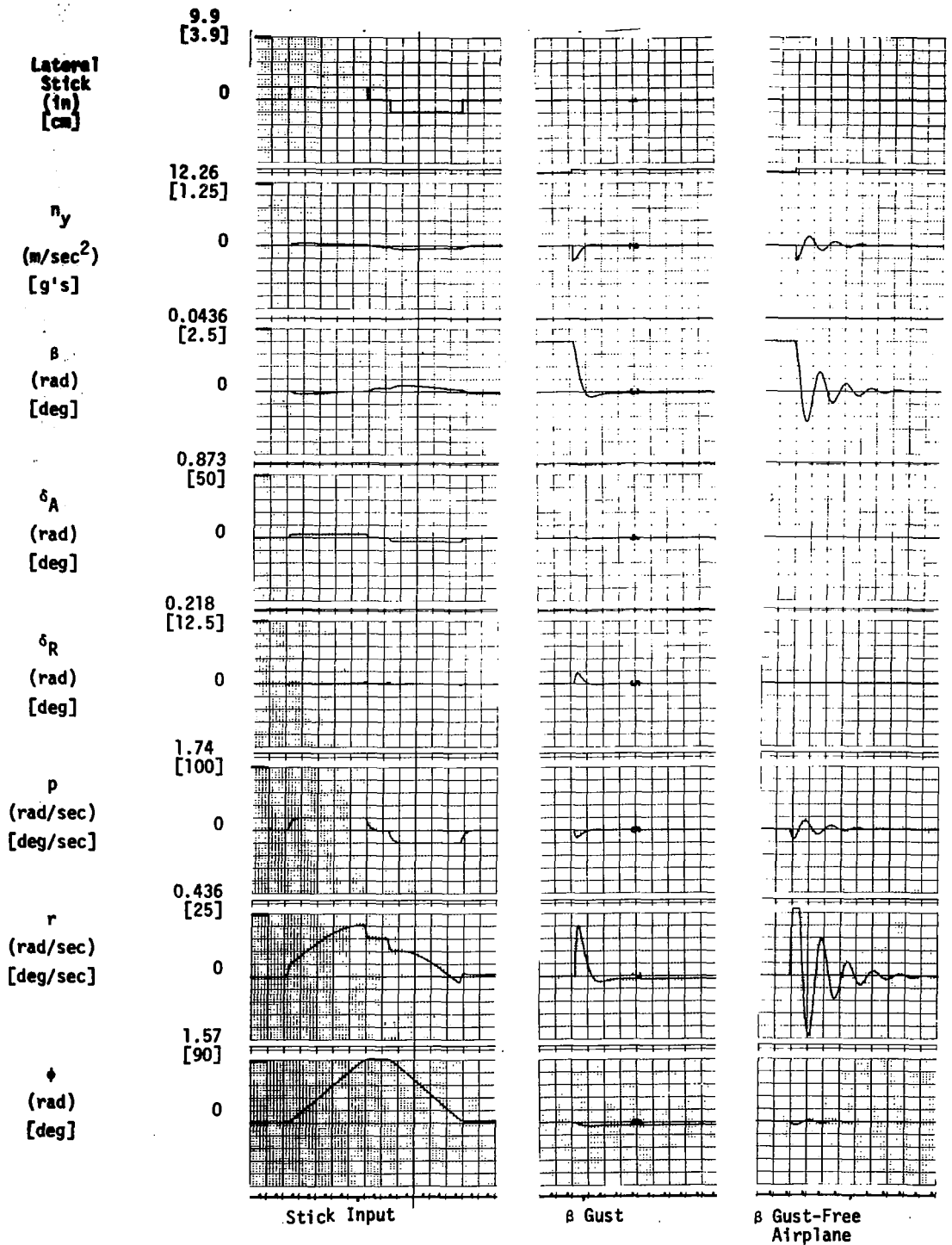


Figure 100. Stick and Gust Responses, Inertially Coordinated CAS, Mach .7, Altitude 1,000 ft.

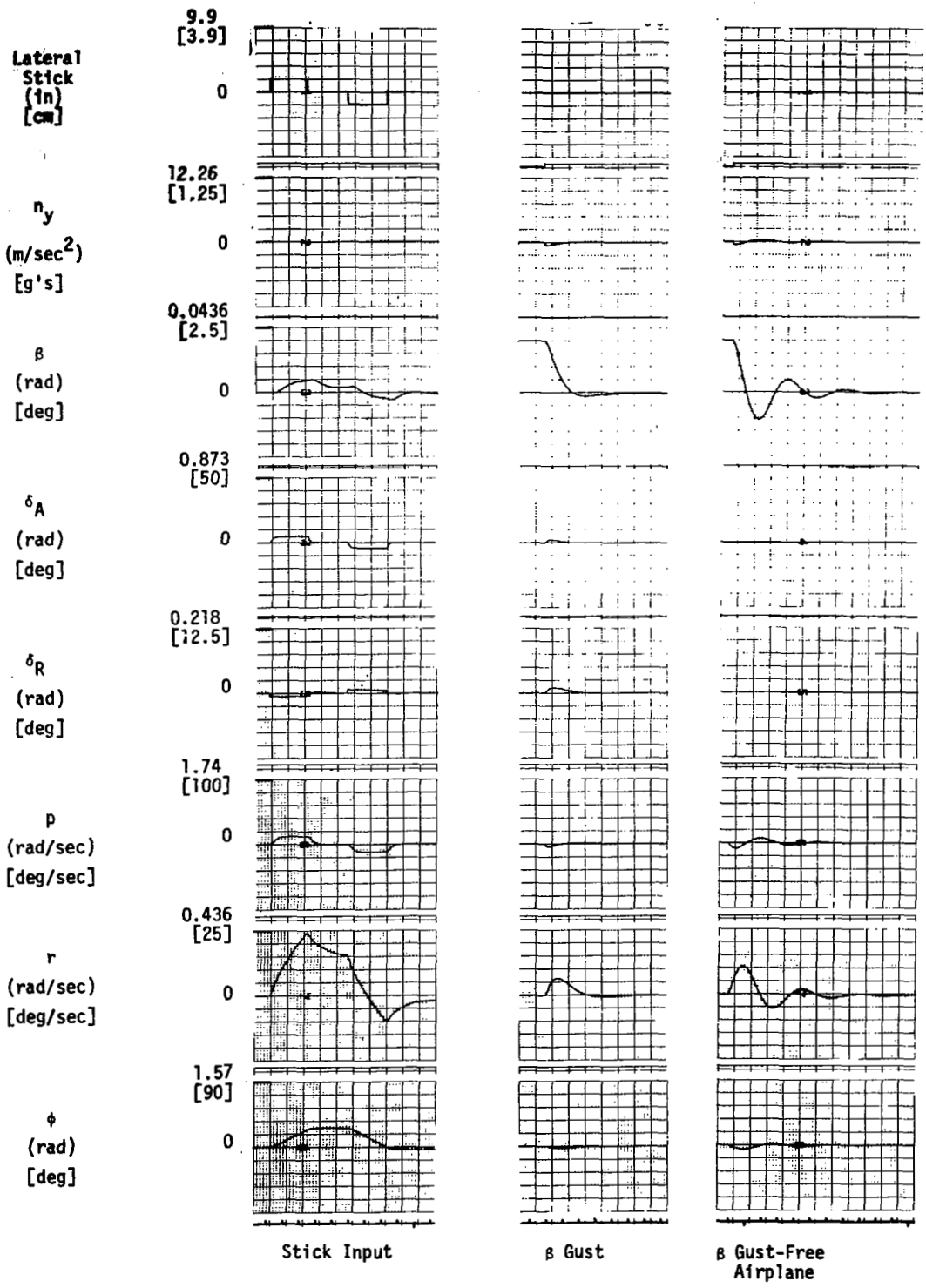


Figure 101. Stick and Gust Responses, Inertially Coordinated CAS, Mach .3, Altitude 1,000 ft.

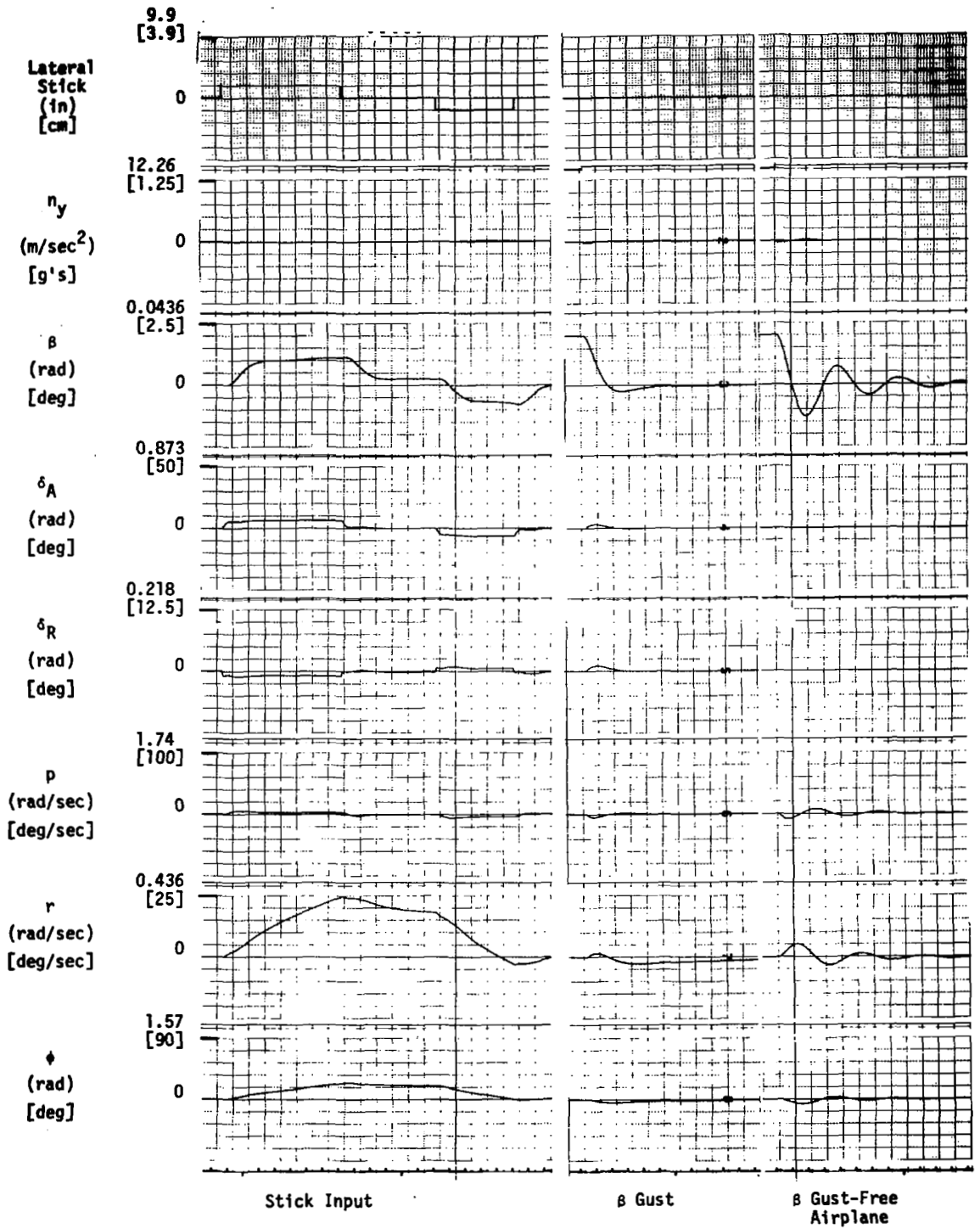


Figure 102. Stick and Gust Responses, Inertially Coordinated CAS, Mach .189, Altitude 1,000 ft.

SECTION 9

SYNTHESIS OF LATERAL-DIRECTIONAL CAS WITH REDUCED MEASUREMENT SET

The design of a control augmentation system for the lateral-directional axis which requires fewer sensors than the system discussed in Section 7 is presented here. The inertially coordinated CAS of Section 8 requires an all attitude reference system to provide the feedback signals ϕ and θ . It was determined that such a sensor complement would not be available on the flight test aircraft. Consequently a second CAS for the lateral-directional axes was designed with reduced requirements for sensors. Specifically, the variables ϕ , θ and V_{T_0} (true airspeed) were not allowed. The allowed feedbacks were p , r , n_{ys} , δ_A and α (for gain scheduling). The practicalization algorithm discussed in Section 5 was employed to develop the new CAS. The starting point or starting gains for the practicalization process were the full state feedback gains used for the inertially coordinated system presented in Section 7. The practicalization algorithm was used to obtain simplified controllers at fixed flight conditions and the resulting gains were then scheduled over the flight envelope. The system design and performance are discussed below.

Fixed Point Designs

As described in the discussion of the practicalization algorithm (FFOC) a set of measurement equations of the form

$$y = Mx,$$

where y is the vector of measurements is formed. The algorithm then determines the gains matrix K' which minimizes the cost functional using a gradient minimization method starting from the full state optimal feedback gains matrix K . The resulting controller is of the form

$$u = K'y = K' Mx$$

Because of the measurement set available, the simplified controller structure must be of the yaw damper type, and thus additional control dynamics are required. In order to obtain Dutch roll damping while at the same time allowing steady turns, washed out yaw rate must be fed back to achieve the damping since a yaw rate feedback would oppose turn coordination. Thus the linear state equation model must be augmented with the washout or high pass dynamics. This was accomplished by augmenting the state vector with a lagged yaw rate state. The new state equation, for r_L , is given by

$$\dot{r}_L = -r_L + r$$

The washout yaw rate signal is then

$$r_w = r - r_L$$

which is the desired high pass. The time constant was chosen based on previous designs of a similar nature. The new state vector is as shown in Table 22.

Table 22. State Vector - Lateral - Directional

Component	Definition
$x_1 =$	p , roll rate, rad/sec
$x_2 =$	r , yaw rate, rad/sec
$x_3 =$	n_{y_s} , sensed lateral acceleration, ft/sec ²
$x_4 =$	ϕ , bank angle, rad
$x_5 =$	δ_A , aileron surface position, deg
$x_6 =$	δ_R , rudder surface position, deg
$x_7 =$	$n_{y_{sl}}$, lagged n_{y_s} , ft/sec ²
$x_8 =$	$n_{y_{sli}}$, integral of $n_{y_{sl}}$, ft/sec
$x_9 =$	p_m , roll rate model state, rad/sec
$x_{10} =$	r_L , lagged yaw rate, rad/sec
$x_{11} =$	u_m , pilot filter state

Because the same cost function and quadratic weights are used for the simplification as for the full state optimization, the same response vector was used.

The measurement vector was as shown in Table 23.

The first six components and the eighth are, in fact, the allowed measurements or feedback signals. Components 7 to 11 (except 8) are added because the initial start-up of the simplification algorithm, as implemented in the FFOC program, requires that the measurement matrix be square and invertable.

In addition to limiting which signals can be used as measurements, the structure of the K' matrix can be specified--that is, within the six allowed measurements, the specific feedbacks to each control can be specified. For the fixed point designs, the following structure was imposed:

Signals allowed to drive the ailerons (5):

$$u_m, p - p_m, r_w, n_{y_{sl}}, n_{y_{sli}}$$

Signals allowed to drive the rudder (5):

$$r_w, n_{y_{sl}}, n_{y_{sli}}, \delta_A, p$$

Table 23. Measurement Vector

Component	Description
$y_1 =$	p
$y_2 =$	r_w
$y_3 =$	δ_A
$y_4 =$	$n_{y_{sl}}$
$y_5 =$	$n_{y_{sli}}$
$y_6 =$	$p - p_m = e$
$y_7 =$	r_L
$y_8 =$	u_m (actual measurement)
$y_9 =$	n_{y_s}
$y_{10} =$	φ
$y_{11} =$	δ_{12}

Prior to selecting this "structure", an investigation (at the five flight conditions used for design iteration of the full state design) of alternative structures was undertaken. The signals r_w , $n_{y_{sl}}$, and $n_{y_{sli}}$ to the aileron and p to the rudder, which normally do not appear in yaw damper, plus accelerometer coordination augmentation systems seemed to improve system performance to a small degree and were allowed in the fixed point design structure. The resulting feedback gains were small, and during gain scheduling no feasible way of scheduling these gains was found so most of them were eliminated eventually.

The results of the simplification algorithm for the power approach flight condition chosen (flight condition 17 in Table 19) were very poor for reasons not immediately obvious. The Dutch roll damping was reduced to an unacceptable level and turn coordination was poor. Because of this, the gains for the power approach condition were ignored during the gain scheduling process. After determining gain schedules based on the other flight conditions the resulting schedules were applied to the power approach condition. Results were better but still not acceptable. Further gain adjustments were made to upgrade the handling qualities at this configuration to an acceptable level.

Gain Scheduling and Block Diagram Definition

Upon determining the desired system structure (allowed feedbacks and form of K') based on the basic five flight conditions used for design iterations, the practicalization algorithm was run on ten different flight conditions which spanned the flight envelope for gain scheduling. The flight conditions were numbers 1, 2, 5, 8, 10, 14, 16, 17, 19, 20 of Table 7.

The gain scheduling was much simpler for this system than the full state case because structural modifications or block diagram manipulation had already been accomplished during the application of the simplification algorithm.

The gains on the measurements to be scheduled were:

Roll Axis

$$K'_{Au_m} = K'_{18} = \text{pilot stick to aileron}$$

$$K'_{Ae} = K'_{16} = \text{roll rate error to aileron}$$

$$K'_{Ar_w} = K'_{12} = \text{washed out yaw rate to aileron}$$

$$K'_{An_{ysl}} = K'_{14} = \text{lagged accelerometer output to aileron}$$

$$K'_{An_{ysli}} = K'_{15} = \int n_{ysl} \text{ to aileron}$$

Yaw Axis

$$K'_{Rr_w} = K'_{22} = \text{washed out yaw rate to rudder}$$

$$K'_{Rn_{ysl}} = K'_{24} = \text{lagged accelerometer output to rudder}$$

$$K'_{Rn_{ysli}} = K'_{25} = \int n_{ysl} \text{ to rudder}$$

$$K'_{R\delta_A} = K'_{23} = \text{aileron surface position to rudder}$$

$$K'_{Rp} = K'_{21} = \text{roll rate to rudder}$$

The candidate scheduling parameters were dynamic pressure \bar{q} , Mach, altitude and angle-of-attack. Each of the above gains was plotted against the candidate scheduling parameters. For three of the gains (K'_{Ar_w} , $K'_{An_{ysl}}$, $K'_{An_{ysli}}$) there was no discernable pattern in any of the plots. Because of this, and since they were small, these gains were dropped. Little performance difference resulted. The remaining seven gains were either scheduled on angle-of-attack or specified as constants. The same comment about the angle-of-attack schedule applies here as in the previous section. Because maneuvering flight conditions were considered, angle-of-attack becomes a better scheduling parameter than dynamic pressure. If the maneuvering flight conditions were not included in the gain schedule considerations, dynamic pressure would likely have been the scheduling parameter. By scheduling on angle-of-attack, some improvement in high angle-of-attack performance was achieved. However, because of the yaw damper structure imposed, high α performance degraded compared to the inertially coordinated system.

The gain schedules for the seven gains, both roll and yaw axis, are presented in Figures 103 to 109. The block diagrams in continuous time form for the roll and yaw axes shown in Figures 110 and 111 respectively. The power approach gains are also shown.

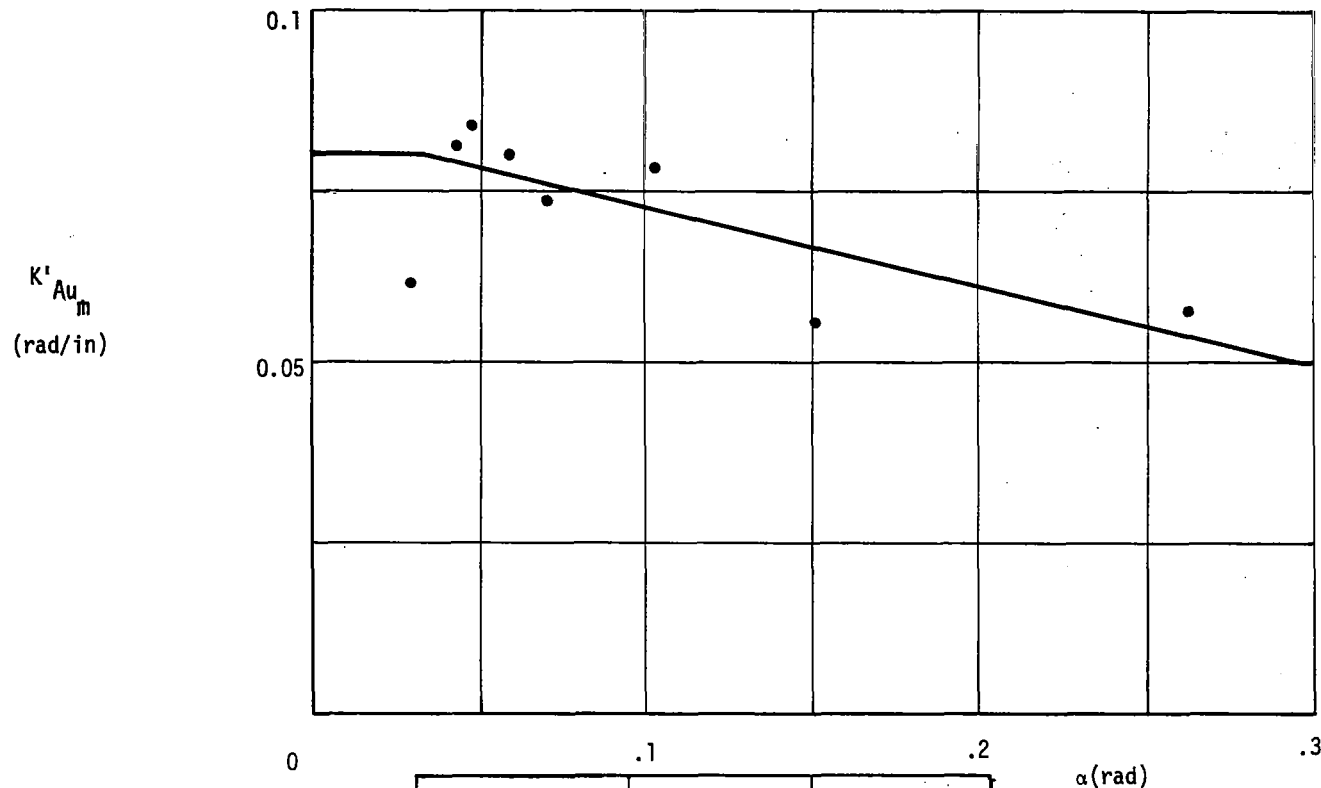
The control system was digitized for checkout on the Langley hardware simulator using the Tustin transformation. The sample rate was 32 samples per second which is the basic sampling rate used in simulator. The digital control laws are shown in Figures 112 and 113.

Performance Summary

The digital control system shown in Figures 112 and 113 was programmed for checkout on the NASA-Langley Research Center hardware simulator in the same manner as described for the inertial coordination system (Section 8).

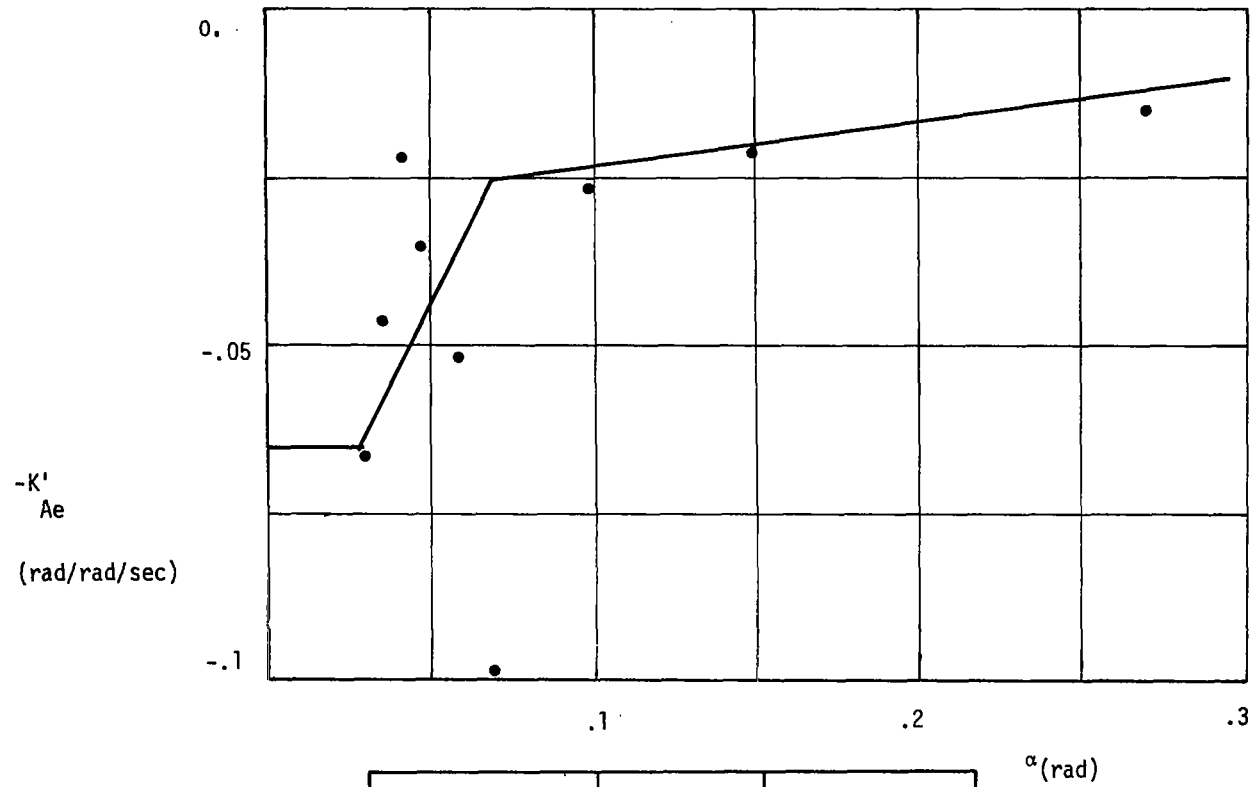
The closed loop roots at flight conditions 1, 5, 10 and 29 are presented in Table 24. Best guesses at identifying the modes are included in the table.

The control system was checked out and flown throughout the flight envelope. Traces are presented below for eight selected flight conditions, which are the same points used for the first CAS presented. Table 25 is a summary of system performance at these flight conditions. At each flight condition three responses were run, a step stick input, a closed loop β gust response and a β gust response of the free airplane. The responses are displayed in Figures 114 through 121. At level flight conditions and moderate to high dynamic pressures the control system performs well with little difference in performance between the two systems designed. For low dynamic pressures (and consequently higher trim angles-of-attack) a degradation in performance is noted over the inertial coordination system, mainly in the Dutch roll damping.



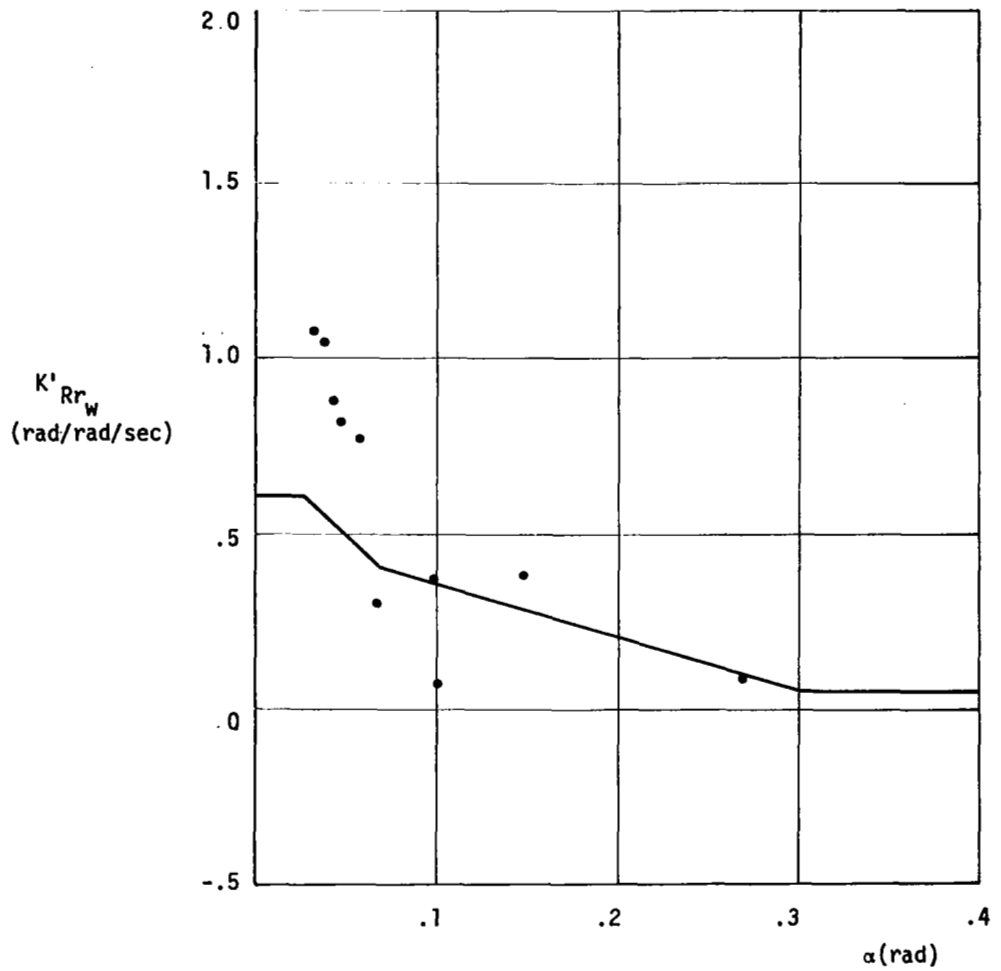
ALPHA	FLIGHT CONDITION	GAIN
.32463E-01	10	.62048F-01
.37001E-01	19	.84106F-01
.43310E-01	14	.82837E-01
.47470E-01	8	.84477E-01
.60213E-01	1	.80370F-01
.71209E-01	16	.73530E-01
.10646E+00	2	.78577E-01
.13055E+00	17	.21047F-01
.15464E+00	5	.56004F-01
.26965E+00	20	.59306F-01

Figure 103. K'_{Au_m} Schedule



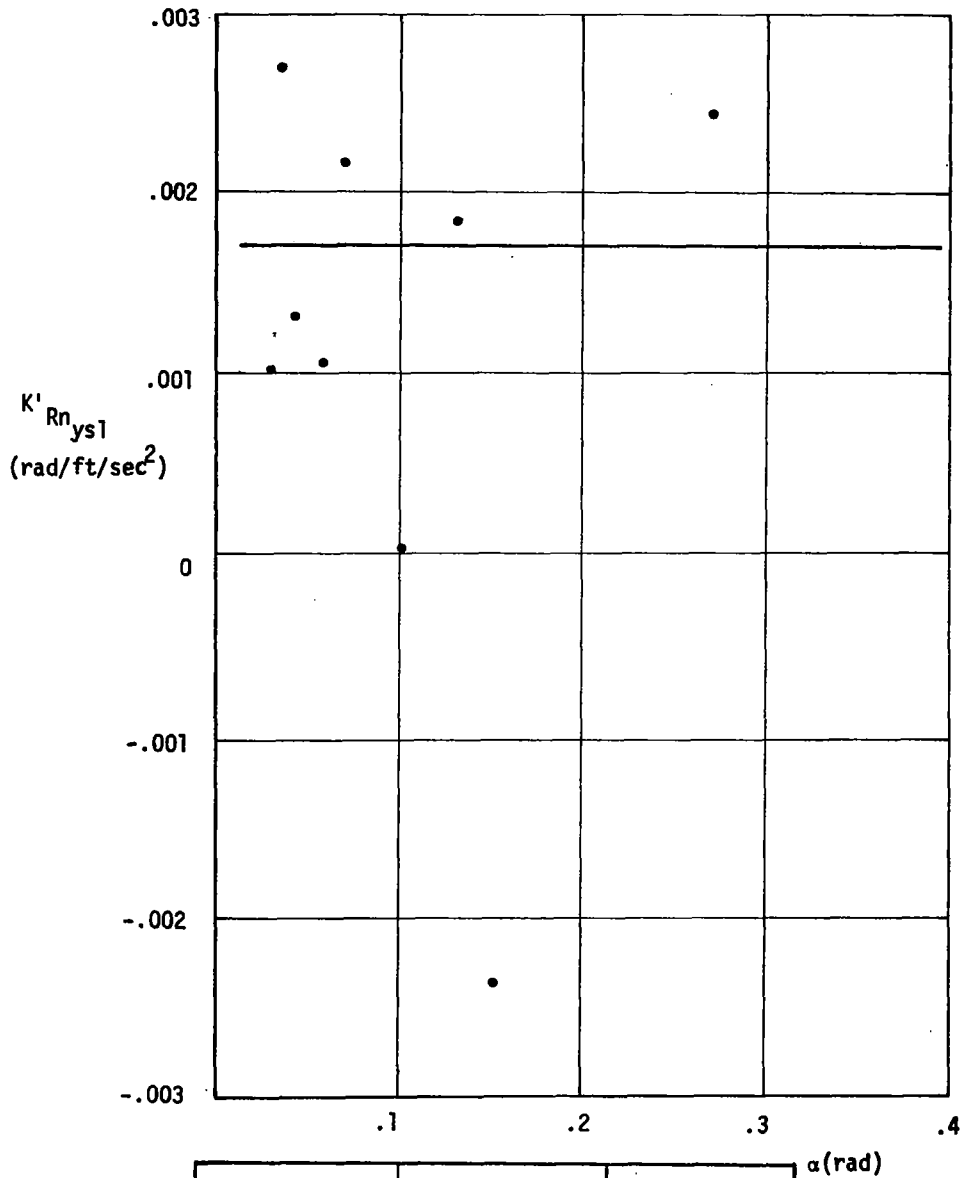
ALPHA	FLIGHT CONDITION	GAIN
.32463E-01	10	-.66940E-01
.37001E-01	19	-.47380E-01
.43310E-01	14	-.21763E-01
.47470E-01	8	-.35111E-01
.60213E-01	1	-.52930E-01
.71209E-01	16	-.99071E-01
.10646E+00	2	-.26541E-01
.13055E+00	17	.74811E-03
.15464E+00	5	-.20131E-01
.26965E+00	20	-.14836E-01

Figure 104. $-K'_{Ae}$ Schedule



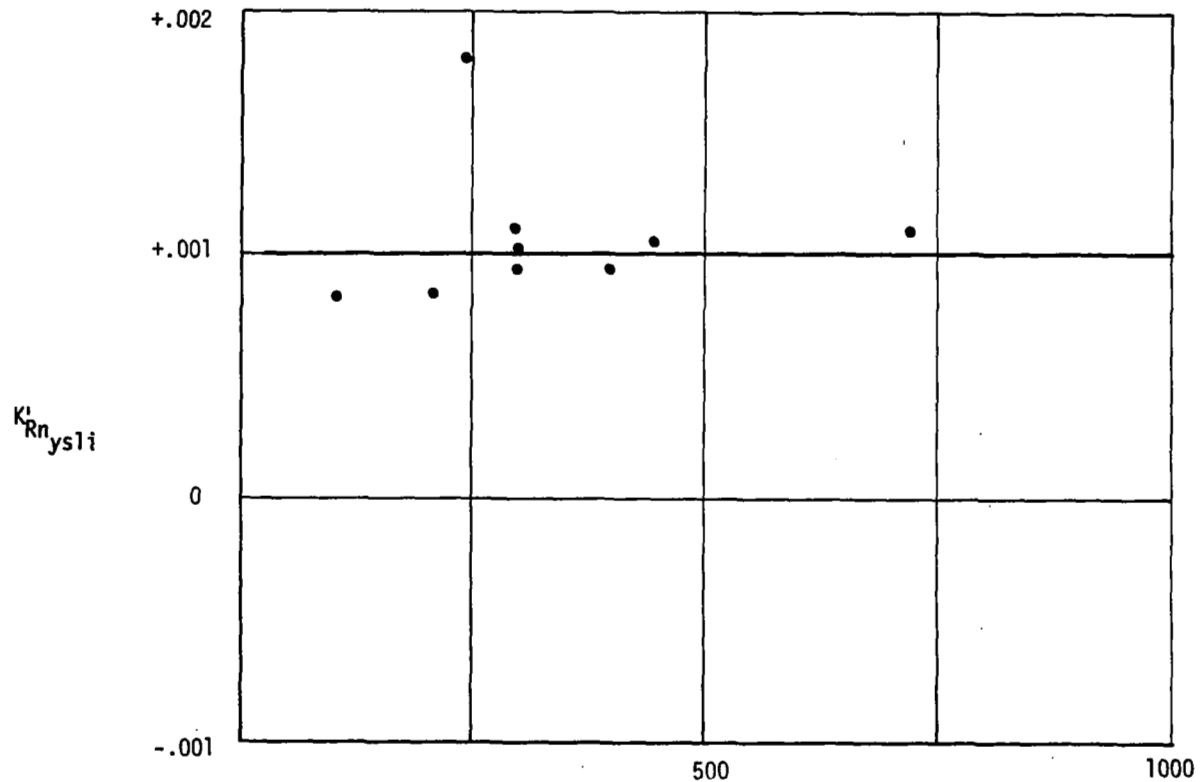
ALPHA	FLIGHT CONDITION	GAIN
.32463E-01	10	.10661F+01
.37001E-01	19	.10467F+01
.43310E-01	14	.86461F+00
.47470E-01	8	.81507F+00
.60213E-01	1	.76539F+00
.71209E-01	16	.29413F+00
.10646E+00	2	.35791E+00
.13055E+00	17	.23249F+01
.15464E+00	5	.37915E+00
.26965E+00	20	.73771F-01

Figure 105. $K' Rr_w$ Schedule



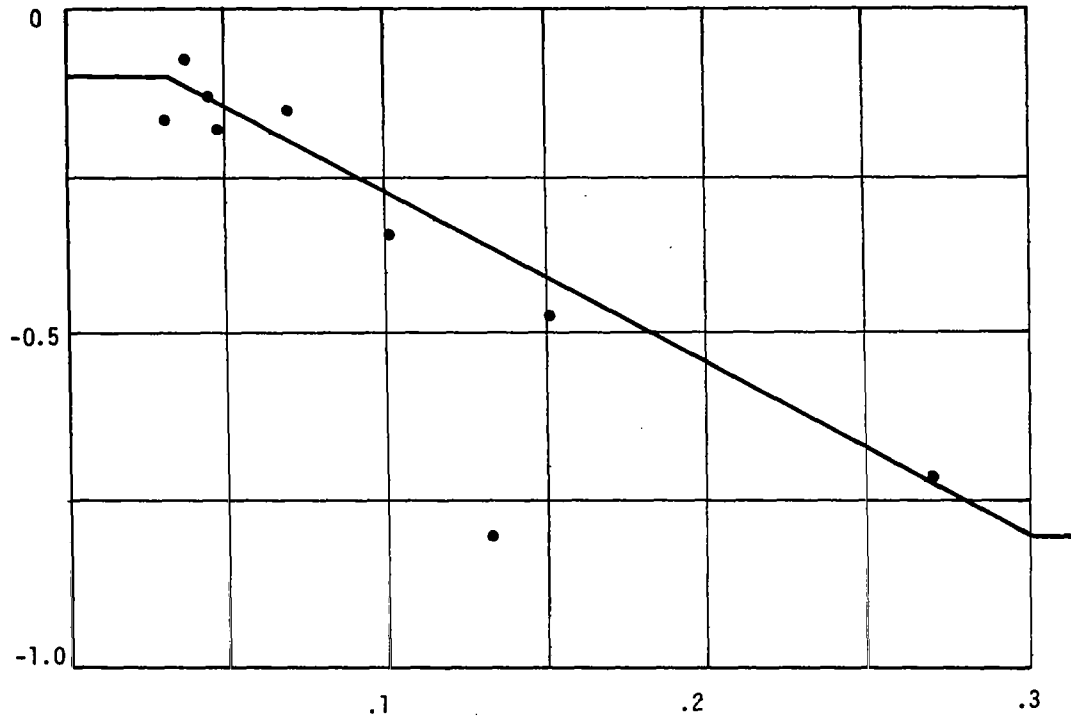
ALPHA	FLIGHT CONDITION	GAIN
.32463E-01	10	.10067E-02
.37001E-01	19	.27223E-02
.43310E-01	14	.13289E-02
.47470E-01	8	-.40742E-03
.60213E-01	1	.10837E-02
.71209E-01	16	.21994E-02
.10646E+00	2	.98939E-04
.13055E+00	17	.18400E-02
.15464E+00	5	-.23760E-02
.26965E+00	20	.24959E-02

Figure 106. $K' Rn_{ys1}$ Schedule



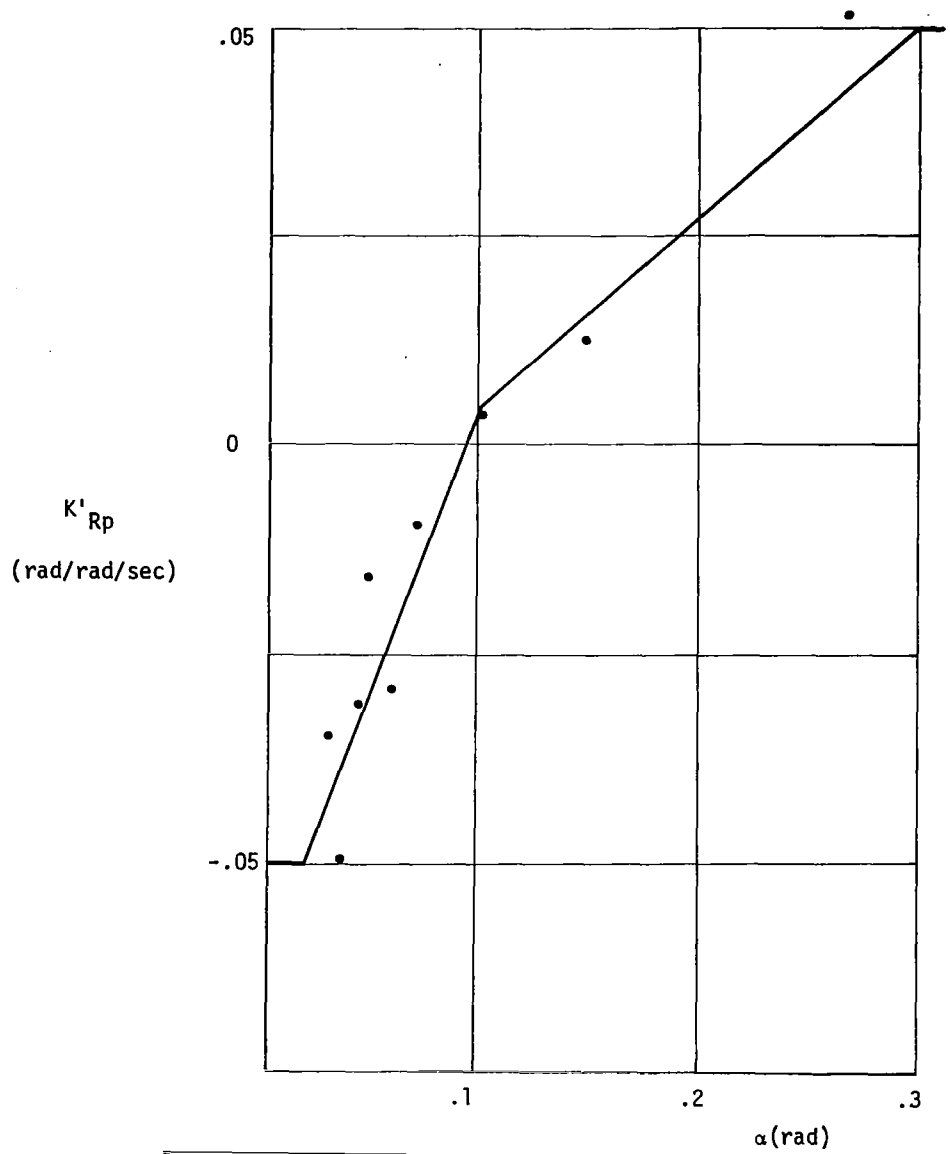
QBAR	FLIGHT CONDITION	GAIN	\bar{q} (psf)
.53000E+02	17	-.22068E-03	170
.10900E+03	5	.81493E-03	200
.22200E+03	16	.84737E-03	220
.24500E+03	20	.18198E-02	245
.30500E+03	1	.10685E-02	305
.30500E+03	19	.95782E-03	305
.30500E+03	2	.11538E-02	305
.39500E+03	8	.92718E-03	395
.43500E+03	14	.10352E-02	435
.72500E+03	10	.11140E-02	725

Figure 107. $K' Rn_{ysli}$ Schedule

$K'_{R\delta_A}$
 (rad/rad)


ALPHA	FLIGHT CONDITION	GAIN
.32463E-01	10	-.17944E+00
.37001E-01	19	-.80815E-01
.43310E-01	14	-.14211E+00
.47470E-01	8	-.18239E+00
.60213E-01	1	-.21126E+00
.71209E-01	16	-.15372E+00
.10646E+00	2	-.35569E+00
.13055E+00	17	-.81452E+00
.15464E+00	5	-.47042E+00
.26965E+00	20	-.72411E+00

 Figure 108. $K'_{R\delta_A}$ Schedule



ALPHA	FLIGHT CONDITION	GAIN
.32463E-01	10	-.34466F-01
.37001E-01	19	-.49706F-01
.43310E-01	14	-.31287F-01
.47470E-01	8	-.15405F-01
.60213E-01	1	-.28110E-01
.71209E-01	16	-.81538F-02
.10646E+00	2	.29709E-02
.13055E+00	17	-.11287E+00
.15464E+00	5	.25119F-01
.26965E+00	20	.53202F-01

Figure 109. K'_{Rp} Schedule

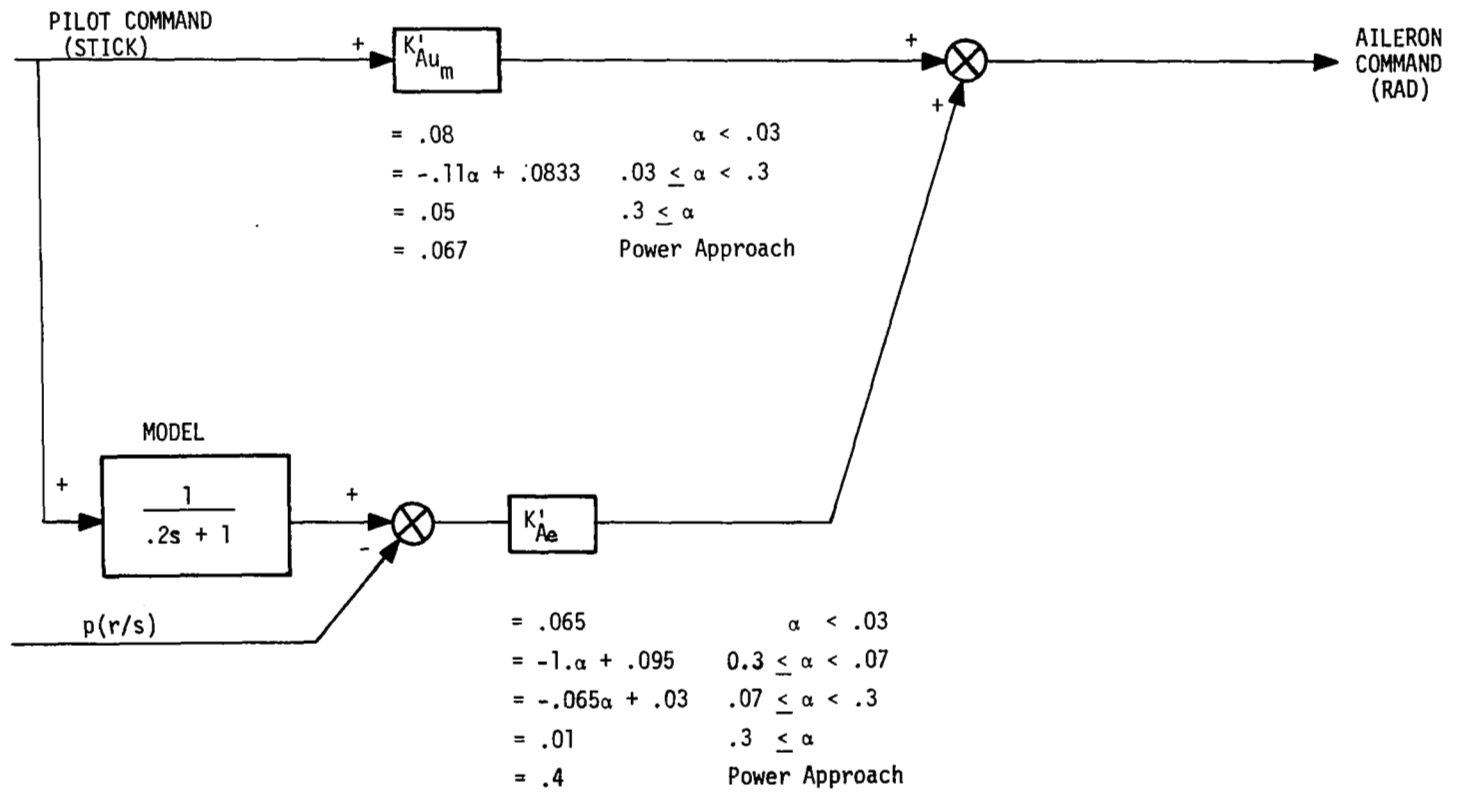


Figure 110. Roll Axis Lateral-Directional CAS with Reduced Measurements

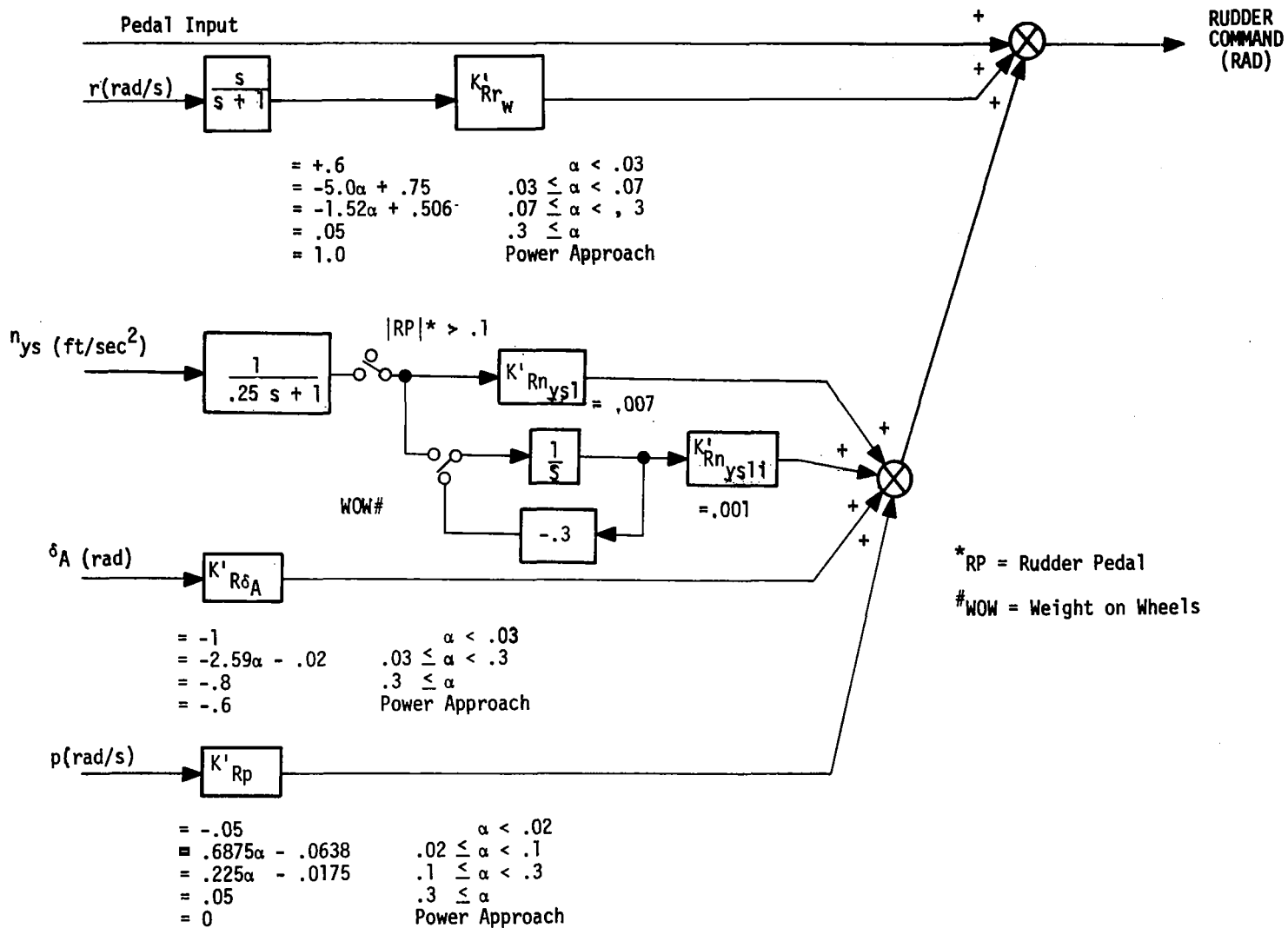
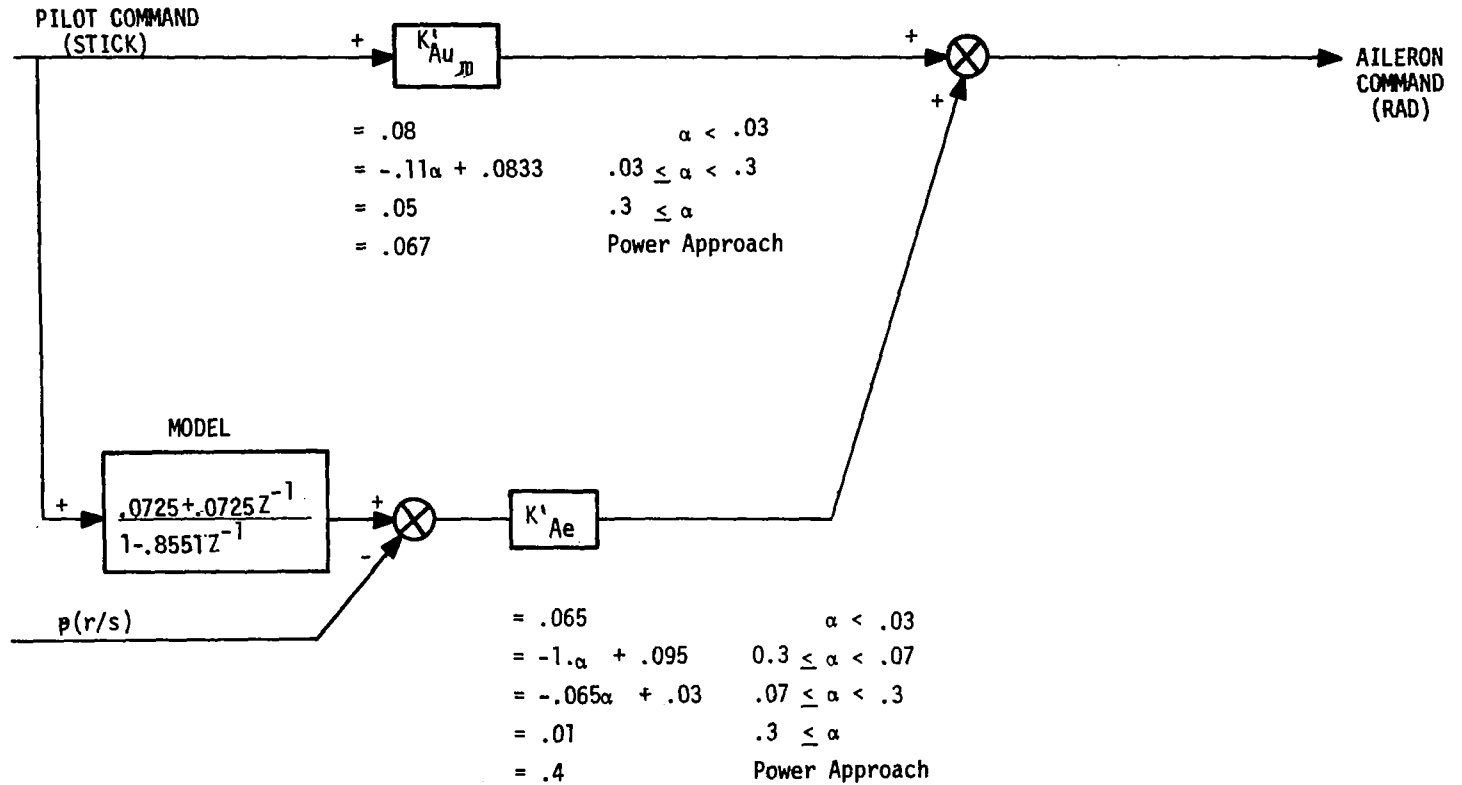


Figure 111. Yaw Axis Lateral Directional CAS with Reduced Measurements



(32 sps)

Figure 112. Digitized Roll Axis Lateral-Directional CAS with Reduced Measurements

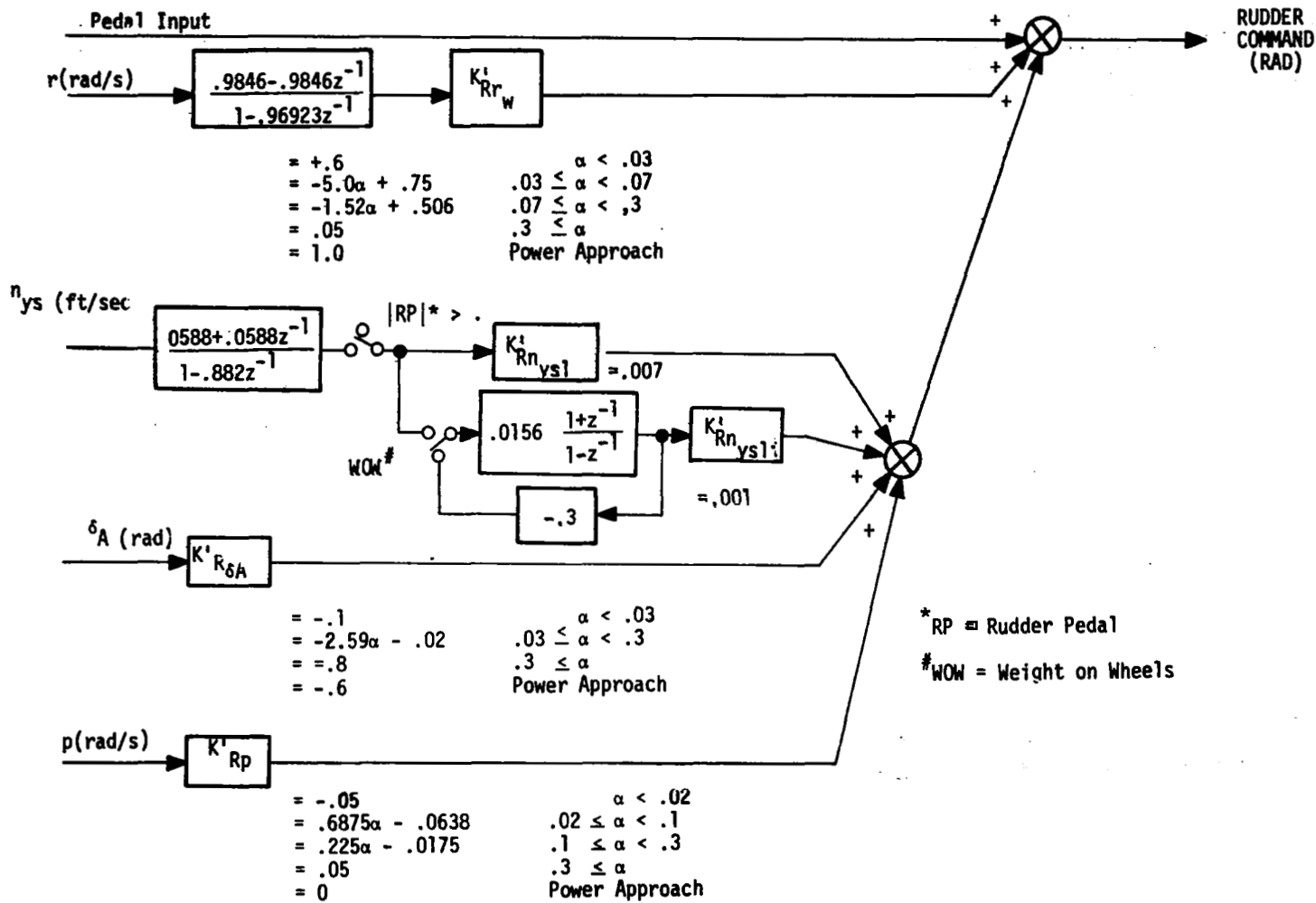


Figure 113. Digitized Yaw Axis Lateral Directional CAS with Reduced Measurements

Table 24. Closed Loop Roots, Reduced Measurements CAS

Flight Condition	Eigenvalues				Mode Identification
	REAL	IMAG	FREQ	DAMP	
1	-5.00000000	0.00000000	5.00000000	+1.00000000	Roll Rate Model ny Integrator Spiral Washout Dutch Roll ny Lag Roll Subsidence Actuator Actuator
	-.00168278	0.00000000	.00168278	+1.00000000	
	-.06965401	0.00000000	.06965401	+1.00000000	
	-1.19159961	0.00000000	1.19159961	+1.00000000	
	-.96476342	2.47157388	2.65319541	+ .36362321	
	-4.86869589	0.00000000	4.86869589	+1.00000000	
	-6.85177019	0.00000000	6.85177019	+1.00000000	
	-20.86617256	0.00000000	20.86617256	+1.00000000	
	-28.63344937	0.00000000	28.63344937	+1.00000000	
5	-5.00000000	0.00000000	5.00000000	+1.00000000	Roll Rate Model ny Integrator Spiral Washout Roll Subsidence Dutch Roll ny Lag Actuator Actuator
	.00516432	0.00000000	.00516432	-1.00000000	
	-.05629992	0.00000000	.05629992	+1.00000000	
	-1.00983804	0.00000000	1.00983804	+1.00000000	
	-2.16342034	0.00000000	2.16342034	+1.00000000	
	-.43645254	1.95409864	2.00224682	+ .21798139	
	-4.57668915	0.00000000	4.57668915	+1.00000000	
	-24.43796548	0.00000000	24.43796548	+1.00000000	
	-29.62795700	0.00000000	29.62795700	+1.00000000	
10	-5.00000000	0.00000000	5.00000000	+1.00000000	Roll Rate Model ny Integrator Spiral ny Lag Dutch Roll Roll Subsidence Actuator Actuator
	-.00026193	0.00000000	.00026193	+1.00000000	
	-.00940583	0.00000000	.00940583	+1.00000000	
	-1.17929951	0.00000000	1.17929951	+1.00000000	
	-1.66775888	2.72469542	3.19458680	+ .52205778	
	-15.25832421	0.00000000	15.25832421	+1.00000000	
	-12.92287268	10.07047284	16.38337760	+ .78877952	
	-23.25827185	0.00000000	23.25827185	+1.00000000	
	20	-5.00000000	0.00000000	5.00000000	
.01088410		0.00000000	.01088410	-1.00000000	
-.09316740		0.00000000	.09316740	+1.00000000	
-.82368297		0.00000000	.82368297	+1.00000000	
-1.67724053		0.00000000	1.67724053	+1.00000000	
-.24554000		3.56010294	3.56856033	+ .06880646	
-5.96723393		0.00000000	5.96723393	+1.00000000	
-24.51311190		0.00000000	24.51311190	+1.00000000	
-29.37058386		0.00000000	29.37058386	+1.00000000	

Table 25. Lateral-Directional CAS with Reduced Measurements Performance Summary

FLIGHT CONDITION							PERFORMANCE							
No.	h ft	Mach	\bar{q} psf	V_o ft/s	α_{trim} deg.	Condition	p_{max} deg/sec	$n_{y_{max}}$ g's	$n_{y_{allowed}}^6$ g's	β_{max}^7 deg.	φ_t deg.	k	β/k deg.	β/k allowed (deg.)
1	20K	.67	305	695	3.45	Cruise	50	+ .03	$\pm .125$	+ .2 - .15	59 ²	.66 ⁴	+ .30 - .22	+6 -2
5	20K	.4	109	415	8.86	Cruise	40	- .05	$\pm .1$	+1.0 0	45 ²	.5 ⁴	+2.0 0	+6 -2
6	20K	.9	551	934	2.18	Cruise	50	+ .1	$\pm .125$	0 - .1	60 ²	.67 ⁴	0 - .15	+6 -2
7	40K	.7	134	678	6.73	Cruise	44	- .05	$\pm .11$	+1.0 - .5	45 ²	.5 ⁴	+2.0 -1.0	+6 -2
8	40K	1.2	395	1163	2.72	Cruise	48	+ .05	$\pm .12$	0 - .02	49 ²	.54 ⁴	0 - .04	-2
10	S. L.	.7	725	782	1.86	Cruise	52	+ .1	$\pm .13$	0 - .1	61 ²	.67 ⁴	0 - .15	
11	S. L.	.3	133	335	7.65	Cruise	36	- .05	$\pm .09$	+ .7 - .7	40 ²	.44 ⁴	+1.57 -1.57	+6 -2
17	S. L.	.189	53	211	7.48	PA ¹	24	- .03	$\pm .06$	+1.0 - .7	22 ³	.73 ⁵	+1.36 - .954	+10

¹ Power approach wing up, gear down

² $\varphi_t = \varphi_{1.3 \text{ sec.}}$

³ $\varphi_t = \varphi_{1.0 \text{ sec.}}$

⁴ $k = \varphi_t/90$

⁵ $k = \varphi_t/30$

⁶ $n_{y_{allowed}} = \frac{p_{max}}{60^\circ} (.15)$

⁷ up to φ of 90°

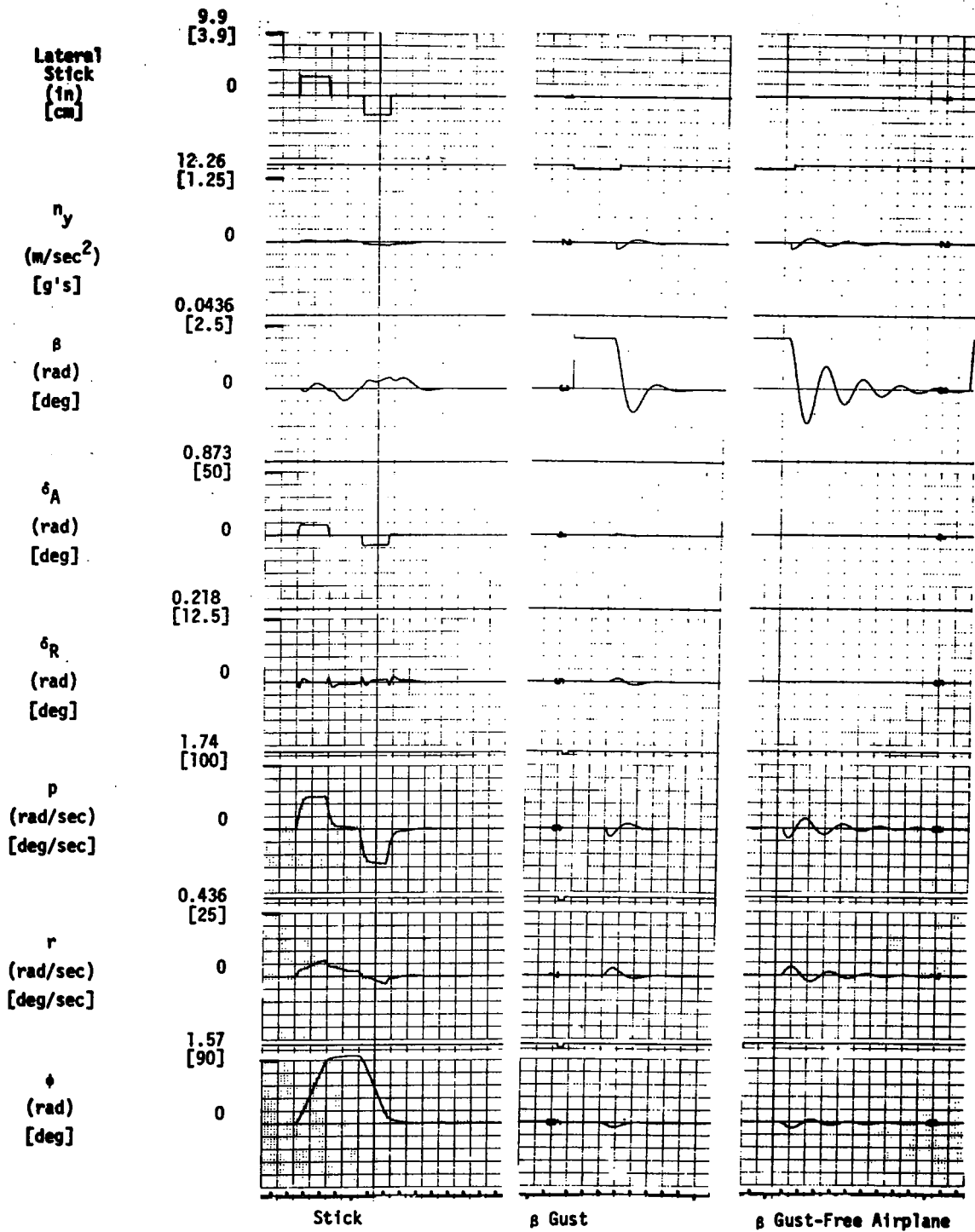


Figure 114. Stick and Gust Responses Reduced Measurement CAS (20,000 ft.; Mach .67)

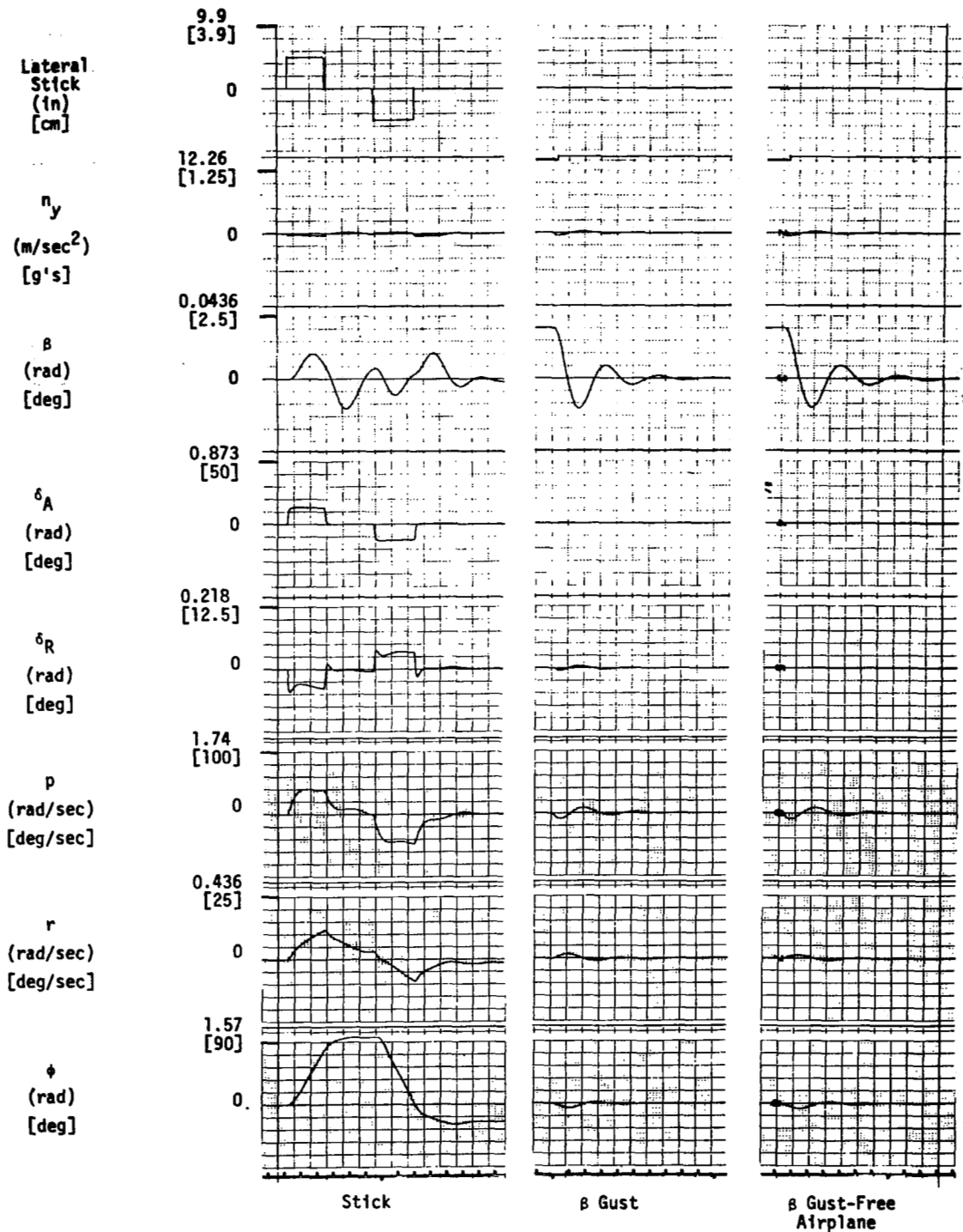


Figure 115. Stick and Gust Responses Reduced Measurement CAS (20,000 ft.; Mach .4)

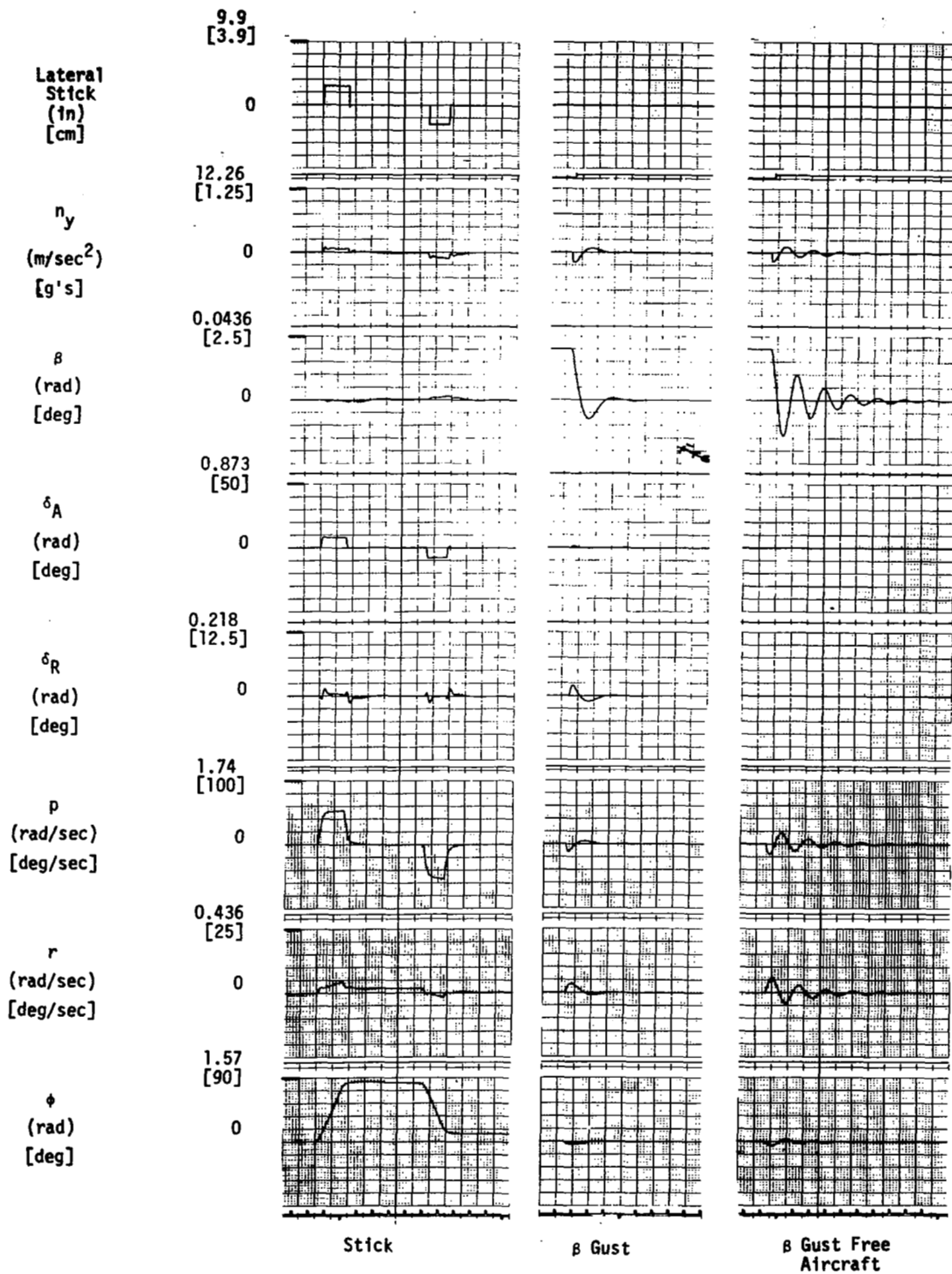


Figure 116. Stick and Gust Responses Reduced Measurement CAS (20,000 ft.; Mach .9)

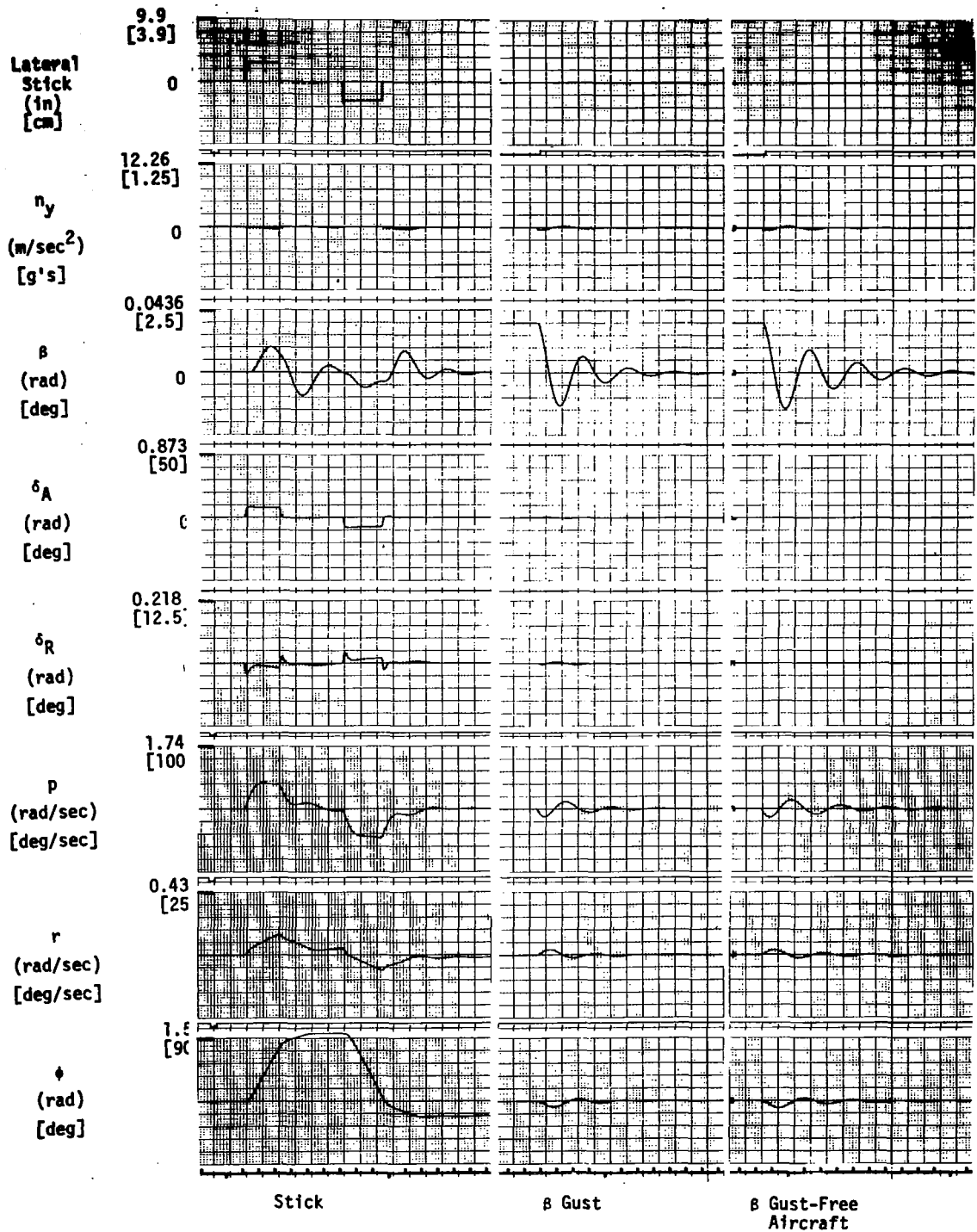


Figure 117. Stick and Gust Responses Reduced Measurement CAS (40,000 ft.; Mach .7)

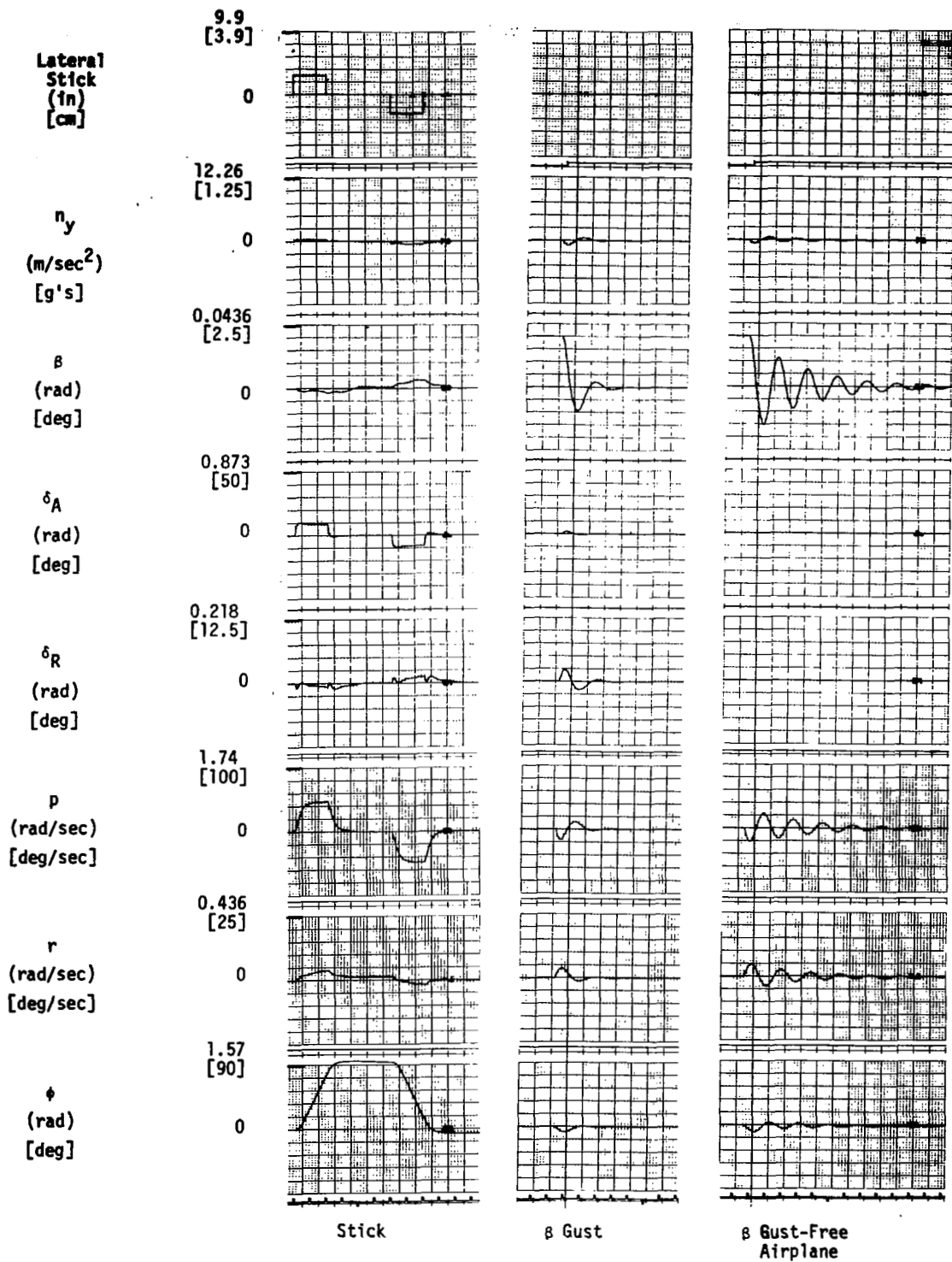


Figure 118. Stick and Gust Responses Reduced Measurement CAS (40,000 ft.; Mach 1.2)

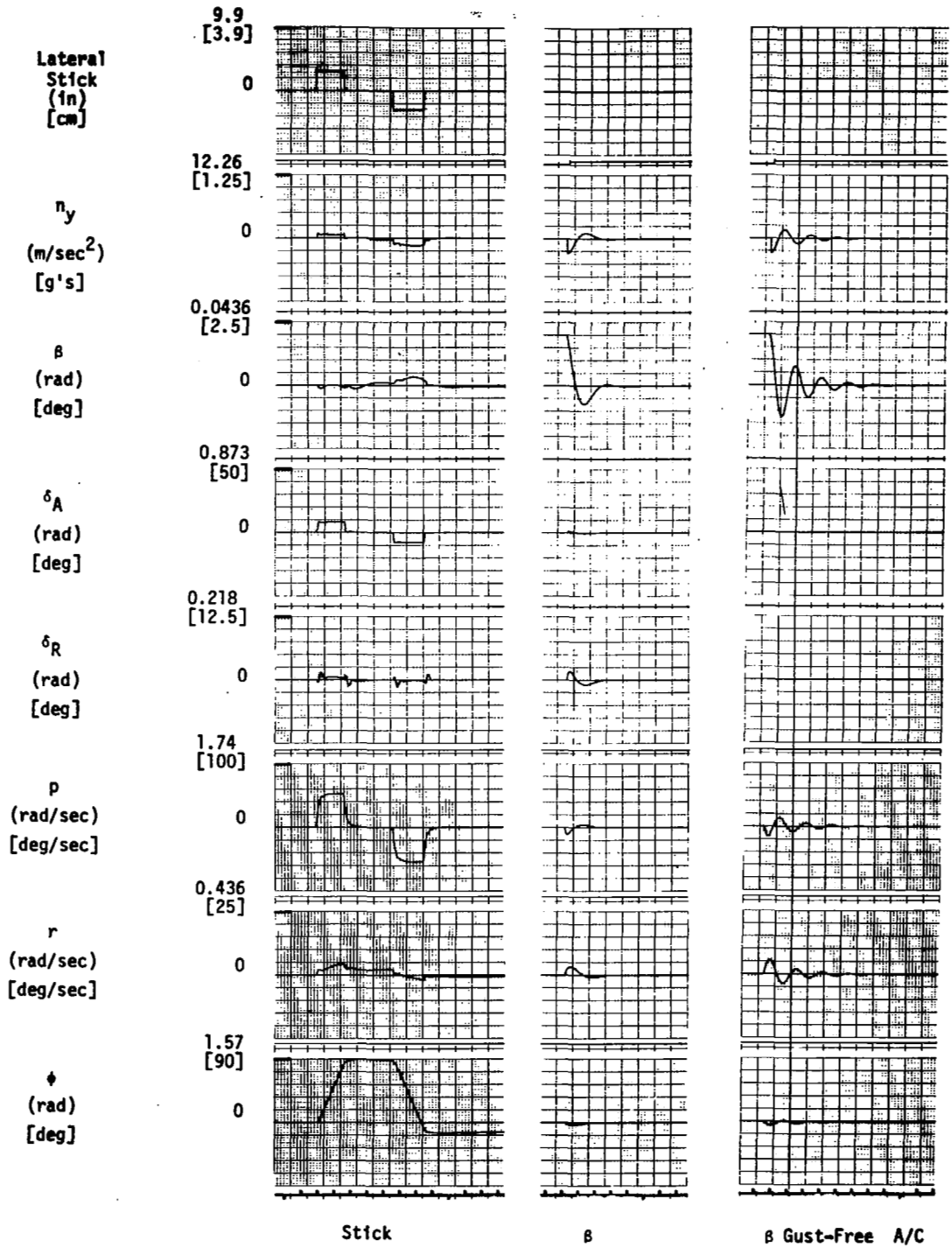


Figure 119. Stick and Gust Responses Reduced Measurement CAS (1,000 ft.; Mach .7)

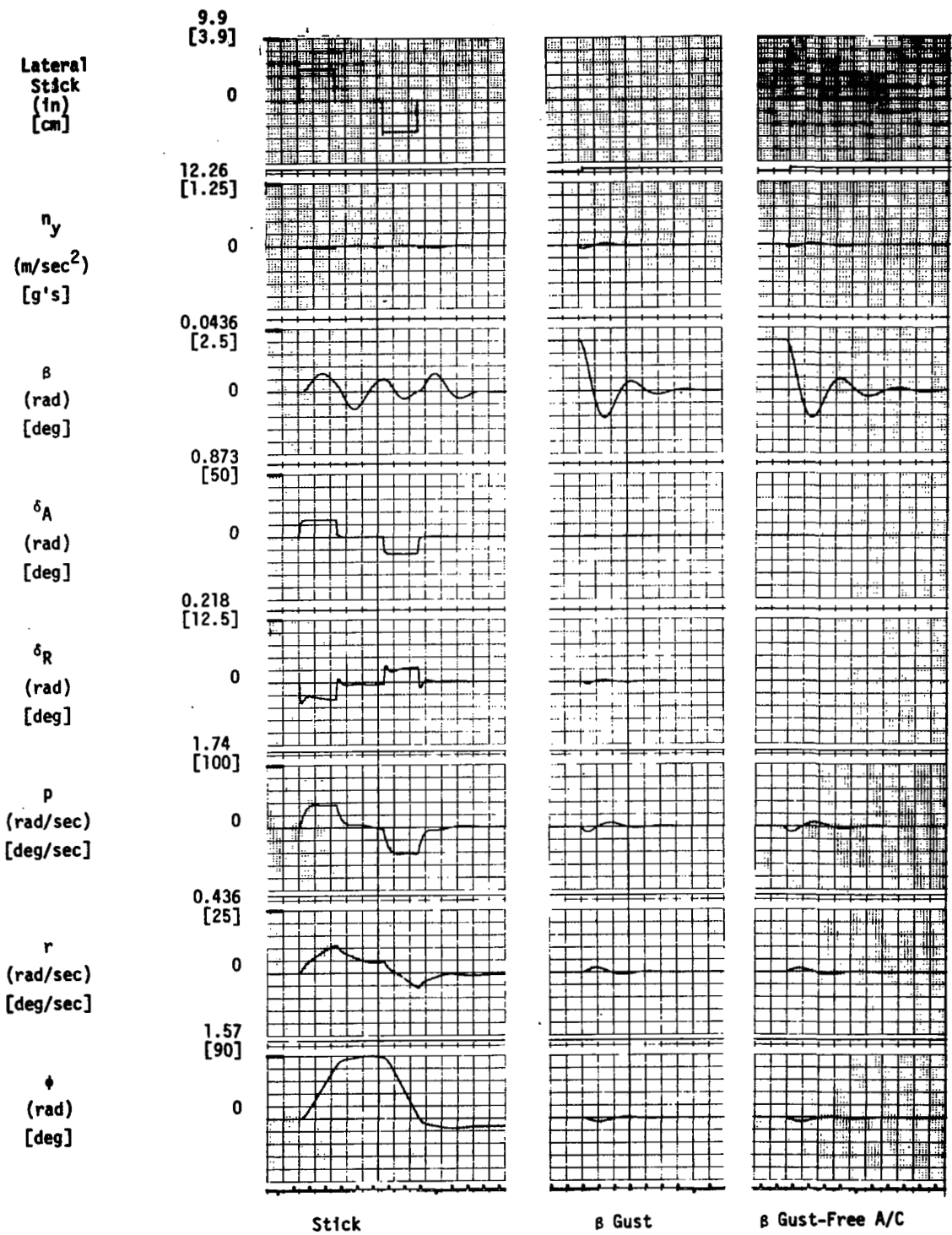


Figure 120. Stick and Gust Responses Reduced Measurement CAS (1,000 ft.; Mach .3)

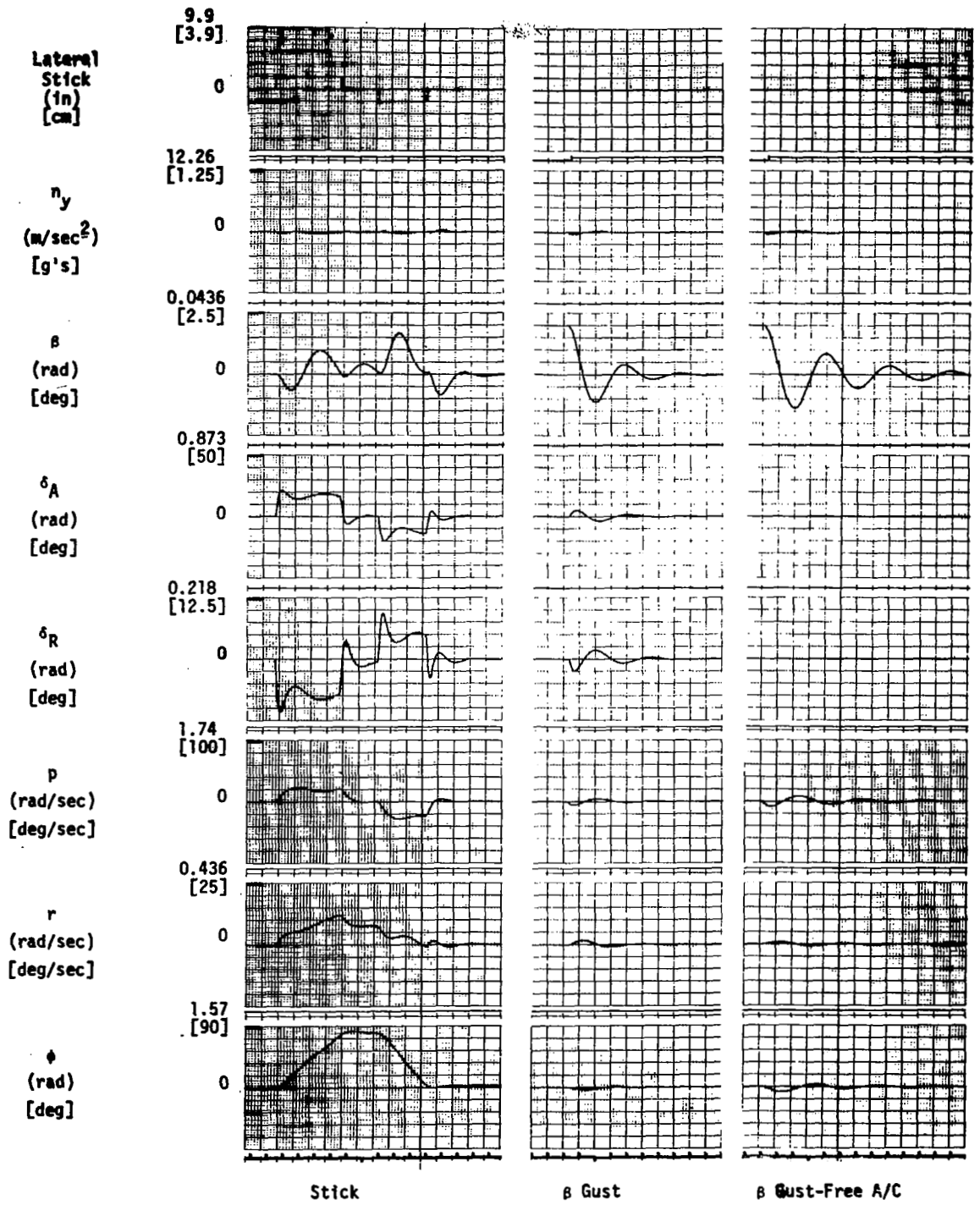


Figure 121. Stick and Gust Responses Reduced Measurement CAS (1,000 ft.; Mach .189)

SECTION 10

LATERAL-DIRECTIONAL SENSOR CONSIDERATIONS AND COMPARISON OF CAS DESIGNS

Recall that the first lateral-directional CAS, presented in Section 8 requires all-attitude inertial reference. It was determined after completion of the design that such a sensor complement would not be available on the F-8C in which the CAS was to be flight tested. Consequently a second CAS was designed which did not require this set of sensors. The second design was accomplished starting with the full state feedback results (of the first design) and applying the simplification algorithm to the system.

The sensor requirements for the two lateral-directional control augmentation systems are reviewed in this section, and the benefits and properties of the two basic candidate sensor complements discussed. A comparison of performance of the two types of systems as applied on this program to the DFBW F8 is made.

Sensor Considerations

The first inertial-directional control augmentation system presented in Section 8 required sensors for the following

p = roll rate

r = yaw rate

n_y = lateral acceleration

φ = bank angle

θ = pitch attitude

V_{T_0} = true air speed

α = angle of attack

δ_A = aileron surface position

Feeding back bank angle and pitch attitude implies a requirement for an all-attitude reference. This has been called the inertial coordination system because of these two signals. The second system, presented in Section 8, employed a reduced sensor set consisting of:

p = roll rate

r = yaw rate

n_y = lateral acceleration

α = angle of attack

δ_A = aileron surface position

This system has been referred to as the reduced measurement CAS. As will be illustrated below, the two sensor complements result in significant differences in system performance. Provision of airframe stability under conditions of low or negative aerodynamic stability requires one or more of the following feedback sensors:

- angular rate
- linear acceleration
- sideslip

The latter sensor is objectionable from the standpoint of vulnerability. Body-mounted devices may also suffer from flow distortions under certain conditions.

Linear accelerometers are relatively reliable, but the rigid body signal content may be difficult to extract, particularly for directional stabilization at low dynamic pressures. Hence, low- q turn coordination often demands unrealizable gain levels.

Angular rate is the preferred sensor, provided that its desired value can be defined during a maneuver. For the directional case, it depends on the object of the control, which in most cases, is turn coordination at zero sideslip. Here the physics of the maneuver require

$$V_{T_0} r_s = g \sin \phi \cos \theta$$

where r_s is stability axis yaw rate, V_{T_0} true airspeed, and ϕ and θ conventional Euler angles. For all-attitude aircraft, this obviously requires all-attitude sensors. Accuracy requirements must be appropriate to usual dynamic lateral acceleration limitations (steady state requirements can be attained through low frequency acceleration feedback of sufficient magnitude).

With dynamic lateral accelerations limited to the 0.1 g area, basic sensors appear to need accuracies within about 2 percent. This is considered to be attainable from current devices provided that power supply variations are compensated appropriately.

In the F-8C DFBW a lateral CAS requiring attitude information could be mechanized with the attitude gyro if the maneuvers were restricted to avoid hitting the pitch gimbal stops. In an all-attitude system we would recommend a primary mode using a single platform properly monitored to detect failures. In the event of a platform error, the system could switch to a lateral CAS not requiring the attitude information (i. e., n_y plus yaw rate feedback).

Application of Acceleration Plus Yaw Rate Control

The least complex sensor complement for the yaw axis consists of lateral acceleration plus yaw rate, the former providing turn coordination and the latter yaw damping. This set also offers compatibility of the sensors with reliability and redundancy objectives, not the least of which is the avoidance of external (airstream) vulnerability. Unfortunately, the use of acceleration plus rate feedback entails limitations for the turn coordination task. These limitations can be exposed by considering some of the basic influences involved in the coordinated turn.

If the basic airplane were assumed to have roll control surfaces which contributed no yawing moment ($N_{\delta A}$) or side forces ($Y_{\delta R}$) and if the yawing moment and side force due to roll rate (N_p and Y_p) were also zero, the relationship between sideslip and bank

angle (for $\delta_R = 0$) would reduce to:

$$\frac{\beta}{\varphi} = \frac{\frac{g}{V_{T_0}} (s - N_R)}{s^2 - s(N_R + Y_V) + (N_\beta + N_R Y_V)}$$

Here the inevitable occurrence of adverse sideslip in the absence of yaw control forces is evident, initiating as the airplane is banked and developing to a sufficient magnitude to counteract the yawing moment due to yaw rate in the turn. The benefit of directional stability (N_β) in minimizing the sideslip is also evident. Development of yaw rate in proportion to bank angle

$$r = \frac{g\varphi}{V_{T_0}}$$

is, of course, essential to turn coordination, and herein lies the first problem in feedback sensor design for the yaw axis.

In using the rate gyro and accelerometer combination, the former generally dominates for the higher frequencies (around the Dutch roll frequency) and the latter is dominant for the lower frequencies. This arrangement offers Dutch roll damping and is preferable from the standpoint of local vibration pickup.

Unfortunately, it usually results in contrary reactions to the initiation of a banked turn, the net feedback opposing the yaw rate essential for the coordinated turn. Placement of the lateral accelerometer can further aggravate the tendency to initially miscoordinate if the location is forward of the center of rotation for sideslip inputs (point where the initial acceleration of the cg is equal and opposite to the local linear acceleration due to yaw angular acceleration). This location equals $-Y_\beta/N_\beta$ which, for typical fighters varies from about 6 feet forward of the c. g. at the landing condition to about 35 feet forward at the high-speed, high-altitude condition. Since lateral accelerometer positions often exceed the former, its initial output during a bank at the low-speed conditions often aggravates an adverse yaw situation.

Perhaps the dominant influence in attaining turn coordination via a lateral accelerometer is the wide variation in its effectiveness as a contributor of lateral "stiffness" over the flight range. A measure of "artificial" directional stability is given by the product $K_{Ny}N_{\delta R}Y_\beta$, where K_{Ny} equals the acceleration gain (rudder deflection per unit acceleration).

The dimensional derivative product $N_{\delta R}Y_\beta$ varies widely over the flight range (by a factor of 100 for the F-8C). Since the minimum value occurs at the landing condition, very high accelerometer gains are required to make significant improvements in coordination. This magnitude is generally well beyond practical loop gain values for frequencies around the Dutch roll.

The inadequacies of a linear accelerometer as a coordination sensor for the low-speed conditions are recognized in the industry. The unavailability of an alternate sensor and the aversion to use of a sideslip sensor have resulted in employment of various cross-feed or feedforward signals, the most popular of which is the aileron-to-rudder

signal. Although these techniques (in conjunction with acceleration) have been used with reasonable success, they do not enjoy the tolerance advantages of the high-bandwidth feedback system which must, of course, be capable of sensing somewhat directly the controlled variable. Lack of this tolerance has contributed to gain-scheduling complexities which are highly dependent on individual airframe peculiarities. Aileron yawing moments can be dominant influences on the coordination problem, varying with flight condition, angle-of-attack, and placement of the roll surfaces relative to the remainder of the airframe.

Benefits of Attitude-Referenced Yaw Control

Use of attitude-related control of angular rate is considered to have the following benefits:

- static stabilization provided with attainable control structures
- superior turn coordination with tolerance to airframe variations
- consistent performance under large angle-of-attack changes
- feedback sensors with realizable redundancy potential
- feedback sensors with predictable characteristics over adequate dynamic range
- superior heading stability under lateral turbulence

Simulation results on this program and for the A-7 multimode indicate that sideslip is reduced, and lateral-directional stability is maintained as N_p is reduced for the mode that includes attitude information in the feedback. [14]

Performance Comparison

The performance of the two types of systems can be compared by referring to the summary tables and the simulator response traces of Section 8 and 9. Table 20 (Section 8) is a summary of the performance of the inertially coordinated system and Table 22 (Section 9) is the analogous table for the reduced measurement system. Figures 95 through 102 of Section 9 are the response traces for the inertially coordinate system, and Figures 114 through 121 are the corresponding responses (same flight conditions) for the second system.

Comparison shows that both systems perform well at medium and high dynamic pressure cruise flight conditions. At the lower dynamic pressure flight conditions, the inertially coordinated system continues to perform well whereas the reduced measurement systems show some performance degradation (compare Figures 96 to 115, 98 to 117, 101 to 128 and 102 to 121). This is unavoidable as pointed out above. A significant difference in the two systems appears during maneuvers at high angle-of-attack. Figure 122 is the response of the inertially coordinated system to a step stick input at flight condition 20 ($h = 20$ K feet, $Mach = .67$, $\bar{q} = 245$, $\alpha_{trim} = 15.45^\circ$, 3g pull up) and Figure 123 is the response of the yaw damper system to a step stick input at the same flight condition. These traces are linear system responses. The linear model of the aircraft was obtained by trimming the 6 DOF F8SIM nonlinear simulation in a 3-g pull up and then linearizing. The lateral-directional equations were then decoupled. (This is precisely the model used for designing at flight condition 20). Linear model responses are used here because similar conditions cannot be duplicated on the hardware simulator. The inertially

coordinated system shows very good Dutch roll damping whereas Dutch roll in the reduced measurement system is very lightly damped. This is also evident from the eigenvalues presented in Tables 21 and 22. The maximum sideslip excursions are roughly equivalent for the critical time period of the first two seconds. Because the reduced measurement system has unacceptably low damping (.06), the maximum sideslip is limited due to the oscillatory nature of the response. The inertially coordinated system has a much more acceptable response, and the advantages of the more complex system are evident.

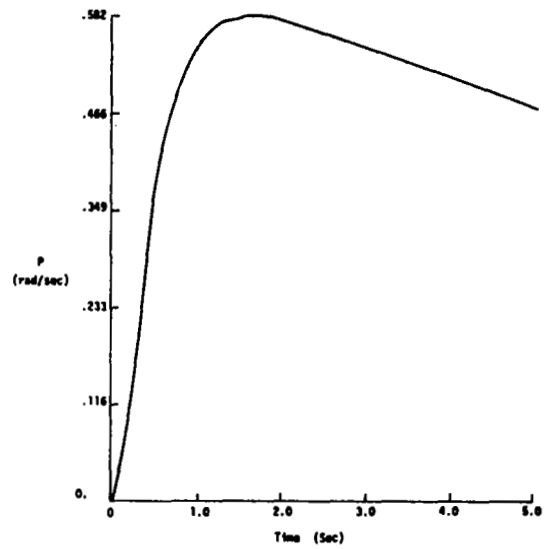
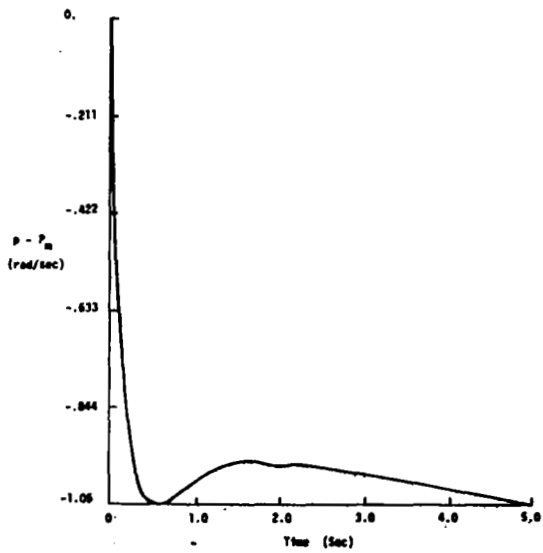
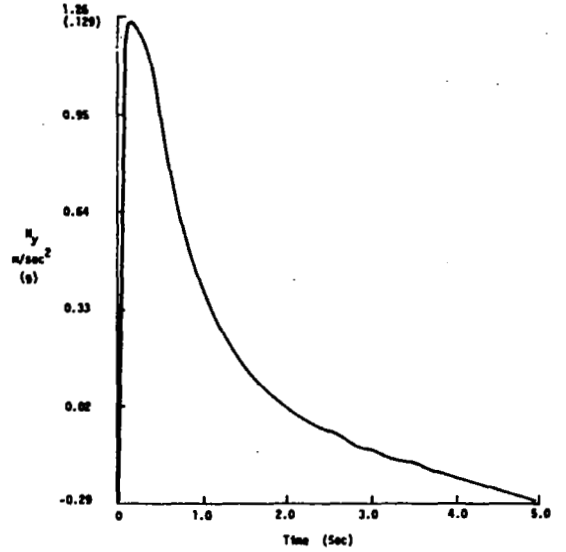
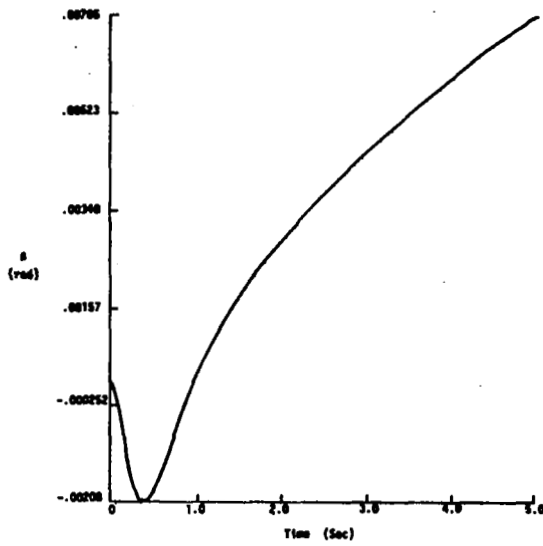


Figure 122. 3-g Pull-up with Inertial Lateral CAS
 $h = 20,000$ $M = 0.6$

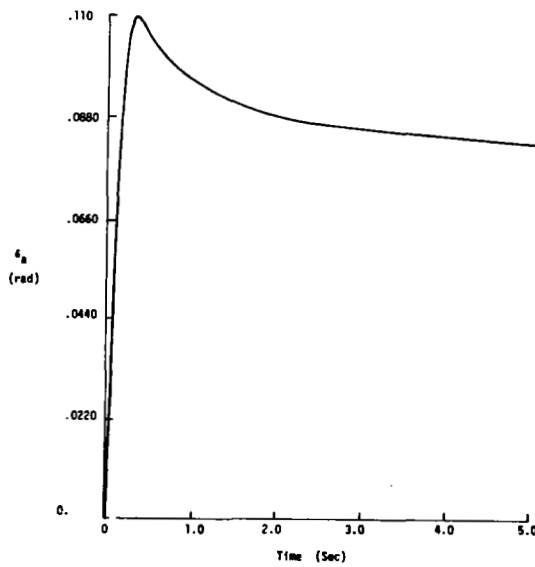
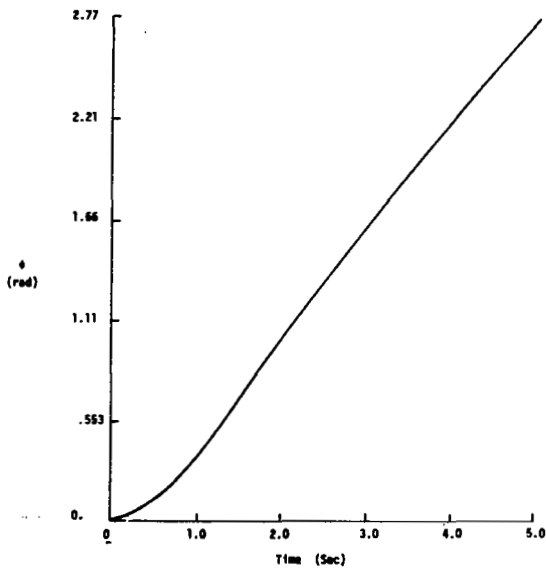
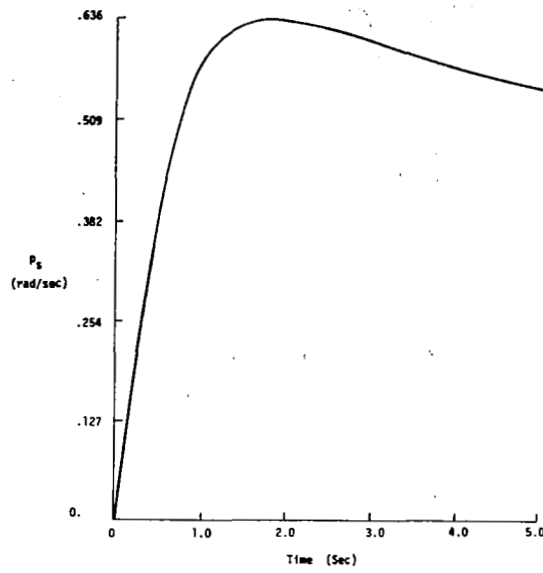
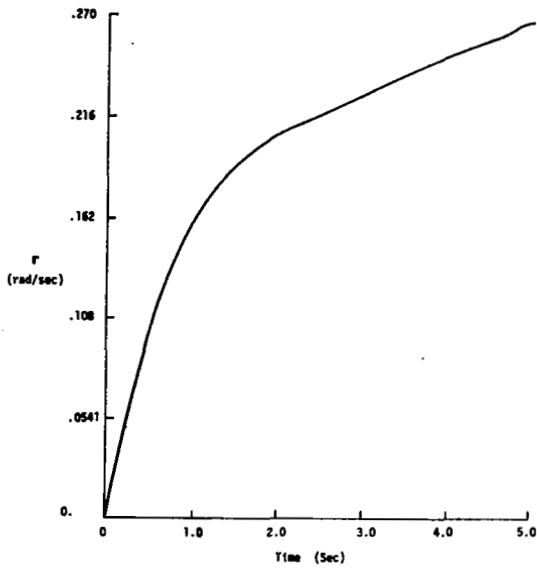


Figure 122. 3-g Pull-up with Inertial Lateral CAS
 $h = 20,000$ $M = 0.6$ (concluded)

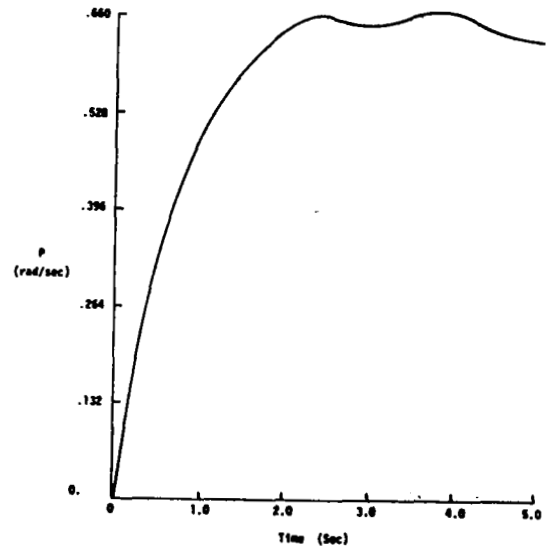
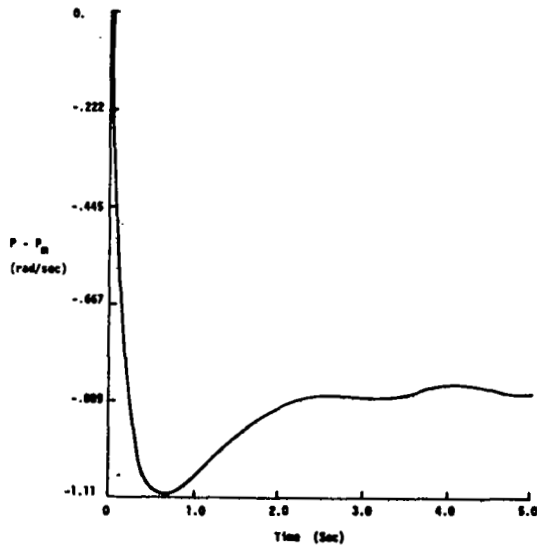
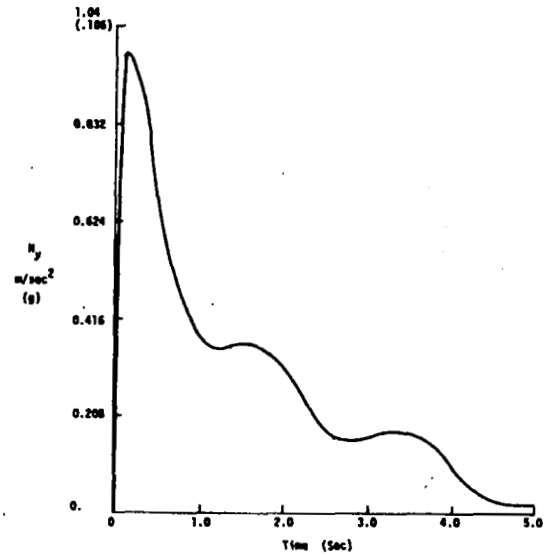
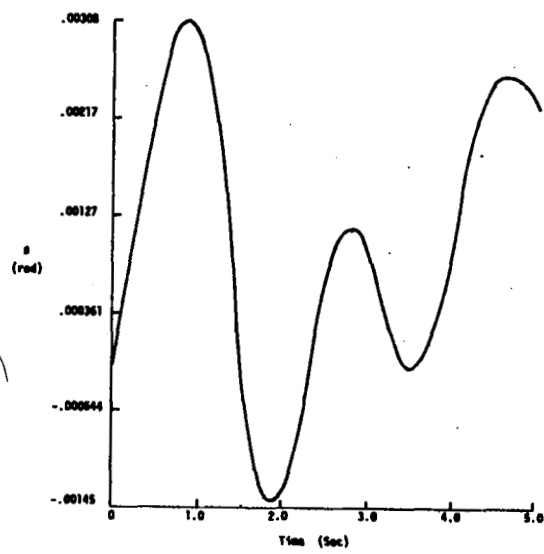


Figure 123. 3-g Pull-up with Reduced Measurement Lateral CAS

$h = 20,000$

$M = 0.6$

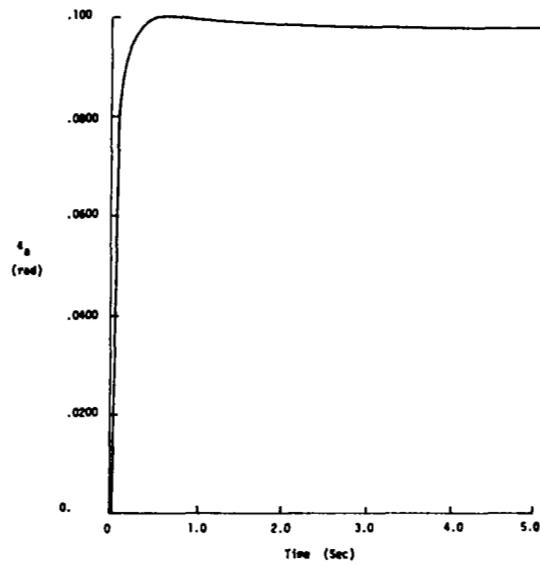
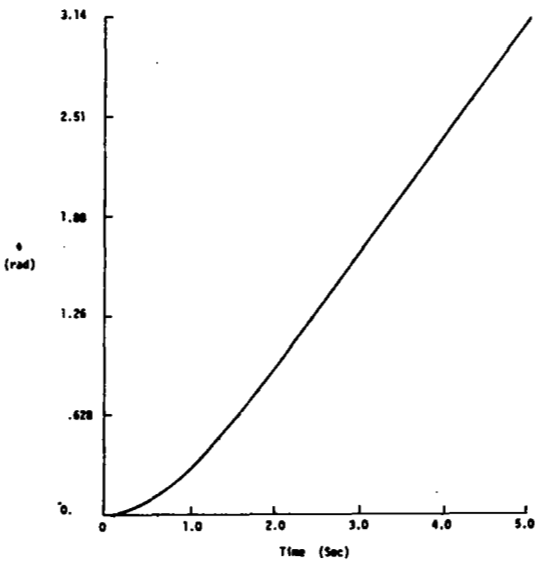
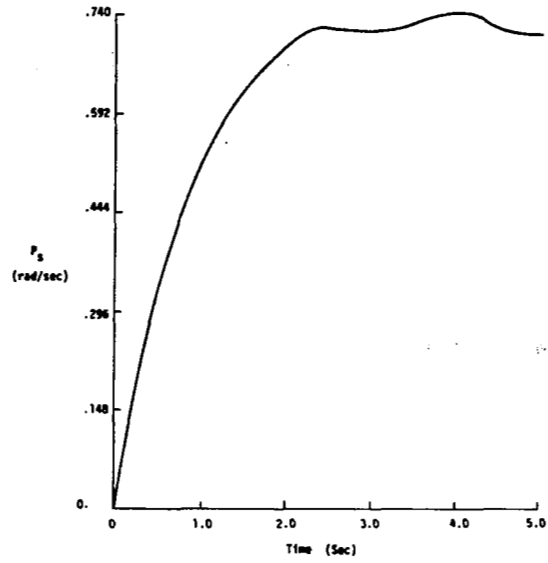
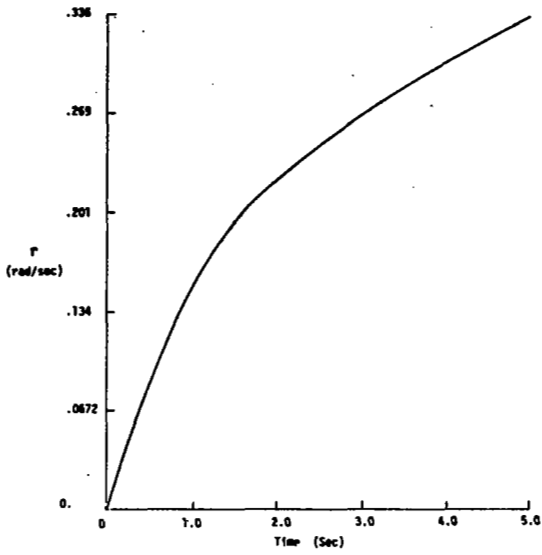


Figure 123. 3-g Pull-up with Reduced Measurement Lateral CAS
 $h = 20,000$ $M = 0.6$ (concluded)

SECTION 11

OUTER LOOP MODES

Conventional outer loops have been incorporated with the CCV inner loops. These functions were designed using classical techniques.

Pitch Axis

Three conventional autopilot modes have been provided:

- Attitude hold
- Altitude hold
- Mach hold

The outer-loop functional block diagram is shown in Figure 124. The three modes are mutually exclusive. Engagement of a selected mode is via a pilot selector switch; disengagement is via a control-stick-steering (CSS) switch or by exceeding preset mode constraints (e.g. a bank angle greater than 1 radian). The CSS switch activates above a preset stick force threshold (e.g. 2 pounds), after which the system reverts to the CAS mode. Various options exist for mode re-engagement upon stick force release, the simplest being to maintain the CAS mode. More complex options provide re-engagement of an autopilot mode upon stick release; usually the re-engaged mode is attitude hold regardless of the originally selected mode. An automatic re-engagement of altitude or Mach hold after making a CSS correction is generally not operationally convenient.

Common to all pitch autopilot modes is the bank angle feedback applied as a CAS command signal through the indicated velocity-scheduled gain. The bank angle function is designed to command the combination of pitch rate and normal acceleration required to approximately maintain the prevailing altitude rate (which is generally zero) up to a bank angle of 1 radian. The scheduled gain term matches the associated CAS feedback signals of acceleration and pitch rate as shown in Figure 125. Since the control roughly maintains altitude during a turn, the transient demands on the outer-loop feedback functions of pitch attitude and altitude are reduced to somewhat of a trim action. Furthermore, the transient performance of the system (e.g. altitude retention during turns) is generally improved. The value of this roll angle function for the Mach hold mode has not been determined at this writing. It is considered to be generally desirable, however, since it counteracts the normal speed increase tendency of the basic augmented airplane as the roll attitude increases.

The bank angle function is limited to that value necessary for the ± 1 radian operating range of the autopilot modes. The absolute value of the $\sec \theta$ function is unnecessary for normal operation, but provides added safety under attitude reference malfunctions.

The pitch attitude hold mode maintains the attitude existing at the time of engagement by storing the reference attitude on integrator I_1 , and holding the reference constant during engagement. The error signal which is formed from the attitude input and reference combination is applied through the velocity scheduled gain and shaping arrangement shown in Figure 124 as a CAS command signal. The net steady-state gain of the attitude error signal is $324 + V_{T_0}$ which combines with the CAS feedbacks to maintain (via the integrating elevator actuator) the following steady-state relationship.

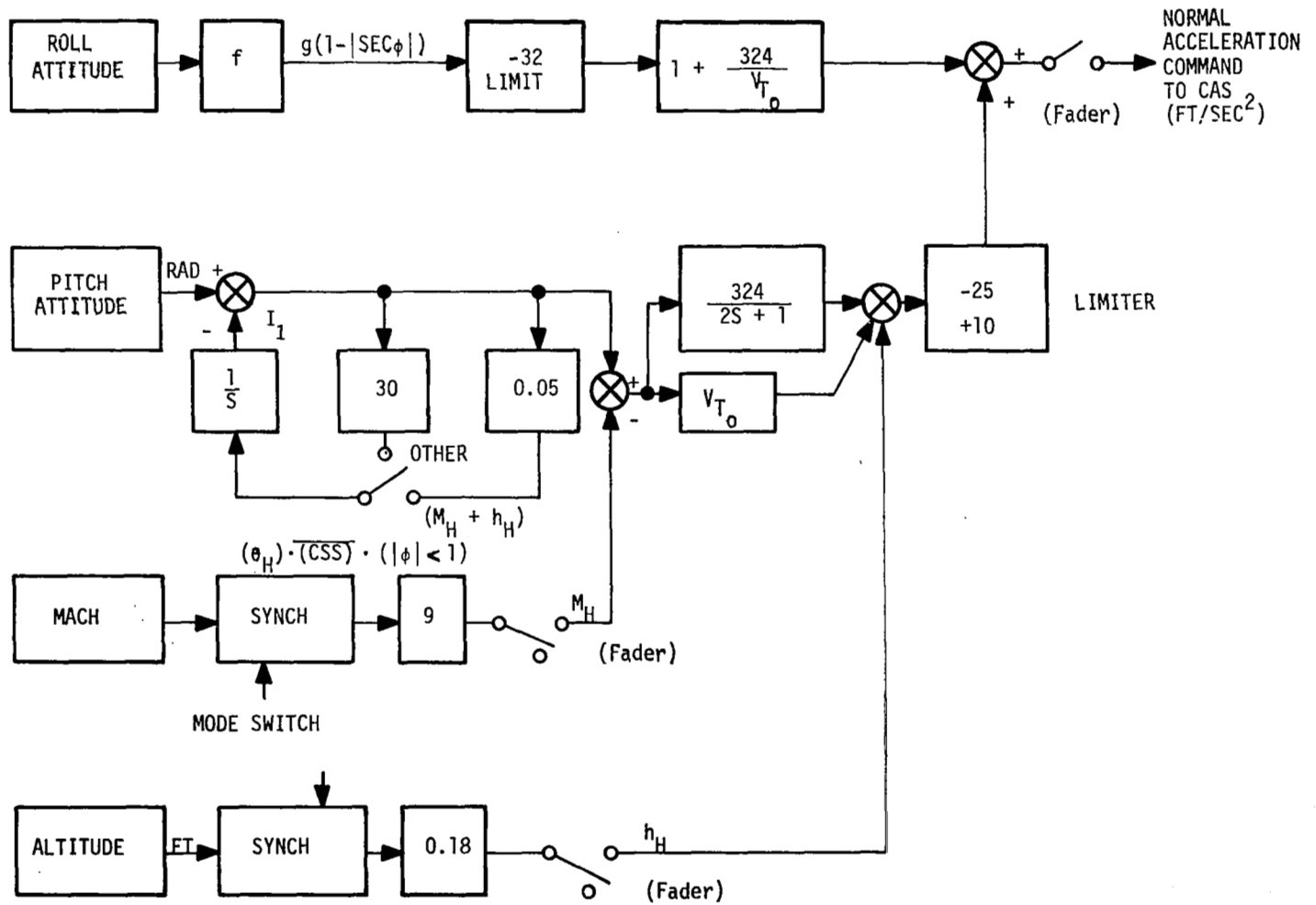


Figure 124. Pitch Outer Loops

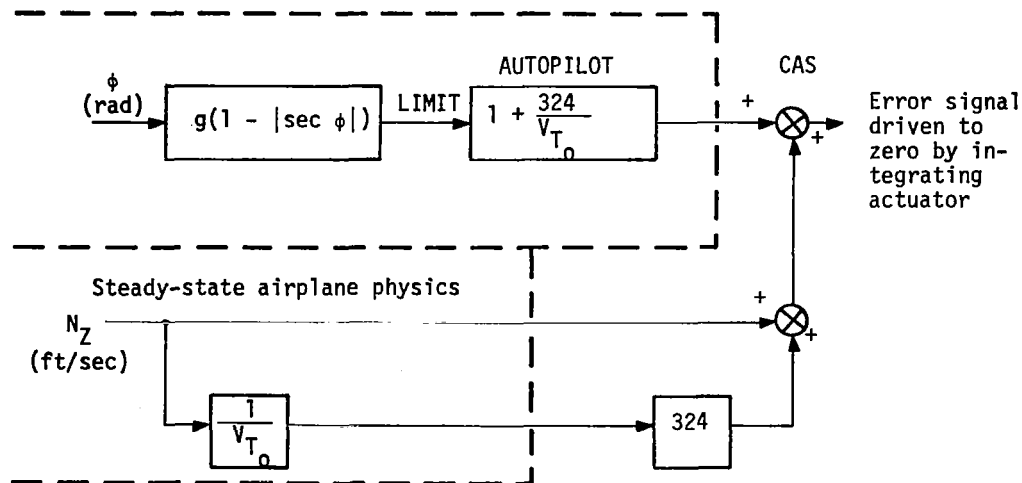


Figure 125. Pitch Autopilot Gain Schedule

$$\theta_E (324 + V_{T_0}) + N_Z + q (324) = 0$$

With the relationship $N_Z = V_{T_0} q$,

$$\theta_E (324 + V_{T_0}) + q (324 + V_{T_0}) = 0$$

resulting in one unit of attitude error (θ_E) producing one unit of pitch rate at all flight conditions. Consequently, ignoring short-period dynamics, the attitude control loop tends toward a desirable one-second time constant. When short-period dynamics are considered, the pitch rate response to an attitude error is characterized by a first-order over a second-order transfer function, the latter constituting the effective augmented short-period frequency. The first-order numerator is the time-constant relating flight path to attitude changes. These inner-loop dynamics approximate the response frequency of the attitude control loop at lower dynamic pressures; hence to avoid undesirable coupling at these flight conditions, a 2-second lag is placed on a portion of the attitude error gain. Because the parallel gain path (which is not lagged) is set equal to velocity, the effect of the lag is reduced as the velocity increases. It is not known whether velocity is the best scheduling parameter in this situation, but it does accomplish the general gain variation desired.

The command signals to the CAS generated by the attitude error signal (and by the other error signals of Mach and altitude when engaged) are limited as indicated (to approximately $-3, +8$ g's). These limits will probably never be encountered except perhaps when engaging altitude hold at high initial altitude rates. They provide, therefore, a controlling element to determine the compromise between altitude overshoot and pilot comfort.

The Mach hold mode controls the Mach number to that which exists upon mode engagement. The associated error signal is generated by the synchronizing arrangement shown in Figure 124. The pitch attitude mode provides an inner loop for the Mach mode, and Mach error signals can be thought of as pitch attitude command signals. To allow attitude trim changes (and achieve low steady-state Mach errors) the attitude reference integrator is slowly reset at an effective time constant (20 seconds) which

is slow compared to the Mach hold response frequencies. The resulting Mach control loop can be approximated as shown in Figure 126.

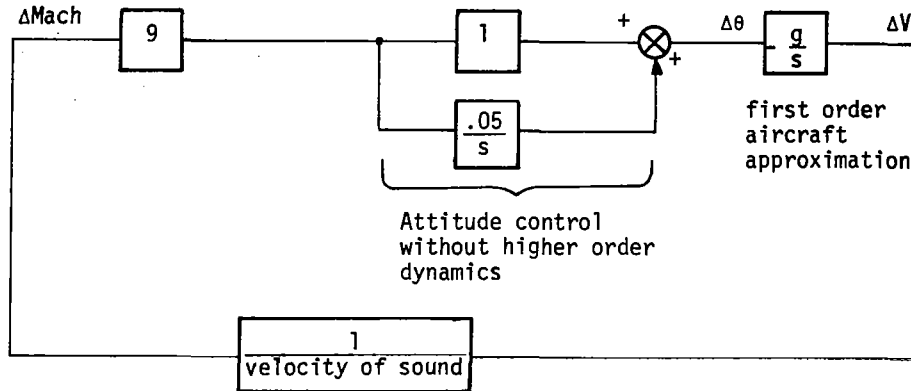


Figure 126. Mach Hold Control

Using nominal values, the Mach loop gain has a bandwidth of approximately 0.3 radians per second, sufficiently below the 1-radian-per-second attitude control loop frequency to avoid stability problems.

An unknown in the above synthesis process is the quality of the Mach signal itself. Noise content may dictate added filtering (with potential gain reduction) or filtering in combination with signal blending (Mach, attitude, and longitudinal acceleration). A similar action may be necessary for the altitude error signal used for the altitude control loop, the blend including barometric altitude, normal acceleration, and roll attitude.

The altitude hold mode maintains the altitude existing at time of engagement, the error signal being generated by the synchronizing element shown in Figure 124. The pitch attitude control forms the inner loop for the altitude mode, with the attitude reference integrator being slowly reset to allow attitude trim changes with low altitude error. At the point in the system where the altitude error is summed with the attitude error function, the latter approximates altitude rate (loosely at low dynamic pressures, closely at high dynamic pressures).

An approximation to the altitude loop is illustrated in Figure 127.

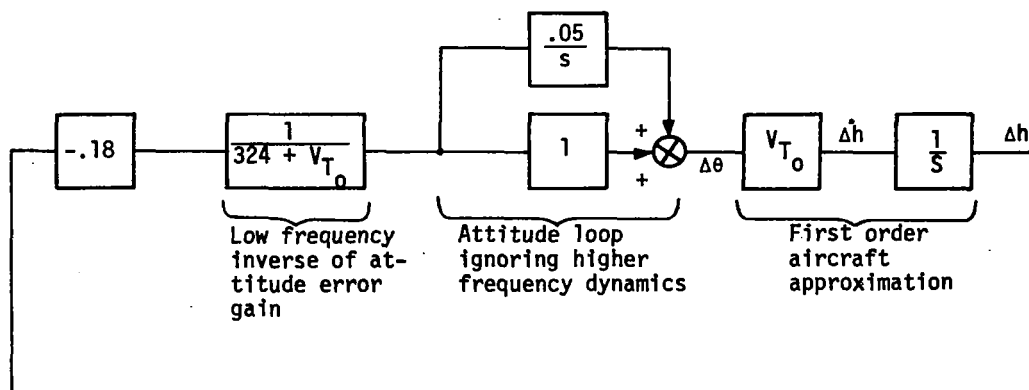


Figure 127. Altitude Hold Dynamics

The altitude loop gain, therefore, remains approximately constant, varying from about $.15 \text{ sec}^{-1}$ at high speed to about half as much at low speed. These values maintain a desirable intermediate position between the higher order attitude loop dynamic range and 20-second attitude reference integrator reset rate.

The switches controlling mode status use two-second faders to eliminate objectionable transients. The attitude reference integrator has the digital form

$$\frac{T}{2} \frac{1 + Z^{-1}}{1 - Z^{-1}}$$

and the 2-second lag has the form

$$\frac{T(1 + Z^{-1})}{(4 + T) - (4 - T)Z^{-1}}$$

where T is the sample period. It is recommended that the sampling rate of the outer loops be one-half the inner loop sampling rate. Therefore, the sampling rate is 20 sps.

Lateral-Directional Outer Loops

Two outer loop autopilot functions are provided:

- roll attitude hold
- heading hold

These modes are mutually exclusive. The block diagrams of the outer loops are shown in Figure 128. Upon engaging roll attitude, the roll synch stores the prevailing value of ψ as the reference. The attitude error is fed back as a roll rate command to the CAS. The roll attitude mode is dropped when roll stick forces exceed $\pm F_{RC}$ (preset constant) or when the roll angle exceeds 1 radian.

A roll attitude error gain of 3 (rad/sec of commanded roll rate per radian of attitude error) is selected to provide a maximum roll attitude loop bandwidth consistent with good damping. An effective roll subsidence time constant up to about 0.4 seconds may be tolerated with this gain, therefore, which appears to be within CAS performance capabilities. The roll rate command limit is set at ± 0.2 rad/sec, primarily as a pilot comfort element if heading select is applied in the alternate mode.

Upon engaging heading hold, the reference value of ψ is stored, and the sum of heading error and bank angle becomes the roll rate command to the CAS. The gain and limiting values of the heading error are switched to smaller values for power approach. The heading error can be generated by the synchronizer as indicated or by a heading select error signal generated by an external source. A limited authority (± 0.1 radian) heading error integrator is provided to minimize steady state error. It is activated only if the heading error is small to avoid undesirable transients under large heading changes when considerable time is spent on the bank limit.

The values of the heading error gains are selected to produce a responsive heading control consistent with good damping. Because the heading rate per unit bank angle varies g/V_{T_0} , the highest loop gain tends to occur at low speed (hence the heading error gain reduction for power approach). Using the higher heading error gain (4) and a minimum velocity of 200 ft/sec, a maximum heading loop gain of 0.64 sec^{-1} results. This is sufficiently below the roll attitude response frequencies (around 3 rad/sec) to maintain good heading damping. The heading integrator operates a decade below the maximum heading loop frequency, maintaining low frequency stability even at the maximum speed end of the flight range.

Two-second faders are used on switches to reduce transients when engaging or disengaging modes. The logic that defines the switch positions is shown in Figure 128. The integrator has the digital form

$$\frac{T}{2} \frac{1 + Z^{-1}}{1 - Z^{-1}}$$

where T is the sample period. It is recommended that the sample rate be one half the inner loop sample rate (i. e., 20 sps).

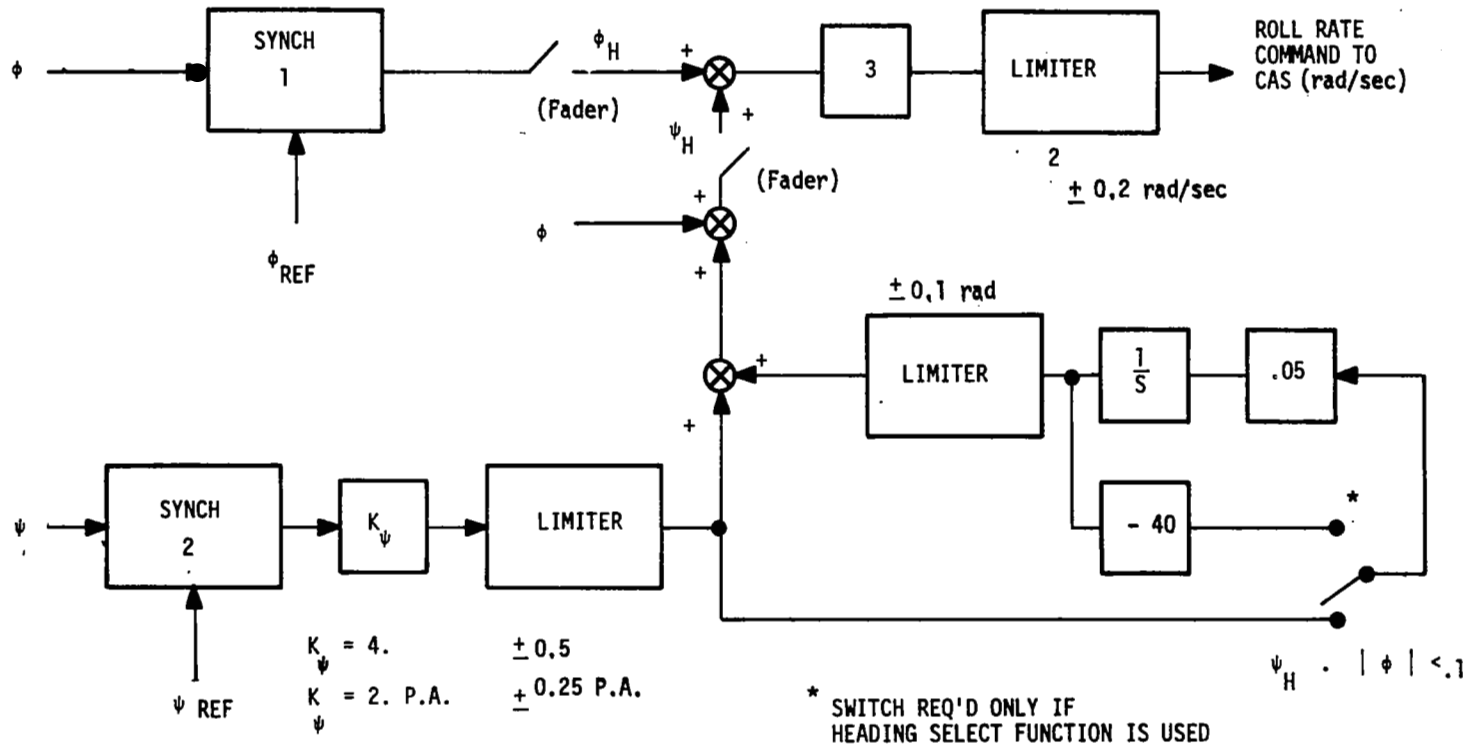


Figure 128. Lateral Outer Loops

SECTION 12

SYSTEM INTEGRATION VERIFICATION

This section presents a series of test operations recommended for verification of proper function of the CCV control laws applied to the F-8C digital fly-by-wire system. The general intent is to demonstrate that the performance is comparable to that determined during prior system synthesis efforts and suitable for further flight test investigation. Related assessments include:

- (1) Performance of actuation elements and related interfaces
- (2) Programming
- (3) Pilot input sensors, control panels, and related interfaces
- (4) Feedback sensor interfaces
- (5) Structural stability during ground operation

Open-Loop Frequency Response Tests

This set of tests is specified by Table 26. Each test is a single input test, with the outputs of all motion sensors (gyros and accelerometers) blocked or otherwise disabled to preclude extra inputs. A single analog sine wave input is applied at the specified sensor input. The output is measured in terms of either actual or simulated surface position, the latter being obtained by simulating servo and surface actuators on a general-purpose computer driven by the analog servo command signal. In one case (test number 7) the actual servo must be used to obtain forward-loop integration characteristics in pitch. In other cases (tests 8 and 9), a simulated servo is specified to avoid this same integration effect.

Note that all functions are specified under the assumption that a zero-order hold output is used and that the programming is such that computation delay effects are negligible.

The functions used to compute the frequency response for each of the sixteen tests are listed in Table 26. Two frequency response plots are given for each test. The first is for a sampling time of 0 (continuous), and the second is for a digital system at a sampling rate of 32 sps. The discrete plots used the Tustin equivalent of the indicated analog filters and include the effects of the zero-order holds (ZOH). Therefore, frequency response checks for operation at other than 32 sps are easily computed with DIGIKON.

Gain Schedule Verification

These operations check proper implementation of gain schedules by a series of open-loop input/output measurements. Each test uses a single analog input with all other inputs nominally zero. Variations in direct-current inputs are made sufficiently slow to preclude dynamic effects (i. e., allow outputs to "settle" before reading). Gains applicable to high-passed paths are checked at discrete frequencies. Table 27 specifies the actual test functions and expected results.

Table 26. Open-Loop Frequency Responses

Test	Conditions	Frequency (rad/sec)	Approximate Amplitudes	Input	Output	Frequency Response	
						Continuous	32 sps
1. Pitch rate to elevator (PA) Figure 129	$\alpha \approx 0$ QF off, NF off $\delta_e \approx 0$ (via trim) PA $\bar{q} < 50$ psf CAS on	0.4 - 30.	$\delta_e = + 2^\circ, \omega < 10$ $= + \frac{20}{\omega}, \omega \geq 10$	Simulated pitch rate (variable)	Elevator position	Figure 130	Figure 131
2. Normal acceleration to elevator Figure 132	(Same as above)	0.4 - 30.	(Same as above)	Simulated normal acceleration (variable)	Elevator position	Figure 133	Figure 134
3. Pitch stick to elevator Figure 135	(Same as above)	0.4 - 30.	(Same as above)	Simulated pitch stick (variable) bias to eliminate dead spot	Elevator position	Figure 136	Figure 137
4. Pitch rate to flaps Figure 138	$\alpha \approx 0$ QF on, NF off $\delta_e \approx 0$ (via trim) PA $\bar{q} < 50$ psf CAS on	0.4 - 10.	$\delta_a = + 4^\circ$	Simulated pitch rate (variable)	Elevator position Flap position	Figure 139 Figure 141	Figure 140 Figure 142
5. Pitch stick to flaps Figure 143	CAS on NF on PA $\bar{q} < 50$ psf $V_o < 59$ KTS	0.4 - 10.	$\delta_a = + 10^\circ, \omega < 3$ $\delta_a = + \frac{30}{\omega}, \omega \geq 3$	Simulated pitch stick (variable) bias to eliminate dead spot	Flap Position	Figure 144	Figure 145

Table 26. Open-Loop Frequency Responses (continued)

Test	Conditions	Frequency (rad/sec)	Approximate Amplitudes	Input	Output	Frequency Response	
						Continuous	32 sps
6. Normal Acceleration to flaps Figure 146	CAS on NF on PA $\bar{q} < 50$ psf	0.4 → 10.	$\delta_a = +10^\circ, \omega < 3$ $\delta_a = +\frac{30}{\omega}, \omega \geq 3$	Simulated normal acceleration (variable)	Flap position	Figure 147	Figure 148
7. Pitch rate to elevator Figure 149	$\alpha \approx 0$ OF off, NF off PA $\bar{q} < 50$ psf CAS on $\delta_e \approx 0$ (via trim) Use actual servo	0.4 → 10.	$\delta_e = +2^\circ$	Simulated pitch rate (variable)	Elevator position	Figure 150	Figure 151
8. Angle of attack to elevator (boundary function) Figure 152	CAS on NF off, QF off PA $\alpha \approx \alpha$ limit simulate servo/ actuator $V_o < 59$ KTS Max. nose up trim	0.4 → 10.	$\alpha = +5^\circ$	Simulated angle of attack	Elevator position	Figure 153	Figure 154
9. Pitch rate to elevator (boundary function) Figure 155	CAS on NF off QF off PA $\alpha \approx \alpha$ limit Simulate servo $V_o < 59$ KTS $\bar{q} < 50$ psf Max. nose up trim	0.4 → 10.	$q = +2^\circ/\text{sec}$	Simulated pitch rate	Elevator position	Figure 156	Figure 157

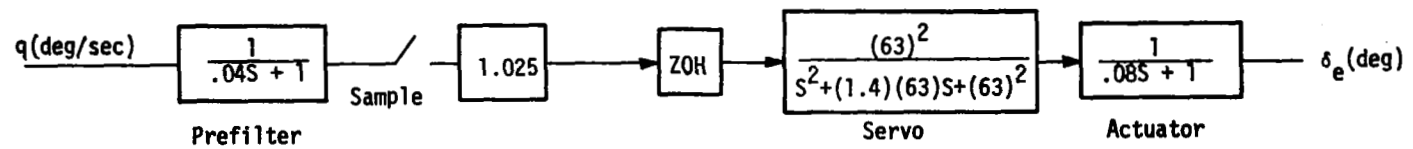
Table 26. Open-Loop Frequency Responses (continued)

Test	Conditions	Frequency (rad/sec)	Approximate Amplitudes	Input	Output	Frequency Response	
						Continuous	32 sps
10. Roll rate to aileron Figure 158	Cas on NF off QF off PA $\delta_a \approx 0$	0.4 → 30.	$p = +10^\circ/\text{sec}$	Simulated roll rate	Aileron position Rudder position	Figure 159 Figure 161	Figure 160 Figure 162
11. Roll stick to aileron Figure 163	$\delta_a \approx 0$ CAS on NF off QF off $\delta_a \approx 0$ PA	0.4 → 10.	$+10^\circ/\text{sec}$ equivalent roll stick	Simulated roll stick. Bias or reprogram to remove stick nonlinearities	Aileron position	Figure 164	Figure 165
12. Yaw rate to rudder Figure 166	CAS on PA $\delta_r \approx 0$	0.4 → 30.	$\delta_r = +2^\circ$	Simulated yaw rate (variable)	Rudder position	Figure 167	Figure 168
13. Lateral acceleration to rudder Figure 169	$\delta_r \approx 0$ CAS on	0.1 → 10.	$\delta_r = +4^\circ$	Simulated lateral acceleration (variable)	Rudder position	Figure 170	Figure 171
14. Roll rate to rudder Figure 172	CAS on $\alpha > 18$ Clean condition	0.1 → 10.	$\delta_r = +2^\circ$	Simulated roll rate (variable)	Rudder position	Figure 173	Figure 174
15. Pitch attitude to elevator Figure 175	Attitude hold on PA $\alpha \approx 0$ $\delta_e \approx 0$ (via trim) $\bar{q} < 50$ psf $V_o < 59$ KTS	0.1 → 10.	$\delta_a = +4^\circ$	Simulated heading angle (variable)	Aileron position	Figure 176	Figure 177

Table 26. Open-Loop Frequency Responses (concluded)

Test	Conditions	Frequency (rad/sec)	Approximate Amplitudes	input	Output	Frequency Response	
						Continuous	32 sps
16. Heading to aileron Figure 178	Heading hold on PA $\delta_a \approx 0$	0.1 - 10.	$\delta_a = +4^\circ$	Simulated heading angle (variable)	Aileron position	Figure 179	Figure 180

* 16 sps



- $\bar{q} < 50$ psf
- PA Condition

Figure 129. Sensed Pitch Rate to Elevator

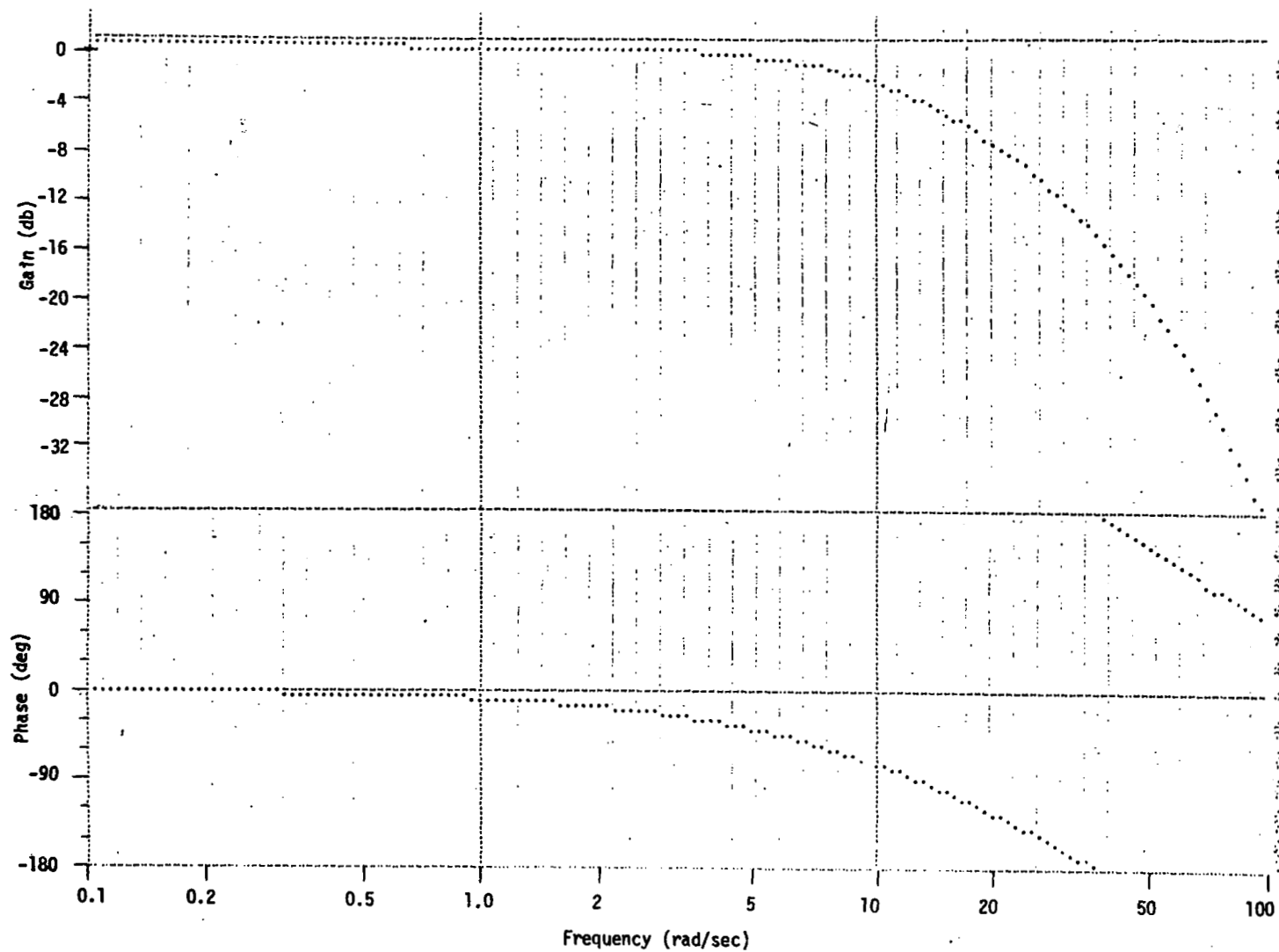


Figure 130. Pitch Rate to Elevator Frequency Response (continuous)

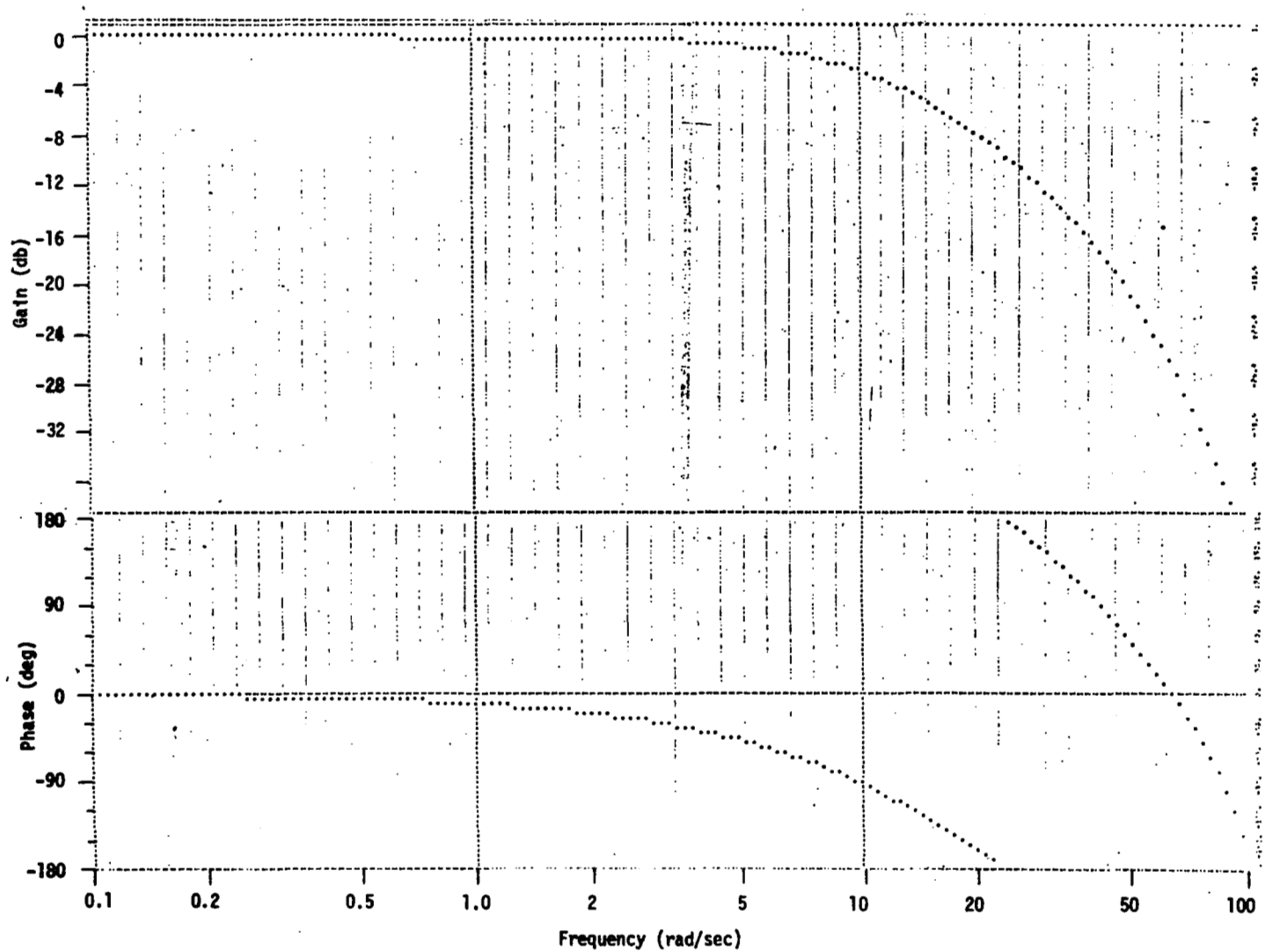
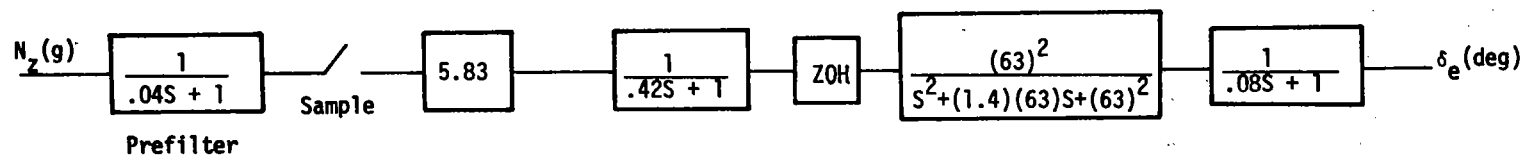


Figure 131. Pitch Rate to Elevator Frequency Response (32 sps)



- $\bar{q} < 50$ psf
- PA Condition

Figure 132. Sensed Normal Acceleration to Elevator

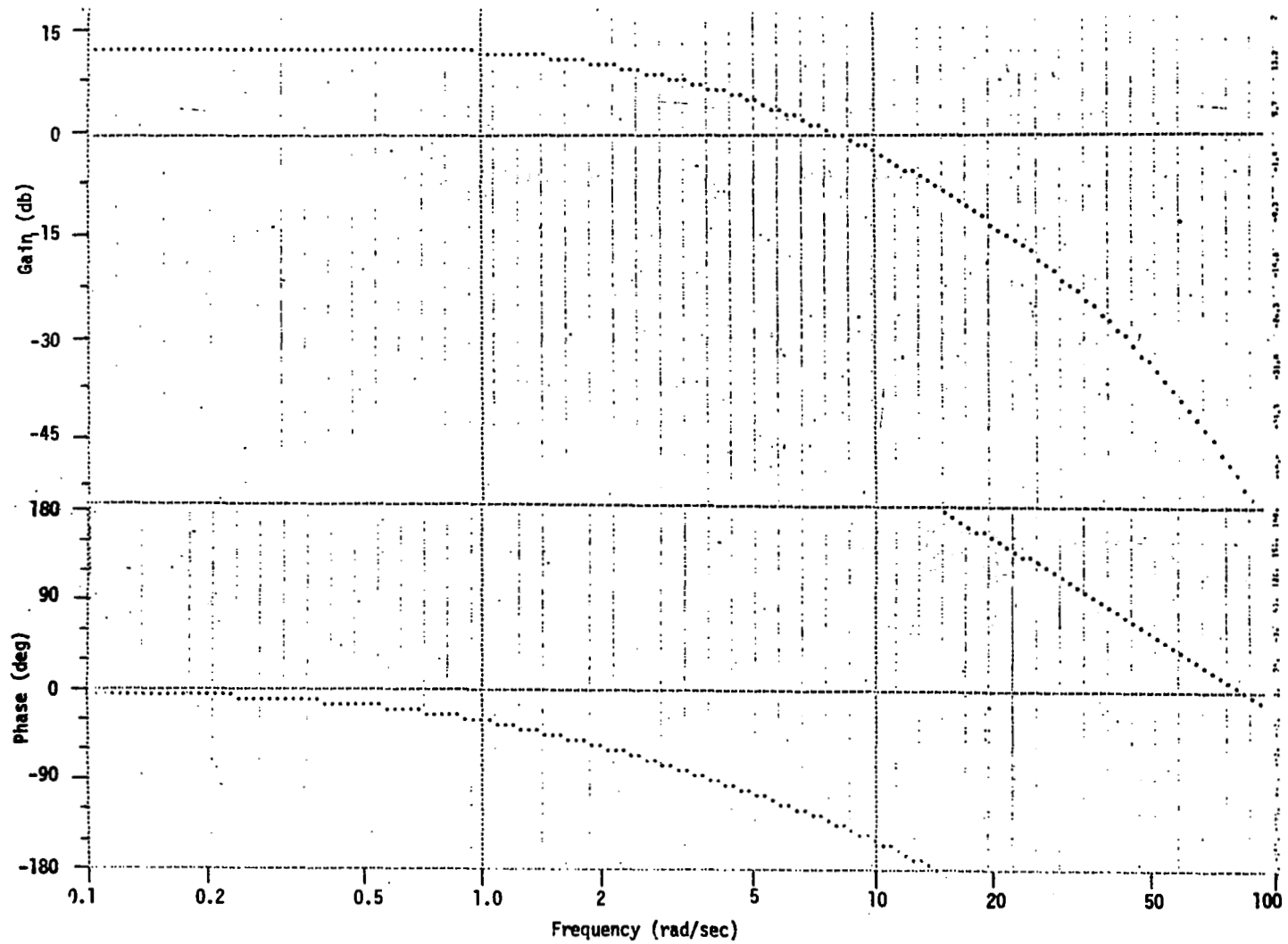


Figure 133. Normal Acceleration to Elevator Frequency Response (continuous)

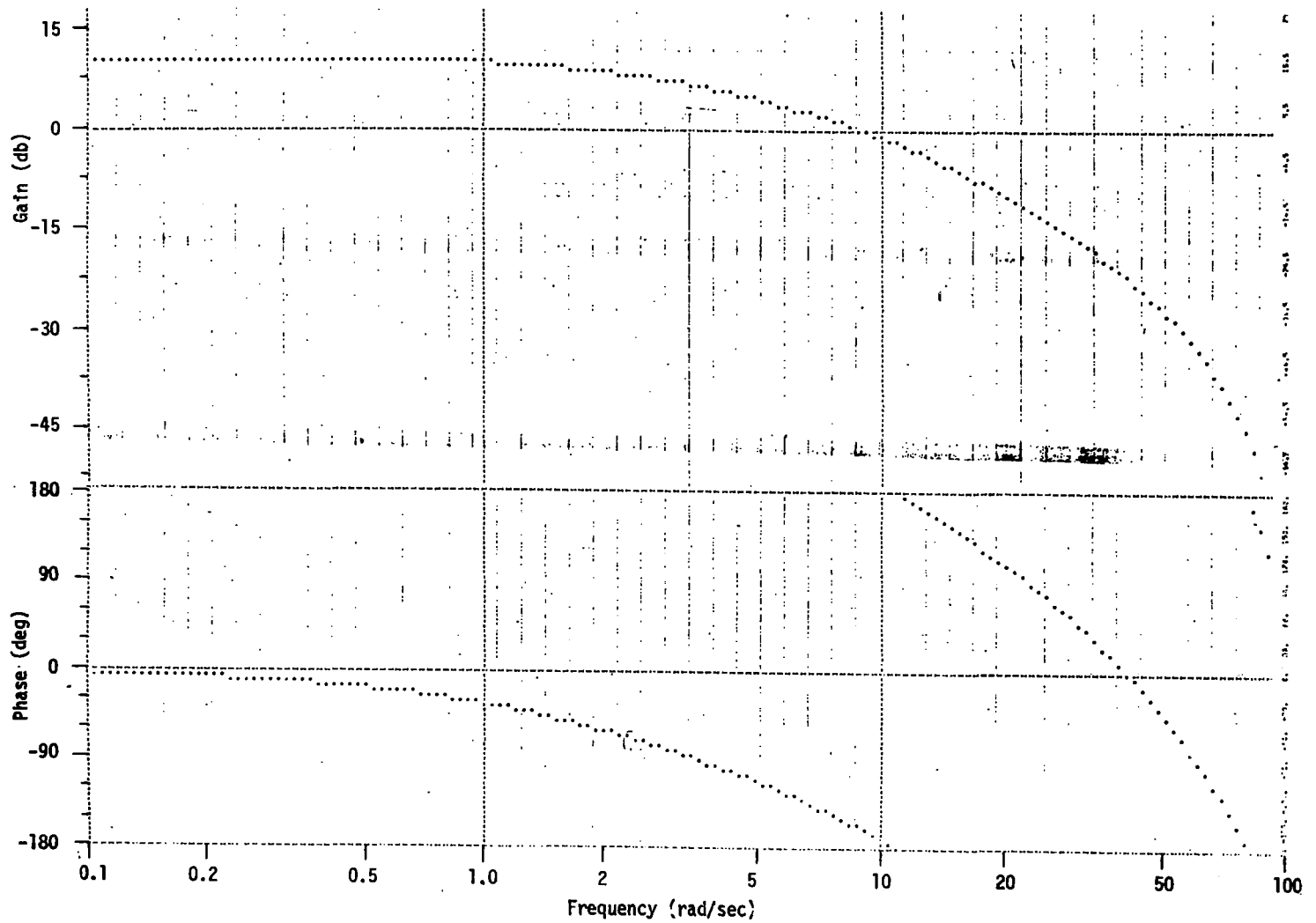
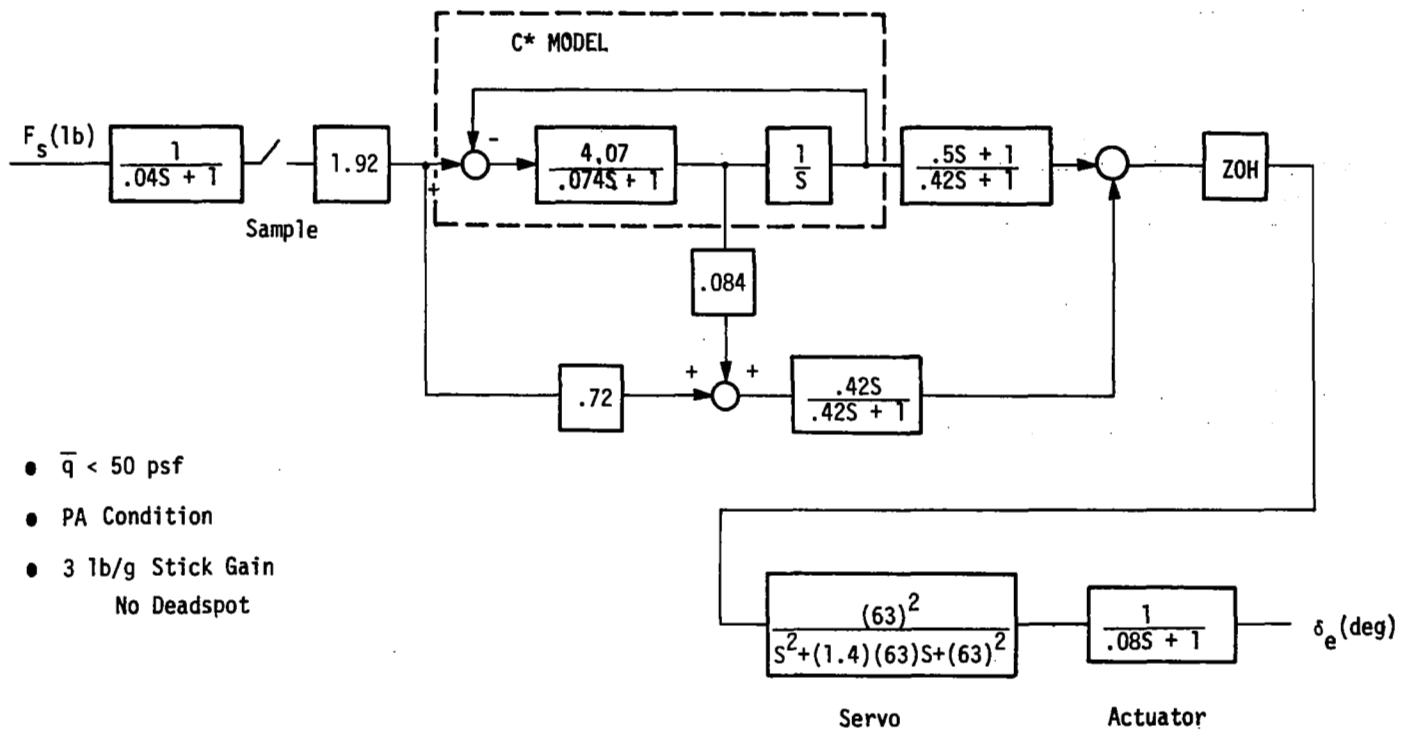


Figure 134. Normal Acceleration to Elevator Frequency Response (32 sps)



- $\bar{q} < 50$ psf
- PA Condition
- 3 lb/g Stick Gain
No Deadspot

Figure 135. Pitch Stick to Elevator

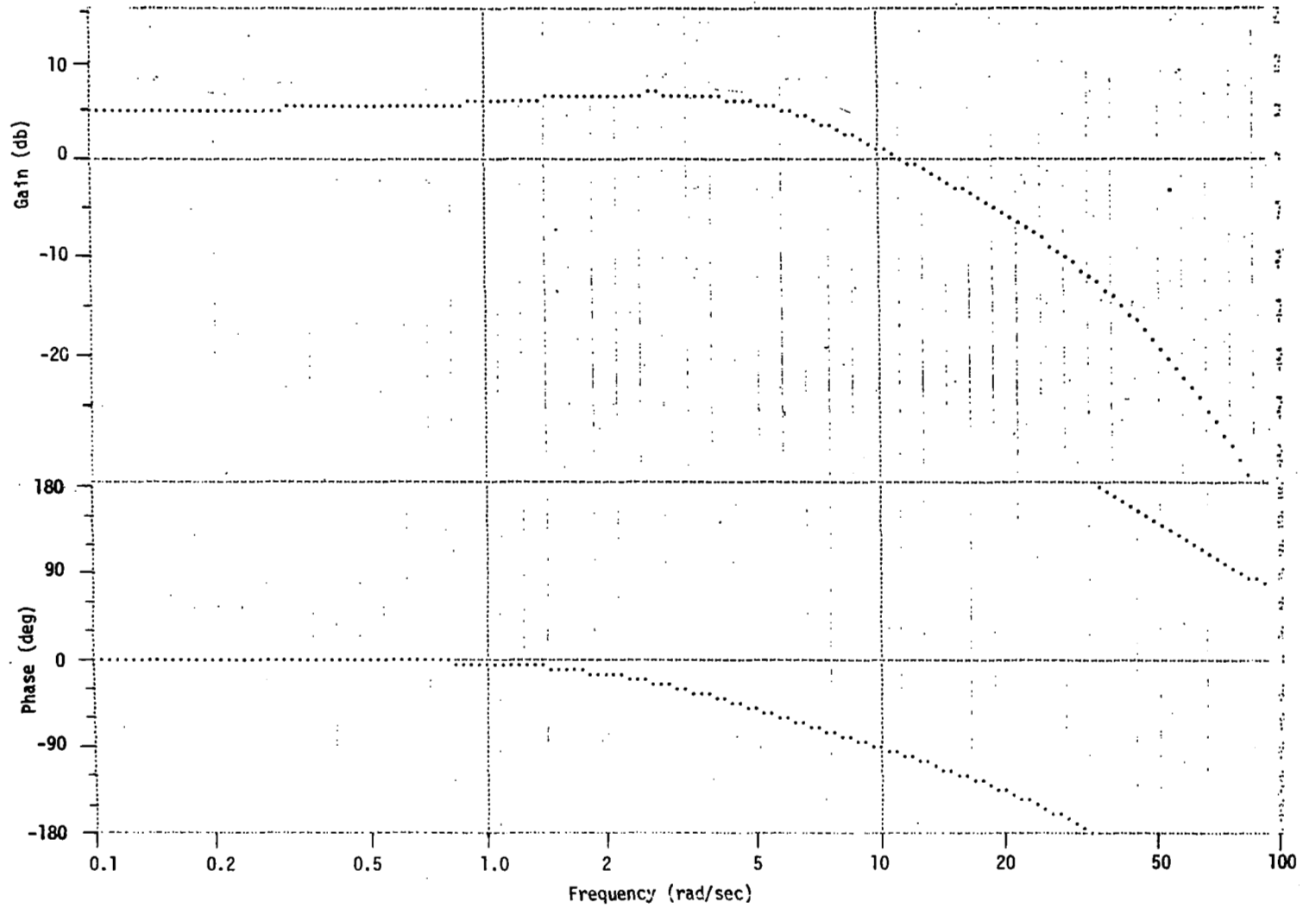


Figure 136. Pitch Stick to Elevator Frequency Response (continuous)

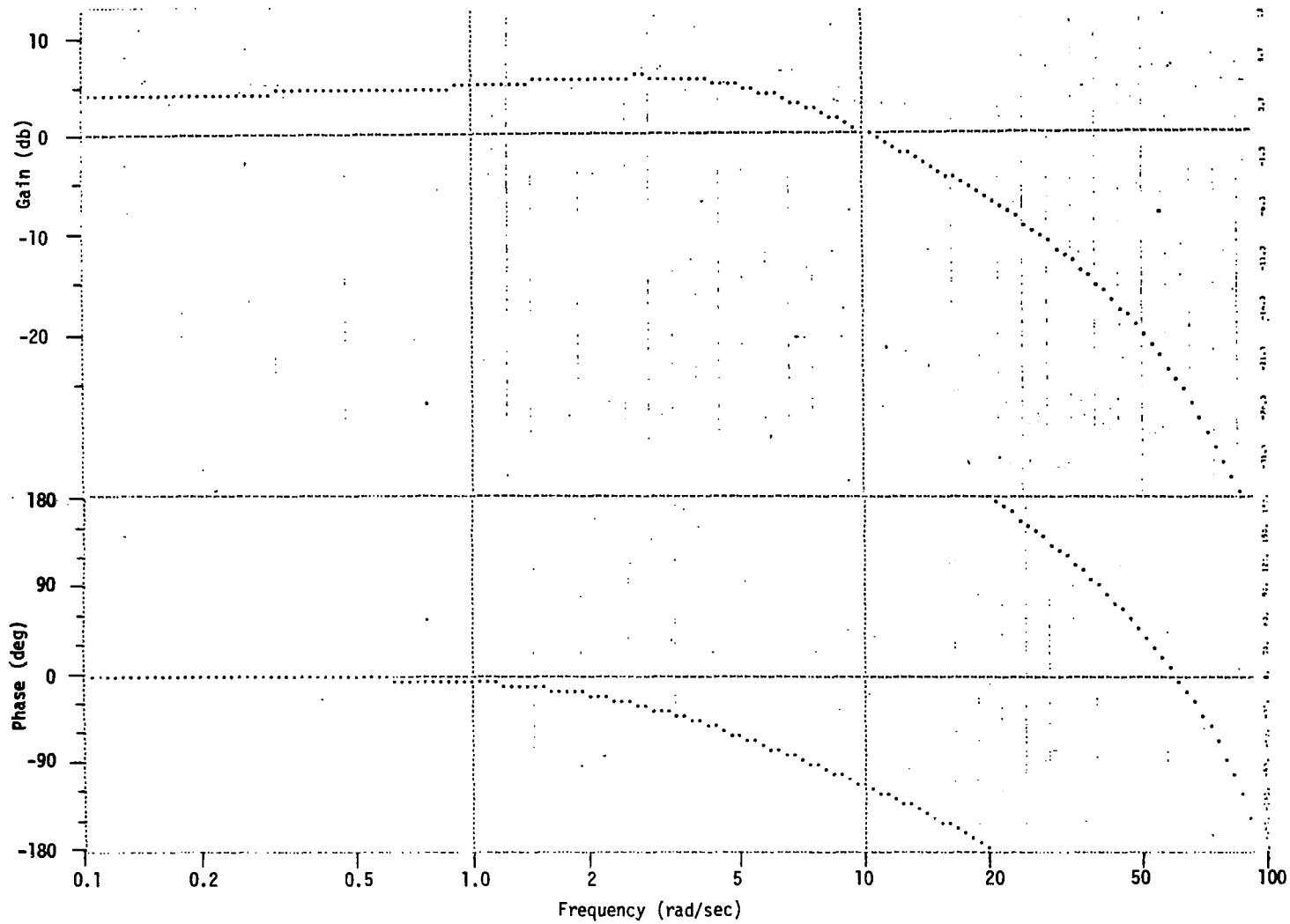


Figure 137. Pitch Stick to Elevator Frequency Response (32 sps)

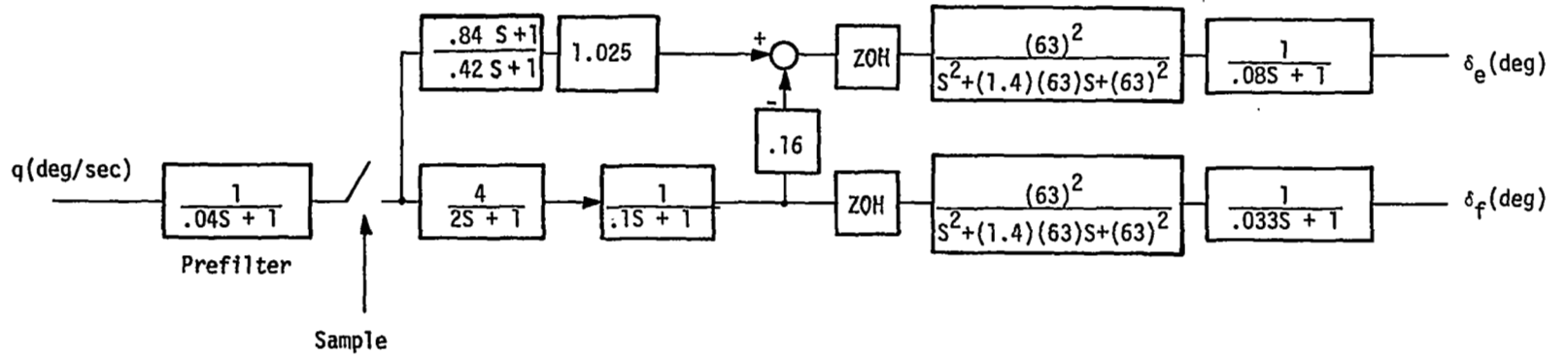


Figure 138. Pitch Rate to Elevator and Flaps

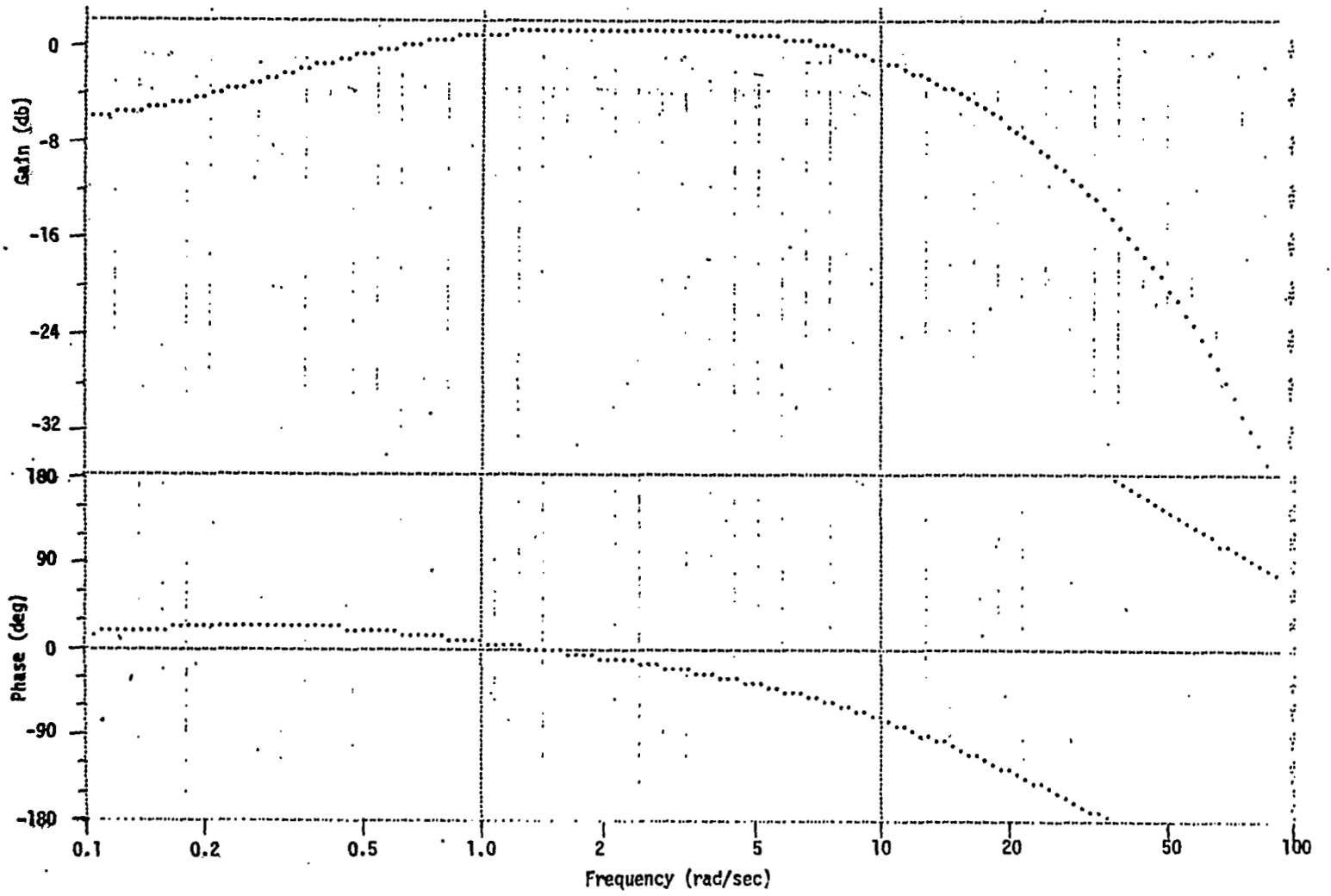


Figure 139. Pitch Rate to Elevator Frequency Response (continuous)

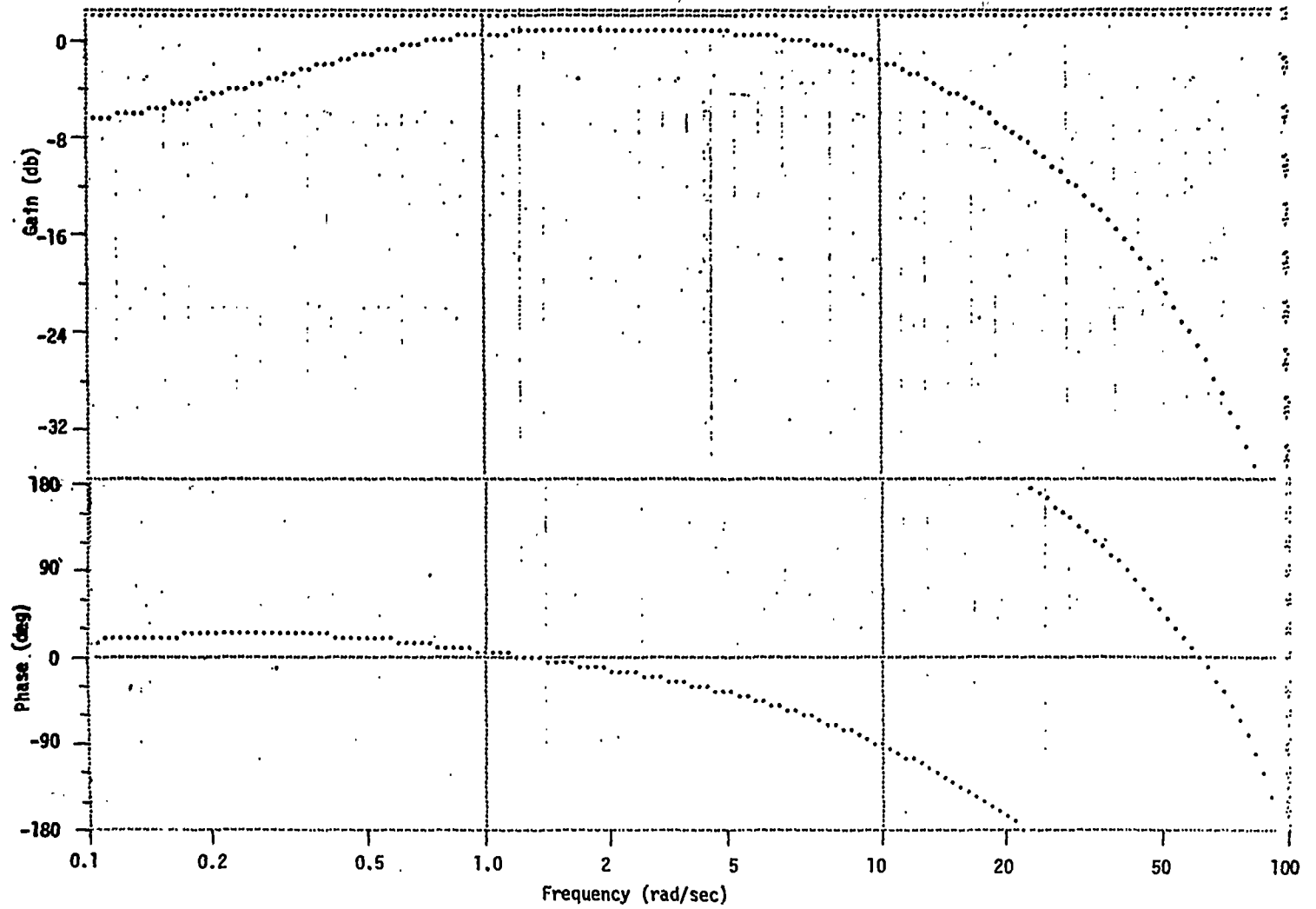


Figure 140. Pitch Rate to Elevator Frequency Response (32 sps)

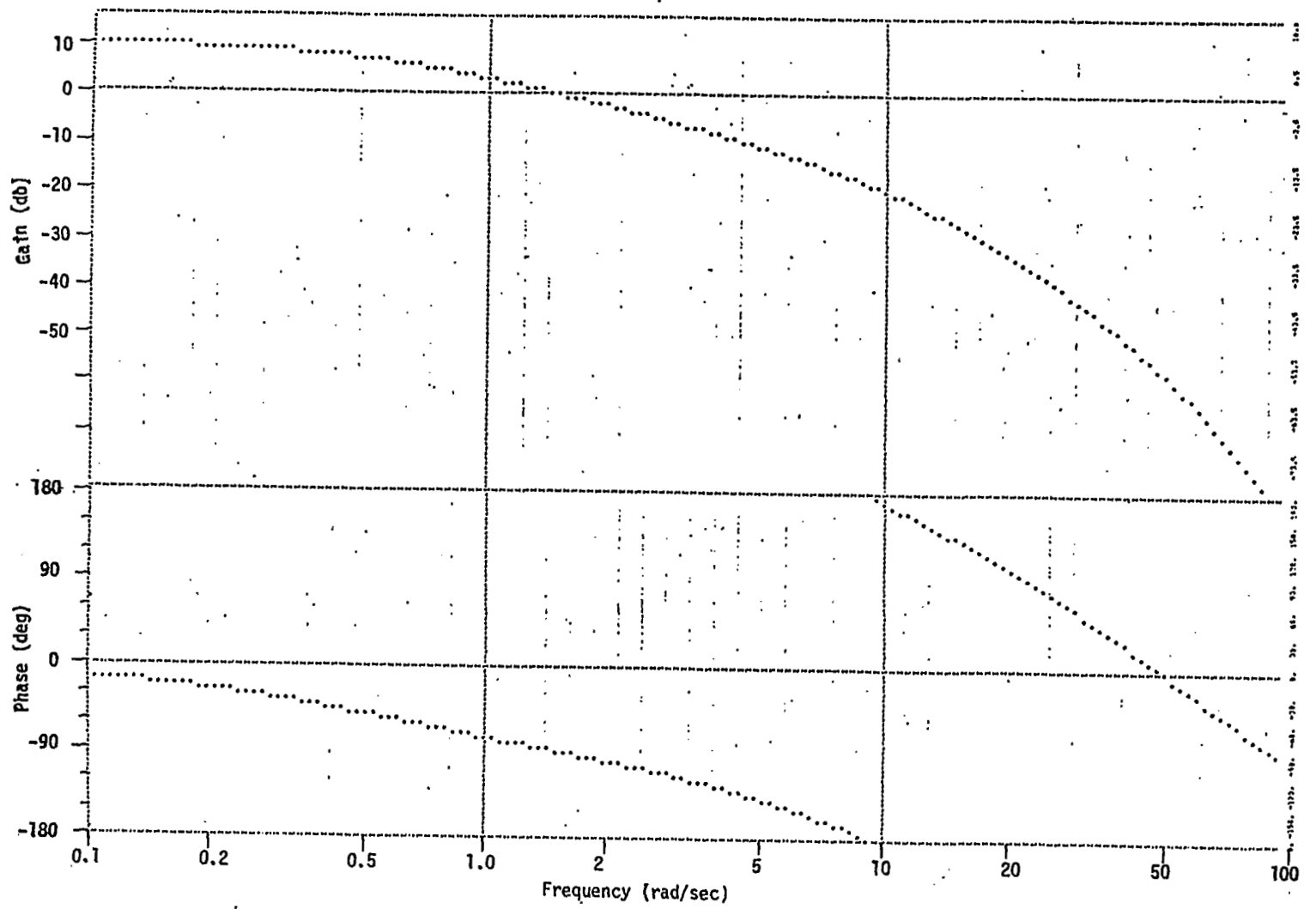


Figure 141. Pitch Rate to Flaps Frequency Response (continuous)

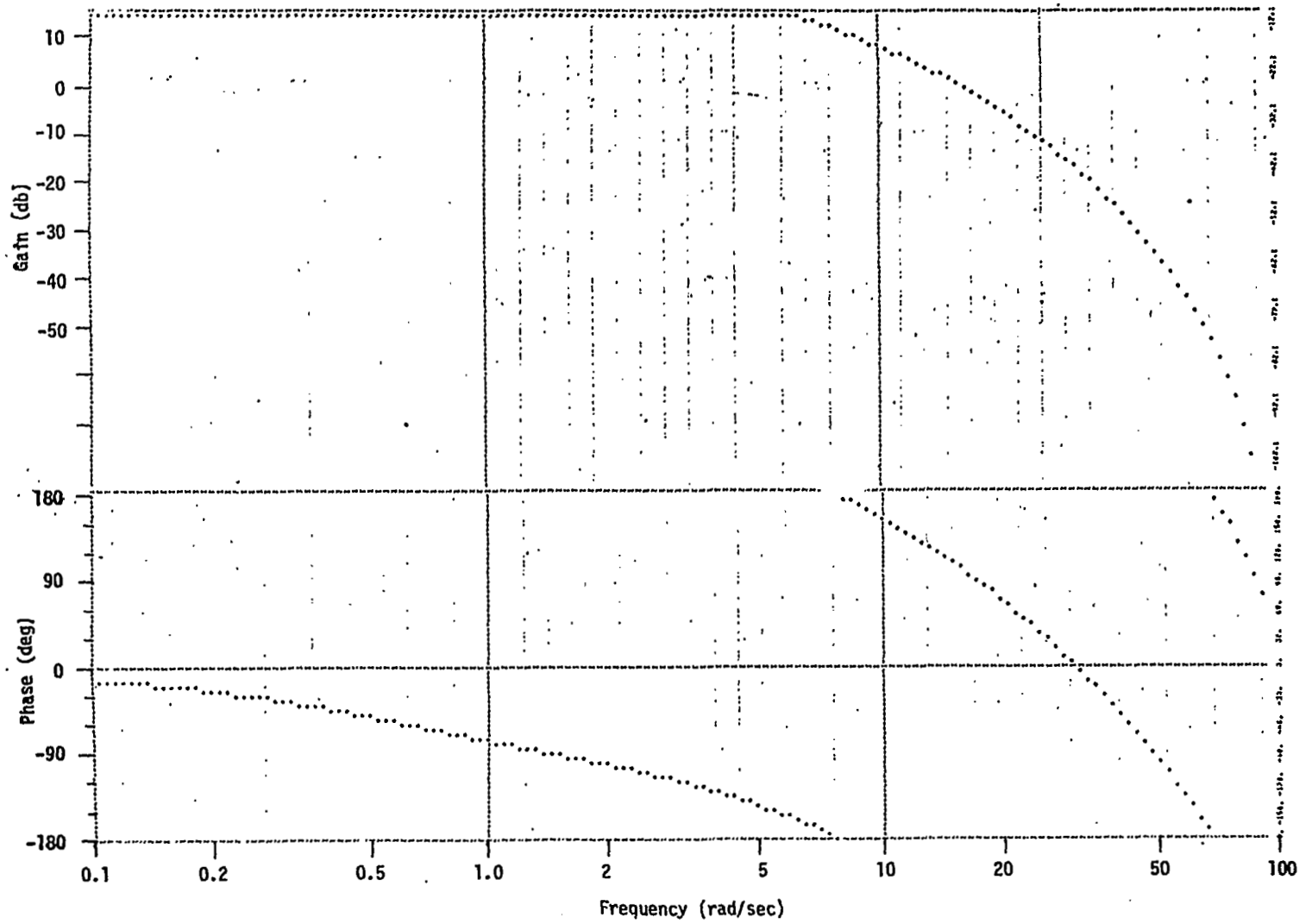
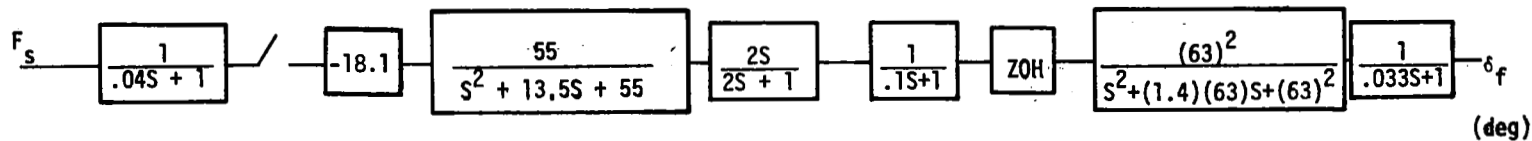


Figure 142. Pitch Rate to Flaps Frequency Response (32 sps)



- $\bar{q} < 50$ psf
- $V_o < 59$ kts
- 3 lb/g Stick Gain
No Deadspot
- N_z Flap Mode Engaged

Figure 143. Pitch Stick to Flaps

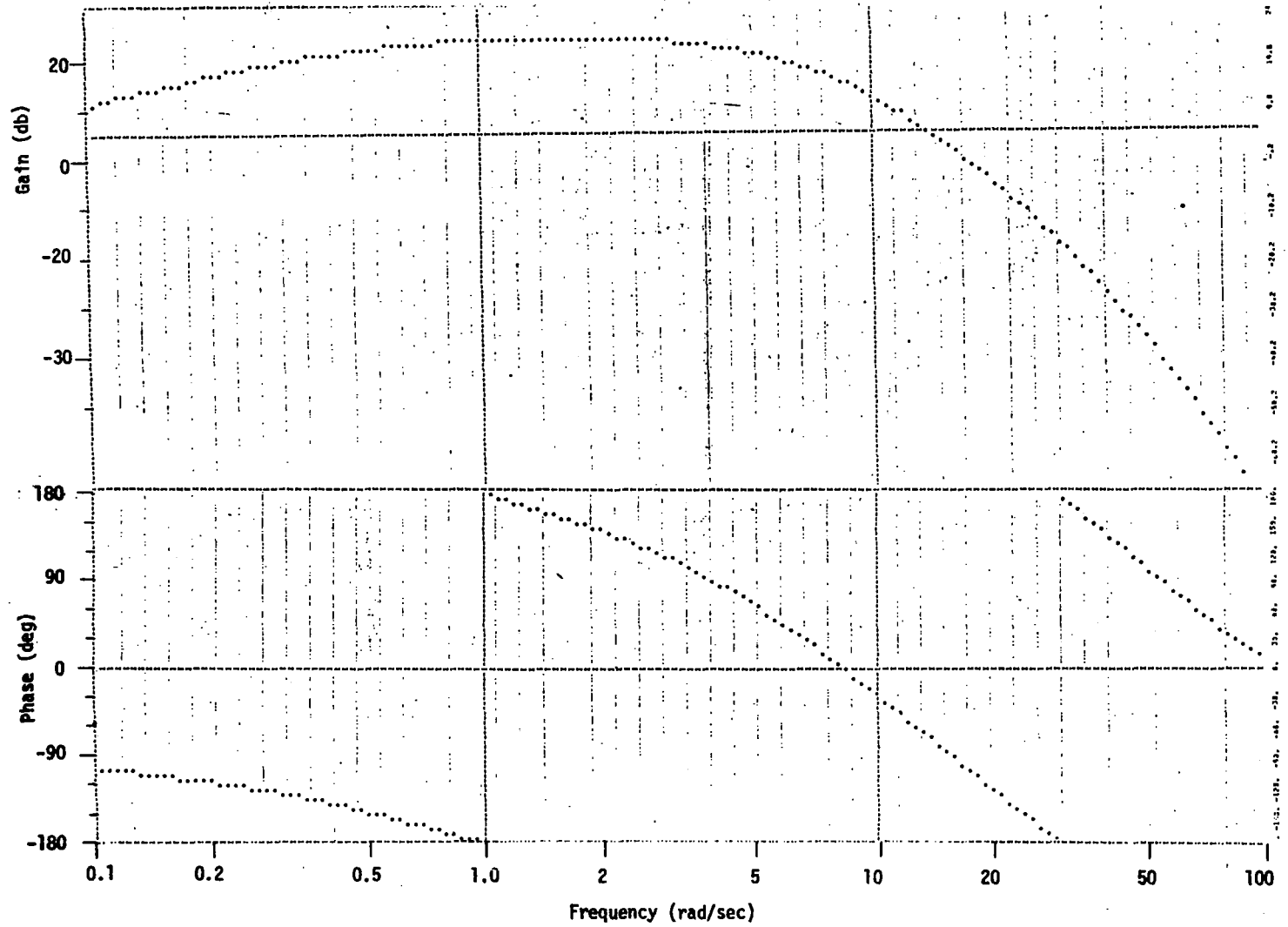


Figure 144. Pitch Stick to Flaps Frequency Response (continuous)

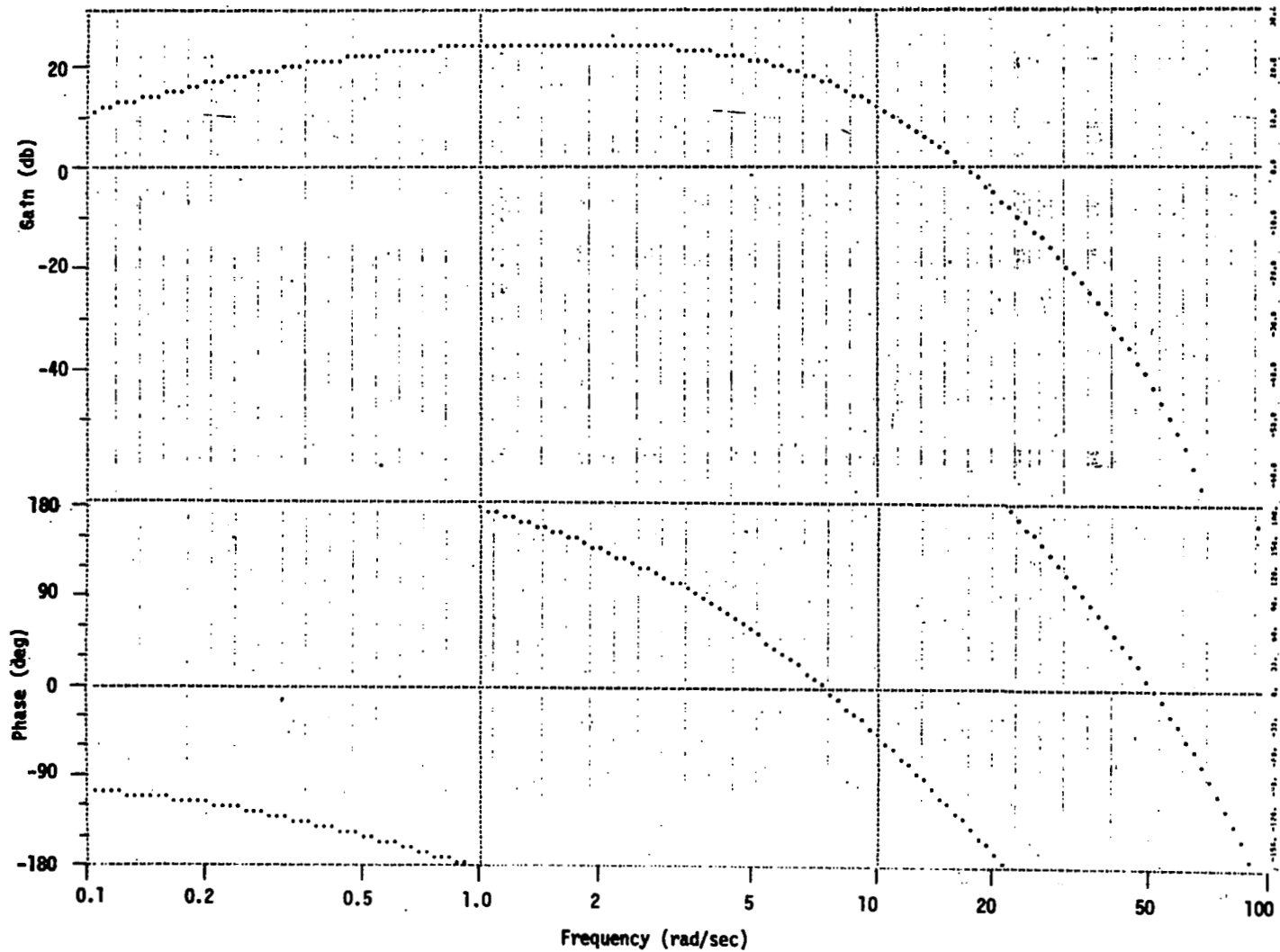
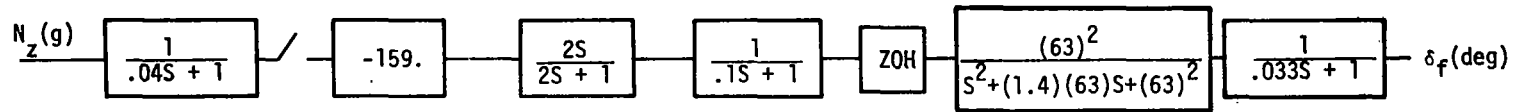


Figure 145. Pitch Stick to Flaps Frequency Response (32 sps)



- $\bar{q} < 50$ psf
- N_z Flap Mode Engaged

Figure 146. Normal Acceleration to Flaps

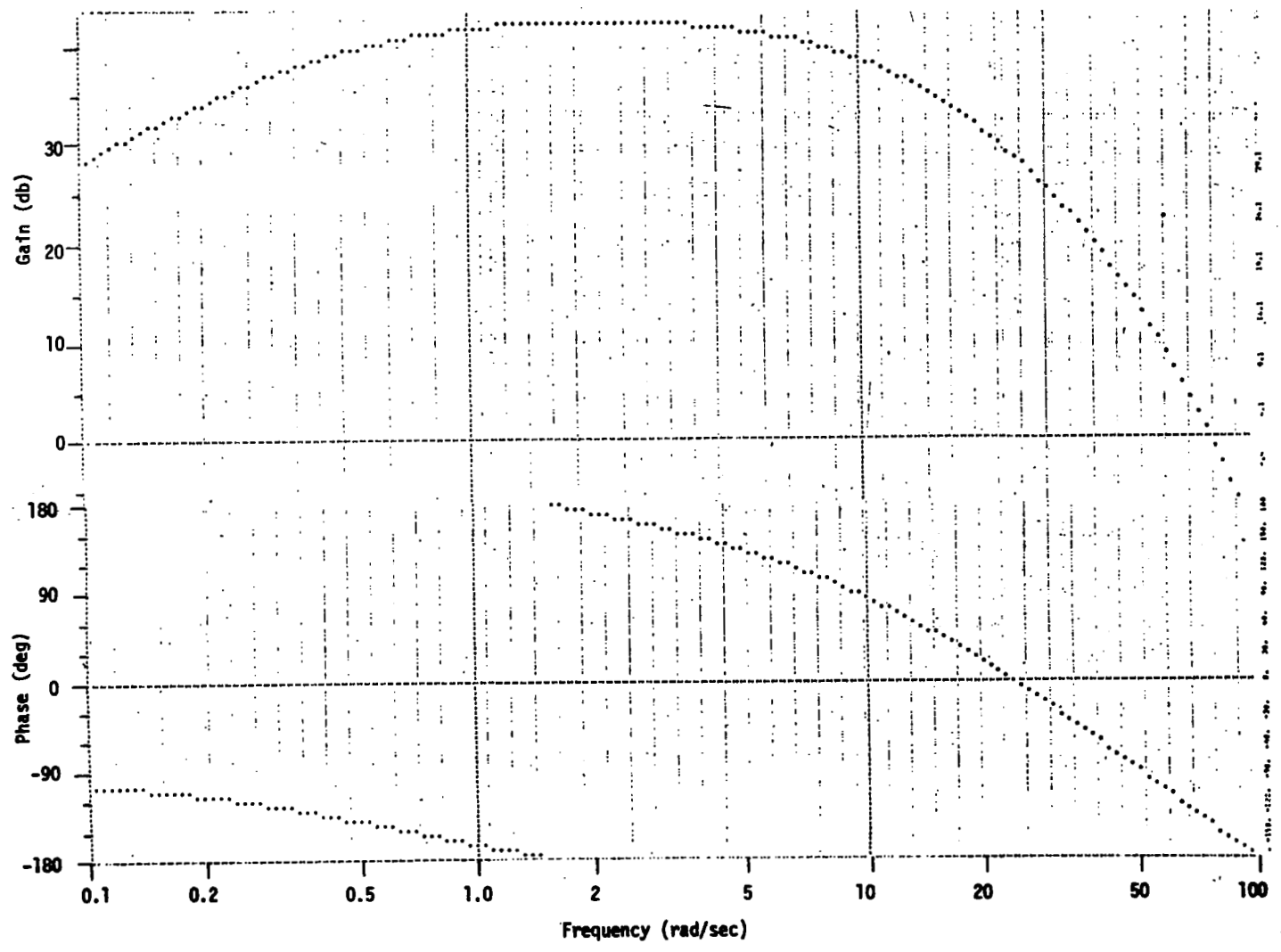


Figure 147. Normal Acceleration to Flaps Frequency Response (continuous)

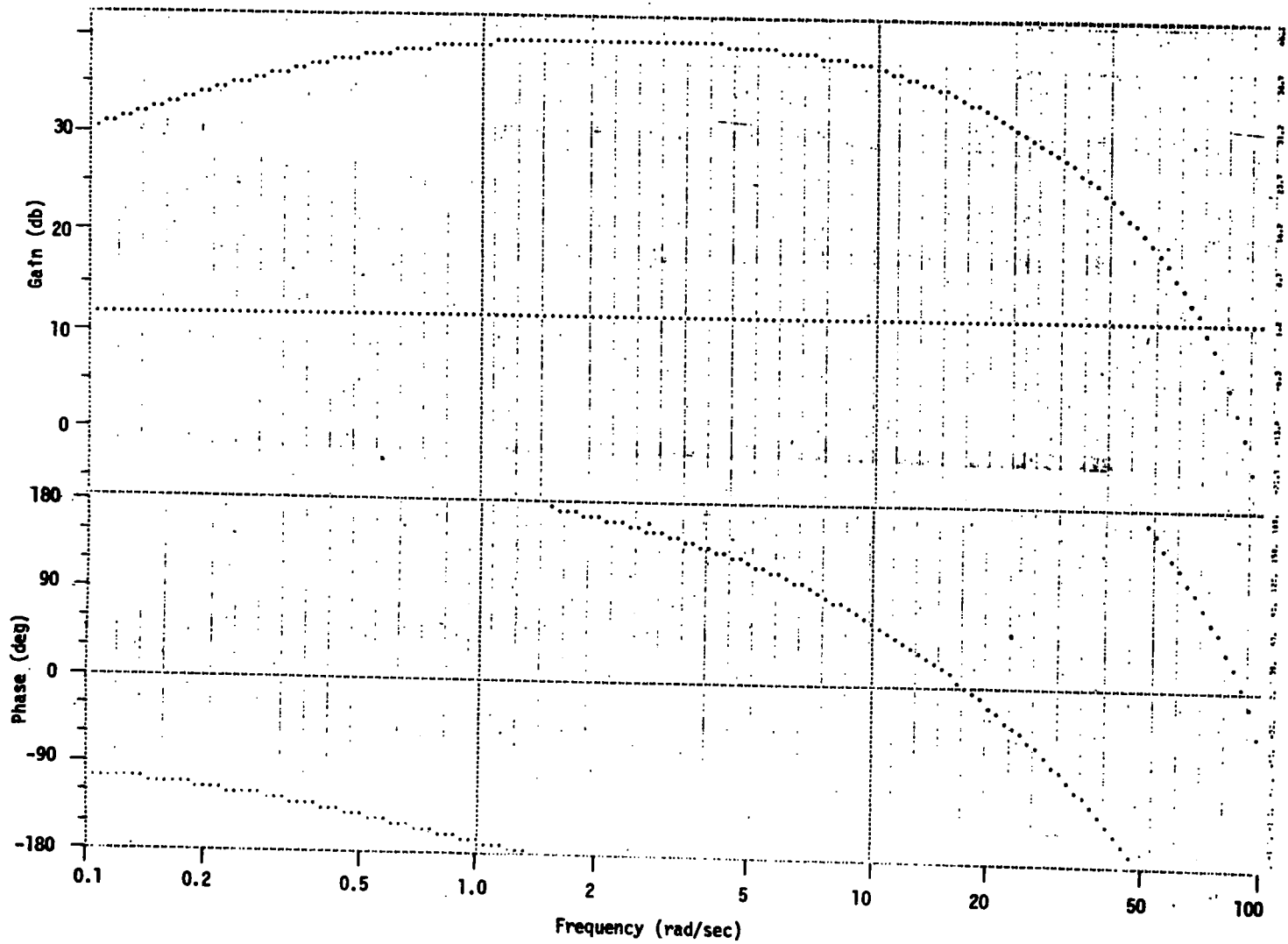
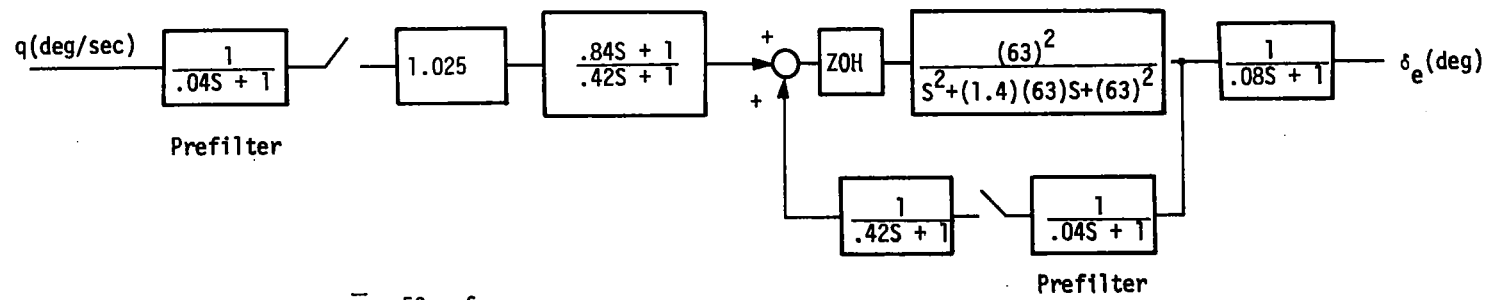


Figure 148. Normal Acceleration to Flaps Frequency Response (32 sps)



- $\bar{q} < 50$ psf
- Clean Condition

Figure 149. Pitch Rate to Elevator

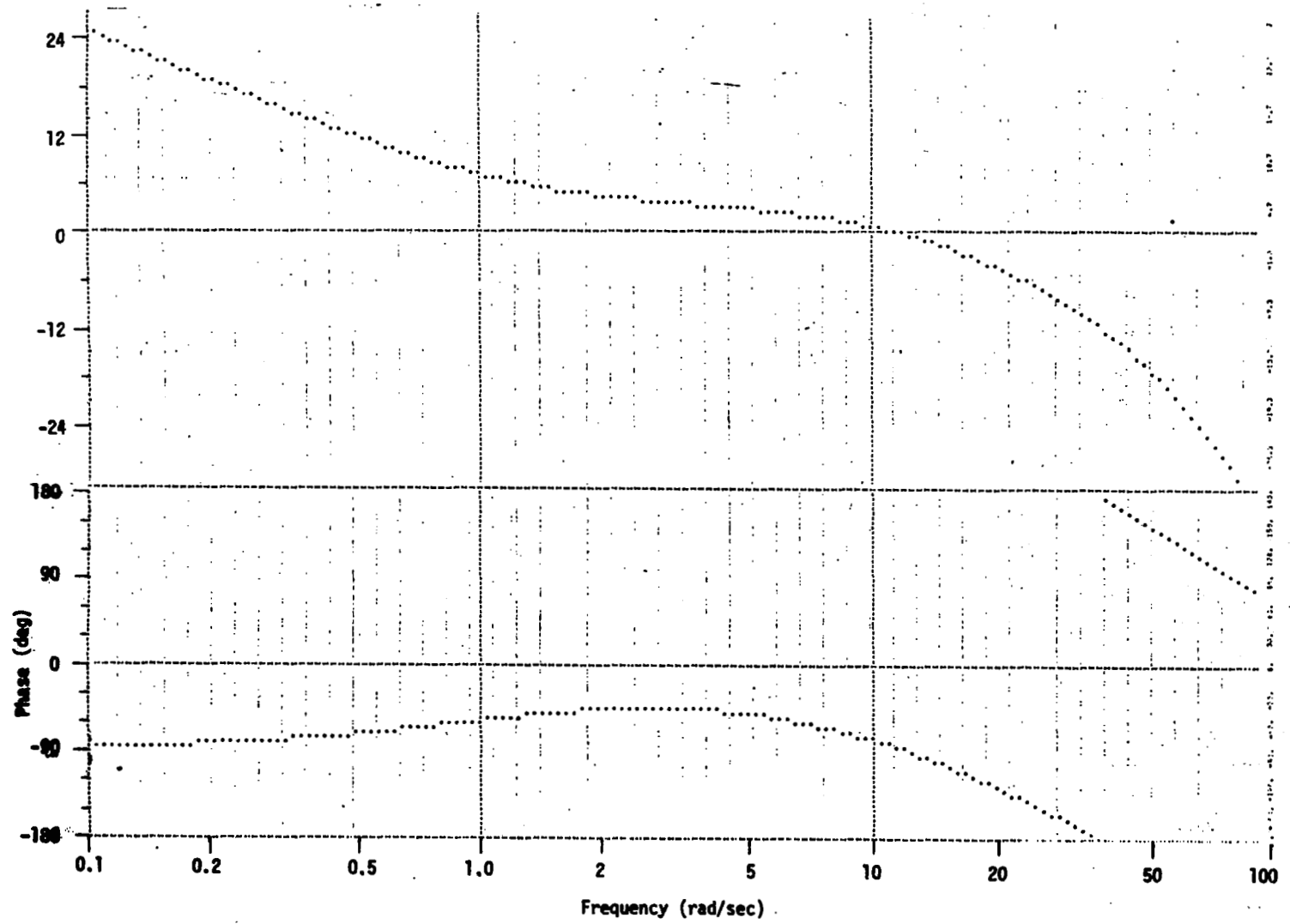


Figure 150. Pitch Rate to Elevator Frequency Response (continuous)

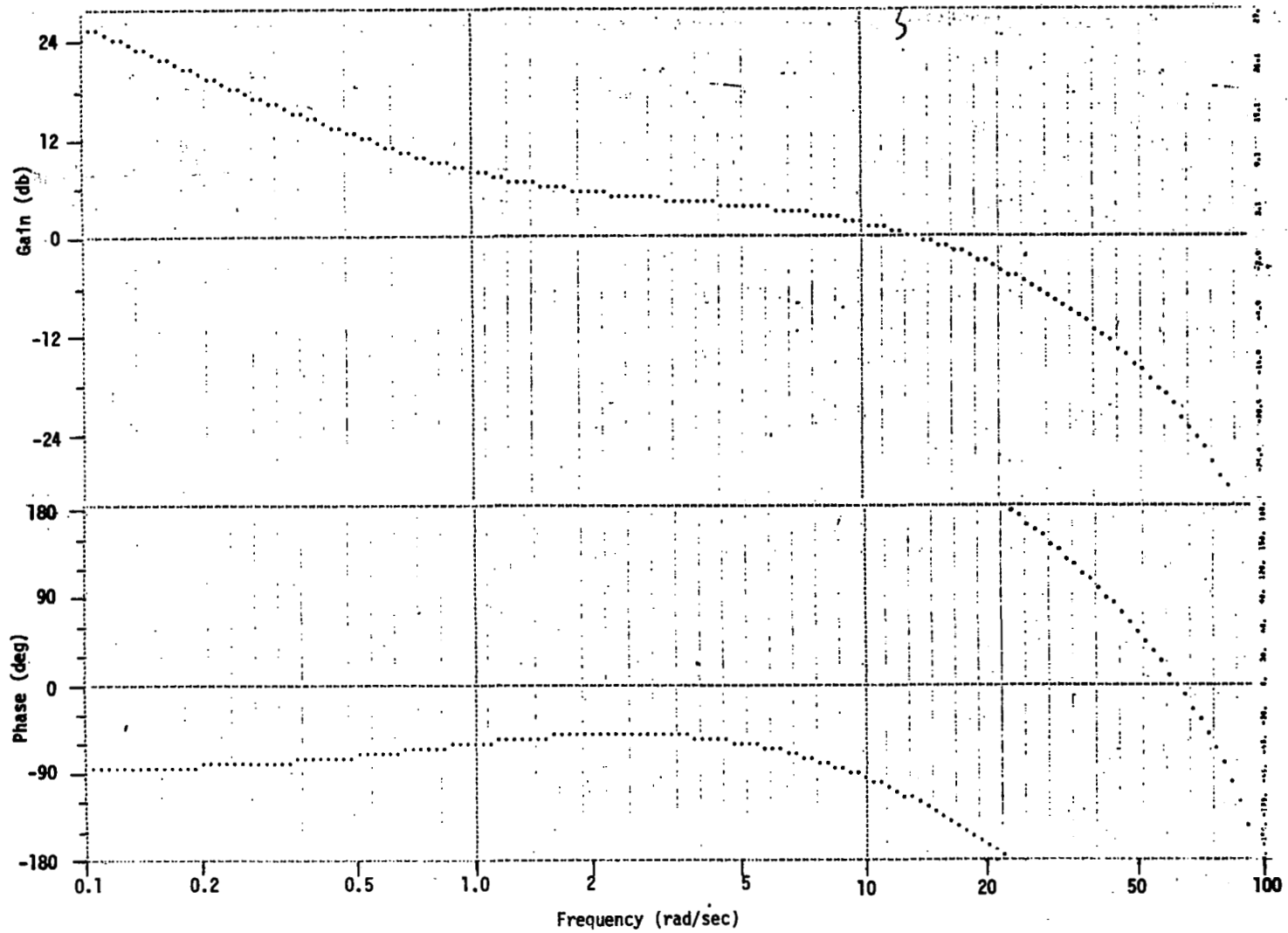
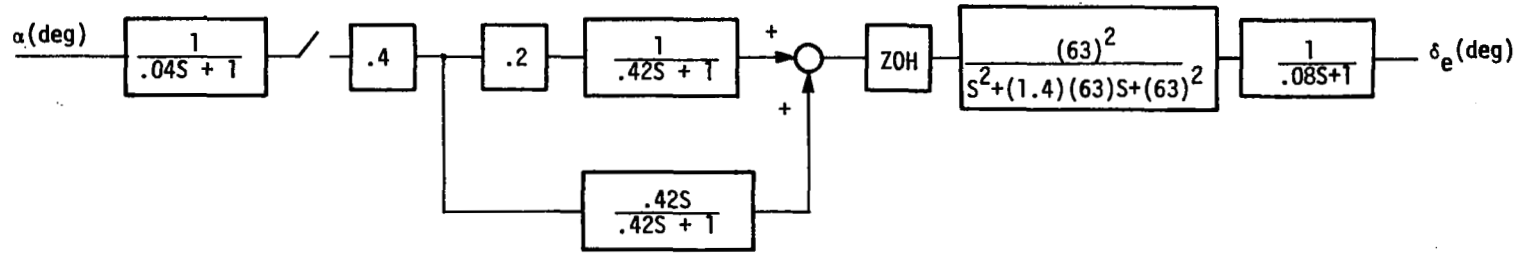


Figure 151. Pitch Rate to Elevator Frequency Response (32 sps)



- $V_0 < 59$ kts
- No Servo Integration (PSS)

Figure 152. Angle-of-Attack to Elevator

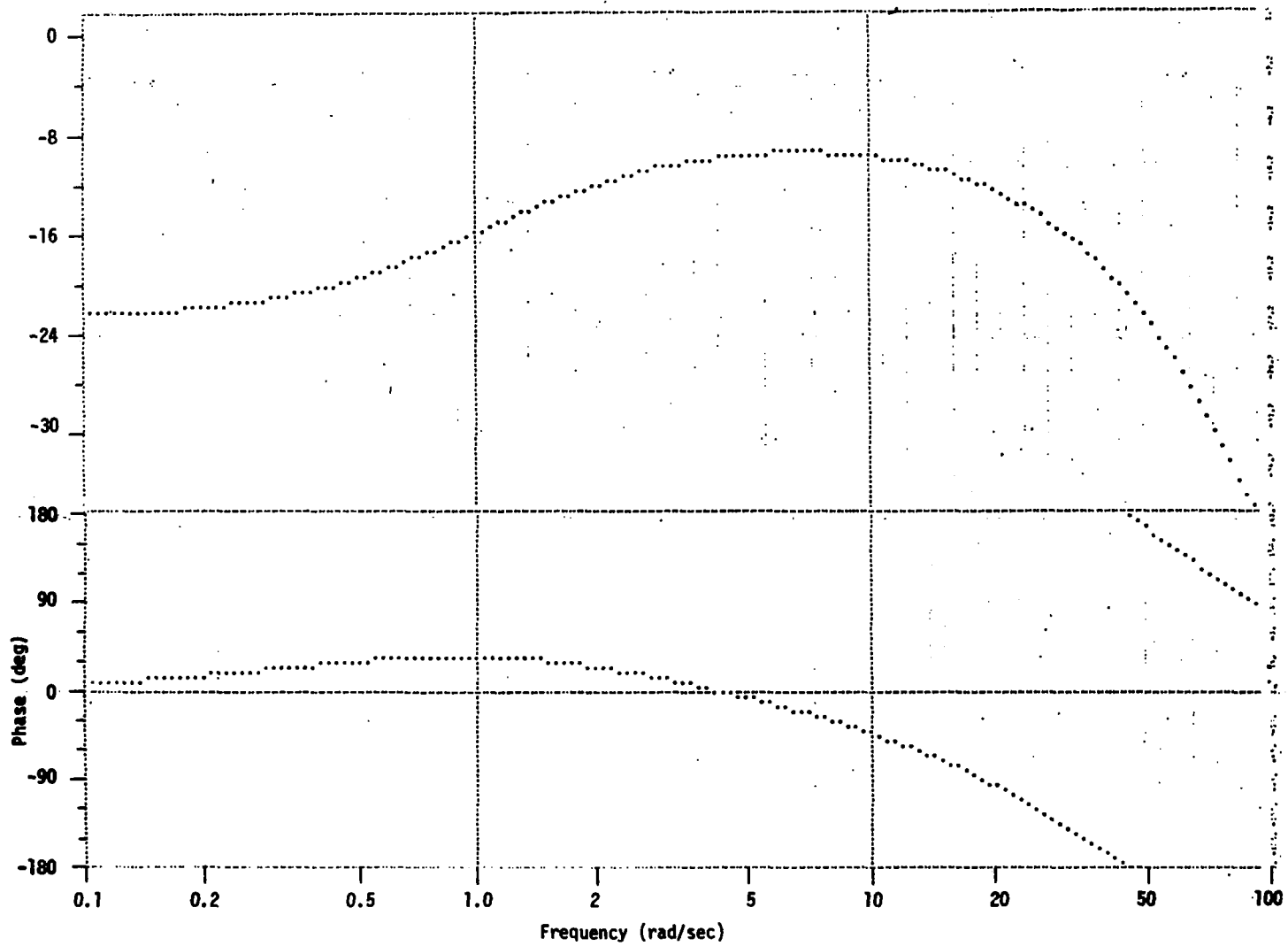


Figure 153. Angle-of-Attack to Elevator Frequency Response (32 sps)

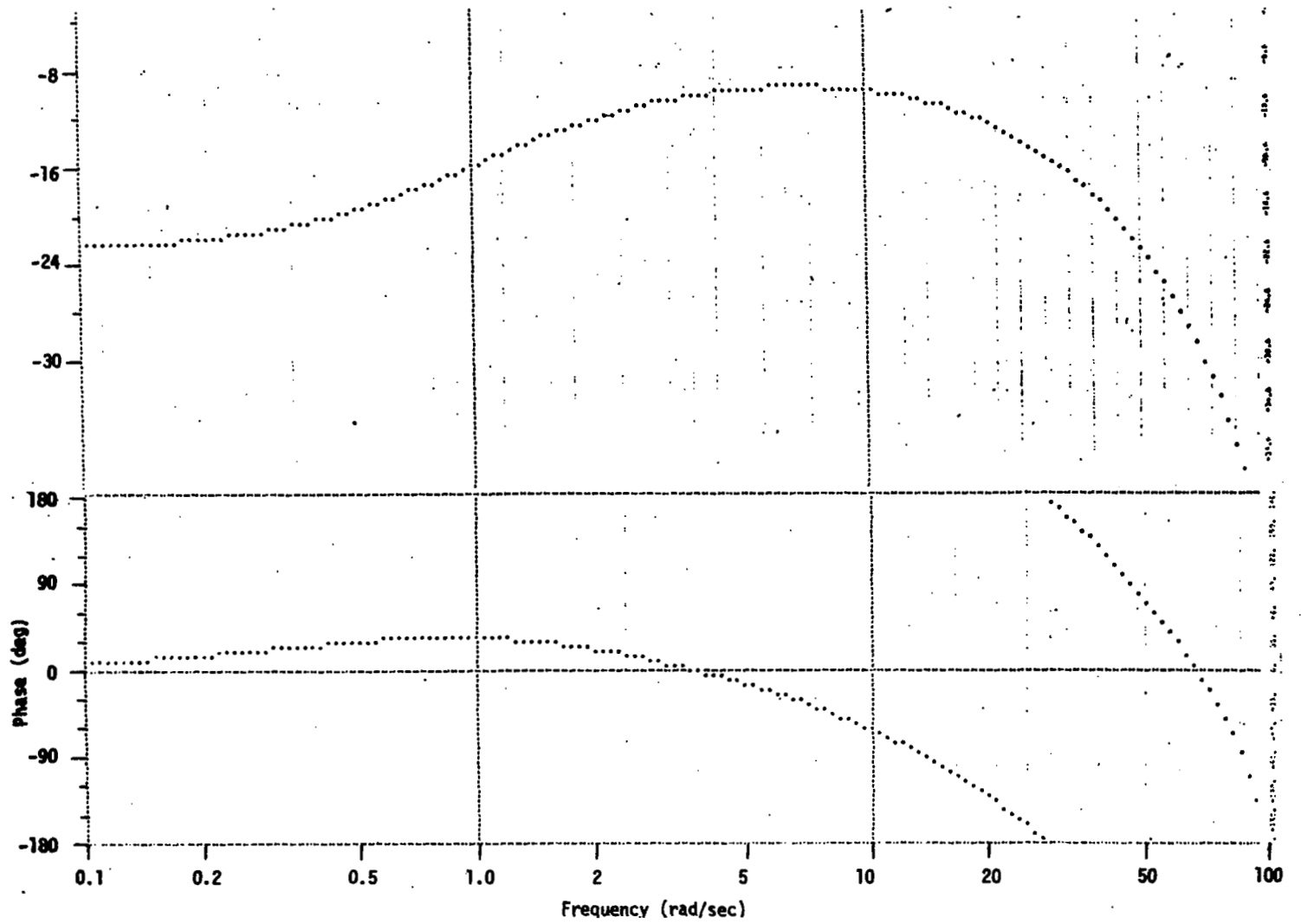
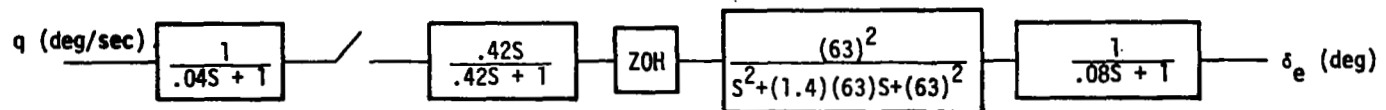


Figure 154. Angle-of-Attack to Elevator Frequency Response (continuous)



- $\bar{q} < 50$ psf
- No Servo Integration

Figure 155. Pitch Rate to Elevator (Boundary Function)

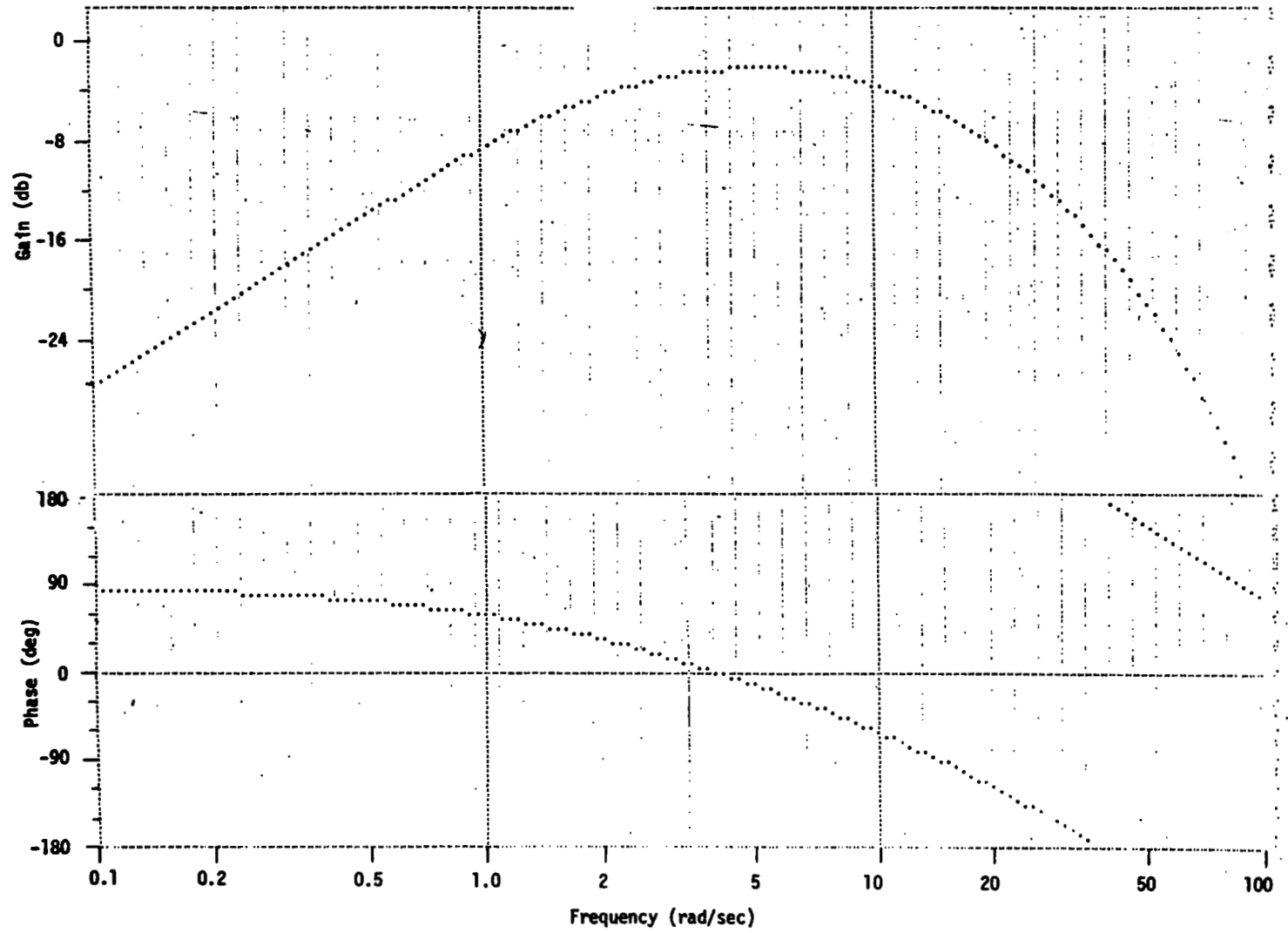


Figure 156. Pitch Rate to Elevator Frequency Response (continuous)

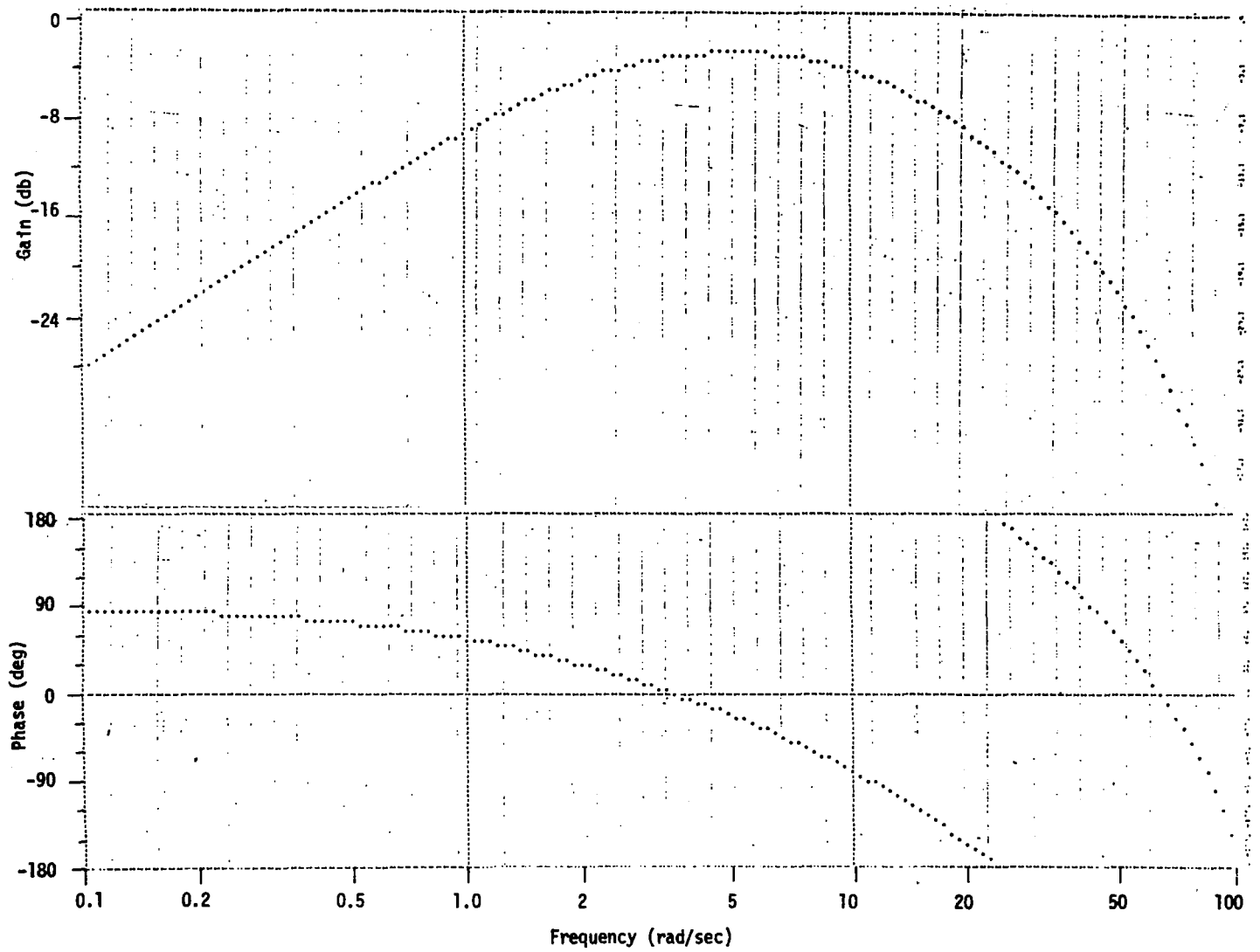


Figure 157. Pitch Rate to Elevator Frequency Response (32 sps)

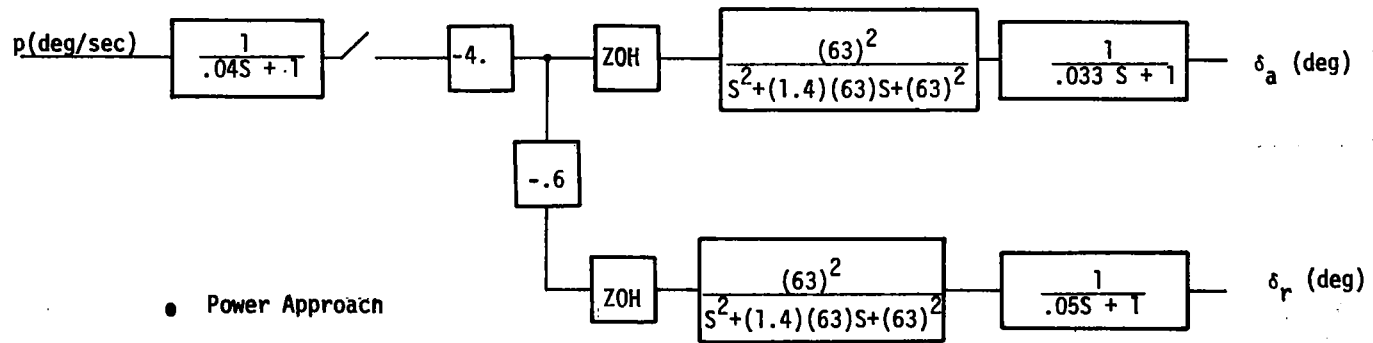


Figure 158. Roll Rate to Aileron and Rudder

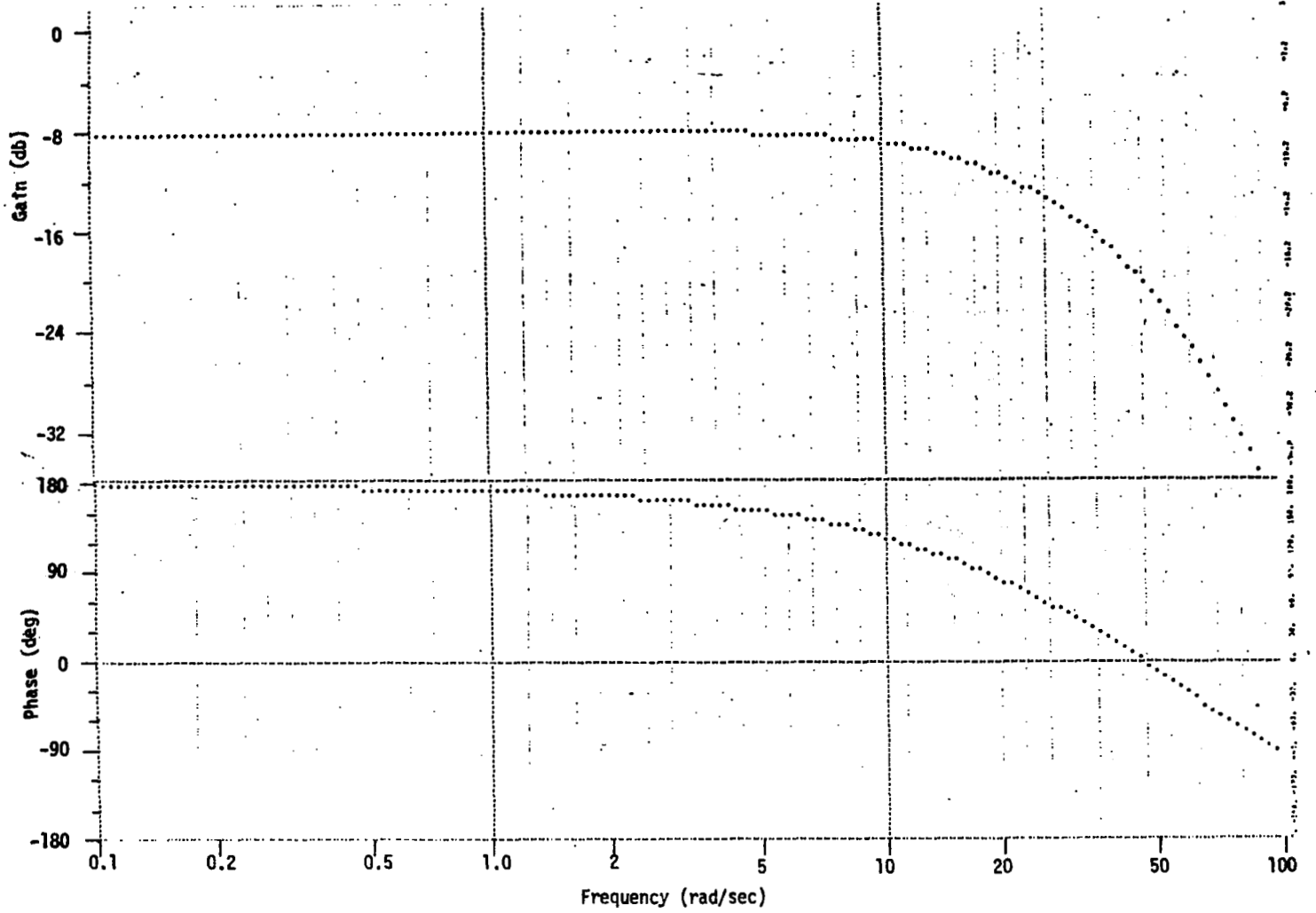


Figure 159. Roll Rate to Aileron Frequency Response (continuous)

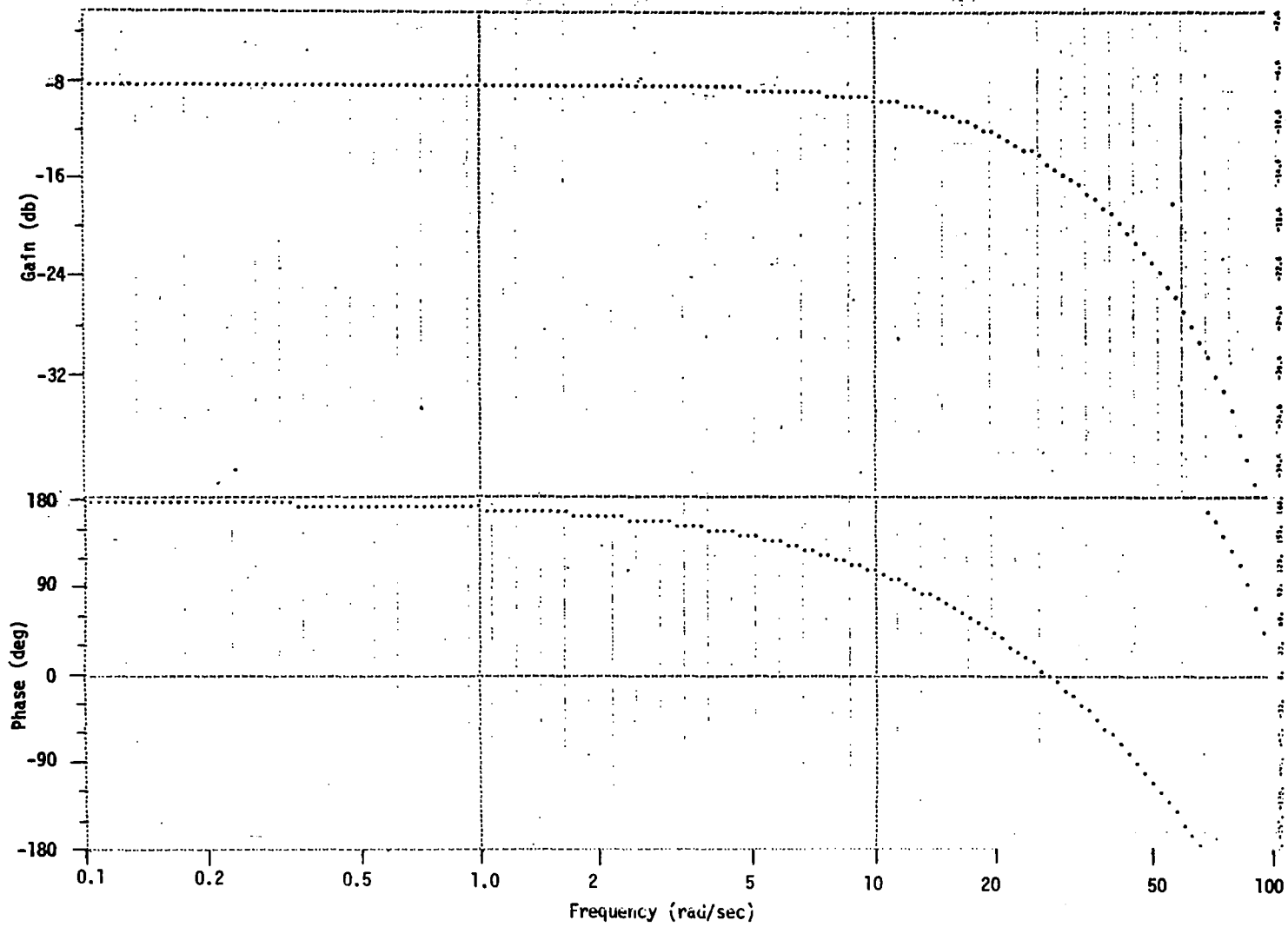


Figure 160. Roll Rate to Aileron Frequency Response (32 sps)

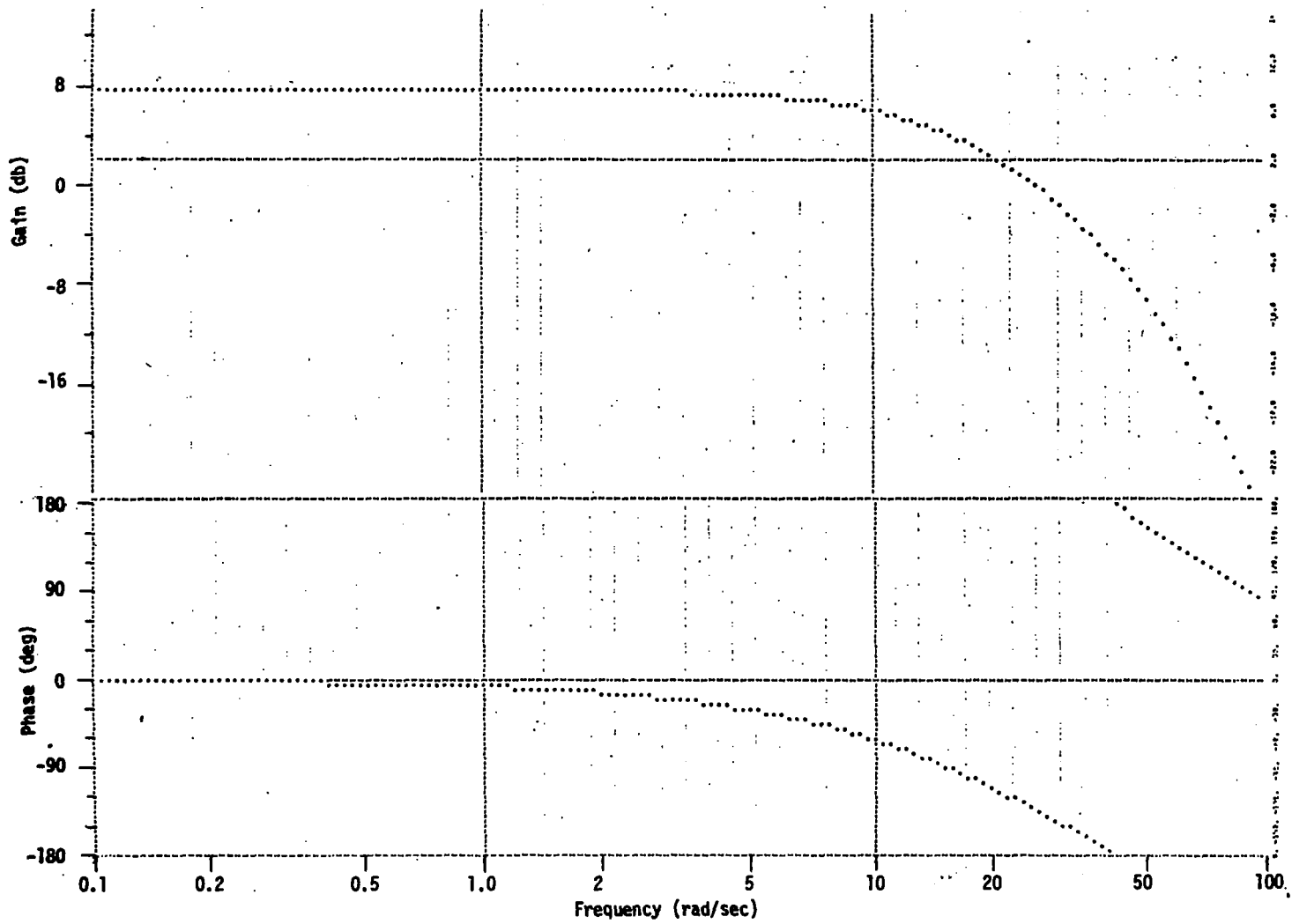


Figure 161. Roll Rate to Rudder Frequency Response (continuous)

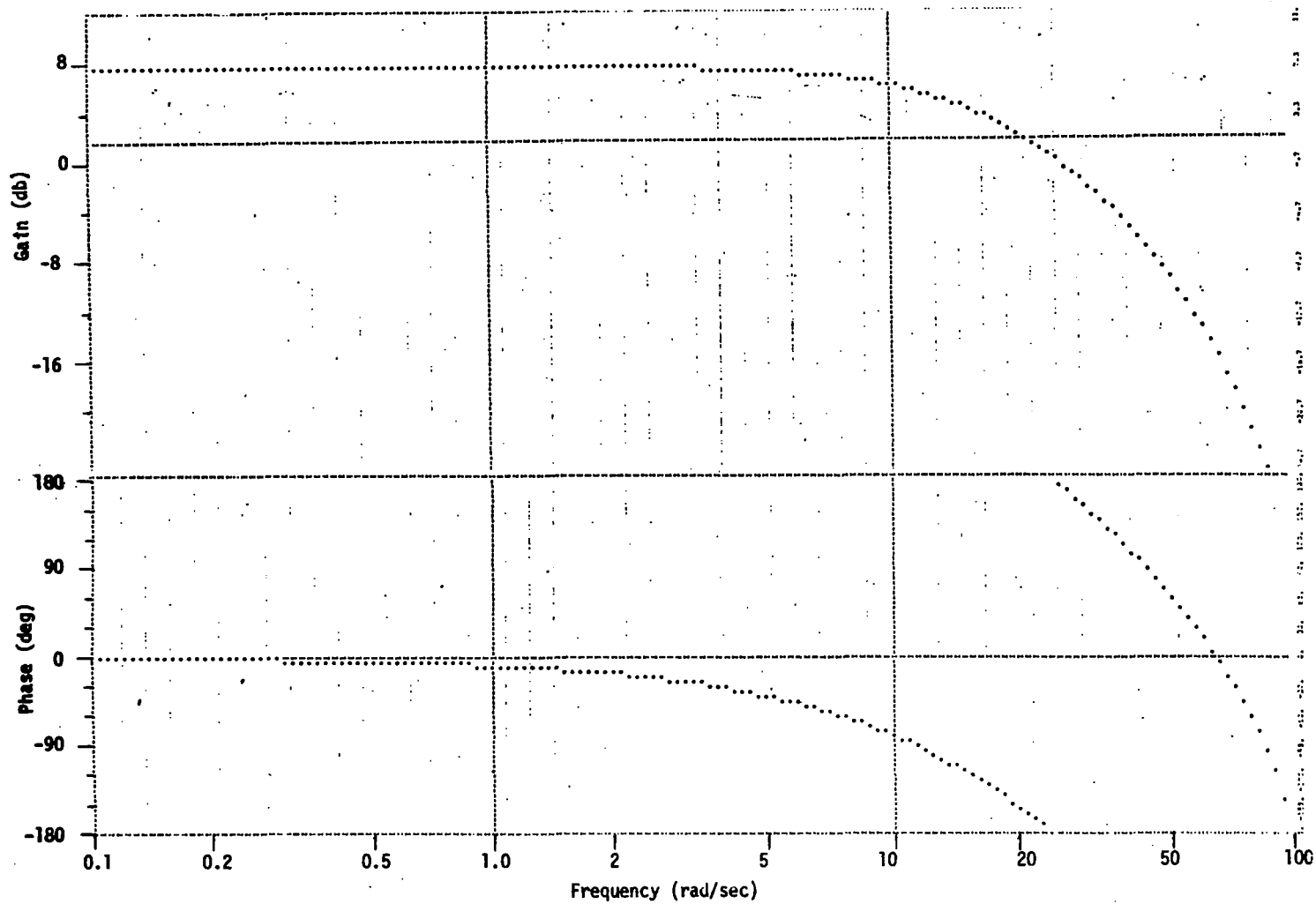
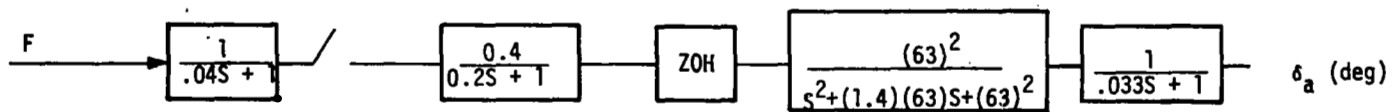


Figure 162. Roll Rate to Rudder Frequency Response (32 sps)



Normalize in terms
of commanded roll rate

- Power Approach Condition
- No Roll Stick Non-Linearities

Figure 163. Roll Stick to Aileron

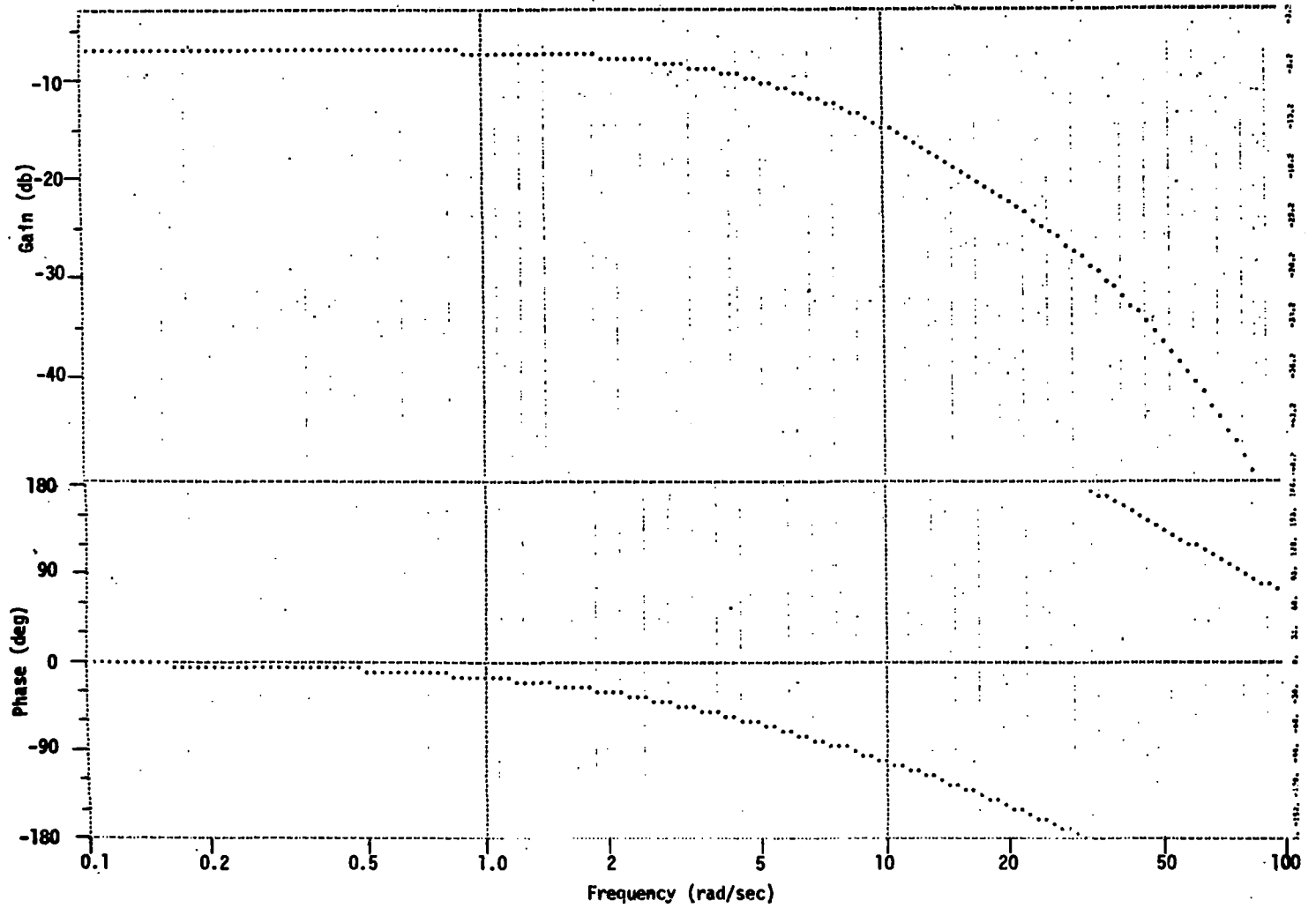


Figure 164. Roll Stick to Aileron Frequency Response (continuous)

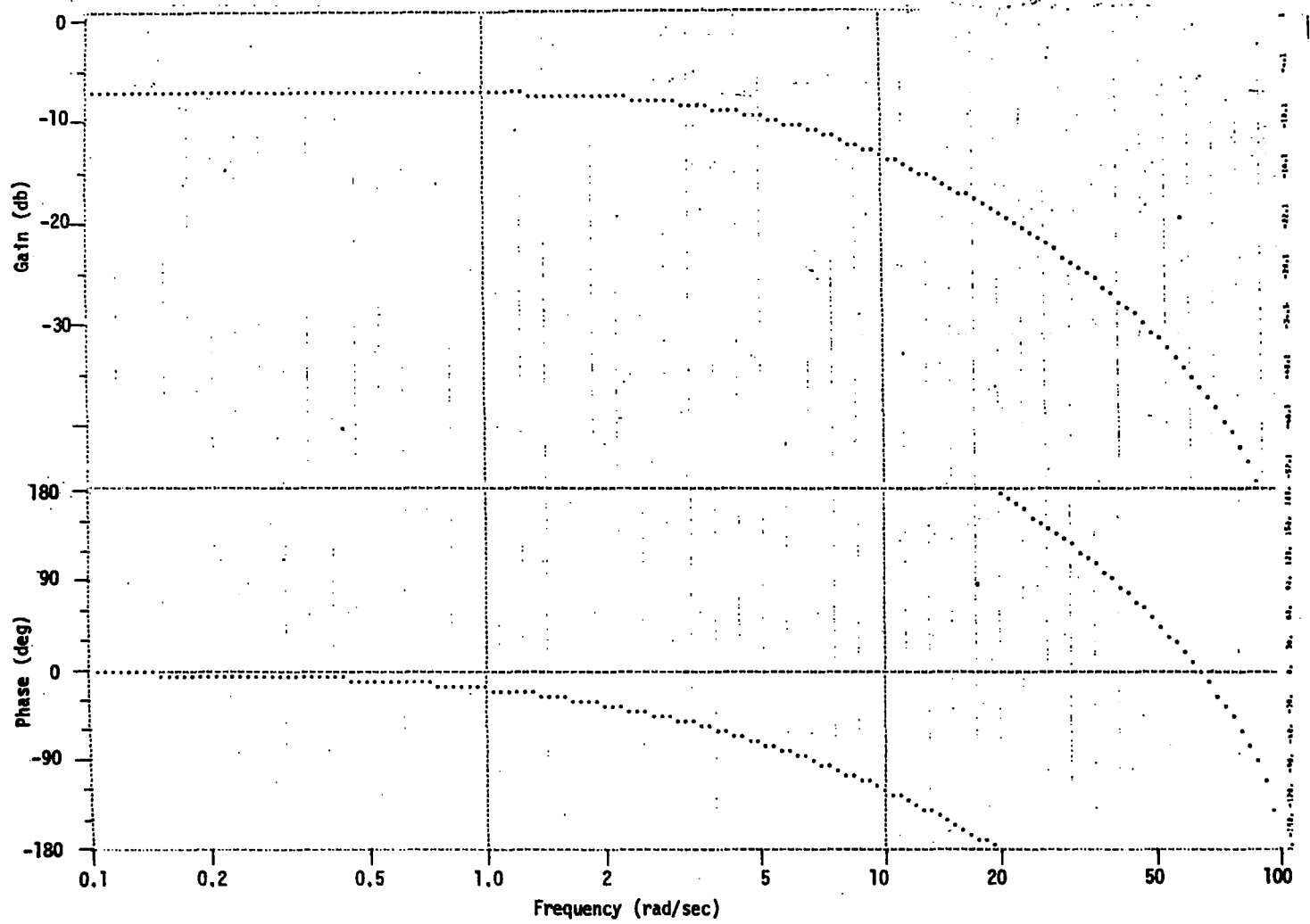
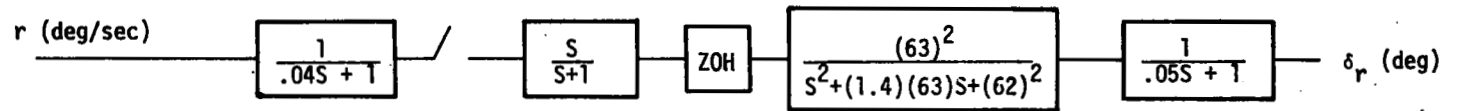


Figure 165. Roll Stick to Aileron Frequency Response (32 sps)



● Power Approach

Figure 166. Yaw Rate to Rudder

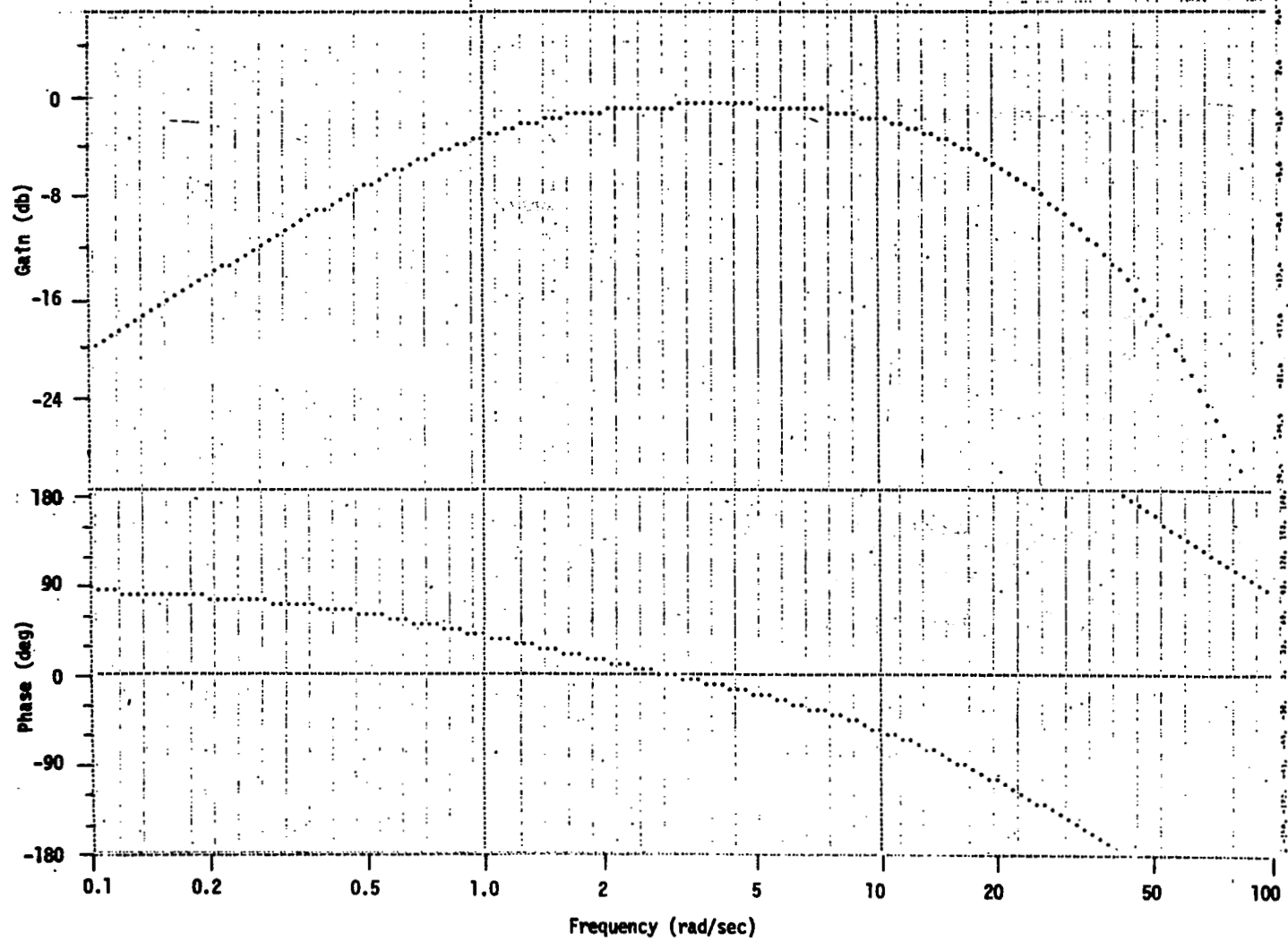


Figure 167. Yaw Rate to Rudder Frequency Response (continuous)

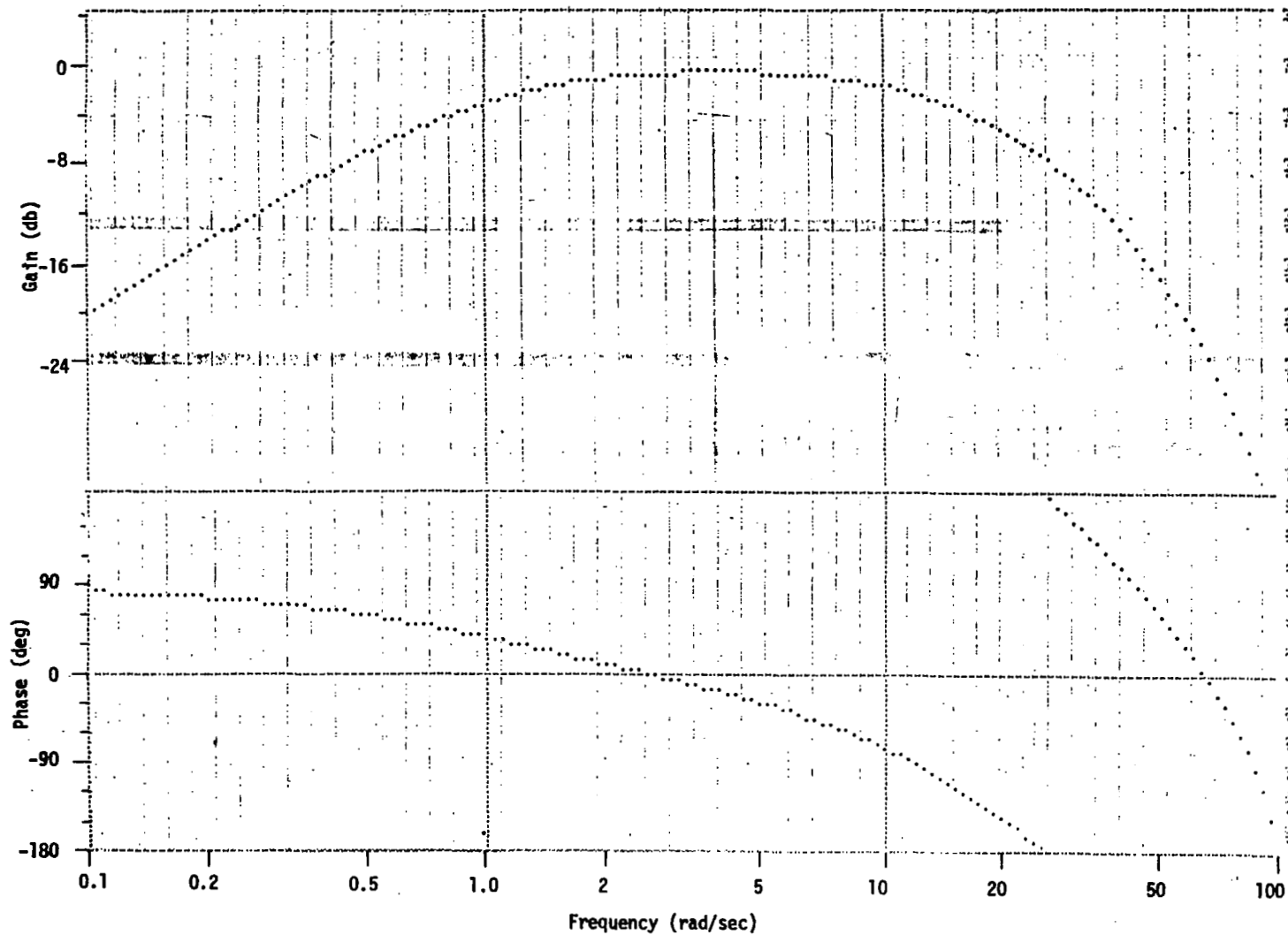


Figure 168. Yaw Rate to Rudder Frequency Response (32 sps)

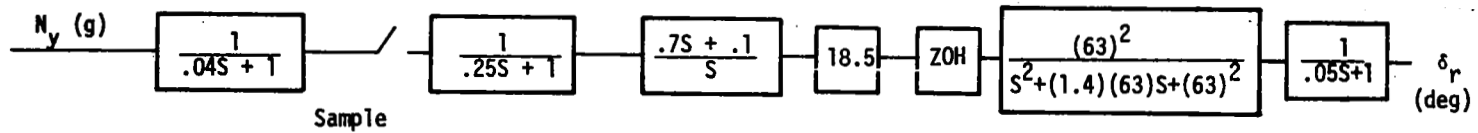


Figure 169. Lateral Acceleration to Rudder

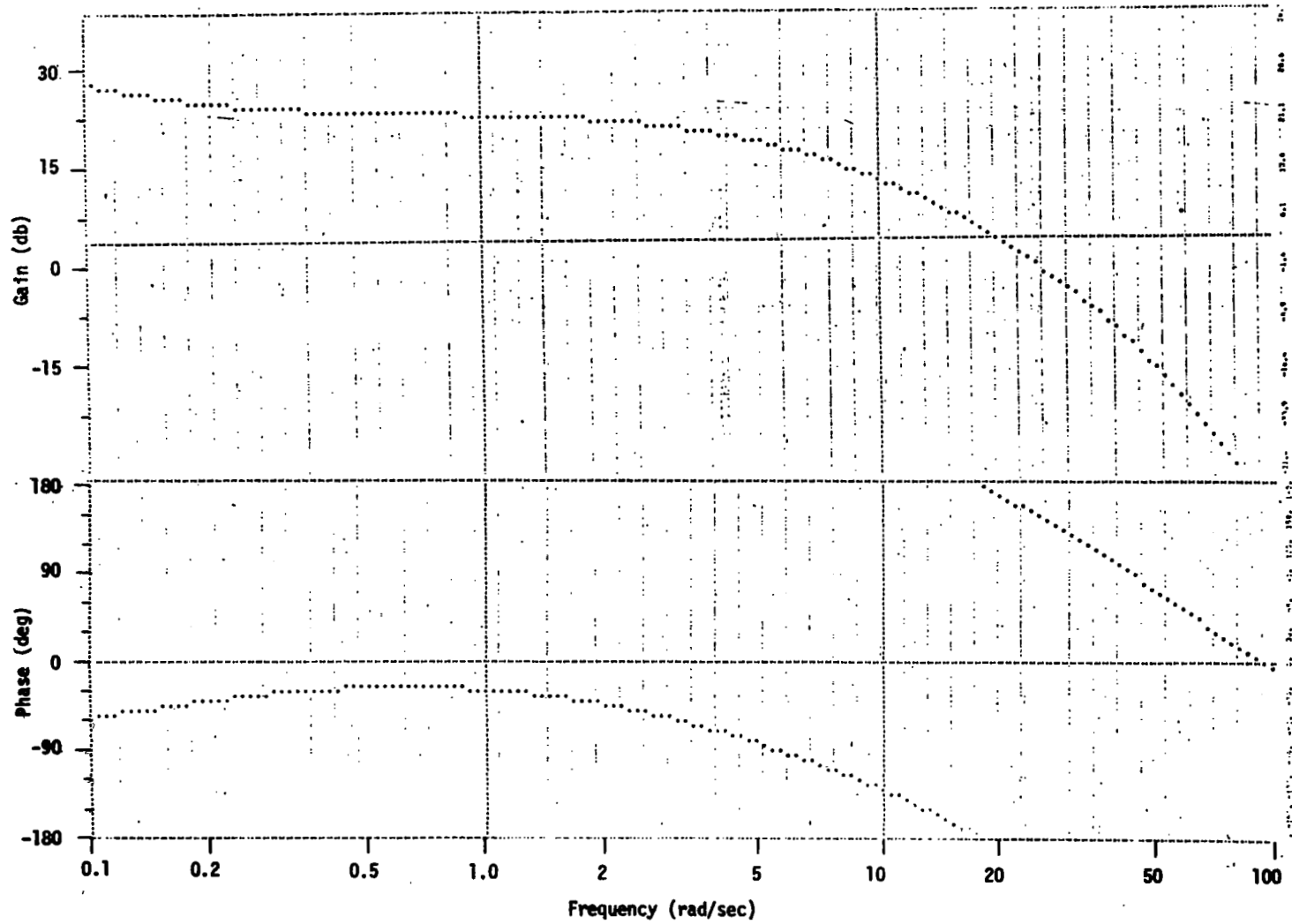


Figure 170. Lateral Acceleration to Rudder Frequency Response (continuous)

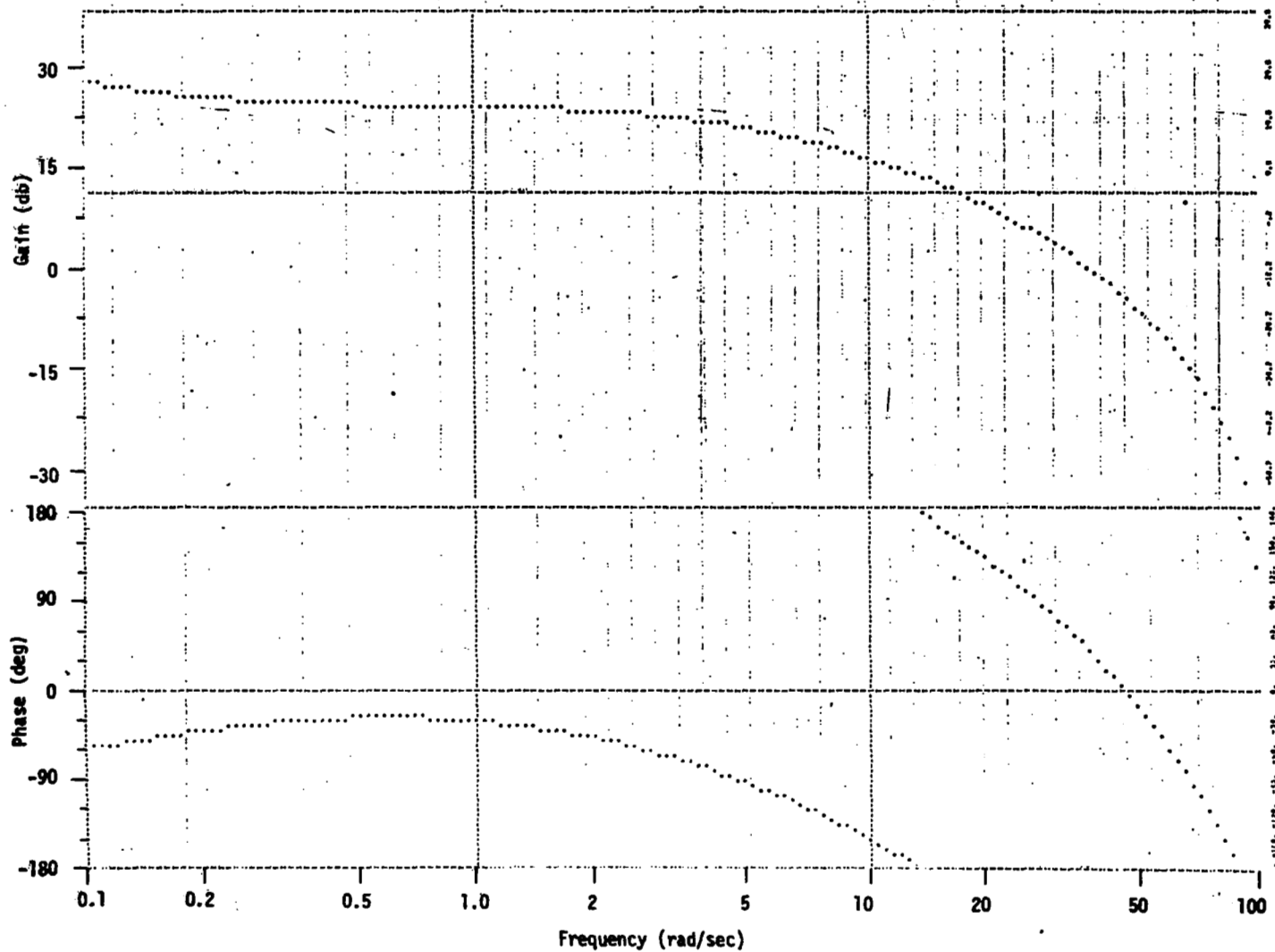
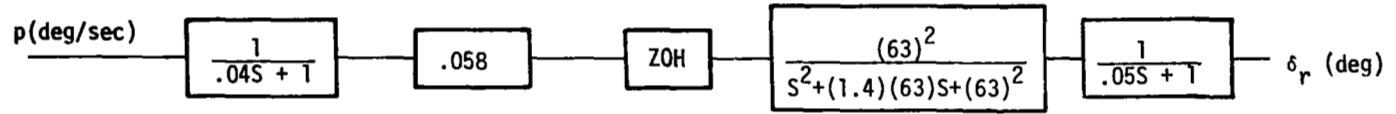


Figure 171. Lateral Acceleration to Rudder Frequency Response (32 sps)



- Angle-of-Attack Above 18 Degrees

Figure 172. Roll Rate to Rudder

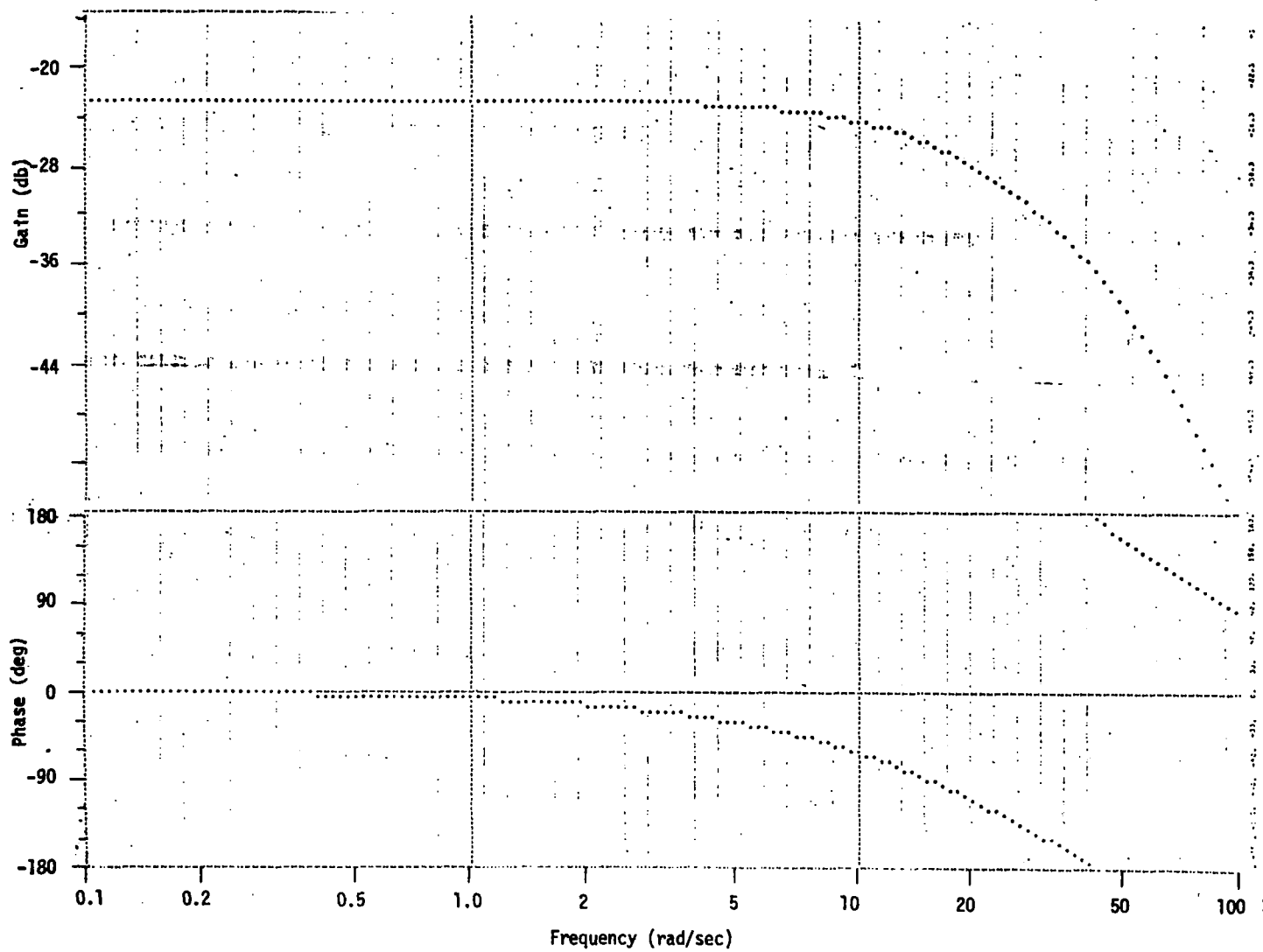


Figure 173. Roll Rate to Rudder Frequency Response (continuous)

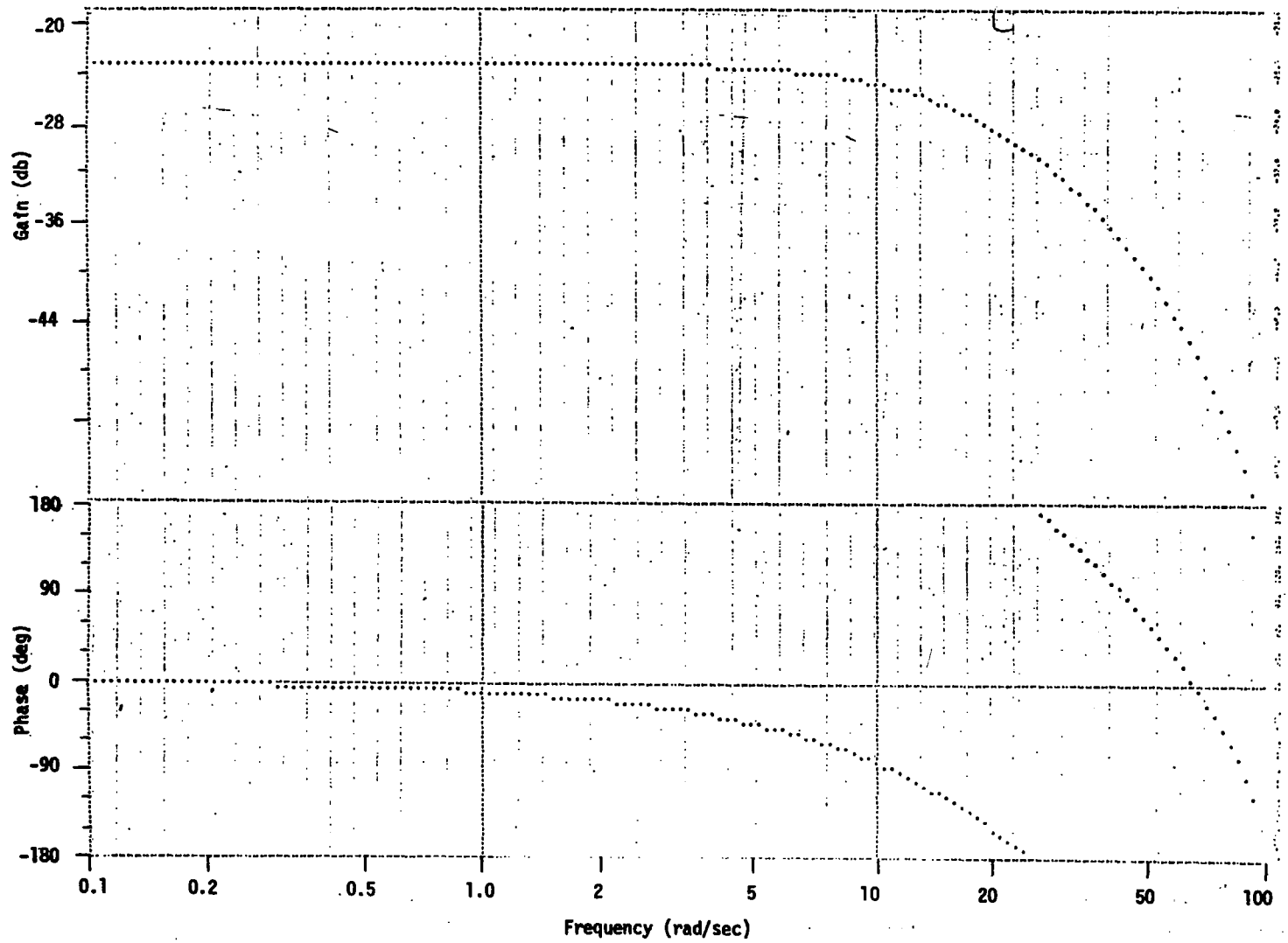
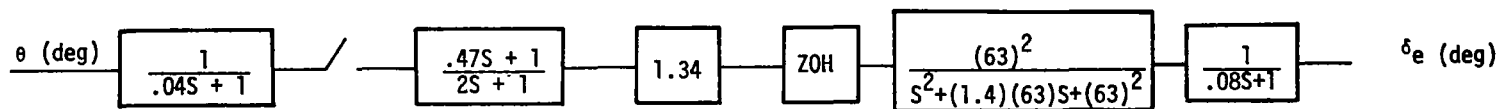


Figure 174. Roll Rate to Rudder Frequency Response (32 sps)

3)



- $\bar{q} < 50$ psf
- PA Condition
- $\alpha \approx 0$
- Airspeed < 59 kts

Figure 175. Pitch Attitude to Elevator

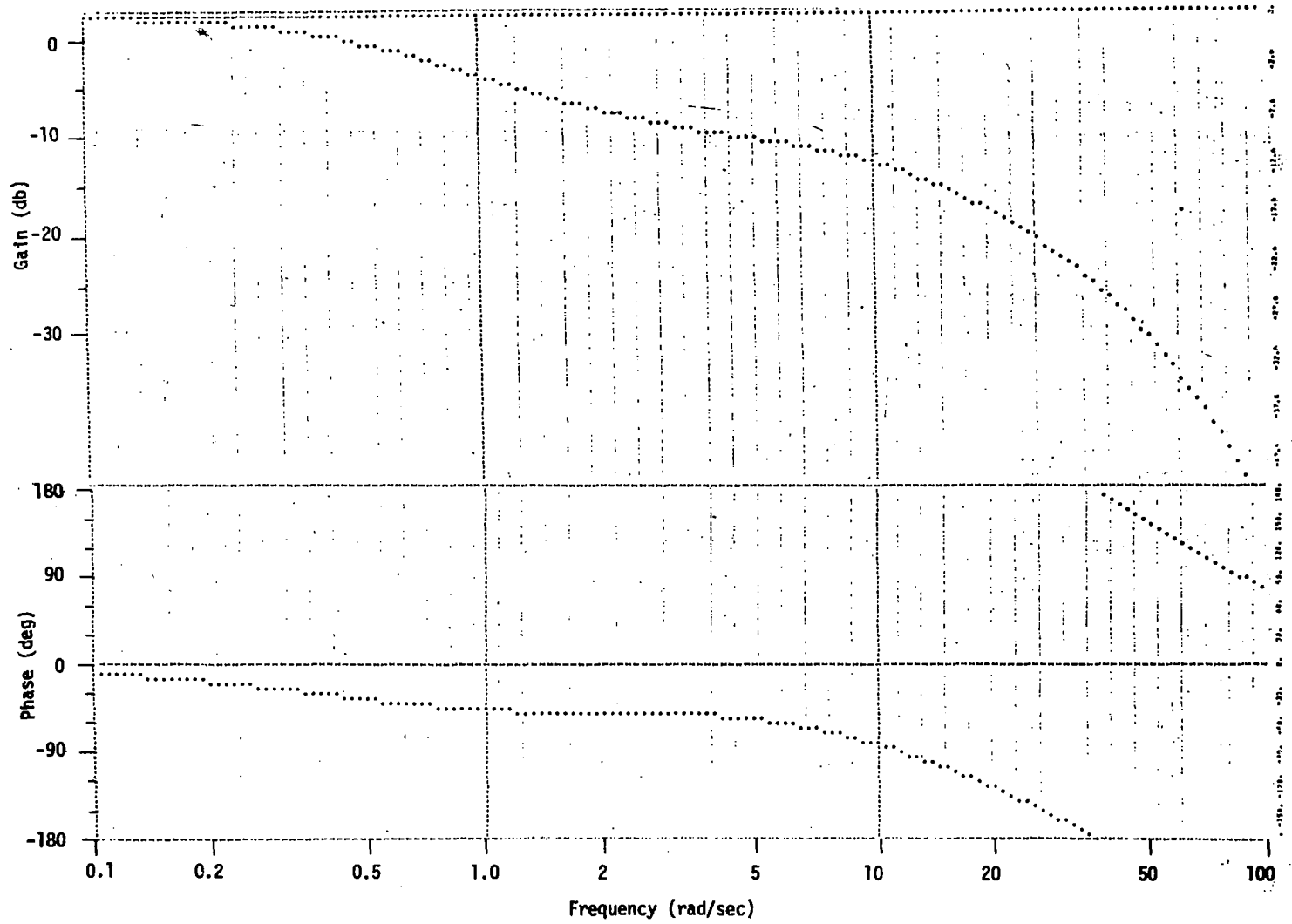


Figure 176. Pitch Attitude to Elevator Frequency Response (continuous)

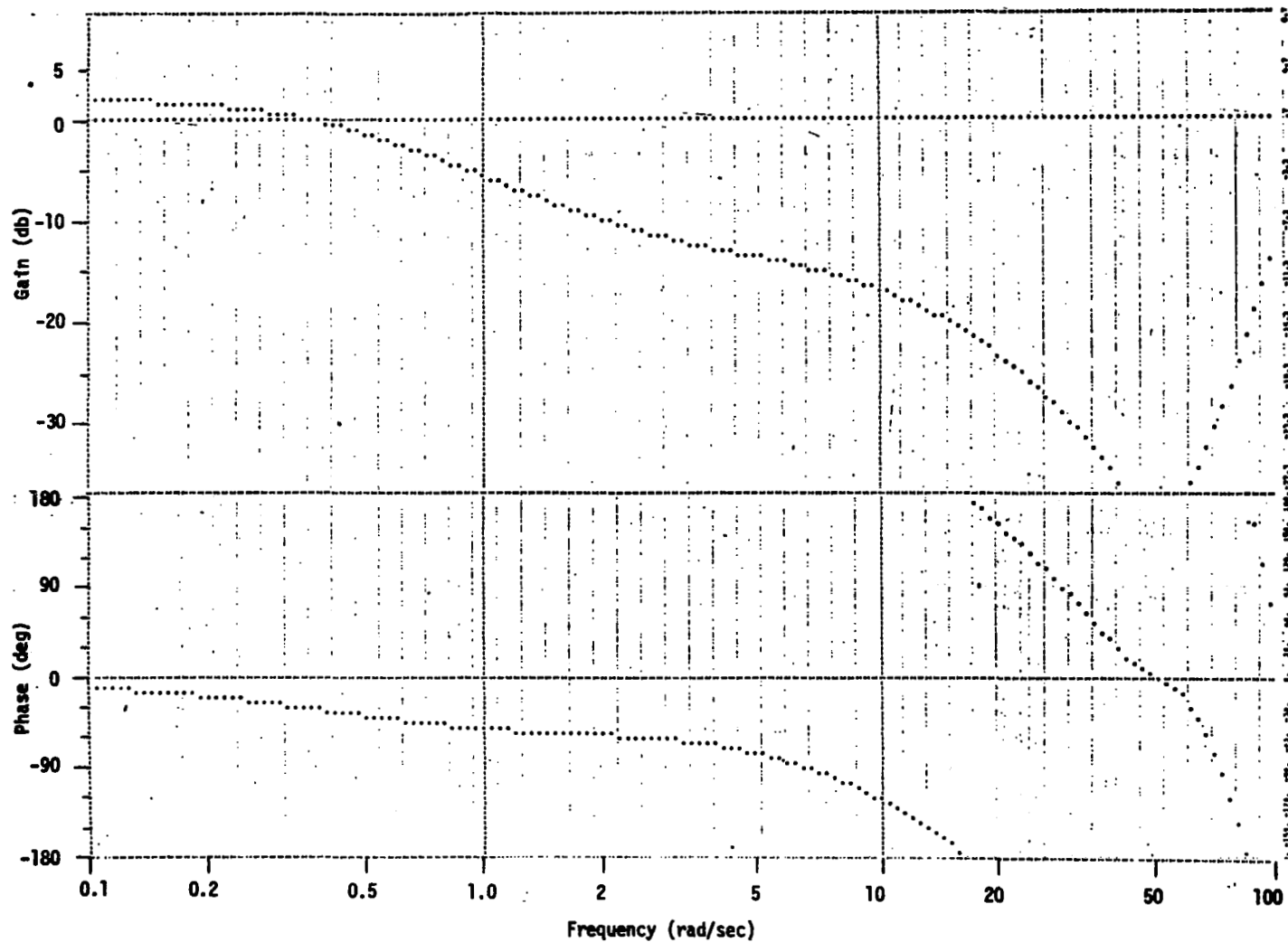
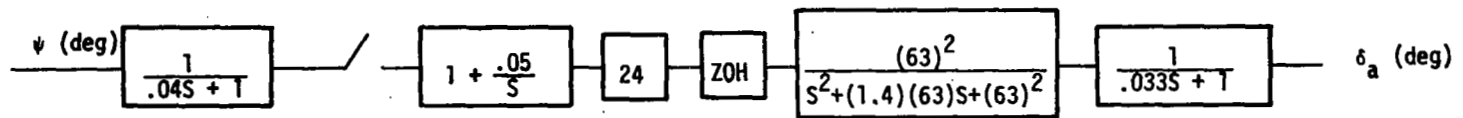


Figure 177. Pitch Attitude to Elevator Frequency Response (16 sps)



● Power Approach

Figure 178. Heading to Ailerons

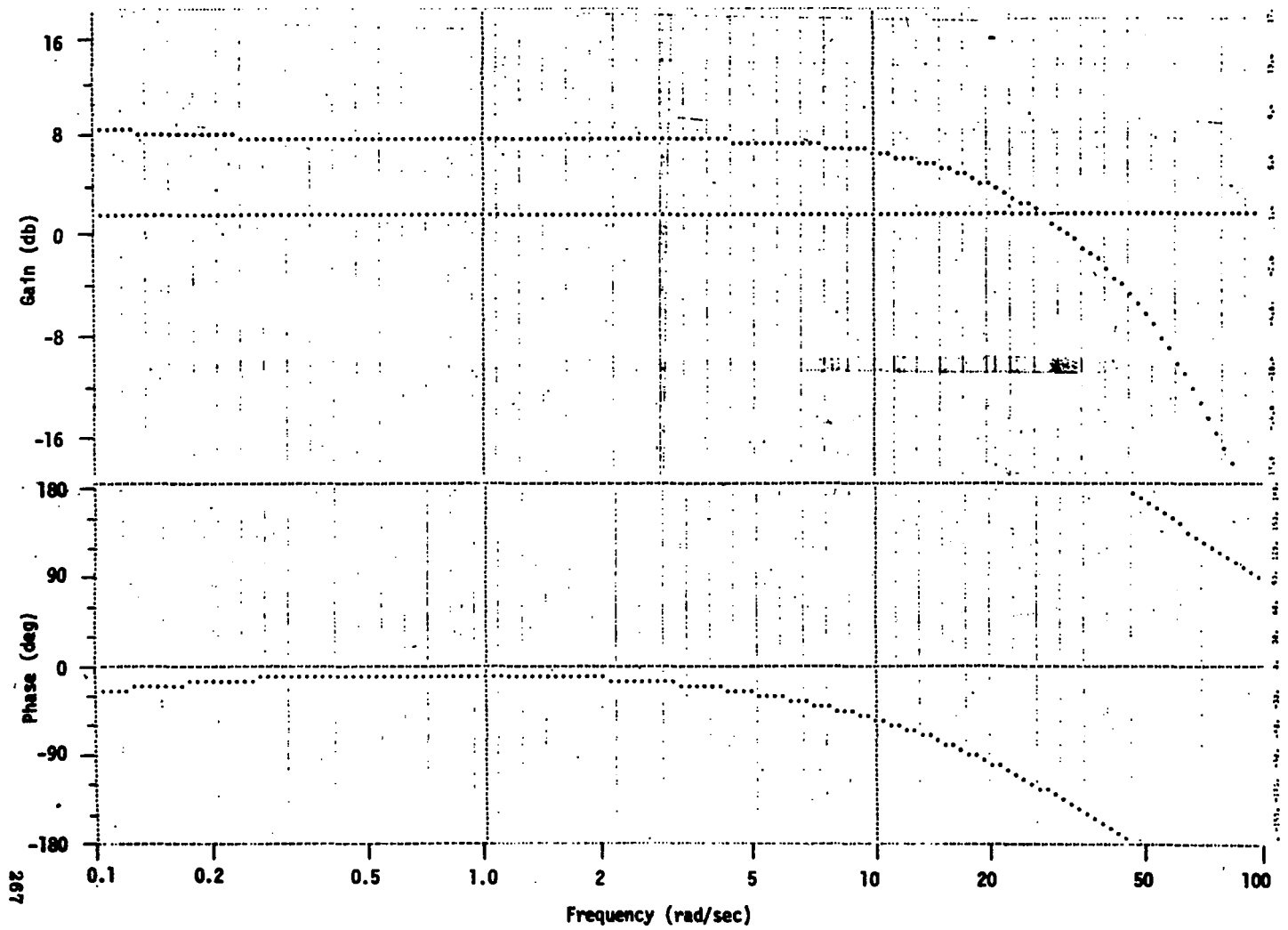


Figure 179. Heading to Aileron Frequency Response (continuous)

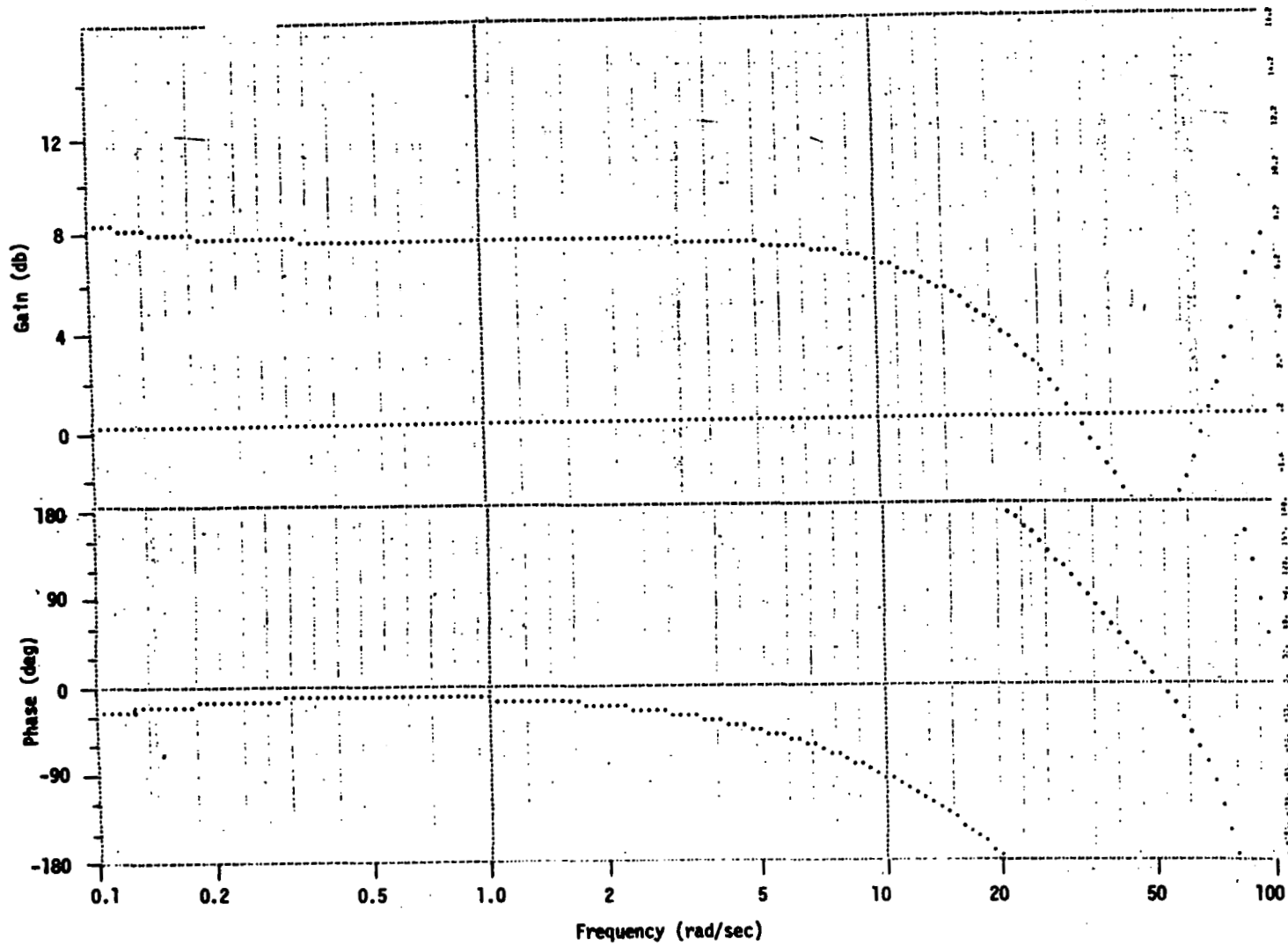


Figure 180. Heading to Aileron Frequency Response (16 sps)

Table 27. Open-Loop Gain Schedule Tests

Test	Initial Conditions	Inputs	Outputs	Expected Results
1. Pitch CAS fwd-loop gain K_{C^*}	PA NF off QF off $\alpha \approx 0$ $\delta_e \approx 0$ (via trim)	$N_z = +1$ g (DC) $\bar{q} = 50 \rightarrow 1200$ psf	Elevator (position or command)	$\Delta\delta_e^* = \frac{292}{\bar{q}}$ deg = 5.8 max * change from $N_z = 0$ value
2. Angle of attack gain $K_{\alpha L}$ (boundary control)	PA NF off QF off Hydraulics off Full nose up trim	$\alpha = 3^\circ$ (DC) above α_{limit} $V_o = 59 \rightarrow 590$ KTS	Elevator position command	$\Delta\delta_e^* = .0040 V_o$ deg * change from $\alpha = \alpha_{\text{limit}}$ value
3. Roll attitude to elevator gain	PA $\alpha \approx 0$ NF off QF off $\delta_e \approx 0$ (via trim) $\bar{q} = 50$ psf Att. mode on	$\varphi = 45^\circ$ DC $V_o = 59 \rightarrow 590$ KTS	Elevator (position or command)	$\Delta\delta_e^* = 1.7 (1 + \frac{192}{V_o})$ deg * change from $\varphi = 0$ value
4. Pitch attitude to elevator gain	PA NF off QF off $\delta_e \approx 0$ (via trim) $\bar{q} = 50$ psf Att. mode on $\alpha \approx 0$	$\theta = -1^\circ$ DC $V_o = 59 \rightarrow 590$ KTS	Elevator (position or command)	$\Delta\delta_e^* = -.00532 (191 + V_o)^\circ$ * change from $\theta = 0$ value

Table 27. Open-Loop Gain Schedule Tests (continued)

270

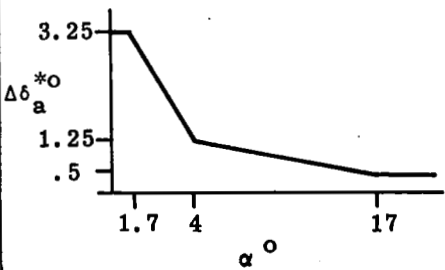
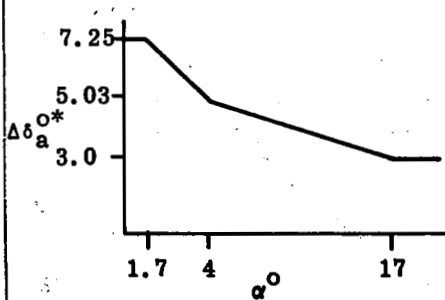
Test	Initial Conditions	Inputs	Outputs	Expected Results
5. Roll rate to aileron gain	CAS on QF off NF off PA condition $\delta_a \approx 0$ (via trim)	$p = -50^\circ/\text{sec}$ (DC) $\alpha = 0 \rightarrow 20^\circ$	Aileron (command or position)	 <p>The graph shows the change in aileron deflection, $\Delta\delta_a$ (in degrees), as a function of the angle of attack, α (in degrees). The y-axis has tick marks at 0.5, 1.25, and 3.25. The x-axis has tick marks at 1.7, 4, and 17. The curve starts at $\alpha = 1.7^\circ$ with $\Delta\delta_a = 3.25^\circ$, drops to $\Delta\delta_a = 1.25^\circ$ at $\alpha = 4^\circ$, and then levels off to approximately 0.5° at $\alpha = 17^\circ$.</p> <p>* change from value at $p = 0$</p>
6. Roll stick to aileron gain	CAS on QF off NF off PA condition $\delta_a \approx 0$ (via trim)	roll stick = $+50^\circ/\text{sec}$ sec equivalent units (DC) $\alpha = 0 \rightarrow 20^\circ$	Aileron (command or position)	 <p>The graph shows the change in aileron deflection, $\Delta\delta_a$ (in degrees), as a function of the angle of attack, α (in degrees). The y-axis has tick marks at 3.0, 5.03, and 7.25. The x-axis has tick marks at 1.7, 4, and 17. The curve starts at $\alpha = 1.7^\circ$ with $\Delta\delta_a = 7.25^\circ$, drops to $\Delta\delta_a = 5.03^\circ$ at $\alpha = 4^\circ$, and then levels off to approximately 3.0° at $\alpha = 17^\circ$.</p> <p>* change from value at $p = 0$</p>

Table 27. Open-Loop Gain Schedule Tests (continued)

Test	Initial Conditions	Inputs	Outputs	Expected Results
7. Roll rate to rudder gain	CAS on QF off NF off PA condition $\delta_a \approx 0$ (via trim) $\delta_r \approx 0$ (via trim)	$p = 50^\circ/\text{sec}$ (DC) $\alpha = 0-20^\circ$	Rudder (command or position)	<p>* change from value at $p = 0$</p>
8. Yaw rate to rudder gain	CAS on QF off NF off PA condition $\delta_r \approx 0$ (via trim)	$r = 10 \sin 3t^\circ/\text{sec}$ $\alpha = 0-20^\circ$	Rudder (position or command)	<p>* \pm sine wave amplitude</p>

Table 27. Open-Loop Gain Schedule Tests (concluded)

Test	Initial Conditions	Inputs	Outputs	Expected Results
9. Pitch rate to elevator (boundary control)	CAS on QF off NF off PA condition $\alpha \approx \alpha_{\text{limit}}$ Full nose up trim Hydraulics off	$q = 10 \sin 3t^\circ / \text{sec}$ $\bar{q} = 50 \rightarrow 1200 \text{ psf}$	Elevator command	$\Delta \delta_e^* = + \frac{94^\circ}{q}, \underline{-} 7.8^\circ \text{ max.}$ * sine wave amplitude
10. Pitch stick to flaps (NF mode)	CAS on NF on PA condition $\bar{q} = 50 \text{ psf}$	pitch stick = $a \sin 3t$ where $A = \text{variable}$ $V_o = 59 \rightarrow 590 \text{ KTS}$	Aileron (position or command) $= + 10^\circ \sin 3t$	$A = A_{(59)} \frac{(191 + V_o)}{2.9(27.4 + V_o)}$ where $A_{(59)} = A(V_o = 59)$
11. Normal acceleration to flaps	CAS on NF on PA condition	$N_z = (.05 \text{ g}) \sin 3t$ $\bar{q} = 50 \rightarrow 1200 \text{ psf}$	Aileron (position or command)	$\Delta \delta_a^* = + \frac{398^\circ}{q}$ * sine wave amplitude

Closed-Loop Ground Tests

This test verifies proper functioning of the system during ground operation including checks for structural resonances. The latter can also indicate low- \bar{q} structural stability in flight, although the value of such indications depends greatly on landing gear support influences and on control surface inertial properties.

Ideally the system and airplane should be in final operational configuration. All hydraulic and electrical power systems should be functioning normally, driven by the aircraft engine. Preliminary tests, however, will use auxiliary power units for hangar testing. It is particularly important that feedback sensors be mounted in flight configuration.

Surface Position Tests--Operation of control stick, rudder pedals, pitch trim, roll trim, and yaw trim are tested. With stick and pedals at neutral positions, all surfaces are operated via the trim inputs. Allocated trim authorities are verified as well as the trim center of all axes. Following this, the trim inputs are neutralized, and the control stick and rudder pedal inputs applied individually. Excluding deadspot or other applied nonlinearities, the following relationships apply:

- Pitch stick to elevator ($\bar{q} \leq 50$ psf) = 5.83 deg per g
- Roll stick to aileron = .47 deg/deg/sec (PA condition)
- Roll stick to rudder = .28 deg/deg/sec (PA condition)
- Rudder pedals to rudder = to be determined

For the pitch and roll stick inputs, the input values have been normalized in terms of the indicated feedback quantities of normal acceleration and roll rate, respectively. Specific stick quantities of force or displacement are currently unknown.

Structural Stability Tests--High control gain values for the critical feedback paths associated with structural coupling exist at the take-off condition. Lack of limit cycles or excessive spurious resonances during ground operation is obviously a requirement. These can be simply detected by operating the system at zero speed in the flight configuration, applying control pulses via stick and pedals, and measuring surface activity. Prime paths for coupling (because of less low-pass filtering and higher-order signals) include pitch rate to elevator (1.025 deg/deg/sec max), roll rate to aileron (0.4 deg/deg/sec max), and yaw rate to rudder (1.0 deg/deg/sec). These values should be doubled and the resonances rechecked to assure adequate margins.

A valid test for low- \bar{q} inflight structural stability requires considerably more effort to eliminate landing gear support effects and to account for lack of surface aerodynamic forces. The former can cause large increases in damping ratios of the structural modes. Reduced gear damping or special support similar to that used for structural shake testing will improve simulation quality.

Lack of surface aerodynamic forces can aggravate lower frequency mode coupling by increasing loop gains if surface inertial forces are being opposed by aerodynamic forces (the usual case). Appropriate compensation can be applied in the ground simulation if the surface inertial properties are known.

Prior F-8C flight experience should be reviewed to compare the gain values quoted above with those used in earlier systems. Given similar sensor locations and loop dynamics, potential structural coupling may be assessed by similarity.

Closed-Loop Rigid-Body Flight Functions

These tests couple the digital controller through either actual or simulated servo actuators to a rigid body simulation of the aircraft and associated motion sensors. Pilot controls are in the active state and may be used to apply inputs. * Actual rate gyros, accelerometers, and angle-of-attack sensors are blocked or otherwise disabled to preclude extraneous inputs. Their outputs are replaced by corresponding signals from simulated sensors. Provision is made to apply either selected values of dynamic pressure and airspeed (in the case of a small perturbation aircraft simulation) or to apply these quantities as added outputs from a full-freedom aircraft simulation.

The major intent of this phase of system verification is to evaluate performance in terms of transient responses to discrete pilot inputs and gust disturbances. Small perturbations are featured to facilitate comparison with prior analyses. Table 28 summarizes a recommended test repertoire. The evaluation should include the following lg flight conditions to cover the aircraft flight regime:

<u>Altitude</u>	<u>Mach</u>	<u>Configuration</u>
20000'	.67	clean
20000'	.40	clean
40000'	1.2	clean
10000'	0.8	clean
0	.189	PA

* To achieve input consistency and freedom from stick or pedal nonlinearities, step input switches paralleling the normal pilot controls are extremely useful, particularly in correlating ground and flight test performance.

Table 28. Closed-Loop Simulated Flight Functions

Test	Control Modes	Inputs	Key Outputs	Critical Performance Qualities
1. Pitch CAS	CAS	<ul style="list-style-type: none"> ● Step stick doublet, $+3$ lb from trim ● Step vertical gust 	<ul style="list-style-type: none"> ● Normal accel. ● Pitch rate ● C* 	<ul style="list-style-type: none"> ● C* response to stick ● Short period damping
2. Lat-Dir. CAS	CAS	<ul style="list-style-type: none"> ● Step stick doublet $+2$ lb from trim ● Step lateral gust ● Step pedal doublet 	<ul style="list-style-type: none"> ● Roll rate ● Yaw rate ● Lateral accel. ● Sideslip 	<ul style="list-style-type: none"> ● Roll rate response to stick ● Turn coordination ● Dutch-roll damping
3. MLC	QF	<ul style="list-style-type: none"> ● Step pitch stick doublet ● Step vertical gust 	<ul style="list-style-type: none"> ● Normal accel. ● Pitch rate ● Flap pos. ● C* 	<ul style="list-style-type: none"> ● C* response to stick ● Flap response ● Short-period damping
4. MLC	NF	<ul style="list-style-type: none"> ● Step pitch stick doublet ● Step vertical gust 	<ul style="list-style-type: none"> ● Normal accel. ● Pitch rate ● C* ● Flap position 	<ul style="list-style-type: none"> ● C*, Nz, & q response to stick ● Flap response ● Short-period damping ● q & Nz gust alleviation
5. Boundary Control	CAS with α boundary control	<ul style="list-style-type: none"> ● step aft pitch stick to exceed α limit, hold on limit, then recenter via step. ● Step vertical gust on limit 	<ul style="list-style-type: none"> ● Angle of attack ● C* ● Pitch rate 	<ul style="list-style-type: none"> ● Achieve limit α without overshoot ● Short-period damping while on limit ● Resumption of normal control

Table 28. Closed-Loop Simulated Flight Functions (continued)

278

Test	Control Modes	Inputs	Key Outputs	Critical Performance Qualities
6. Pitch Attitude Control	Pitch Attitude Hold	<ul style="list-style-type: none"> • Pitch stick, pull up to desired attitude & release force, push over to new attitude & release. • Step vertical gust • Roll stick, bank 45°, hold 10 sec, and return to wings level 	<ul style="list-style-type: none"> • Pitch rate • Pitch attitude 	<ul style="list-style-type: none"> • Attitude lock-on & release • Mode stability under gust • Attitude retention during turns
7. Mach Control	Mach Hold	<ul style="list-style-type: none"> • Roll stick, bank 45°, hold 10 sec, and return to level. • Step vertical gust • Step longitudinal gust 	<ul style="list-style-type: none"> • Mach • Attitude 	<ul style="list-style-type: none"> • Mach error during turns • Mode stability under gust
8. Altitude Control	Altitude Hold	<ul style="list-style-type: none"> • Engage mode during 5000 fpm climb • Roll stick, bank 45°, hold 10 sec, and return to level • Step vertical gust 	<ul style="list-style-type: none"> • Altitude • Attitude • Normal Acceleration 	<ul style="list-style-type: none"> • Transient g's & altitude error when engaged in climb • Altitude error during turns • Mode stability under gusts

Table 28. Closed-Loop Simulated Flight Functions (concluded)

Test	Control Modes	Inputs	Key Outputs	Critical Performance Qualities
9. Roll Attitude Control	Attitude Hold	<ul style="list-style-type: none"> • Roll stick, roll to 45° & release, roll back to level & release. • Step lateral gust 	<ul style="list-style-type: none"> • Bank angle • Roll rate • Yaw rate 	<ul style="list-style-type: none"> • Attitude lock-on & release • Mode stability under gust
10. Heading Hold	Heading Hold	<ul style="list-style-type: none"> • Engage mode during 45° bank turn • Step lateral gust 	<ul style="list-style-type: none"> • Bank angle • Heading 	<ul style="list-style-type: none"> • Bank transient following engage • Mode stability under gust

SECTION 13

SIMULATOR PROGRAM DEFINITION

Overview

This section defines an experimental program to evaluate controlled configured vehicle (CCV) laws on the NASA/LRC F-8C simulator. The objective is to provide NASA with a tool for quantitatively measuring and comparing pilot performance and to aid NASA in planning a more efficient flight test program. [22]

The design and methodology for two specific experiments are defined. In the first experiment, the effects of gust levels on pilot performance with the CCV controlled F-8C and a base-line controller* for the F-8C are compared. In the second experiment, gust level is held constant and the effects of speed and altitude on pilot performance with the two structures are compared. Since the CCV control laws are to enhance stability, the response to turbulence is considered a major consideration.

The independent and dependent variables associated with the two experimental designs are discussed next. The reduction of subject variability is then discussed followed by a definition of simulation tasks. Next the procedure and instructions used to conduct the experiments are defined. This section concludes with a summary of data analysis and interpretation.

Experimental Design

The purpose of having an experimental design is to provide a structure through which data may be obtained in a systematic manner relatively free from unwanted effects. The data are indicators of the existence and strength of a relationship between two or more variables. Further, in order to be able to state with some level of certainty that the relationship exists, it is necessary to repeat the observation(s) a number of times.

There are two essential elements involved in specifying an experimental situation--one or more independent variables (IV) and one or more dependent variables (DV). An IV has its value set prior to and remains constant during the experiment. In a DV changes are being observed and recorded. These changes are a function of or "dependent" upon controlled changes in the IV's.

There are many variations of experimental design which exist in the literature. For purposes of the present studies a basic mixed design using repeated measures has been chosen. The choice and recommendation was based almost entirely on economic considerations. This particular design yields the largest amount of data with a minimal expenditure of resources. In addition, it directly accounts for the variability in performance which exists between pilots.

An example of this design is depicted in Figure 181. An experiment utilizing this design would compare the performance of three pilots flying both the CCV controlled F-8C and a base structure F-8C* under varying values of a flight condition. With this

* A structure designated by NASA/LRC. This could be the unaugmented F8-C.

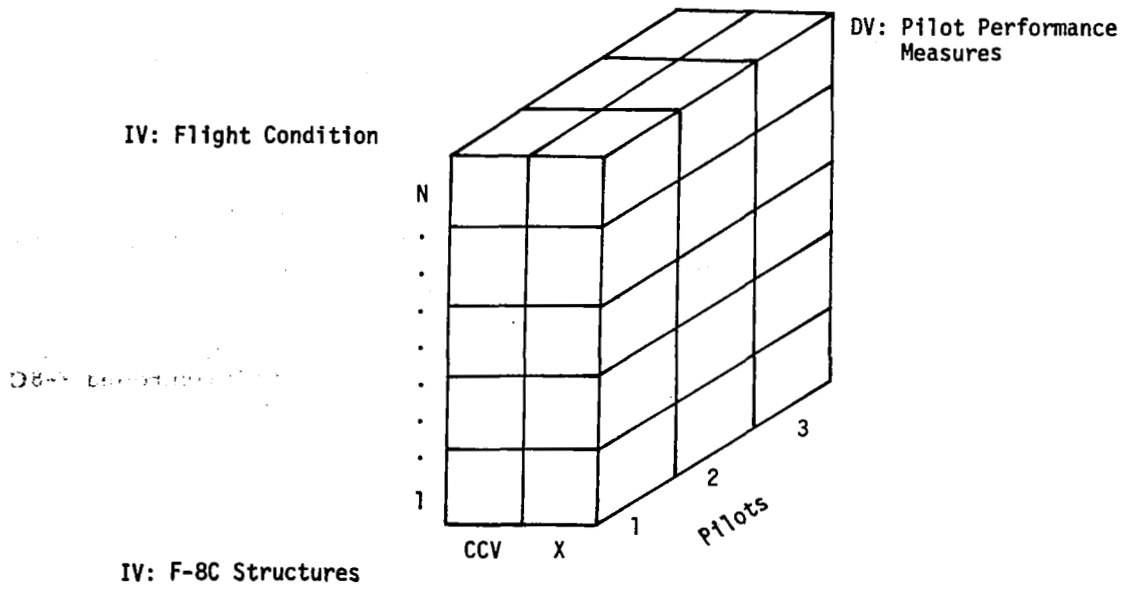


Figure 181. Experimental Design

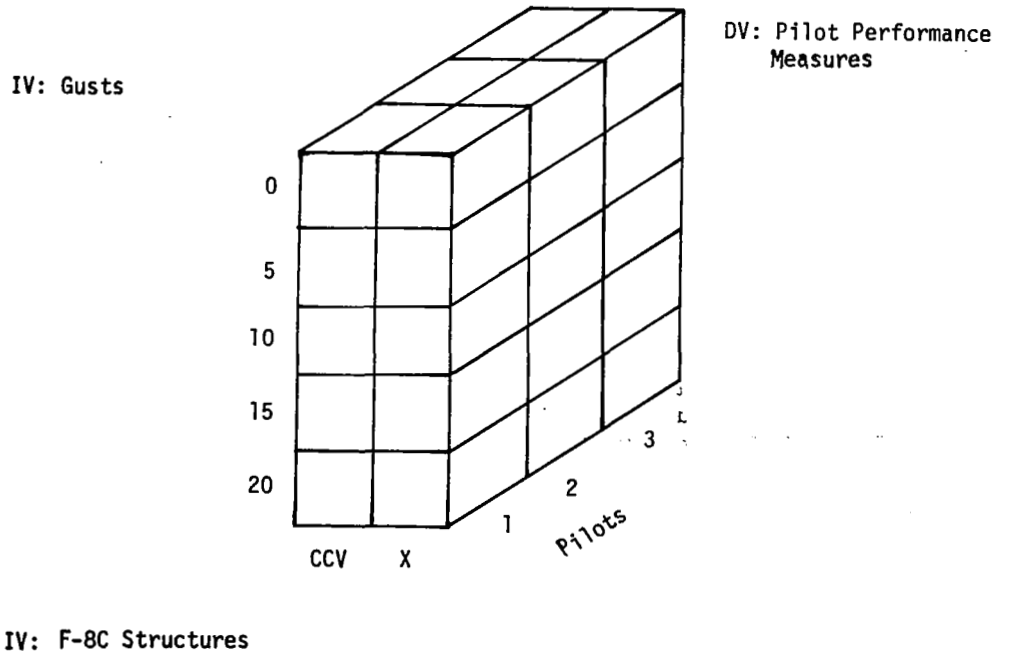


Figure 182. Experimental Design for Comparison of Gust Effects on Pilot Performance

design any condition for which values can be pre-set (IV) could be used. Pilot performance (DV) could be measured using:

- Altitude error
- Velocity error
- Lateral error
- Bank angle
- Sideslip
- Pilot aileron stick command
- Pilot rudder command
- Single-axis rms errors
- Multi-axis rms errors

In addition two pilot opinion ratings could be used:

- Cooper-Harper Ratings [23]
- Global Ratings [24]

In the evaluation of flight systems, one major consideration is how the system operates under various levels of gusts. The first experiment will, therefore, use gust levels as the flight condition in the experimental design. Five velocities of gusts were determined by taking equal interval velocities between zero, or no gusts, and 20 knots, the maximum disturbance which the F-8C could be expected to encounter. The design for the first experiment is shown in Figure 182.

Another major consideration is the evaluation of the system while flying at typical speeds and altitudes. Figure 183 contains the design of the second experiment. The design has remained the same as in the first experiment. However, the independent variable of gusts has been replaced with five values of speed and altitude.

Subjects

In experiments using human subjects, two types of subject variability must be tolerated and accounted for: intersubject variability such as training differences and experience differences; and intrasubject variability such as motivation, attitude, fatigue, or boredom. Variability is computed as error and thus, in a sense, is subtracted from the results. Therefore, large variability can have the effect of suppressing real differences between the variables being tested.

Intersubject variability can be reduced by increasing the number of subjects. However, experimental situations, such as the present one, impose certain minimum requirements upon subject acceptability (i. e., being able to fly an F-8C). The number of available subjects is thus reduced and often these subjects are not homogeneous. These factors contribute to inter-subject variability.

The experimental design described in the previous section treats the subject pilots as a separate independent variable. Fewer subjects can be tolerated in a design of this type because the variability introduced by each subject can be directly examined. However, this technique can only determine the amount of variability--it does not or cannot control it. Therefore, subjects should be matched to the extent possible on factors such as:

IV: Speed + Altitude

DV: Pilot Performance

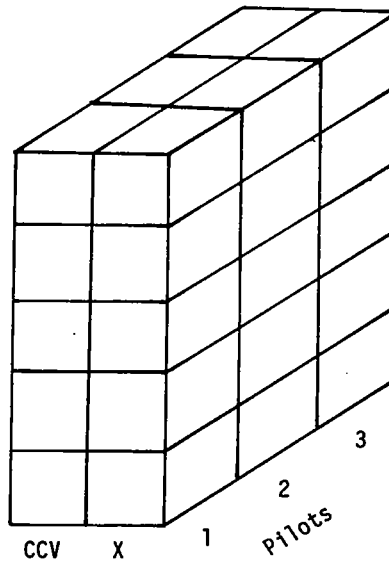
Mach = 1.2; 40,000 ft.

Mach = 0.8; 10,000 ft.

Mach = 0.67; 20,000 ft.

Mach = 0.4; 20,000 ft.

Power Approach



IV: F-8C Structures

Figure 183. Experimental Design for Comparison of Speed and Altitude Effects on Pilot Performance

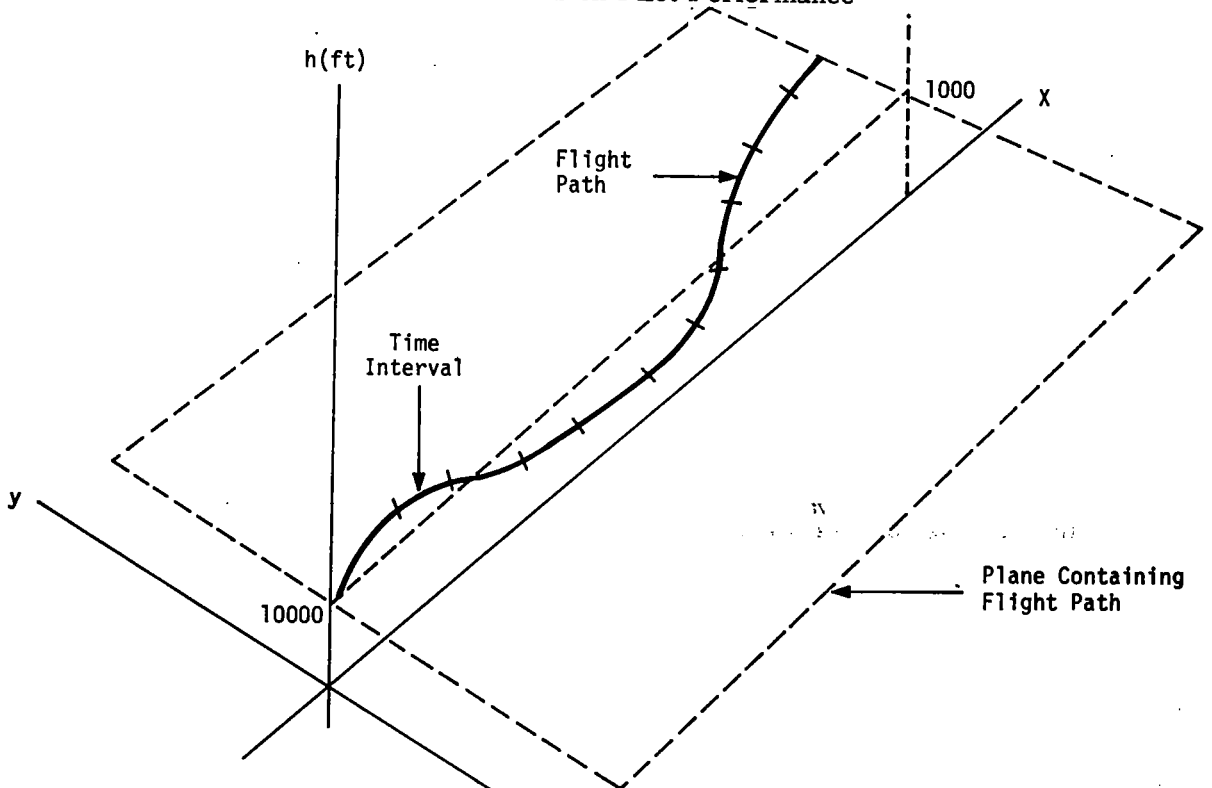


Figure 184. Typical Flight Profile

- Service branch
- Age
- Rank
- F-8C flying hours
- Total flying hours
- Education

Intrasubject variability is reduced through an increase in the number of observations. Since the number of subjects is small, the number of observations on each subject must be increased. However, factors such as boredom and motivation must also be taken into account. A procedure developed to balance these factors to reduce the intrasubject variability is described in the subsection on Procedure.

Task

A task used by Stein and Henke [25] meets the crucial requirements for the present type of experimentation:

- New learning or interference from prior learning is kept to a minimum.
- The task includes the use of full cockpit instrumentation and controls.
- The task provides a structure for controlling intrasubject variability; i. e., all subjects should perceive, understand, and perform the task in a similar manner and are subject to the same experimental controls.

The task consists of a series of flight profiles which can be randomly used for each flight condition (i. e., gust or speed and altitude). The profiles consist of timed intervals during which constant bank angle turns or wings--level flight are commanded. A typical flight profile is pictorially represented in Figure 184.

The primary display of the flight path course to the pilot is the flight director. The task is thus a perceptual motor tracking task in which deviations from appropriate pitch and lateral commands must be detected and corrected for.

Procedure

Instructions--Instructions must be developed which will insure that the subject clearly understands what is required of him. From the standpoint of the experimenter, the instructions must be as explicit as possible to insure consistency between subjects.

In general, instructions should incorporate the following sequence and sections:

- 1) Introduction includes who is conducting the research; a generalized statement of the purpose.
- 2) Overview includes in general terms what the task will be; what equipment is used; approximately how long it will take; if more than one session--how many; and importance of continuity in attendance.

- 3) Specific explanation of the task and subject role includes demonstration of equipment and performance of a typical task; number and length of trials.
- 4) Practice trial includes a complete run through of all aspects of the task by the experimenter, conducted in the same manner as a formal data session.
- 5) Answering of questions

Practice Session--In experimentation involving a highly complex task, such as the present one, it is necessary to have all subjects begin with approximately the same skill level and yet, at a level at which results are based upon a typical level of operators of the task. Practice sessions are used to insure that subjects are operating at a prescribed level.

The practice session should be handled in a manner as close to the formal data collection sessions as possible. All of the flight conditions (in a randomized order) should be flown twice. Throughout the practice session the pilots should receive immediate feedback about their performance errors. Particular care should be taken by the experimenter to insure that the subjects are maintaining a high performance level on all parameters.

Data Collection--Using the dependent measures previously described in the experimental design subsection, two data collection phases would be required. Phase I would be used for collection of the pilot performance measures, and Phase II would consist of the pilot opinion ratings.

Each subject pilot would participate in five sessions consisting of 40 trials each--20 in Phase I and 20 in Phase II. In each phase would be presented a random sequence of 20 trials containing two trials for each of the 20 experimental conditions, (e.g., the two F-8C structures by the five conditions of either gust of speed and altitude - 2x5x2). The pilots would not be told which condition they were flying.

The task and procedure would be the same for both Phase I and Phase II with the exception of the time interval between trials. In Phase II the pilots would be asked to rate each system under each condition as it was flown. Thus, the intertrial interval has to be longer to give the pilots time to fill out the forms.*

Data Analysis

Once an experimental design is selected, much of the analysis can be performed on-line if data point or data summary requirements are considered early enough to be included in the software set-up. The value of performing these analyses on-line lies in being able to detect trends in the data during the training and formal data collection. Thus, changes in pilot strategy that do not meet the requirements of the simulation can be detected and corrected.

In addition, the establishment of standard data formats and headings reduces the probability of losing cell entries and avoids the problem of unequal observations.

Once the data have been collected, the data should be manipulated for the computation and displaying of such things as:

*The two scale forms are contained in Appendix E.

- Histograms
- Graphics
- Means
- Standard deviations
- Analysis of variance tables

Recall that in the present experimental design the main effects of interest are the fixed effects of system type and flight condition and the random effect of pilots. The analysis of variance is designed to determine the level of statistical significance of these effects in the experiment. An analysis of variance output format (analysis of variance table) for this experimental design is contained in Table 29.

The histograms and graphics provide a pictorial representation of the data, while the means and standard deviations provide a numerical summary of the data. These are, therefore, the key to interpreting the results indicated by the analyses of variance.

Data Interpretation

An analysis of variance would be computed on the data from each of the pilot performance measures and output in a format similar to that contained in Table 32. The F-statistic (contained in the last column) is used for two types of interpretation--the main effects and interactions. The main effects terms consist of:

- Systems (A)
CCV controlled F-8C and Base structure F-8C
- Flight condition (B)
Gust levels or speed and altitude
- Subjects (C)

The interaction terms represent all possible combinations of the main effects:

- Systems (A) x Flight condition (B)
- Flight condition (B) x Subjects (C)
- Systems (A) x Subjects (C)
- Systems (A) x Flight condition (B) x Subjects (C)

The output of an analysis of variance is an F-statistic ($F \geq 0$), which is computed under the statistical hypothesis (H_0) that all the means of a particular main effect are identical. Under this hypothesis, the F-statistic is distributed according to the F-distribution law^[27]. Critical values (F_p) can thus be determined such that (under H_0) probability is ($F \geq F_p$) = p, for p = 0.05 or p = 0.01. Then, if the F-statistic (under F in Table 29) comes out greater than F_p , it can be concluded that H_0 is refuted (i. e., the means are different) or a rare event of probability, p, has been observed. This is condensed by saying that the means are different at a level of significance equal to p (or, more simply, the effect is significant at level p). If F comes out less than F_p , the hypothesis (H_0) that the means were identical would have to be accepted (or, more simply, the effect is not significant at level p).

For example, if the F-statistic for the main effect of systems (A) came out greater than F_p on any of the pilot performance measures, it would have to be concluded that for that measure, there was a significant difference (at level p) between the CCV controlled F-8C and the base structure F-8C. The histograms, graphics, means, and standard deviations would be used to isolate this difference. Inferences about the difference could then be drawn.

Table 29. Analysis of Variance Output Format

Source of Variance	Degrees of Freedom	Mean Square	F
Systems (A)			
Flight condition (B)			
Subjects (C)			
A x B			
B x C			
A x C			
A x B x C			
Residual			
Total			

$a_p \leq 0.01$

$b_p \leq 0.05$

^cN.S. = Nonsignificant

SECTION 14

FLIGHT TEST INVESTIGATION

This section presents recommended flight test procedures to evaluate the control laws developed under this study. Major emphasis is placed on the basic "inner-loop" functions (augmentation, boundary control, direct lift, and maneuver load control) in contrast to the relatively conventional "autopilot" modes of attitude, heading, Mach, and altitude hold. It is recognized that the recommended procedures and conditions are subject to constraints imposed by prevailing aircraft status as well as overall flight test safety. Particular conflicts may arise in probing flight envelope extremes which is desirable in evaluating overall control system performance. Figure 185 illustrates the general flight condition repertoire envisioned for control assessment, including specific points having past analytical emphasis.

Table 30 lists the recommended mode test sequence. Each mode is discussed in following paragraphs.

Table 30. Mode Test Sequence

1. Primary Flight Control System
2. Boundary Control
3. Maneuver Load Control (Q-Flaps)
4. MLC plus Response Augmentation (N-Flaps)
5. Autopilot
• Attitude
• Heading
• Altitude
• Mach

Digital Flight Control System (DFCS)

The DFCS is the fundamental control mode which incorporates the so-called "control augmentation" functions. The only possible "lower" mode would be an emergency backup mode normally engaged only after a sequence of failures. The DFCS is engaged on the ground and functions throughout takeoff and landing.

Table 31 shows the suggested DFCS test sequence. It begins with the low-dynamic pressure conditions and proceeds to higher q 's as system performance is verified. Each condition has nearly the same general test repertoire designed to evaluate nominal system performance. The special tests are more flight research oriented, attempting to optimize system characteristics through parametric investigations.

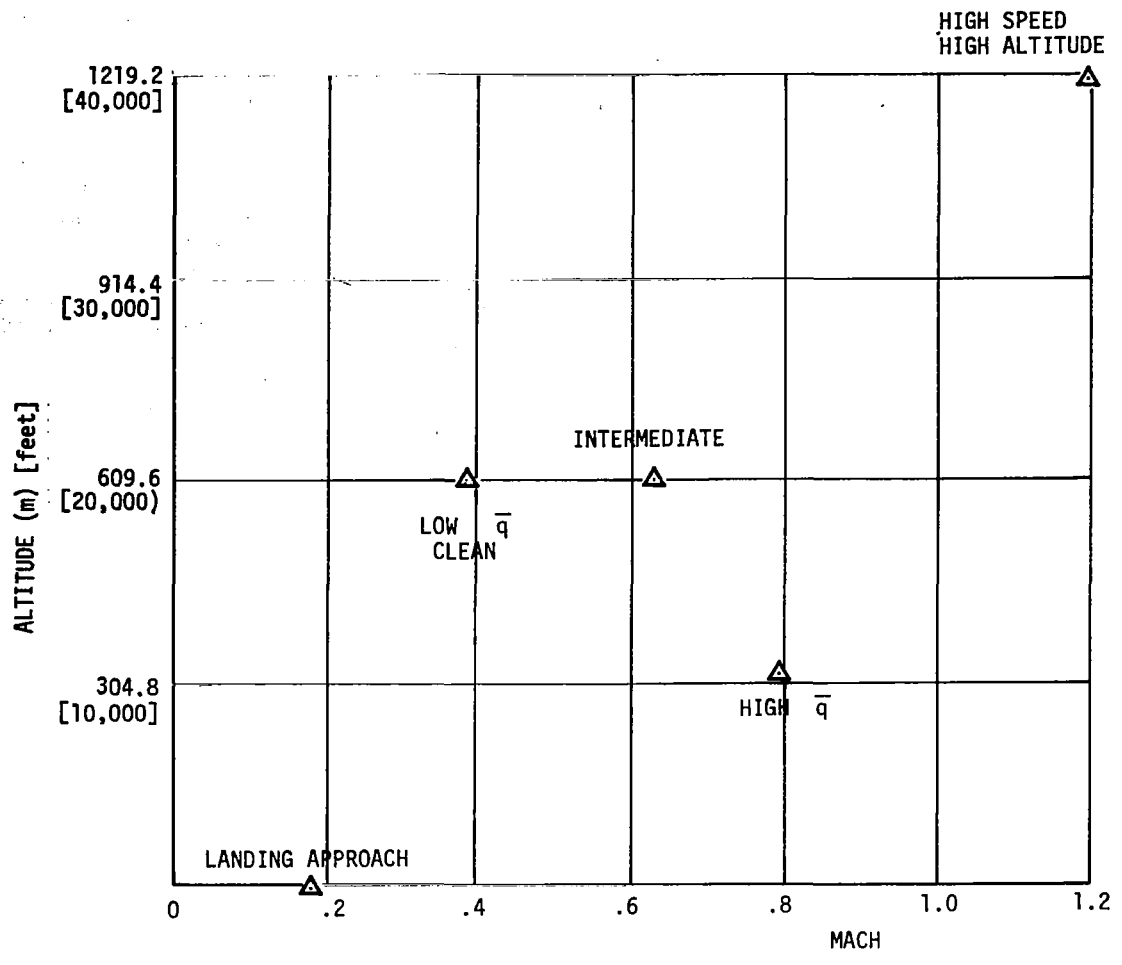


Figure 185. Flight Control Test Conditions

The general test sequence begins with trim capability trials. The trim elements in pitch, roll, and yaw are operated to verify that a desired trim state can be easily achieved without repeated efforts. Both "straight and level" and intentionally mistrimmed states should be established. It is noted that the trim objective is not to enable "hands-off" flight (autopilot modes provide this function) but rather to achieve and hold a desired trim state within acceptably low (around breakout levels) control forces. At clean flight conditions (where the so-called "neutral speed stability function" is provided) a pitch axis with near-neutral speed stability is expected.

Table 31. DFCS Test Sequence

1.0	Low - \bar{q} Testing
1.1	Approach Configuration
1.1.1	General Test Repertoire
	<ul style="list-style-type: none">• Trim Capability (3 axes)• Stability margins & mode damping• Transient command response• Apparent speed stability• Configuration change transients• Overall flight acceptability
1.1.2	Special Test Repertoire
	<ul style="list-style-type: none">• Stick gradient optimization• Stick nonlinearities investigation• Response speed investigation
1.2	Clean Configuration
1.2.1	General Test Repertoire
1.2.2	Special Test Repertoire
2.0	Increasing - \bar{q} Testing
	(Repeat test 1.2 at higher \bar{q} flight conditions)

A trim related issue particularly relevant to fly-by-wire systems is the general acceptability of series trim methods*. Because the series trim action involves a

*A series trim input is added to the stick input, whereas a parallel trim input alters the prevailing stick force level only.

closed-loop response through the aircraft, a somewhat more difficult trim task usually results. This is compensated to a degree by having to trim much less frequently (if at all) with an integrating system.

Stability margins and airframe damping are the next tests. These are conducted from a trimmed straight and level condition. Control stick pulses and rudder kicks are the primary means of excitation. It is assumed that pilot adjustment of forward-loop control gains (proportionally affecting rudder, aileron, and elevator command signals) is possible on an incremental basis (up to +6 db) from nominal. The gains should be perturbed individually around their nominal value with the other gains at their nominal values. An appropriate series would be:

- (1) pitch, roll, and yaw pulses, gains nominal (including scheduled gains)
- (2) pitch stick pulse, pitch gain + 3 db
- (3) pitch stick pulse, pitch gain + 6 db
- (4) pitch stick pulse, pitch gain - 3 db
- (5) pitch stick pulse, pitch gain - 6 db
- (6) Roll stick pulse, roll gain + 3 db
- (7) Roll stick pulse, roll gain + 6 db
- (8) Roll stick pulse, roll gain - 3 db
- (9) Roll stick pulse, roll gain - 6 db
- (10) Rudder Pedal pulse, yaw gain + 3 db
- (11) Rudder Pedal pulse, yaw gain + 6 db
- (12) Rudder Pedal pulse, yaw gain - 3 db
- (13) Rudder Pedal pulse, yaw gain - 6 db

The primary variables to be recorded during these tests are the 3-axes body rates and surface positions. Any tendency towards limit cycles should be noted, as well as associated amplitudes and frequency. Prevailing values of apparent short-period damping and Dutch-roll damping are estimated from the pitch rate and yaw rate recordings, respectively.

Measurement of transient command responses follows. Here the use of step input switches in pitch and roll is recommended to enable precise inputs and avoid stick nonlinearities. Pitch inputs between 0.25 and 0.5 g are applied, held for 3 to 5 seconds, then removed. Recordings of pitch rate and normal acceleration are made to enable comparison with ground simulation results and related response envelopes. Roll inputs of 20 degrees per second are applied, held until 40 to 50 degrees bank, removed for 3 seconds, reversed and removed to achieve wings level. Recordings of roll rate, bank angle, yaw rate, lateral acceleration, and sideslip angle are taken.

To investigate higher angle-of-attack performance, a constant altitude turn ($\phi = 45^\circ$) can be established. Roll inputs causing a $\pm 20^\circ$ change in bank angle are applied and similar recordings are made as in the wings level case. From these data, lateral-directional performance is measured in terms of roll subsidence, spiral stability, and turn coordination.

Apparent speed stability tests consist of applying power changes to achieve speed increments of 5 to 10% of nominal while holding constant altitude flight. The resulting

time histories of stick input, speed, normal acceleration, pitch rate, and elevator positions are recorded.

Transients resulting from changes in aircraft configuration are measured at appropriate conditions. Usual operational changes in gear position, wing position, and flap position are applied. Recordings are made of stick input, normal acceleration, pitch rate, and elevator position. Comparison with conventional F-8C transients are made by pilot opinion.

After the above formal test sequence is completed, a series of operationally-relevant maneuvers appropriate to the prevailing flight condition should be made to assess overall flight acceptability. Landing/take-off trials, aerobatics, simulated in-flight refueling, and formation flight are candidates.

The special test sequence of Table 31 identifies three technical areas which continue to merit additional handling qualities investigation. They are listed in a preferred order of test, although the interactive nature of their properties dictates an iterative approach. The stick gradient variations are accomplished first, using a nominal type of stick non-linearity (e. g. + .5 pound deadspot) and nominal response dynamics. After selecting a preferred gradient, various stick deadspot values are investigated. The best value is probably task-oriented, so the investigation should include a range of flying tasks, from simple cruise control to small amplitude tracking. Additional nonlinearity types can also be studied. In place of or in addition to a simple stick deadspot, a stick output varying as the square of the stick input (deflection or force) has proven advantageous in certain situations. Finally, the system response speed can be adjusted via prefiltered on the pitch and roll stick inputs using nominal gradients and stick nonlinearities.

Boundary Control

The boundary control system is designed to prevent inadvertent excesses in angle-of-attack. As currently studied, a "hard" angle-of-attack limit is applied, although the system can be adjusted to merely effect an increase in apparent stick force above the preset α limit. For purposes of initial flight testing, the α limit should be set at a conservative low value for the prevailing condition, perhaps via cockpit adjustment. As confidence develops, the limit can be set to increasing values. The major use of the boundary control is at the lower \bar{q} conditions, although the system will function over the flight range. Both approach and clean configurations should be tested where appropriate. The testing should begin at low \bar{q} 's and progress higher. At each condition the following test sequence is recommended. In addition to the usual pitch variables, the limit α (if cockpit adjustable) and the input signals to the signal selection algorithm should be recorded. The following test sequence investigates the switching characteristics of the boundary controller, and not the dependence of the alpha boundary on sideslip.

Unaccelerated Limiting--Slowly reduce speed (or reduce the α limit value) until the limit is encountered. Continue to reduce speed (or the limit) and observe that the actual angle of attack follows the limit. Apply aft stick inputs when on the limit and note no reaction. Apply forward stick inputs until the angle of attack moves below the limit. Restore speed (or raise the α limit) to restore trimmed flight.

Accelerated Limiting - Slow Approach--Beginning at trimmed flight, apply aft pitch stick inputs until the limit α is encountered, taking 3 to 6 seconds to achieve a stick input corresponding to about twice that necessary to reach the limit. Note that the α limit is accomplished without overshoot. Reduce stick input to the trimmed value, and note that normal control is smoothly restored. Vary bank angle and power as required during the

maneuver to roughly maintain speed and altitude. Finally, vary stick inputs around trim within the α limit and note that DFCS operation is normal.

Accelerated Limiting - Fast Approach--Repeat the above tests using rapid stick inputs (essentially steps) and verify that the α limit is observed smoothly and without overshoot, and that normal control is properly restored.

General Acceptability--At appropriate conditions apply typical operational maneuvers to make a general pilot assessment of boundary control effectiveness and utility. Attempt to determine control utility as a maneuver aid in achieving maximum performance without upset. Judge the acceptability of a limiting action without associated stick force cues. Observe boundary maintenance while performing gross speed changes by applying full power at low speed, pull to achieve limit, and accelerate until speed, power, or g limited. Adjust bank angle to maintain approximate altitude.

Maneuver Load Control (Q-Flaps)

This mode is designed to produce minimum drag flap positions without appreciably affecting normal DFCS transient performance. To verify the latter, the following elements of the "general test repertoire" should be repeated in the pitch axis at conditions where the QF mode is pertinent.

- trim capability
- transient command response
- apparent speed stability
- overall flight acceptability

Results are compared to those of the DFCS.

After these tests have proved satisfactory, the effectiveness of the flap schedule in reducing drag during sustained maneuvers may be determined by a series of coordinated turns. With 12 degrees of flap allocated to the MLC function, a 3 degree per-second pitch rate produces full flap deflection. Bank angles should be selected to produce slightly in excess of the full 12 degree deflection to produce maximum effect. A steady turn is held between 10 and 30 seconds to allow study conditions to develop. Two techniques may be employed:

- (1) Perform the turn at constant power setting. Record the speed time history with and without the QF mode.
- (2) Perform the turn at as constant speed as possible. Record power setting with and without the QF mode.

From the above data, drag reduction due to the QF mode can be determined.

MLC Plus Response Augmentation (Nz-Flaps)

This mode produces the same steady-state flap settings as the QF mode, but in addition is designed to improve pitch transient response to stick inputs and alleviate gusts in terms of reduced normal acceleration and/or pitch rate. To evaluate the former qualities, portions of the pitch DFCS testing described earlier should be repeated, namely:

- transient command response
- overall flight acceptability

The step input responses of pitch rate and normal acceleration are of particular interest, and these should be recorded with and without the N_z flap mode engaged in two adjacent runs to assure common conditions as much as possible. A combination of less pitch rate overshoot and faster normal acceleration response should be the dominant quality of the N_z flap mode when compared to the basic DFCS.

The gust alleviation qualities of the N_z flap mode must be determined as air turbulence conditions permit. Pitch rate, pitch attitude, and normal acceleration recordings are desired at various turbulence conditions, run with the DFCS and N_z flap modes engaged alternately. Relative RMS values can then be computed.

Autopilot Modes

The autopilot mode complement consists of a fairly conventional set of outer loop control laws for an airplane of the F-8C class. They are all "hold" modes in that the desired value of the major controlled variable (attitude, heading, Mach, or altitude) must be attained before mode engagement, upon which the current value becomes the control reference point. Flight test of each mode is discussed in following paragraphs. Flight conditions defined in Figure 185 are applicable.

Pitch and Roll Attitude Hold--Engage the mode after establishing trimmed unaccelerated flight at the desired attitude. Apply rudder kicks and check damping (record body rates and surface positions).

Apply roll stick inputs to achieve roll rates of about 30 deg/sec. Avoid pitch inputs to preclude pitch attitude CCS (control stick steering) switching. Bank to about 45 degrees and release roll stick to lock on new bank angle. Hold bank for 30 seconds, then apply opposite roll stick to roll to opposite bank angle. Hold for 30 seconds, then roll to wings level and hold. Assess roll engage and disengage properties of above maneuver (record roll attitude and roll stick). Record pitch attitude to measure attitude error during maneuver.

Flying at wings level, apply pitch stick inputs of approximately + 0.25 g to achieve pitch attitudes of about + 45 degrees. Hold each attitude for about 10 seconds. Assess pitch attitude engage and disengage properties (record pitch attitude and pitch stick).

Assess general mode performance under typical operational maneuvers. Include full-roll and loop maneuvers to verify accommodation of large amplitude anomalies. Judge acceptability of stick-force properties during large maneuvers.

Heading Hold--Engage mode at trimmed flight. Apply rudder kicks to check damping. Note heading retention qualities. Apply roll stick inputs, bank to 45 degrees, and hold. Engage heading hold in band and observe roll out and recovery of initial heading. Record heading error and bank angle. Repeat at opposite bank angle.

Altitude Hold--Engage mode at level flight and record steady-state performance for 30 seconds (altitude error, pitch attitude, and elevator position). Apply configuration and power changes appropriate to the flight condition and measure altitude error time history. Make bank CSS maneuvers without dropping altitude mode, holding + 45 degree banks for 30 seconds each. Record altitude error and bank angle.

Check altitude engage transients at initial rate conditions. Via pitch attitude hold, establish initial rates of climb of + 5000 fpm. Engage altitude mode at selected altitude and measure attitude, altitude, and normal acceleration. Assess trade-off between altitude recovery and normal acceleration.

Mach Hold--Engage mode at selected speed and record steady-state performance for 1 minute (Mach error, pitch attitude, elevator position). Perform CSS banking maneuvers without dropping Mach mode and assess performance during the turn. With the autopilot on attitude hold, establish a rapid Mach rate (plus & minus). Engage Mach hold and record transient.

SECTION 15

CONCLUDING REMARKS

The design program described in this report has successfully generated flight-worthy digital CCV control laws. These laws meet all handling quality requirements for fighter-category aircraft. They provide automatic boundary limiting, 40 percent reduction in gust load accelerations, and 15 percent maneuver load drag reduction. The capability for flying with reduced static stability has been included. These benefits were realized without any modification of the test aircraft. Careful integration of the various quadratic controllers with mode transition logic and minimum drag schedules results in no conflicts among the CCV objectives.

A test plan for verifying proper flight system integration was formulated based on frequency response characteristics. A number of experiments were also suggested for evaluating handling qualities on the simulator. Finally, flight test investigations were specified for assessing performance in the air.

The design process made extensive use of modern quadratic optimal control design methodology. To ensure flight worthiness, the signal shaping and integrators essential to good CAS design were included in the optimum control formulation. In addition, many classical performance and sensitivity measures (such as gain and phase margins) were used in evaluating the designs during the synthesis process. Finally, better understanding and acceptance of the designs were achieved by presenting them in standard block diagram form. The resulting control laws are basically linear gains and signal compensation, with key parameters scheduled on external air data measurements to achieve stability and good performance throughout the flight envelope.

Two lateral-directional CAS designs were produced using different sensor complements. The first CAS mechanizes "inertial turn coordination." It commands theoretical yaw rates required to maintain coordinated turns and uses deviations to damp Dutch roll. This results in ideal lateral coordination and good damping regardless of the angle-of-attack.

Unfortunately, these feedbacks require several difficult to measure signals. In addition to rates and attitudes, angle-of-attack and true air speed are required. The second lateral CAS eliminates the attitude and true-air-speed signals, yet performs nearly as well as the full-measurement design.

APPENDIX A

**DEFINITION OF "A" ARRAY
PARAMETERS USED IN F8SIM**

COMPLETE SIMULATION DICTIONARY NUMERICALLY

A()	MNEMONIC	DESCRIPTION	INITIAL VALUE	SET BY	UNITS
1	TM	SIMULATION TIME	0.	EXEK	SEC
2	X	BODY POS. ALONG EARTH AXIS XE	0.	DYNK	FT
3	Y	BODY POS. ALONG EARTH AXIS YE	0.	DYNK	FT
4	H	BODY POS. ALONG EARTH AXIS ZE		DYNK	FT
5	MACH	MACH NUMBER = VEL/SOS	C	AERO	
6	SOS	SPEED OF SOUND - COMP. IN ATMOS	C	DYNK	FT/SEC
7	U	VEL COMP OF CG-X AXIS WRT EARTH		DYNK	FT/SEC
8	V	VEL COMP OF CG-Y AXIS WRT EARTH		DYNK	FT/SEC
9	W	VEL COMP OF CG-Z AXIS WRT EARTH		DYNK	FT/SEC
10	UA	VEL COMP OF CG-X AXIS WRT AIR	C	DYNK	FT/SEC
11	VA	VEL COMP OF CG-Y AXIS WRT AIR	C	DYNK	FT/SEC
12	WA	VEL COMP OF CG-Z AXIS WRT AIR	C	DYNK	FT/SEC
13	XDOT	VEL COMP ALONG XE	C	DYNK	FT/SEC
14	YDOT	VEL COMP ALONG YE	C	DYNK	FT/SEC
15	HDOT	VEL COMP ALONG ZE	C	DYNK	FT/SEC
16	VEL	MAGNITUDE OF VELOCITY VECTOR	C	DYNK	FT/SEC
17	UDOT	TIME DERIVATIVE OF U	C	DYNK	FT/S/S
18	VDOT	TIME DERIVATIVE OF V	C	DYNK	FT/S/S
19	WDOT	TIME DERIVATIVE OF W	C	DYNK	FT/S/S
20	ACGX	ACCEL OF BODY (WO G) - BODY X AXIS	C	DYNK	FT/S/S
21	ACGY	ACCEL OF BODY (WO G) - BODY Y AXIS	C	DYNK	FT/S/S
22	AXGZ	ACCEL OF BODY (WO G) - BODY Z AXIS	C	DYNK	FT/S/S
23	AXI	OUTPUT ACCEL PKG BODY X AXIS	C	DYNK	
24	AYI	OUTPUT ACCEL PKG BODY Y AXIS		DYNK	
25	AZI	OUTPUT ACCEL PKG BODY Z AXIS	C	DYNK	
28	GAM	FLIGHT PATH ANGLE WRT EARTH AXIS	C	DYNK	RAD
29	AL (ALD)	ANGLE OF ATTACK WRT INS AIR MASS	C	TRIM	RAD
30	BET	SIDE-SLIP ANGLE WRT INS AIR MASS	C	DYNK	RAD
31	TH	EULER PITCH ANGLE		DYNK	RAD
32	PHI	EULER ROLL ANGLE		DYNK	RAD
33	PSI	EULER YAW ANGLE		DYNK	RAD
36	GAMDOT	NOT USED IN F8	0	DYNK	
37	ALDOT	SCALAR TIME DERIVATIVE OF AL	C	DYNK	RAD/SEC
38	BETDOT	SCALAR TIME DERIVATIVE OF BET	C	DYNK	RAD/SEC
39	THDOT	TIME DERIV OF TH	C	DYNK	RAD/SEC
40	PHIDOT	TIME DERIV OF PHI	C	DYNK	RAD/SEC
41	PSIDOT	TIME DERIV OF PSI	C	DYNK	RAD SEC
42	P	BODY ANGULAR RATE-BODY AXIS X		DYNK	RAD/SEC
43	Q	BODY ANGULAR RATE-BODY AXIS Y		DYNK	RAD/SEC
44	R	BODY ANGULAR RATE-BODY AXIS Z		DYNK	RAD/SEC
45	PDOT	BODY ANGULAR ACC -BODY AXIS X	C	DYNK	RAD/S/S
46	QDOT	BODY ANGULAR ACC -BODY AXIS Y	C	DYNK	RAD/S/S
47	RDOT	BODY ANGULAR ACC -BODY AXIS Z	C	DYNK	RAD/S/S
48	STH	SINE THETA	C	DYNK	--
49	CTH	COSINE THETA	C	DYNK	--
50	SPHI	SINE PHI	C	DYNK	--
51	CPHI	COS PHI	C	DYNK	--
52	SPSI	SINE PSI	C	DYNK	--
53	CPSI	COSINE PSI	C	DYNK	--
54	E11	ELEM DIR. COS MAT.-EARTH TO BODY	C.	DYNK	--
55	E21	ELEM DIR. COS MAT.-EARTH TO BODY	C	DYNK	--
56	E31	ELEM DIR. COS MAT.-EARTH TO BODY	C	DYNK	--

COMPLETE SIMULATION DICTIONARY NUMERICALLY
(continued)

A ()	MNEMONIC	DESCRIPTION	INITIAL VALUE	SET BY	UNITS
57	E12	ELEM DIR. COS MAT.-EARTH TO BODY	C	DYNK	--
58	E22	ELEM DIR. COS MAT.-EARTH TO BODY	C	DYNK	--
59	E32	ELEM DIR. COS MAT.-EARTH TO BODY	C	DYNK	--
60	E13	ELEM DIR. COS MAT.-EARTH TO BODY	C	DYNK	--
61	E23	ELEM DIR. COS MAT. EARTH TO BODY	C	DYNK	--
62	E33	ELEM DIR. COS MAT.-EARTH TO BODY	C	DYNK	--
66	CHI	HEADING ANGLE	C	DYNK	RAD
67	RX	ACCELEROMETER LOCATION-X COORD	0.	DYNK	FT
68	RY	ACCELEROMETER LOCATION Y COORD	0.	DYNK	FT
69	RZ	ACCELEROMETER LOCATION Z COORD	0.	DYNK	FT
70	QBAR	DYNAMIC PRESSURE	C	AERO	LB/SQ FT
71	FX	AERO FORCE ALONG X BODY AXIS	C	AERO	LB
72	FY	AERO FORCE ALONG Y BODY AXIS	C	AERO	LB
73	FZ	AERO FORCE ALONG Z BODY AXIS	C	AERO	LB
77	L	AERO MOMENT ABOUT X BODY AXIS	C	AERO	FT-LB
78	M	AERO MOMENT ABOUT Y BODY AXIS	C	AERO	FT-LB
79	N	AERO MOMENT ABOUT Z BODY AXIS	C	AERO	FT-LB
80	PA	P + ANG. WIND COMP. (ROLL)	C	DYNK	RAD/SEC
81	QA	Q + ANG. WIND COMP. (PITCH)	C	DYNK	RAD/SEC
82	RA	R + ANG. WIND COMP. (YAW)	C	DYNK	RAD/SEC
83	IX	MOM OF INERT ABOUT BODY AX AT CG	C	DYNK	SL-FT*FT
84	IY	MOM OF INERT ABOUT BODY AX AT CG	C	DYNK	SL-FT*FT
85	IZ	MOM OF INERT ABOUT BODY AX AT CG	C	DYNK	SL-FT*FT
86	IXY	CROSS PROD OF INERT-AXES X-Y	0.	DYNK	SL-FT*FT
87	IYZ	CROSS PROD OF INERT-AXES Y-Z	0.	DYNK	SL-FT*FT
88	IXZ	CROSS PROD OF INERT-AXES X-Z	C	DYNK	SL-FT*FT
89	DELT	SIM TIME INCREMENT=A(132)/A(131)	C	EXEK	SEC
90	G	ACCELERATION DUE TO GRAVITY	32.18	DYNK	FT/S/S
91	MASS	VEHICLE MASS -- MASS WO FUEL=	583.88	DYNK	SLUG
92	TRIMCNT	MAX NO. TRIM LOOP ITERATIONS	10.	TRIM	--
94	FLG	FLAG = 1 IF BODY MOMENTS CHANGE	0.	DYNK	--
95	XCG	CG LOCATION	C	DYNK	--
96	IMOM	ENGINE MOMENTUM (DT)	C	AERO	SL-FT*FT
101	UG	WIND GUST VEL ALONG X-AXIS	0.	DYNK	FT/SEC
102	UG	WIND GUST VEL ALONG Y-AXIS	0.	DYNK	FT/SEC
103	WG	WIND GUST VEL ALONG Z-AXIS	0.	DYNK	FT/SEC
104	PG	WIND GUST ANG VEL ABOUT X-AXIS	0.	DYNK	RAD/SEC
105	QG	WIND GUST ANG VEL ABOUT Y-AXIS	0.	DYNK	RAD/SEC
106	RG	WIND GUST ANG VEL ABOUT Z-AXIS	0.	DYNK	RAD/SEC
108	HDOT1	PAST VALUE OF HDOT	C	DYNK	FT/SEC
111	XT	NOT USED IN F8 DYNK SETS XT=0.	C	DYNK	LB
112	ZT	NOT USED IN F8-DYNK SETS ZT=0.	C	DYNK	LB
113	YT	NOT USED IN F8-DYNK SETS YT=0.	C	DYNK	LB
117	S	WING SURFACE AREA	376.	AERO	FT*FT
118	CDDG	DEL CD/DEL LANDING GEAR-CONSTANT	.025	AERO	1/100PCT
119	CLDF	DEL CL/DEL FLAPS -CONSTANT	.480	AERO	1/RAD
120	CLDG	DEL CL/DEL LANDING GEAR-CONSTANT	.026	AERO	1/100PCT
121	CMDF	DEL CM/DEL FLAPS -CONSTANT	-.1457	AERO	1/RAD
122	CMDG	DEL CM/DEL LANDING GEAR-CONSTANT	-.017	AERO	1/100PCT
123	FMAX(1)	MAX X FORCE TO TRIM (+ OR -)	270.	TRIM	LB
124	FMAX(2)	MAX Z FORCE TO TRIM (+ OR -)	270.	TRIM	LB
125	FMAX(3)	MAX Y MOM. TO TRIM (+ OR -)	1000.	TRIM	FT-LB
128	CBAR	MEAN CHORD	11.78	AERO	FT
129	RLE	MOMENT ARM OF DRT -CONSTANT	5.	AERO	FT

COMPLETE SIMULATION DICTIONARY NUMERICALLY
(continued)

A ()	MNEMONIC	DESCRIPTION	INITIAL VALUE	SET BY	UNITS
131	ANN	=1.	1.	EXEK	--
132	DELT	DELT/ANN = BASIC TIME INCREMENT	.1	EXEK	SEC
134	DTOUT	A ARRAY DUMP INTERVAL TO LP	.1	EXEK	SEC
138	RUN	RUN NUMBER - SET AUTOMATICALLY	C	EXEK	--
142	TAPE	OUTPUT DEVICE NO -TAPE OR DISC	7.	LINK	--
143	DTLNK1	TAPE DUMP INTERVAL (A AND L DATA)	0.	EXEK	SEC
144	DTLNK2	LINEAR DATA DUMP INTERVAL TO LP	0.	EXEK	SEC
145	N1	START INDEX FOR A DUMP =1.	C	EXEK	--
146	N2	END INDEX FOR A DUMP =1000.	C	EXEK	--
147	DV(1)	ALPHA INCREMENT IN TRIM LOOP	.001	TRIM	RAD
148	DV(2)	ELEVATOR INCREMENT IN TRIM LOOP	.001	TRIM	RAD
149	DV(3)	THROTTLE INCREMENT IN TRIM LOOP	.0	TRIM	PCT*100
151	AF	ACCELERATION DUE TO GRAVITY	32.2	EVAL	FT/S/S
161	W1	1ST COMP OF QUATERN. (ANG COORD)	C	DYNK	--
162	W2	2ND COMP OF QUATERN. (ANG COORD)	C	DYNK	--
163	W3	3RD COMP OF QUATERN. (ANG COORD)	C	DYNK	--
164	W4	4TH COMP OF QUATERN. (ANG COORD)	C	DYNK	--
165	W1DOT	TIME DERIV. OF W1	C	DYNK	--
166	W2DOT	TIME DERIV. OF W2	C	DYNK	--
167	W3DOT	TIME DERIV. OF W3	C	DYNK	--
168	W4DOT	TIME DERIV. OF W4	C	DYNK	--
171	ANU	NUMBER OF CONTROL INPUTS	9.	LINK	--
172	ANW	NUMBER OF DISTURBANCE INPUTS	3.	LINK	--
170	ANX	NUMBER OF STATES	12	LINK	--
176	DSB	SPEED BRAKE POSITION		AERO	RAD
177	DE	ELEVATOR SURFACE POSITION	C	TRIM	RAD
178	DLE	CRUISE DROOP POSITION		AERO	RAD
179	DF	MANEUVER FLAP POSITION		AERO	RAD
180	DG	LANDING GEAR POS=1 FOR GEAR OUT		AERO	PCT*100
181	DA	AILERON SURFACE POSITION		AERO	RAD
182	DR	RUDDER SURFACE POSITION		AERO	RAD
183	DT	THROTTLE POSITION	C	TRIM	PCT*100
184	DRT	ROLLING TAIL POSITION		AERO	RAD
189	PCTF	PERCENT FUEL		DYNK	PERCENT
197	B	WING SPAN	35.67	AERO	FT
201	DX(01)	PERTURBATION ON STATE -P	.1	LINK	RAD/SEC
202	DX(02)	PERTURBATION ON STATE -R	.1	LINK	RAD/SEC
203	DX(03)	PERTURBATION ON STATE -V	10.	LINK	FT/SEC
204	DX(04)	PERTURBATION ON STATE -PHI	.02	LINK	RAD
205	DX(05)	PERTURBATION ON STATE -PSI	.02	LINK	RAD
206	DX(06)	PERTURBATION ON STATE -Y	100.	LINK	FT
207	DX(07)	PERTURBATION ON STATE -Q	.1	LINK	RAD/SEC
208	DX(08)	PERTURBATION ON STATE -W	.5	LINK	FT/SEC
209	DX(09)	PERTURBATION ON STATE -U	1.	LINK	FT/SEC
210	DX(10)	PERTURBATION ON STATE -THETA	.02	LINK	RAD
211	DX(11)	PERTURBATION ON STATE -H	100.	LINK	FT
212	DX(12)	PERTURBATION ON STATE -X	100.	LINK	FT
221	DU(01)	PERTURBATION ON CONTROLS -DA	.02	LINK	RAD
222	DU(02)	PERTURBATION ON CONTROLS -DR	.02	LINK	RAD
223	DU(03)	PERTURBATION ON CONTROLS -DRT	.02	LINK	RAD
224	DU(04)	PERTURBATION ON CONTROLS -DE	.0025	LINK	RAD
225	DU(05)	PERTURBATION ON CONTROLS -DF	.02	LINK	RAD
226	DU(06)	PERTURBATION ON CONTROLS -DLE	.02	LINK	RAD
227	DU(07)	PERTURBATION ON CONTROLS -DSB	.06	LINK	RAD

COMPLETE SIMULATION DICTIONARY NUMERICALLY
(continued)

A ()	MNEMONIC	DESCRIPTION	INITIAL VALUE	SET BY	UNITS
228	DU(08)	PERTURBATION ON CONTROLS -DG	.1	LINK	PCT*100
229	DU(09)	PERTURBATION ON CONTROLS -DT	.01	LINK	PCT*100
259	ELIN	NOT USED IN F8	0.	DYNK	
260	GAMN	NOT USED IN F8	0.	EXEK	
265	DELT4	DELT/4.	C	DYNK	SEC
266	DHDLT	DELT/2.	C	DYNK	SEC
274	HMIN	NOT USED IN F8		MAIN	
283	TMAX	MAX TIME FOR TIME VARYING RUNS		MAIN	SEC
330	VMIN(1)	MIN. LIMIT ON ALPHA (-8 DEG)	-.14	TRIM	RAD
331	VMIN(2)	MIN. LIMIT ON ELEVATOR (-25 DEG)	-.43	TRIM	RAD
332	VMIN(3)	MIN. LIMIT ON THROTTLE (CLOSED)	0.	TRIM	PCT*100
333	VMAX(1)	MAX. LIMIT ON ALPHA (30 DEG)	.523	TRIM	RAD
334	VMAX(2)	MAX. LIMIT ON ELEVATOR (5 DEG)	.0873	TRIM	RAD
335	VMAX(3)	MAX. LIMIT ON THROTTLE (WITH AB)	2.	TRIM	PCT*100
485	ANY	NUMBER OF MEASUREMENTS	9.	LINK	--
486	EE	DEF. OF ZERO-IF (ABS(-).LT.EE)--0	1.E-7	LINK	--
498	APERT	PERTURBATION COEFFICIENT	1.	LINK	--
600	RLT	TOTAL THRUST MOM. ABOUT X-AXIS	0.	DYNK	FT-LB
601	RMT	TOTAL THRUST MOM. ABOUT Y-AXIS	0.	DYNK	FT-LB
602	RNT	TOTAL THRUST MOM. ABOUT Z-AXIS	0.	DYNK	FT-LB
700	THD	EULER PITCH ANGLE	C	DYNK	DEG
701	PHID	EULER ROLL ANGLE	C	DYNK	DEG
702	PSID	EULER YAW ANGLE	C	DYNK	DEG
703	GAMD	FLIGHT PATH ANGLE WRT EARTH	C	DYNK	DEG
704	RDOTD	BODY ANGULAR ACC -BODY AXIS Z	C	DYNK	DEG/S/S
705	QDOTD	BODY ANGULAR ACC -BODY AXIS Y	C	DYNK	DEG/S/S
706	ALD	ANGLE OF ATTACK WRT INS AIR MASS	C	DYNK	DEG
707	BETD	SIDE-SLIP ANGLE WRT INS AIR MASS	C	DYNK	DEG
708	GAMDOT	NOT USED IN F8 =GAMDOT*57.3	C	DYNK	
709	ALDOTD	SCALAR TIME DERIVATIVE OF ALD	C	DYNK	DEG/SEC
710	BETDOTD	SCALAR TIME DERIVATIVE OF BETD	C	DYNK	DEG/SEC
711	PD	BODY ANGULAR RATE-BODY AXIS X	C	DYNK	DEG/SEC
712	QD	BODY ANGULAR RATE-BODY AXIS Y	C	DYNK	DEG/SEC
713	RD	BODY ANGULAR RATE BODY AXIS Z	C	DYNK	DEG/SEC
714	CHID	HEADING ANGLE	C	DYNK	DEG
715	PDOTD	BODY ANGULAR ACC -BODY AXIS X	C	DYNK	DEG/S/S
801	T	MILITARY RATED THRUST F(1)	C	AERO	LB
802	TAB	THRUST DUE TO AFTERBURNER F(2)	C	AERO	LB
803	CD	DRAG COEFF. F(3)	C	AERO	--
804	CDSB	DEL CD DUE TO SPEED BRAKE F(4)	C	AERO	--
805	CDDE	DEL CD DUE TO ELEVATOR F(5)	C	AERO	--
806	CDDLE	DEL CD/DEL LGAD EDGE DROOP F(6)	C	AERO	1/RAD
807	CDDF	DEL CD/DEL AIL MANUVR FLAP F(7)	C	AERO	1/RAD
808	CYB	DEL CY/BETA F(8)	C	AERO	1/RAD
809	CYR	DEL CY/R F(9)	C	AERO	1/RAD
810	CYP	DEL CY/P F(10)	C	AERO	1/RAD
811	RHO	AIR DENSITY(SUBROUT ATMOS) F(11)	C	AERO	SL/CU FT
812	SOS	SPEED OF SOUND(SUB. ATMOS) F(12)	C	AERO	FT/SEC
813	CYDA	DEL CY/TOT AILER SURE POS. F(13)	C	AERO	1/RAD
814	CYDR	DEL CY/RUDDER SURFACE POS. F(14)	C	AERO	1/RAD
815	CL	LIFT COEFF. F(15)	C	AERO	--
816	CLSB	DEL CL DUE TO SPEED BRAKE F(16)	C	AERO	--
817	CLDLE	DEL CL/DEL LEAD EDGE DROOP F(17)	C	AERO	1/RAD
818	CLLB	DEL CLL/BETA F(18)	C	AERO	1/RAD

COMPLETE SIMULATION DICTIONARY NUMERICALLY
(continued)

A()	MNEMONIC	DESCRIPTION	INITIAL VALUE	SET BY	UNITS	
819	CLLR	DEL CLL/R	F(19)	C	AERO	1/RAD
820	CLLP	DEL CLL/P	F(20)	C	AERO	1/RAD
821	CLLDA	DEL CLL/TOT AILER SURF. POS	F(21)	C	AERO	1/RAD
822	CLDE	DEL CL/DEL ELEV SURF. POS.	F(22)	C	AERO	1/RAD
823	CM	CM	F(23)	C	AERO	--
824	CMQ	DEL CM/Q	F(24)	C	AERO	1/RAD
825	CMAD	DEL CM/ALDOT	F(25)	C	AERO	1/RAD
826	CMDLE	DEL CM/DEL LEAD EDGE DROOP	F(26)	C	AERO	1/RAD
827	CMSB	DEL CM DUE TO SPEED BRAKE	F(27)	C	AERO	--
828	XCG	CG LOCATION	F(28)	C	DYNK	--
829	IX	MOMENT OF INERTIA ABOUT X	F(29)	C	DYNK	SL-FT*FT
830	IY	MOMENT OF INERTIA ABOUT Y	F(30)	C	DYNK	SL-FT*FT
831	IZ	MOMENT OF INERTIA ABOUT Z	F(31)	C	DYNK	SL-FT*FT
832	IXZ	CROSS PRODUCT OF INERT. XZ	F(32)	C	DYNK	SL-FT*FT
833	CNB	DEL CN/BETA	F(33)	C	AERO	1/RAD
834	CNR	DEL CN/R	F(34)	C	AERO	1/RAD
835	CNP	DEL CN/P	F(35)	C	AERO	1/RAD
836	CNDA	DEL CN/TOT AILER SURF POS.	F(36)	C	AERO	1/RAD
837	CNDR	DEL CN/RUDDER SURF. POS.	F(37)	C	AERO	1/RAD
838	CLLDR	DEL CLL/RUDDER SURF. POS.	F(38)	C	AERO	1/RAD
839	F(39)	NOT USED IN F8	F(39)	0.	FLOOK	
840	F(40)	NOT USED IN F8	F(40)	0.	FLOOK	
841	F(41)	NOT USED IN F8	F(41)	0.	FLOOK	
842	F(42)	NOT USED IN F8	F(42)	0.	FLOOK	
843	F(43)	NOT USED IN F8	F(43)	0.	FLOOK	
844	F(44)	NOT USED IN F8	F(44)	0.	FLOOK	
845	F(45)	NOT USED IN F8	F(45)	0.	FLOOK	
846	F(46)	NOT USED IN F8	F(46)	0.	FLOOK	
847	F(47)	NOT USED IN F8	F(47)	0.	FLOOK	
848	F(48)	NOT USED IN F8	F(48)	0.	FLOOK	
849	F(49)	NOT USED IN F8	F(49)	0.	FLOOK	
850	F(50)	NOT USED IN F8	F(50)	0.	FLOOK	
861	DW(01)	PERTURBATION ON DIST 1 (X-GUST)	1.	LINK	FT/SEC	
862	DW(02)	PERTURBATION ON DIST 2 (Y-GUST)	10.	LINK	FT/SEC	
863	DW(03)	PERTURBATION ON DIST 3 (Z-GUST)	.5	LINK	FT/SEC	
864	DW(04)	NOT USED IN F8	0.	LINK		
865	DW(05)	NOT USED IN F8	0.	LINK		
866	DW(06)	NOT USED IN F8	0.	LINK		
867	DW(07)	NOT USED IN F8	0.	LINK		
868	DW(08)	NOT USED IN F8	0.	LINK		
869	DW(09)	NOT USED IN F8	0.	LINK		
870	DW(10)	NOT USED IN F8	0.	LINK		
871	DW(11)	NOT USED IN F8	0.	LINK		
872	DW(12)	NOT USED IN F8	0.	LINK		
901	AI(01)	A LOC. OF STATE	-P	42	LINK	--
902	AI(02)	A LOC. OF STATE	-R	44.	LINK	--
903	AI(03)	A LOC. OF STATE	-V	8.	LINK	--
904	AI(04)	A LOC. OF STATE	-PHI	32.	LINK	--
905	AI(05)	A LOC. OF STATE	-PSI	33.	LINK	--
906	AI(06)	A LOC. OF STATE	-Y	3.	LINK	--
907	AI(07)	A LOC. OF STATE	-Q	43.	LINK	--
908	AI(08)	A LOC. OF STATE	-W	9.	LINK	--
909	AI(09)	A LOC. OF STATE	-U	7.	LINK	--
910	AI(10)	A LOC. OF STATE	-THETA	31.	LINK	--

COMPLETE SIMULATION DICTIONARY NUMERICALLY
(concluded)

A ()	MNEMONIC	DESCRIPTION	INITIAL VALUE	SET BY	UNITS	
911	AI(11)	A LOC. OF STATE	-H	4.	LINK	--
912	AI(12)	A LOC. OF STATE	-X	2.	LINK	--
913	AI(13)	DA LOC OF STATE DERIV.	-PDOT	1.	LINK	--
914	AI(14)	DA LOC OF STATE DERIV.	-RDOT	2.	LINK	--
915	AI(15)	DA LOC OF STATE DERIV.	-VDOT	3.	LINK	--
916	AI(16)	DA LOC OF STATE DERIV.	-PHIDOT	4.	LINK	--
917	AI(17)	DA LOC OF STATE DERIV.	-PSIDOT	5.	LINK	--
918	AI(18)	DA LOC OF STATE DERIV.	-VDOT	6.	LINK	--
919	AI(19)	DA LOC OF STATE DERIV.	-QDOT	7.	LINK	--
920	AI(20)	DA LOC OF STATE DERIV.	-WDOT	8.	LINK	--
921	AI(21)	DA LOC OF STATE DERIV.	-UDOT	9.	LINK	--
922	AI(22)	DA LOC OF STATE DERIV.	-THDOT	10.	LINK	--
923	AI(23)	DA LOC OF STATE DERIV.	-HDOT	11.	LINK	--
924	AI(24)	DA LOC OF STATE DERIV.	-XDOT	12.	LINK	--
925	AI(25)	A LOC. OF CONTROL SURFACE	-DA	181.	LINK	--
926	AI(26)	A LOC. OF CONTROL SURFACE	-DR	182.	LINK	--
927	AI(27)	A LOC. OF CONTROL SURFACE	-DRT	184.	LINK	--
928	AI(28)	A LOC. OF CONTROL SURFACE	-DE	177.	LINK	--
929	AI(29)	A LOC. OF CONTROL SURFACE	-DF	179.	LINK	--
930	AI(30)	A LOC. OF CONTROL SURFACE	-DLE	178.	LINK	--
931	AI(31)	A LOC. OF CONTROL SURFACE	-DSB	176.	LINK	--
932	AI(32)	A LOC. OF CONTROL SURFACE	-DG	180.	LINK	--
933	AI(33)	A LOC. OF THRUST CONTROL	-DT	183.	LINK	--
934	AI(34)	A LOC. OF DISTURBANCE	-X GUST	101.	LINK	--
935	AI(35)	A LOC. OF DISTURBANCE	-Y GUST	102.	LINK	--
936	AI(36)	A LOC. OF DISTURBANCE	-Z GUST	103.	LINK	--
937	AI(37)	DA LOC OF MEASUREMENT	-BET	13.	LINK	--
938	AI(38)	DA LOC OF MEASUREMENT	-AY1	14.	LINK	--
939	AI(39)	DA LOC OF MEASUREMENT	-AL	15.	LINK	--
940	AI(40)	DA LOC OF MEASUREMENT	-AZ1	16.	LINK	--
941	AI(41)	DA LOC OF MEASUREMENT	-VEL	17.	LINK	--
942	AI(42)	DA LOC OF MEASUREMENT	-CLDE	18.	LINK	--
943	AI(43)	DA LOC OF MEASUREMENT	-CL	19.	LINK	--
944	AI(44)	DA LOC OF MEASUREMENT	-CYDR	20.	LINK	--
945	AI(45)	DA LOC OF MEASUREMENT	-CYB	21	LINK	--
946	AI(46)	NOT USED IN F8			LINK	--
947	AI(47)	NOT USED IN F8			LINK	--
948	AI(48)	NOT USED IN F8			LINK	--
949	AI(49)	NOT USED IN F8			LINK	--
950	AI(50)	NOT USED IN F8			LINK	--
951	AI(51)	NOT USED IN F8			LINK	--
952	AI(52)	NOT USED IN F8			LINK	--
953	AI(53)	NOT USED IN F8			LINK	--
954	AI(54)	NOT USED IN F8			LINK	--
955	AI(55)	NOT USED IN F8			LINK	--
956	AI(56)	NOT USED IN F8			LINK	--
957	AI(57)	NOT USED IN F8			LINK	--
958	AI(58)	NOT USED IN F8			LINK	--
959	AI(59)	NOT USED IN F8			LINK	--
960	AI(60)	NOT USED IN F8			LINK	--
997	TABRD	FUNCTION TABLE READ IN FLAG =0	0.	FLOOK	--	

APPENDIX B

TWENTY FLIGHT CONDITIONS

Consists of:

- Nominal Trim Point
- "A" Array Values at Trim
- System Matrices
- Eigenvalues of Free Aircraft

Note

The coefficients corresponding to elevator surface effectiveness were subsequently scaled by the following factor (K_1).

$M < 1$

$$K_1 = [9.5 \times 10^{-6}h - 0.575]M + [-1.6 \times 10^{-6}h + 1.12]$$

$M > 1$

$$K_1 = 8.8 \times 10^{-6}h + 0.41$$

where h = altitude (ft)

NOMINAL TRAJECTORY PARAMETERS (T= 0.00)

NX = 12
 NU = 9
 NV = 3
 NY = 9
 APERT = .1000E+01

X3 VECTOR

0. 0. 0. 0. 0. 0. 0. .4183E+02 .6941E+03 .6020E-01
 .2000E+05 0.

U3 VECTOR

0. 0. 0. -.4186E-01 0. 0. 0. 0. .3990E+00

W3 VECTOR

0. 0. 0.

YN VECTOR

0. 0. .6020E-01 -.3214E+02 .6953E+03 .4974E+00 .1787E+00 .1951E+00 .1987E-01

DYNAMIC PRESSURE # .30544E+03

MACH # .67

ANGLE-OF-ATTACK # 3.45

FB-SIM

FLIGHT CONDITION 1

LIST OF NON-ZERO ELEMENTS IN A(1), THRU, A(1000)

4	.2000E+05	5	.6700E+00	7	.6941E+03	9	.4183E+02	10	.6941E+03	12	.4183E+02	13	.6953E+03
16	.6953E+03	17	.2641E-03	19	-.3045E-03	20	.1938E+01	22	-.3214E+02	23	.1938E+01	25	-.3214E+02
29	.6020E-01	31	.6020E-01	37	-.4599E-06	46	.4854E-05	51	.1000E+01	54	.9982E+00	56	.6016E-01
58	.1000E+01	60	-.6016E-01	62	-.9982E+00	70	.3054E+03	71	-.1240E+04	73	-.2056E+05	78	.4201E+00
83	.9200E+04	84	.8655E+05	85	.9126E+05	88	.2953E+04	89	.1000E+00	90	.3220E+02	91	.6398E+03
92	.1000E+02	95	.3035E+00	96	.4977E+04	117	.3750E+03	118	.2500E-01	119	.4300E+00	120	.2600E-01
121	-.1457E+00	122	-.1700E-01	123	.2700E+03	124	.2700E+03	125	.1000E+04	128	.1178E+02	129	.5000E+01
131	.1000E+01	132	.1000E+00	134	.1000E+00	138	.6000E+01	142	.7000E+01	145	.1000E+01	146	.1000E+04
147	.1000E-02	148	.1000E-02	149	.1000E-01	151	.3220E+02	152	.1987E-01	154	.1787E+00	156	.3114E-06
161	.9995E+00	163	.3010E-01	170	.1200E+02	171	.9000E+01	172	.3000E+01	177	-.4186E-01	183	.3990E+00
189	.2100E+02	197	.3567E+02	201	.1000E+00	202	.1000E+00	203	.1000E+02	204	.2000E-01	205	.2000E-01
206	.1000E+03	207	.1000E+00	208	.5000E+00	209	.1000E+01	210	.2000E-01	211	.1000E+03	212	.1000E+03
221	.2000E-01	222	.2000E-01	223	.2000E-01	224	.2500E-02	225	.2000E-01	226	.2000E-01	227	.5000E-01
228	.1000E+00	229	.1000E-01	265	.2500E-01	266	.5000E-01	283	.2500E+00	330	-.1400E+00	331	-.4370E+00
333	.5230E+00	334	.8730E-01	335	.2000E+01	485	.9000E+01	486	.1000E-06	498	.1000E+01	700	.3449E+01
705	.2781E-03	706	.3449E+01	709	-.2635E-04	801	.5716E+04	802	.2387E+04	803	.1980E-01	805	.7677E-04
806	-.1117E-01	807	.6467E-02	808	-.1056E+01	809	.4123E+00	810	.2750E-01	811	.1266E-02	812	.1038E+04
813	.1945E-01	814	.1951E+00	815	.1787E+00	817	-.1406E+00	818	-.1200E+00	819	.1367E-01	820	-.3282E+00
821	.5521E-01	822	.4974E+00	823	-.3107E-02	824	-.4262E+01	825	-.4060E+00	826	-.1459E+00	828	.3035E+00
829	.9200E+04	830	.8655E+05	831	.9126E+05	832	.2953E+04	833	.1378E+00	834	-.3135E+00	835	-.1019E-01
836	.1093E-01	837	-.1007E+00	838	.2514E-01	861	.1000E+01	862	.1000E+02	863	.5000E+00	901	.4200E+02
902	.4400E+02	903	.8000E+01	904	.3200E+02	905	.3300E+02	906	.3000E+01	907	.4300E+02	908	.9000E+01
909	.7000E+01	910	.3100E+02	911	.4000E+01	912	.2000E+01	913	.1000E+01	914	.2000E+01	915	.3000E+01
916	.4000E+01	917	.5000E+01	918	.6000E+01	919	.7000E+01	920	.8000E+01	921	.9000E+01	922	.1000E+02
923	.1100E+02	924	.1200E+02	925	.1810E+03	926	.1820E+03	927	.1840E+03	928	.1770E+03	929	.1790E+03
930	.1780E+03	931	.1760E+03	932	.1800E+03	933	.1830E+03	934	.1010E+03	935	.1020E+03	936	.1030E+03
937	.1300E+02	938	.1400E+02	939	.1500E+02	940	.1600E+02	941	.1700E+02	942	.1800E+02	943	.1900E+02
944	.2000E+02	945	.2100E+02	961	.1295E+05	962	.9300E+05	963	.1010E+06	964	.2080E+04	965	.5839E+03
966	.5000E+00												

LINEAR-DYNAMICS

F MATRIX(12X12)

-3.78	.406E-01	-.747E-01	0.	0.	0.	.177E-01	0.	0.	0.	0.	0.
-.134	-.359	.609E-02	0.	0.	0.	.551E-01	0.	0.	0.	0.	0.
42.0	-692.	-.272	32.1	0.	0.	0.	0.	0.	0.	0.	0.
1.00	.603E-01	0.	0.	0.	0.	0.	0.	0.	0.	0.	0.
0.	1.00	0.	0.	0.	0.	0.	0.	0.	0.	0.	0.
0.	0.	1.000	-41.8	695.	0.	0.	0.	0.	0.	0.	0.
0.	-.575E-01	0.	0.	0.	0.	-.616	-.914E-02	.625E-03	0.	.193E-06	0.
0.	0.	0.	0.	0.	0.	.694.	-1.05	-.458E-01	-1.94	.104E-02	0.
0.	0.	0.	0.	0.	0.	-41.8	.832E-01	-.104E-01	-32.1	-.286E-04	0.
0.	0.	0.	0.	0.	0.	1.000	0.	0.	0.	0.	0.
0.	0.	0.	0.	0.	0.	0.	-.998	.602E-01	695.	0.	0.
0.	0.	0.	0.	0.	0.	0.	.602E-01	.998	0.	0.	0.

G1 MATRIX(12X 9)

24.9	9.82	15.6	0.	0.	0.	0.	0.	0.	G2 MATRIX(12X 3)		
1.30	-4.19	.506	0.	0.	0.	0.	0.	0.	ROW 1	0.	0.
3.48	34.9	0.	0.	0.	0.	0.	0.	0.	ROW 2	-.7472E-01	0.
0.	0.	0.	0.	0.	0.	0.	0.	0.	ROW 3	.6087E-02	0.
0.	0.	0.	0.	0.	0.	0.	0.	0.	ROW 4	-.2719E+00	0.
0.	0.	0.	0.	0.	0.	0.	0.	0.	ROW 5	0.	0.
0.	0.	0.	0.	0.	0.	0.	0.	0.	ROW 6	0.	0.
0.	0.	0.	-13.8	-2.27	-2.28	.120E-01	-.265	.414E-04	ROW 7	0.	0.
0.	0.	0.	-109.	-76.9	25.3	-1.47	-4.92	0.	ROW 8	.6249E-03	0.
0.	0.	0.	.542	3.48	.481	-3.94	-4.19	8.93	ROW 9	-.4584E-01	0.
0.	0.	0.	0.	0.	0.	0.	0.	0.	ROW 10	-.1036E-01	0.
0.	0.	0.	0.	0.	0.	0.	0.	0.	ROW 11	0.	0.
0.	0.	0.	0.	0.	0.	0.	0.	0.	ROW 12	0.	0.

HX MATRIX(9X12)

0.	0.	.144E-02	0.	0.	0.	0.	0.	0.	0.	0.	0.
.126	1.89	-.272	0.	0.	0.	0.	0.	0.	0.	0.	0.
0.	0.	0.	0.	0.	0.	0.	.144E-02	-.865E-04	0.	0.	0.
0.	0.	0.	0.	0.	0.	0.	-1.05	-.458E-01	0.	.104E-02	0.
0.	0.	0.	0.	0.	0.	0.	.602E-01	.998	0.	0.	0.
0.	0.	0.	0.	0.	0.	0.	-.464E-06	-.769E-05	0.	0.	0.
0.	0.	0.	0.	0.	0.	0.	.582E-02	-.259E-03	0.	.253E-06	0.
0.	0.	0.	0.	0.	0.	0.	-.930E-05	-.154E-03	0.	.208E-05	0.
0.	0.	0.	0.	0.	0.	0.	.142E-03	.155E-05	0.	0.	0.

HU MATRIX(9X 9)

0.	0.	0.	0.	0.	0.	0.	0.	0.
3.48	34.9	0.	0.	0.	0.	0.	0.	0.
0.	0.	0.	0.	0.	0.	0.	0.	0.
0.	0.	0.	-109.	-76.9	25.3	-1.47	-4.92	0.
0.	0.	0.	0.	0.	0.	0.	0.	0.
0.	0.	0.	0.	0.	0.	0.	0.	0.
0.	0.	0.	.608	.430	-.141	.687E-02	.260E+01	0.
0.	0.	0.	0.	0.	0.	0.	0.	0.
0.	0.	0.	.336E-01	.647E-02	-.112E-01	.225E-01	.250E-01	0.

HW MATRIX(9X 3)

ROW 1	0.	.1438E-02	0.
ROW 2	0.	-.2719E+00	0.
ROW 3	-.8653E-04	0.	.1436E-02
ROW 4	-.4584E-01	0.	-.1049E+01
ROW 5	.9982E+00	0.	.6016E-01
ROW 6	-.7695E-05	0.	-.4638E-06
ROW 7	-.2592E-03	0.	.5819E-02
ROW 8	-.1543E-03	0.	-.9299E-05
ROW 9	.1554E-05	0.	.1417E-03

EIGENVALUES OF FREE A/C

REAL	IMAG	DAMPING	FREQ
-.749741E-14	0.		
-.274691E-12	0.		
-.274691E-12	0.		
-.139911E-02	0.		
-.298476E-01	0.		
-.484620E-02	.761816E-01	.634855E-01	.763356E-01
-.831551E+00	.251314E+01	.314132E+00	.264714E+01
-.345453E+00	.265455E+01	.129048E+00	.267694E+01
-.369385E+01	0.		

EIGENVALUES FOR LATERAL AXES

REAL	IMAG	DAMPING	FREQ
-.129896E-13	0.		
-.129896E-13	0.		
-.298446E-01	0.		
-.344389E+00	.265380E+01	.128693E+00	.267605E+01
-.369393E+01	0.		

EIGENVALUES FOR PITCH AXIS

REAL	IMAG	DAMPING	FREQ
-.156125E-15	0.		
-.130910E-02	0.		
-.482708E-02	.761902E-01	.632288E-01	.763429E-01
-.832598E+00	.251357E+01	.314440E+00	.264787E+01

NOMINAL TRAJECTORY PARAMETERS(T= 0.00)

NX = 12
NU = 9
NW = 3
NY = 9
APERT = .1000E+01

X3 VECTOR

0. 0. 0. 0. 0. 0. 0. .7386E+02 .6914E+03 .1064E+00
.2000E+05 0.

U3 VECTOR

0. 0. 0. -.6459E-01 0. 0. 0. 0. .8680E+00

W3 VECTOR

0. 0. 0.

YN VECTOR

0. 0. .1064E+00 -.6402E+02 .6953E+03 .4974E+00 .3551E+00 .1951E+00 .4306E-01

DYNAMIC PRESSURE = .30544E+03
MACH = .67
ANGLE-OF-ATTACK = 6.10

F8-SIM

FLIGHT CONDITION 2

LIST OF NON-ZERO ELEMENTS IN A(1), THRU, A(1000)													
4	.2000E+05	5	.6700E+00	7	.6914E+03	9	.7386E+02	10	.6914E+03	12	.7386E+02	13	.6953E+03
15	.4547E-12	16	.6953E+03	17	.3421E+01	19	.3201E+02	20	.6842E+01	22	.6402E+02	23	.6842E+01
25	.6402E+02	28	.6540E-15	29	.1064E+00	31	.1064E+00	37	.4629E-01	46	.1777E-03	51	.1000E+01
54	.9943E+00	56	.1062E+00	58	.1000E+01	60	.1062E+00	62	.9943E+00	70	.3054E+03	71	.4377E+04
73	.4096E+05	78	.1538E+02	83	.9200E+04	84	.8655E+05	85	.9126E+05	88	.2953E+04	89	.1000E+00
90	.3220E+02	91	.6398E+03	92	.1000E+02	95	.3035E+00	96	.1083E+05	117	.3750E+03	118	.2500E-01
119	.4300E+00	120	.2600E-01	121	.1457E+00	122	.1700E-01	123	.2700E+03	124	.2700E+03	125	.1000E+04
128	.1178E+02	129	.5000E+01	131	.1000E+01	132	.1000E+00	134	.1000E+00	138	.2000E+01	142	.7000E+01
145	.1000E+01	146	.1000E+04	147	.1000E-02	148	.1000E-02	149	.1000E-01	151	.6440E+02	152	.4306E-01
154	.3551E+00	156	.1140E-04	161	.9986E+00	163	.5319E-01	170	.1200E+02	171	.9000E+01	172	.3000E+01
177	.6459E-01	183	.8680E+00	189	.2100E+02	197	.3567E+02	201	.1000E+00	202	.1000E+00	203	.1000E+02
204	.2000E-01	205	.2000E-01	206	.1000E+03	207	.1000E+00	208	.5000E+00	209	.1000E+01	210	.2000E-01
211	.1000E+03	212	.1000E+03	221	.2000E-01	222	.2000E-01	223	.2000E-01	224	.2500E-02	225	.2000E-01
226	.2000E-01	227	.5000E-01	228	.1000E+00	229	.1000E-01	265	.2500E-01	266	.5000E-01	283	.2500E+00
330	.1400E+00	331	.4370E+00	333	.5230E+00	334	.8730E-01	335	.2000E+01	485	.9000E+01	486	.1000E-06
498	.1000E+01	700	.6098E+01	703	.3747E-13	705	.1018E-01	706	.6098E+01	709	.2652E+01	801	.5716E+04
802	.2387E+04	803	.4238E-01	805	.6768E-03	806	.7875E-01	807	.2701E-01	808	.1088E+01	809	.4217E+00
810	.8277E-01	811	.1264E-02	812	.1038E+04	813	.1591E-01	814	.1951E+00	815	.3551E+00	817	.1578E+00
818	.1346E+00	819	.2078E-01	820	.3256E+00	821	.5521E-01	822	.4974E+00	823	.6166E-02	824	.4262E+01
825	.4060E+00	826	.1580E+00	828	.3035E+00	829	.9200E+04	830	.8655E+05	831	.9126E+05	832	.2953E+04
833	.1329E+00	834	.3138E+00	835	.2404E-01	836	.9513E-02	837	.9997E-01	838	.2511E-01	861	.1000E+01
862	.1000E+02	863	.5000E+00	901	.4200E+02	902	.4400E+02	903	.8000E+01	904	.3200E+02	905	.3300E+02
906	.3000E+01	907	.4300E+02	908	.9000E+01	909	.7000E+01	910	.3100E+02	911	.4000E+01	912	.2000E+01
913	.1000E+01	914	.2000E+01	915	.3000E+01	916	.4000E+01	917	.5000E+01	918	.6000E+01	919	.7000E+01
920	.8000E+01	921	.9000E+01	922	.1000E+02	923	.1100E+02	924	.1200E+02	925	.1810E+03	926	.1820E+03
927	.1840E+03	928	.1770E+03	929	.1790E+03	930	.1780E+03	931	.1760E+03	932	.1800E+03	933	.1830E+03
934	.1010E+03	935	.1020E+03	936	.1030E+03	937	.1300E+02	938	.1400E+02	939	.1500E+02	940	.1600E+02
941	.1700E+02	942	.1800E+02	943	.1900E+02	944	.2000E+02	945	.2100E+02	961	.1295E+05	962	.9300E+05
963	.1010E+06	964	.2080E+04	965	.5839E+03	966	.5000E+00						

LINEAR DYNAMICS

F MATRIX(12X12)

-3.76	.122	-.842E-01	0.	0.	0.	.385E+01	0.	0.	0.	0.	0.
-.149	-.356	.545E-02	0.	0.	0.	.120	0.	0.	0.	0.	0.
74.2	-689.	-.280	32.0	0.	0.	0.	0.	0.	0.	0.	0.
1.00	.107	0.	0.	0.	0.	0.	0.	0.	0.	0.	0.
0.	1.01	0.	0.	0.	0.	0.	0.	0.	0.	0.	0.
0.	0.	1.000	-73.9	695.	0.	0.	0.	0.	0.	0.	0.
0.	-.125	0.	0.	0.	0.	-.616	-.981E-02	.140E-02	0.	.946E-06	0.
0.	0.	0.	0.	0.	0.	691.	-1.09	-.948E-01	-3.42	.210E-02	0.
0.	0.	0.	0.	0.	0.	-73.9	.416E+01	-.101E-01	-32.0	-.156E-03	0.
0.	0.	0.	0.	0.	0.	1.000	0.	0.	0.	0.	0.
0.	0.	0.	0.	0.	0.	0.	-.994	.106	695.	0.	0.
0.	0.	0.	0.	0.	0.	0.	.106	.994	0.	0.	0.

G1 MATRIX(12X 9)

24.9	9.82	15.6	0.	0.	0.	0.	0.	0.
1.23	-4.16	-.506	0.	0.	0.	0.	0.	0.
2.85	34.9	0.	0.	0.	0.	0.	0.	0.
0.	0.	0.	0.	0.	0.	0.	0.	0.
0.	0.	0.	0.	0.	0.	0.	0.	0.
0.	0.	0.	0.	0.	0.	0.	0.	0.
0.	0.	0.	-14.7	-2.27	-2.47	-.198E-01	-.265	.732E-04
0.	0.	0.	-110.	-76.0	29.6	-1.17	-5.10	0.
0.	0.	0.	-1.19	13.0	11.0	-3.92	-3.96	8.93
0.	0.	0.	0.	0.	0.	0.	0.	0.
0.	0.	0.	0.	0.	0.	0.	0.	0.
0.	0.	0.	0.	0.	0.	0.	0.	0.

G2 MATRIX(12X 3)

ROW 1	0.	0.
ROW 2	-.8423E-01	0.
ROW 3	.5451E-02	0.
ROW 4	-.2801E+00	0.
ROW 5	0.	0.
ROW 6	0.	0.
ROW 7	0.	0.
ROW 8	.1402E-02	-.9807E-02
ROW 9	-.9476E-01	-.1091E+01
ROW 10	-.1005E+01	.4162E-01
ROW 11	0.	0.
ROW 12	0.	0.

HX MATRIX(9X12)

0.	0.	.144E-02	0.	0.	0.	0.	0.	0.	0.	0.	0.	0.
.380	1.94	-.280	0.	0.	0.	0.	0.	0.	0.	0.	0.	0.
0.	0.	0.	0.	0.	0.	0.	.143E-02	-.153E-03	0.	0.	0.	0.
0.	0.	0.	0.	0.	0.	0.	-1.09	-.948E-01	0.	.210E-02	0.	0.
0.	0.	0.	0.	0.	0.	0.	.106	.994	0.	0.	0.	0.
0.	0.	0.	0.	0.	0.	0.	-.819E-06	-.767E-05	0.	0.	0.	0.
0.	0.	0.	0.	0.	0.	0.	.592E-02	-.489E-03	0.	.394E-06	0.	0.
0.	0.	0.	0.	0.	0.	0.	-.164E-04	-.154E-03	0.	.208E-05	0.	0.
0.	0.	0.	0.	0.	0.	0.	.911E-03	-.633E-04	0.	0.	0.	0.

HU MATRIX(9X 9)

0.	0.	0.	0.	0.	0.	0.	0.	0.
2.85	34.9	0.	0.	0.	0.	0.	0.	0.
0.	0.	0.	0.	0.	0.	0.	0.	0.
0.	0.	0.	-110.	-76.0	29.6	-1.17	-5.10	0.
0.	0.	0.	0.	0.	0.	0.	0.	0.
0.	0.	0.	0.	0.	0.	0.	0.	0.
0.	0.	0.	.609	.430	-.158	.418E-02	.260E-01	0.
0.	0.	0.	0.	0.	0.	0.	0.	0.
0.	0.	0.	.718E-01	-.270E-01	-.787E-01	.225E-01	.250E-01	0.

HW MATRIX(9X 3)

ROW 1	0.	.1438E-02	0.
ROW 2	0.	-.2801E+00	0.
ROW 3	-.1528E-03	0.	.1430E-02
ROW 4	-.9476E-01	0.	-.1091E+01
ROW 5	.9943E+00	0.	.1062E+00
ROW 6	-.7665E-05	0.	-.8189E-06
ROW 7	-.4888E-03	0.	.5915E-02
ROW 8	-.1537E-03	0.	-.1642E-04
ROW 9	-.6334E-04	0.	.9111E-03

EIGENVALUES OF FREE A/C

REAL	IMAG	DAMPING	FREQ
-.89A637E-14	0.		
-.443515E-13	0.		
-.443515E-13	0.		
-.376569E-02	0.		
-.299112E-01	0.		
-.122049E-01	.109668E+00	.110607E+00	.110345E+00
-.843605E+00	.260338E+01	.308262E+00	.273665E+01
-.586097E+00	.289057E+01	.198718E+00	.294939E+01
-.319361E+01	0.		

EIGENVALUES FOR LATERAL AXES

REAL	IMAG	DAMPING	FREQ
.162093E-13	0.		
.162093E-13	0.		
-.299026E-01	0.		
-.586621E+00	.288337E+01	.198713E+00	.294204E+01
-.319430E+01	0.		

EIGENVALUES FOR PITCH AXIS

REAL	IMAG	DAMPING	FREQ
-.587308E-13	0.		
-.376568E-02	0.		
-.121167E-01	.109728E+00	.109758E+00	.110395E+00
-.844828E+00	.260896E+01	.308069E+00	.274234E+01

NOMINAL TRAJECTORY PARAMETERS (T= 0.00)

NX = 12

NU = 9

NW = 3

NY = 9

APERT = .1000E+01

X3 VECTOR

0.	0.	0.	0.	0.	0.	0.	0.	.1460E+03	.6798E+03	.2115E+00
.2000E+05	0.									

U3 VECTOR

0.	0.	0.	-.1424E+00	0.	0.	0.	0.	0.	.2000E+01	
----	----	----	------------	----	----	----	----	----	-----------	--

W3 VECTOR

0.	0.	0.								
----	----	----	--	--	--	--	--	--	--	--

YN VECTOR

0.	0.	.2115E+00	-.1259E+03	.6953E+03	.4974E+00	.6873E+00	.1951E+00	.1498E+00		
----	----	-----------	------------	-----------	-----------	-----------	-----------	-----------	--	--

DYNAMIC PRESSURE = .30544E+03

MACH = .67

ANGLE-OF-ATTACK = 12.12

F8-SIM

FLIGHT CONDITION 3

LIST OF NON-ZERO ELEMENTS IN A(1), THRU, A(1000)

4	.2000E+05	5	.6700E+00	7	.6798E+03	9	.1460E+03	10	.6798E+03	12	.1460E+03	13	.6953E+03
15	-.2728E-11	16	.6953E+03	17	.5517E+01	19	-.9445E+02	20	.1228E+02	22	-.1259E+03	23	.1228E+02
25	-.1259E+03	28	-.3924E-14	29	.2115E+00	31	.2115E+00	37	-.1345E+00	46	-.2390E-03	51	.1000E+01
54	.9777E+00	56	.2099E+00	58	.1000E+01	60	-.2099E+00	62	.9777E+00	70	.3054E+03	71	.7855E+04
73	-.8057E+05	78	-.2069E+02	83	.9200E+04	84	.8655E+05	85	.9126E+05	88	.2953E+04	89	.1000E+00
90	.3220E+02	91	.6398E+03	92	.1000E+02	95	.3035E+00	96	.1248E+05	117	.3750E+03	118	.2500E-01
119	.4300E+00	120	.2600E-01	121	-.1457E+00	122	-.1700E-01	123	.2700E+03	124	.2700E+03	125	.1000E+04
128	.1178E+02	129	.5000E+01	131	.1000E+01	132	.1000E+00	134	.1000E+00	138	.3000E+01	142	.7000E+01
145	.1000E+01	146	.1000E+04	147	.1000E-02	148	.1000E-02	149	.1000E-01	151	.1288E+03	152	.1498E+00
154	.6873E+00	156	-.1533E-04	161	.9944E+00	163	.1056E+00	170	.1200E+02	171	.9000E+01	172	.3000E+01
177	-.1424E+00	183	.2000E+01	189	.2100E+02	197	.3567E+02	201	.1000E+00	202	.1000E+00	203	.1000E+02
204	.2000E-01	205	.2000E-01	206	.1000E+03	207	.1000E+00	208	.5000E+00	209	.1000E+01	210	.2000E-01
211	.1000E+03	212	.1000E+03	221	.2000E-01	222	.2000E-01	223	.2000E-01	224	.2500E-02	225	.2000E-01
226	.2000E-01	227	.5000E-01	228	.1000E+00	229	.1000E-01	265	.2500E-01	266	.5000E-01	283	.2500E+00
330	-.1400E+00	331	-.4370E+00	333	.5230E+00	334	.8730E-01	335	.2000E+01	485	.9000E+01	486	.1000E-06
498	.1000E+01	700	.1212E+02	703	-.2248E-12	705	-.1369E-01	706	-.1212E+02	709	.7705E+01	801	.5716E+04
802	.2387E+04	803	.1467E+00	805	.3082E-02	806	-.2265E+00	807	-.1453E+00	808	-.1188E+01	809	.4383E+00
810	.9295E-01	811	.1264E-02	812	.1038E+04	813	.7622E-02	814	.1951E+00	815	.6873E+00	817	.1214E-01
818	-.1196E+00	819	.5534E-01	820	-.2410E+00	821	.4725E-01	822	.4974E+00	823	-.1198E-01	824	-.4262E+01
825	-.4060E+00	826	.1563E+00	828	-.3035E+00	829	.9200E+04	830	.8655E+05	831	.9126E+05	832	.2953E+04
833	.1181E+00	834	-.3428E+00	835	-.1124E-01	836	.5756E-02	837	-.9898E-01	838	.2490E-01	861	.1000E+01
862	.1000E+02	863	.5000E+00	901	.4200E+02	902	.4400E+02	903	.8000E+01	904	.3200E+02	905	.3300E+02
906	.3000E+01	907	.4300E+02	908	.9000E+01	909	.7000E+01	910	.3100E+02	911	.4000E+01	912	.2000E+01
913	.1000E+01	914	.2000E+01	915	.3000E+01	916	.4000E+01	917	.5000E+01	918	.6000E+01	919	.7000E+01
920	.8000E+01	921	.9000E+01	922	.1000E+02	923	.1100E+02	924	.1200E+02	925	.1810E+03	926	.1820E+03
927	.1840E+03	928	.1770E+03	929	.1790E+03	930	.1780E+03	931	.1760E+03	932	.1800E+03	933	.1830E+03
934	.1810E+03	935	.1820E+03	936	.1830E+03	937	.1300E+02	938	.1400E+02	939	.1500E+02	940	.1600E+02
941	.1700E+02	942	.1800E+02	943	.1900E+02	944	.2000E+02	945	.2100E+02	961	.1295E+05	962	.9300E+05
963	.1010E+06	964	.2080E+04	965	.5839E+03	966	.5000E+00						

LINEAR DYNAMICS

F MATRIX(12X12)

-2.78	.509	-.750E-01	0.	0.	0.	.443E-01	0.	0.	0.	0.	0.
-.103	-.377	.425E-02	0.	0.	0.	.138	0.	0.	0.	0.	0.
146.	-678.	-.306	31.5	0.	0.	0.	0.	0.	0.	0.	0.
1.98	.215	0.	0.	0.	0.	0.	0.	0.	0.	0.	0.
0.	1.02	0.	0.	0.	0.	0.	0.	0.	0.	0.	0.
0.	0.	1.000	-146.	695.	0.	0.	0.	0.	0.	0.	0.
0.	-.144	0.	0.	0.	0.	-.616	-.178E-01	.272E-02	0.	-.301E-05	0.
0.	0.	0.	0.	0.	0.	680.	-.923	-.184	-6.76	.424E-02	0.
0.	0.	0.	0.	0.	0.	-146.	-.830E-01	.222E-02	-31.5	-.162E-03	0.
0.	0.	0.	0.	0.	0.	1.000	0.	0.	0.	0.	0.
0.	0.	0.	0.	0.	0.	0.	-.978	.210	695.	0.	0.
0.	0.	0.	0.	0.	0.	0.	.210	.978	0.	0.	0.

G1 MATRIX(12X 9)

21.3	9.73	15.6	0.	0.	0.	0.	0.	0.		G2 MATRIX(12X 3)	
.947	-4.12	.506	0.	0.	0.	0.	0.	0.	ROW 1	0.	0.
1.36	34.9	0.	0.	0.	0.	0.	0.	0.	ROW 2	-.7502E-01	0.
0.	0.	0.	0.	0.	0.	0.	0.	0.	ROW 3	.4245E-02	0.
0.	0.	0.	0.	0.	0.	0.	0.	0.	ROW 4	-.3059E+00	0.
0.	0.	0.	0.	0.	0.	0.	0.	0.	ROW 5	0.	0.
0.	0.	0.	0.	0.	0.	0.	0.	0.	ROW 6	0.	0.
0.	0.	0.	-13.8	-2.27	-2.44	-.925E-01	-.265	.604E-04	ROW 7	0.	0.
0.	0.	0.	-115.	-69.8	6.39	-.381	-5.49	0.	ROW 8	.2721E-02	-.1779E-01
0.	0.	0.	22.9	41.6	40.1	-4.04	-3.40	3.73	ROW 9	-.1840E+00	-.9228E+00
0.	0.	0.	0.	0.	0.	0.	0.	0.	ROW 10	.2220E-02	-.8297E-01
0.	0.	0.	0.	0.	0.	0.	0.	0.	ROW 11	0.	0.
0.	0.	0.	0.	0.	0.	0.	0.	0.	ROW 12	0.	0.

HX MATRIX(9X12)

0.	0.	.144E-02	0.	0.	0.	0.	0.	0.	0.	0.	0.	0.
.427	2.01	-.306	0.	0.	0.	0.	0.	0.	0.	0.	0.	0.
0.	0.	0.	0.	0.	0.	0.	.141E-02	-.302E-03	0.	0.	0.	0.
0.	0.	0.	0.	0.	0.	0.	-.923	-.184	0.	.424E-02	0.	0.
0.	0.	0.	0.	0.	0.	0.	.210	.978	0.	0.	0.	0.
0.	0.	0.	0.	0.	0.	0.	-.162E-05	-.754E-05	0.	0.	0.	0.
0.	0.	0.	0.	0.	0.	0.	.432E-02	-.868E-03	0.	.161E-06	0.	0.
0.	0.	0.	0.	0.	0.	0.	-.324E-04	-.151E-03	0.	.208E-05	0.	0.
0.	0.	0.	0.	0.	0.	0.	.240E-02	-.480E-03	0.	0.	0.	0.

HU MATRIX(9X 9)

0.	0.	0.	0.	0.	0.	0.	0.	0.
1.36	34.9	0.	0.	0.	0.	0.	0.	0.
0.	0.	0.	0.	0.	0.	0.	0.	0.
0.	0.	0.	-115.	-69.8	6.39	-.381	-5.49	0.
0.	0.	0.	0.	0.	0.	0.	0.	0.
0.	0.	0.	0.	0.	0.	0.	0.	0.
0.	0.	0.	.654	.430	-.121E-01	-.265E-02	.260E-01	0.
0.	0.	0.	0.	0.	0.	0.	0.	0.
0.	0.	0.	.956E-02	-.145	-.227	.225E-01	.250E-01	0.

HW MATRIX(9X 3)

ROW 1	0.	.1438E-02	0.
ROW 2	0.	-.3059E+00	0.
ROW 3	-.3019E-03	0.	.1406E-02
ROW 4	-.1840E+00	0.	-.9228E+00
ROW 5	.9777E+00	0.	.2099E+00
ROW 6	-.7537E-05	0.	-.1618E-05
ROW 7	-.8681E-03	0.	.4319E-02
ROW 8	-.1511E-03	0.	-.3245E-04
ROW 9	-.4800E-03	0.	.2400E-02

EIGENVALUES OF FREE A/C

REAL	IMAG	DAMPING	FREQ
0.	0.		
-.310257E-13	0.		
-.310257E-13	0.		
-.426839E-02	0.		
-.360887E-01	0.		
-.327846E-01	.129564E+00	.245307E+00	.133647E+00
-.148127E+01	0.		
-.736867E+00	.352729E+01	.204490E+00	.360344E+01
-.968948E+00	.345510E+01	.270022E+00	.358840E+01

EIGENVALUES FOR LATERAL AXES

REAL	IMAG	DAMPING	FREQ
-.888178E-15	0.		
-.888178E-15	0.		
-.360693E-01	0.		
-.148187E+01	0.		
-.971907E+00	.346088E+01	.270368E+00	.359476E+01

EIGENVALUES FOR PITCH AXIS

REAL	IMAG	DAMPING	FREQ
.129850E-13	0.		
-.426868E-02	0.		
-.327608E-01	.129664E+00	.244961E+00	.133739E+00
-.733642E+00	.351906E+01	.204089E+00	.359472E+01

NOMINAL TRAJECTORY PARAMETERS (T= 0.00)

NX = 12

NU = 9

NW = 3

NY = 9

APERT = .1000E+01

X3 VECTOR

0. 0. 0. 0. 0. 0. 0. .5234E+02 .6933E+03 .7535E-01
.2000E+05 0.

U3 VECTOR

0. 0. 0. -.5359E-01 0. 0. 0. 0. .4797E+00

W3 VECTOR

0. 0. 0.

YN VECTOR

0. 0. .7535E-01 -.3211E+02 .6953E+03 .4974E+00 .2335E+00 .1951E+00 .2387E-01

DYNAMIC PRESSURE = .30544E+03

MACH = .67

ANGLE-OF-ATTACK = 4.32

F8-SIM

FLIGHT CONDITION A

LIST OF NON-ZERO ELEMENTS IN A(1), THRU, A(1000)

4	.2000E+05	5	.6700E+00	7	.6933E+03	9	.5234E+02	10	.6933E+03	12	.5234E+02	13	.6953E+03
15	-.4547E-12	16	.6953E+03	17	.2983E-03	19	.6236E-03	20	.2424E+01	22	-.3211E+02	23	.2424E+01
25	-.3211E+02	28	-.6540E-15	29	.7535E-01	31	.7535E-01	37	.8620E-06	46	.6951E-04	51	.1000E+01
54	.9972E+00	56	.7528E-01	58	.1000E+01	60	-.7528E-01	62	.9972E+00	70	.3054E+03	71	.2029E+04
73	-.2687E+05	78	.6412E+01	83	.1290E+05	84	.9225E+05	85	.1000E+06	88	.2270E+04	89	.1000E+00
90	.3220E+02	91	.8369E+03	92	.1000E+02	95	.2870E+00	96	.5985E+04	117	.3750E+03	118	.2500E-01
119	.4300E+00	120	.2600E-01	121	-.1457E+00	122	-.1700E-01	123	.2700E+03	124	.2700E+03	125	.1000E+04
128	.1178E+02	129	.5000E+01	131	.1000E+01	132	.1000E+00	134	.1000E+00	138	.4000E+01	142	.7000E+01
145	.1000E+01	146	.1000E+04	147	.1000E-02	148	.1000E-02	149	.1000E-01	151	.3220E+02	152	.2387E-01
154	.2335E+00	156	.4752E-05	161	.9993E+00	163	.3767E-01	170	.1200E+02	171	.9000E+01	172	.3000E+01
177	-.5359E-01	183	.4797E+00	189	.9500E+02	197	.3567E+02	201	.1000E+00	202	.1000E+00	203	.1000E+02
204	.2000E-01	205	.2000E-01	206	.1000E+03	207	.1000E+00	208	.5000E+00	209	.1000E+01	210	.2000E-01
211	.1090E+03	212	.1090E+03	221	.2000E-01	222	.2000E-01	223	.2000E-01	224	.2500E-02	225	.2000E-01
226	.2000E-01	227	.5000E-01	228	.1000E+00	229	.1000E-01	265	.2500E-01	266	.5000E-01	283	.2500E+00
330	-.1400E+00	331	-.4370E+00	333	.5230E+00	334	.8730E-01	335	.2000E+01	485	.9000E+01	486	.1000E-06
498	.1000E+01	700	.4317E+01	703	-.3747E-13	705	.3982E-02	706	.4317E+01	709	.4939E+04	801	.5716E+04
802	.2387E+04	803	.2410E-01	805	-.2308E-03	806	-.2435E-01	807	.3936E-03	808	-.1063E+01	809	.4141E+00
810	.4759E-01	811	.1264E-02	812	.1038E+04	813	.1834E-01	814	.1951E+00	815	.2335E+00	817	-.1459E+00
818	-.1278E+00	819	.1591E-01	820	-.3303E+00	821	.5526E-01	822	.4974E+00	823	-.1545E-03	824	-.4262E+01
825	-.4060E+00	826	-.1510E+00	828	.2870E+00	829	.1290E+05	830	.9225E+05	831	.1000E+06	832	.2270E+04
833	.1356E+00	834	-.3136E+00	835	-.1771E-01	836	.1037E-01	837	-.1004E+00	838	.2514E-01	861	.1000E+01
862	.1000E+02	863	.5000E+00	901	.4200E+02	902	.4400E+02	903	.8000E+01	904	.3200E+02	905	.3300E+02
906	.3000E+01	907	.4300E+02	908	.9000E+01	909	.7000E+01	910	.3100E+02	911	.4000E+01	912	.2000E+01
913	.1000E+01	914	.2000E+01	915	.3000E+01	916	.4000E+01	917	.5000E+01	918	.6000E+01	919	.7000E+01
920	.8000E+01	921	.9000E+01	922	.1000E+02	923	.1100E+02	924	.1200E+02	925	.1810E+03	926	.1820E+03
927	.1840E+03	928	.1770E+03	929	.1790E+03	930	.1780E+03	931	.1760E+03	932	.1800E+03	933	.1830E+03
934	.1010E+03	935	.1020E+03	936	.1030E+03	937	.1300E+02	938	.1400E+02	939	.1500E+02	940	.1600E+02
941	.1700E+02	942	.1800E+02	943	.1900E+02	944	.2000E+02	945	.2100E+02	961	.1295E+05	962	.9300E+05
963	.1010E+06	964	.2080E+04	965	.5839E+03	966	.5000E+00						

LINEAR DYNAMICS

F MATRIX(12X12)

-2.70	.717E-01	-.570E-01	0.	0.	0.	.106E-01	0.	0.	0.	0.	0.
-.798E-01	-.327	.673E-02	0.	0.	0.	.601E-01	0.	0.	0.	0.	0.
52.5	-.692.	-.209	32.1	0.	0.	0.	0.	0.	0.	0.	0.
1.00	.755E-01	0.	0.	0.	0.	0.	0.	0.	0.	0.	0.
0.	1.00	0.	0.	0.	0.	0.	0.	0.	0.	0.	0.
0.	0.	1.000	-52.3	695.	0.	0.	0.	0.	0.	0.	0.
0.	-.649E-01	0.	0.	0.	0.	-.578	-.111E-01	.945E-03	0.	.287E-06	0.
0.	0.	0.	0.	0.	0.	693.	-.827	-.469E-01	-2.42	.104E-02	0.
0.	0.	0.	0.	0.	0.	-52.3	-.190E-01	-.166E-02	-32.1	-.482E-04	0.
0.	0.	0.	0.	0.	0.	1.000	0.	0.	0.	0.	0.
0.	0.	0.	0.	0.	0.	0.	-.997	.753E-01	695.	0.	0.
0.	0.	0.	0.	0.	0.	0.	.753E-01	.997	0.	0.	0.

G1 MATRIX(12X 9)

17.6	7.27	11.1	0.	0.	0.	0.	0.	0.
.824	-3.94	.252	0.	0.	0.	0.	0.	0.
2.51	26.7	0.	0.	0.	0.	0.	0.	0.
0.	0.	0.	0.	0.	0.	0.	0.	0.
0.	0.	0.	0.	0.	0.	0.	0.	0.
0.	0.	0.	0.	0.	0.	0.	0.	0.
0.	0.	0.	-13.2	-2.13	-2.21	.100E-01	-.248	.372E-04
0.	0.	0.	-82.3	-58.7	20.3	-1.18	-3.81	0.
0.	0.	0.	-.349	4.38	1.81	-3.00	-3.14	6.83
0.	0.	0.	0.	0.	0.	0.	0.	0.
0.	0.	0.	0.	0.	0.	0.	0.	0.
0.	0.	0.	0.	0.	0.	0.	0.	0.

G2 MATRIX(12X 3)

ROW 1	0.	-.5705E-01	0.
ROW 2	0.	.6731E-02	0.
ROW 3	0.	-.2092E+00	0.
ROW 4	0.	0.	0.
ROW 5	0.	0.	0.
ROW 6	0.	0.	0.
ROW 7	0.	.9446E-03	0.
ROW 8	0.	-.1107E-01	0.
ROW 9	0.	-.8271E+00	0.
ROW 10	0.	-.1659E-02	0.
ROW 11	0.	0.	0.
ROW 12	0.	0.	0.

HX MATRIX(9X12)

0.	0.	.144E-02	0.	0.	0.	0.	0.	0.	0.	0.	0.
.167	1.45	-.209	0.	0.	0.	0.	0.	0.	0.	0.	0.
0.	0.	0.	0.	0.	0.	0.	.143E-02	-.108E-03	0.	0.	0.
0.	0.	0.	0.	0.	0.	0.	-.827	-.469E-01	0.	.104E-02	0.
0.	0.	0.	0.	0.	0.	0.	.753E-01	.997	0.	0.	0.
0.	0.	0.	0.	0.	0.	0.	-.580E-06	-.769E-05	0.	0.	0.
0.	0.	0.	0.	0.	0.	0.	.593E-02	-.326E-03	0.	.336E-06	0.
0.	0.	0.	0.	0.	0.	0.	-.116E-04	-.154E-03	0.	.208E-05	0.
0.	0.	0.	0.	0.	0.	0.	.923E-03	-.547E-04	0.	0.	0.

HW MATRIX(9X 9)

0.	0.	0.	0.	0.	0.	0.	0.	0.
2.51	26.7	0.	0.	0.	0.	0.	0.	0.
0.	0.	0.	0.	0.	0.	0.	0.	0.
0.	0.	0.	-.823	-.587	20.3	-1.18	-3.81	0.
0.	0.	0.	0.	0.	0.	0.	0.	0.
0.	0.	0.	0.	0.	0.	0.	0.	0.
0.	0.	0.	.600	.430	-.147	.693E-02	.260E-01	0.
0.	0.	0.	0.	0.	0.	0.	0.	0.
0.	0.	0.	.478E-01	.394E-03	-.244E-01	.225E-01	.250E-01	0.

HW MATRIX(9X 3)

ROW 1	0.	.1438E-02	0.
ROW 2	0.	-.2092E+00	0.
ROW 3	-.1083E-03	0.	.1434E-02
ROW 4	-.4691E-01	0.	-.8271E+00
ROW 5	.9972E+00	0.	.7528E-01
ROW 6	-.7687E-05	0.	-.5803E-06
ROW 7	-.3263E-03	0.	.5931E-02
ROW 8	-.1541E-03	0.	-.1164E-04
ROW 9	-.5474E-04	0.	.9233E-03

EIGENVALUES OF FREE A/C

REAL	IMAG	DAMPING	FREQ
-.504669E-15	0.		
-.291703E-12	0.		
-.291703E-12	0.		
-.150699E-02	0.		
-.287051E-01	0.		
-.471234E-02	.775761E-01	.606330E-01	.777191E-01
-.695112E+00	.277430E+01	.249371E+00	.286030E+01
-.349896E+00	.268603E+01	.129174E+00	.270873E+01
-.250937E+01	0.		

EIGENVALUES FOR LATERAL AXES

REAL	IMAG	DAMPING	FREQ
.165978E-13	0.		
.165978E-13	0.		
-.287005E-01	0.		
-.250946E+01	0.		
-.347866E+00	.268599E+01	.128439E+00	.270842E+01

EIGENVALUES FOR PITCH AXIS

REAL	IMAG	DAMPING	FREQ
.731325E-13	0.		
-.150699E-02	0.		
-.469672E-02	.775870E-01	.604242E-01	.777291E-01
-.698112E+00	.277393E+01	.244058E+00	.286043E+01

NOMINAL TRAJECTORY PARAMETERS(T= 0.00)

NX = 12

NU = 9

NW = 3

NY = 9

APERT = .1000E+01

X3 VECTOR

0.	0.	0.	0.	0.	0.	0.	0.	.6391E+02	.4102E+03	.1546E+00
.2000E+05	0.									

U3 VECTOR

0.	0.	0.	-.7695E-01	0.	0.	0.	0.		.4842E+00	
----	----	----	------------	----	----	----	----	--	-----------	--

W3 VECTOR

0.	0.	0.								
----	----	----	--	--	--	--	--	--	--	--

YN VECTOR

0.	0.	.1546E+00	-.3180E+02	.4151E+03	.5200E+00	.4940E+00	.2172E+00	.6610E-01		
----	----	-----------	------------	-----------	-----------	-----------	-----------	-----------	--	--

DYNAMIC PRESSURE = .10887E+03

MACH = .40

ANGLE-OF-ATTACK = 0.86

F8-SIM.

FLIGHT CONDITION 5

LIST OF NON-ZERO ELEMENTS IN A(1), THRU, A(1000)

4	.2000E+05	5	.4000E+00	7	.4102E+03	9	.6391E+02	10	.4102E+03	12	.6391E+02	13	.4151E+03
15	-.1137E-11	16	.4151E+03	17	-.2379E-02	19	.2048E-01	20	.4955E+01	22	-.3180E+02	23	.4955E+01
25	-.3180E+02	28	-.2739E-14	29	.1546E+00	31	.1546E+00	37	.4962E-04	46	-.6202E-04	51	.1000E+01
54	.9881E+00	56	.1540E+00	58	.1000E+01	60	-.1540E+00	62	.9881E+00	70	.1089E+03	71	.3170E+04
73	-.2034E+05	78	-.5368E+01	83	.9200E+04	84	.8655E+05	85	.9126E+05	88	.2953E+04	89	.1000E+00
90	.3220E+02	91	.6398E+03	92	.1000E+02	95	.3035E+00	96	.6041E+04	117	.3750E+03	118	.2500E-01
119	.4300E+00	120	.2600E-01	121	-.1457E+00	122	-.1700E-01	123	.2700E+03	124	.2700E+03	125	.1000E+04
128	.1178E+02	129	.5000E+01	131	.1000E+01	132	.1000E+00	134	.1000E+00	138	.5000E+01	142	.7000E+01
145	.1000E+01	146	.1000E+04	147	.1000E-02	148	.1000E-02	149	.1000E-01	151	.3220E+02	152	.6610E-01
154	.4940E+00	156	-.1116E-04	161	.9970E+00	163	.7721E-01	170	.1200E+02	171	.9000E+01	172	.3000E+01
177	-.7695E-01	183	.4842E+00	199	.2100E+02	197	.3567E+02	201	.1000E+00	202	.1000E+00	203	.1000E+02
204	.2000E-01	205	.2000E-01	206	.1000E+03	207	.1000E+00	208	.5000E+00	209	.1000E+01	210	.2000E-01
211	.1000E+03	212	.1000E+03	221	.2000E-01	222	.2000E-01	223	.2000E-01	224	.2500E-02	225	.2000E-01
226	.2000E-01	227	.5000E-01	228	.1000E+00	229	.1000E-01	265	.2500E-01	266	.5000E-01	283	.2500E+00
330	-.1400E+00	331	-.4370E+00	333	.5230E+00	334	.8730E-01	335	.2000E+01	485	.9000E+01	486	.1000E-06
488	.1000E+01	700	.8856E+01	703	-.1569E-12	705	-.3553E-02	706	.8856E+01	709	.2843E-02	801	.5642E+04
802	.4304E+04	803	.6453E-01	805	.1565E-02	806	-.1392E+00	807	-.8683E-01	808	-.1034E+01	809	.4144E+00
810	.1070E+00	811	.1264E-02	812	.1038E+04	813	.8327E-02	814	.2172E+00	815	.4940E+00	817	-.1619E+00
818	-.1354E+00	819	.4729E-01	820	-.3455E+00	821	.5802E-01	822	.5200E+00	823	-.8719E-02	824	-.4088E+01
825	-.5057E+00	826	-.1138E+00	828	.3035E+00	829	.9200E+04	830	.8655E+05	831	.9126E+05	832	.2953E+04
833	.9883E-01	834	-.3020E+00	835	-.3628E-01	836	.5112E-02	837	-.1046E+00	838	.2633E-01	861	.1000E+01
862	.1000E+02	863	.5000E+00	901	.4200E+02	902	.4400E+02	903	.8000E+01	904	.3200E+02	905	.3300E+02
906	.3000E+01	907	.4300E+02	908	.9000E+01	909	.7000E+01	910	.3100E+02	911	.4000E+01	912	.2000E+01
913	.1000E+01	914	.2000E+01	915	.3000E+01	916	.4000E+01	917	.5000E+01	918	.6000E+01	919	.7000E+01
920	.8000E+01	921	.9000E+01	922	.1000E+02	923	.1100E+02	924	.1200E+02	925	.1810E+03	926	.1820E+03
927	.1840E+03	928	.1770E+03	929	.1790E+03	930	.1780E+03	931	.1760E+03	932	.1800E+03	933	.1830E+03
934	.1010E+03	935	.1020E+03	936	.1030E+03	937	.1300E+02	938	.1400E+02	939	.1500E+02	940	.1600E+02
941	.1700E+02	942	.1800E+02	943	.1900E+02	944	.2000E+02	945	.2100E+02	961	.1295E+05	962	.9300E+05
963	.1010E+06	964	.2080E+04	965	.5839E+03	966	.5000E+00						

LINEAR DYNAMICS

F MATRIX(12X12)

-2.38	.258	-.510E-01	0.	0.	0.	.215E-01	0.	0.	0.	0.	0.
-.102	-.199	.193E-02	0.	0.	0.	.669E-01	0.	0.	0.	0.	0.
64.2	-409.	-.159	31.8	0.	0.	0.	0.	0.	0.	0.	0.
1.00	.156	0.	0.	0.	0.	0.	0.	0.	0.	0.	0.
0.	1.01	0.	0.	0.	0.	0.	0.	0.	0.	0.	0.
0.	0.	1.000	-63.9	415.	0.	0.	0.	0.	0.	0.	0.
0.	-.698E-01	0.	0.	0.	0.	-.362	-.777E-02	.788E-03	0.	-.760E-06	0.
0.	0.	0.	0.	0.	0.	410.	-.637	-.683E-01	-4.96	.106E-02	0.
0.	0.	0.	0.	0.	0.	-63.9	.253E-01	-.671E-03	-31.8	-.133E-03	0.
0.	0.	0.	0.	0.	0.	1.000	0.	0.	0.	0.	0.
0.	0.	0.	0.	0.	0.	0.	-.988	.154	415.	0.	0.
0.	0.	0.	0.	0.	0.	0.	.154	.988	0.	0.	0.

G1 MATRIX(12X 9)

9.31	3.67	5.83	0.	0.	0.	0.	0.	0.
.383	-1.55	.189	0.	0.	0.	0.	0.	0.
.531	13.9	0.	0.	0.	0.	0.	0.	0.
0.	0.	0.	0.	0.	0.	0.	0.	0.
0.	0.	0.	0.	0.	0.	0.	0.	0.
0.	0.	0.	0.	0.	0.	0.	0.	0.
0.	0.	0.	-4.85	-.807	-.633	-.258E-01	-.943E-01	.130E-03
0.	0.	0.	-38.5	-26.3	11.6	-.341	-1.88	0.
0.	0.	0.	-.572	9.70	7.19	-1.40	-1.32	8.82
0.	0.	0.	0.	0.	0.	0.	0.	0.
0.	0.	0.	0.	0.	0.	0.	0.	0.
0.	0.	0.	0.	0.	0.	0.	0.	0.

G2 MATRIX(12X 3)

ROW 1	0.	0.
ROW 2	-.5103E-01	0.
ROW 3	.1933E-02	0.
ROW 4	-.1590E+00	0.
ROW 5	0.	0.
ROW 6	0.	0.
ROW 7	0.	0.
ROW 8	.7884E-03	0.
ROW 9	-.6832E-01	0.
ROW 10	-.6710E-03	0.
ROW 11	0.	0.
ROW 12	0.	0.

HX MATRIX(9X12)

0.	0.	.241E-02	0.	0.	0.	0.	0.	0.	0.	0.	0.
.293	1.14	-.159	0.	0.	0.	0.	0.	0.	0.	0.	0.
0.	0.	0.	0.	0.	0.	0.	.238E-02	-.371E-03	0.	0.	0.
0.	0.	0.	0.	0.	0.	0.	-.637	-.683E-01	0.	.106E-02	0.
0.	0.	0.	0.	0.	0.	0.	.154	.988	0.	0.	0.
0.	0.	0.	0.	0.	0.	0.	-.164E-04	-.105E-03	0.	-.176E-06	0.
0.	0.	0.	0.	0.	0.	0.	.941E-02	-.127E-02	0.	.318E-06	0.
0.	0.	0.	0.	0.	0.	0.	-.809E-05	-.519E-04	0.	.104E-05	0.
0.	0.	0.	0.	0.	0.	0.	.227E-02	-.320E-03	0.	0.	0.

HU MATRIX(9X 9)

0.	0.	0.	0.	0.	0.	0.	0.	0.
.531	13.9	0.	0.	0.	0.	0.	0.	0.
0.	0.	0.	0.	0.	0.	0.	0.	0.
0.	0.	0.	-38.5	-26.3	11.6	-.341	-1.88	0.
0.	0.	0.	0.	0.	0.	0.	0.	0.
0.	0.	0.	.595	.430	-.162	.191E-02	.260E-01	0.
0.	0.	0.	0.	0.	0.	0.	0.	0.
0.	0.	0.	.102	-.868E-01	-.139	.224E-01	.250E-01	0.

HW MATRIX(9X 3)

ROW 1	0.	.2409E-02	0.
ROW 2	0.	-.1590E+00	0.
ROW 3	-.3709E-03	0.	.2380E-02
ROW 4	-.6832E-01	0.	-.6373E+00
ROW 5	.9881E+00	0.	.1540E+00
ROW 6	-.1050E-03	0.	-.1635E-04
ROW 7	-.1271E-02	0.	.9406E-02
ROW 8	-.5191E-04	0.	-.8089E-05
ROW 9	-.3196E-03	0.	.2273E-02

EIGENVALUES OF FREE A/C

REAL	IMAG	DAMPING	FREQ
-.198606E-13	0.		
-.709385E-14	0.		
-.709385E-14	0.		
-.894024E-03	0.		
-.422109E-01	0.		
-.503103E-02	.102739E+00	.489104E-01	.102862E+00
-.485334E+00	.178810E+01	.262449E+00	.185306E+01
-.430061E+00	.177035E+01	.236059E+00	.182184E+01
-.185412E+01	0.		

EIGENVALUES FOR LATERAL AXES

REAL	IMAG	DAMPING	FREQ
.832667E-14	0.		
.832667E-14	0.		
-.421830E-01	0.		
-.185447E+01	0.		
-.421627E+00	.176681E+01	.232120E+00	.181642E+01

EIGENVALUES FOR PITCH AXIS

REAL	IMAG	DAMPING	FREQ
-.148520E-12	0.		
-.894036E-03	0.		
-.494634E-02	.102808E+00	.480566E-01	.102927E+00
-.494689E+00	.179076E+01	.266272E+00	.185784E+01

NOMINAL TRAJECTORY PARAMETERS (T= 0.00)

X = 12

U = 9

M = 3

Y = 9

PERT = .1000E+01

J VECTOR

0. 0. 0. 0. 0. 0. 0. .3559E+02 .9333E+03 .3011E-01
-2000E-05 0.

I3 VECTOR

0. 0. 0. -.3228E-01 0. 0. 0. 0. .7184E+00

I2 VECTOR

2. 0. 0.

I1 VECTOR

0. 0. .3011E-01 -.3218E+02 .9340E+03 .4870E+00 .9890E-01 .1433E+00 .2050E-01

DYNAMIC PRESSURE = .95115E+02

MACH = .90

ANGLE-OF-ATTACK = 2.18

FB-SIM

FLIGHT CONDITION 6

LIST OF NON-ZERO ELEMENTS IN A(1), THRU, A(1000)

4	.2000E+05	5	.9000E+00	7	.9333E+03	9	.3559E+02	10	.9333E+03	12	.3559E+02	13	.9340E+03
15	-.2274E-12	16	.9340E+03	17	.1924E-02	19	-.7238E-03	20	.1229E+01	22	-.3218E+02	23	.1229E+01
25	-.3218E+02	28	-.2434E-15	29	.3811E-01	31	.3811E-01	37	-.8529E-06	46	-.4829E-04	51	.1000E+01
54	.9993E+00	56	.3810E-01	58	.1000E+01	60	-.3810E-01	62	.9993E+00	70	.5511E+03	71	.7862E+03
73	-.2059E+05	78	-.4180E+01	83	.9200E+04	84	.8655E+05	85	.9126E+05	88	.2953E+04	89	.1000E+00
90	.3720E+02	91	.6398E+03	92	.1000E+02	95	.3035E+00	96	.8963E+04	117	.3750E+03	118	.2500E-01
119	.4300E+00	120	.2600E-01	121	-.1457E+00	122	-.1700E-01	123	.2700E+03	124	.2700E+03	125	.1000E+04
128	.1178E+02	129	.5000E+01	131	.1000E+01	132	.1000E+00	134	.1000E+00	138	.6000E+01	142	.7000E-01
145	.1000E+01	146	.1000E+04	147	.1000E-02	148	.1000E-02	149	.1000E-01	151	.3220E+02	152	.2050E-01
154	.9890E-01	156	-.1717E-05	161	.9996E+00	163	.1906E-01	170	.1200E+02	171	.9000E+01	172	.3000E+01
177	-.3228E-01	183	.7184E+00	189	.2100E+02	197	.3567E+02	201	.1000E+00	202	.1000E+00	203	.1000E+02
204	.2000E-01	205	.2000E-01	206	.1000E+03	207	.1000E+00	208	.5000E+00	209	.1000E+01	210	.2000E-01
211	.1000E+03	212	.1000E+03	221	.2000E-01	222	.2000E-01	223	.2000E-01	224	.2500E-02	225	.2000E-01
226	.2000E-01	227	.5000E-01	228	.1000E+00	229	.1000E-01	265	.2500E-01	266	.5000E-01	283	.2500E+00
330	-.1400E+00	331	-.4370E+00	333	.5230E+00	334	.8730E-01	335	.2000E+01	485	.9000E+01	486	.1000E-06
498	.1000E+01	700	.2184E+01	703	-.1395E-13	705	-.2767E-02	706	.2184E+01	709	-.4887E-04	861	.5905E+04
832	.1763E+04	803	.2010E-01	805	.4082E-03	806	-.5667E-02	807	.9194E-02	808	-.1104E+01	809	.4451E+00
810	-.5554E-02	811	.1264E-02	812	.1038E+04	813	.2438E-01	814	.1433E+00	815	.9890E-01	817	-.1154E+00
818	-.1054E+00	819	.5629E-02	820	-.3711E+00	821	.4480E-01	822	.4870E+00	823	-.1703E-02	824	-.4600E+01
825	-.3200E+00	826	-.1668E+00	828	.3035E+00	829	.9200E+04	830	.8655E+05	831	.9126E+05	832	.2953E+04
833	.1764E+00	834	-.3323E+00	835	.2978E-02	836	.1010E-01	837	-.8244E-01	838	.1932E-01	861	.1000E+01
862	.1000E+02	863	.5000E+00	901	.4200E+02	902	.4400E+02	903	.8000E+01	904	.3200E+02	905	.3000E+02
906	.3000E+01	907	.4300E+02	908	.9000E+01	909	.7000E+01	910	.3100E+02	911	.4000E+01	912	.2000E+01
913	.1000E+01	914	.2000E+01	915	.3000E+01	916	.4000E+01	917	.5000E+01	918	.6000E+01	919	.7000E+01
920	.8000E+01	921	.9000E+01	922	.1000E+02	923	.1100E+02	924	.1200E+02	925	.1810E+03	926	.1820E+03
927	.1840E+03	928	.1770E+03	929	.1790E+03	930	.1780E+03	931	.1760E+03	932	.1800E+03	933	.1830E+03
934	.1010E+03	935	.1020E+03	936	.1030E+03	937	.1300E+02	938	.1400E+02	939	.1500E+02	940	.1600E+02
941	.1700E+02	942	.1800E+02	943	.1900E+02	944	.2000E+02	945	.2100E+02	961	.1295E+05	962	.9300E+05
963	.1010E+06	964	.2080E+04	965	.5839E+03	966	.5000E+00						

LINEAR DYNAMICS

F MATRIX(12X12)

-5.74	-.792E-01	-.866E-01	0.	0.	0.	.319E-01	0.	0.	0.	0.	0.
-.181	-.515	.119E-01	0.	0.	0.	.992E-01	0.	0.	0.	0.	0.
35.6	-931.	-.382	32.2	0.	0.	0.	0.	0.	0.	0.	0.
1.00	.381E-01	0.	0.	0.	0.	0.	0.	0.	0.	0.	0.
0.	1.00	0.	0.	0.	0.	0.	0.	0.	0.	0.	0.
0.	0.	1.000	-35.6	934.	0.	0.	0.	0.	0.	0.	0.
0.	-.104	0.	0.	0.	0.	-.873	-.136E-01	-.131E-03	0.	-.234E-05	0.
0.	0.	0.	0.	0.	0.	933.	-1.65	-.395E-01	-1.23	.968E-03	0.
0.	0.	0.	0.	0.	0.	-35.6	.476E-01	-.418E-01	-32.2	-.602E-04	0.
0.	0.	0.	0.	0.	0.	1.000	0.	0.	0.	0.	0.
0.	0.	0.	0.	0.	0.	0.	-.999	.381E-01	934.	0.	0.
0.	0.	0.	0.	0.	0.	0.	.381E-01	.999	0.	0.	0.

G1 MATRIX(12X 9)

36.5	13.5	27.6	0.	0.	0.	0.	0.	0.	0.		
2.00	-6.22	.894	0.	0.	0.	0.	0.	0.	0.		
7.88	46.3	0.	0.	0.	0.	0.	0.	0.	0.		
0.	0.	0.	0.	0.	0.	0.	0.	0.	0.		
0.	0.	0.	0.	0.	0.	0.	0.	0.	0.		
0.	0.	0.	0.	0.	0.	0.	0.	0.	0.		
0.	0.	0.	-27.7	-4.09	-4.69	-.780E-01	-.478	.214E-04			
0.	0.	0.	-215.	-139.	37.3	-1.74	-8.70	0.			
0.	0.	0.	4.73	2.32	.409	-7.25	-7.75	9.23			
0.	0.	0.	0.	0.	0.	0.	0.	0.			
0.	0.	0.	0.	0.	0.	0.	0.	0.			
0.	0.	0.	0.	0.	0.	0.	0.	0.			
0.	0.	0.	0.	0.	0.	0.	0.	0.			
0.	0.	0.	0.	0.	0.	0.	0.	0.			

G2 MATRIX(12X 3)

ROW 1		
0.	-.8658E-01	0.
ROW 2		
0.	.1194E-01	0.
ROW 3		
0.	-.3818E+00	0.
ROW 4		
0.	0.	0.
ROW 5		
0.	0.	0.
ROW 6		
0.	0.	0.
ROW 7		
0.	-.1312E-03	-.1356E-01
ROW 8		
0.	-.3948E-01	-.1652E+01
ROW 9		
0.	-.4183E-01	.4764E-01
ROW 10		
0.	0.	0.
ROW 11		
0.	0.	0.
ROW 12		
0.	0.	0.

MX MATRIX(9X12)

0.	0.	.107E-02	0.	0.	0.	0.	0.	0.	0.	0.	0.
-.343E-01	2.75	-.382	0.	0.	0.	0.	0.	0.	0.	0.	0.
0.	0.	0.	0.	0.	0.	0.	.107E-02	-.408E-04	0.	0.	0.
0.	0.	0.	0.	0.	0.	0.	-1.65	-.395E-01	0.	.968E-03	0.
0.	0.	0.	0.	0.	0.	0.	.381E-01	.999	0.	0.	0.
0.	0.	0.	0.	0.	0.	0.	-.860E-05	-.225E-03	0.	-.839E-06	0.
0.	0.	0.	0.	0.	0.	0.	.509E-02	-.940E-04	0.	.372E-06	0.
0.	0.	0.	0.	0.	0.	0.	-.183E-04	-.479E-03	0.	.165E-05	0.
0.	0.	0.	0.	0.	0.	0.	.152E-03	.888E-04	0.	.352E-06	0.

MU MATRIX(9X 9)

0.	0.	0.	0.	0.	0.	0.	0.	0.
7.88	46.3	0.	0.	0.	0.	0.	0.	0.
0.	0.	0.	0.	0.	0.	0.	0.	0.
0.	0.	0.	-215.	-139.	37.3	-1.74	-8.70	0.
0.	0.	0.	0.	0.	0.	0.	0.	0.
0.	0.	0.	0.	0.	0.	0.	0.	0.
0.	0.	0.	.667	.430	-.115	.452E-02	.260E-01	0.
0.	0.	0.	0.	0.	0.	0.	0.	0.
0.	0.	0.	.108E-01	.919E-02	-.567E-02	.226E-01	.250E-01	0.

MW MATRIX(9X 3)

ROW 1	0.	.1071E-02	0.
ROW 2	0.	-.3818E+00	0.
ROW 3	-.4080E-04	0.	.1070E-02
ROW 4	-.3948E-01	0.	-.1652E+01
ROW 5	.9993E+00	0.	.3810E-01
ROW 6	-.2251E-03	0.	-.8596E-05
ROW 7	-.9399E-04	0.	.5087E-02
ROW 8	-.4793E-03	0.	-.1829E-04
ROW 9	.8878E-04	0.	.1518E-03

EIGENVALUES OF FREE A/C

REAL	IMAG	DAMPING	FREQ
0.	0.		
.776254E-13	0.		
.776254E-13	0.		
-.316303E-01	0.		
-.163228E-01	0.		
-.491535E-02	.382526E-01	.127449E+00	.385671E-01
-.126044E+01	.353500E+01	.335849E+00	.375299E+01
-.429087E+00	.378363E+01	.112684E+00	.380788E+01
-.576406E+01	0.		

EIGENVALUES FOR LATERAL AXES

REAL	IMAG	DAMPING	FREQ
.729417E-13	0.		
.729417E-13	0.		
-.163115E-01	0.		
-.426668E+00	.378212E+01	.112101E+00	.380611E+01
-.576416E+01	0.		

EIGENVALUES FOR PITCH AXIS

REAL	IMAG	DAMPING	FREQ
.103857E-14	0.		
-.316434E-01	0.		
-.489420E-02	.382624E-01	.126878E+00	.385742E-01
-.126283E+01	.353580E+01	.336347E+00	.375455E+01

NOMINAL TRAJECTORY PARAMETERS(T= 0.00)

NX = 12

NU = 9

NW = 3

NY = 9

APERT = .1000E+01

X3 VECTOR

0.	0.	0.	0.	0.	0.	0.	0.	.7954E+02	.6736E+03	.1175E+00
.4000E+05	0.									

U3 VECTOR

0.	0.	0.	-.6885E-01	0.	0.	0.	0.	0.	.8623E+00	
----	----	----	------------	----	----	----	----	----	-----------	--

W3 VECTOR

0.	0.	0.								
----	----	----	--	--	--	--	--	--	--	--

YN VECTOR

0.	0.	.1175E+00	-.3197E+02	.6783E+03	.4972E+00	.4030E+00	.2252E+00	.5103E-01		
----	----	-----------	------------	-----------	-----------	-----------	-----------	-----------	--	--

DYNAMIC PRESSURE = .13429E+03

MACH = .70

ANGLE-OF-ATTACK = 8.73

F8-SIN

FLIGHT CONDITION 7

LIST OF NON-ZERO ELEMENTS IN A(1), THRU, A(1000)

4	.4000E+05	5	.7000E+00	7	.6736E+03	9	.7954E+02	10	.6736E+03	12	.7954E+02	13	.6783E+03
15	-.9095E-12	16	.6783E+03	17	.1646E-02	19	.8514E-02	20	.3778E+01	22	-.3197E+02	23	.3778E+01
25	-.3197E+02	28	-.1341E-14	29	.1175E+00	31	.1175E+00	37	.1218E-04	46	.4263E-03	51	.1000E+01
54	.9931E+00	56	.1173E+00	58	.1000E+01	60	-.1173E+00	62	.9931E+00	70	.1343E+03	71	.2417E+04
73	-.2045E+05	78	.3689E+02	83	.9200E+04	84	.8655E+05	85	.9126E+05	88	.2953E+04	89	.1000E+00
90	.3220E+02	91	.6398E+03	92	.1000E+02	95	.3035E+00	96	.1076E+05	117	.3750E+03	118	.2500E-01
119	.4300E+00	120	.2600E-01	121	-.1457E+00	122	-.1700E-01	123	.2700E+03	124	.2700E+03	125	.1000E+04
128	.1178E+02	129	.5000E+01	131	.1000E+01	132	.1000E+00	134	.1000E+00	138	.7000E+01	142	.7000E+01
145	.1000E+01	146	.1000E+04	147	.1000E-02	148	.1000E-02	149	.1000E-01	151	.3220E+02	152	.5103E-01
154	.4030E+00	156	.6219E-04	161	.9983E+00	163	.5874E-01	170	.1200E+02	171	.9000E+01	172	.3000E+01
177	-.6885E-01	183	.8623E+00	189	.2100E+02	197	.3567E+02	201	.1000E+00	202	.1000E+00	203	.1000E+02
204	.2000E-01	205	.2000E-01	206	.1000E+03	207	.1000E+00	208	.5000E+00	209	.1000E+01	210	.2000E-01
211	.1000E+03	212	.1000E+03	221	.2000E-01	222	.2000E-01	223	.2000E-01	224	.2500E-02	225	.2000E-01
226	.2000E-01	227	.5000E-01	228	.1000E+00	229	.1000E-01	265	.2500E-01	266	.5000E-01	283	.2500E+00
330	-.1400E+00	331	-.4370E+00	333	.5230E+00	334	.8730E-01	335	.2000E+01	485	.9000E+01	486	.1000E-06
498	.1000E+01	700	.6734E+01	703	-.7683E-13	705	.2442E-01	706	.6734E+01	709	.6980E-03	801	.3003E+04
802	.3654E+04	803	.5019E-01	805	.8469E-03	806	-.9595E-01	807	-.3682E-01	808	-.1106E+01	809	.4291E+00
810	.9479E-01	811	.5938E-03	812	.9690E+03	813	.1579E-01	814	.2252E+00	815	.4030E+00	817	-.1473E+00
818	-.1414E+00	819	.3752E-01	820	-.3245E+00	821	.6096E-01	822	.4972E+00	823	-.6851E-02	824	-.4610E+01
825	-.6400E+00	826	-.1661E+00	828	.3035E+00	829	.9200E+04	830	.8655E+05	831	.9126E+05	832	.2953E+04
833	.1402E+00	834	-.3172E+00	835	-.2615E-01	836	.1029E-01	837	-.1138E+00	838	.2869E-01	861	.1000E+01
862	.1000E+02	863	.5000E+00	901	.4200E+02	902	.4400E+02	903	.8000E+01	904	.3200E+02	905	.3300E+02
966	.3000E+01	907	.4300E+02	908	.9000E+01	909	.7000E+01	910	.3100E+02	911	.4000E+01	912	.2900E+01
913	.1000E+01	914	.2000E+01	915	.3000E+01	916	.4000E+01	917	.5000E+01	918	.6000E+01	919	.7000E+01
920	.8000E+01	921	.9000E+01	922	.1000E+02	923	.1100E+02	924	.1200E+02	925	.1810E+03	926	.1820E+03
927	.1840E+03	928	.1770E+03	929	.1790E+03	930	.1780E+03	931	.1760E+03	932	.1800E+03	933	.1830E+03
934	.1010E+03	935	.1020E+03	936	.1030E+03	937	.1300E+02	938	.1400E+02	939	.1500E+02	940	.1600E+02
941	.1700E+02	942	.1800E+02	943	.1900E+02	944	.2000E+02	945	.2100E+02	961	.1295E+05	962	.9300E+05
963	.1010E+06	964	.2080E+04	965	.5839E+03	966	.5000E+00						

LINEAR DYNAMICS

F MATRIX(12X12)

-1.69	.141	-.399E-01	0.	0.	0.	.382E-01	0.	0.	0.	0.	0.
-.682E-01	-.160	.260E-02	0.	0.	0.	.119	0.	0.	0.	0.	0.
72.7	-673.	-.128	32.0	0.	0.	0.	0.	0.	0.	0.	0.
1.00	.118	0.	0.	0.	0.	0.	0.	0.	0.	0.	0.
0.	1.01	0.	0.	0.	0.	0.	0.	0.	0.	0.	0.
0.	0.	1.000	-79.5	678.	0.	0.	0.	0.	0.	0.	0.
0.	-.124	0.	0.	0.	0.	-.312	-.424E-02	.731E-03	0.	0.	0.
0.	0.	0.	0.	0.	0.	674.	-.496	-.494E-01	-3.78	.154E-02	0.
0.	0.	0.	0.	0.	0.	-79.5	.282E-01	-.500E-02	-32.0	-.185E-03	0.
0.	0.	0.	0.	0.	0.	1.000	0.	0.	0.	0.	0.
0.	0.	0.	0.	0.	0.	0.	-.993	.117	678.	0.	0.
0.	0.	0.	0.	0.	0.	0.	.117	.993	0.	0.	0.

G1 MATRIX(12X 9)

12.1	4.93	6.88	0.	0.	0.	0.	0.	0.	0.	G2 MATRIX(12X 3)	
.594	-2.00	.222	0.	0.	0.	0.	0.	0.	0.	ROW 1	0.
1.24	17.7	0.	0.	0.	0.	0.	0.	0.	0.	ROW 2	-.3988E-01
0.	0.	0.	0.	0.	0.	0.	0.	0.	0.	ROW 3	.2604E-02
0.	0.	0.	0.	0.	0.	0.	0.	0.	0.	ROW 4	-.1284E+00
0.	0.	0.	0.	0.	0.	0.	0.	0.	0.	ROW 5	0.
0.	0.	0.	0.	0.	0.	0.	0.	0.	0.	ROW 6	0.
0.	0.	0.	-6.84	-.997	-1.14	-.134E-01	-.116	.309E-04	0.	ROW 7	0.
0.	0.	0.	-48.7	-33.3	12.4	-.440	-2.26	0.	0.	ROW 8	.7314E-03
0.	0.	0.	-.620	6.85	6.14	-1.73	-1.71	4.69	0.	ROW 9	-.4237E-02
0.	0.	0.	0.	0.	0.	0.	0.	0.	0.	ROW 10	-.4937E-01
0.	0.	0.	0.	0.	0.	0.	0.	0.	0.	ROW 11	-.4962E+00
0.	0.	0.	0.	0.	0.	0.	0.	0.	0.	ROW 12	-.4997E-02
0.	0.	0.	0.	0.	0.	0.	0.	0.	0.	ROW 12	.2823E-01
0.	0.	0.	0.	0.	0.	0.	0.	0.	0.	ROW 12	0.
0.	0.	0.	0.	0.	0.	0.	0.	0.	0.	ROW 12	0.
0.	0.	0.	0.	0.	0.	0.	0.	0.	0.	ROW 12	0.

HX MATRIX(9X12)

0.	0.	.147E-02	0.	0.	0.	0.	0.	0.	0.	0.	0.
.196	.888	-.128	0.	0.	0.	0.	0.	0.	0.	0.	0.
0.	0.	0.	0.	0.	0.	0.	.146E-02	-.173E-03	0.	0.	0.
0.	0.	0.	0.	0.	0.	0.	-.496	-.494E-01	0.	.154E-02	0.
0.	0.	0.	0.	0.	0.	0.	.117	.993	0.	0.	0.
0.	0.	0.	0.	0.	0.	0.	-.968E-06	-.820E-05	0.	0.	0.
0.	0.	0.	0.	0.	0.	0.	.609E-02	-.557E-03	0.	0.	0.
0.	0.	0.	0.	0.	0.	0.	-.833E-05	-.705E-04	0.	.660E-06	0.
0.	0.	0.	0.	0.	0.	0.	.957E-03	-.693E-04	0.	0.	0.

HU MATRIX(9X 9)

0.	0.	0.	0.	0.	0.	0.	0.	0.
1.24	17.7	0.	0.	0.	0.	0.	0.	0.
0.	0.	0.	0.	0.	0.	0.	0.	0.
0.	0.	0.	-48.7	-33.3	12.4	-.440	-2.26	0.
0.	0.	0.	0.	0.	0.	0.	0.	0.
0.	0.	0.	0.	0.	0.	0.	0.	0.
0.	0.	0.	.613	.430	-.147	.297E-02	.260E-01	0.
0.	0.	0.	0.	0.	0.	0.	0.	0.
0.	0.	0.	.804E-01	-.368E-01	-.959E-01	.225E-01	.250E-01	0.

HW MATRIX(9X 3)

ROW 1	0.	0.
ROW 2	.1474E-02	0.
ROW 3	-.1284E+00	0.
ROW 4	-.1729E-03	0.
ROW 5	-.4937E-01	0.
ROW 6	.9931E+00	0.
ROW 7	-.8199E-05	0.
ROW 8	-.5573E-03	0.
ROW 9	-.7051E-04	0.
	-.6929E-04	0.
		.1464E-02
		-.4962E+00
		.1173E+00
		-.9682E-06
		.6089E-02
		-.8327E-05
		.9571E-03

EIGENVALUES OF FREE A/C

REAL	IMAG	DAMPING	FREQ
-.258579E-14	0.		
-.148563E-13	0.		
-.148563E-13	0.		
-.370646E-02	0.		
-.256853E-01	0.		
-.636333E-02	.857555E-01	.739998E-01	.859912E-01
-.400194E+00	.169971E+01	.229181E+00	.174619E+01
-.138975E+01	0.		
-.278658E+00	.213565E+01	.129383E+00	.215375E+01

EIGENVALUES FOR LATERAL AXES

REAL	IMAG	DAMPING	FREQ
.130451E-13	0.		
.130451E-13	0.		
-.256574E-01	0.		
-.139094E+01	0.		
-.279625E+00	.213109E+01	.130097E+00	.214936E+01

EIGENVALUES FOR PITCH AXIS

REAL	IMAG	DAMPING	FREQ
-.725947E-13	0.		
-.370666E-02	0.		
-.616663E-02	.858881E-01	.716140E-01	.861092E-01
-.398843E+00	.170139E+01	.228234E+00	.174752E+01

NOMINAL TRAJECTORY PARAMETERS (T= 0.00)

NX = 12
NU = 9
NW = 3
NY = 9
APERI = .1000E+01

X3 VECTOR

0. 0. 0. 0. 0. 0. 0. .5511E+02 .1161E+04 .4741E-01
.4000E+05 0.

U3 VECTOR

0. 0. 0. -.5886E-01 0. 0. 0. 0. .2000E+01

W3 VECTOR

0. 0. 0.

YN VECTOR

0. 0. .4741E-01 -.3216E+02 .1163E+04 .4530E+00 .1371E+00 .8020E-01 .4339E-01

DYNAMIC PRESSURE = .39465E+03
MACH = 1.20
ANGLE-OF-ATTACK = 2.72

F8-SIM

FLIGHT CONDITION 8

LIST OF NON-ZERO ELEMENTS IN A(1), THRU, A(1000)

4	.4000E+05	5	.1200E+01	7	.1161E+04	9	.5511E+02	10	.1161E+04	12	.5511E+02	13	.1163E+04
15	-.4547E-12	16	.1163E+04	17	-.1492E+01	19	-.1455E-10	20	.3409E-01	22	-.3216E+02	23	.3409E-01
25	-.3216E+02	28	-.3911E-15	29	.4741E-01	31	.4741E-01	37	.6082E-04	46	.8067E-05	51	.1000E+01
54	.9989E+00	56	.4739E-01	58	.1000E+01	60	-.4739E-01	62	.9989E+00	70	.3946E+03	71	.2181E+02
73	-.2058E+05	78	.6982E+00	83	.9200E+04	84	.8655E+05	85	.9126E+05	88	.2953E+04	89	.1000E+00
90	.3220E+02	91	.6398E+03	92	.1000E+02	95	.3035E+00	96	.1248E+05	117	.3750E+03	118	.2500E-01
119	.4300E+00	120	.2600E-01	121	-.1457E+00	122	-.1700E-01	123	.2700E+03	124	.2700E+03	125	.1000E+04
128	.1178E+02	129	.5000E+01	131	.1000E+01	132	.1000E+00	134	.1000E+00	139	.8000E+01	142	.7000E+01
145	.1000E+01	146	.1000E+04	147	.1000E-02	148	.1000E-02	149	.1000E-01	151	.3220E+02	152	.4339E-01
154	.1371E+00	156	.4005E-06	161	.9997E+00	163	.2370E-01	170	.1200E+02	171	.9000E+01	172	.3000E+01
177	-.5886E-01	183	.2000E+01	189	.2100E+02	197	.3567E+02	201	.1000E+00	202	.1000E+00	203	.1000E+02
204	.2000E-01	205	.2000E-01	206	.1000E+03	207	.1000E+00	208	.5000E+00	209	.1000E+01	210	.2000E-01
211	.1000E+03	212	.1000E+03	221	.2000E-01	222	.2000E-01	223	.2000E-01	224	.2500E-02	225	.2000E-01
226	.2000E-01	227	.5000E-01	228	.1000E+00	229	.1000E-01	265	.2500E-01	266	.5000E-01	283	.2500E+00
330	-.1400E+00	331	-.4370E+00	333	.5230E+00	334	.8730E-01	335	.2000E+01	485	.9000E+01	486	.1000E-06
498	.1000E+01	700	.2717E+01	703	-.2241E-13	705	.4622E-03	706	.2717E+01	709	.3484E-02	801	.3523E+04
802	.1952E+04	803	.4353E-01	805	-.1376E-03	806	-.9050E-02	807	.8046E-02	808	-.1101E+01	809	.5444E+00
810	.2801E-02	811	.5838E-03	812	.9690E+03	813	.1249E-01	814	.8020E-01	815	.1371E+00	817	-.1296E+00
818	-.1193E+00	819	.1473E-01	820	-.3012E+00	821	.2433E-01	822	.4530E+00	823	-.2081E-02	824	-.4350E-01
825	.1300E+01	826	-.1717E+00	828	.3035E+00	829	.9200E+04	830	.8655E+05	831	.9126E+05	832	.2953E+04
833	.1886E+00	834	-.4212E+00	835	.2694E-02	836	.3804E-02	837	-.4416E-01	838	.1243E-01	861	.1000E+01
862	.1000E+02	863	.5000E+00	901	.4200E+02	902	.4400E+02	903	.8000E+01	904	.3200E+02	905	.3300E+02
906	.3000E+01	907	.4300E+02	908	.9000E+01	909	.7000E+01	910	.3100E+02	911	.4000E+01	912	.2000E+01
913	.1000E+01	914	.2000E+01	915	.3000E+01	916	.4000E+01	917	.5000E+01	918	.6000E+01	919	.7000E+01
920	.8000E+01	921	.9000E+01	922	.1000E+02	923	.1100E+02	924	.1200E+02	925	.1810E+03	926	.1820E+03
927	.1840E+03	928	.1770E+03	929	.1790E+03	930	.1780E+03	931	.1760E+03	932	.1800E+03	933	.1830E+03
934	.1010E+03	935	.1020E+03	936	.1030E+03	937	.1300E+02	938	.1400E+02	939	.1500E+02	940	.1600E+02
941	.1700E+02	942	.1800E+02	943	.1900E+02	944	.2000E+02	945	.2100E+02	961	.1295E+05	962	.9300E+05
963	.1010E+06	964	.2080E+04	965	.5839E+03	966	.5000E+00						

LINEAR DYNAMICS

F MATRIX(12X12)

-2.68	.982E-02	-.565E-01	0.	0.	0.	.443E-01	0.	0.	0.	0.	0.
-.843E-01	-.373	.726E-02	0.	0.	0.	.138	0.	0.	0.	0.	0.
55.1	-.116E+04	-.219	32.2	0.	0.	0.	0.	0.	0.	0.	0.
1.00	.474E-01	0.	0.	0.	0.	0.	0.	0.	0.	0.	0.
0.	1.00	0.	0.	0.	0.	0.	0.	0.	0.	0.	0.
0.	0.	1.000	-55.1	.116E+04	0.	0.	0.	0.	0.	0.	0.
0.	-.144	0.	0.	0.	0.	-.311	-.256E-01	.198E-02	0.	.203E-06	0.
0.	0.	0.	0.	0.	0.	.116E+04	-.905	.321E-01	-1.53	.155E-02	0.
0.	0.	0.	0.	0.	0.	-55.1	.531E-01	-.173E-01	-32.2	.277E-03	0.
0.	0.	0.	0.	0.	0.	1.000	0.	0.	0.	0.	0.
0.	0.	0.	0.	0.	0.	0.	-.999	.474E-01	.116E+04	0.	0.
0.	0.	0.	0.	0.	0.	0.	.474E-01	.999	0.	0.	0.

G1 MATRIX(12X 9)

14.2	6.38	18.4	0.	0.	0.	0.	0.	0.
.679	-2.35	.596	0.	0.	0.	0.	0.	0.
2.89	18.6	0.	0.	0.	0.	0.	0.	0.
0.	0.	0.	0.	0.	0.	0.	0.	0.
0.	0.	0.	0.	0.	0.	0.	0.	0.
0.	0.	0.	0.	0.	0.	0.	0.	0.
0.	0.	0.	-17.5	-2.95	-3.45	.389	-.343	-.165E-04
0.	0.	0.	-113.	-99.4	30.0	.277	-6.28	0.
0.	0.	0.	.657	2.85	.671	-6.03	-5.49	3.05
0.	0.	0.	0.	0.	0.	0.	0.	0.
0.	0.	0.	0.	0.	0.	0.	0.	0.
0.	0.	0.	0.	0.	0.	0.	0.	0.

G2 MATRIX(12X 3)

ROW 1	0.	0.
ROW 2	-.5653E-01	0.
ROW 3	.7255E-02	0.
ROW 4	-.2189E+00	0.
ROW 5	0.	0.
ROW 6	0.	0.
ROW 7	0.	0.
ROW 8	.1084E-02	-.2559E-01
ROW 9	.3209E-01	-.9050E+00
ROW 10	-.1735E-01	.5311E-01
ROW 11	0.	0.
ROW 12	0.	0.

HX MATRIX(9X12)

0.	0.	.860E-03	0.	0.	0.	0.	0.	0.	0.	0.	0.
.994E-02	1.93	-.219	0.	0.	0.	0.	0.	0.	0.	0.	0.
0.	0.	0.	0.	0.	0.	0.	.859E-03	-.408E-04	0.	0.	0.
0.	0.	0.	0.	0.	0.	0.	-.905	.321E-01	0.	.155E-02	0.
0.	0.	0.	0.	0.	0.	0.	.474E-01	.999	0.	0.	0.
0.	0.	0.	0.	0.	0.	0.	-.198E-04	-.418E-03	0.	0.	0.
0.	0.	0.	0.	0.	0.	0.	.387E-02	-.375E-03	0.	0.	0.
0.	0.	0.	0.	0.	0.	0.	-.771E-05	-.163E-03	0.	.100E-05	0.
0.	0.	0.	0.	0.	0.	0.	.697E-04	-.259E-04	0.	0.	0.

HU MATRIX(9X 9)

0.	0.	0.	0.	0.	0.	0.	0.	0.
2.89	18.6	0.	0.	0.	0.	0.	0.	0.
0.	0.	0.	0.	0.	0.	0.	0.	0.
0.	0.	0.	-113.	-99.4	30.0	.277	-6.28	0.
0.	0.	0.	0.	0.	0.	0.	0.	0.
0.	0.	0.	0.	0.	0.	0.	0.	0.
0.	0.	0.	.489	.430	-.130	-.243E-02	.260E-01	0.
0.	0.	0.	0.	0.	0.	0.	0.	0.
0.	0.	0.	.204E-01	.805E-02	-.905E-02	.260E-01	.250E-01	0.

HW MATRIX(9X 3)

ROW 1	0.	.8600E-03	0.
ROW 2	0.	-.2189E+00	0.
ROW 3	-.4076E-04	0.	.8591E-03
ROW 4	.3209E-01	0.	-.9050E+00
ROW 5	.9989E+00	0.	.4739E-01
ROW 6	-.4175E-03	0.	-.1979E-04
ROW 7	-.3753E-03	0.	.3871E-02
ROW 8	-.1626E-03	0.	-.7706E-05
ROW 9	-.2587E-04	0.	.6970E-04

EIGENVALUES OF FREE A/C

REAL	IMAG	DAMPING	FREQ
0.	0.		
.110877E-13	0.		
.110877E-13	0.		
-.129209E-01	0.		
-.206614E-01	0.		
-.114133E-02	.403593E-01	.282679E-01	.403754E-01
-.267222E+01	0.		
-.289189E+00	.339038E+01	.849882E-01	.340269E+01
-.608723E+00	.545171E+01	.110968E+00	.548559E+01

EIGENVALUES FOR LATERAL AXES

REAL	IMAG	DAMPING	FREQ
.579536E-13	0.		
.579536E-13	0.		
-.206570E-01	0.		
-.267238E+01	0.		
-.288634E+00	.339175E+01	.847925E-01	.340401E+01

EIGENVALUES FOR PITCH AXIS

REAL	IMAG	DAMPING	FREQ
-.218813E-13	0.		
-.129198E-01	0.		
-.112670E-02	.403676E-01	.279000E-01	.403833E-01
-.609217E+00	.544910E+01	.111109E+00	.548305E+01

NOMINAL TRAJECTORY PARAMETERS(T= 0.00)

NX = 12
 NU = 9
 NW = 3
 NY = 9
 APERT = .1000E+01

X3 VECTOR

0. 0. 0. 0. 0. 0. 0. .2948E+02 .8622E+03 .3418E-01
 .1000E+05 0.

U3 VECTOR

0. 0. 0. -.2991E-01 0. 0. 0. 0. .6209E+00

W3 VECTOR

0. 0. 0.

YN VECTOR

0. 0. .3418E-01 -.3219E+02 .8627E+03 .4964E+00 .8369E-01 .1370E+00 .1821E-01

DYNAMIC PRESSURE = .65169E+03
 MACH = .80
 ANGLE-OF-ATTACK = 1.96

F8-SIM

FLIGHT CONDITION 9

LIST OF NON-ZERO ELEMENTS IN A(1)• THRU, A(1000)

4	.1000E+05	5	.8000E+00	7	.8622E+03	9	.2948E+02	10	.8622E+03	12	.2948E+02	13	.8627E+03
15	-.2274E-12	16	.8627E+03	17	.5689E-02	19	-.5627E-02	20	.1106E+01	22	-.3219E+02	23	.1106E+01
25	-.3219E+02	28	-.2636E-15	29	.3418E-01	31	.3418E-01	37	-.6745E-05	46	.3181E-05	51	.1000E+01
54	.9994E+00	56	.3417E-01	58	.1000E+01	60	-.3417E-01	62	.9994E+00	70	.6517E+03	71	.7076E+03
73	-.2059E+05	78	.2754E+00	83	.9200E+04	84	.8655E+05	85	.9126E+05	88	.2953E+04	89	.1000E+00
90	.3220E+02	91	.6398E+03	92	.1000E+02	95	.3035E+00	96	.7747E+04	117	.3750E+03	118	.2500E-01
119	.4300E+00	120	.2600E-01	121	-.1457E+00	122	-.1700E-01	123	.2700E+03	124	.2700E+03	125	.1000E+04
128	.1178E+02	129	.5000E+01	131	.1000E+01	132	.1000E+00	134	.1000E+00	138	.9000E+01	142	.7000E+01
145	.1000E+01	146	.1000E+04	147	.1000E-02	148	.1000E-02	149	.1000E-01	151	.3220E+02	152	.1821E-01
154	-.8369E-01	156	.9565E-07	161	.9999E+00	163	.1709E-01	170	.1200E+02	171	.9000E+01	172	.3000E+01
177	-.2991E-01	183	.6209E+00	189	.2100E+02	197	.3567E+02	201	.1000E+00	202	.1000E+00	203	.1000E+02
204	.2000E-01	205	.2000E-01	206	.1000E+03	207	.1000E+00	208	.5000E+00	209	.1000E+01	210	.2000E-01
211	.1000E+03	212	.1000E+03	221	.2000E-01	222	.2000E-01	223	.2000E-01	224	.2500E-02	225	.2000E-01
226	.2000E-01	227	.5000E-01	228	.1000E+00	229	.1000E-01	265	.2500E-01	266	.5000E-01	283	.2500E+00
330	-.1400E+00	331	-.4370E+00	333	.5230E+00	334	.8730E-01	335	.2000E+01	485	.9000E+01	486	.1000E-06
428	.1000E+01	700	.1958E+01	703	-.1510E-13	705	.1823E-03	706	.1958E+01	709	-.3864E-03	801	.7177E+04
802	.1751E+04	803	.1779E-01	805	.4257E-03	806	-.3140E-02	807	.9680E-02	808	-.1088E+01	809	.4311E+00
810	-.1060E-01	811	.1751E-02	812	.1078E+04	813	.2349E-01	814	.1370E+00	815	.8369E-01	817	-.1179E+00
818	-.9722E-01	819	.6092E-02	820	-.3308E+00	821	.4482E-01	822	.4964E+00	823	-.1437E-02	824	-.4140E-01
825	-.2200E+00	826	-.1520E+00	828	.3035E+00	829	.9200E+04	830	.8655E+05	831	.9126E+05	832	.2953E+04
833	.1825E+00	834	-.3158E+00	835	.6465E-02	836	.9330E-02	837	-.7855E-01	838	.1868E-01	861	.1000E+01
862	.1000E+02	863	.5000E+00	901	.4200E+02	902	.4400E+02	903	.8000E+01	904	.3200E+02	905	.3300E+02
906	.3000E+01	907	.4300E+02	908	.9000E+01	909	.7000E+01	910	.3100E+02	911	.4000E+01	912	.2000E+01
913	.1000E+01	914	.2000E+01	915	.3000E+01	916	.4000E+01	917	.5000E+01	918	.6000E+01	919	.7000E+01
920	.8000E+01	921	.9000E+01	922	.1000E+02	923	.1100E+02	924	.1200E+02	925	.1810E+03	926	.1820E+03
927	.1840E+03	928	.1770E+03	929	.1790E+03	930	.1780E+03	931	.1760E+03	932	.1800E+03	933	.1830E+03
934	.1010E+03	935	.1020E+03	936	.1030E+03	937	.1300E+02	938	.1400E+02	939	.1500E+02	940	.1600E+02
941	.1700E+02	942	.1800E+02	943	.1900E+02	944	.2000E+02	945	.2100E+02	961	.1295E+05	962	.9300E+05
963	.1010E+06	964	.2080E+04	965	.5839E+03	966	.5000E+00						

LINEAR DYNAMICS

F MATRIX(12X12)

-6.54	-.817E-01	-.102	0.	0.	0.	.275E-01	0.	0.	0.	0.	0.
-.199	-.626	.163E-01	0.	0.	0.	.858E-01	0.	0.	0.	0.	0.
29.4	-859.	-.482	32.2	0.	0.	0.	0.	0.	0.	0.	0.
1.00	.342E-01	0.	0.	0.	0.	0.	0.	0.	0.	0.	0.
0.	1.00	0.	0.	0.	0.	0.	0.	0.	0.	0.	0.
0.	0.	1.000	-29.5	863.	0.	0.	0.	0.	0.	0.	0.
0.	-.895E-01	0.	0.	0.	0.	-.999	-.155E-01	.493E-03	0.	0.	0.
0.	0.	0.	0.	0.	0.	862.	-1.96	-.155E-01	-1.10	.987E-03	0.
0.	0.	0.	0.	0.	0.	-29.5	.452E-01	-.169E-01	-32.2	.393E-04	0.
0.	0.	0.	0.	0.	0.	1.000	0.	0.	0.	0.	0.
0.	0.	0.	0.	0.	0.	0.	-.999	.342E-01	863.	0.	0.
0.	0.	0.	0.	0.	0.	0.	.342E-01	.999	0.	0.	0.

G1 MATRIX(12X 9)

43.2	15.5	33.3	0.	0.	0.	0.	0.	0.			
2.29	-7.00	1.08	0.	0.	0.	0.	0.	0.			
8.97	52.3	0.	0.	0.	0.	0.	0.	0.			
0.	0.	0.	0.	0.	0.	0.	0.	0.			
0.	0.	0.	0.	0.	0.	0.	0.	0.			
0.	0.	0.	0.	0.	0.	0.	0.	0.			
0.	0.	0.	-30.9	-4.84	-5.06	-.527E-01	-.565	.222E-04			
0.	0.	0.	-246.	-164.	45.1	-2.10	-10.3	0.			
0.	0.	0.	5.84	1.92	-.340	-8.55	-9.20	11.2			
0.	0.	0.	0.	0.	0.	0.	0.	0.			
0.	0.	0.	0.	0.	0.	0.	0.	0.			
0.	0.	0.	0.	0.	0.	0.	0.	0.			
0.	0.	0.	0.	0.	0.	0.	0.	0.			

G2 MATRIX(12X 3)		
ROW 1		
0.	-.1016E+00	0.
ROW 2		
0.	.1627E-01	0.
ROW 3		
0.	-.4819E+00	0.
ROW 4		
0.	0.	0.
ROW 5		
0.	0.	0.
ROW 6		
0.	0.	0.
ROW 7		
.4929E-03	0.	-.1552E-01
ROW 8		
-.1546E-01	0.	-.1959E+01
ROW 9		
-.1686E-01	0.	.4520E-01
ROW 10		
0.	0.	0.
ROW 11		
0.	0.	0.
ROW 12		
0.	0.	0.

HX MATRIX(9X12)

0.	0.	.116E-02	0.	0.	0.	0.	0.	0.	0.	0.	0.
-.837E-01	3.40	-.482	0.	0.	0.	0.	0.	0.	0.	0.	0.
0.	0.	0.	0.	0.	0.	0.	.116E-02	-.396E-04	0.	0.	0.
0.	0.	0.	0.	0.	0.	0.	-1.96	-.155E-01	0.	.987E-03	0.
0.	0.	0.	0.	0.	0.	0.	.342E-01	.999	0.	0.	0.
0.	0.	0.	0.	0.	0.	0.	-.253E-06	-.741E-05	0.	0.	0.
0.	0.	0.	0.	0.	0.	0.	.510E-02	-.154E-03	0.	0.	0.
0.	0.	0.	0.	0.	0.	0.	-.690E-05	-.202E-03	0.	.202E-05	0.
0.	0.	0.	0.	0.	0.	0.	.153E-03	.614E-06	0.	0.	0.

HU MATRIX(9X 9)

0.	0.	0.	0.	0.	0.	0.	0.	0.
8.97	52.3	0.	0.	0.	0.	0.	0.	0.
0.	0.	0.	0.	0.	0.	0.	0.	0.
0.	0.	0.	-246.	-164.	45.1	-2.10	-10.3	0.
0.	0.	0.	0.	0.	0.	0.	0.	0.
0.	0.	0.	0.	0.	0.	0.	0.	0.
0.	0.	0.	.643	.430	-.118	.473E-02	.260E-01	0.
0.	0.	0.	0.	0.	0.	0.	0.	0.
0.	0.	0.	.669E-02	.968E-02	-.314E-02	.226E-01	.250E-01	0.

HW MATRIX(9X 3)

ROW 1	0.	.1159E-02	0.
ROW 2	0.	-.4819E+00	0.
ROW 3	-.3961E-04	0.	.1158E-02
ROW 4	-.1546E-01	0.	-.1959E+01
ROW 5	.9994E+00	0.	.3417E-01
ROW 6	-.7414E-05	0.	-.2535E-06
ROW 7	-.1543E-03	0.	.5103E-02
ROW 8	-.2017E-03	0.	-.6895E-05
ROW 9	.6143E-06	0.	.1525E-03

EIGENVALUES OF FREE A/C

REAL	IMAG	DAMPING	FREQ
0.	0.		
-.829497E-13	0.		
-.829497E-13	0.		
-.316690E-02	0.		
-.168868E-01	0.		
-.707593E-02	.572494E-01	.122665E+00	.576850E-01
-.147326E+01	.362622E+01	.376400E+00	.391408E+01
-.520904E+00	.415337E+01	.124442E+00	.418590E+01
-.659559E+01	0.		

EIGENVALUES FOR LATERAL AXES

REAL	IMAG	DAMPING	FREQ
-.299760E-14	0.		
-.299760E-14	0.		
-.168869E-01	0.		
-.519606E+00	.415212E+01	.124174E+00	.410451E+01
-.659564E+01	0.		

EIGENVALUES FOR PITCH AXIS

REAL	IMAG	DAMPING	FREQ
.136002E-14	0.		
-.316682E-02	0.		
-.706189E-02	.572533E-01	.122417E+00	.576872E-01
-.147454E+01	.362698E+01	.376614E+00	.391526E+01

NOMINAL TRAJECTORY PARAMETERS (T= 0.00)

NX = 12

NU = 9

NW = 3

NY = 9

APERT = .1000E+01

X3 VECTOR

0. 0. 0. 0. 0. 0. 0. .2542E+02 .7818E+03 .3250E-01
0. 0.

U3 VECTOR

0. 0. 0. -.2903E-01 0. 0. 0. 0. .5482E+00

W3 VECTOR

0. 0. 0.

YN VECTOR

0. 0. .3250E-01 -.3218E+02 .7822E+03 .4972E+00 .7516E-01 .1450E+00 .1739E-01

DYNAMIC PRESSURE = .72553E+03

MACH = .70

ANGLE-OF-ATTACK = 1.86

F8-SIM.

FLIGHT CONDITION 10

LINEAR DYNAMICS

F MATRIX(12X12)

-7.57	-.871E-01	-.121	0.	0.	0.	.243E-01	0.	0.	0.	0.	0.
-.226	-.743	.156E-01	0.	0.	0.	.757E-01	0.	0.	0.	0.	0.
25.3	-778.	-.576	32.2	0.	0.	0.	0.	0.	0.	0.	0.
1.00	.325E-01	0.	0.	0.	0.	0.	0.	0.	0.	0.	0.
0.	1.00	0.	0.	0.	0.	0.	0.	0.	0.	0.	0.
0.	0.	1.000	-25.5	782.	0.	0.	0.	0.	0.	0.	0.
0.	-.790E-01	0.	0.	0.	0.	-1.10	-.195E-01	.569E-03	0.	-.112E-06	0.
0.	0.	0.	0.	0.	0.	782.	-2.25	-.157E-01	-1.05	.924E-03	0.
0.	0.	0.	0.	0.	0.	-25.4	.501E-01	-.203E-01	-32.2	.117E-03	0.
0.	0.	0.	0.	0.	0.	1.000	0.	0.	0.	0.	0.
0.	0.	0.	0.	0.	0.	0.	-.999	.325E-01	782.	0.	0.
0.	0.	0.	0.	0.	0.	0.	.325E-01	.999	0.	0.	0.

G1 MATRIX(12X 9)

48.4	15.2	37.1	0.	0.	0.	0.	0.	0.
2.54	-7.68	1.20	0.	0.	0.	0.	0.	0.
9.32	61.6	0.	0.	0.	0.	0.	0.	0.
0.	0.	0.	0.	0.	0.	0.	0.	0.
0.	0.	0.	0.	0.	0.	0.	0.	0.
0.	0.	0.	0.	0.	0.	0.	0.	0.
0.	0.	0.	-32.9	-5.39	-5.13	-.137E-01	-.629	.156E-04
0.	0.	0.	-272.	-183.	53.4	-2.48	-11.4	0.
0.	0.	0.	6.72	1.74	-1.12	-9.49	-10.3	13.5
0.	0.	0.	0.	0.	0.	0.	0.	0.
0.	0.	0.	0.	0.	0.	0.	0.	0.
0.	0.	0.	0.	0.	0.	0.	0.	0.

G2 MATRIX(12X 3)

ROW 1	0.	0.
ROW 2	-.1211E+00	0.
ROW 3	.1564E-01	0.
ROW 4	-.5756E+00	0.
ROW 5	0.	0.
ROW 6	0.	0.
ROW 7	.5692E-03	0.
ROW 8	-.1945E-01	0.
ROW 9	-.1572E-01	0.
ROW 10	-.2030E-01	0.
ROW 11	.5007E-01	0.
ROW 12	0.	0.

HX MATRIX(9X12)

0.	0.	.128E-02	0.	0.	0.	0.	0.	0.	0.	0.	0.
-.121	4.03	-.576	0.	0.	0.	0.	0.	0.	0.	0.	0.
0.	0.	0.	0.	0.	0.	0.	.128E-02	-.415E-04	0.	0.	0.
0.	0.	0.	0.	0.	0.	0.	-2.25	-.157E-01	0.	.924E-03	0.
0.	0.	0.	0.	0.	0.	0.	.325E-01	.999	0.	0.	0.
0.	0.	0.	0.	0.	0.	0.	-.233E-06	-.716E-05	0.	0.	0.
0.	0.	0.	0.	0.	0.	0.	.527E-02	-.156E-03	0.	0.	0.
0.	0.	0.	0.	0.	0.	0.	-.699E-05	-.215E-03	0.	.111E-06	0.
0.	0.	0.	0.	0.	0.	0.	.149E-03	.545E-06	0.	0.	0.

HU MATRIX(9X 9)

0.	0.	0.	0.	0.	0.	0.	0.	0.
9.32	61.6	0.	0.	0.	0.	0.	0.	0.
0.	0.	0.	0.	0.	0.	0.	0.	0.
0.	0.	0.	-272.	-183.	53.4	-2.48	-11.4	0.
0.	0.	0.	0.	0.	0.	0.	0.	0.
0.	0.	0.	0.	0.	0.	0.	0.	0.
0.	0.	0.	.639	.430	-.125	.511E-02	.260E-01	0.
0.	0.	0.	0.	0.	0.	0.	0.	0.
0.	0.	0.	.496E-02	.989E-02	-.144E-02	.225E-01	.250E-01	0.

HW MATRIX(9X 3)

ROW 1	0.	.1278E-02	0.
ROW 2	0.	-.5756E+00	0.
ROW 3	-.4154E-04	0.	.1278E-02
ROW 4	-.1572E-01	0.	-.2251E+01
ROW 5	.9995E+00	0.	.3249E-01
ROW 6	-.7155E-05	0.	-.2326E-06
ROW 7	-.1559E-03	0.	.5266E-02
ROW 8	-.2150E-03	0.	-.6990E-05
ROW 9	.5449E-06	0.	.1489E-03

EIGENVALUES OF FREE A/C

REAL	IMAG	DAMPING	FREQ
0.	0.		
.225553E-13	0.		
.225553E-13	0.		
-.189181E-02	0.		
-.228214E-01	0.		
-.936949E-02	.595275E-01	.155483E+00	.602604E-01
-.167339E+01	.385811E+01	.397916E+00	.420539E+01
-.617573E+00	.395430E+01	.154307E+00	.400224E+01
-.763141E+01	0.		

EIGENVALUES FOR LATERAL AXES

REAL	IMAG	DAMPING	FREQ
.549560E-13	0.		
.549560E-13	0.		
-.228211E-01	0.		
-.616284E+00	.395376E+01	.154013E+00	.400151E+01
-.763144E+01	0.		

EIGENVALUES FOR PITCH AXIS

REAL	IMAG	DAMPING	FREQ
-.654338E-14	0.		
-.189179E-02	0.		
-.935762E-02	.595315E-01	.155281E+00	.602625E-01
-.167468E+01	.385827E+01	.398159E+00	.420605E+01

NOMINAL TRAJECTORY PARAMETERS (T= 0.00)

NX = 12

NU = 9

NW = 3

NY = 9

APERT = .1000E+01

X3 VECTOR

0.	0.	0.	0.	0.	0.	0.	0.	.4457E+02	.3323E+03	.1333E+00
0.	0.									

U3 VECTOR

0.	0.	0.	-.5492E-01	0.	0.	0.	0.	0.	.2619E+00	

W3 VECTOR

0.	0.	0.								

YM VECTOR

0.	0.	.1333E+00	-.3191E+02	.3352E+03	.5311E+00	.4050E+00	.2120E+00	.4744E-01		

DYNAMIC PRESSURE = .13326E+03

MACH = .30

ANGLE-OF-ATTACK = 7.64

F8-SIM

FLIGHT CONDITION: 11

LIST OF NON-ZERO ELEMENTS IN A(1), THRU, A(1000)

5	.3000E+00	7	.3323E+03	9	.4457E+02	10	.3323E+03	12	.4457E+02	13	.3352E+03	15	.9095E-12
16	.3352E+03	17	-.2062E-02	19	.5269E-02	20	.4279E+01	22	-.3191E+02	23	.4279E+01	25	-.3191E+02
28	-.2713E-14	29	.1333E+00	31	.1333E+00	37	.1639E-04	46	-.5091E-04	51	.1000E+01	54	.9911E+00
56	.1330E+00	58	.1000E+01	60	-.1330E+00	62	.9911E+00	70	.1333E+03	71	.2738E+04	73	-.2042E+05
78	-.4400E+01	83	.9200E+04	84	.8655E+05	85	.9126E+05	88	.2953E+04	89	.1000E+00	90	.3220E+02
91	-.6398E+03	92	.1000E+02	95	.3035E+00	96	.3267E+04	117	.3750E+03	118	.2500E-01	119	.4300E+00
120	.2600E-01	121	-.1457E+00	122	-.1700E-01	123	.2700E+03	124	.2700E+03	125	.1000E+04	128	.1178E+02
129	.5000E+01	131	.1000E+01	132	.1000E+00	134	.1000E+00	138	.1100E+02	142	.7000E+01	145	.1000E+01
146	.1000E+04	147	.1000E-02	148	.1000E-02	149	.1000E-01	151	.3220E+02	152	.4744E-01	154	.4058E+00
156	-.7485E-05	161	.9978E+00	163	.6662E-01	170	.1200E+02	171	.9000E+01	172	.3000E+01	177	-.5492E-01
183	.2619E+00	189	.2100E+02	197	.3567E+02	201	.1000E+00	202	.1000E+00	203	.1000E+02	204	.2000E-01
205	.2000E-01	206	.1000E+03	207	.1000E+00	208	.5000E+00	209	.1000E+01	210	.2000E-01	211	.1000E+03
212	.1000E+03	221	.2000E-01	222	.2000E-01	223	.2000E-01	224	.2500E-02	225	.2000E-01	226	.2000E-01
227	.5000E-01	228	.1000E+00	229	.1000E-01	265	.2500E-01	266	.5000E-01	283	.2500E+00	330	-.1400E+00
331	-.4370E+00	333	.5230E+00	334	.8730E-01	335	.2000E+01	485	.9000E+01	486	.1000E-06	498	.1000E+01
700	.7640E+01	703	-.1554E-12	705	-.2917E-02	706	.7640E+01	709	.9394E-03	801	.9131E+04	802	.4252E+04
803	.4463E-01	805	.2814E-02	806	-.9424E-01	807	-.5076E-01	808	-.9589E+00	809	.4104E+00	810	.1157E+00
811	.2372E-02	812	.1117E+04	813	.8755E-02	814	.2120E+00	815	.4058E+00	817	-.1663E+00	818	-.1332E+00
819	.4020E-01	820	-.3503E+00	821	.5896E-01	822	.5311E+00	823	-.7523E-02	824	-.3957E+01	825	-.4857E+00
826	-.9183E-01	828	.3035E+00	829	.9200E+04	830	.8655E+05	831	.9126E+05	832	.2953E+04	833	.9886E-01
834	-.2991E+00	835	-.3597E-01	836	.7276E-02	837	-.1007E+00	838	.2502E-01	861	.1000E+01	862	.1000E+02
863	.5000E+00	901	.4200E+02	902	.4400E+02	903	.8000E+01	904	.3200E+02	905	.3300E+02	906	.3000E+01
907	.4300E+02	908	.9000E+01	909	.7000E+01	910	.3100E+02	911	.4000E+01	912	.2000E+01	913	.1000E+01
914	.2000E+01	915	.3000E+01	916	.4000E+01	917	.5000E+01	918	.6000E+01	919	.7000E+01	920	.8000E+01
921	.9000E+01	922	.1000E+02	923	.1100E+02	924	.1200E+02	925	.1810E+03	926	.1820E+03	927	.1840E+03
928	.1770E+03	929	.1790E+03	930	.1780E+03	931	.1760E+03	932	.1800E+03	933	.1830E+03	934	.1010E+03
935	.1020E+03	936	.1030E+03	937	.1300E+02	938	.1400E+02	939	.1500E+02	940	.1600E+02	941	.1700E+02
942	.1800E+02	943	.1900E+02	944	.2000E+02	945	.2100E+02	961	.1295E+05	962	.9300E+05	963	.1010E+06
964	.2080E+04	965	.5839E+03	966	.5000E+00								

LINEAR DYNAMICS

F MATRIX(12X12)

-3.66	.318	-.761E-01	0.	0.	0.	.116E-01	0.	0.	0.	0.	0.
-.156	-.300	.300E-02	0.	0.	0.	.362E-01	0.	0.	0.	0.	0.
45.1	-331.	-.224	31.9	0.	0.	0.	0.	0.	0.	0.	0.
1.00	.134	0.	0.	0.	0.	0.	0.	0.	0.	0.	0.
0.	1.01	0.	0.	0.	0.	0.	0.	0.	0.	0.	0.
0.	0.	1.000	-44.6	335.	0.	0.	0.	0.	0.	0.	0.
0.	-.378E-01	0.	0.	0.	0.	-.531	-.864E-02	.700E-03	0.	-.669E-06	0.
0.	0.	0.	0.	0.	0.	.332.	-.913	-.827E-01	-4.28	.919E-03	0.
0.	0.	0.	0.	0.	0.	-44.6	.102	-.122E-01	-31.9	-.531E-04	0.
0.	0.	0.	0.	0.	0.	1.000	0.	0.	0.	0.	0.
0.	0.	0.	0.	0.	0.	0.	-.991	.133	335.	0.	0.
0.	0.	0.	0.	0.	0.	0.	.133	.991	0.	0.	0.

G1 MATRIX(12X 9)

11.6	4.26	7.29	0.	0.	0.	0.	0.	0.
.517	-1.83	.236	0.	0.	0.	0.	0.	0.
.684	16.6	0.	0.	0.	0.	0.	0.	0.
0.	0.	0.	0.	0.	0.	0.	0.	0.
0.	0.	0.	0.	0.	0.	0.	0.	0.
0.	0.	0.	0.	0.	0.	0.	0.	0.
0.	0.	0.	-5.90	-.985	-.627	-.224E-01	-.115	.329E-03
0.	0.	0.	-47.4	-32.8	13.8	-.421	-2.27	0.
0.	0.	0.	-.931	8.39	5.57	-1.71	-1.67	14.3
0.	0.	0.	0.	0.	0.	0.	0.	0.
0.	0.	0.	0.	0.	0.	0.	0.	0.
0.	0.	0.	0.	0.	0.	0.	0.	0.

G2 MATRIX(12X 3)

ROW 1	0.	0.
ROW 2	-.7609E-01	0.
ROW 3	.2997E-02	0.
ROW 4	-.2236E+00	0.
ROW 5	0.	0.
ROW 6	0.	0.
ROW 7	0.	0.
ROW 8	.7000E-03	0.
ROW 9	-.8267E-01	0.
ROW 10	-.1217E-01	0.
ROW 11	0.	0.
ROW 12	0.	0.
U.	0.	0.

HX MATRIX(9X12)

0.	0.	.298E-02	0.	0.	0.	0.	0.	0.	0.	0.	0.
.481	1.71	-.224	0.	0.	0.	0.	0.	0.	0.	0.	0.
0.	0.	0.	0.	0.	0.	0.	.296E-02	-.397E-03	0.	0.	0.
0.	0.	0.	0.	0.	0.	0.	-.913	-.827E-01	0.	.919E-03	0.
9.	0.	0.	0.	0.	0.	0.	.133	.991	0.	0.	0.
0.	0.	0.	0.	0.	0.	0.	-.131E-04	-.978E-04	0.	-.114E-06	0.
0.	0.	0.	0.	0.	0.	0.	.113E-01	-.135E-02	0.	.188E-06	0.
0.	0.	0.	0.	0.	0.	0.	-.171E-04	-.127E-03	0.	0.	0.
0.	0.	0.	0.	0.	0.	0.	.141E-02	-.160E-03	0.	0.	0.

HU MATRIX(9X 9)

0.	0.	0.	0.	0.	0.	0.	0.	0.
.684	16.6	0.	0.	0.	0.	0.	0.	0.
0.	0.	0.	0.	0.	0.	0.	0.	0.
0.	0.	0.	-47.4	-32.8	13.8	-.421	-2.27	0.
0.	0.	0.	0.	0.	0.	0.	0.	0.
0.	0.	0.	0.	0.	0.	0.	0.	0.
0.	0.	0.	.600	.430	-.166	.243E-02	.260E-01	0.
0.	0.	0.	0.	0.	0.	0.	0.	0.
0.	0.	0.	.926E-01	-.508E-01	-.942E-01	.224E-01	.250E-01	0.

HW MATRIX(9X 3)

ROW 1	0.	0.
ROW 2	.298E-02	0.
ROW 3	-.2236E+00	0.
ROW 4	-.3966E-03	.2956E-02
ROW 5	-.8267E-01	-.9127E+00
ROW 6	.9911E+00	.1330E+00
ROW 7	-.9778E-04	-.1312E-04
ROW 8	-.1351E-02	.1129E-01
ROW 9	-.1271E-03	-.1705E-04
ROW 9	-.1598E-03	.1415E-02

EIGENVALUES OF FREE A/C

REAL	IMAG	DAMPING	FREQ
-.211009E-13	0.		
-.135183E-13	0.		
-.135183E-13	0.		
-.457592E-03	0.		
-.691988E-02	.116260E+00	.594156E-01	.116466E+00
-.553918E-01	0.		
-.724178E+00	.169221E+01	.391596E+00	.183909E+01
-.443990E+00	.177627E+01	.242496E+00	.183092E+01
-.324261E+01	0.		

EIGENVALUES FOR LATERAL AXES

REAL	IMAG	DAMPING	FREQ
-.147660E-13	0.		
-.147660E-13	0.		
-.553832E-01	0.		
-.443415E+00	.177564E+01	.242281E+00	.183017E+01
-.324266E+01	0.		

EIGENVALUES FOR PITCH AXIS

REAL	IMAG	DAMPING	FREQ
-.216840E-16	0.		
-.457592E-03	0.		
-.689689E-02	.116280E+00	.591234E-01	.116483E+00
-.720765E+00	.169261E+01	.391787E+00	.183969E+01

NONINAL TRAJECTORY PARAMETERS(T= 0.00)

NX = 12
NU = 9
NY = 3
NY = 9
APERT = .1000E+01

X3 VECTOR

0. 0. 0. 0. 0. 0. 0. .2971E+02 .5915E+03 .5019E-01
0. 0.

U3 VECTOR

0. 0. 0. -.3223E-01 0. 0. 0. 0. .3230E+00

W3 VECTOR

0. 0. 0.

YN VECTOR

0. 0. .5019E-01 -.3216E+02 .5922E+03 .5057E+00 .1312E+00 .1790E+00 .1815E-01

DYNAMIC PRESSURE = .41592E+03
MACH = .53
ANGLE-OF-ATTACK = 2.88

F8-SIM

FLIGHT CONDITION 12

LINEAR DYNAMICS

MATRIX(12X12)

5.70	.431E-01	-.104	0.	0.	0.	.143E-01	0.	0.	0.	0.	0.
.191	-.552	.770E-02	0.	0.	0.	.446E-01	0.	0.	0.	0.	0.
29.8	-589.	-.414	32.2	0.	0.	0.	0.	0.	0.	0.	0.
1.00	.502E-01	0.	0.	0.	0.	0.	0.	0.	0.	0.	0.
1.	1.00	0.	0.	0.	0.	0.	0.	0.	0.	0.	0.
2.	0.	1.000	-29.7	592.	0.	0.	0.	0.	0.	0.	0.
2.	-.466E-01	0.	0.	0.	0.	-.866	-.144E-01	-.487E-03	0.	-.250E-05	0.
0.	0.	0.	0.	0.	0.	592.	-1.58	-.552E-01	-1.62	.889E-03	0.
0.	0.	0.	0.	0.	0.	-29.7	.964E-01	-.146E-01	-32.2	.423E-04	0.
0.	0.	0.	0.	0.	0.	1.000	0.	0.	0.	0.	0.
0.	0.	0.	0.	0.	0.	0.	-.999	.502E-01	592.	0.	0.
0.	0.	0.	0.	0.	0.	0.	.502E-01	.999	0.	0.	0.

G1 MATRIX(12X 9)

32.6	11.1	21.7	0.	0.	0.	0.	0.	0.
1.71	-5.20	.701	0.	0.	0.	0.	0.	0.
4.27	43.6	0.	0.	0.	0.	0.	0.	0.
0.	0.	0.	0.	0.	0.	0.	0.	0.
0.	0.	0.	0.	0.	0.	0.	0.	0.
0.	0.	0.	0.	0.	0.	0.	0.	0.
0.	0.	0.	-18.1	-3.08	-2.61	.293E-01	-.360	.654E-04
0.	0.	0.	-150.	-105.	33.5	-1.87	-6.64	0.
0.	0.	0.	1.84	3.38	-.271	-5.38	-5.77	13.7
0.	0.	0.	0.	0.	0.	0.	0.	0.
0.	0.	0.	0.	0.	0.	0.	0.	0.
0.	0.	0.	0.	0.	0.	0.	0.	0.

G2 MATRIX(12X 3)

ROW 1	0.	-.1036E+00	0.
ROW 2	0.	.7699E-02	0.
ROW 3	0.	-.4136E+00	0.
ROW 4	0.	0.	0.
ROW 5	0.	0.	0.
ROW 6	0.	0.	0.
ROW 7	0.	-.4868E-03	0.
ROW 8	0.	-.5521E-01	0.
ROW 9	0.	-.1463E-01	0.
ROW 10	0.	.9638E-01	0.
ROW 11	0.	0.	0.
ROW 12	0.	0.	0.

MX MATRIX (9X12)

0.	0.	.169E-02	0.	0.	0.	0.	0.	0.	0.	0.	0.	0.
.101	2.93	-.414	0.	0.	0.	0.	0.	0.	0.	0.	0.	0.
0.	0.	0.	0.	0.	0.	0.	.169E-02	-.847E-04	0.	0.	0.	0.
0.	0.	0.	0.	0.	0.	0.	-1.58	-.552E-01	0.	.889E-03	0.	0.
0.	0.	0.	0.	0.	0.	0.	.502E-01	.999	0.	0.	0.	0.
0.	0.	0.	0.	0.	0.	0.	-.495E-05	-.985E-04	0.	-.201E-06	0.	0.
0.	0.	0.	0.	0.	0.	0.	.643E-02	-.218E-03	0.	.214E-06	0.	0.
0.	0.	0.	0.	0.	0.	0.	-.644E-05	-.128E-03	0.	.218E-06	0.	0.
0.	0.	0.	0.	0.	0.	0.	.148E-03	-.299E-05	0.	0.	0.	0.

HW MATRIX (9X 9)

0.	0.	0.	0.	0.	0.	0.	0.	0.
4.27	43.6	0.	0.	0.	0.	0.	0.	0.
0.	0.	0.	0.	0.	0.	0.	0.	0.
0.	9.	0.	-150.	-105.	33.5	-1.87	-6.64	0.
0.	0.	0.	0.	0.	0.	0.	0.	0.
0.	0.	0.	0.	0.	0.	0.	0.	0.
0.	0.	0.	.613	.430	-.137	.657E-02	.260E-01	0.
0.	0.	0.	0.	0.	0.	0.	0.	0.
0.	0.	0.	.233E-01	.770E-02	-.579E-02	.224E-01	.250E-01	0.

HW MATRIX (9X 3)

ROW 1	0.	.1688E-02	0.
ROW 2	0.	-.4136E+00	0.
ROW 3	-.8471E-04	0.	.1636E-02
ROW 4	-.5521E-01	0.	-.1577E+01
ROW 5	.9987E+00	0.	.5017E-01
ROW 6	-.9853E-04	0.	-.4949E-05
ROW 7	-.2176E-03	0.	.6428E-02
ROW 8	-.1281E-03	0.	-.6435E-05
ROW 9	-.2992E-05	0.	.1477E-03

EIGENVALUES OF FREE A/C

REAL	IMAG	DAMPING	FREQ
.496956E-15	0.		
-.362353E-12	0.		
-.367353E-12	0.		
-.130024E-01	0.		
-.546620E-03	.320323E-01	.139415E-01	.320354E-01
-.390392E-01	0.		
-.122145E+01	.289288E+01	.388976E+00	.314017E+01
-.482838E+00	.272121E+01	.174706E+00	.276371E+01
-.566342E+01	0.		

EIGENVALUES FOR LATERAL AXES

REAL	IMAG	DAMPING	FREQ
.797140E-13	0.		
.797140E-13	0.		
-.399182E-01	0.		
-.482240E+00	.272113E+01	.174501E+00	.276353E+01
-.566345E+01	0.		

EIGENVALUES FOR PITCH AXIS

REAL	IMAG	DAMPING	FREQ
.103923E-14	0.		
-.130016E-01	0.		
-.440674E-03	.320388E-01	.137531E-01	.320418E-01
-.122205E+01	.289277E+01	.389151E+00	.314030E+01

NOMINAL TRAJECTORY PARAMETERS(T= 0.00)

NX = 12

NU = 9

NW = 3

NY = 9

APERF = .1000E+01

X3 VECTOR

0.	0.	0.	0.	0.	0.	0.	0.	.4617E+02	.6210E+03	.7421E-01
.2000E+05	0.									

U3 VECTOR

0.	0.	0.	-.4923E-01	0.	0.	0.	0.	0.	.3606E+00	
----	----	----	------------	----	----	----	----	----	-----------	--

W3 VECTOR

0.	0.	0.								
----	----	----	--	--	--	--	--	--	--	--

YN VECTOR

0.	0.	.7421E-01	-.3211E+02	.6227E+03	.4980E+00	.2226E+00	.2063E+00	.2231E-01		
----	----	-----------	------------	-----------	-----------	-----------	-----------	-----------	--	--

DYNAMIC PRESSURE = .24495E+03

MACH = .60

ANGLE-OF-ATTACK = 4.25

FB-SIM

FLIGHT CONDITION 13

LIST OF NON-ZERO ELEMENTS IN A(I), THRU, A(1000)

4	.2000E+05	5	.6000E+00	7	.6210E+03	9	.4617E+02	10	.6210E+03	12	.4617E+02	13	.6227E+03
15	-.4547E-12	16	.6227E+03	17	-.6869E-03	19	-.1424E-03	20	.2387E+01	22	-.3211E+02	23	.2387E+01
25	-.3211E+02	28	-.7303E-15	29	.7421E-01	31	.7421E-01	37	-.1463E-06	46	-.1789E-04	51	.1000E+01
54	.9972E+00	56	.7415E-01	58	.1000E+01	60	-.7415E-01	62	.9972E+00	70	.2450E+03	71	.1527E+04
73	-.2055E+05	78	-.1548E+01	83	.9200E+04	84	.8655E+05	85	.9126E+05	88	.2953E+04	89	.1000E+00
90	.3220E+02	91	.6398E+03	92	.1000E+02	95	.3035E+00	96	.4499E+04	117	.3750E+03	118	.2500E-01
119	.4300E+00	120	.2600E-01	121	-.1457E+00	122	-.1700E-01	123	.2700E+03	124	.2700E+03	125	.1000E+04
128	.1178E+02	129	.5000E+01	131	.1000E+01	132	.1000E+00	134	.1000E+00	138	.1300E+02	142	.7000E+01
145	.1000E+01	146	.1000E+04	147	.1000E-02	148	.1000E-02	149	.1000E-01	151	.3220E+02	152	.2231E-01
154	.2226E+00	156	-.1431E-05	161	.9993E+00	163	.3710E-01	170	.1200E+02	171	.9000E+01	172	.3000E+01
177	-.4923E-01	183	.3606E+00	189	.2100E+02	197	.3567E+02	201	.1000E+00	202	.1000E+00	203	.1000E+02
204	.2000E-01	205	.2000E-01	206	.1000E+03	207	.1000E+00	208	.5000E+00	209	.1000E+01	210	.2000E-01
211	.1000E+03	212	.1000E+03	221	.2000E-01	222	.2000E-01	223	.2000E-01	224	.2500E-02	225	.2000E-01
226	.2000E-01	227	.5000E-01	228	.1000E+00	229	.1000E-01	265	.2500E-01	266	.5000E-01	283	.2500E+00
330	-.1400E+00	331	-.4370E+00	333	.5230E+00	334	.8730E-01	335	.2000E+01	485	.9000E+01	486	.1000E-06
498	.1000E+01	700	.4252E+01	703	-.4184E-13	705	-.1025E-02	706	.4252E+01	709	-.8380E-05	801	.5697E+04
802	.2884E+04	803	.2240E-01	805	-.8868E-04	806	-.2216E-01	807	.1397E-02	808	-.1041E+01	809	.4030E+00
810	.4713E-01	811	.1764E-02	812	.1038E+04	813	.1684E-01	814	.2063E+00	815	.2226E+00	817	-.1444E+00
818	-.1273E+00	819	.1767E-01	820	-.3224E+00	821	.5699E-01	822	.4980E+00	823	-.3880E-02	824	-.4150E+01
825	-.4200E+00	826	-.1403E+00	828	.3035E+00	829	.9200E+04	830	.8655E+05	831	.9126E+05	832	.2953E+04
833	.1141E+00	834	-.3090E+00	835	-.1749E-01	836	.1066E-01	837	-.1043E+00	838	.2639E-01	861	.1000E+01
862	.1000E+02	863	.5000E+00	901	.4200E+02	902	.4400E+02	903	.8000E+01	904	.3200E+02	905	.3300E+02
906	.3000E+01	907	.4300E+02	908	.9000E+01	909	.7000E+01	910	.3100E+02	911	.4000E+01	912	.2000E+01
913	.1000E+01	914	.2000E+01	915	.3000E+01	916	.4000E+01	917	.5000E+01	918	.6000E+01	919	.7000E+01
920	.8000E+01	921	.9000E+01	922	.1000E+02	923	.1100E+02	924	.1200E+02	925	.1810E+03	926	.1820E+03
927	.1840E+03	928	.1770E+03	929	.1790E+03	930	.1780E+03	931	.1760E+03	932	.1800E+03	933	.1830E+03
934	.1010E+03	935	.1020E+03	936	.1030E+03	937	.1300E+02	938	.1400E+02	939	.1500E+02	940	.1600E+02
941	.1700E+02	942	.1800E+02	943	.1900E+02	944	.2000E+02	945	.2100E+02	961	.1295E+05	962	.9300E+05
963	.1010E+06	964	.2080E+04	965	.5839E+03	966	.5000E+00						

LINEAR DYNAMICS

F MATRIX(12X12)

-3.33	.791E-01	-.716E-01	0.	0.	0.	.160E-01	0.	0.	0.	0.	0.
-.126	-.315	.394E-02	0.	0.	0.	.498E-01	0.	0.	0.	0.	0.
46.4	-619.	-.240	32.1	0.	0.	0.	0.	0.	0.	0.	0.
1.00	.744E-01	0.	0.	0.	0.	0.	0.	0.	0.	0.	0.
0.	1.00	0.	0.	0.	0.	0.	0.	0.	0.	0.	0.
0.	0.	1.000	-46.2	623.	0.	0.	0.	0.	0.	0.	0.
0.	-.520E-01	0.	0.	0.	0.	-.540	-.933E-02	.335E-03	0.	-.920E-06	0.
0.	0.	0.	0.	0.	0.	621.	-.956	-.501E-01	-2.39	.105E-02	0.
0.	0.	0.	0.	0.	0.	-46.2	-.173E-01	-.158E-02	-32.1	-.485E-04	0.
0.	0.	0.	0.	0.	0.	1.000	0.	0.	0.	0.	0.
0.	0.	0.	0.	0.	0.	0.	-.997	.741E-01	623.	0.	0.
0.	0.	0.	0.	0.	0.	0.	.741E-01	.997	0.	0.	0.

G1 MATRIX(12X 9)

20.6	8.28	12.6	0.	0.	0.	0.	0.	0.
1.05	-3.48	.406	0.	0.	0.	0.	0.	0.
2.42	29.6	0.	0.	0.	0.	0.	0.	0.
0.	0.	0.	0.	0.	0.	0.	0.	0.
0.	0.	0.	0.	0.	0.	0.	0.	0.
0.	0.	0.	0.	0.	0.	0.	0.	0.
0.	0.	0.	-10.8	-1.82	-1.76	.194E-01	-.212	.527E-04
0.	0.	0.	-86.0	-61.6	20.9	-1.28	-3.99	0.
0.	0.	0.	-.362	4.38	1.64	-3.14	-3.30	8.90
0.	0.	0.	0.	0.	0.	0.	0.	0.
0.	0.	0.	0.	0.	0.	0.	0.	0.
0.	0.	0.	0.	0.	0.	0.	0.	0.

G2 MATRIX(12X 3)

ROW 1	0.	0.
ROW 2	-.7157E-01	0.
ROW 3	.3939E-02	0.
ROW 4	-.2400E+00	0.
ROW 5	0.	0.
ROW 6	0.	0.
ROW 7	0.	0.
ROW 8	.3347E-03	-.9333E-02
ROW 9	-.5008E-01	-.9562E+00
ROW 10	-.1575E-02	-.1733E-01
ROW 11	0.	0.
ROW 12	0.	0.

HX MATRIX(9X12)

0.	0.	.161E-02	0.	0.	0.	0.	0.	0.	0.	0.	0.	0.
.194	1.66	-.240	0.	0.	0.	0.	0.	0.	0.	0.	0.	0.
0.	0.	0.	0.	0.	0.	0.	.160E-02	-.119E-03	0.	0.	0.	0.
0.	0.	0.	0.	0.	0.	0.	-.956	-.501E-01	0.	.105E-02	0.	0.
0.	0.	0.	0.	0.	0.	0.	.741E-01	.997	0.	0.	0.	0.
0.	0.	0.	0.	0.	0.	0.	-.420E-05	-.568E-04	0.	-.141E-06	0.	0.
0.	0.	0.	0.	0.	0.	0.	.654E-02	-.363E-03	0.	.305E-06	0.	0.
0.	0.	0.	0.	0.	0.	0.	-.770E-05	-.103E-03	0.	.189E-05	0.	0.
0.	0.	0.	0.	0.	0.	0.	.965E-03	-.601E-04	0.	0.	0.	0.

HU MATRIX(9X 9)

0.	0.	0.	0.	0.	0.	0.	0.	0.
2.42	29.6	0.	0.	0.	0.	0.	0.	0.
0.	0.	0.	0.	0.	0.	0.	0.	0.
0.	0.	0.	-86.0	-61.6	20.9	-1.28	-3.99	0.
0.	0.	0.	0.	0.	0.	0.	0.	0.
0.	0.	0.	0.	0.	0.	0.	0.	0.
0.	0.	0.	.597	.430	-.144	.728E-02	.260E-01	0.
0.	0.	0.	0.	0.	0.	0.	0.	0.
0.	0.	0.	.469E-01	.140E-02	-.222E-01	.224E-01	.250E-01	0.

HW MATRIX(9X 3)

ROW 1	0.	.1606E-02	0.
ROW 2	0.	-.2400E+00	0.
ROW 3	-.1191E-03	0.	.1602E-02
ROW 4	-.5008E-01	0.	-.9562E+00
ROW 5	.9972E+00	0.	.7415E-01
ROW 6	-.5681E-04	0.	-.4204E-05
ROW 7	-.3635E-03	0.	.6544E-02
ROW 8	-.1033E-03	0.	-.7698E-05
ROW 9	-.6012E-04	0.	.9655E-03

EIGENVALUES OF FREE A/C

REAL	IMAG	DAMPING	FREQ
-.288455E-13	0.		
.338833E-12	0.		
.338833E-12	0.		
-.686860E-03	0.		
-.212363E-02	.709415E-01	.292215E-01	.709733E-01
-.389875E-01	0.		
-.745587E+00	.240015E+01	.296658E+00	.251329E+01
-.344303E+00	.229270E+01	.148509E+00	.231840E+01
-.315850E+01	0.		

EIGENVALUES FOR LATERAL AXES

REAL	IMAG	DAMPING	FREQ
.213163E-13	0.		
.213163E-13	0.		
-.389759E-01	0.		
-.343191E+00	.229249E+01	.148052E+00	.231804E+01
-.315859E+01	0.		

EIGENVALUES FOR PITCH AXIS

REAL	IMAG	DAMPING	FREQ
.268721E-12	0.		
-.686862E-03	0.		
-.210497E-02	.709565E-01	.296526E-01	.709877E-01
-.746682E+00	.240004E+01	.297068E+00	.251351E+01

NOMINAL TRAJECTORY PARAMETERS(T= 0.00)

NX = 12
NU = 9
NW = 3
NY = 9
APERT = .1000E+01

X3 VECTOR

0. 0. 0. 0. 0. 0. 0. 0. .3673E+02 .8294E+03 .4425E-01
.2000E+05 0.

U3 VECTOR

0. 0. 0. -.3426E-01 0. 0. 0. 0. .5470E+00

W3 VECTOR

0. 0. 0.

YN VECTOR

0. 0. .4425E-01 -.3217E+02 .8302E+03 .4964E+00 .1253E+00 .1742E+00 .1946E-01

DYNAMIC PRESSURE = .43547E+03
MACH = .80
ANGLE-OF-ATTACK = 2.54

FB-S14

FLIGHT CONDITION 14

LIST OF NON-ZERO ELEMENTS IN A(1), THRU, A(1000)													
4	.2000E+05	5	.8000E+00	7	.8294E+03	9	.3673E+02	10	.8294E+03	12	.3673E+02	13	.8302E+03
15	-.2274E-12	16	.8302E+03	17	.5536E-02	19	-.5518E-02	20	.1430E+01	22	-.3217E+02	23	.1430E+01
25	-.3217E+02	28	-.2739E-15	29	.4425E-01	31	.4425E-01	37	-.6935E-05	46	.3155E-05	51	.1000E+01
54	.9990E+00	56	.4424E-01	58	.1000E+01	60	-.4424E-01	62	.9990E+00	70	.4355E+03	71	.9149E+03
73	-.2059E+05	78	.2730E+00	83	.9200E+04	84	.8655E+05	85	.9126E+05	88	.2953E+04	89	.1000E+00
90	.3220E+02	91	.6398E+03	92	.1000E+02	95	.3035E+00	96	.6825E+04	117	.3750E+03	118	.2500E-01
119	.4300E+00	120	.2600E-01	121	-.1457E+00	122	-.1700E-01	123	.2700E+03	124	.2700E+03	125	.1000E+04
129	.1178E+02	129	.5003E+01	131	.1000E+01	132	.1000E+00	134	.1000E+00	138	.1400E+02	142	.7000E+01
145	.1000E-01	146	.1000E+04	147	.1000E-02	148	.1000E-02	149	.1000E-01	151	.3220E+02	152	.1946E-01
154	.1253E+00	156	.1419E-06	161	.9998E+00	163	.2212E-01	170	.1200E+02	171	.9000E+01	172	.3000E-01
177	-.3426E-01	183	.5470E+00	189	.2100E+02	197	.3567E+02	201	.1000E+00	202	.1000E+00	203	.1000E+02
204	.2000E-01	205	.2000E-01	206	.1000E+03	207	.1000E+00	208	.5000E+00	209	.1000E+01	210	.2000E-01
211	.1000E+03	212	.1000E+03	221	.7000E-01	222	.2000E-01	223	.2000E-01	224	.2500E-02	225	.2000E-01
226	.2000E-01	227	.5000E-01	228	.1000E+00	229	.1000E-01	265	.2500E-01	266	.5000E-01	283	.2500E+00
330	-.1400E+00	331	-.4370E+00	333	.5230E+00	334	.8730E-01	335	.2000E+01	485	.9000E+01	486	.1000E-06
498	.1000E+01	700	.2535E+01	703	-.1559E-13	705	.1807E-03	706	.2535E+01	709	-.3973E-03	801	.5822E+04
802	.2025E+04	803	.1909E-01	805	.3716E-03	806	-.6792E-02	807	.8436E-02	808	-.1091E+01	809	.4316E+00
810	.3661E-02	811	.1264E-02	812	.1038E+04	813	.2298E-01	814	.1742E+00	815	.1253E+00	817	-.1286E+00
819	-.1085E+00	819	.8491E-02	820	-.3414E+00	821	.5099E-01	822	.4964E+00	823	-.2172E-02	824	-.4470E+01
825	-.3800E+00	826	-.1567E+00	828	.3035E+00	829	.9200E+04	830	.8655E+05	831	.9126E+05	832	.2953E+04
833	.1815E+00	834	-.3220E+00	835	-.1098E-03	836	.1094E-01	837	-.9370E-01	838	.2275E-01	861	.1000E+01
862	.1000E+02	863	.9000E+00	901	.4200E+02	902	.4400E+02	903	.8000E+01	904	.3200E+02	905	.3300E+02
936	.3000E+01	907	.4300E+02	908	.9000E+01	909	.7000E+01	910	.3100E+02	911	.4000E+01	912	.2000E+01
913	.1000E+01	914	.2000E+01	915	.3000E+01	916	.4000E+01	917	.5000E+01	918	.6000E+01	919	.7000E+01
920	.8000E+01	921	.9000E+01	922	.1000E+02	923	.1100E+02	924	.1200E+02	925	.1810E+03	926	.1820E+03
927	.1840E+03	928	.1770E+03	929	.1790E+03	930	.1780E+03	931	.1760E+03	932	.1800E+03	933	.1830E+03
934	.1610E+03	935	.1020E+03	936	.1030E+03	937	.1300E+02	938	.1400E+02	939	.1500E+02	940	.1600E+02
941	.1700E+02	942	.1800E+02	943	.1900E+02	944	.2000E+02	945	.2100E+02	961	.1295E+05	962	.9300E+05
963	.1010E+06	964	.2080E+04	965	.5839E+03	966	.5000E+00						

LINEAR DYNAMICS

F MATRIX(12X12)

-4.69	-.265E-01	-.793E-01	0.	0.	0.	.243E-01	0.	0.	0.	0.	0.
-.152	-.442	.109E-01	0.	0.	0.	.756E-01	0.	0.	0.	0.	0.
36.7	-827.	-.335	32.2	0.	0.	0.	0.	0.	0.	0.	0.
1.00	.443E-01	0.	0.	0.	0.	0.	0.	0.	0.	0.	0.
0.	1.00	0.	0.	0.	0.	0.	0.	0.	0.	0.	0.
0.	0.	1.000	-36.7	830.	0.	0.	0.	0.	0.	0.	0.
0.	-.789E-01	0.	0.	0.	0.	-.765	-.107E-01	.502E-03	0.	0.	0.
0.	0.	0.	0.	0.	0.	829.	-1.36	-.296E-01	-1.42	.105E-02	0.
0.	0.	0.	0.	0.	0.	-36.7	.592E-01	-.119E-01	-32.2	.917E-05	0.
0.	0.	0.	0.	0.	0.	1.000	0.	0.	0.	0.	0.
0.	0.	0.	0.	0.	0.	0.	-.999	.442E-01	830.	0.	0.
0.	0.	0.	0.	0.	0.	0.	.442E-01	.999	0.	0.	0.

G1 MATRIX(12X 9)

32.9	12.6	22.3	0.	0.	0.	0.	0.	0.	G2 MATRIX(12X 3)
1.76	-5.57	.720	0.	0.	0.	0.	0.	0.	ROW 1
5.86	44.5	0.	0.	0.	0.	0.	0.	0.	0.
0.	0.	0.	0.	0.	0.	0.	0.	0.	ROW 2
0.	0.	0.	0.	0.	0.	0.	0.	0.	0.
0.	0.	0.	0.	0.	0.	0.	0.	0.	ROW 3
0.	0.	0.	0.	0.	0.	0.	0.	0.	0.
0.	0.	0.	0.	0.	0.	0.	0.	0.	ROW 4
0.	0.	0.	0.	0.	0.	0.	0.	0.	0.
0.	0.	0.	0.	0.	0.	0.	0.	0.	ROW 5
0.	0.	0.	0.	0.	0.	0.	0.	0.	0.
0.	0.	0.	-20.6	-3.23	-3.49	-.290E-01	-.377	.290E-04	ROW 6
0.	0.	0.	-161.	-110.	32.9	-1.63	-6.91	0.	0.
0.	0.	0.	2.76	2.70	.280	-5.69	-6.08	9.10	ROW 7
0.	0.	0.	0.	0.	0.	0.	0.	0.	0.
0.	0.	0.	0.	0.	0.	0.	0.	0.	ROW 8
0.	0.	0.	0.	0.	0.	0.	0.	0.	0.
0.	0.	0.	0.	0.	0.	0.	0.	0.	ROW 9
0.	0.	0.	0.	0.	0.	0.	0.	0.	0.
0.	0.	0.	0.	0.	0.	0.	0.	0.	ROW 10
0.	0.	0.	0.	0.	0.	0.	0.	0.	0.
0.	0.	0.	0.	0.	0.	0.	0.	0.	ROW 11
0.	0.	0.	0.	0.	0.	0.	0.	0.	0.
0.	0.	0.	0.	0.	0.	0.	0.	0.	ROW 12
0.	0.	0.	0.	0.	0.	0.	0.	0.	0.

HX MATRIX(9X12)

0.	0.	.120E-02	0.	0.	0.	0.	0.	0.	0.	0.	0.	0.
.291E-01	2.37	-.335	0.	0.	0.	0.	0.	0.	0.	0.	0.	0.
0.	0.	0.	0.	0.	0.	0.	.120E-02	-.533E-04	0.	0.	0.	0.
0.	0.	0.	0.	0.	0.	0.	-1.36	-.296E-01	0.	.105E-02	0.	0.
0.	0.	0.	0.	0.	0.	0.	.442E-01	.999	0.	0.	0.	0.
0.	0.	0.	0.	0.	0.	0.	-.341E-06	-.770E-05	0.	0.	0.	0.
0.	0.	0.	0.	0.	0.	0.	.531E-02	-.187E-03	0.	.159E-06	0.	0.
0.	0.	0.	0.	0.	0.	0.	-.684E-05	-.154E-03	0.	.267E-05	0.	0.
0.	0.	0.	0.	0.	0.	0.	.153E-03	.837E-06	0.	0.	0.	0.

HU MATRIX(9X 9)

0.	0.	0.	0.	0.	0.	0.	0.	0.
5.86	44.5	0.	0.	0.	0.	0.	0.	0.
0.	0.	0.	0.	0.	0.	0.	0.	0.
0.	0.	0.	-161.	-110.	32.9	-1.63	-6.91	0.
0.	0.	0.	0.	0.	0.	0.	0.	0.
0.	0.	0.	0.	0.	0.	0.	0.	0.
0.	0.	0.	.631	.430	-.129	.538E-02	.260E-01	0.
0.	0.	0.	0.	0.	0.	0.	0.	0.
0.	0.	0.	.171E-01	.844E-02	-.679E-02	.226E-01	.250E-01	0.

HW MATRIX(9X 3)

ROW 1	0.	.1204E-02	0.
ROW 2	0.	-.3354E+00	0.
ROW 3	-.5328E-04	0.	.1203E-02
ROW 4	-.2961E-01	0.	-.1363E+01
ROW 5	.9990E+00	0.	.4424E-01
ROW 6	-.7701E-05	0.	-.3410E-06
ROW 7	-.1868E-03	0.	.5308E-02
ROW 8	-.1544E-03	0.	-.6837E-05
ROW 9	.8369E-06	0.	.1532E-03

EIGENVALUES OF FREE A/C

REAL	IMAG	DAMPING	FREQ
-.210233E-13	0.		
-.331648E-13	0.		
-.331648E-13	0.		
-.190899E-02	0.		
-.184847E-01	0.		
-.531497E-02	.641054E-01	.826264E-01	.643253E-01
-.106244E+01	.297250E+01	.336570E+00	.315666E+01
-.381980E+00	.345566E+01	.109869E+00	.347670E+01
-.469031E+01	0.		

EIGENVALUES FOR LATERAL AXES

REAL	IMAG	DAMPING	FREQ
-.109912E-13	0.		
-.109912E-13	0.		
-.184838E-01	0.		
-.380869E+00	.345434E+01	.109594E+00	.347527E+01
-.469039E+01	0.		

EIGENVALUES FOR PITCH AXIS

REAL	IMAG	DAMPING	FREQ
-.520417E-16	0.		
-.190897E-02	0.		
-.529708E-02	.641111E-01	.823429E-01	.643295E-01
-.106353E+01	.297334E+01	.336792E+00	.315782E+01

NOMINAL TRAJECTORY PARAMETERS(IT= 0.00)

NX = 12

NU = 9

NW = 3

NY = 9

APERT= .1000E+01

X3 VECTOR

0.	0.	0.	0.	0.	0.	0.	0.	.6952E+02	.7720E+03	.8981E-01
.4000E+05	0.									

U3 VECTOR

0.	0.	0.	-.5514E-01	0.	0.	0.	0.	0.	.7727E+00	
----	----	----	------------	----	----	----	----	----	-----------	--

W3 VECTOR

0.	0.	0.								
----	----	----	--	--	--	--	--	--	--	--

YN VECTOR

0.	0.	.8981E-01	-.3207E+02	.7752E+03	.4964E+00	.3099E+00	.2183E+00	.3627E-01		
----	----	-----------	------------	-----------	-----------	-----------	-----------	-----------	--	--

DYNAMIC PRESSURE = .17540E+03

MACH = .80

ANGLE-OF-ATTACK = 5.15

F8-SIM

FLIGHT CONDITION 15

LIST OF NON-ZERO ELEMENTS IN A(1), THRU, A(1000)

4	.4000E+05	5	.8000E+00	7	.7720E+03	9	.6952E+02	10	.7720E+03	12	.6952E+02	13	.7752E+03
15	-.4547E-12	16	.7752E+03	17	.3578E-02	19	.4557E-02	20	.2892E+01	22	-.3207E+02	23	.2892E+01
25	-.3207E+02	28	-.5866E-15	29	.8981E-01	31	.8981E-01	37	.5441E-05	46	.1724E-02	51	.1000E+01
54	.9960E+00	56	.8969E-01	58	.1000E+01	60	-.8969E-01	62	.9960E+00	70	.1754E+03	71	.1850E+04
73	-.2052E+05	78	.1492E+03	83	.9200E+04	84	.8655E+05	85	.9126E+05	88	.2953E+04	89	.1000E+00
90	.3220E+02	91	.6398E+03	92	.1000E+02	95	.3035E+00	96	.9640E+04	117	.3750E+03	118	.2500E-01
119	.4300E+00	120	.2600E-01	121	-.1457E+00	122	-.1700E-01	123	.2700E+03	124	.2700E+03	125	.1000E+04
128	.1178E+02	129	.5000E+01	131	.1000E+01	132	.1000E+00	134	.1000E+00	138	.1500E+02	142	.7000E+01
145	.1000E+01	146	.1000E+04	147	.1000E-02	148	.1000E-02	149	.1000E-01	151	.3220E+02	152	.3627E-01
154	.3099E+00	156	.1926E-03	161	.9990E+00	163	.4489E-01	170	.1200E+02	171	.9000E+01	172	.3000E+01
177	-.5514E-01	183	.7727E+00	189	.2100E+02	197	.3567E+02	201	.1000E+00	202	.1000E+00	203	.1000E+02
204	.2000E-01	205	.2000E-01	206	.1000E+03	207	.1000E+00	208	.5000E+00	209	.1000E+01	210	.2000E-01
211	.1000E+03	212	.1000E+03	221	.2000E-01	222	.2000E-01	223	.2000E-01	224	.2500E-02	225	.2000E-01
226	.2000E-01	227	.5000E-01	228	.1000E+00	229	.1000E-01	265	.2500E-01	266	.5000E-01	283	.2500E+00
330	-.1400E+00	331	-.4370E+00	333	.5230E+00	334	.8730E-01	335	.2000E+01	485	.9000E+01	486	.1000E-06
498	.1000E+01	700	.5146E+01	703	-.3361E-13	705	.9879E-01	706	.5146E+01	709	.3118E+03	801	.3104E+04
802	.3216E+04	803	.3581E-01	805	.4675E-03	806	-.4639E-01	807	-.1236E-01	808	-.1113E+01	809	.4379E+00
810	.6210E-01	811	.5838E-03	812	.9690E+03	813	.2025E-01	814	.2183E+00	815	.3099E+00	817	-.1321E+00
818	-.1401E+00	819	.2541E-01	820	-.3323E+00	821	.6057E-01	822	.4964E+00	823	-.5135E-02	824	-.4870E+01
825	-.6800E+00	826	-.1753E+00	828	.3035E+00	829	.9200E+04	830	.8655E+05	831	.9126E+05	832	.2953E+04
833	.1751E+00	834	-.3256E+00	835	-.1930E-01	836	.1162E-01	837	-.1131E+00	838	.2810E-01	861	.1000E+01
862	.1000E+02	863	.5000E+00	901	.4200E+02	902	.4400E+02	903	.8000E+01	904	.3200E+02	905	.3300E+02
906	.3000E+01	907	.4300E+02	908	.9000E+01	909	.7000E+01	910	.3100E+02	911	.4000E+01	912	.2000E+01
913	.1000E+01	914	.2000E+01	915	.3000E+01	916	.4000E+01	917	.5000E+01	918	.6000E+01	919	.7000E+01
920	.8000E+01	921	.9000E+01	922	.1000E+02	923	.1100E+02	924	.1200E+02	925	.1810E+03	926	.1820E+03
927	.1840E+03	928	.1770E+03	929	.1790E+03	930	.1780E+03	931	.1760E+03	932	.1800E+03	933	.1830E+03
934	.1010E+03	935	.1020E+03	936	.1030E+03	937	.1300E+02	938	.1400E+02	939	.1500E+02	940	.1600E+02
941	.1700E+02	942	.1800E+02	943	.1900E+02	944	.2000E+02	945	.2100E+02	961	.1295E+05	962	.9300E+05
963	.1010E+06	964	.2080E+04	965	.5839E+03	966	.5000E+00						

LINEAR DYNAMICS

F MATRIX(12X12)

-1.97	.882E-01	-.448E-01	0.	0.	0.	.343E-01	0.	0.	0.	0.	0.
-.753E-01	-.190	.416E-02	0.	0.	0.	.107	0.	0.	0.	0.	0.
69.7	-771.	-.148	32.1	0.	0.	0.	0.	0.	0.	0.	0.
1.00	.901E-01	0.	0.	0.	0.	0.	0.	0.	0.	0.	0.
0.	1.00	0.	0.	0.	0.	0.	0.	0.	0.	0.	0.
0.	0.	1.000	-69.5	775.	0.	0.	0.	0.	0.	0.	0.
0.	-.111	0.	0.	0.	0.	-.378	-.510E-02	.576E-03	0.	-.152E-06	0.
0.	0.	0.	0.	0.	0.	.772.	-.574	-.461E-01	-2.89	.154E-02	0.
0.	0.	0.	0.	0.	0.	-.69.5	-.420E-02	-.180E-02	-32.1	-.144E-03	0.
0.	0.	0.	0.	0.	0.	1.000	0.	0.	0.	0.	0.
0.	0.	0.	0.	0.	0.	0.	-.996	.897E-01	775.	0.	0.
0.	0.	0.	0.	0.	0.	0.	.897E-01	.996	0.	0.	0.

G1 MATRIX(12X 9)

15.7	6.30	8.97	0.	0.	0.	0.	0.	0.			
.807	-2.70	.290	0.	0.	0.	0.	0.	0.			
2.08	22.4	0.	0.	0.	0.	0.	0.	0.			
0.	0.	0.	0.	0.	0.	0.	0.	0.			
0.	0.	0.	0.	0.	0.	0.	0.	0.			
0.	0.	0.	0.	0.	0.	0.	0.	0.			
0.	0.	0.	-9.05	-1.30	-1.57	-.103E-01	-.152	.260E-04			
0.	0.	0.	-62.7	-43.9	13.9	-.722	-2.89	0.			
0.	0.	0.	-.440	5.23	3.53	-2.26	-2.32	4.85			
0.	0.	0.	0.	0.	0.	0.	0.	0.			
0.	0.	0.	0.	0.	0.	0.	0.	0.			
0.	0.	0.	0.	0.	0.	0.	0.	0.			
0.	0.	0.	0.	0.	0.	0.	0.	0.			
0.	0.	0.	0.	0.	0.	0.	0.	0.			

G2 MATRIX(12X 3)

ROW 1	0.	0.
ROW 2	-.4477E-01	0.
ROW 3	.4160E-02	0.
ROW 4	-.1477E+00	0.
ROW 5	0.	0.
ROW 6	0.	0.
ROW 7	0.	0.
ROW 8	.5762E-03	-.5100E-02
ROW 9	-.4606E-01	-.5738E+00
ROW 10	-.1803E-02	-.4200E-02
ROW 11	0.	0.
ROW 12	0.	0.

HX MATRIX(9X12)

0.	0.	.129E-02	0.	0.	0.	0.	0.	0.	0.	0.	0.	0.
.147	1.04	-.148	0.	0.	0.	0.	0.	0.	0.	0.	0.	0.
0.	0.	0.	0.	0.	0.	0.	.128E-02	-.116E-03	0.	0.	0.	0.
0.	0.	0.	0.	0.	0.	0.	-.574	-.461E-01	0.	.154E-02	0.	0.
0.	0.	0.	0.	0.	0.	0.	.897E-01	.996	0.	0.	0.	0.
0.	0.	0.	0.	0.	0.	0.	-.741E-06	-.822E-05	0.	0.	0.	0.
0.	0.	0.	0.	0.	0.	0.	.544E-02	-.349E-03	0.	0.	0.	0.
0.	0.	0.	0.	0.	0.	0.	-.637E-05	-.707E-04	0.	.890E-06	0.	0.
0.	0.	0.	0.	0.	0.	0.	.932E-03	-.585E-04	0.	0.	0.	0.

HW MATRIX(9X 9)

0.	0.	0.	0.	0.	0.	0.	0.	0.
2.08	22.4	0.	0.	0.	0.	0.	0.	0.
0.	0.	0.	0.	0.	0.	0.	0.	0.
0.	0.	0.	-62.7	-43.9	13.9	-.722	-2.89	0.
0.	0.	0.	0.	0.	0.	0.	0.	0.
0.	0.	0.	0.	0.	0.	0.	0.	0.
0.	0.	0.	.607	.430	-.132	.501E-02	.260E-01	0.
0.	0.	0.	0.	0.	0.	0.	0.	0.
0.	0.	0.	.590E-01	-.124E-01	-.464E-01	.226E-01	.250E-01	0.

HW MATRIX(9X 3)

ROW 1	0.	.1290E-02	0.
ROW 2	0.	-.1477E+00	0.
ROW 3	-.1157E-03	0.	.1285E-02
ROW 4	-.4606E-01	0.	-.5738E+00
ROW 5	.9960E+00	0.	.8969E-01
ROW 6	-.8223E-05	0.	-.7405E-06
ROW 7	-.3487E-03	0.	.5437E-02
ROW 8	-.7072E-04	0.	-.6368E-05
ROW 9	-.5846E-04	0.	.9322E-03

EIGENVALUES OF FREE A/C

REAL	IMAG	DAMPING	FREQ
-.293043E-14	0.		
-.215971E-13	0.		
-.215971E-13	0.		
-.340864E-02	0.		
-.209953E-01	0.		
-.404327E-02	.759206E-01	.534435E-01	.760293E-01
-.470705E+00	.198737E+01	.230472E+00	.204236E+01
-.178232E+01	0.		
-.254189E+00	.245568E+01	.102960E+00	.246880E+01

EIGENVALUES FOR LATERAL AXES

REAL	IMAG	DAMPING	FREQ
.927036E-14	0.		
.927036E-14	0.		
-.209797E-01	0.		
-.178297E+01	0.		
-.253783E+00	.245161E+01	.102967E+00	.246471E+01

EIGENVALUES FOR PITCH AXIS

REAL	IMAG	DAMPING	FREQ
.133227E-13	0.		
-.340885E-02	0.		
-.397153E-02	.759785E-01	.522004E-01	.760823E-01
-.470886E+00	.198969E+01	.230301E+00	.204465E+01

NOMINAL TRAJECTORY PARAMETERS (T= 0.00)

NX = 12

NU = 9

NW = 3

NY = 9

APERI = .1000E+01

X3 VECTOR

0. 0. 0. 0. 0. 0. 0. .6203E+02 .8698E+03 .7119E-01
.4000E+05 0.

U3 VECTOR

0. 0. 0. -.4794E-01 0. 0. 0. 0. .6575E+00

W3 VECTOR

0. 0. 0.

YN VECTOR

0. 0. .7119E-01 -.3212E+02 .8721E+03 .4870E+00 .2457E+00 .1940E+00 .2529E-01

DYNAMIC PRESSURE = .22199E+03

MACH = .90

ANGLE-OF-ATTACK = 4.08

F8-SIM

FLIGHT CONDITION 16

LINEAR DYNAMICS

F MATRIX(12X12)

-2.69	.978E-02	-.498E-01	0.	0.	0.	.292E-01	0.	0.	0.	0.	0.
-.100	-.225	.553E-02	0.	0.	0.	.908E-01	0.	0.	0.	0.	0.
62.1	-.869	-.166	32.1	0.	0.	0.	0.	0.	0.	0.	0.
1.00	.713E-01	0.	0.	0.	0.	0.	0.	0.	0.	0.	0.
0.	1.00	0.	0.	0.	0.	0.	0.	0.	0.	0.	0.
0.	0.	1.000	-62.0	872.	0.	0.	0.	0.	0.	0.	0.
0.	-.998E-01	0.	0.	0.	0.	-.448	-.988E-02	-.791E-03	0.	0.	0.
0.	0.	0.	0.	0.	0.	870.	-.698	-.489E-01	-2.29	.154E-02	0.
0.	0.	0.	0.	0.	0.	-62.0	-.317E-01	-.106E-01	-32.1	-.116E-03	0.
0.	0.	0.	0.	0.	0.	1.000	0.	0.	0.	0.	0.
0.	0.	0.	0.	0.	0.	0.	-.997	.711E-01	872.	0.	0.
0.	0.	0.	0.	0.	0.	0.	.711E-01	.997	0.	0.	0.

G1 MATRIX(12X 9)

19.4	7.31	11.1	0.	0.	0.	0.	0.	0.	G2 MATRIX(12X 3)		
1.04	-3.16	.360	0.	0.	0.	0.	0.	0.	ROW 1	0.	0.
3.01	25.3	0.	0.	0.	0.	0.	0.	0.	ROW 2	-.4976E-01	0.
0.	0.	0.	0.	0.	0.	0.	0.	0.	ROW 3	.5528E-02	0.
0.	0.	0.	0.	0.	0.	0.	0.	0.	ROW 4	-.1661E+00	0.
0.	0.	0.	0.	0.	0.	0.	0.	0.	ROW 5	0.	0.
0.	0.	0.	0.	0.	0.	0.	0.	0.	ROW 6	0.	0.
0.	0.	0.	-11.0	-1.65	-2.89	-.216E-01	-.192	.235E-04	ROW 7	0.	0.
0.	0.	0.	-84.8	-55.8	21.0	-1.06	-3.61	0.	ROW 8	-.7910E-03	-.9876E-02
0.	0.	0.	.225	3.45	.986	-2.88	-3.00	5.02	ROW 9	-.4892E-01	0.
0.	0.	0.	0.	0.	0.	0.	0.	0.	ROW 10	-.1063E-01	0.
0.	0.	0.	0.	0.	0.	0.	0.	0.	ROW 11	0.	0.
0.	0.	0.	0.	0.	0.	0.	0.	0.	ROW 12	0.	0.

LIST OF NON-ZERO ELEMENTS IN A(I), THRU, A(1000)

4	.4000E+05	5	.9000E+00	7	.8698E+03	9	.6203E+02	10	.8698E+03	12	.6203E+02	13	.8721E+03
15	-.9095E-12	16	.8721E+03	17	.1166E-02	19	.2841E-03	20	.2292E+01	22	-.3212E+02	23	.2292E+01
25	-.3212E+02	28	-.1043E-14	29	.7119E-01	31	.7119E-01	37	.2298E-06	46	-.7520E-04	51	.1000E+01
54	.9975E+00	56	.7113E-01	58	.1000E+01	60	-.7113E-01	62	.9975E+00	70	.2220E+03	71	.1466E+04
73	-.2055E+05	78	-.6508E+01	83	.9200E+04	84	.8655E+05	85	.9126E+05	88	.2953E+04	89	.1000E+00
90	.3220E+02	91	-.6398E+03	92	.1000E+02	95	.3035E+00	96	.8203E+04	117	.3750E+03	118	.2500E-01
119	.4300E+00	120	.2600E-01	121	-.1457E+00	122	-.1700E-01	123	.2700E+03	124	.2700E+03	125	.1000E+04
128	.1178E+02	129	.5900E+01	131	.1000E+01	132	.1000E+00	134	.1000E+00	138	.1600E+02	142	.7000E-01
145	.1000E+01	146	.1000E+04	147	.1000E-02	148	.1000E-02	149	.1000E-01	151	.3220E+02	152	.2529E-01
154	.2457E+00	156	-.6637E-05	161	.9994E+00	163	.3559E-01	170	.1200E+02	171	.9000E+01	172	.3000E+01
177	-.4794E-01	183	.6575E+00	189	.2100E+02	197	.3567E+02	201	.1000E+00	202	.1000E+00	203	.1000E+02
204	.2000E-01	205	.2000E-01	206	.1000E+03	207	.1000E+00	208	.5000E+00	209	.1000E+01	210	.2000E-01
211	.1000E+03	212	.1000E+03	221	.2000E-01	222	.2000E-01	223	.2000E-01	224	.2500E-02	225	.2000E-01
225	.2000E-01	227	.5000E-01	228	.1000E+00	229	.1000E-01	265	.2500E-01	266	.5000E-01	283	.2500E+00
330	-.1400E+00	331	-.4370E+00	333	.5230E+00	334	.8730E-01	335	.2000E+01	485	.9000E+01	486	.1000E-06
498	.1000E+01	700	.4079E+01	703	-.5976E-13	705	-.4308E-02	706	.4079E+01	709	.1317E-04	801	.3211E+04
802	.2895E+04	803	.2550E-01	805	-.2053E-03	806	-.1904E-01	807	.4064E-02	808	-.1113E+01	809	-.4471E+00
810	.4041E-01	811	.5838E-03	812	.9690E+03	813	.2312E-01	814	.1948E+00	815	.2457E+00	817	-.1605E+00
818	-.1392E+00	819	.1244E-01	820	-.4022E+00	821	.5920E-01	822	.4870E+00	823	-.4247E-02	824	-.5100E+01
825	-.7500E+00	826	-.1839E+00	828	.3035E+00	829	.9200E+04	830	.8655E+05	831	.9126E+05	832	.2953E+04
833	.1974E+00	834	-.3392E+00	835	-.2016E-01	836	.1265E-01	837	-.1045E+00	838	.2581E-01	861	.1000E+01
862	.1000E+02	863	.5000E+00	901	.4200E+02	902	.4400E+02	903	.8000E+01	904	.3200E+02	905	.3300E+02
906	.3000E+01	907	.4300E+02	908	.9000E+01	909	.7000E+01	910	.3100E+02	911	.4000E+01	912	.2000E+01
913	.1000E+01	914	.2000E+01	915	.3000E+01	916	.4000E+01	917	.5000E+01	918	.6000E+01	919	.7000E+01
920	.8000E+01	921	.9000E+01	922	.1000E+02	923	.1100E+02	924	.1200E+02	925	.1810E+03	926	.1820E+03
927	.1840E+03	928	.1770E+03	929	.1790E+03	930	.1780E+03	931	.1760E+03	932	.1800E+03	933	.1830E+03
934	.1010E+03	935	.1020E+03	936	.1030E+03	937	.1300E+02	938	.1400E+02	939	.1500E+02	940	.1600E+02
941	.1700E+02	942	.1800E+02	943	.1900E+02	944	.2000E+02	945	.2100E+02	961	.1295E+05	962	.9300E+05
963	.1010E+06	964	.2080E+04	965	.5839E+03	966	.5000E+00						

HX MATRIX(9X12)

0.	0.	.115E-02	0.	0.	0.	0.	0.	0.	0.	0.	0.
.108	1.19	-.166	0.	0.	0.	0.	0.	0.	0.	0.	0.
0.	0.	0.	0.	0.	0.	0.	.114E-02	-.816E-04	0.	0.	0.
0.	0.	0.	0.	0.	0.	0.	-.698	-.489E-01	0.	.154E-02	0.
0.	0.	0.	0.	0.	0.	0.	.711E-01	.997	0.	0.	0.
0.	0.	0.	0.	0.	0.	0.	-.172E-04	-.241E-03	0.	0.	0.
0.	0.	0.	0.	0.	0.	0.	.526E-02	-.192E-03	0.	0.	0.
0.	0.	0.	0.	0.	0.	0.	-.345E-04	-.484E-03	0.	.115E-05	0.
0.	0.	0.	0.	0.	0.	0.	.902E-03	.389E-04	0.	0.	0.

HU MATRIX(9X 9)

0.	0.	0.	0.	0.	0.	0.	0.	0.
3.01	25.3	0.	0.	0.	0.	0.	0.	0.
0.	0.	0.	0.	0.	0.	0.	0.	0.
0.	0.	0.	-84.8	-55.8	21.0	-1.06	-3.61	0.
0.	0.	0.	0.	0.	0.	0.	0.	0.
0.	0.	0.	0.	0.	0.	0.	0.	0.
0.	0.	0.	.650	.430	-.160	.653E-02	.260E-01	0.
0.	0.	0.	0.	0.	0.	0.	0.	0.
0.	0.	0.	.446E-01	.406E-02	-.190E-01	.226E-01	.250E-01	0.

HW MATRIX(9X 3)

ROW 1	0.	.1147E-02	0.
ROW 2	0.	-.1661E+00	0.
ROW 3	-.8157E-04	0.	.1144E-02
ROW 4	-.4892E-01	0.	-.6977E+00
ROW 5	.9975E+00	0.	.7113E-01
ROW 6	-.2406E-03	0.	-.1718E-04
ROW 7	-.1916E-03	0.	.5263E-02
ROW 8	-.4836E-03	0.	-.3450E-04
ROW 9	.3894E-04	0.	.9022E-03

EIGENVALUES OF FREE A/C

REAL	IMAG	DAMPING	FREQ
0.	0.		
-.578843E-13	0.		
-.578843E-13	0.		
-.242066E-02	0.		
-.160739E-01	0.		
.103787E-03	.349764E-01	.296734E-02	.349765E-01
-.572727E+00	.292232E+01	.192325E+00	.297791E+01
-.259571E+00	.275005E+01	.939700E-01	.276227E+01
-.255204E+01	0.		

EIGENVALUES FOR LATERAL AXES

REAL	IMAG	DAMPING	FREQ
.546785E-14	0.		
.546785E-14	0.		
-.160681E-01	0.		
-.255227E+01	0.		
-.255266E+00	.275091E+01	.923965E-01	.276273E+01

EIGENVALUES FOR PITCH AXIS

REAL	IMAG	DAMPING	FREQ
.108386E-12	0.		
-.242086E-02	0.		
.129027E-03	.349842E-01	.368813E-02	.349844E-01
-.576944E+00	.292058E+01	.193799E+00	.297702E+01

NOMINAL TRAJECTORY PARAMETERS(T= 0.00)

NX = 12
 NU = 9
 NW = 3
 NY = 9

APERT = .1000E+01

X3 VECTOR

0. 0. 0. 0. 0. 0. 0. .2912E+02 .2092E+03 .1383E+00
 0. 0.

U3 VECTOR

0. 0. 0. -.2500E+00 .3490E+00 .4370E+00 0. .1000E+01 .3647E+00

W3 VECTOR

0. 0. 0.

YN VECTOR

0. 0. .1383E+00 -.3199E+02 .2112E+03 .5443E+00 .9363E+00 .2349E+00 .1746E+00

DYNAMIC PRESSURE = .52891E+02
 MACH = .19
 ANGLE-OF-ATTACK = 7.93

F8-SIM

FLIGHT CONDITION 17

LIST OF NON-ZERO ELEMENTS IN A(1), THRU, A(1000)

5	.1890E+00	7	.2092E+03	9	.2912E+02	10	.2092E+03	12	.2912E+02	13	.2112E+03	15	-.4547E-12
16	.2112E+03	17	-.6721E-01	19	-.9289E-01	20	.4372E+01	22	-.3199E+02	23	.4372E+01	25	-.3199E+02
28	-.2153E-14	29	.1383E+00	31	.1383E+00	37	-.3917E-03	46	-.6258E-02	51	.1000E+01	54	.9904E+00
56	.1379E+00	58	.1000E+01	60	-.1379E+00	62	.9904E+00	70	.5289E+02	71	.2580E+04	73	-.1887E+05
78	-.5326E+03	83	.9011E+04	84	.8511E+05	85	.8973E+05	88	.2569E+04	89	.1000E+00	90	.3220E+02
91	.5900E+03	92	.1000E+02	95	.3354E+00	96	.4551E+04	117	.3750E+03	118	.2500E-01	119	.4300E+00
120	.2600E-01	121	-.1457E+00	122	-.1700E-01	123	.2700E+03	124	.2700E+03	125	.1000E+04	128	.1178E+02
129	.5000E+01	131	.1000E+01	132	.1000E+00	134	.1000E+00	138	.1700E+02	142	.7000E+01	145	.1000E+01
146	.1000E+04	147	.1000E-02	148	.1000E-02	149	.1000E-01	151	.3220E+02	152	.1746E+00	154	.9363E+00
156	-.2280E-02	161	.9976E+00	163	.6910E-01	170	.1200E+02	171	.9000E+01	172	.3000E+01	177	-.2500E+00
178	.4370E+00	179	.3490E+00	180	.1000E+01	183	.3647E+00	189	.2300E+01	190	.1000E+01	197	.3567E+02
201	.1000E+00	202	.1000E+00	203	.1000E+02	204	.2000E-01	205	.2000E-01	206	.1000E+03	207	.1000E+00
208	.5000E+00	209	.1000E+01	210	.2000E-01	211	.1000E+03	212	.1000E+03	221	.2000E-01	222	.2000E-01
223	.2000E-01	224	.2500E-02	225	.2000E-01	226	.2000E-01	227	.5000E-01	228	.1000E+00	229	.1000E-01
265	.2500E-01	266	.5900E-01	283	.2500E+00	330	-.1400E+00	331	-.4370E+00	333	.5230E+00	334	.8730E-01
335	.2000E+01	485	.9090E+01	486	.1000E-06	498	.1000E+01	700	.7925E+01	703	-.1234E-12	705	-.3585E+00
736	.7925E+01	769	-.2245E-01	801	.9457E+04	802	.5042E+04	803	.1996E+00	805	.6629E-02	806	-.8564E-01
807	-.5514E-01	808	-.1239E+01	809	.2820E+00	810	.3705E+00	811	.2372E-02	812	.1117E+04	813	.2153E-01
814	.2349E+00	815	.8253E+00	817	-.1488E+00	818	-.2093E+00	819	.1523E+00	820	-.2935E+00	821	.3695E-01
822	.5443E+00	823	-.1054E+00	824	-.4020E+01	825	-.6000E+00	826	-.6940E-01	828	.3354E+00	829	.9011E+04
830	.8511E+05	831	.8973E+05	832	.2569E+04	833	.1392E+00	834	-.3104E+00	835	-.3239E-01	836	-.7228E-02
837	-.1220E+00	838	.2542E-01	861	.1000E+01	862	.1000E+02	863	.5000E+00	901	.4200E+02	902	.4400E+02
903	.8000E+01	904	.3200E+02	905	.3300E+02	906	.3000E+01	907	.4300E+02	908	.9000E+01	909	.7000E+01
910	.3100E+02	911	.4000E+01	912	.2000E+01	913	.1000E+01	914	.2000E+01	915	.3000E+01	916	.4000E+01
917	.5000E+01	918	.6000E+01	919	.7000E+01	920	.8000E+01	921	.9000E+01	922	.1000E+02	923	.1100E+02
924	.1200E+02	925	.1810E+03	926	.1820E+03	927	.1840E+03	928	.1770E+03	929	.1790E+03	930	.1780E+03
931	.1760E+03	932	.1800E+03	933	.1830E+03	934	.1010E+03	935	.1020E+03	936	.1030E+03	937	.1300E+02
938	.1400E+02	939	.1500E+02	940	.1600E+02	941	.1700E+02	942	.1800E+02	943	.1900E+02	944	.2000E+02
945	.2100E+02	961	.1295E+05	962	.9300E+05	963	.1010E+06	964	.2080E+04	965	.5839E+03	966	.5000E+00

LINEAR DYNAMICS

F MATRIX(12X12)

-1.97	.959	-.770E-01	0.	0.	0.	.146E-01	0.	0.	0.	0.	0.
-.779E-01	-.179	.322E-02	0.	0.	0.	.511E-01	0.	0.	0.	0.	0.
30.2	-208.	-.198	31.9	0.	0.	0.	0.	0.	0.	0.	0.
1.00	.139	0.	0.	0.	0.	0.	0.	0.	0.	0.	0.
0.	1.01	0.	0.	0.	0.	0.	0.	0.	0.	0.	0.
0.	0.	1.000	-29.1	211.	0.	0.	0.	0.	0.	0.	0.
0.	-.535E-01	0.	0.	0.	0.	-.354	-.297E-02	.111E-03	0.	-.175E-06	0.
0.	0.	0.	0.	0.	0.	209.	-.501	-.234	-4.44	.938E-03	0.
0.	0.	0.	0.	0.	0.	-29.1	.162	-.406E-01	-31.9	-.139E-04	0.
0.	0.	0.	0.	0.	0.	1.000	0.	0.	0.	0.	0.
0.	0.	0.	0.	0.	0.	0.	-.990	.138	211.	0.	0.
0.	0.	0.	0.	0.	0.	0.	.138	.990	0.	0.	0.

G1 MATRIX(12X 9)

2.91	1.74	3.02	0.	0.	0.	0.	0.	0.	G2 MATRIX(12X 3)		
.263E-01	-.912	.865E-01	0.	0.	0.	0.	0.	0.	ROW 1	0.	0.
.724	7.90	0.	0.	0.	0.	0.	0.	0.	ROW 2	-.7701E-01	0.
0.	0.	0.	0.	0.	0.	0.	0.	0.	0.	.3222E-02	0.
0.	0.	0.	0.	0.	0.	0.	0.	0.	ROW 3	0.	0.
0.	0.	0.	0.	0.	0.	0.	0.	0.	ROW 4	-.1976E+00	0.
0.	0.	0.	0.	0.	0.	0.	0.	0.	0.	0.	0.
0.	0.	0.	0.	0.	0.	0.	0.	0.	ROW 5	0.	0.
0.	0.	0.	0.	0.	0.	0.	0.	0.	0.	0.	0.
0.	0.	0.	-1.86	-.397	-.192	-.102E-01	-.465E-01	.481E-03	ROW 6	0.	0.
0.	0.	0.	-17.0	-14.1	5.35	-.171	-.982	0.	0.	.1110E-03	0.
0.	0.	0.	3.75	3.83	2.16	-.738	-.712	16.0	ROW 7	0.	-.2972E-02
0.	0.	0.	0.	0.	0.	0.	0.	0.	ROW 8	-.2337E+00	0.
0.	0.	0.	0.	0.	0.	0.	0.	0.	ROW 9	0.	-.5012E+00
0.	0.	0.	0.	0.	0.	0.	0.	0.	0.	-.4057E-01	0.
0.	0.	0.	0.	0.	0.	0.	0.	0.	ROW 10	0.	.1618E+00
0.	0.	0.	0.	0.	0.	0.	0.	0.	0.	0.	0.
0.	0.	0.	0.	0.	0.	0.	0.	0.	ROW 11	0.	0.
0.	0.	0.	0.	0.	0.	0.	0.	0.	0.	0.	0.
0.	0.	0.	0.	0.	0.	0.	0.	0.	ROW 12	0.	0.
									0.	0.	0.

HX MATRIX (9X12)

0.	0.	.473E-02	0.	0.	0.	0.	0.	0.	0.	0.	0.
1.05	.800	-.198	0.	0.	0.	0.	0.	0.	0.	0.	0.
0.	0.	0.	0.	0.	0.	0.	.469E-02	-.653E-03	0.	0.	0.
0.	0.	0.	0.	0.	0.	0.	-.501	-.234	0.	.938E-03	0.
0.	0.	0.	0.	0.	0.	0.	.138	.990	0.	0.	0.
0.	0.	0.	0.	0.	0.	0.	0.	0.	0.	0.	0.
0.	0.	0.	0.	0.	0.	0.	.134E-01	-.194E-02	0.	0.	0.
0.	0.	0.	0.	0.	0.	0.	0.	0.	0.	0.	0.
0.	0.	0.	0.	0.	0.	0.	.145E-02	-.143E-03	0.	0.	0.

HU MATRIX (9X 9)

0.	0.	0.	0.	0.	0.	0.	0.	0.
.724	7.90	0.	0.	0.	0.	0.	0.	0.
0.	0.	0.	0.	0.	0.	0.	0.	0.
0.	0.	0.	-17.0	-16.1	5.35	-.171	-.982	0.
0.	0.	0.	0.	0.	0.	0.	0.	0.
0.	0.	0.	0.	0.	0.	0.	0.	0.
0.	0.	0.	.515	.430	-.149	.202E-02	.260E-01	0.
0.	0.	0.	0.	0.	0.	0.	0.	0.
0.	0.	0.	-.410E-01	-.551E-01	-.856E-01	.224E-01	.250E-01	0.

HW MATRIX (9X 3)

ROW 1	0.	.4731E-02	0.
ROW 2	0.	-.1976E+00	0.
ROW 3	-.6528E-03	0.	.4690E-02
ROW 4	-.2337E+00	0.	-.5012E+00
ROW 5	.9904E+00	0.	.1379E+00
ROW 6	0.	0.	0.
ROW 7	-.1943E-02	0.	.1339E-01
ROW 8	0.	0.	0.
ROW 9	-.1427E-03	0.	.1445E-02

EIGENVALUES OF FREE A/C

REAL	IMAG	DAMPING	FREQ
-.108214E-13	0.		
-.465960E-13	0.		
-.465960E-13	0.		
-.583330E-03	0.		
-.548778E-01	0.		
-.189253E-01	.170831E+00	.104932E+00	.171780E+00
-.429620E+00	.794587E+00	.475614E+00	.903295E+00
-.234744E+00	.167694E+01	.138632E+00	.169329E+01
-.182000E+01	0.		

EIGENVALUES FOR LATERAL AXES

REAL	IMAG	DAMPING	FREQ
.754952E-14	0.		
.754952E-14	0.		
-.549737E-01	0.		
-.182021E+01	0.		
-.234807E+00	.167653E+01	.138702E+00	.169289E+01

EIGENVALUES FOR PITCH AXIS

REAL	IMAG	DAMPING	FREQ
-.107553E-15	0.		
-.583322E-03	0.		
-.176054E-01	.170820E+00	.102621E+00	.171725E+00
-.429822E+00	.794093E+00	.476016E+00	.902956E+00

NOMINAL TRAJECTORY PARAMETERS(IT= 0.00)

NX = 12
NU = 9
NW = 3
NY = 9
APERT = .1000E+01

X3 VECTOR

0. 0. 0. 0. 0. 0. 0. .1340E+02 .2444E+03 .5478E-01
0. 0.

U3 VECTOR

0. 0. 0. -.2247E+00 .3490E+00 .4370E+00 0. .1000E+01 .4524E+00

W3 VECTOR

0. 0. 0.

YN VECTOR

0. 0. .5478E-01 -.3215E+02 .2447E+03 .5443E+00 .7046E+00 .2349E+00 .1589E+00

DYNAMIC PRESSURE = .71014E+02

MACH = .22

ANGLE-OF-ATTACK = 3.14

F8-SIN

FLIGHT CONDITION 18

LIST OF NON-ZERO ELEMENTS IN A(1), THRU, A(1000)

5	.2190E+00	7	.2444E+03	9	.1340E+02	10	.2444E+03	12	.1340E+02	13	.2447E+03	15	-.5684E-13
16	.2447E+03	17	.2693E-02	19	.6371E-02	20	.1766E+01	22	-.3215E+02	23	.1756E+01	25	-.3215E+02
28	-.2323E-15	29	.5478E-01	31	.5478E-01	37	.2539E-04	46	.5088E-03	51	.1000E+01	54	.9985E+00
56	.5475E-01	58	.1000E+01	60	-.5475E-01	62	.9985E+00	70	.7101E+02	71	.1042E+04	73	-.1897E+05
78	.4331E+02	83	.9011E+04	84	.8511E+05	85	.8973E+05	88	.2569E+04	89	.1000E+00	90	.3220E+02
91	.5900E+03	92	.1000E+02	95	.3354E+00	96	.5644E+04	117	.3750E+03	118	.2500E-01	119	.4300E+00
120	.2600E-01	121	-.1457E+00	122	-.1700E-01	123	.2700E+03	124	.2700E+03	125	.1000E+04	128	.1178E+02
129	.5000E+01	131	.1000E+01	132	.1000E+00	134	.1000E+00	138	.1800E+02	142	.7000E+01	145	.1000E+01
146	.1000E+04	147	.1000E-02	148	.1000E-02	149	.1000E-01	151	.3220E+02	152	.1589E+00	154	.7046E+00
156	.1381E-03	161	.9996E+00	163	.2738E-01	170	.1200E+02	171	.9000E+01	172	.3000E+01	177	-.2247E+00
178	.4370E+00	179	.3490E+00	180	.1000E+01	183	.4524E+00	189	.2300E+01	190	.1000E+01	197	.3567E+02
201	.1000E+00	202	.1000E+00	203	.1000E+02	204	.2000E-01	205	.2000E-01	206	.1000E+03	207	.1000E+00
208	.5000E+00	209	.1000E+01	210	.2000E-01	211	.1000E+03	212	.1000E+03	221	.2000E-01	222	.2000E-01
223	.2000E-01	224	.2500E-02	225	.2000E-01	226	.2000E-01	227	.5000E-01	228	.1000E+00	229	.1000E-01
265	.2500E-01	266	.5000E-01	283	.2500E+00	330	-.1400E+00	331	-.4370E+00	333	.5230E+00	334	.8730E-01
335	.2000E+01	485	.9000E+01	486	.1000E-06	498	.1000E+01	700	.3138E+01	703	-.1331E-13	705	.2915E-01
766	.3138E+01	709	.1455E-02	801	.9369E+04	802	.4829E+04	803	.1208E+00	805	.1169E+01	806	-.2618E-02
807	.7137E-02	808	-.1316E+01	809	.3428E+00	810	.2823E+00	811	.2372E-02	812	.1117E+04	813	.2290E-01
814	.2349E+00	815	.5904E+00	817	-.1416E+00	818	-.2106E+00	819	.1281E+00	820	-.3130E+00	821	.4928E-01
822	.5443E+00	823	.1102E+00	824	.4020E+01	825	.6000E+00	826	-.8126E-01	828	.3354E+00	829	.9011E+04
830	.8511E+05	831	.8973E+05	832	.2569E+04	833	.1870E+00	834	-.2939E+00	835	-.2970E-01	836	-.8980E-02
837	-.1220E+00	838	.2649E-01	861	.1000E+01	862	.1000E+02	863	.5000E+00	901	.4200E+02	902	.4400E+02
903	.8000E+01	904	.3200E+02	905	.3300E+02	906	.3000E+01	907	.4300E+02	908	.9000E+01	909	.7000E+01
910	.3100E+02	911	.4000E+01	912	.2000E+01	913	.1000E+01	914	.2000E+01	915	.3000E+01	916	.4000E+01
917	.5000E+01	918	.6000E+01	919	.7000E+01	920	.8000E+01	921	.9000E+01	922	.1000E+02	923	.1100E+02
924	.1200E+02	925	.1810E+03	926	.1820E+03	927	.1840E+03	928	.1770E+03	929	.1790E+03	930	.1780E+03
931	.1760E+03	932	.1800E+03	933	.1830E+03	934	.1010E+03	935	.1020E+03	936	.1030E+03	937	.1300E+02
938	.1400E+02	939	.1500E+02	940	.1600E+02	941	.1700E+02	942	.1800E+02	943	.1900E+02	944	.2000E+02
945	.2100E+02	961	.1295E+05	962	.9300E+05	963	.1010E+06	964	.2080E+04	965	.5839E+03	966	.5000E+00

LINEAR DYNAMICS

F MATRIX(12X12)

-2.43	.927	-.092E-01	0.	0.	0.	.181E-01	0.	0.	0.	0.	0.
-.925E-01	-.200	.582E-02	0.	0.	0.	.634E-01	0.	0.	0.	0.	0.
14.3	-243.	-.243	32.1	0.	0.	0.	0.	0.	0.	0.	0.
1.00	.548E-01	0.	0.	0.	0.	0.	0.	0.	0.	0.	0.
0.	1.00	0.	0.	0.	0.	0.	0.	0.	0.	0.	0.
0.	0.	1.000	-13.4	245.	0.	0.	0.	0.	0.	0.	0.
0.	-.663E-01	0.	0.	0.	0.	-.410	-.664E-02	.168E-03	0.	-.386E-06	0.
0.	0.	0.	0.	0.	0.	244.	-.618	-.229	-1.76	.940E-03	0.
0.	0.	0.	0.	0.	0.	-13.4	.112	-.522E-01	-32.1	.877E-04	0.
0.	0.	0.	0.	0.	0.	1.000	0.	0.	0.	0.	0.
0.	0.	-0.	0.	0.	0.	0.	-.999	.547E-01	245.	0.	0.
0.	0.	0.	0.	0.	0.	0.	.547E-01	.999	0.	0.	0.

G1 MATRIX(12X 9)

4.25	2.44	4.05	0.	0.	0.	0.	0.	0.
.267E-01	-1.22	.116	0.	0.	0.	0.	0.	0.
1.03	10.6	0.	0.	0.	0.	0.	0.	0.
0.	0.	0.	0.	0.	0.	0.	0.	0.
0.	0.	0.	0.	0.	0.	0.	0.	0.
0.	0.	0.	0.	0.	0.	0.	0.	0.
0.	0.	0.	-2.41	-.533	-.301	.559E-02	-.624E-01	.189E-03
0.	0.	0.	-21.2	-19.4	6.39	-.363	-1.23	0.
0.	0.	0.	5.38	.741	-.232	-.995	-1.06	15.9
0.	0.	0.	0.	0.	0.	0.	0.	0.
0.	0.	0.	0.	0.	0.	0.	0.	0.
0.	0.	0.	0.	0.	0.	0.	0.	0.

G2 MATRIX(12X 3)

ROW 1	0.	0.
ROW 2	-.8916E-01	0.
ROW 3	.5822E-02	0.
ROW 4	-.2430E+00	0.
ROW 5	0.	0.
ROW 6	0.	0.
ROW 7	0.	0.
ROW 8	.1676E-03	-.6637E-02
ROW 9	-.2294E+00	-.6181E+00
ROW 10	-.5222E-01	.1118E+00
ROW 11	0.	0.
ROW 12	0.	0.

HX MATRIX(9X12)

0.	0.	.408E-02	0.	0.	0.	0.	0.	0.	0.	0.	0.
.929	1.13	-.243	0.	0.	0.	0.	0.	0.	0.	0.	0.
0.	0.	0.	0.	0.	0.	0.	.408E-02	-.224E-03	0.	0.	0.
0.	0.	0.	0.	0.	0.	0.	-.618	-.229	0.	.940E-03	0.
0.	0.	0.	0.	0.	0.	0.	.547E-01	.999	0.	0.	0.
0.	0.	0.	0.	0.	0.	0.	0.	0.	0.	0.	0.
0.	0.	0.	0.	0.	0.	0.	.128E-01	-.700E-03	0.	0.	0.
0.	0.	0.	0.	0.	0.	0.	0.	0.	0.	0.	0.
0.	0.	0.	0.	0.	0.	0.	.108E-02	-.650E-04	0.	0.	0.

HU MATRIX(9X 9)

0.	0.	0.	0.	0.	0.	0.	0.	0.
1.03	10.6	0.	0.	0.	0.	0.	0.	0.
0.	0.	0.	0.	0.	0.	0.	0.	0.
0.	0.	0.	-21.2	-19.4	6.39	-.363	-1.23	0.
0.	0.	0.	0.	0.	0.	0.	0.	0.
0.	0.	0.	0.	0.	0.	0.	0.	0.
0.	0.	0.	.476	.430	-.142	.682E-02	.260E-01	0.
0.	0.	0.	0.	0.	0.	0.	0.	0.
0.	0.	0.	-.933E-01	.714E-02	-.262E-02	.224E-01	.250E-01	0.

HW MATRIX(9X 3)

ROW 1	0.	.4084E-02	0.
ROW 2	0.	-.2430E+00	0.
ROW 3	-.2237E-03	0.	.4080E-02
ROW 4	-.2294E+00	0.	-.6181E+00
ROW 5	.9985E+00	0.	.5475E-01
ROW 6	0.	0.	0.
ROW 7	-.7001E-03	0.	.1285E-01
ROW 8	0.	0.	0.
ROW 9	-.6504E-04	0.	.1077E-02

EIGENVALUES OF FREE A/C

REAL	IMAG	DAMPING	FREQ
-.165970E-13	0.		
.148682E-12	0.		
.148682E-12	0.		
-.693571E-03	0.		
-.426089E-01	0.		
-.239632E-01	.166547E+00	.142416E+00	.168262E+00
-.515338E+00	.127012E+01	.375972E+00	.137068E+01
-.106407E+00	.179505E+01	.591741E-01	.179820E+01
-.261975E+01	0.		

EIGENVALUES FOR LATERAL AXES

REAL	IMAG	DAMPING	FREQ
.494049E-14	0.		
.494049E-14	0.		
-.426471E-01	0.		
-.105901E+00	.179406E+01	.589264E-01	.179718E+01
-.261986E+01	0.		

EIGENVALUES FOR PITCH AXIS

REAL	IMAG	DAMPING	FREQ
-.139778E-16	0.		
-.693562E-03	0.		
-.237182E-01	.166559E+00	.140979E+00	.168239E+00
-.516018E+00	.127020E+01	.376376E+00	.137102E+01

NOMINAL TRAJECTORY PARAMETERS(T= 0.00)

NX = 12

NU = 9

NM = 3

NY = 9

APERT = .1000E+01

X3 VECTOR

0.	0.	0.	0.	0.	0.	0.	0.	.2568E+02	.6948E+03	.3695E-01
.2000E+05	0.									

U3 VECTOR

0.	0.	0.	-.3129E-01	0.	0.	0.	0.	0.	.3425E+00	
----	----	----	------------	----	----	----	----	----	-----------	--

W3 VECTOR

0.	0.	0.								
----	----	----	--	--	--	--	--	--	--	--

YN VECTOR

0.	0.	.3695E-01	-.1643E+02	.6953E+03	.4974E+00	.9117E-01	.1951E+00	.1769E-01		
----	----	-----------	------------	-----------	-----------	-----------	-----------	-----------	--	--

DYNAMIC PRESSURE = .30544E+03

MACH = .67

ANGLE-OF-ATTACK = 2.12

F8-SIM

FLIGHT CONDITION 19

LIST OF NON-ZERO ELEMENTS IN A(1), THRU, A(1000)

4	.2000E+05	5	.6700E+00	7	.6948E+03	9	.2568E+02	10	.6948E+03	12	.2568E+02	13	.6953E+03
15	-.1137E-12	16	.6953E+03	17	-.6913E+00	19	.1575E+02	20	.4981E+00	22	-.1643E+02	23	.4981E+00
25	-.1643E+02	28	-.1635E-15	29	-.3695E-01	31	.3695E-01	37	.2267E-01	46	.3661E-02	51	.1000E+01
54	.9993E+00	56	.3694E-01	58	.1000E+01	60	-.3694E-01	62	.9993E+00	70	.3054E+03	71	.3187E+03
73	-.1051E+05	78	.3169E+03	83	.9200E+04	84	.8655E+05	85	.9126E+05	88	.2953E+04	89	.1000E+00
90	.3220E+02	91	.6398E+03	92	.1000E+02	95	.3035E+00	96	.4273E+04	117	.3750E+03	118	.2500E-01
119	.4300E+00	120	.2600E-01	121	-.1457E+00	122	-.1700E-01	123	.2700E+03	124	.2700E+03	125	.1000E+04
128	-.1178E+02	129	.5000E+01	131	.1000E+01	132	.1000E+00	134	.1000E+00	138	.1900E+02	142	.7000E+01
145	.1000E+01	146	.1000E+04	147	.1000E-02	148	.1000E-02	149	.1000E-01	151	.1610E+02	152	.1769E-01
154	.9117E-01	156	.2348E-03	161	.9998E+00	163	.1847E-01	170	.1200E+02	171	.9000E+01	172	.3000E+01
177	-.3129E-01	183	.3425E+00	189	.2100E+02	197	.3567E+02	201	.1000E+00	202	.1000E+00	203	.1000E+02
204	.2000E-01	205	.2900E-01	206	.1000E+03	207	.1000E+00	208	.5000E+00	209	.1000E+01	210	.2000E-01
211	.1000E+03	212	.1000E+03	221	.2000E-01	222	.2000E-01	223	.2000E-01	224	.2500E-02	225	.2000E-01
226	.2000E-01	227	.5000E-01	228	.1000E+00	229	.1000E-01	265	.2500E-01	266	.5000E-01	283	.2500E+00
330	-.1400E+00	331	-.4370E+00	333	.5230E+00	334	.8730E-01	335	.2000E+01	485	.9000E+01	486	.1000E-06
498	.1000E+01	700	.2117E+01	703	-.9368E-14	705	.2698E+00	706	.2117E+01	709	.1299E+01	801	.5716E+04
802	.2387E+04	803	.1727E-01	805	.4181E-03	806	-.2728E-02	807	.9338E-02	808	-.1051E+01	809	.4110E+00
810	-.5912E-02	811	.1264E-02	812	.1038E+04	813	.2110E-01	814	.1951E+00	815	.9117E-01	817	-.1303E+00
818	-.1041E+00	819	.1035E-01	820	-.3211E+00	821	.5507E-01	822	.4974E+00	823	-.1351E-02	824	-.4262E+01
825	-.4050E+00	826	-.1365E+00	828	.3035E+00	829	.9200E+04	830	.8655E+05	831	.9126E+05	832	.2953E+04
833	.1392E+00	834	-.3135E+00	835	.5265E-02	836	.1192E-01	837	-.1012E+00	838	.2515E-01	861	.1000E+01
862	.1000E+02	863	.5000E+00	901	.4200E+02	902	.4400E+02	903	.8000E+01	904	.3200E+02	905	.3300E+02
906	.3000E+01	907	.4300E+02	908	.9000E+01	909	.7000E+01	910	.3100E+02	911	.4000E+01	912	.2000E+01
913	.1000E+01	914	.2000E+01	915	.3000E+01	916	.4000E+01	917	.5000E+01	918	.6000E+01	919	.7000E+01
920	.8000E+01	921	.9000E+01	922	.1000E+02	923	.1100E+02	924	.1200E+02	925	.1810E+03	926	.1820E+03
927	.1840E+03	928	.1770E+03	929	.1790E+03	930	.1780E+03	931	.1760E+03	932	.1800E+03	933	.1830E+03
934	.1010E+03	935	.1020E+03	936	.1030E+03	937	.1300E+02	938	.1400E+02	939	.1500E+02	940	.1600E+02
941	.1700E+02	942	.1800E+02	943	.1900E+02	944	.2000E+02	945	.2100E+02	961	.1295E+05	962	.9300E+05
963	.1010E+06	964	.2080E+04	965	.5839E+03	966	.5000E+00						

LINEAR DYNAMICS

F MATRIX(12X12)

-3.69	.234E-02	-.644E-01	0.	0.	0.	.152E-01	0.	0.	0.	0.	0.
-.113	-.360	.651E-02	0.	0.	0.	.473E-01	0.	0.	0.	0.	0.
25.7	-693.	-.271	32.2	0.	0.	0.	0.	0.	0.	0.	0.
1.00	.370E-01	0.	0.	0.	0.	0.	0.	0.	0.	0.	0.
0.	1.00	0.	0.	0.	0.	0.	0.	0.	0.	0.	0.
0.	0.	1.000	-25.7	695.	0.	0.	0.	0.	0.	0.	0.
0.	-.494E-01	0.	0.	0.	0.	-.616	-.920E-02	.345E-03	0.	-.147E-06	0.
0.	0.	0.	0.	0.	0.	695.	-1.05	-.138E-01	-1.19	.543E-03	0.
0.	0.	0.	0.	0.	0.	-25.7	.336E-01	-.944E-02	-32.2	.142E-04	0.
0.	0.	0.	0.	0.	0.	1.000	0.	0.	0.	0.	0.
0.	0.	0.	0.	0.	0.	0.	-.999	.369E-01	695.	0.	0.
0.	0.	0.	0.	0.	0.	0.	.369E-01	.999	0.	0.	0.

G1 MATRIX(12X 9)

24.9	9.82	15.6	0.	0.	0.	0.	0.	0.
1.34	-4.21	.506	0.	0.	0.	0.	0.	0.
3.78	34.9	0.	0.	0.	0.	0.	0.	0.
0.	0.	0.	0.	0.	0.	0.	0.	0.
0.	0.	0.	0.	0.	0.	0.	0.	0.
0.	0.	0.	0.	0.	0.	0.	0.	0.
0.	0.	0.	-13.7	-2.27	-2.13	.208E-02	-.265	.254E-04
0.	0.	0.	-113.	-77.0	23.3	-1.14	-4.82	0.
0.	0.	0.	2.47	1.17	-.373	-3.99	-4.30	8.93
0.	0.	0.	0.	0.	0.	0.	0.	0.
0.	0.	0.	0.	0.	0.	0.	0.	0.
0.	0.	0.	0.	0.	0.	0.	0.	0.

G2 MATRIX(12X 3)

ROW 1	0.	0.
ROW 2	-.6441E-01	0.
ROW 3	.6515E-02	0.
ROW 4	-.2706E+00	0.
ROW 5	0.	0.
ROW 6	0.	0.
ROW 7	0.	0.
ROW 8	.3446E-03	-.9203E-02
ROW 9	-.1379E-01	-.1045E+01
ROW 10	-.9445E-02	.3361E-01
ROW 11	0.	0.
ROW 12	0.	0.
G.	0.	0.

HX MATRIX(9X12)											
0.	0.	.144E-02	0.	0.	0.	0.	0.	0.	0.	0.	0.
-.271E-01	1.89	-.271	0.	0.	0.	0.	0.	0.	0.	0.	0.
0.	0.	0.	0.	0.	0.	0.	.144E-02	-.531E-04	0.	0.	0.
0.	0.	0.	0.	0.	0.	0.	-1.05	-.138E-01	0.	.543E-03	0.
0.	0.	0.	0.	0.	0.	0.	.369E-01	.999	0.	0.	0.
0.	0.	0.	0.	0.	0.	0.	-.285E-06	-.770E-05	0.	0.	0.
0.	0.	0.	0.	0.	0.	0.	.581E-02	-.186E-03	0.	0.	0.
0.	0.	0.	0.	0.	0.	0.	-.571E-05	-.154E-03	0.	.208E-05	0.
0.	0.	0.	0.	0.	0.	0.	.157E-03	.676E-06	0.	0.	0.

HU MATRIX(9X 9)									HW MATRIX(9X 3)		
0.	0.	0.	0.	0.	0.	0.	0.	0.	ROW 1		
3.78	34.9	0.	0.	0.	0.	0.	0.	0.	ROW 2	.1438E-02	0.
0.	0.	0.	0.	0.	0.	0.	0.	0.	ROW 3	0.	-.2706E+00
0.	0.	0.	-113.	-77.0	23.3	-1.14	-4.82	0.	ROW 4	-.5312E-04	0.
0.	0.	0.	0.	0.	0.	0.	0.	0.	ROW 5	-.1379E-01	0.
0.	0.	0.	0.	0.	0.	0.	0.	0.	ROW 6	.9993E+00	0.
0.	0.	0.	0.	0.	0.	0.	0.	0.	ROW 7	-.7703E-05	0.
0.	0.	0.	.632	.430	-.130	.551E-02	.260E-01	0.	ROW 8	-.1861E-03	0.
0.	0.	0.	0.	0.	0.	0.	0.	0.	ROW 9	-.1545E-03	0.
0.	0.	0.	.956E-02	.934E-02	-.273E-02	.225E-01	.250E-01	0.		.6758E-06	0.
											.1572E-23

EIGENVALUES OF FREE A/C

REAL	IMAG	DAMPING	FREQ
-.495115E-14	0.		
-.147195E-11	0.		
-.147195E-11	0.		
-.128484E-02	0.		
-.281937E-01	0.		
-.413723E-02	.518698E-01	.795092E-01	.520346E-01
-.829876E+00	.252112E+01	.312666E+00	.265419E+01
-.262186E+00	.253592E+01	.102841E+00	.254543E+01
-.377268E+01	0.		

EIGENVALUES FOR LATERAL AXES

REAL	IMAG	DAMPING	FREQ
.582867E-14	0.		
.582867E-14	0.		
-.288888E-01	0.		
-.261327E+00	.253567E+01	.102517E+00	.254910E+01
-.377271E+01	0.		

EIGENVALUES FOR PITCH AXIS

REAL	IMAG	DAMPING	FREQ
-.131839E-15	0.		
-.128484E-02	0.		
-.412532E-02	.518765E-01	.792718E-01	.520403E-01
-.830732E+00	.252112E+01	.312957E+00	.265446E+01

NOMINAL TRAJECTORY PARAMETERS(T= 0.00)

NK = 12

NU = 9

NW = 3

NY = 9

APERT = .1000E+01

X3 VECTOR

0. 0. 0. 0. 0. 0. 0. 0. .1659E+03 .6002E+03 .2697E+00
.2000E+05 0.

U3 VECTOR

0. 0. 0. -.1857E+00 0. 0. 0. 0. .2000E+01

W3 VECTOR

0. 0. 0.

YN VECTOR

0. 0. .2697E+00 -.1241E+03 .6227E+03 .4980E+00 .8283E+00 .2063E+00 .2491E+00

DYNAMIC PRESSURE = .24495E+03

MACH = .60

ANGLE-OF-ATTACK = 15.45

FB-SIM

FLIGHT CONDITION 21

LIST OF NON-ZERO ELEMENTS IN A(1) THRU A(1000)

4	.2000E+05	5	.5000E+00	7	.6002E+03	9	.1659E+03	10	.6002E+03	12	.1659E+03	13	.6227E+03
15	-.3638E-11	16	-.6227E+03	17	-.1854E+00	19	-.9311E+02	20	.8395E+01	22	-.1241E+03	23	.8395E+01
25	-.1241E+03	28	-.8243E-14	29	.2697E+00	31	.2697E+00	37	-.1440E+00	46	-.5511E-03	51	.1000E+01
54	.9638E+00	56	.2665E+00	58	.1000E+01	60	-.2665E+00	62	.9638E+00	70	.2450E+03	71	.5371E+04
73	-.7943E+05	78	-.4769E+02	83	.9200E+04	84	.8655E+05	85	.9126E+05	88	.2953E+04	89	.1000E+00
90	.3220E+02	91	.6398E+03	92	.1000E+02	95	.3035E+00	96	.1248E+05	117	.3750E+03	118	.7500E-01
119	.4300E+00	120	.2600E-01	121	-.1457E+00	122	-.1700E-01	123	.2700E+03	124	.2700E+03	125	.1000E+04
128	-.1178E+02	129	.5000E+01	131	.1000E+01	132	.1000E+00	134	.1000E+00	138	.2000E+02	142	.7000E+01
145	.1000E+01	146	.1000E+04	147	.1000E-02	148	.1000E-02	149	.1000E-01	151	.1288E+03	152	.2491E+00
154	.8283E+00	156	-.4408E-04	161	.9909E+00	163	.1345E+00	170	.1200E+02	171	.9000E+01	172	.3000E+01
177	-.1857E+00	183	.2000E+01	189	.2100E+02	197	.3567E+02	201	.1000E+00	202	.1000E+00	203	.1000E+02
204	.2000E-01	205	.2000E-01	206	.1000E+03	207	.1000E+00	208	.5000E+00	209	.1000E+01	210	.2000E-01
211	.1000E+03	212	.1000E+03	221	.2000E-01	222	.2000E-01	223	.2000E-01	224	.2500E-02	225	.2000E-01
226	.2000E-01	227	.5000E-01	228	.1000E+00	229	.1000E-01	265	.2500E-01	266	.5000E-01	283	.2500E+00
330	-.1400E+00	331	-.4370E+00	333	.5230E+00	334	.8730E-01	335	.2000E+01	485	.9000E+01	486	.1000E-05
408	.1000E+01	700	.1545E+02	703	-.3348E-12	705	-.3157E-01	706	.1545E+02	709	-.8253E+01	801	.4269E+04
802	.2884E+04	803	.2444E+00	805	.4732E-02	806	-.2970E+00	807	-.1494E+00	808	-.1228E+01	809	.4490E+00
810	.1300E+00	811	.1264E-02	812	.1038E+04	813	.7920E-03	814	.2063E+00	815	.8283E+00	817	.1019E+00
818	-.1018E+00	819	.8723E-01	820	-.2170E+00	821	.4175E-01	822	.4980E+00	823	-.1449E-01	824	-.4150E+01
825	-.4200E+00	826	-.1234E+00	828	.3035E+00	829	.9200E+04	830	.8655E+05	831	.9126E+05	832	.2953E+04
833	.3774E-01	834	-.4183E+00	835	.2439E-02	836	.1533E-01	837	-.1027E+00	838	.9193E-03	861	.1000E+01
902	.1000E+02	863	.5000E+00	901	.4200E+02	902	.4400E+02	903	.8000E+01	904	.3200E+02	905	.3300E+02
906	.3000E+01	907	.4300E+02	908	.9000E+01	909	.7000E+01	910	.3100E+02	911	.4000E+01	912	.2000E+01
913	.1000E+01	914	.2000E+01	915	.3000E+01	916	.4000E+01	917	.5000E+01	918	.6000E+01	919	.7000E+01
920	.2000E+01	921	.9000E+01	922	.1000E+02	923	.1100E+02	924	.1200E+02	925	.1810E+03	926	.1820E+03
927	.1840E+03	928	.1770E+03	929	.1790E+03	930	.1780E+03	931	.1760E+03	932	.1800E+03	933	.1830E+03
934	.1610E+03	935	.1620E+03	936	.1630E+03	937	.1640E+03	938	.1650E+03	939	.1660E+03	940	.1670E+03
941	.1700E+02	942	.1800E+02	943	.1900E+02	944	.2000E+02	945	.2100E+02	961	.1295E+05	962	.9300E+05
963	.1010E+06	964	.2080E+04	965	.5839E+03	966	.5000E+00						

LINEAR DYNAMICS

F MATRIX(12X12)

-2.24	.760	-.583E-01	0.	0.	0.	.443E-01	0.	0.	0.	0.	0.
-.699E-01	-.406	-.933E-04	0.	0.	0.	.138	0.	0.	0.	0.	0.
166.	-.998.	-.283	31.0	0.	0.	0.	0.	0.	0.	0.	0.
1.04	.276	0.	0.	0.	0.	0.	0.	0.	0.	0.	0.
0.	1.04	0.	0.	0.	0.	0.	0.	0.	0.	0.	0.
0.	0.	1.000	-166.	623.	0.	0.	0.	0.	0.	0.	0.
0.	-.144	0.	0.	0.	0.	-.540	-.151E-01	.257E-02	0.	-.391E-05	0.
0.	0.	0.	0.	0.	0.	600.	-.805	-.199	-8.58	.419E-02	0.
0.	0.	0.	0.	0.	0.	-166.	-.211E-01	-.258E-01	-31.0	.167E-03	0.
0.	0.	0.	0.	0.	0.	1.000	0.	0.	0.	0.	0.
0.	0.	0.	0.	0.	0.	0.	-.964	.266	623.	0.	0.
0.	0.	0.	0.	0.	0.	0.	.266	.964	0.	0.	0.

G1 MATRIX(12X 9)

15.2	-.865	12.6	0.	0.	0.	0.	0.	0.
1.04	-3.71	.406	0.	0.	0.	0.	0.	0.
.114	29.6	0.	0.	0.	0.	0.	0.	0.
0.	0.	0.	0.	0.	0.	0.	0.	0.
0.	0.	0.	0.	0.	0.	0.	0.	0.
0.	0.	0.	0.	0.	0.	0.	0.	0.
0.	0.	0.	-11.0	-1.82	-1.54	-.665E-02	-.212	.958E-04
0.	0.	0.	-92.7	-53.8	-2.74	.643	-4.55	0.
0.	0.	0.	17.6	37.1	45.0	-3.52	-2.46	4.51
0.	0.	0.	0.	0.	0.	0.	0.	0.
0.	0.	0.	0.	0.	0.	0.	0.	0.
0.	0.	0.	0.	0.	0.	0.	0.	0.

G2 MATRIX(12X 3)

ROW 1	0.	0.
ROW 2	-.5827E-01	0.
ROW 3	-.9334E-04	0.
ROW 4	-.2833E+00	0.
ROW 5	0.	0.
ROW 6	0.	0.
ROW 7	0.	0.
ROW 8	.2568E-02	-.1510E-01
ROW 9	-.1993E+00	-.8050E+00
ROW 10	-.2583E-01	-.2111E-01
ROW 11	0.	0.
ROW 12	0.	0.
0.	0.	0.

HX MATRIX(9X12)

0.	0.	.161E-02	0.	0.	0.	0.	0.	0.	0.	0.	0.	0.
.535	1.85	-.283	0.	0.	0.	0.	0.	0.	0.	0.	0.	0.
0.	0.	0.	0.	0.	0.	0.	.155E-02	-.428E-03	0.	0.	0.	0.
0.	0.	0.	0.	0.	0.	0.	-.805	-.199	0.	.419E-02	0.	0.
0.	0.	0.	0.	0.	0.	0.	.266	.964	0.	0.	0.	0.
0.	0.	0.	0.	0.	0.	0.	-.152E-04	-.549E-04	0.	-.141E-06	0.	0.
0.	0.	0.	0.	0.	0.	0.	.428E-02	-.112E-02	0.	.150E-06	0.	0.
0.	0.	0.	0.	0.	0.	0.	-.276E-04	-.998E-04	0.	.189E-05	0.	0.
0.	0.	0.	0.	0.	0.	0.	.266E-02	-.746E-03	0.	0.	0.	0.

HU MATRIX(9X 9)

0.	0.	0.	0.	0.	0.	0.	0.	0.
.114	29.6	0.	0.	0.	0.	0.	0.	0.
0.	0.	0.	0.	0.	0.	0.	0.	0.
0.	0.	0.	-92.7	-53.8	-2.74	.643	-4.55	0.
0.	0.	0.	0.	0.	0.	0.	0.	0.
0.	0.	0.	0.	0.	0.	0.	0.	0.
0.	0.	0.	.655	.430	.102	-.108E-01	.260E-01	0.
0.	0.	0.	0.	0.	0.	0.	0.	0.
0.	0.	0.	.538E-01	-.149	-.297	.224E-01	.250E-01	0.

HW MATRIX(9X 3)

ROW 1	0.	.1606E-02	0.
ROW 2	0.	-.2833E+00	0.
ROW 3	-.4279E-03	0.	.1548E-02
ROW 4	-.1993E+00	0.	-.8050E+00
ROW 5	.9638E+00	0.	.2665E+00
ROW 6	-.5490E-04	0.	-.1516E-04
ROW 7	-.1122E-02	0.	.4283E-02
ROW 8	-.9981E-04	0.	-.2761E-04
ROW 9	-.7463E-03	0.	.2659E-02

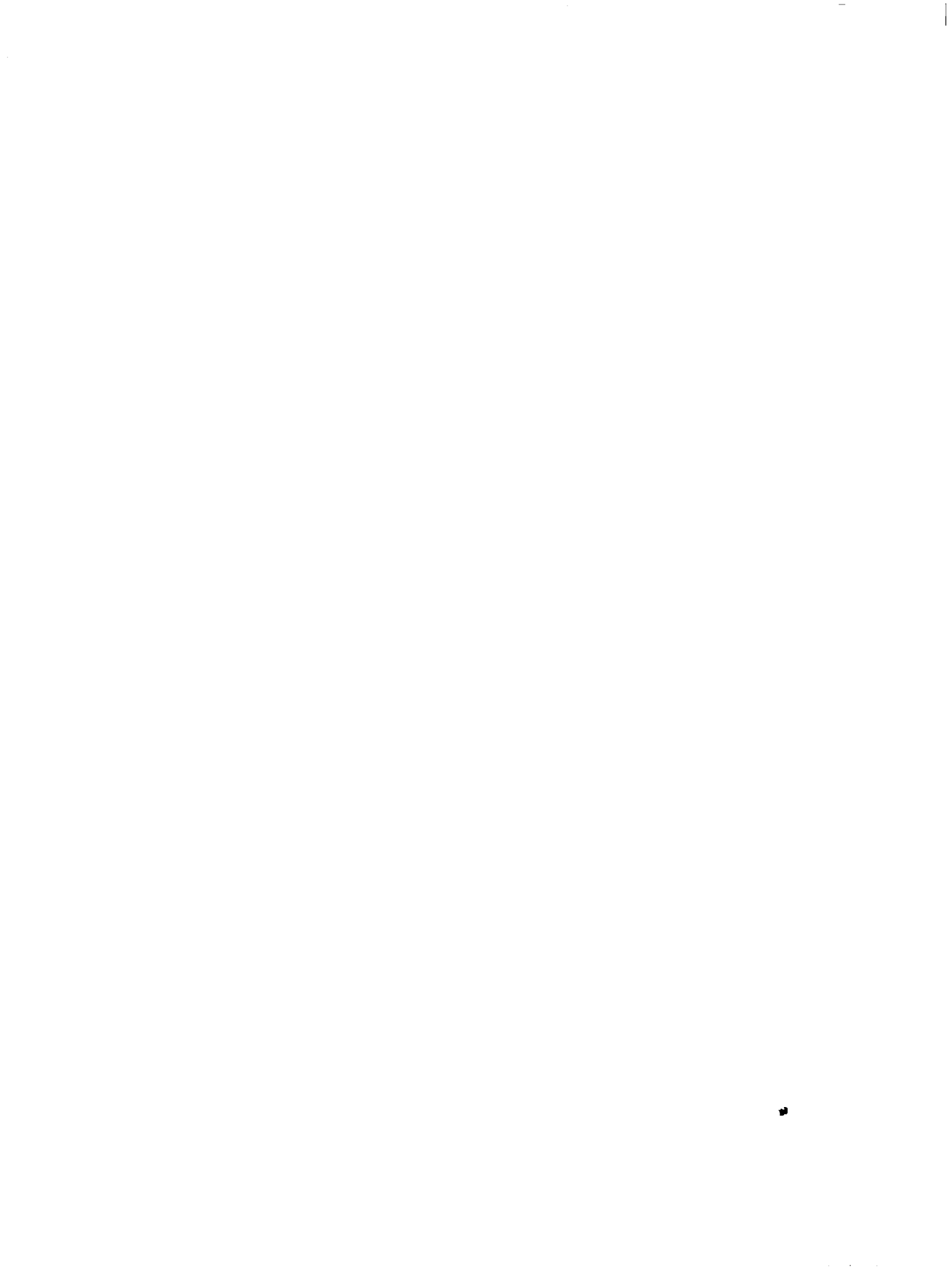
REAL	IMAG	DAMPING	FREQ
0.	0.		
.97187E-14	0.		
.97187E-14	0.		
-.227692E-02	0.		
-.967621E-01	0.		
-.521744E-01	.129260E+00	.374322E+00	.139394E+00
-.764985E+00	0.		
-.631661E+00	.307034E+01	.201510E+00	.313465E+01
-.107242E+01	.290366E+01	.335012E+00	.308174E+01

EIGENVALUES FOR LATERAL AXES

REAL	IMAG	DAMPING	FREQ
.464906E-14	0.		
.464906E-14	0.		
-.966880E-01	0.		
-.764903E+00	0.		
-.103181E+01	.290443E+01	.334758E+00	.308226E+01

EIGENVALUES FOR PITCH AXIS

REAL	IMAG	DAMPING	FREQ
-.218575E-14	0.		
-.227693E-02	0.		
-.527050E-01	.129474E+00	.373955E+00	.139602E+00
-.632320E+00	.306628E+01	.201962E+00	.313080E+01



APPENDIX C

F8SIM

APPENDIX C

F8SIM

The flow diagram of F8SIM is shown in Figure C-1. The main program makes a series of calls to appropriate subroutines. The subroutines are summarized in Table C-1. An executive subroutine, EXEK, performs input/output and other house-keeping chores and the linearization. The MODE flag, stored in blank COMMON, causes routines to perform in various modes of operation, as will be described below.

F8SIM is programmed to evaluate and/or integrate the equations of motion at a series of any number of flight conditions specified by the user. This is accomplished by processing an input deck consisting of control cards followed by data cards. The primary types of flow control cards are "C", "PCC", "RUN" and "STOP". Their functions are summarized in Table C-2.

The operation of F8SIM will now be briefly explained. All information to be transferred between subroutines is stored in an array called the A-array. This contains the current values of all variables used in the simulation. The aero functions are stored in a tabular form containing up to three dependent arguments. The 38 functions associated with the F-8C are listed in Table C-3. [21]

The program starts by zeroing the A-array. Then EXEK calls PREAD to read parameter cards and the aero data consisting of 38 functions. Calls to FLOOK then evaluate the functions corresponding to the related parameters. All constants are set in other subroutines.

Next EXEK calls AERO, which computes the aerodynamic forces and moments in body axes.

TRIM is then called to determine the throttle setting, elevator position and angle-of-attack for the selected conditions.

AERO is then called to update the forces and moments with the trimmed values.

Next DYNK is called. This subroutine combines the externally applied forces and moments with the aircraft kinematics and integrates the resulting differential equations of motion. The external forces and moments consist of components due to gravity, engine, wind, and aerodynamics. The kinematics include all cross-products of inertia. All computations are performed in body axes.

After taking one integration step the A-array is dumped, and LINK is called to generate linear models in state variable form.

These operations in the various modes will now be explained using simplified flow charts for F8SIM and EXEK, TRIM, AERO, and DYNK subroutines.

When F8SIM (Figure C-1) is entered, the A-array, a buffer in blank common for transfer of information between subroutines, is zeroed out. The MODE flag is then set to -1. EXEK (Figure C-2) is called which in turn calls PREAD to read cards from the input deck. The first card to be read will be a "PCC" card, which means there are data cards to follow. On the first flight condition there will be many data cards to define elements of the A-array. However, on succeeding flight conditions, most of these

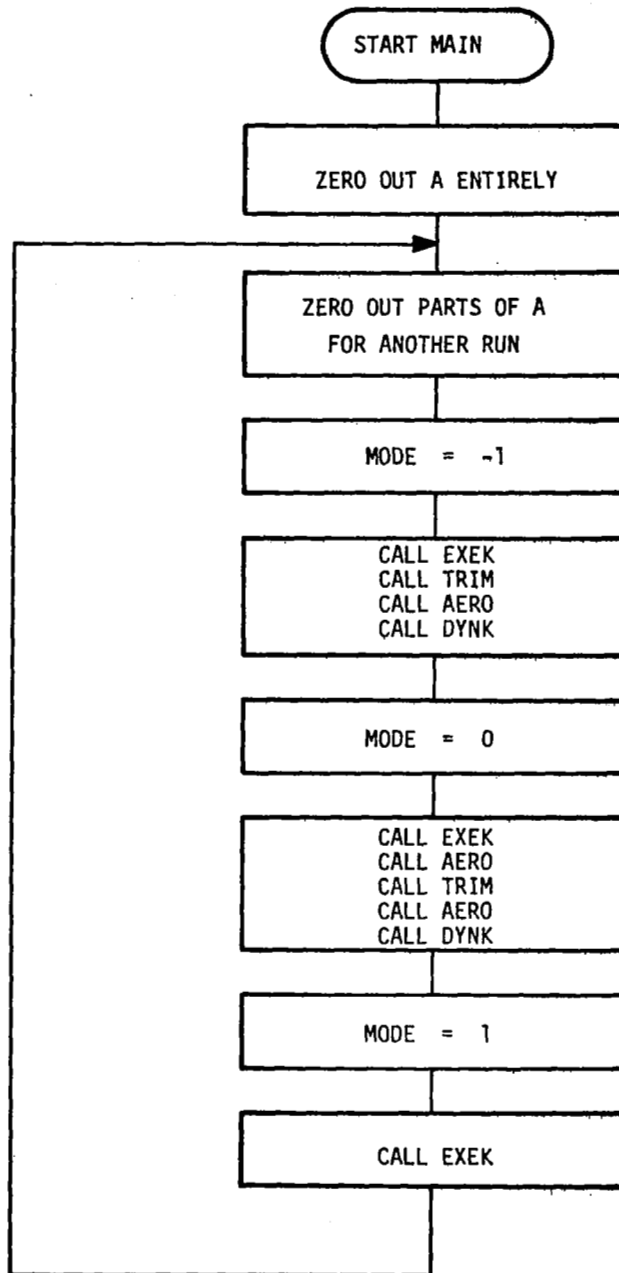


Figure C-1. F8SIM Flow Diagram

Table C-1. F8SIM Subroutine Summary

Subroutine	Description
F8SIM (Main program)	Nonlinear simulation and linearization of aircraft
EXEC	Executive
DYNK	Aircraft dynamics for six degrees of freedom
LINK	Linearization of aircraft dynamics for six degrees of freedom using numerical differentiation
PREAD	A-array parameter input
DDUMP	A-array data dump
MDUMP	Matrix printout
FLOOK	Table input look-up and linear interpolation
AERO	Compute aerodynamic forces and moments and thrust forces and moments in body axes
ATMOS	1962 Standard Atmosphere, computes air density and speed of sound as function of altitude
TRIM	Trims throttle, elevator and angle of attack at specified flight conditions
EVAL	Used with TRIM to compute X forces, Z forces and pitching moments in stability axes.

Table C-2. F8SIM Control Cards

Control Card Type	Function
C	Cause the commentary information on the card to be printed on the line printer output.
PCC	Signal that subsequent cards will be data cards to be read in.
RUN	Causes data input to stop and starts program execution.
STOP	Causes program execution to terminate.

Table C-3. F-8C Aerodynamic Functions

FUNCTION NUMBER	FUNCTION NAME AND VARIABLES	FUNCTION NUMBER	FUNCTION NAME AND VARIABLES
1	$T(\text{vel}, H)$	20	$C_{L_p}(H, M, \alpha)$
2	$\Delta T_{AB}(\text{vel}, H)$	21	$C_{L_{\delta a}}(H, M, \alpha)$
3	$C_D(M, \alpha)$	22	$C_{L_{\delta e}}(M)$
4	$C_{D_{\Delta SB}}(SB, M)$	23	$C_M(M, \delta e, \alpha)$
5	$C_{D_{\Delta R}}(\delta e, \alpha)$	24	$C_m(H, M)$
6	$C_{D_{\delta LE}}(M, \alpha)$	25	$C_{m_{\dot{\alpha}}}(H, M)$
7	$C_{D_{\delta f}}(\alpha)$	26	$C_{m_{\delta LE}}(M, \alpha)$
8	$C_{y_{\beta}}(M, \alpha)$	27	$C_{m_{\Delta SB}}(M, \delta SB, \alpha)$
9	$C_{y_r}(M, \alpha)$	28	h(% FUEL)
10	$C_{y_p}(M, \alpha)$	29	IX(% FUEL)
11	HI Simulation	30	IY(% FUEL)
12	HI Simulation	31	IZ(% FUEL)
13	$C_{y_{\delta a}}(M, \alpha)$	32	$I_{XZ}(\% \text{ FUEL})$
14	$C_{y_{\delta r}}(H, M)$	33	$C_{N_{\beta}}(H, M, \alpha)$
15	$C_L(M, \delta e, \alpha)$	34	$C_{N_r}(H, M, \alpha)$
16	$C_{L_{\Delta SB}}(M, \delta SB, \alpha)$	35	$C_{N_p}(H, M, \alpha)$
17	$C_{L_{\delta LE}}(M, \alpha)$	36	$C_{N_{\delta a}}(H, M, \alpha)$
18	$C_{L_{\beta}}(H, M, \alpha)$	37	$C_{N_{\delta r}}(H, M)$
19	$C_{L_r}(H, M, \alpha)$	38	$C_{L_{\delta r}}(H, M, \alpha)$

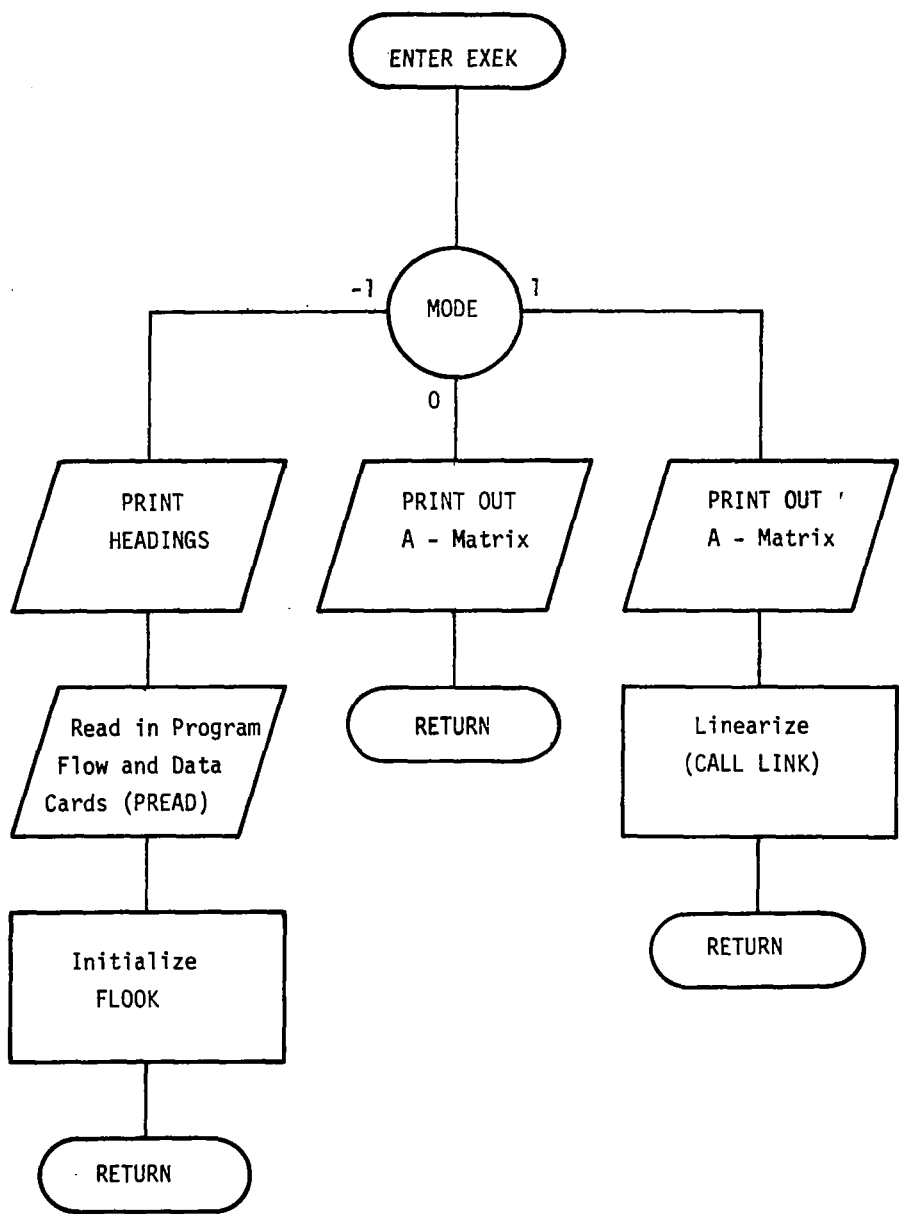


Figure C-2. Subroutine EXEK Flow Diagram

elements remain defined as before, and only a minimum set of parameters need be specified. As soon as a "RUN" card is encountered on the input deck, control returns to EXEK, which calls FLOOK, the linear table look-up routine, to initialize itself. Control returns to MAIN which calls TRIM (Figure C-3) to initialize itself by setting its maximum iterations count. AERO (Figure C-4) is then called, and it uses an atmosphere model and current flight condition input data to find the speed of sound from which aircraft velocity is computed. Then DYNK (Figure C-5) is called to find aircraft mass properties for the current flight condition. Control returns to MAIN.

The MODE flag is set to 0. EXEK is called, and it prints out the A-matrix values for the untrimmed aircraft. After return to MAIN, AERO (Figure C-4) is called to evaluate the aerodynamic forces and moments on the aircraft. MAIN then calls TRIM which computes the elevator position, throttle setting, and angle-of-attack to reduce the aero forces and moments to values below a certain trim tolerance. AERO is called again to evaluate the aero loads with the new flight control settings. At this point the aircraft is trimmed. DYNK is called to integrate the equations of motion one step forward, thus yielding aircraft translational and rotational velocities, and describing the state of the aircraft at the current flight condition.

The MODE flag is now set to 1. EXEK is called, which dumps the trimmed A-matrix and then calls LINK, the linearization routine. LINK perturbs the nonlinear equations of motion about the current flight condition to approximate the system by a linear set of differential equations. [2] After the approximate linear system is evaluated, the eigenvalues of this system are computed, and then control returns to MAIN. At this point, the F-8SIM program readies itself to read in another flight condition by zeroing out certain elements of the A-matrix. The MODE flag is reset to -1, and EXEK routine again reads in data cards for the next flight condition. If a "STOP" card is encountered, the program terminates.

Subroutine AERO--AERO evaluates the forces and moments on the aircraft at a given flight condition.

First, with altitude known, the atmosphere density, ρ , and speed of sound, S_{OS} , are determined using an atmospheric model. With those two numbers plus all components of the aircraft's velocity, u , v and w , the following quantities, i. e. total velocity, dynamic pressure, Mach, angle-of-attack, and sideslip angle are obtained

$$V = (u^2 + v^2 + w^2)^{\frac{1}{2}}$$

$$\bar{q} = \frac{1}{2} \rho V^2$$

$$M = V/S_{OS}$$

$$\alpha = \tan^{-1} (w/u)$$

$$\beta = \sin^{-1} (v/V)$$

The aerodynamic coefficients are obtained by calls to FLOOK, a linear table lookup routine, which will interpolate a dependent variable in up to three independent variables. The aero data which FLOOK interpolates exists as card images on a permanent disk file.

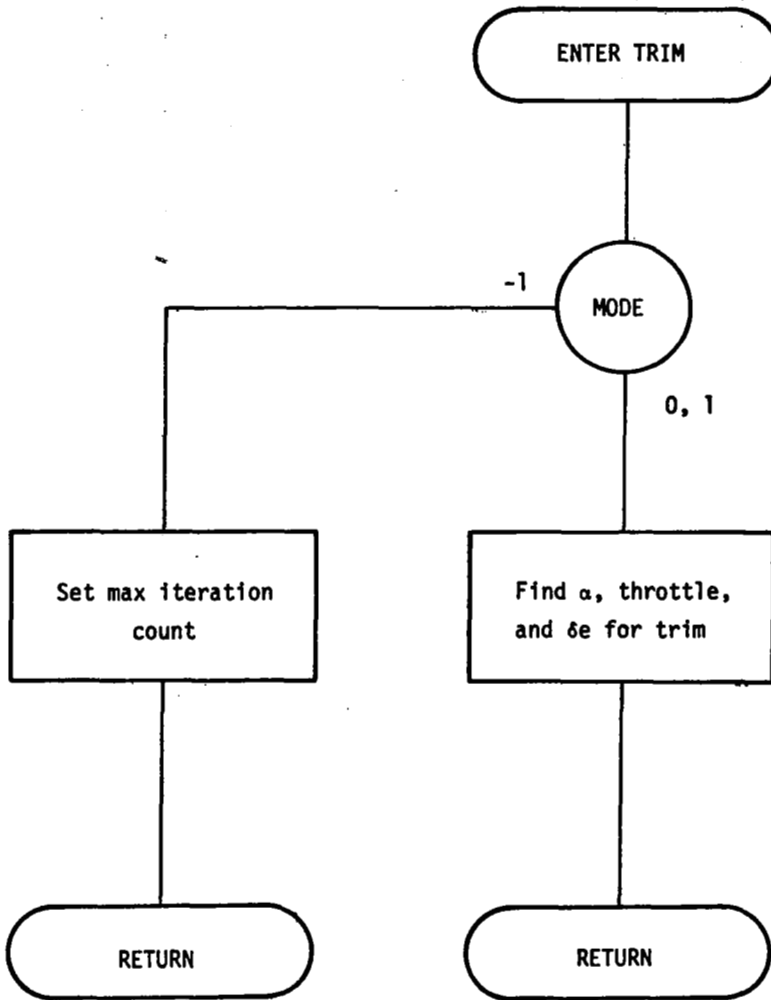


Figure C-3. Subroutine TRIM Flow Diagram

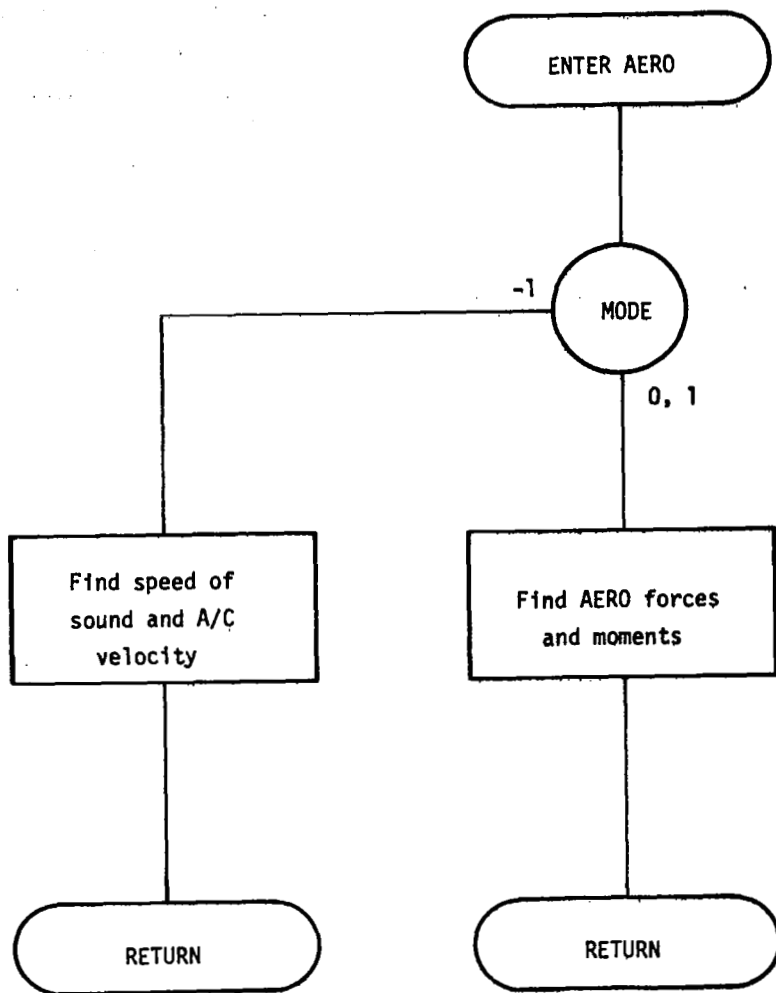


Figure C-4. Subroutine AERO Flow Diagram

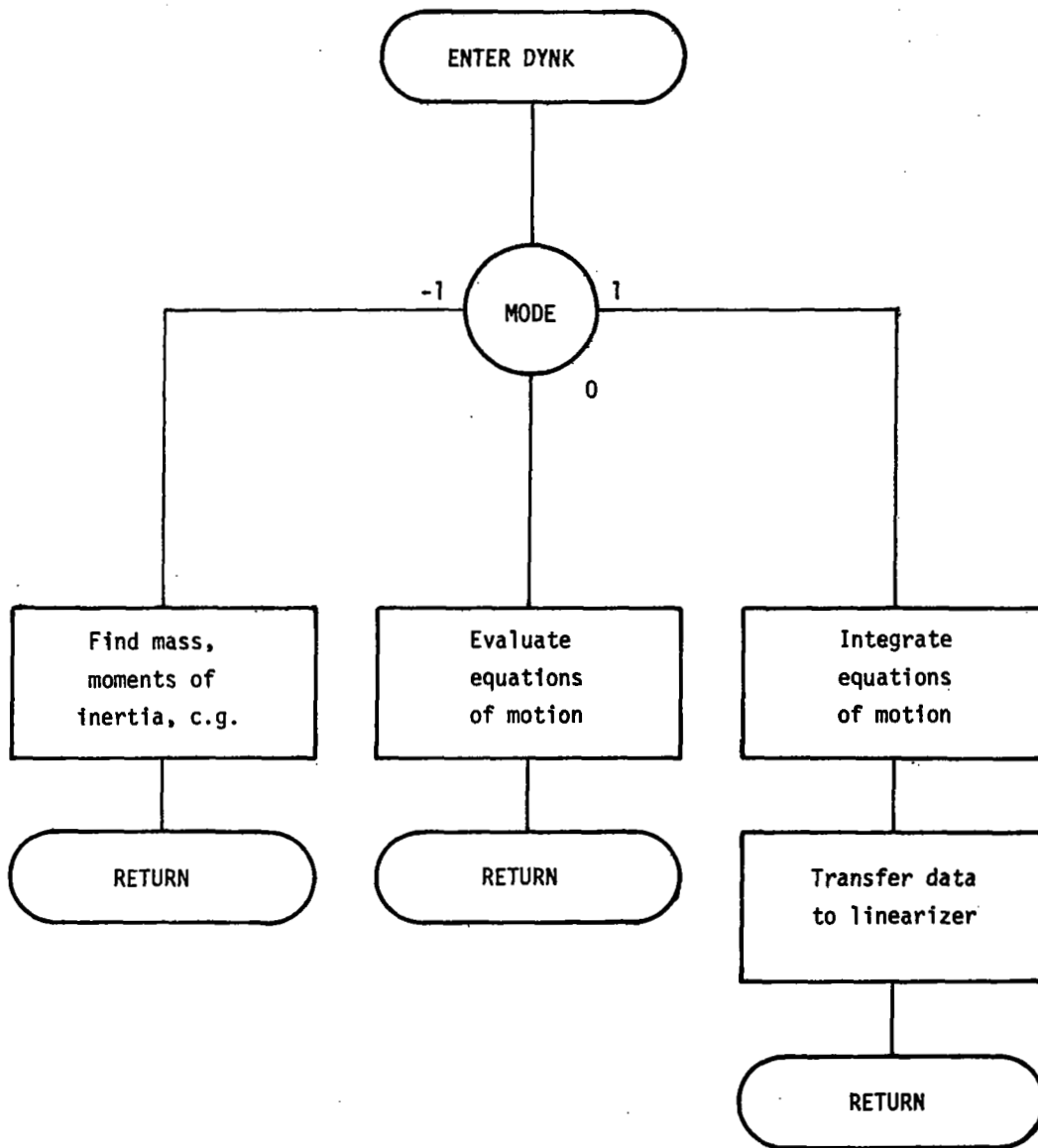


Figure C-5. Subroutine DYNK Flow Diagram

After all the aero coefficients have been determined, either through table lookup or direct input, forces and moments on the aircraft excluding weight contributions can be found. For the translational forces

$$\text{Drag coefficient} = \Sigma C_D = C_D + C_{D\Delta SB} + C_{D\delta e} + C_{D\delta LE} + C_{D\delta f} \delta f + C_{D\delta g} \delta g$$

$$\text{Lift coefficient} = \Sigma C_L = C_L + C_{L\Delta SB} + C_{L\Delta LE} \Delta LE + C_{L\delta f} \delta f + C_{L\delta g} \delta g$$

$$\text{Side Force coefficient} = \Sigma C_Y = C_{Y\beta} \beta + \frac{b}{2V} (C_{Yr} r + C_{Yp} p) + C_{Y\delta a} \delta a + C_{Y\delta r} \delta r$$

where b = wingspan (ft.)

V = total velocity

If percent throttle is less than 100,

$$T_p = T \cdot \text{percent throttle}/100$$

otherwise

$$T_p = T + \Delta T_{AB} \cdot (\text{percent throttle} - 100)/100$$

Therefore,

$$F_x = T_p + \bar{q} S (\Sigma C_L \sin \alpha - \Sigma C_D \cos \alpha)$$

$$F_y = \bar{q} S \Sigma C_Y$$

$$F_z = -\bar{q} S (\Sigma C_D \sin \alpha + \Sigma C_L \cos \alpha)$$

For the moments

$$\begin{aligned} \text{Roll Moment Coefficient} = \Sigma C_l = C_{l\beta} \beta + \frac{b}{2V} (C_{lr} r + C_{lp} p) + C_{l\delta a} \delta a + C_{l\delta r} \delta r \\ + \frac{l_e}{2b} C_{l\delta e} \delta RT \end{aligned}$$

$$\begin{aligned} \text{Pitch Moment Coefficient} = \Sigma C_m = C_m + \frac{\bar{c}}{2V} (C_{mq} q + C_{m\dot{\alpha}} \dot{\alpha}) + C_{m\Delta LE} \Delta LE \\ + C_{m\delta F} \delta F + C_{m\delta g} \delta g + C_{m\Delta SB} + C_L (x_{cg} - x_{mrc}) \end{aligned}$$

$$\begin{aligned} \text{Yaw Moment Coefficient} = \Sigma C_n = C_{n\beta} \beta + \frac{b}{2V} (C_{nr} r + C_{np} p) + C_{n\delta a} \delta a + C_{n\delta r} \delta r \\ + \bar{c} (x_{cg} - x_{mrc}) C_{Y\beta} \beta / b \end{aligned}$$

where

l_e = rolling tail moment arm (ft.)

$$\dot{\alpha} = \frac{d\alpha}{dt} \approx q(p \cos \alpha + r \sin \alpha) \tan \beta + (F_z \cos \alpha - F_x \sin \alpha) / m V \cos \beta$$

x_{cg} = non-dimensional cg x coordinate

x_{mrc} = non-dimensional moment reference center x -coordinate

\bar{c} = mean chord.

Finally, the moments are computed

$$L = \bar{q} S b \Sigma C_l$$

$$M = \bar{q} S \bar{c} \Sigma C_m$$

$$N = \bar{q} S b \Sigma C_n$$

Subroutine TRIM--When trimming the aircraft, it is necessary to find trim values of angle-of-attack, thrust, and elevator position, which cause the net forces and moments on the airframe to be below a specified tolerance. Mathematically, the trim condition of the aircraft can be expressed as a nonlinear vector function in u

$$F(u) < F_{tol}$$

Finding the roots of this set of inequalities defines the trim condition. An equivalent procedure is to find the roots of the following set of nonlinear equations

$$F(x) = 0$$

Applying Taylor's Theorem yields

$$\begin{aligned} F_1(x_1^{i+1}, x_2^{i+1}, \dots, x_n^{i+1}) &= F_1(x_1^i, \dots, x_n^i) + \frac{\partial F_1}{\partial x_1} (x_1^{i+1} - x_1^i) \\ &+ \frac{\partial F_1}{\partial x_2} (x_2^{i+1} - x_2^i) + \dots + \frac{\partial F_1}{\partial x_n} (x_n^{i+1} - x_n^i) + \text{H.O.T.} \end{aligned}$$

$$\begin{aligned} F_2(x_1^{i+1}, x_2^{i+1}, \dots, x_n^{i+1}) &= F_2(x_1^i, \dots, x_n^i) + \frac{\partial F_2}{\partial x_1} (x_1^{i+1} - x_1^i) \\ &+ \frac{\partial F_2}{\partial x_2} (x_2^{i+1} - x_2^i) + \dots + \frac{\partial F_2}{\partial x_n} (x_n^{i+1} - x_n^i) + \text{H.O.T.} \end{aligned}$$

$$\begin{aligned} F_n(x_1^{i+1}, x_2^{i+1}, \dots, x_n^{i+1}) &= F_n(x_1^i, \dots, x_n^i) + \frac{\partial F_n}{\partial x_1} (x_1^{i+1} - x_1^i) \\ &+ \frac{\partial F_n}{\partial x_2} (x_2^{i+1} - x_2^i) + \dots + \frac{\partial F_n}{\partial x_n} (x_n^{i+1} - x_n^i) + \text{H.O.T.} \end{aligned}$$

where H. O. T. = higher order terms

In matrix notation -

$$\begin{bmatrix} F_1(x_1^{i+1}, \dots, x_n^{i+1}) \\ F_n(x_1^{i+1}, \dots, x_n^{i+1}) \end{bmatrix} = \begin{bmatrix} F_1(x_1^i, \dots, x_n^i) \\ F_n(x_1^i, \dots, x_n^i) \end{bmatrix} + \begin{bmatrix} \frac{\partial F_1}{\partial x_1} & \dots & \frac{\partial F_1}{\partial x_n} \\ \frac{\partial F_n}{\partial x_1} & \dots & \frac{\partial F_n}{\partial x_n} \end{bmatrix} \begin{bmatrix} x_1^{i+1} - x_1^i \\ \dots \\ x_n^{i+1} - x_n^i \end{bmatrix} + \text{H. O. T.}$$

or

$$F^{i+1} = F^i + J_F(x^{i+1} - x^i) + \text{H. O. T.}$$

If x is close to a root, then F^{i+1} and the higher order terms will be negligible, and the following approximation can be made -

$$F^i = J_F(x^{i+1} - x^i) \approx 0$$

$$x^{i+1} - x^i = \Delta x \approx -J_F^{-1} F^i$$

Experience has shown that if a reasonably good starting guess is made for x , convergence occurs within 5 or 6 iterations.

Subroutine TRIM implements this procedure by solving the 3×3 linear system of equations

$$-J_F \Delta x = F^i$$

$$x_{i+1} = x_i + \Delta x$$

for Δx . The Jacobian matrix J_F is evaluated, using a backward difference formula

$$\frac{\partial F_i}{\partial x_j} \approx \frac{F_i - F_{i-1}}{x_j - x_{j-1}}$$

The function vector F , whose components represent axial force, normal force, and pitching moment, is evaluated by calls to subroutine AERO. The vector x represents angle-of-attack, elevator position, and throttle position. When the Newton loop described above has sufficiently converged, the solution x will be the control input required to trim the aircraft.

Subroutine DYNK--Subroutine DYNK integrates the equations of motion of the aircraft at a specified flight condition. The equations of motion are composed of the force and moment calculations performed by AERO as well as mass properties computed or looked up in DYNK.

The following mass properties are looked up by FLOOK

I_x (% fuel)	x-Moment of inertia
I_y (% fuel)	y-Moment of inertia
I_z (% fuel)	z-Moment of inertia
I_{xz} (% fuel)	xz cross-moment
M (% fuel)	mass
x_{cg} (% fuel)	c. g. x-coordinate.

Accelerations are computed from force and moment calculations and mass properties.

Translational -

$$\dot{u} = F_x/M - g \sin \theta - wq + vr$$

$$\dot{v} = F_y/M + g \sin \phi - ur + wp$$

$$\dot{w} = F_z/M + g \cos \phi - vp + uq$$

Angular -

$$\dot{p} = qr \left(\frac{I_y - I_z}{I_x} \right) + (\dot{r} + pq) \frac{I_{xz}}{I_z} + L$$

$$\dot{q} = rp \left(\frac{I_z - I_x}{I_y} \right) + (r^2 - p^2) \frac{I_{xz}}{I_z} + M$$

$$\dot{r} = pq \left(\frac{I_x - I_y}{I_z} \right) + (\dot{p} - qr) \frac{I_{xz}}{I_z} + N$$

Also, by transformation, earth velocities are obtained

$$\dot{x} = u \cos \theta \cos \psi + v(\sin \phi \sin \theta \cos \psi + \cos \phi \sin \psi) + w(\sin \phi \sin \psi + \cos \phi \sin \theta \cos \psi)$$

$$\dot{y} = u \cos \theta \sin \psi + v(\cos \phi \cos \psi + \sin \phi \sin \theta \sin \psi) + w(\cos \phi \sin \theta \sin \psi - \sin \phi \cos \psi)$$

$$\dot{h} = -u \sin \theta + v \sin \phi \cos \theta + w \cos \phi \cos \theta$$

where

θ = pitch angle

ψ = heading angle

ϕ = roll angle

h = altitude

The preceding nine differential equations constitute the nonlinear equations of motion to be integrated. DYNK performs this integration using a single-step Euler formula

$$y_n = y_{n-1} + \frac{h}{2} (3f_n - f_{n-1}) + O(h^2)$$

where

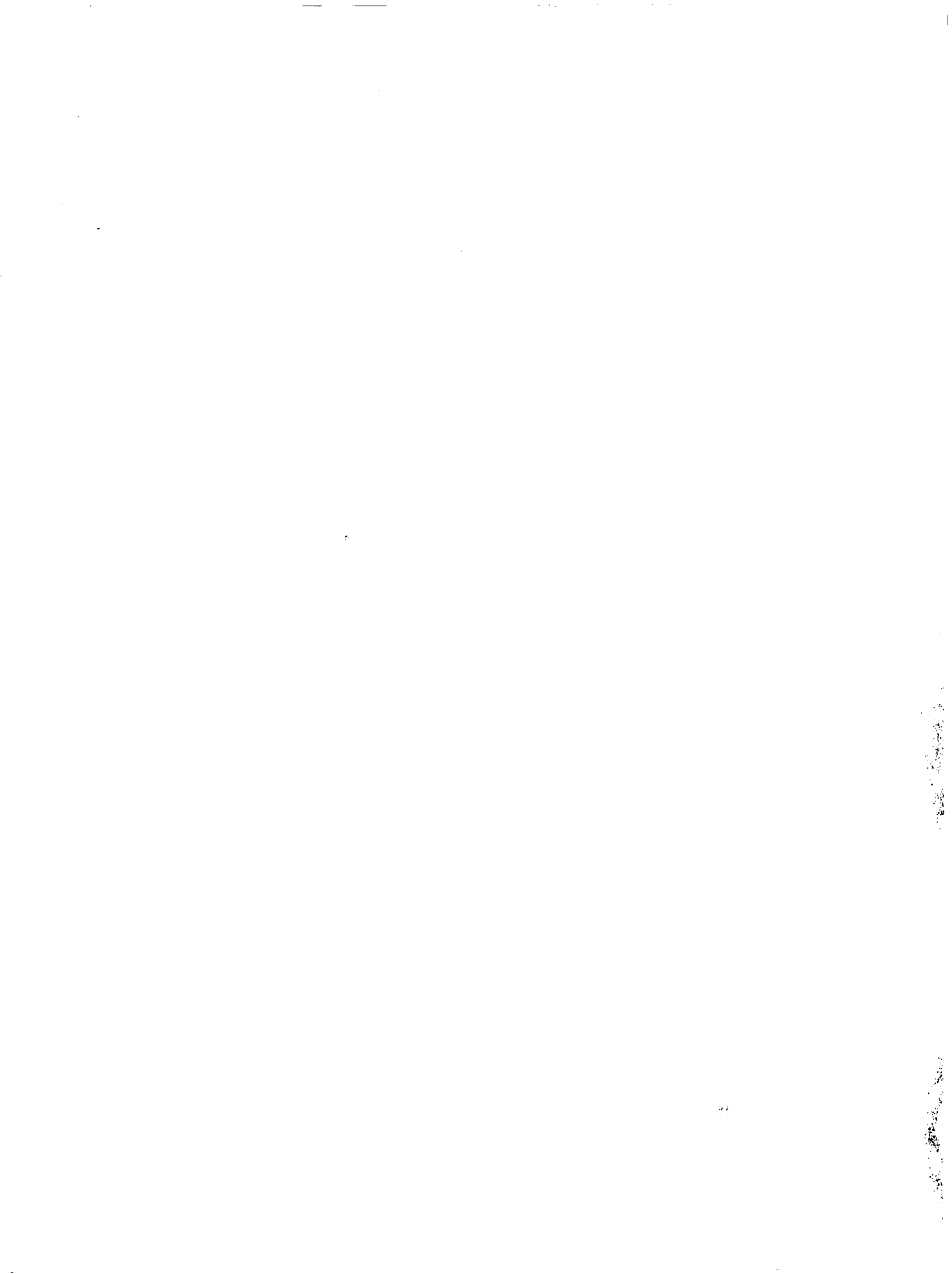
y = integral

h = step size

f = derivative function

Subroutine DYNK is also used to evaluate the equations of motion after state perturbation by the linearization routine LINK. In this mode, specified by entering DYNK with the formal parameter LIN \neq 0, no integration is performed.

A Array Dictionary -- A complete tabulation of the variables assigned to in A array in F8SIM is given in Appendix A.



APPENDIX D

F-8C WING ROOT LOADS

APPENDIX D

F-8C WING ROOT LOADS

INTRODUCTION

Data were not available to determine wing root loads from a model incorporating flexure. However, perturbation loads equations were developed for a rigid aircraft under symmetric, short-period motion.

Inertial forces are generated from section mass and inertia data are taken from LTV data [29]. Aero dynamic loads are generated by using thin-airfoil, two-dimensional strip estimates for $C_L[y]$ and $C_m[y]$, by assuming $C_L[y]$ is the average between elliptical and two-dimensional (the Schrenk approximation), and by forcing the results to yield the correct wing $C_{L\alpha}$.

Finally, numerical values are presented for the aircraft operating at $M = 0.67$ at 20,000 ft.

SUMMARY OF RESULTS

Formulas are presented for the wing root shear (S), bending moment (B), and torsion moment (T). The shear is taken to be the load outboard of panel 1 (cf Figure D-1). The torsion and bending moments are taken about Λ_R and orthogonal to it. The reference Λ_R is arbitrarily taken to be midway between the two spars. It should more logically be taken about the elastic axis (assuming there is one). Since this location is not known, the axis midway between the two spars should be sufficient for the intended purposes.

The forces are the sum of inertial and aerodynamic forces, i. e.,

$$S + S_I + S_A \quad (1)$$

$$T + T_I + T_A \quad (2)$$

$$B = B_I + B_A \quad (3)$$

The inertial forces are given by equations (4) through (6). Aerodynamic forces are given by equations (7) through (9). All symbols are defined in Table D-1.

To evaluate equations (4) through (6) the data of Table D-2 will have to be converted for dimensions. In addition, since our equations are cast in a NACA coordinate system centered at the center of gravity, the shop coordinate system data needs to be converted in an obvious way.

In equations (7) through (9) the tildes over the numbers in the first summations indicate inclusion over the entire chord, e.g., $\tilde{2} = 2 + 19$, $\tilde{3} = 3 + 20$, $\tilde{4} = 4 + 21 + 36$, $\tilde{10} = 10 + 27 + 42$, $\tilde{11} = 11 + 28$, etc. The hat notation is similar

$$\begin{aligned} & \hat{i} \text{ for } i \text{ 3-19} \\ i = & \hat{\quad} \\ & 2 \text{ chordwise extension of section 19} \end{aligned}$$

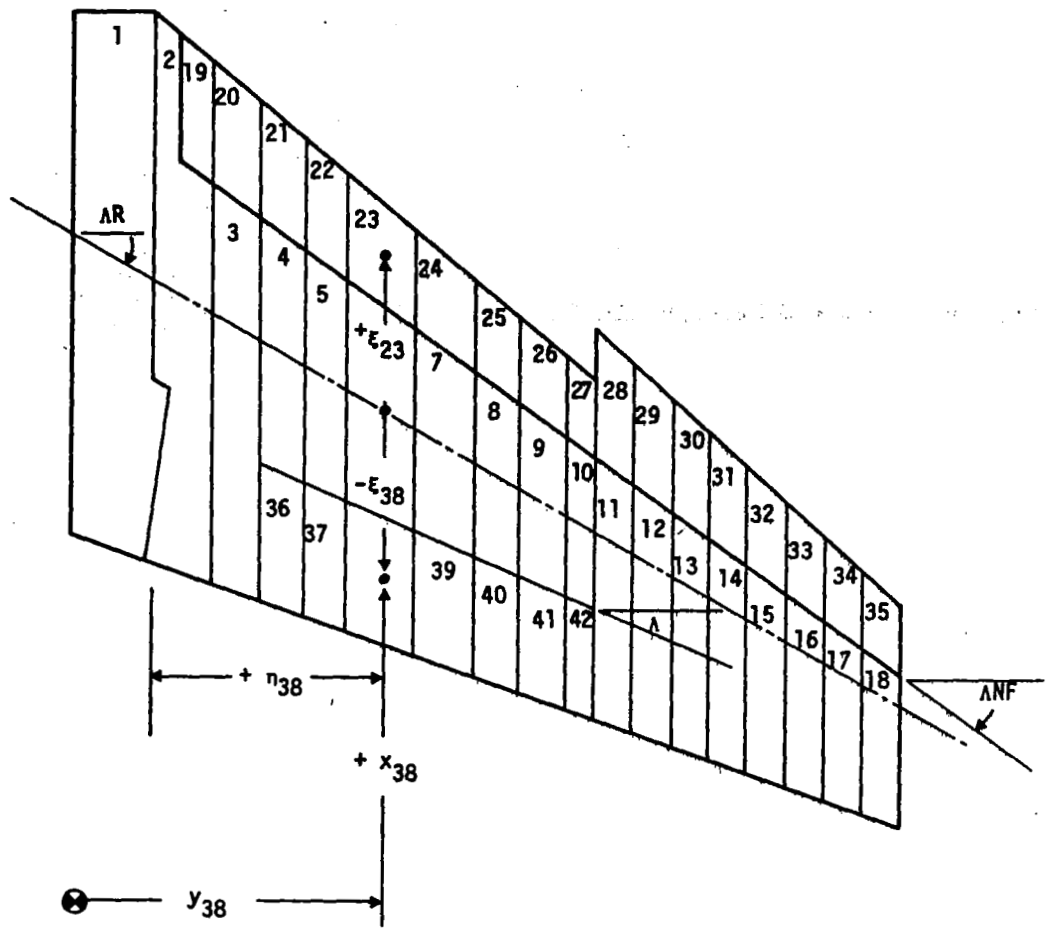


Figure D-1. Right Wing Panel

100-7011-8

Table D-1. Symbol Definition

Symbol	Description	Units
B	Right wing down root bending moment about axis orthogonal to ΔR (cf Figure D-1)	ft-lb
Both	T. E. or L. E. (cf Figure D-1)	
C_L	Airplane (wing) lift coefficient	
$C_{L_i} = C_{L_i}[y]$	Wing section lift coefficient	
C_m	Wing section moment coefficient	
I_{xx}	Section x-axis inertia about its cg	slug ft ²
I_{xy}	Section cross product inertia about its cg	slug ft ²
I_{yy}	Section y-axis inertia about its cg	slug ft ²
L. E.	Leading edge (cf Figure D-1)	
S	Shear force (positive down)	lb
S	Wing area	ft ²
T	Nose up root torsion moment about ΔR	ft-lb
T. E.	Trailing edge (cf Figure D-1)	
b	Wing span	ft
c	Chord length	ft
m	Mass	slug
q	Body axis nose up perturbation pitch rate	rad/sec
\bar{q}	Dynamic pressure	lb/ft ²
u_o	Body axis forward equilibrium speed	ft/sec
w	Body axis downward perturbation velocity	ft/sec
$\sim w$	Wind velocity (positive up)	ft/sec
x	Body axis distance forward of cg	ft
x_H	Hinge line position back of L. E.	ft
y	Body axis distance (right positive)	ft

Table D-1. (Cont.)

Symbol	Description	Units
ΔB	Bending due to moments (cf equation 32)	ft-lb
Δ_{RA}	Distance .25c is ahead of AR (cf Figure D-1)	ft
Δ_T	Torsion due to moments (cf equation 31)	ft-lb
ΔX_{NF_1}	Distance nose flap cg is forward of hinge line	ft
$\Delta X_{\delta a_1}$	Distance aileron cg is forward of hinge line	ft
ANF	Sweep angle of nose flap hinge line (cf Figure D-1)	rad
ΔR	Sweep angle of reference (elastic) axis (cf Figure D-1)	rad
$\Delta \delta a$	Sweep angle of aileron hinge line (cf Figure D-1)	rad
Ω_x	Angular velocity about x axis	rad/sec
Ω_y	Angular velocity about y axis	rad/sec
α	Angle of attack	rad
δB	Bending due to forces (cf equation 34)	ft-lb
δ_{NF}	Nose flap downward deflection about hinge	rad
δ_T	Torsion due to forces (cf equation 33)	ft-lb
δa	Aileron downward deflection about hinge	rad
η	Deflection of δa or δ_{NF} about constant chord line (positive downward)	rad
η	Δ_y from section 1 (cf Figure D-1)	ft
ξ_1	Distance section cg is forward of AR (cf Figure D-1)	ft
θ_H	Hinge line position (cf equation 41)	rad

SPECIAL SUBSCRIPTS

I Inertial
 A Aerodynamic

SPECIAL SUPERSCRIPTS

~ on numbers
 ^ on numbers

Table D-2. XF8U-1 Wing Inertial Data

SL	Wt. Lb.	\bar{X} In.	\bar{Y} In.	I XX Lb. -In. ²	I YY Lb. -In. ²	P XY Lb. -In. ²
01	305.310	418.6635	009.543414	14558.92000	341064.5000	0451.600000
02	259.370	435.0787	026.463620	06257.09300	274626.9000	7270.230000
03	104.350	449.5705	041.140490	03126.40700	159516.6000	-0984.100000
04	178.220	455.0061	053.765290	02933.23200	098760.9600	0250.980000
05	172.900	464.2249	065.807400	02982.62000	088254.7400	0305.610000
06	274.100	475.0020	079.537030	11349.15000	133321.0000	0350.200000
07	299.310	488.1441	095.736680	09987.90000	118957.4000	-0440.510000
08	126.270	494.1393	109.464400	02060.71200	034437.5100	0150.870000
09	153.390	505.9262	121.111800	03184.55400	037439.8400	1424.140000
10	060.090	511.1077	130.406200	00502.33990	014298.9400	-0628.011000
11	032.150	510.8065	139.714700	00338.85530	013107.0300	-0148.072000
12	030.130	525.1201	150.060000	00307.52080	012253.7000	-0165.356000
13	026.850	534.2037	160.000000	00269.19790	008021.2880	0000.001000
14	027.220	539.2781	169.591100	00387.27120	009558.0120	0275.997000
15	017.900	551.7424	180.000000	00188.99600	004046.5160	0000.001000
16	016.840	558.9428	190.121100	00194.69640	003331.6850	-0094.905000
17	014.510	566.2468	199.434100	00188.69510	002900.3230	0130.086000
18	009.880	571.7939	209.385600	00095.65945	001756.4920	-0060.131400
19	007.570	380.4241	030.499330	00114.10780	001573.4050	-0000.053100
20	010.860	392.3207	041.654690	00180.13020	002231.9380	0069.532200
21	010.350	403.8261	053.316420	00172.33770	001932.8400	-0012.870500
22	007.960	415.3681	065.500000	00121.02000	001116.2720	-0000.025100
23	024.310	431.2615	077.137800	00587.80110	002414.9850	-0090.766120
24	010.780	446.9326	096.585340	00446.99250	001553.2870	0086.322980
25	007.170	459.4908	108.892600	00117.60760	000833.7164	-0004.801120
26	007.030	471.3301	121.499200	00107.05010	000905.7369	0000.011640
27	003.560	481.4276	131.491500	00055.28104	000304.2213	-0028.800000
28	008.520	485.0148	140.000000	00071.00000	001200.0070	0000.019900
29	010.830	496.3992	150.528100	00098.45000	001156.2020	0014.868600
30	007.430	505.7150	160.000000	00061.99130	000989.2953	-0000.000100
31	009.030	518.3155	170.969200	00090.14444	001036.9410	0058.764290
32	010.740	520.4850	180.000000	00052.99160	001033.4210	-0000.000100
33	007.210	538.7101	190.951400	00086.64653	000557.4673	0054.086800
34	006.670	547.0079	198.962500	00081.25636	000391.8979	0002.740000
35	003.800	557.9236	209.500000	00030.99800	000264.1199	-0000.080000
36	009.120	524.8184	053.150210	00101.80350	001604.7230	0030.034000
37	014.580	523.6945	066.157060	00133.55620	002231.7820	-0105.202000
38	015.710	536.1441	079.735830	00509.31610	002442.5890	0012.695000
39	017.430	538.4967	094.728050	00426.99370	002180.2330	0095.963000
40	006.980	548.5696	109.091600	00061.74745	000785.7750	0014.683800
41	000.740	551.0862	121.454800	00069.53230	001150.6220	-0013.436700
42	003.270	557.5960	130.409700	00023.11011	000342.7052	0000.919500

$C_{L\alpha}$ is a function of y , i. e., the section value. It is given by equation (10). $C_{L\alpha}$ should be the wing only value. For present purposes the value of $C_{L\alpha}$ for the entire aircraft should be acceptable.

Section values of $C_{L\delta_a}$, $C_{L\delta_{NF}}$, $C_{m\delta_a}$, and $C_{m\delta_{NF}}$ are given by equations (11) through (14). Values of $C_{L_n}/2\pi$ T. E., $C_{L_n}/2\pi$ L. E., and $C_{m\eta}$ both are presented in Figure D-2 and Table D-3.

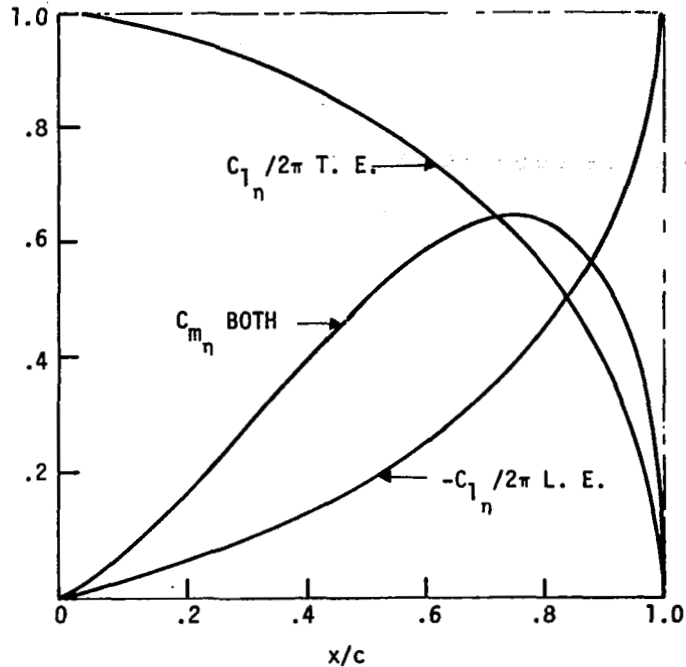


Figure D-2. Thin Airfoil Characteristics

Table D-3. Thin Airfoil Characteristics

x	cos θ	sin θ	θ	$C_{l_{\eta/2\pi}}$ T. E.	C_{m2} BOTH	$C_{l_{\eta/2\pi}}$ L. E.
0.00	1.0	0.0000	0.0000	1.0000	0.0000	-0.0000
0.10	0.8	0.6000	0.6435	0.9862	-0.0600	-0.0138
0.20	0.6	0.8000	0.9273	0.9595	-0.1600	-0.0405
0.30	0.4	0.9165	1.1593	0.9227	-0.2750	-0.0773
0.40	0.2	0.9798	1.3694	0.8760	-0.3919	-0.1240
0.50	0.0	1.0000	1.5701	0.8185	-0.5000	-0.1818
0.60	-0.2	0.9798	1.7722	0.7478	-0.5879	-0.2522
0.70	-0.4	0.9165	1.9823	0.6607	-0.6416	-0.3393
0.80	-0.6	0.8000	2.2143	0.5498	-0.6400	-0.1502
0.90	-0.8	0.6000	2.4981	0.3958	-0.5400	-0.6042
0.95	-0.9	0.4359	2.6906	0.2823	-0.4141	-0.7177
1.00	-1.0	0.0000	3.1416	0.0000	0.0000	-1.0000

ROOT D'ALEMBERT INERTIAL SHEAR

$$\begin{aligned}
 S_I = & \dot{w} \sum_2^{42} m_i + q (u_o) \sum_2^{42} m_i + q \sum_2^{42} m_i x_i \\
 & - \ddot{\delta}_{NF} \{ \cos(\Delta NF) \} \sum_{19}^{35} m_i (\Delta x NF)_i \\
 & + \ddot{\delta}_a \{ \cos(\Delta \delta a) \} \sum_{36}^{42} m_i (\Delta x \delta a)_i
 \end{aligned} \tag{4}$$

ROOT D'ALEMBERT INERTIAL TORSION

$$\begin{aligned}
 T_I = & + \dot{w} \{ \cos(\Delta R) \} \sum_2^{42} m_i \xi_i \\
 & - q (u_o) \{ \cos(\Delta R) \} \sum_2^{42} m_i \xi_i
 \end{aligned}$$

$$\begin{aligned}
& \left\{ -\dot{q} \sum_2^{42} \left[(\cos \Delta R) m_{i i} x_i \xi_i + \sin (\Delta R) I_{x y_i} + \cos (\Delta R) I_{y y_i} \right] \right\} \\
& + \delta_{NF} \left\{ \sum_{19}^{35} \left[(\cos \Delta R) \cos (\Delta N F) m_i (\Delta X N F)_i \xi_i \right. \right. \\
& \quad + (\sin \Delta R \cos \Delta N F + \cos \Delta R \sin \Delta N F) I_{x y_i} \\
& \quad \left. \left. + \sin \Delta N F \sin \Delta R I_{x x_i} + \cos \Delta N F \cos \Delta R I_{y y_i} \right] \right\} \\
& + \delta_a \left\{ \sum_{36}^{42} \left[-(\cos \Delta R) \cos (\Delta \delta a) m_i (\Delta x \delta a)_i \xi_i \right. \right. \\
& \quad \left. \left. - (\sin \Delta R) (\cos \Delta \delta a) - (\cos \Delta R) (\sin \Delta \delta a) I_{x y_i} \right. \right. \\
& \quad \left. \left. - \cos \Delta \delta a \sin \Delta R I_{x x_i} - \cos \Delta \delta a \cos \Delta R I_{y y_i} \right] \right\} \quad (5)
\end{aligned}$$

ROOT D'ALEMBERT INERTIAL BENDING

$$\begin{aligned}
B_I &= -\dot{w} \left\{ \sec(\Delta R) \sum_2^{42} m_i \eta_i \right. \\
& + q(u_o) \sec(\Delta R) \sum_2^{42} m_i \eta_i \\
& \left. + \dot{q} \sum_2^{42} \left[\sec(\Delta R) m_{i i} x_i \eta_i + \cos \Delta R I_{x y_i} - \sin \Delta R I_{y y_i} \right] \right\} \\
& + \delta_{NF} \left\{ \sum_{19}^{35} \left[-(\sec \Delta R) (\cos \Delta N F) m_i (\Delta X N F)_i \eta_i \right. \right. \\
& \quad \left. \left. - (\cos \Delta R \cos \Delta N F + \sin \Delta R \sin \Delta N F) I_{x y_i} \right] \right\}
\end{aligned}$$

$$\begin{aligned}
& -(\cos \Lambda NF) (\cos \Lambda R) I_{xx_i} + (\cos \Lambda NF) (\sin \Lambda R) I_{yy_i} \Big\} \\
& + \delta a \left[\begin{array}{l} 42 \\ \Sigma + (\sec \Lambda R) (\cos \Lambda \delta a) m_i (\Delta x \delta a)_i \eta_i \\ 36 \end{array} \right. \\
& (+ \cos \Lambda R \cos \Lambda \delta a - \sin \Lambda R \sin \Lambda \delta a) I_{xy_i} \\
& \left. + (\sin \Lambda \delta a) (\cos \Lambda R) I_{xx_i} - (\cos \Lambda \delta a) (\sin \Lambda R) I_{yy_i} \right] \Big\} \quad (6)
\end{aligned}$$

ROOT AERODYNAMIC SHEAR

$$\begin{aligned}
S_A = - \{w + \tilde{w}\} \frac{\bar{q}}{V} \frac{\tilde{I}8}{\Sigma} C_{L_{\alpha_i}} \Delta S_i \\
- \delta a \bar{q} \frac{\tilde{I}0}{\Sigma} C_{L_{\delta a_i}} \Delta S_i \\
- \delta NF \bar{q} \frac{\hat{1}8}{\Sigma} C_{L_{\delta NF_i}} \Delta S_i \quad (7)
\end{aligned}$$

ROOT AERODYNAMIC TORSION

$$\begin{aligned}
T_A = + \{w + \tilde{w}\} \frac{\bar{q}}{V} \cos(\Lambda R) \frac{\tilde{I}8}{\Sigma} \{C_{L_{\alpha_i}} (\Delta RA)_i\} \Delta S_i \\
+ \delta a \bar{q} \cos \Lambda R \frac{\tilde{I}0}{\Sigma} \{C_{L_{\delta a_i}} (\Delta RA)_i + c C_{m_{\delta a_i}}\} \Delta S_i \\
+ \delta NF \bar{q} \cos \Lambda R \frac{\hat{1}8}{\Sigma} \{C_{L_{\delta NF_i}} (\Delta RA)_i + c C_{m_{\delta NF_i}}\} \Delta S_i \quad (8)
\end{aligned}$$

ROOT AERODYNAMIC BENDING

$$\begin{aligned}
 B_A = \{w + \tilde{w}\} \frac{\bar{q}}{V} \frac{\hat{18}}{2} \sum \{(-\sec \Lambda R) C_{L\alpha_i} \eta_i \Delta S_i\} \\
 + \delta a \frac{\tilde{10}}{4} \sum \{(-\sec \Lambda R) C_{L\delta a_i} \eta_i + c C_{m\delta a_i} \sin \Lambda R\} \Delta S_i \\
 + \delta_{NF} \frac{\hat{18}}{2} \sum \{(-\sec \Lambda R) C_{L\delta_{NF}_i} \eta_i + c C_{m\delta_{NF}_i} \sin \Lambda R\} \Delta S_i
 \end{aligned} \tag{9}$$

$$C_{L\alpha} = \frac{C_{L\alpha}}{2} \left\{ 1 + \frac{4S}{\pi cb} \sqrt{1 - (2y/b)^2} \right\} \tag{10}$$

$$C_{L\delta a} + \cos(\Lambda \delta a) \left\{ \frac{C_{L\eta}}{2\pi} \text{T. E.} \right\} C_{L\alpha} \tag{11}$$

$$C_{L\delta_{NF}} = \cos(\Lambda \delta_{NF}) \left\{ \frac{C_{L\eta}}{2\pi} \text{L. E.} \right\} C_{L\alpha} \tag{12}$$

$$C_{m\delta a} = \cos(\Lambda \delta a) \left\{ C_{m\eta} \text{BOTH} \right\}_{\delta a} \tag{13}$$

$$C_{m\delta_{NF}} = \cos(\Lambda \delta_{NF}) \left\{ C_{m\eta} \text{BOTH} \right\}_{\delta_{NF}} \tag{14}$$

DERIVATION OF EQUATIONS

The inertial forces are derived first; then the aerodynamic forces are presented.

Inertial

Consider a hinged section A on the otherwise rigid aircraft (Figure D-3). The linearized local inertial forces are given by equations (15) through (17). Ω_x and Ω_y are the angular rates about hinge lines oriented with x and y.

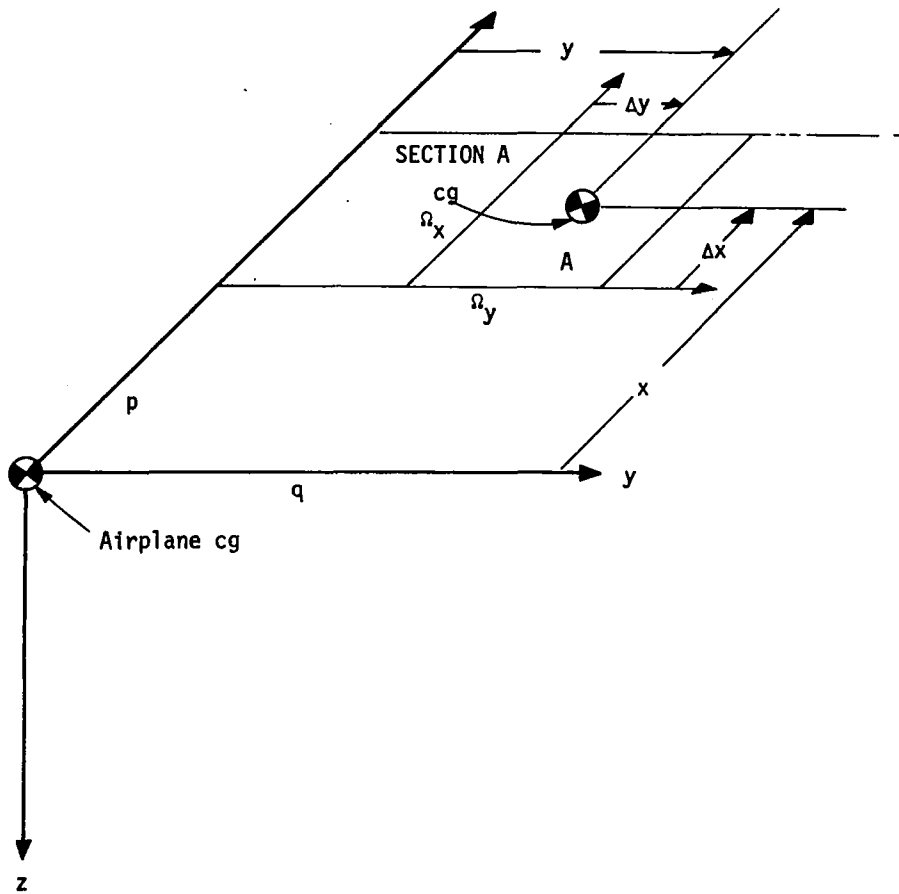


Figure D-3. Coordinate System.

These forces and angles need to be resolved. The resolution formulae are given by equations (27) through (34).

Equations (15) through (34) are combined in an obvious way to yield equations (4) through (6).

TRIM LINEARIZED SYMMETRIC D'ALEMBERT FORCES ABOUT LOCAL CG

$$F_{z_i} = m_i \{-\dot{w} + u_o \dot{q} + x_i \dot{q} + (\Delta x)_i \dot{\Omega}_y - (\Delta y)_i \dot{\Omega}_x\} \quad (15)$$

$$M_{x_i} = I_{xy_i} \dot{q} + I_{xy_i} \dot{\Omega}_y - I_{xx_i} \dot{\Omega}_x \quad (16)$$

$$M_{y_i} = -I_{yy_i} \dot{q} - I_{yy_i} \dot{\Omega}_y + I_{xy_i} \dot{\Omega}_x \quad (17)$$

On a Fixed Portion of the Wing

$$F_{z_i} = m_i \{-\dot{w} + u_o \dot{q} + x_i \dot{q}\} \quad (18)$$

$$M_{x_i} = I_{xy_i} \dot{q} \quad (19)$$

$$M_{y_i} = -I_{yy_i} \dot{q} \quad (20)$$

On the Aileron

$$F_{z_i} = m_i \{-\dot{w} + u_o \dot{q} + x_i \dot{q} + (\Delta x)_i \cos \Lambda \delta a \ddot{\delta a}\} \quad (21)$$

$$M_{x_i} = I_{xy_i} \dot{q} + I_{xy_i} (\cos \Lambda \delta a) \ddot{\delta a} + I_{xx_i} (\sin \Lambda \delta a) \ddot{\delta a} \quad (22)$$

$$M_{y_i} = -I_{yy_i} \dot{q} - I_{yy_i} (\cos \Lambda \delta a) \ddot{\delta a} - I_{xy_i} (\sin \Lambda \delta a) \ddot{\delta a} \quad (23)$$

On the Nose Flap

$$F_{z_i} = M_i \{-\dot{w} + u_o \dot{q} + x_i \dot{q} - (\Delta x)_i (\cos \Lambda NF) \delta NF\} \quad (24)$$

$$M_{x_i} = I_{xy_i} \dot{q} - I_{xy_i} (\cos \Lambda NF) \delta NF - I_{xx_i} (\sin \Lambda NF) \delta NF \quad (25)$$

$$M_{y_i} = -I_{yy_i} \ddot{q} + I_{yy_i} (\cos \Lambda NF) \ddot{\delta NF} + I_{x_{y_i}} (\sin \Lambda NF) \ddot{\delta NF} \quad (26)$$

Resolution Formulae

$$\dot{\Omega}_x = + (\sin \Lambda NF) \ddot{\delta NF} \quad (27)$$

$$\dot{\Omega}_y = - (\cos \Lambda NF) \ddot{\delta NF} \quad (28)$$

$$\dot{\Omega}_x = - (\sin \Lambda \delta a) \ddot{\delta a} \quad (29)$$

$$\dot{\Omega}_y = + (\cos \Lambda \delta a) \ddot{\delta a} \quad (30)$$

$$\Delta T = (\cos \Lambda R) M_y - (\sin \Lambda R) M_x \quad (31)$$

$$\Delta B = (\cos \Lambda R) M_x + (\sin \Lambda R) M_y \quad (32)$$

$$\delta T = - (\cos \Lambda R) \xi F_z \quad (33)$$

$$\delta B = + (\sec \Lambda R) \eta F_z \quad (34)$$

AERODYNAMIC

Thin airfoil theory yields the following [30]:

Wing Section

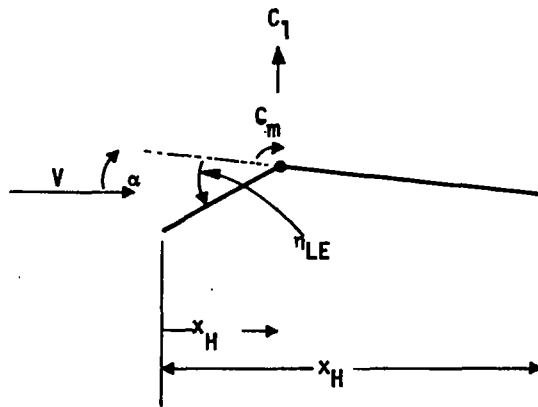
$$C_{L_\alpha} / 2\pi = 1.0 \quad (35)$$

$$C_{m_\alpha} = 0 \quad (36)$$

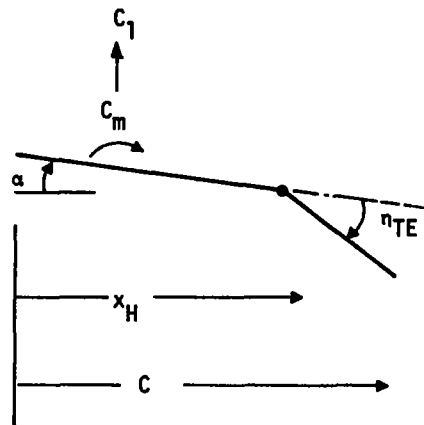
Trailing Edge Flap (Figure D-4)

$$C_{L_\eta} / 2\pi = 1 - \frac{\theta_H}{\pi} + \frac{\sin \theta_H}{\pi} \quad (37)$$

$$C_{m_\eta} = \frac{1}{2} \sin \theta_H (\cos \theta_H - 1) \quad (38)$$



LE FLAP



TE FLAP

Figure D-4. Flapped Airfoil Section

Leading Edge Flap (Figure D-4)

$$C_{L\eta} / 2\pi = -\frac{\theta_H}{\pi} + \frac{\sin \theta_H}{\pi} \quad (39)$$

$$C_{m\eta} = \frac{1}{2} \sin \theta_H (\cos \theta_H - 1) \quad (40)$$

where

C_m is the .25 chord value and

$$x_H = \frac{c}{2} (1 - \cos \theta_H) \quad (41)$$

$$x = 0 \quad \text{Leading edge (L. E.)} \quad (42)$$

$$x_h \quad \text{Hinge line} \quad (43)$$

$$X = c \quad \text{Trailing edge} \quad (44)$$

These formulas may be found in most any book on subsonic aerodynamics (in particular on pp. 84-87 of reference [30]).

The crudest approximation would assume

$$C_{L\alpha} = C_{L\alpha} \text{ wing} \quad (45)$$

$$C_{L\delta} = (\cos \Lambda) \frac{C_{L\alpha}}{2\pi} (C_{L\eta} \text{ thin airfoil data}) \quad (46)$$

$$C_{m\delta} = (\cos \Lambda) C_{m\eta} \text{ thin airfoil} \quad (47)$$

The wing, however, has a tendency toward the ideal lift distribution. We therefore assume the Schrenk approximation midway between the crudest and elliptical. The results are given by equations (10) through (14).

NUMERICAL EXAMPLE

The preceding equations were evaluated at Flight Condition 1 ($M = 0.67$ at 20,000 ft).

Inertial

Shear (cf equation 4)

$$S_I = -73.896 \dot{w} + 51,264. \dot{q} - 666.41 \ddot{q} - 2.6920 \delta_{NF}'' - 2.2593 \delta_a''$$

Torsion (cf equation 5)

$$T_I = +33.066 \dot{w} - 22,939. \dot{q} - 55.070 \ddot{q} + 10.729 \ddot{\delta}_{NF} - 9.9544 \ddot{\delta}_a$$

Bending (cf equation 6)

$$B_I = -418.93 \dot{w} + 290,630. \dot{q} - 4968.7 \ddot{q} - 23.641 \ddot{\delta}_{NF} - 16.345 \ddot{\delta}_a$$

Aerodynamic

At this flight condition $C_{L\alpha} = 3.78/\text{rad}$. Strip coefficients (cf. equations 10-14) are presented in Table D-4.

Shear (cf equation 7)

$$S_A = -268.36 w - 53,567. \delta_a + 11,294. \delta_{NF}$$

Torsion (cf equation 8)

$$T_A = +209.61 w - 91636. \delta_a - 52190. \delta_{NF}$$

Bending (cf equation 9)

$$B_A = -2212.7 w - 473940. \delta_a + 71904. \delta_{NF}$$

Finally steady-state bending (B_I) was evaluated for a maneuver using only the elevator (Mode I) and then the minimum drag positions for the leading and trailing edge flaps (see Table D-5).

These results show that B_I is reduced, indicating that minimum drag positioning of the surfaces probably does not adversely affect wing bending. It is felt that more complete modeling including flexure is needed to address this issue completely.

Table D-4. Aerodynamic Section Coefficients

STRIP	CLA	CLDA	CLNF	CMDA	CMNF
1	.34301E+01	.18261E+01	-.19984E+00	-.57748E+00	-.11652E+00
2	.35206E+01	.18742E+01	-.20510E+00	-.57748E+00	-.11652E+00
3	.3600 E+01	.19166E+01	-.20974E+00	-.57748E+00	-.11652E+00
4	.36695E+01	.19867E+01	-.21378E+00	-.57748E+00	-.11652E+00
5	.37362E+01	.20228E+01	-.21767E+00	-.57748E+00	-.11652E+00
6	.38126E+01	.20985E+01	-.22212E+00	-.58651E+00	-.11652E+00
7	.39021E+01	.21478E+01	-.22575E+00	-.58651E+00	-.11652E+00
8	.39758E+01	.22242E+01	-.26058E+00	-.58651E+00	-.11652E+00
9	.40349E+01	.22937E+01	-.26445E+00	-.57748E+00	-.11652E+00
10	.40782E+01	.23551E+01	-.26729E+00	-.57748E+00	-.12380E+00
11	.41478E+01	.23953E+01	-.27185E+00	-.57748E+00	-.12380E+00
12	.41159E+01	.24140E+01	-.26976E+00	-.57748E+00	-.12380E+00
13	.41626E+01	.24789E+01	-.30313E+00	-.57297E+00	-.12380E+00
14	.41532E+01	.25109E+01	-.30245E+00	-.56846E+00	-.12380E+00
15	.40993E+01	.25153E+01	-.29853E+00	-.55944E+00	-.12380E+00
16	.39691E+01	.25070E+01	-.28904E+00	-.55041E+00	-.12380E+00
17	.37153E+01	.24137E+01	-.27056E+00	-.54139E+00	-.12380E+00
18	.30716E+01	.20510E+01	-.22369E+00	-.53237E+00	-.12380E+00

Table D-5. Maneuver Parameters - F. C. 1

MODE I	MINIMUM DRAG
$\dot{w} \approx 0$	$\dot{w} \approx 0$
$q = -0.03 \text{ rad/sec}$	$q = -0.03 \text{ rad/sec}$
$\alpha = -.032 \text{ rad}$	$\alpha = -.02 \text{ rad}$
$u_o = 694 \text{ ft/sec}$	$u_o = 694 \text{ ft/sec}$
$w = 22.2 \text{ ft/sec}$	$w = 13.8 \text{ ft/sec}$
$\delta_F = 0$	$\delta_f = -.1 \text{ rad}$
$\delta_{t_e} = 0$	$\delta_{t_e} = +.12 \text{ rad}$

APPENDIX E
EXPERIENCE QUESTIONNAIRE AND GLOBAL AND
COOPER-HARPER RATING SCALES

APPENDIX E

EXPERIENCE QUESTIONNAIRE, AND GLOBAL AND
COOPER-HARPER RATING SCALES

Date _____

Name _____

Address _____

Highest Military Rank _____

Current Job Title _____

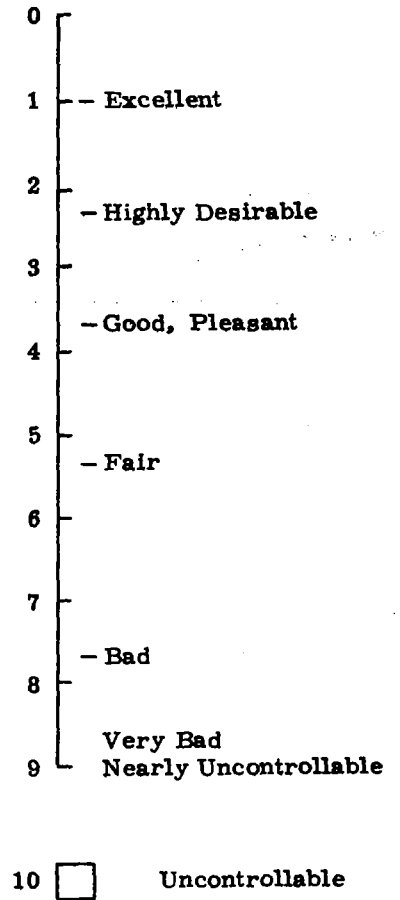
FLYING HISTORY

<u>Type of Aircraft</u>	<u>No. of Total Hours/ No. of Instrument Hours</u>	<u>Currently Qualified? (Yes/No)</u>
1. _____	_____	_____
2. _____	_____	_____
3. _____	_____	_____
4. _____	_____	_____
5. _____	_____	_____
6. _____	_____	_____

Answer the following questions in order:

HANDLING QUALITIES

- | | Yes | No |
|---|--------------------------|--------------------------|
| 1. Is the vehicle controllable during this task? | <input type="checkbox"/> | <input type="checkbox"/> |
| 2. Is the vehicle acceptable for the task? (May have deficiencies which warrant improvement, but is adequate for the task.) | <input type="checkbox"/> | <input type="checkbox"/> |
| 3. Is the vehicle satisfactory for the task? (i. e., adequate for the task without improvement.) | <input type="checkbox"/> | <input type="checkbox"/> |



RESPONSE CHARACTERISTICS

CONTROL

- 0
- 1 - Excellent, pure (i. e., no accidental excitation) primary and secondary response characteristics
- 2
- 3
- 4 - Good, relatively pure, primary and secondary response characteristics
- 5
- 6 { Fair, somewhat impure, primary or secondary response characteristics
- 7 { Quite sensitive, sluggish, or uncomfortable in primary or secondary responses
- 8 { Extremely sensitive, sluggish, or uncomfortable in primary or secondary responses
- 9 - Nearly uncontrollable

- 0
- 1 - Extremely easy to control with excellent precision
- 2
- 3 - Very easy to control with good precision
- 4
- 5 - Easy to control with fair precision
- 6 - { Controllable with somewhat inadequate precision
- 7 - { Controllable, but only very imprecisely
- 8 - Difficult to control
- 8 - Very difficult to control
- 9 - Nearly uncontrollable

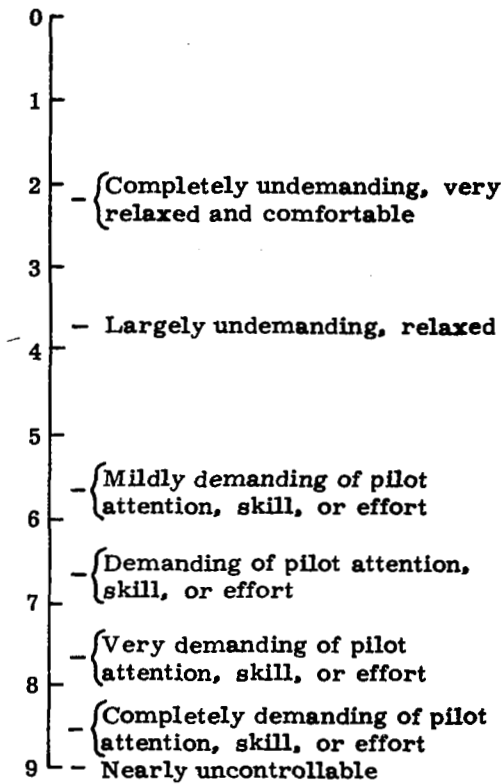
10 Uncontrollable

Not Applicable

10 Uncontrollable

Not Applicable

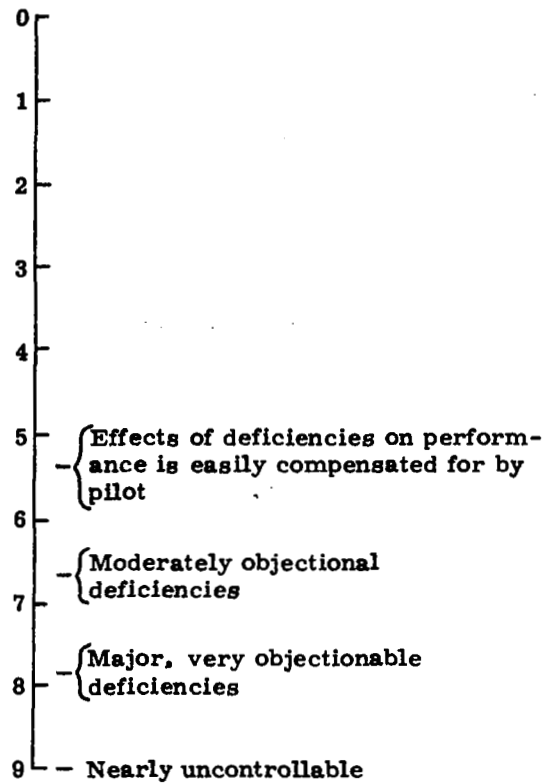
DEMANDS ON PILOT



10 Uncontrollable

Not Applicable

EFFECTS OF DEFICIENCIES



10 Uncontrollable

Not Applicable

REFERENCES

1. Deets, D. A. and Szalai, K. J., "Design and Flight Experience with a Digital Fly-by-wire Control System Using Apollo Guidance System Hardware on an F-8 Aircraft," AIAA Paper 72-881, Guidance and Control Conference, Stanford, California, August 1972.
2. Konar, A. F. and Ward, M. D., Development of Weapon Delivery Models and Analysis Programs, Volume II, "Documentation of the Armament Delivery Analysis Programming System (ADAPS)," AFFDL-TR-71-123, April 1972.
3. VanDierendonck, A. J. and Hartmann, G. L., Quadratic Methodology, Honeywell Report F0161-FR, October 1973.
4. Konar, A. F., et al., "Digital Flight Control System Analysis," Technical Report AFFDL-TR-73-119, Air Force Flight Dynamics Laboratory, Wright-Patterson Air Force Base, December 1973.
5. "New Short Period Handling Quality for Fighter Aircraft," Boeing Document D6-17841T/N, October 1965.
6. Kisslinger, R. L. and Wendl, M., Survivable Flight Control System Interim Report No. 1, Studies Analysis and Approach, AFFDL-TR-71-20 Supplement 1, Wright-Patterson Air Force Base, May 1971.
7. Military Specification -- Flying Qualities of Piloted Airplanes, MIL-F-8785B(ASG), 7 August 1969.
8. Sisk, T. R. et al, Use of Maneuver Flaps to Enhance the Transonic Maneuverability of Fighter Aircraft: NASA TM X-2844 (Confidential) Flight Research Center, Edwards, California, July 1973.
9. Jarvis, C. R., "An Overview of NASA's Digital Fly-by-wire Technology Development Program", in NASA TN D-7843 Flight Research Center, Edwards, California, February 1975.
10. Yore, E. E. and Gunderson, D. C., "Active Control System Trends," NASA Symposium on Advanced Control Technology and its Potential for Future Transport Aircraft, Los Angeles, California, July 9-11, 1974.
11. VanDierendonck, A. J., Stone, C. R., Ward, M. D., "Application of Practical Optimal Control Theory to the C-5A Load Improvement Control System (LICS), Wright-Patterson Air Force Base, AFFDL-TR-73-122, October 1973.
12. Monaghan, R. C. and Friend, E. L., Effects of Flaps on Buffet Characteristics and Wing-rock Onset of an F-8C Airplane at Subsonic and Transonic Speeds: NASA TM X-2873, Flight Research Center, Edwards, California, August 1973.
13. Fischel, J. and Friend, E. L., Preliminary Assessment of Effects of Wing Flaps on High Subsonic Flight Buffet Characteristics of Three Airplanes: NASA TM X-2011 (Confidential) Flight Research Center, Edwards, California, May 1970.

14. Sisk, T. R. et al, Factors Affecting Tracking Precision of Fighter Aircraft: NASA TM X-2844, (Confidential) Flight Research Center, Edwards, California, March 1971.
15. Bassett, K., Yechout, T., Oelschaeger, D., and Hendrick, R., "A Digital Multi-mode Flight Control System for Tactical Fighters," presented at NEACON, Dayton, Ohio, May 13-15, 1974.
16. Athans, M., and Falb, P., Optimal Control, McGraw Hill, New York, 1966.
17. Bryson, A. E., and Ho, Y. E., Applied Optimal Control, Blaisdell Publishing Company, Waltham, Massachusetts, 1969.
18. Kwakernaak, H., and Sivan, R., Linear Optimal Control Systems, John Wiley and Sons, New York, 1972.
19. VanDierendonck, A. J., "Design Method for Fully Augmented Systems for Variable Flight Conditions," AFFDL-TR-71-162, Wright-Patterson Air Force Base, January 1972.
20. Deets, D. A., "Design and Development Experience with a Digital Fly-by-wire Control System in an F-8C Airplane", in NASA TN D-7843 Flight Research Center, Edwards, California, February 1975.
21. "Research and Development of Automatic Flight Control System: Design Installation and Flight Evaluation in Model, F84-IP," Report No. E9R 12185, Chance Vought Aircraft, Inc., June 30, 1959.
22. Krier, G. E., "A Pilot's Opinion of the F-8 Digital Fly-by-wire Airplane" in NASA TN D-7843 Flight Research Center, Edwards, California, February 1975.
23. Cooper, G. E. and Harper, R. P., Jr., "The Use of Pilot Rating in the Evaluation of Aircraft Handling Qualities," NASA TND-5153, April 1969.
24. Anderson, B. F., The Psychological Experiment: An Introduction to the Scientific Method. Brooks-Cole Publishing Company, Belmont, California, 1966.
25. Stein, G., Henke, A. H., "A Design Procedure and Handling-Quality Criteria for Lateral-Directional Flight Control Systems," Air Force Flight Dynamics Laboratory Technical Report AFFDL-TR-70-152, Wright-Patterson Air Force Base, Ohio, February 1971.
26. Scheffe, H. A., The Analysis of Variance, Wiley, New York, 1969.
27. McDonnell, J. D., "Pilot Rating Techniques for the Estimation and Evaluation of Handling Qualities." Air Force Flight Dynamics Laboratory Technical Report No. AFFDL-TR-68-76, Wright-Patterson Air Force Base, Ohio, December 1968.
28. XF8U-1 and F8U-1 Airplanes Ground Vibration Test Report, Chance Vought Report 9616, 29 April 1955, Dallas, Texas.
29. Kuethe, A. M. and Schetzser, J. D., "Foundations of Aerodynamics," John Wiley and Sons, 1950.